The Development of New Molecular Scaffolds for Nucleic Acid Condensation

Natasha McStay B.Sc.

PhD Thesis

Assoc. Prof. Andrew Kellett
School of Chemical Sciences
Faculty of Science and Health
Dublin City University
Ireland

Prof. Nicholas Gathergood
Tallinn University of Technology
School of Science, Department
of Chemistry and Biotechnology
Estonia

January 2019

Declaration

I hereby certify that this material, which I now submit for assessment on the programme of study leading to the award of Doctor of Philosophy (PhD) is entirely my own work, and that I have exercised reasonable care to ensure that the work is original, and does not to the best of my knowledge breach any law of copyright, and has not been taken from the work of others save and to the extent that such work has been cited and acknowledged within the text of my work.

Signed: _____ ID No.: 10305089 Date:_____

Acknowledgements

I would like to express my sincere gratitude to my supervisor Assoc. Prof. Andrew Kellett for all his help and giving me the opportunity to work in his group. I am deeply grateful for being adopted into his group at the early stage of my PhD. I cannot truly express through words how thankful I am for everything. His kind words of encouragement and patience is endless. It has been a privilege working in the Kellett group under such an outstanding motivational supervisor.

I would like to especially thank Dr Zara Molphy for being my mentor and for providing me with much-needed advice in the early days of my PhD. I wish her all the best. Thanks to my fellow Kellett Research Group colleagues both past and present.

I gratefully acknowledge the funding received towards my PhD from the Marie Sklodowska-Curie Innovative Training Network (ITN) ClickGene [H2020-MSCA-ITN-2014−642023]. This work was also supported by the Synthesis and Solid-State Pharmaceutical Centre (SSPC) and Science Foundation Ireland (SFI) under grant number 12/RC/2275.

I would like to thank Prof Nicholas Gathergood for spiking my interest in opioid research and providing help and support throughout my project. To Tony for his kind patience in teaching me the delicate skill of atomic force microscopy. The AFM will always be my favourite instrument to work on no matter how frustrating it can be. Thank you, Vickie, for all your help and advice. I would like to acknowledge Prof Niall Barron and his group for their cell culture support in assessing the preliminary toxicity of the tripodal opioids. A special thanks to the technical staff in the School of Chemical Sciences and the NRF, they have always gone above and beyond to help. Ambrose is my hero.

I would like to thank my parents and family for their unconditional love, support and belief in me. Especially my crazy sister who has been so amazing. To my best friends Sinead, Tara, and Aisling. The most challenging days are made easy with such great friends around.

“Just keep swimming”

Lastly and most importantly I cannot express how amazing and supportive my partner Paul has been. He has stood by me through all the frustration and helped me in more ways than ever, not only by helping with the cell culture experiments and reading paper drafts but all your kind words of encouragement.

Publications

- **N. McStay**, A. Reilly, N. Gathergood and A. Kellett. Efficient DNA Condensation by a C_3-Symmetric Codeine Scaffold. ChemPlusChem, **2019**, 84 (1), 38-42.

- **N. McStay**, Z. Molphy, A. Coughlan, A. Cafolla, V. McKee, N. Gathergood and A. Kellett. C_3-Symmetric Opioid Scaffolds are pH-Responsive DNA Condensation Agents, Nucleic Acids Res. **2017**, 45 (2), 527–540

- **N. McStay**, Z. Molphy, N. Gathergood, and A. Kellett, Symmetry: Culture and Science, **2017**, 28, 195-198. (conference paper)

Awards

- Colin Barnes award for postgraduate excellence 2017 received on the School of Chemical Sciences Research Day 2017, Dublin City University.

- Outstanding Graduate Researcher Award 2018, Faculty of Science and Health, Dublin City University.

Poster and Scientific Talks

Poster Title:

- **McStay, N**.; Molphy, Z.; Cafolla, T.; Coughlan, A.; Gathergood, N. and Kellett, A. 2016. Opioid Architectures as New DNA Binding Molecules. 68thIrish Universities Chemistry Research Colloquium, University College Cork 23rd and 24th June 2016.

Scientific Talks:

- **N. McStay**, Z. Molphy, A. Coughlan, A. Cafolla, V. McKee, N. Gathergood and A. Kellett. C_3-Symmetric Opioid Scaffolds are pH-Responsive DNA Condensation Chemistry Research Colloquium, Dublin City University 22rd and 23th June 2017

- **N. McStay**, Z. Molphy, A. Coughlan, A. Cafolla, V. McKee, N. Gathergood and A. Kellett. C_3-Symmetric Opioid Scaffolds are pH-Responsive DNA Condensation Agents. School of Chemical Sciences Research Day 2017, Dublin City University, 12th May.

- **McStay, N.;** Molphy, Z.; Gathergood, N. and Kellett, A. 2016. Opioid Architectures as New DNA Binding Molecules. Symmetry Festival 2016, Vienna University of Technology, 18-22nd July.

Table of Contents

Table of Figures

Table of Schemes

Abbreviations

A	Adenine
ACN	Acetonitrile
Boc	tert-Butyloxycarbonyl
Bp	Base pair
C	Cytosine
CD	Circular dichroism spectroscopy
$CDCl_3$	Deuterated chloroform
CHN	Carbon, hydrogen, and nitrogen elemental analysis
ctDNA	Calf thymus DNA
CSD	Cambridge Structural Database
CuAAC	Copper(I)-catalysed azide alkyne cycloaddition
DCM	Dichloromethane
DLS	Dynamic light scattering
DIPEA	*N,N*-Diisopropylethylamine
DMF	Dimethylformamide
DMSO-$_{d6}$	Deuterated dimethyl sulfoxide
DMSO	Dimethylsulfoxide
DNA	Deoxyribose nucleic acid
dsDNA	Double stranded DNA
D_2O	Deuterated water
EDTA	Ethylenediaminetetraacetic acid
EtBr	Ethidium Bromide
EtOH	Ethanol
G	Guanine
HPLC	High pressure liquid chromatography
H_2O	Water
IR	Infrared spectroscopy
K_{app}	Apparent binding constant
lcDNA	Linear DNA
MeOH	Methanol
MP	Melting point
MS	Mass spectroscopy
N.D.	Not detected
NMR	Nuclear magnetic resonance

PCR	Polymerase chain reaction
Phen	1,10-phenanthroline
Poly[(A-T)$_2$]	Poly(deoxyadenylic-thymidylic) acid sodium salt
Poly[(G-C)$_2$]	Poly(deoxyguanylic-deoxycytidylic) acid sodium salt
RNA	Ribonucleic acid
SAR	Structure-Activity-Relationship
stDNA	Salmon testes DNA
T	Thymine
TFA	Trifluoroacetic acid
THF	Tetrahydrofuran
TLC	Thin layer chromatography
T_M	Thermal melting
tRNA	Transfer RNA
rt	Room temperature
ξ	Zelta potential

Units of Measurement

Å	Angstrom
bp	base pair
cm	Centimetre
cm^{-1}	Reciprocal wavelength
C_{50}	Concentration required to reduce 50% fluorescence
˚C	Degrees Celsius
δ	NMR chemical shift
T_M	Thermal melting
ε_{max}	molar absorption coefficient
g	gram
h	Hour
Hz	Hertz
J	Coupling constant
K_{app}	Apparent binding constant on DNA
Kb	kilobase
L	Litre
M	Molar

mol	Mole
mg	Milligram
min	Minute
ml	Millilitre
mM	Millimolar
Mp	Melting point
ng	Nanogram
pH	Potential of hydrogen
ppm	Parts per million
Q	Fluorescence quenching
r	[drug]/[DNA] ratio
s	Seconds
V	Volt
ν	Frequency
µL	Microliter
µM	Micromolar

Abstract

Natasha McStay B.Sc.

The Development of New Molecular Scaffolds for Nucleic Acid Condensation

The discovery of new synthetic DNA recognition agents is an area of considerable research interest. The aim of this research was to develop novel trivalent scaffolds for the purpose of DNA condensation and examine through structure-activity relationships how these compounds bind and collapse the helical structure of DNA into particles suitable for passing through biological barriers.

A major objective of this study was to investigate the use of synthetic tripodal C_3-symmetric opioid scaffolds as efficient condensation agents of double stranded DNA (dsDNA). Morphine, codeine, heterocodeine, and oripavine C_3-opioids were generated and showed comparable condensation capabilities. Condensation was achieved on both superhelical and linear dsDNA conformations and identified by agarose electrophoresis, viscosity, turbidity, and atomic force microscopy (AFM) measurements. Tripodal opioid aggregation was identified as pH dependent and strongly influenced by ionic strength with further evidence of cationic amine-phosphate backbone coordination.

Since preliminary screening of the C_3-oripavine opioid with selected mammalian cell lines indicated poor tolerance, the second aspect of this project focused on developing non-opioid DNA condensation agents. Tripodal imidazolium salts containing the same mesitylene core as the C_3-opioids were therefore screened for potential activity. Results showed some evidence of DNA condensation but not at the same threshold as C_3-opioids.

Building on these results, a new library of terminal polyamine C_3-scaffolds was prepared using the copper-catalysed azide-alkyne cycloaddition reaction. This new series, called “Tri-Click”, was developed as potential non-viral vectors for gene delivery with potentially lower cytotoxicity compared to tripodal opioids. The solubility of Tri-Click compounds was greatly improved compared to C_3-opioids scaffolds but evidence of nucleic acid damage was also identified. This DNA damage mechanism was then probed using a variety of biophysical methods with specific trapping agents for reactive oxygen species (ROS) indicating single stranded DNA breaks mediated by copper-catalysed free radicals.

Chapter I

DNA Structure, Function, and Condensation

I. 1. Nucleic Acids as Molecular Targets

Nucleic acids are an important target molecule for the development of new biologically active therapeutics. An important aspect of targeting a molecule is understanding its structural and functional components in great detail. This introduction will focus on the structure and function of deoxyribonucleic acid (DNA), gene therapy and applications of gene delivery with a focus on nucleic acid condensation.

I. 1.1. DNA primary and secondary structure

DNA is comprised of two chains made of nucleotides where each nucleotide contains a phosphate group, a sugar and a nitrogenous base. These two strands are known as polynucleotides that coil around each other to form a double helix which codes for the genetic makeup of living cells. In ribonucleic acid (RNA), the sugar unit is ribose while in DNA the sugar is deoxyribose and the difference between these two structures is a single oxygen atom. There are four heterocyclic bases in DNA which are grouped as purines (adenine (A) and guanine (G)) and pyrimidines (cytosine (C) and thymine (T)). The secondary structure of DNA arises from each of the four nucleobases pairing with a specific complementary base through hydrogen bond donor and acceptor properties,[1] Figure I-1A. DNA bases follow Chargaff's rules whereby a 1:1 (purine:pyrimidine) relationship exists between A and T as well as G and C.[2,3] The biologically predominant B-form of duplex DNA comprises of two antiparallel sugar-phosphate chains, where the heteroaromatic bases lie in the centre of the helix and hydrogen bonding between them effectively binds the two helical chains together.[4] The phosphodiester backbone is highly negatively charged, the pK_a of phosphate groups are near 0 at physiological pH (7.2). The Watson-Crick arrangement stabilises the structure through both inter-chain base pair hydrogen bond interactions and π-π stacking interactions between complimentary base pairs.[1] The angle between the glycosidic bonds and the hydrogen bonds results in unequal grooves in the helical structure referred to as the minor and major grooves. Structural characteristics of B-DNA highlight key aspects such as the major groove (10.5 Å) is wider than the minor groove (4.8 Å), although their depths are generally identical. Between the base pairs of B-DNA there is an axial rise of 3.4 Å (0.34 nm) and a 34.5 ° twist angle associated with every residue rotation while the width of the helix diameter is 20 Å (Figure I-1C).[5]

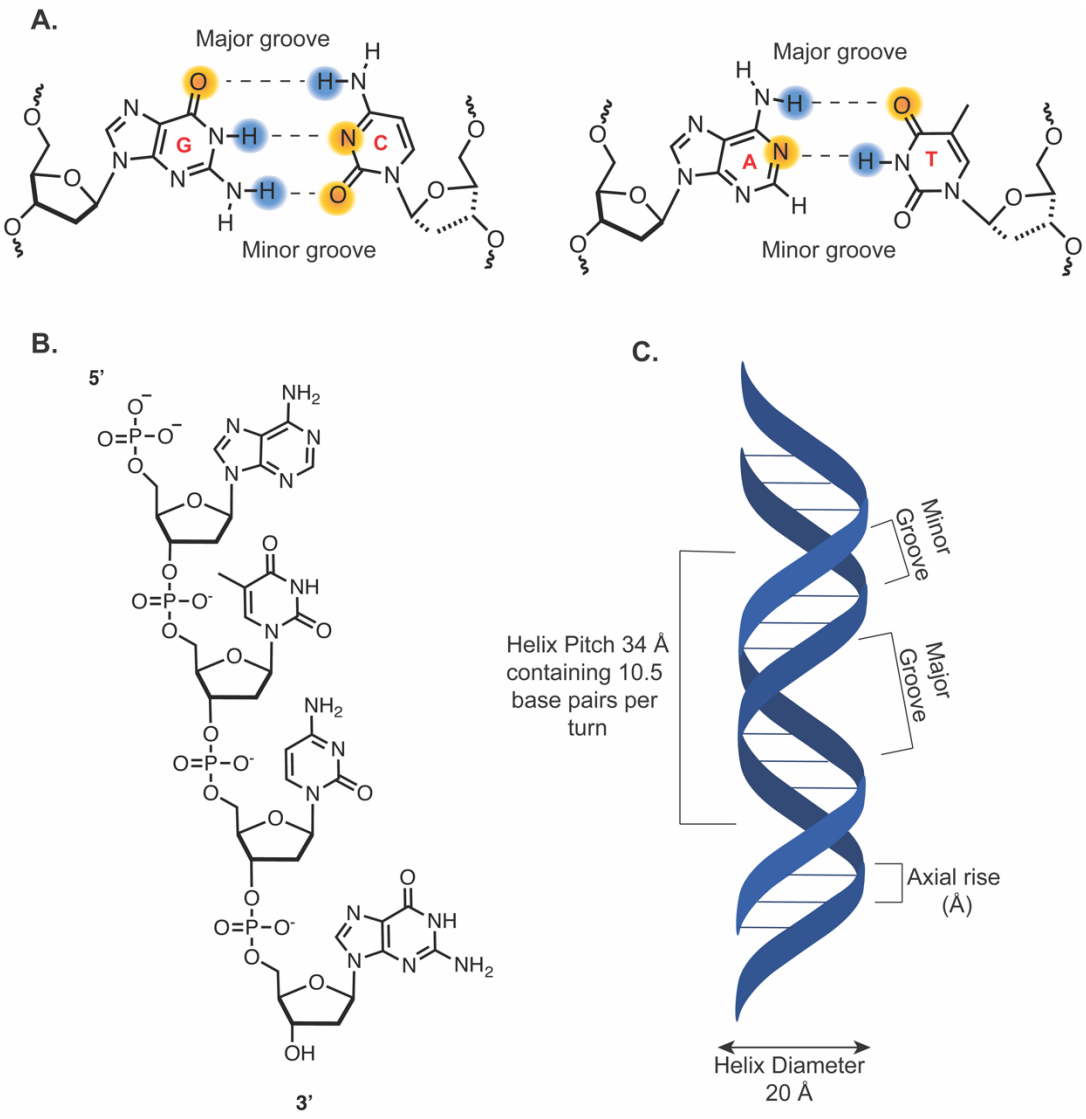

Figure I-1. A. DNA base pairs, guanine-cytosine (G-C) and adenine-thymine (A-T) highlighting hydrogen bond donor (blue) and acceptor (orange) relationships. **B.** Sequence 5'-ATCG-3', phosphate group. **C.** DNA ribbon display illustrating main structural features of B-DNA.

I. 1.2. DNA tertiary structure

Most DNA double helices are right-handed however there is still a certain degree of plasticity and conformational arrangements associated with the tertiary structure. There are three main subtypes studied in solution including A-DNA, B-DNA and Z-DNA, Figure I-2. A-DNA is a short, wide, right-handed helix resulting from dehydrated DNA and is rarely observed under normal physiological circumstances. A-DNA has a similar but more rigid and compacted structure consisting of 11 base pairs per helical turn with a axial rise of 2.3 Å between bases pairs.[5] B-DNA, the structure proposed by Watson and Crick, is the most common conformation in most living cells.

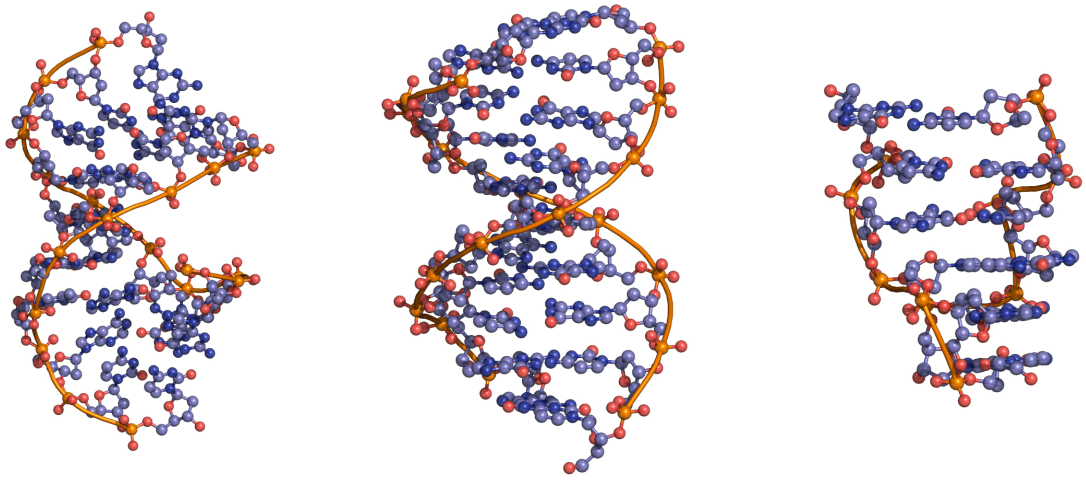

Figure I-2. X-ray structures of A-, B- and Z-DNA from PDB files 1VJ4, 1BNA and 2DCG.

Z-DNA, unlike A- and B-DNA, is a left-handed helix. Z-DNA was first discovered in 1979,[6] and is a transient form of DNA, only occasionally existing in response to certain types of biological activity such as during transcriptional processes *in-vivo*, due to the torsional strains generated as negative supercoils are created by RNA polymerase moving along the sequence of the DNA double helix. This drastic conformational change is due to bases alternating between the syn- and anti-conformations. Z-DNA is elongated and narrow with a diameter of 18 Å, and is composed of only one single narrow groove which resembles that of the minor groove of B-DNA resulting in a zigzag arrangement of the backbone (hence Z-DNA). Recently, certain proteins where shown to bind very strongly to Z-DNA, suggesting that Z-DNA plays an important biological role in protection against viral disease.[7] A number of parameters are used to define distortions from ideal DNA conformations and can be distinguished by a number of factors including; helical sense, number of nucleotides within one pitch (residues per turn), helical pitch (distance between two base pairs within a 360° turn), helix diameter, distance between base pairs (axial rise), and the angle of rotation between residues (Table I-1).[8] The structural form of DNA is not limited to helices described, other forms of DNA such as triplexes, G-quadruplexes, and I-motifs have recognised importance for gene-specific drug targeting.[9,10]

Table I-1. Summary of the main structural differences between A-, B-, and Z-DNA.[8]

Parameter	A-DNA	B-DNA	Z-DNA
Helical sense	Right	Right	Left
Residues per helical turn	11	10	12
Helix Pitch (Å)	28	34	45
Helix Diameter (Å)	23	20	18
Axial Rise (Å)	2.55	3.4	3.7
Rotation per Residue (Å)	33	36	-30

When the two ends of DNA are covalently closed to form a circular molecule (ccDNA or scDNA) the total number of times DNA chains can twist around one another is based on the total number of base pairs in the sequence and the DNA is said to be topologically constrained (Figure I-3). The twist of the helix is defined as the number of helical turns of one DNA strand around the other and the writhe is the number of times the DNA is interwound. The sum of the twist number (Tw) and the writhe number (Wr) must equal the link number (Lk), such that Lk = Tw + Wr. DNA supercoiling is generated by DNA metabolism and typically tends to be overwound (positively supercoiled) upstream of replication or transcription forks and underwound (negatively supercoiled) downstream of these forks.[11] Cellular processes such as transcription, translation recombination and chromatin compaction can only proceed if topological entanglements are relaxed in order to maintain cellular function. There are two ways in which topological constraints can be relieved enzymatically including treatment with DNaseI or DNA topoisomerases.[12] DNaseI is a double strand specific restriction endonuclease that hydrolytically cleaves the phosphodiester backbone of DNA in the presence of divalent cations (Ca^{2+} and Mg^{2+}) inducing single stranded nicks via the hydrolysis of P-O3′ bond in the minor groove producing 5′-phosphorylated and 3′-hydroxylated fragments. This restriction enzyme digests all phosphodiester bonds and is involved in cellular processes including DNA degradation.[13]

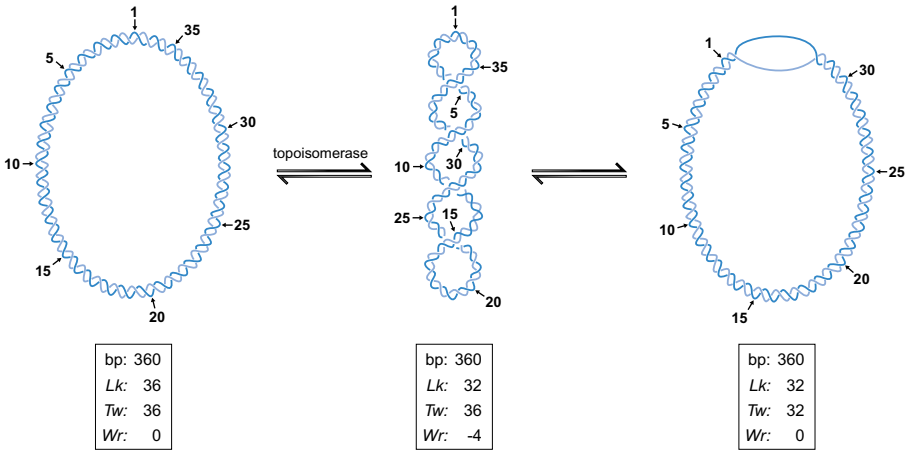

Figure I-3. Topological constraints of supercoiled DNA. Conversion of relaxed, to negatively supercoiled and local disruption of base pairing by an enzyme.[11]

I. 1.3. DNA damage

DNA damage can result from metabolic or hydrolytic processes in cells, including reactive oxygen species (ROS), reactive nitrogen species (RNS), reactive carbonyl species, alkylating agents, and hydrolysis which can cleave along the phosphodiester bond. Cleavage of DNA is an important process in normal functionalisation of living cells. Enzymes such as topoisomerase introduce temporarily single or double strand breaks for DNA replication, transcription, recombination and chromatin remodelling. Restriction endonucleases protect against foreign DNA by cleaving the affected DNA sequence.[14]

Examples of chemical damages to DNA bases include but are not limited to: the deamination of cytosine, the methylation of guanine or cytosine, and the oxidation of the 8-position of adenine or guanine by hydroxyl radicals generated by oxidizing agents or γ-radiation, Figure I-4. These chemical damages are counteracted by specific DNA repair processes. The conversion of cytosine to uracil gives rise to transition mutations if left uncorrected (Figure I-4A). Uracil is a foreign base in DNA, and is converted back to cytosine by a specific enzyme, uracil DNA glycosylase (UDG). O(6)-Methylguanine can be formed when DNA is exposed to alkylnitrosoureas, such as *N*-nitrosodimethylamine (NDMA) and *N*-methyl-*N*-nitrosourea. The major product of the reaction is *N*(7)-methylguanine (Figure I-4B), which is not mutagenic, because the modification does not disturb base pairing; but the O-methylated product, O(6)-methylguanine, is mutagenic (Figure I-4C).

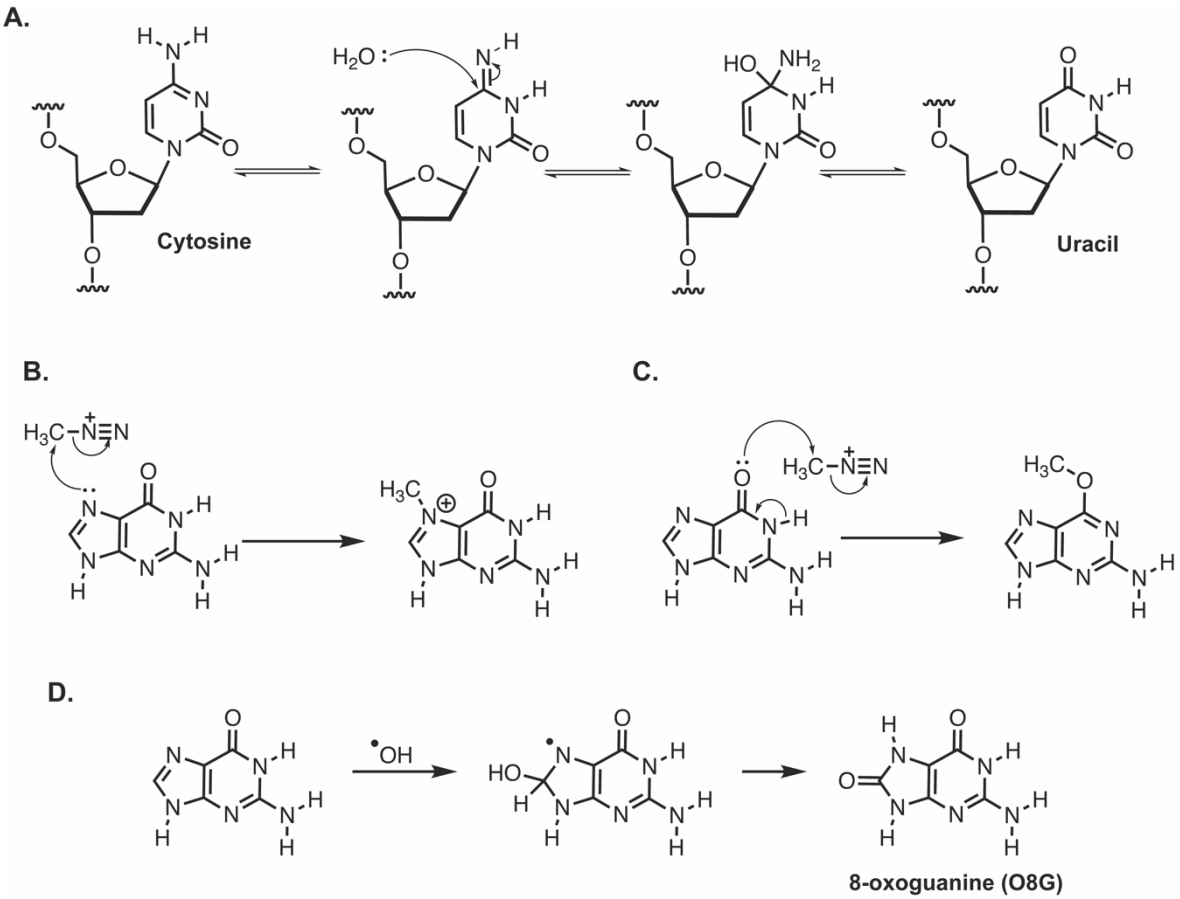

Figure I-4. Hydrolytic cytosine deamination to uracil (**A.**); Methylation of guanine by the diazonium cation formed from alkynitrosourea, major product *N*(7)-methyl dG (**B.**) and minor product O(6)-methyl dG (**C.**); Oxidation of guanine to 8-oxoguanine (O8G) (**D.**).

The reaction of the purine bases of DNA with ROS such as hydroxyl radicals can result in the formation of 8-oxoguanine (O8G) Figure I-4D, which base-pairs preferentially with adenine rather than cytosine and thus generates transversion mutations after replication and is considered one of the major mutagenic base lesions generated by hydroxyl radicals. The activities of many anticancer drugs rely on the ability to introduce extensive damage to DNA which in-turn triggers cellular apoptosis. The reduction of molecular oxygen can generate reactive intermediates such as superoxide anion ($O_2^{\bullet-}$) and hydrogen peroxide (H_2O_2), which in turn through redox reactions gives rise to the production of hydroxyl radicals ($^{\bullet}OH$). Although the superoxide anion is indirectly toxic to DNA, in the presence biologically relevant transition metals such as copper(II), a one electron redox reaction results in the production of oxygen radicals. $^{\bullet}OH$ generation can be driven by the reduction of Cu^{2+} by superoxide under oxidative stress promoting Fenton-like chemistry.[15,16]

These reactions couple to produce copper catalysed Haber-Weiss processes.[17,18] The development of artificial metal-based chemical nucleases (*e.g*. copper(II) 1,10-phenanthroline complexes) has gained increased attention in recent years and this research stemmed, largely, from observations reported by Sigman.[19] The Kellett group has carried out extensive research on the development of artificial chemical nucleases with a focus on copper(II) phenanthrene oxidative damage.[15–18,20–22] Compounds capable of inducing site selective double strand cleavage are of great importance not only as anticancer therapeutics but also aiding in the development of gene editing technology.

I. 2. Gene Editing

Gene therapy is the therapeutic delivery of nucleic acids into a patient to achieve a therapeutic effect. Broadly, its functions can be classified as *i*.) replacing a mutated gene, *ii*.) inactivating a mutated gene, or *iii*.) introducing a therapeutic gene to combat disease. Gene editing technologies such as homologous recombination (HR)[23] and Cre-Lox site specific recombination[24] where the first methods available for gene editing, however these techniques suffered from poor site selective activity and efficiency. The development of site selective cleavage was introduced by zinc-finger nucleases (ZFNs),[25,26] and transcription activator like effector nucleases (TALENs)[27,28] which greatly improved on the current methodologies. However, the recent development of clustered regularly interspaced short palindromic repeat sequences (CRISPRs) has overshadowed these techniques, Figure I-5.[29,30]

DNA recognition by zinc fingers occurs in the presence of a zinc atom. The zinc finger protein domain forms a compact $\beta\beta\alpha$–structure with the α-helical portion of each finger making contact with 3 or 4 bp in the major groove of the DNA.[31] Tandem fingers in a zinc finger array wrap around the DNA to bind extended target sequences such that a three-finger protein binds a 9 bp target site. Zinc finger nucleases are classified as chimeric as they are comprised of a FokI restriction endonuclease where the domain has been replaced with a zinc finger domain. The FokI nuclease functions as a dimer allowing two ZFNs to bind to opposite strands of DNA containing three zinc-finger domains, which is required to induce double strand breaks, Figure I-6.[25] The advancement of ZFNs occurred when synthetic arrays containing more than three domains that could recognize DNA sequences of 9-18 bp in length were developed. Since oligonucleotides of 18 bp is sufficient to

offer specificity within the human genome, ZFNs technology enables targeting of virtually any sequence.[32] However, ZFNs are challenging to build and assembly of finger domains is frequently unsuccessful along with combining the two domains to form a dimer with the correct orientation, spacing and protein packing.[31]

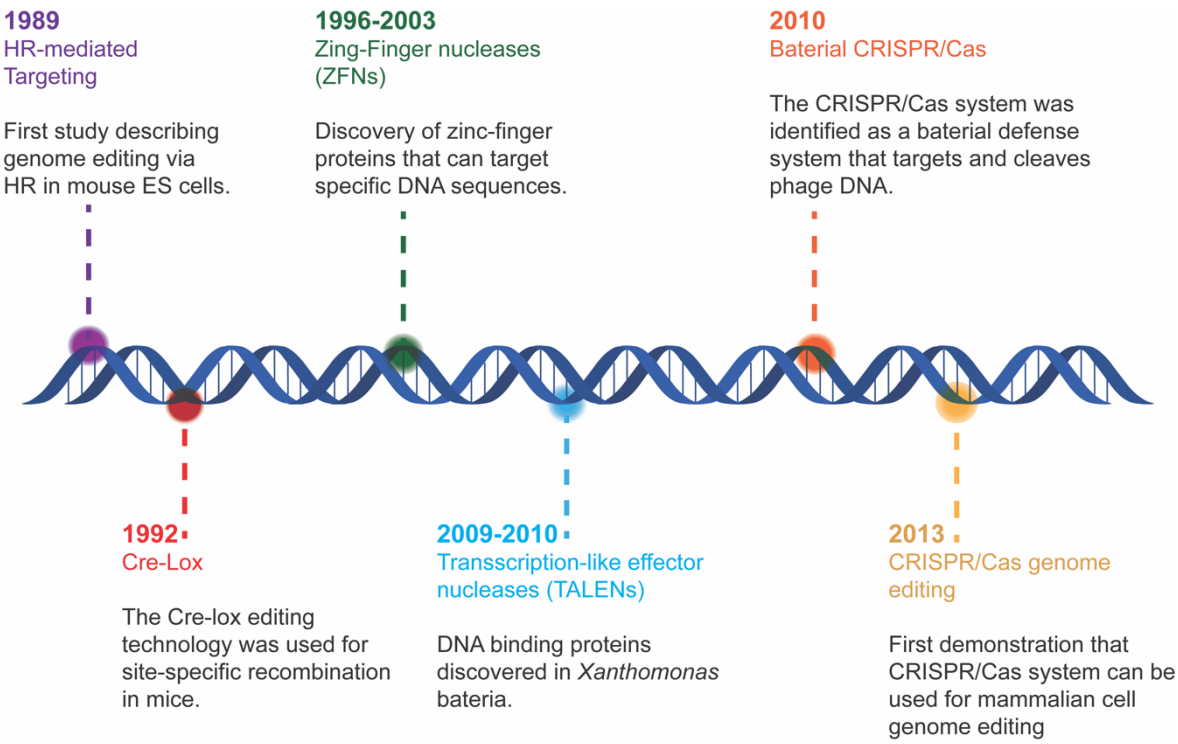

Figure I-5. A timeline of breakthrough discoveries in gene editing technology.

Close to ten years after ZFNs, TALENs were discovered and highlighted an alternative platform for engineering DNA-binding proteins.[27] TALE proteins isolated from the plant pathogen Xanthromonas highlighted highly conserved 33-35 amino acid repeats, each of which binds to a single base pair of DNA with specificity dictated by two hypervariable residues. Each repeat forms a two-helix structure connected by a loop into the major groove of DNA as the protein wraps around in a superhelical structure.[33] Similar to ZFNs, TALEN repeats are linked together to recognize contiguous DNA sequences, however, the cloning repeat of TALEN arrays can be troublesome to generate, requiring a binding sequence to begin with thymine base recognition.[28]

The discovery of clustered DNA repeats lead to the identification of CRISPRs[34] and from there researchers identified nearby CRISPR associated genes and Cas proteins, CRISPR/Cas9 system.[35] Unlike ZFNs and TALENs which use protein-DNA

interactions for targeting, CRISPR/Cas systems use RNA-guiding nucleases which are governed by base-pairing rules between the engineered RNA and the target DNA site, Figure I-6. Two components must be introduced into and/or expressed in cells to perform genome editing: the Cas9 nuclease and a guide RNA (gRNA), consisting of a fusion of CRISPR RNA and a fixed transactivating CRISPR RNA (crRNA).[36] Twenty nucleotides at the 5′ end of the gRNA corresponding to the protospacer portion of the crRNA, directs the Cas9 nuclease to cleave complementary target-DNA sequences. Cas9 nuclease activity can be engineered to any DNA sequence in the form of N_{20}-NGG, simply by altering the first 20 nucleotides of the gRNA to correspond to the target DNA sequence.[29,37,38] The simplicity of the Cas9 nucleases has allowed for multiple gRNAs to be introduced simultaneously, inducing small and large deletions or inversions between double strand breaks.[39,40] A current issue associated with this system has been identified by Cas9-induced off target mutations. High rates of mutagenesis have been observed for off-target sites which can be variable in frequency and challenging to predict as they arise due to mismatch pairing and prolonged expression. The off-target mutations are a major concern when applying CRISPR/Cas9 system to clinical applications, however new tools are becoming readily available for the reduction of these off-target mutations.[41]

Recent reports have indicated that while CRISPR/Cas9 worked quite effectively in editing cancer cells, it was remarkably inefficient when targeting healthy cells.[42,43] This stems from the association of protein p53 being activated when CRISPR/Cas9 systems induces double strand breaks on the target DNA strand. This protein activates the repair systems in the cell when DNA is damaged, making editing much more difficult. The absence of p53 in cells may result in CRISPR systems being more effective, but puts a cell at risk to become cancerous. Mutations, or deficiencies in p53 gene have been found in the majority of cancer types, often known as a tumour suppressor gene.[44] What if the p53 gene could be restored? Chira *et al*. proposed a concept of restoring the p53 genotype in cancer cells by entirely replacing the mutant p53 locus within the tumour genome with a functional copy, resulting in cell death and possible tumour regression.[45] The p53 locus measures 20.5 kb in length,[44] where previously the CRISPR/Cas9 system has efficiently replaced a large genomic fragment of 65 kb which could make this concept come into reality very soon.[46]

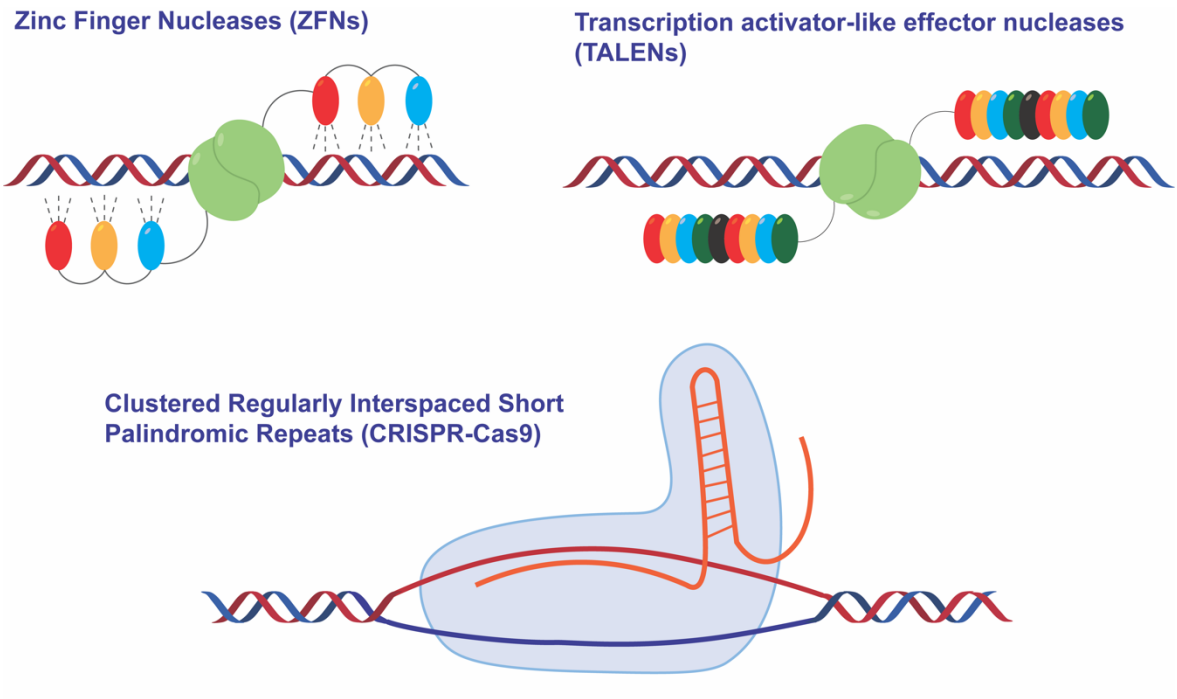

Figure I-6. Representation of gene editing technologies: zinc finger nucleases (ZFNs); transcription activator like effector nucleases (TALENs); clustered regularly interspaced short palindromic repeat (CRISPR) sequences.

Gene therapy has become one of the most promising strategies for treating genetic diseases and has gained increased attention since the discovery of the CRISPR/Cas9 system; significant research is ongoing in this field.[37] However, a major limitation for gene editing by ZFNs, TALENs and CRISPR/Cas9 systems is the *in vivo* delivery of these large proteins and plasmids. Focusing on CRISPR/Cas9 systems, this requires the delivery of a specified plasmid which encodes for the Cas9 enzyme and one or more RNAs rather than large protein complexes required for ZFNs and TALENs.

I. 2.1. Gene delivery

Gene delivery methods are classified as either viral or non-viral, where non-viral applications can be further categorised by physical or chemical methods. A summary of some of the current methods of gene delivery is highlighted in Figure I-2. Physical methods include: microinjection; electroporation; sonoporation; and gene gun delivery.[47] However, these forms of gene delivery are limited to *in vitro* or *ex vivo* applications only and will not be discussed further.

Table I-2. Methods of gene delivery.[47-49]

Viral Vectors	Non-Viral	
	Physical	**Chemical**
Lentivirus	Microinjection	Cationic Polymers
Retrovirus	Electroporation	Neutral crowding
Adenovirus	Sonoporation	Dendrimers
Adeno-associated virus	Gene gun	Liposomes
Herpes simplex virus		Inorganic-complexes

I. 2.2. Viral vectors

Lentiviral, retroviral, adenoviral, and adeno-associated viral (AAV) vectors have been extensively studied as model systems and in clinical applications. Most approved clinical trials for gene therapy so far have utilised viral vectors as the delivery system. The majority of these trials are currently in early proof of concept phases (phase I or II) where only a small percentage have reached phase IV. Viral vectors are efficient in DNA/RNA packing and delivery for *in vitro*, *ex vivo* and *in vivo* applications. Viruses have evolved very efficient mechanisms to deliver genetic material into cells. Retroviral and lentiviral systems package their cargo within a protein like capsid surrounded by a lipid membrane envelope, which can fuse with the plasma membrane of a cell delivering the payload into the cytoplasm. Retroviral vectors are limited to *ex vivo* applications and dividing cells, however, lentiviral vectors can mediate gene transfer in both dividing and non-dividing cells.[50] Other viruses, such as adenovirus and AAV have a proteinaceous capsid that is taken up by endocytosis and have evolved to escape the endosome/lysosome compartment to deliver the cargo DNA directly to the nuclease. Adenoviral vectors have a high-capacity with regard to viral vectors mentioned above, up to 36 kb capacity.[51]

The preparation of these viral-vectors where viral genomic DNA is completely removed can be difficult to prepare in high volume. A major limitation, is the strong innate immune response to the adenoviral capsid itself, as well as continuing low-level expression of viral genes producing a secondary viral gene-dependent immune response. The severity and risk of evoking a harmful immune response and other toxic side effects is a direct result of vector dose, where, *in vivo* delivery at high doses can result in severe inflammation and cytotoxicity.[52] Viral-vectors suffer from site-selective integration and more work is required to develop specific target-cell populations for in vivo applications.

I. 2.3. Non-viral vectors

Thus, the most rate limiting step for gene therapy is the delivery mechanism. Although viral-vectors have shown promising applications in pre-clinical trials they suffer from serious immune responses, toxicity and carcinogenesis. More recently non-viral vectors are receiving increased attention as a plausible substitution.[48,53,54] Despite the rapid discovery and recent development of various synthetic non-viral vectors, only a small fraction have been used in clinical stages of research. Nevertheless, there are several advantages of non-viral vectors such as ease of preparation, large scale production, stability, low cost, safety, lower immunogenicity and reduced toxicity.[53] The first step in the preparation of a non-viral vector is nucleic acid condensation/packing. The ability of a condensation agent to efficiently pack and protect DNA cargo from endonuclease activity in cells, along with aiding in cellular uptake is essential.

I. 3. DNA Condensation

The majority of DNA in all living organisms is present as well-ordered and compact structures. This packing is essential for the organising of long genome sizes of ~3 billion bp and natural examples include the formation of chromatin which is a result of condensed DNA/protein complexes.[55] Other forms of compaction can be highlighted through DNA packing in viruses and bacteria. Important early research questions included the study of DNA packing in the heads of bacteriophages, however now there is a greater interest in nucleic acid condensation as it is an important step in the nucleic acid delivery for gene therapy applications. DNA condensation is defined as “the collapse of extended DNA chains into compact, orderly particles containing only one or a few molecules” either *in vitro* or *in vivo*.[56]

I. 3.1. Mechanism of condensation

DNA is a highly charged molecule and cationic charge density plays a critical role in DNA aggregation where the majority of cationic condensation agents carry a 3+ or higher charge to fully collapse the helical backbone.[57,58] A common mechanism of synthetic and naturally occurring surface binders is the ability to bind the electron rich phosphate backbone, primarily through H-bonding and electrostatic interactions. Electrostatic binding by polycationic molecules can directly lead to a collapse in the B-DNA conformation with which results in the condensation or aggregation of DNA structures.[59] Cationic charge density is essential for the

neutralisation of anionic phosphate charge and the reorganisation of water dipoles adjacent to DNA surfaces resulting in nucleic acid condensation. DNA collapse occurs once ~90% of phosphate charge neutralisation has occurred[57] where the structure and charge density of the condensation agent plays a key role within collapsing transitions.[60] Although DNA condensation has been reviewed extensively by Bloomfield[59] and others including theoretical descriptions into the dynamics of polymer collapse,[56,61] it is important to consider recent advances to this field. Exceptions to the ≥3+ cationic valence requirement for DNA collapse are rare, both Mn^{2+} and the putrescine^{2+} cations are known to aggregate DNA but only at high (millimolar) concentration.[62]

I. 3.2. Structure and morphology of condensed DNA

The morphology of DNA aggregates depends on the solution properties, condensing agent structure and DNA length. The compaction of DNA is considered to be highly ordered and Atomic Force Microscopy (AFM) has allowed for the study and visualisation of these structural variations of plasmid DNA. Condensed DNA commonly forms toroid structures, similar in shape to a doughnut. These condensed forms of nucleic acid were once believed to have a specific outer radius of 50 nm,[59] however DNA can aggregate into toroid structures of varying sizes, along with non-toroidal structures such as rods. Golan *et al.*[63] reported detailed AFM images on the various stages of plasmid condensation into toroid and rod structures by a positively charged polylysine compound covalently bound to a glycoprotein, acting as a cationic condensing agent. A representation of the reported AFM images shown in Figure I-7(I-IV) highlights the stages of condensation from open circular plasmid DNA to flattened, compact and then the tightly packed toroid and rod structures. Classical toroid DNA compaction as shown in Figure I-7 (a-d) and compared to elongated toroid structures present in Figure I-7 (e-h), which lie outside the expected parameters and highlight that condensation is not a strict process. The DNA content of toroids and rods is based on the assumption that the toroid or rod contains B-DNA packing throughout.[64,65] The relationship between toroids and rods has been of great interest in the understanding of nucleic acid condensation,[66–69] the formation of these aggregates being influenced by both kinetic and thermodynamic factors under experimental conditions. Shorter DNA strands have been shown to favour rod like condensates while larger plasmids form toroid and non-toroidal aggregates.[67] The formation of condensed DNA is not restricted to toroids or rod

like structures and, through AFM imaging, aggregates of varying shapes and sizes are possible.[70] Polycations can induce alternative changes in B-DNA configuration; a reversible B ⟶ A transition, regulated by dehydration, was recently shown in short G-C rich oligonucleotide sequences exposed to a poly(allylamine)-*graft*-dextran synthetic cationic polymer.[71]

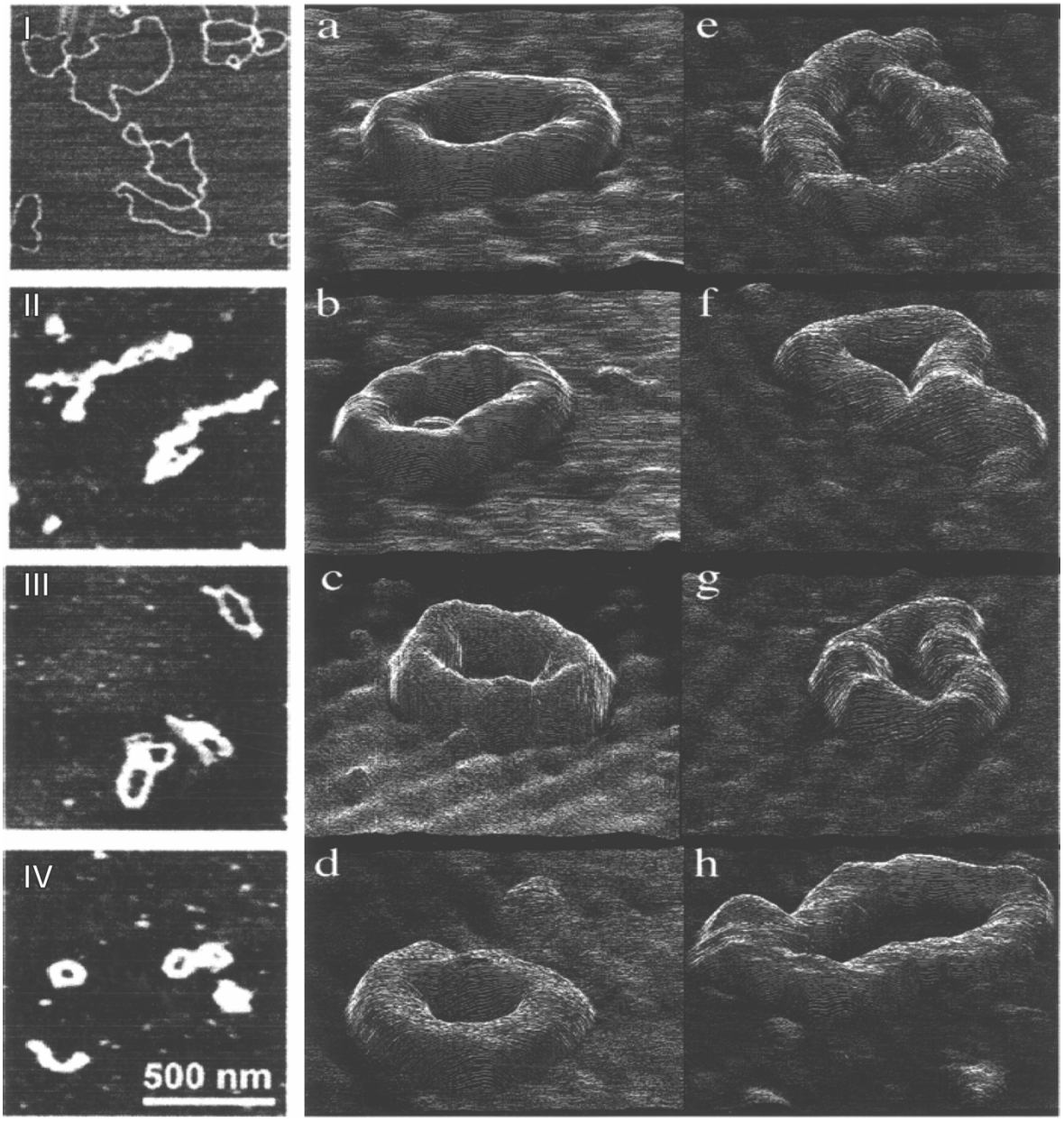

Figure I-7. AFM images reported by Golan *et al*.[63] Stages in DNA condensation, (I) circular plasmid DNA; (II) thick flattened; (III) compact; (IV) toroid and rods. Variability in toroid size and shape; (a-d) toroid of uniform shape and contour length. AFM images (e-h) highlight toroids of irregular shape and variable contour length.[63]

I. 3.3. Cellular uptake and targeting

Cationic vectors condense negatively charged DNA into compact particles by electrostatic interactions which results in positively charged particles. These particles can also facilitate cellular uptake via electrostatic interactions with anionic cell surface groups, such as proteoglycans. Interactions with proteoglycans may be essential for the process of internalization of the complexes. Internalization takes place by a non-specific adsorptive endocytosis.[72] Improvements to cellular uptake has been undertaken by adapting receptor-mediated surface binding, through incorporation of cell-binding ligands into transfection complexes. These cell binding ligands can be proteins,[73] peptides,[74] vitamins,[75] or antibodies[76] that specifically recognize a cell surface receptor. Receptor-mediated targeting is limited by the level of expression of the receptor on the cell surface, the affinity of the ligand-receptor binding and most importantly, whether binding to the receptor is followed by internalization.[77] Polylysine has been shown, when coupled to transfection agents, to have enhanced cell targeting and uptake properties. This was first shown by Wu *et al.* who demonstrated the targeting of asialoglycoprotein receptors by polylysine/DNA complexes.[78–80] In most cases, efficient internalization of ligand/DNA complexes was found, however DNA complexes often remained trapped in the endolysosomes. These form as a result of fusions between late endosomes and lysosomes during endocytosis; due to the high acid hydrolase activity that can result in DNA degradation.[81] However, in cell types with an excess presence of negatively charged cell-surface proteoglycans receptor mediated delivery is not required.

I. 4. Condensation Agents

I. 4.1. Naturally occurring polyamines

Naturally occurring polyamines spermidine^{3+} and spermine^{4+} are abundantly found in living organisms and aid in the packaging of cellular DNA by lowering the free energy of transition required for condensation.[56,60] In rare cases putrescine^{2+} has been shown to induce DNA condensation at high loading, structures shown in Figure I-8. Ionization of polyamines is an important factor in these interactions with nucleic acids to induce condensation. The pK_a values for these polyamines are as follows: putrescine, 10.8 and 9.4; spermidine, 10.8, 9.94 and 8.4; spermine, 10.9, 10.1, 8.9 and 8.1, supporting the view that the predominant mode of interaction is electrostatic in nature.[82] DNA condensation studies in the presence of polyamines bearing the

same degree of positive charge showed that chemical structure had a significant influence on DNA condensation and the nature of the aggregates formed.[60] Rowatt *et al.* investigated the strength of polyamine binding to DNA of polyamines with varying methylene spacer lengths and observed that the presence of the butylene rather than the propylene group is preferable for tight binding.[83] Stereospecific effects were also found in the case of dimethyl-spermine analogues. Hydrodynamic radii of nanoparticles formed in the presence of α,α'-dimethyl-spermine differed significantly from those produced by spermine, forming larger aggregates.[84]

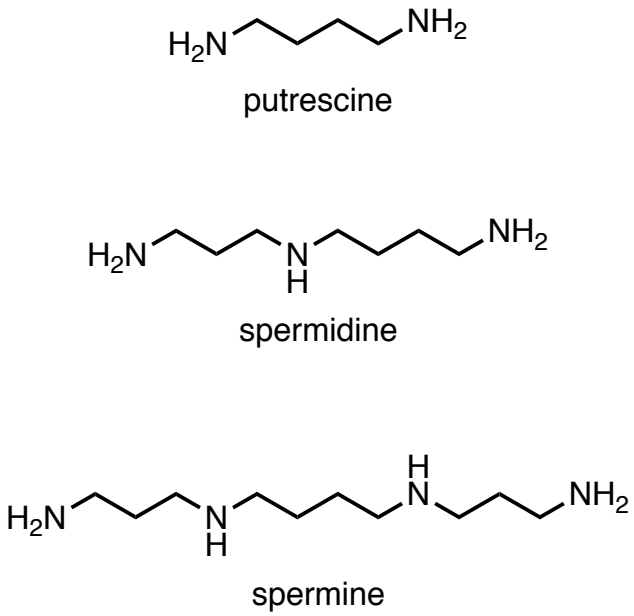

Figure I-8. Chemical structures of natural polyamines

I. 4.2. Cationic polymers

Cationic polymers offer an immense chemical diversity and potential for functionalization and are an ideal scaffold to build from. Early examples of cationic polymers capable of condensing DNA include polylysine and polyethylenimines (PEIs). Highly cationic charge density polymers PEIs have shown particularly promising efficacy for the compaction and transfection of nucleic acids in cell culture as well as applications *in vivo*. PEIs are synthetic polymers that can be prepared either in linear or branched forms and are the most studied polymeric material for gene delivery. The ethylamine repeating units provide every third atom as a potential protonate-able amino nitrogen giving rise to the high cationic charge, however under physiological pH only every 5th or 6th amino nitrogen is protonated.[85,86] DNA condensation by cationic polymers can be described as a function of the cation-to-anion ratio, PEI nitrogen-to-DNA phosphate (N/P) ratio; where complete

condensation of DNA occurs at N/P ratios of 2-3 forming neutral particles, higher ratios (>4) results in complexes forming with a strong positive charge.[77]

Gene delivery vectors suffer from cytotoxicity due to poor biocompatibility and non-degradable structures under physiological conditions. The degree of transfection must overcome the degree of toxicity and thus preparing non-viral vectors to provide sufficient stability with reduced toxicity is of great importance.[87] Functional group modification can increase polymer activity, cellular uptake, and reduce toxicity. Guanidinium groups are important in cellular penetrating peptides, shown to facilitate the cellular internalization and when incorporated can enhance cellular uptake of polymers/DNA complexes. Carboxyl groups can influence the net average charge which can affect their cellular uptake, endosomal escape, and transfection efficiency in gene delivery. Disulfide bonds increases biodegradability and decrease cytotoxicity. Hydrophobic groups influence hydrophobic/hydrophilic balance, gene encapsulation, and gene dissociation from polyplexes and cellular uptake of the polymers. Branching polymers can enhance transfection efficiency to some extent.[88] However, it is important to note that different functional groups may affect polymer properties in the different stages of gene delivery.

I. 4.3. Neutral crowding polymers

Neutral polymers such as polyethylene glycol (PEG) have been shown under high concentrations to provoke DNA condensation. This process is a result of an excluded volume mechanism.[89] Conjugation of PEG has shown to increase water solubility and stability of some complexes, along with preventing nonspecific protein adsorption.[90] PEG has been extensively used for PEI modification as it provides shielding and stealth properties to PEI/DNA complexes, however this can lead to a reduction of non-specific ionic interactions between the complex and target cells, leading to a decrease in transfection efficiency.[91]

I. 4.4. Dendrimers

Dendrimers are an important class of synthetic condensing agents, in particular polyamine scaffolds. They are composed of hyperbranched architectures with symmetric repetition of inner layers, these repetitions are commonly known as “generations”. The increment of generations confers an increase not only in structure but also overall charge density. The use of dendrimers has been

extensively studied as an important class of non-viral vectors.[92–95] Poly(amidoamine) (PAMAM) is a commercially available dendrimer commonly used as a starting point in the synthesis of these large complexes. The basic PAMAM dendrimer up to the second-generation dendrimer is shown in Figure I-9, where each subsequent generation is attached via the primary terminal amine on each amidoamine chain. The ethylenediamine core can be replaced by alternative diamines such as 1,5-diaminohexane and bis(3-aminopropyl) ether. This had a significant impact on dendrimer size and structural symmetry under varying pH conditions.[96]

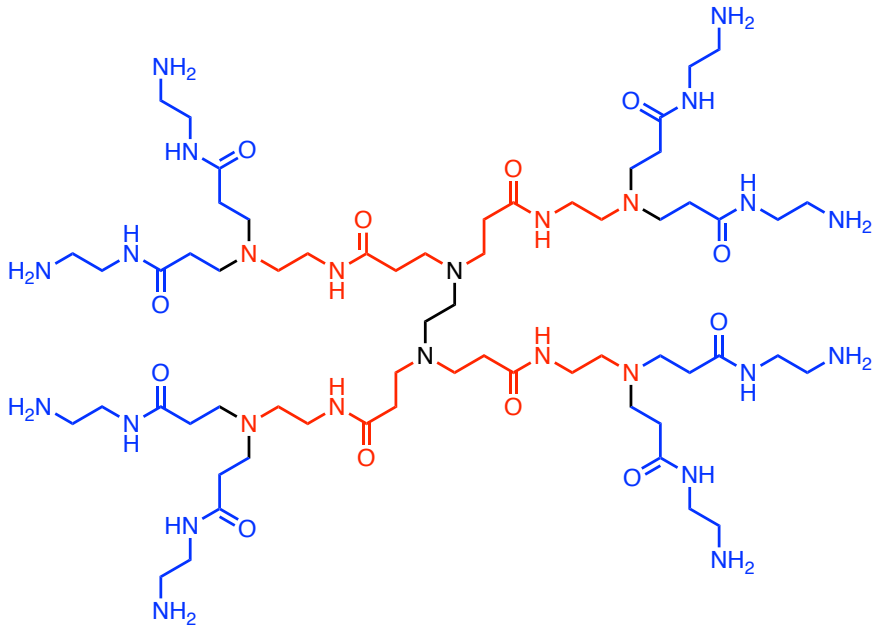

Figure I-9. Basic PAMAM dendrimer, highlight core (black), generation 1 (red) and generation 2 (blue).

I. 4.5. Liposomes

Cationic lipids are a family of small molecules containing a hydrophilic cationic headgroup, hydrophobic tails and a linking moiety, and have been recognized as promising gene delivery agents. Cationic lipids spontaneously self-assemble with nucleic acids into nano-sized complexes. The liposome complex offers protection from nucleases and allows for greater cellular uptake as membrane penetration predominantly occurs through endocytosis. There is a substantial number of cationic liposome/micelle systems reported to mediate nucleic acid delivery and are currently commercialised. A number of these transfection agents were nicely summarised by Miller,[97] and this report also highlighted the inconsistencies within the literature regarding *in vitro* and *in vivo* testing. The commercially available lipid

reagents include dioleoylphosphatidylethanolamine (DOPE), dioctadecylamido-glycylspermine (DOGS), Figure I-10 and 2,3-bis(oleoyl)oxypropyltrimethyl ammonium chloride (DOTMA), Figure I-11.

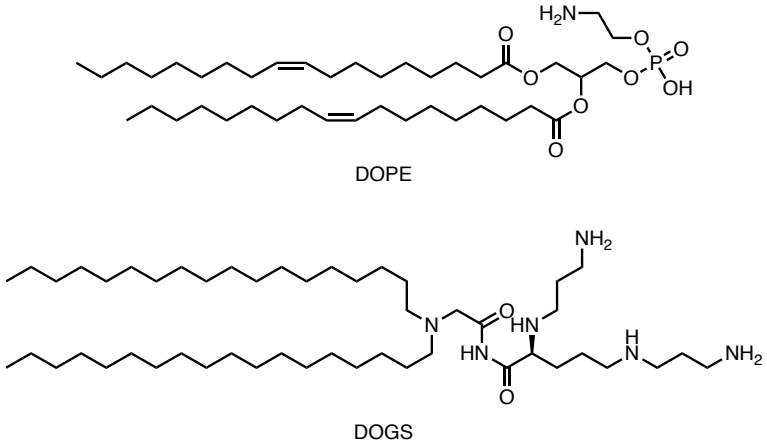

Figure I-10. Chemical structures of dioleoylphosphatidylethanolamine (DOPE) and dioctadecylamidoglycylspermine (DOGS).

Felgner and co-workers first utilized cationic liposomes as nucleic acid delivery vehicles by using the cationic lipid, *N*-[1-(2,3-dioleyloxy)propyl]-*N,N,N*-trimethylammonium (DOTMA) Figure I-11 and the neutral, naturally occurring phospholipid, dioleoylphosphatidylethanolamine, Figure I-10.[98] When combined in a 1:1 molar ratio this formulation subsequently became commercially available as Lipofectin. Lipofectin and the subsequent analogues of Lipofectin are the most commonly used transfection agents used in cell culture. Their chemical makeup generally consists of a neutral lipid alongside a highly cationic lipid. Cationic lipids are characterised structurally by three components: a cationic head group, a hydrophobic tail, and a linking group. Limitations of liposomes include low efficacy as a result of poor stability and rapid clearance as well as the generation of inflammatory or anti-inflammatory responses.[99,100]

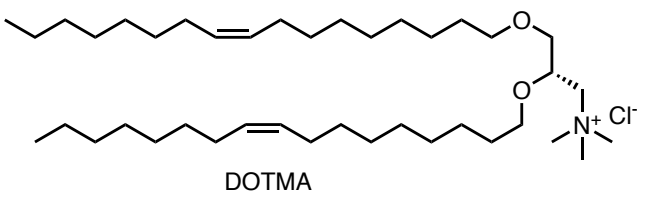

Figure I-11. Chemical structures of cationic lipid, *N*-[1-(2,3-dioleyloxy)propyl]-*N,N,N*-trimethylammonium (DOTMA).

I. 4.5. Inorganic complexes

Cationic inorganic complexes are a promising kind of non-viral delivery systems that have become more prominent due to the early studies of inorganic cations such as cobalt hexammine ($[Co(NH_3)_6]^{3+}$) which are capable of inducing DNA condensation.[101,102] Metal complexes exhibit a high positive charge density to neutralise the negative charge of the DNA backbone, which is a prerequisite for DNA condensation. $[Co(NH_3)_6]^{3+}$ has undergone extensive study for its ionic surface-binding, condensation and dehydration properties with DNA.[103,104] Although $[Co(NH_3)_6]^{3+}$ can also induce a B ⟶ ψ transitions in short oligonucleotide sequences, aggregation of long DNA polymers occurs without modification to the secondary B-DNA conformation.[102] X-ray crystallographic analysis showed that the $[Co(NH_3)_6]^{3+}$ ion adopts a novel binding mode, binding directly to phosphate groups and connecting to N7 and O6 atoms of guanines by water bridges.[105] Ethanol is commonly used to precipitate DNA when used in high loading (>80 %) however, small additions of 15-20% ethanol will induce condensation if in the presence of $[Co(NH_3)_6]^{3+}$. This is believed to be a synergistic relationship.[101] Huang *et al*. reported a series of Co(II) and Ca(II) complexes with polybenzimidazoles as efficient complexes capable of mediating nucleic acid packing via electrostatic interactions.[106] The aromatic ligands are capable of intercalating into DNA base pairs which can increase the binding affinity of these complexes. Other metals have been shown to induce DNA condensation such as Ni(II) and Rh(II) complexes.[107,108]

Li *et al*.[109] nicely summarised a series of cobalt and ruthenium complexes capable of inducing DNA damage supported by intercalative ligands such as 1,10-phenanthroline (Phen). Phen is a highly documented semi-intercalator ligand. In the case of *tris*(Phen)-cobalt(III) complex one of the phenanthroline ligands partially intercalates into the adjacent DNA base pairs and the others interact along the major groove of the DNA molecule, resulting in hydrophobic interactions that facilitate electrostatic interactions.[110] A further example of metal complex-promoted DNA condensation was recently identified with *di*-Fe^{2+} supramolecular helicases; these 4+ cationic agents bind DNA non-covalently and are capable of inhibiting DNA-processing enzymes including RNA polymerase, DNA topoisomerase I, deoxyribonuclease I, along with a variety of restriction endonucleases.[111]

Trinuclear platinum complexes show efficient DNA binding activity via noncovalent hydrogen bonding, and electrostatic interactions that induce the collapse of the helical backbone of DNA forming tightly aggregated particles.[112] These polynuclear platinum complexes were developed by Farrell and co-workers and bind DNA using a unique phosphate clamp binding mode. These highly cationic compounds are characterised by three *trans*-Pt(II) ions linked through diamine linkers of varying carbon chain lengths (5-7) shown in Figure I-12.

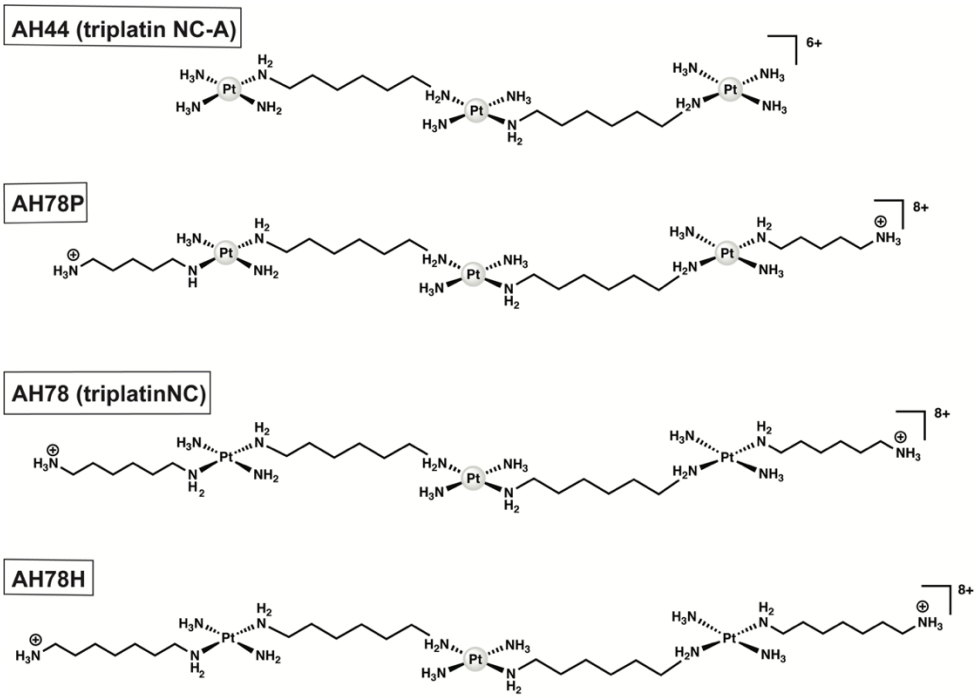

Figure I-12. Chemical structures of Tri-platinum series.[115]

These platinum complexes do not display typical covalent binding like those of cisplatin or transplatin, rather the protonated amine groups bind to the oxygens of the phosphate back bone resulting in either groove spanning or backbone tracking, Figure I-13, depending on the DNA sequence context.[114] Various techniques such as UV/visible spectroscopy, light scattering, gel electrophoresis and atomic force microscopy were employed to show the effects of DNA condensation by TriplatinNC. Interestingly, the concentration required to induce condensation was estimated to be 27% lower than that of spermine under the same conditions.[115]

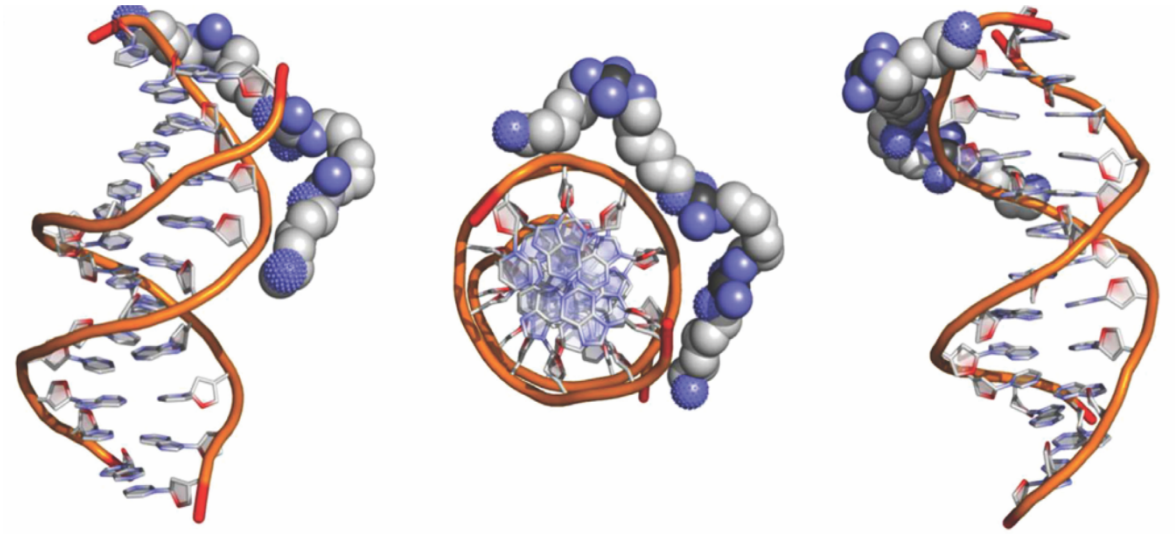

Figure I-13. Perspective views of the double-stranded B-DNA Dickerson-Drew dodecamer bound to TriplatinNC via backone tracking.[113]

I. 5. Conclusions

Nucleic acids have immense potential as therapeutics and the development of safe and effective delivery vectors is of great interest. Gene editing technology has taken a significant leap forward as demonstrated with ongoing research into CRISPR/Cas-9 systems. This form of gene editing surpasses previous methods such as ZFNs and TALENs which require protein-DNA recognition. CRISPR/Cas-9 utilises RNA-guiding nucleases which are governed by base-pairing rules between the engineered RNA and the target DNA site. Unlike ZFNs and TALENs, which are large protein complexes, the CRISPR/Cas-9 system requires a specific engineered plasmid coded for Cas-9 along with gRNAs for cellular delivery, reducing the need to deliver a large complex cargo. Viral-vectors have been predominantly used in clinical-trials in early phases, nevertheless, they suffer from immunogenicity, large scale production issue, carcinogenicity and lack of site-selectivity. The development of non-viral synthetic systems to overcome these issues associated with viral-vectors are ongoing within the field.

Non-viral vectors rely on nucleic acid condensation for efficient packing and delivery. DNA condensation typically arises due to cationic species inducing the collapse of the tertiary structure of DNA. A common mechanism of synthetic and naturally occurring surface binders is the ability to bind the electron rich phosphate backbone, primarily through H-bonding and electrostatic interactions. Electrostatic binding by polycationic molecules can directly lead to a collapse in the B-DNA

conformation with results in the condensation or aggregation of DNA structures into nanoparticles. Condensation agents discussed here included: cationic polyamines; neutral crowding polymers; liposomes; dendrimers; and cationic inorganic complexes. The most common trend between these agents is the highly positive cationic charge, except for neural crowding polymers. DNA collapse occurs once ~90% of phosphate charge neutralisation has occurred where the structure and charge density of the condensation agent plays a key role within collapsing nucleic acid transitions.

An upsurge in the development gene therapy technology has required the need for the development of safe and efficient delivery systems. As viral-vectors are accompanied with immunogenicity, the risk factors associated out-weigh the benefits. Non-viral vectors are currently in the early stages of research and require increased attention. Three key aspects of vector design should include: i) simple formulation and preparation; ii) they must demonstrate nontoxicity, biocompatibility and biodegradability; iii) the materials should possess tune-able properties that will allow accurate control over release of the genetic payload.

I. 6. References

1 J. D. Watson and F. H. C. Crick, *Nature*, **1953**, 171, 737–738.

2 E. Chargaff, R. Lipshitz and C. Green, *J. Biol. Chem.*, **1952**, 195, 155–160.

3 D. Elson and E. Chargaff, *Experientia*, **1952**, 8, 143–145.

4 A. Travers and G. Muskhelishvili, *FEBS J.*, **2015**, 282, 2279–2295.

5 S. Harteis and S. Schneider, *Int. J. Mol. Sci.*, **2014**, 15, 12335–12363.

6 A. H.-J. Wang, G. J. Quigley, F. J. Kolpak, J. L. Crawford, J. H. van Boom, G. van der Marel and A. Rich, *Nature*, **1979**, 282, 680–686.

7 A. Rich and S. Zhang, *Nat. Rev. Genet.*, **2003**, 4, 566–572.

8 D. W. Ussery, in *eLS*, American Cancer Society, **2002**, pp. 1–11.

9 J. Zhao, A. Bacolla, G. Wang and K. M. Vasquez, *Cell. Mol. Life Sci.*, **2010**, 67, 43–62.

10 R. Satange, C. Chang and M.-H. Hou, *Nucleic Acids Res.*, **2018**, 46, 6416–6434.

11 J. D. Watson, T. A. Baker, S. P. Bell, A. Gann, M. Levine and R. Losick, in *Molecular Biology of the Gene, 5th Ed, Pearson Education, 2004: Gene*, Pearson Education, United States, 5th edn., **2004,** pp. 98–128.

12 J. D. Watson, A. Baker, S. P. Bell, A. Gann, M. Levine and R. Losick, in *Molecular Biology of the Gene*, ed. D. Sabic, Pearson, United States, 7th Edition., **2013**, pp. 77–106.

13 W. Kabsch, H. G. Mannherz, D. Suck, E. F. Pai and K. C. Holmes, *Nature*, 1990, **347**, 37–44.

14 T. Lindahl, *Nature*, **1993**, 362, 709–715.

15 Z. Molphy, A. Prisecaru, C. Slator, N. Barron, M. McCann, J. Colleran, D. Chandran, N. Gathergood and A. Kellett, *Inorg. Chem.*, **2014**, 53, 5392–5404.

16 Z. Molphy, C. Slator, C. Chatgilialoglu and A. Kellett, *Front. Chem.*, **2015**, 3, 1–9.

17 Z. Molphy, D. Montagner, S. S. Bhat, C. Slator, C. Long, A. Erxleben and A. Kellett, *Nucleic Acids Res.*, **2018**, DOI:10.1093/nar/gky806.

18 C. Slator, Z. Molphy, V. McKee, C. Long, T. Brown and A. Kellett, *Nucleic Acids Res.*, **2018**, 46, 2733–2750.

19 D. S. Sigman, A. Mazumder and D. M. Perrin, *Chem. Rev.*, **1993**, 93, 2295–2316.

20 N. Z. Fantoni, Z. Molphy, C. Slator, G. Menounou, G. Toniolo, G. Mitrikas, V. McKee, C. Chatgilialoglu and A. Kellett, *Chem. – Eur. J.*, **2018**, DOI:10.1002/chem.201804084.

21 A. Prisecaru, M. Devereux, N. Barron, M. McCann, J. Colleran, A. Casey, V. McKee and A. Kellett, *Chem. Commun.*, **2012**, 48, 6906.

22 C. Slator, N. Barron, O. Howe and A. Kellett, *ACS Chem. Biol.*, **2016**, 11, 159–171.

23 M. R. Capecchi, *Science*, **1989**, 244, 1288–1292.

24 M. Lakso, B. Sauer, B. Mosinger, E. J. Lee, R. W. Manning, S. H. Yu, K. L. Mulder and H. Westphal, *Proc. Natl. Acad. Sci.*, **1992**, 89, 6232–6236.

25 Y. G. Kim, J. Cha and S. Chandrasegaran, *Proc. Natl. Acad. Sci.*, **1996**, 93, 1156–1160.

26 M. Bibikova, K. Beumer, J. K. Trautman and D. Carroll, *Science*, **2003**, 300, 764–764.

27 M. Christian, T. Cermak, E. L. Doyle, C. Schmidt, F. Zhang, A. Hummel, A. J. Bogdanove and D. F. Voytas, *Genetics*, **2010**, 186, 757–761.

28 M. J. Moscou and A. J. Bogdanove, *Science*, **2009**, 326, 1501–1501.

29 J. E. Garneau, M.-È. Dupuis, M. Villion, D. A. Romero, R. Barrangou, P. Boyaval, C. Fremaux, P. Horvath, A. H. Magadán and S. Moineau, *Nature*, **2010**, 468, 67–71.

30 L. Cong, F. A. Ran, D. Cox, S. Lin, R. Barretto, N. Habib, P. D. Hsu, X. Wu, W. Jiang, L. A. Marraffini and F. Zhang, *Science*, **2013**, 339, 819–823.

31 D. Carroll, *Genetics*, **2011**, 188, 773–782.

32 M. H. Porteus and D. Carroll, *Nat. Biotechnol.*, **2005**, 23, 967–973.

33 J. K. Joung and J. D. Sander, *Nat. Rev. Mol. Cell Biol.*, **2013**, 14, 49-59.

34 Y. Ishino, H. Shinagawa, K. Makino, M. Amemura and A. Nakata, *J. Bacteriol.*, **1987**, 169, 5429–5433.

35 R. Jansen, J. D. A. van Embden, W. Gaastra and L. M. Schouls, *Mol. Microbiol.*, **2002**, 43, 1565–1575.

36 J. A. Doudna and E. Charpentier, *Science*, **2014**, 346, 1258096.

37 J. D. Sander and J. K. Joung, *Nat. Biotechnol.*, **2014**, 32, 347–355.

38 B. P. Kleinstiver, V. Pattanayak, M. S. Prew, S. Q. Tsai, N. T. Nguyen, Z. Zheng and J. K. Joung, *Nature*, **2016**, 529, 490.

39 L.-E. Jao, S. R. Wente and W. Chen, *Proc. Natl. Acad. Sci.*, **2013**, 110, 13904–13909.

40 R. Sekine, T. Kawata and T. Muramoto, *Sci. Rep.*, **2018**, 8, 8471.

41 X.-H. Zhang, L. Y. Tee, X.-G. Wang, Q.-S. Huang and S.-H. Yang, *Mol. Ther. - Nucleic Acids*, **2015**, 4, e264.

42 E. Haapaniemi, S. Botla, J. Persson, B. Schmierer and J. Taipale, *Nat. Med.*, **2018**, 24, 927–930.

43 R. J. Ihry, K. A. Worringer, M. R. Salick, E. Frias, D. Ho, K. Theriault, S. Kommineni, J. Chen, M. Sondey, C. Ye, R. Randhawa, T. Kulkarni, Z. Yang, G. McAllister, C. Russ, J. Reece-Hoyes, W. Forrester, G. R. Hoffman, R. Dolmetsch and A. Kaykas, *Nat. Med.*, **2018**, 24, 939–946.

44 M. Olivier, M. Hollstein and P. Hainaut, *Cold Spring Harb. Perspect. Biol.*, **2010**, 2, 1–17.

45 S. Chira, D. Gulei, A. Hajitou and I. Berindan-Neagoe, *Trends Biotechnol.*, **2018**, 36, 653–660.

46 L. Zhang, R. Jia, N. J. Palange, A. C. Satheka, J. Togo, Y. An, M. Humphrey, L. Ban, Y. Ji, H. Jin, X. Feng and Y. Zheng, *PLOS ONE*, **2015**, 10, 1-14.

47 M. J. Herrero, L. Sendra, A. Miguel and S. F. Aliño, in *Safety and Efficacy of Gene-Based Therapeutics for Inherited Disorders*, ed. N. Brunetti-Pierri, Springer International Publishing, Cham, **2017**, pp. 113–135.

48 I. Slivac, D. Guay, M. Mangion, J. Champeil and B. Gaillet, *Expert Opin. Biol. Ther.*, **2017**, 17, 105–118.

49 M. A. Kotterman, T. W. Chalberg and D. V. Schaffer, *Annu. Rev. Biomed. Eng.*, **2015**, 17, 63–89.

50 S. R. Choudhury, E. Hudry, C. A. Maguire, M. Sena-Esteves, X. O. Breakefield and P. Grandi, *Neuropharmacology*, **2017**, 120, 63–80.

51 M. F. Naso, B. Tomkowicz, W. L. Perry and W. R. Strohl, *BioDrugs*, **2017**, 31, 317–334.

52 M. B. Appaiahgari and S. Vrati, *Expert Opin. Biol. Ther.*, **2015**, 15, 337–351.

53 L. De Laporte, J. Cruz Rea and L. D. Shea, *Biomaterials*, **2006**, 27, 947–954.

54 H. Yin, R. L. Kanasty, A. A. Eltoukhy, A. J. Vegas, J. R. Dorkin and D. G. Anderson, *Nat. Rev. Genet.*, **2014**, 15, 541–555.

55 L. Sperling and A. Klug, *J. Mol. Biol.*, **1977**, 112, 253–263.

56 V. A. Bloomfield, *Biopolymers*, **1997**, 44, 269–282.

57 R. W. Wilson and V. A. Bloomfield, *Biochemistry*, **1979**, 18, 2192–2196.

58 G. S. Manning, *Q. Rev. Biophys.*, **1978**, 11, 179–246.

59 V. A. Bloomfield, *Curr. Opin. Struct. Biol.*, **1996**, 6, 334–341.

60 V. Vijayanathan, T. Thomas, A. Shirahata and T. J. Thomas, *Biochemistry*, **2001**, 40, 13644–13651.

61 A. Y. Grosberg and D. V. Kuznetsov, *Macromolecules*, **1992**, 25, 1970–1979.

62 V. Andrushchenko, H. van de Sande and H. Wieser, *Biopolymers*, **2003**, 69, 529–545.

63 R. Golan, L. I. Pietrasanta, W. Hsieh and H. G. Hansma, *Biochemistry*, **1999**, 38, 14069–14076.

64 P. G. Arscott, A.-Z. Li and V. A. Bloomfield, *Biopolymers*, **1990**, 30, 619–630.

65 V. A. Bloomfield, *Biopolymers*, **1991**, 31, 1471–1481.

66 M. R. Shen, K. H. Downing, R. Balhorn and N. V. Hud, *J. Am. Chem. Soc.*, **2000**, 122, 4833–4834.

67 I. D. Vilfan, C. C. Conwell, T. Sarkar and N. V. Hud, *Biochemistry*, **2006**, 45, 8174–8183.

68 B. van den Broek, M. C. Noom, J. van Mameren, C. Battle, F. C. MacKintosh and G. J. L. Wuite, *Biophys. J.*, **2010**, 98, 1902–1910.

69 R. Cortini, B. R. Caré, J.-M. Victor and M. Barbi, *J. Chem. Phys.*, **2015**, 142, 105102.

70 N. McStay, Z. Molphy, A. Coughlan, A. Cafolla, V. McKee, N. Gathergood and A. Kellett, *Nucleic Acids Res.*, **2017**, 45, 527–540.

71 N. Yamaguchi, Y. Zouzumi, N. Shimada, S. Nakano, N. Sugimoto, A. Maruyama and D. Miyoshi, *Chem Commun*, **2016**, 52, 7446–7449.

72 J. P. Leonetti, G. Degols and B. Lebleu, *Bioconjug. Chem.*, **1990**, 1, 149–153.

73 E. Wagner, M. Cotten, R. Foisner and M. L. Birnstiel, *Proc. Natl. Acad. Sci. U. S. A.*, **1991**, 88, 4255–4259.

74 S. Deshayes, M. C. Morris, G. Divita and F. Heitz, *Cell. Mol. Life Sci. CMLS*, **2005**, 62, 1839–1849.

75 C. P. Leamon and P. S. Low, *Drug Discov. Today*, **2001**, 6, 44–51.

76 E. Song, P. Zhu, S.-K. Lee, D. Chowdhury, S. Kussman, D. M. Dykxhoorn, Y. Feng, D. Palliser, D. B. Weiner, P. Shankar, W. A. Marasco and J. Lieberman, *Nat. Biotechnol.*, **2005**, 23, 709–717.

77 R. Kircheis, L. Wightman and E. Wagner, *Adv. Drug Deliv. Rev.*, **2001**, 53, 341–358.

78 G. Y. Wu and C. H. Wu, *Biochemistry*, **1988**, 27, 887–892.

79 G. Y. Wu and C. H. Wu, *J. Biol. Chem.*, **1988**, 263, 14621–14624.

80 T. D. McKee, M. E. DeRome, G. Y. Wu and M. A. Findeis, *Bioconjug. Chem.*, **1994**, 5, 306–311.

81 N. A. Bright, L. J. Davis and J. P. Luzio, *Curr. Biol.*, **2016**, 26, 2233–2245.

82 I. S. Blagbrough, A. A. Metwally and A. J. Geall, in *Polyamines: Methods and Protocols*, eds. A. Pegg and J. R. Casero, Humana Press, Totowa, NJ, **2011**, pp. 493–503.

83 E. Rowatt and R. J. P. Williams, *J. Inorg. Biochem.*, **1992**, 46, 87–97.

84 I. Nayvelt, M. T. Hyvönen, L. Alhonen, I. Pandya, T. Thomas, A. R. Khomutov, J. Vepsäläinen, R. Patel, T. A. Keinänen and T. J. Thomas, *Biomacromolecules*, **2010**, 11, 97–105.

85 O. Boussif, F. Lezoualc'h, M. A. Zanta, M. D. Mergny, D. Scherman, B. Demeneix and J. P. Behr, *Proc. Natl. Acad. Sci. U. S. A.*, **1995**, 92, 7297–7301.

86 M. X. Tang and F. C. Szoka, *Gene Ther.*, **1997**, 4, 823–832.

87 T. J. Thomas, H. A. Tajmir-Riahi and T. Thomas, *Amino Acids*, **2016**, 48, 2423–2431.

88 Y. Sun, L. Xian, J. Yu, T. Yang, J. Zhang, Z. Yang, J. Jiang, C. Cai, X. Zhao, L. Yang and P. Ding, *Macromol. Biosci.*, **2017**, 17, 1600297.

89 L. S. Lerman, *Proc. Natl. Acad. Sci. U. S. A.*, **1971**, 68, 1886–1890.

90 J. Benns and S. Kim, *J. Drug Target.*, **2000**, 8, 1–12.

91 T. J. Thomas and T. Thomas, *Int. J. Biol. Macromol.*, **2018**, 109, 36–48.

92 M.-L. Ainalem, A. M. Carnerup, J. Janiak, V. Alfredsson, T. Nylander and K. Schillén, *Soft Matter*, **2009**, 5, 2310–2320.

93 K. Fant, E. K. Esbjörner, P. Lincoln and B. Nordén, *Biochemistry*, **2008**, 47, 1732–1740.

94 E. Froehlich, J. S. Mandeville, C. M. Weinert, L. Kreplak and H. A. Tajmir-Riahi, *Biomacromolecules*, **2011**, 12, 511–517.

95 M. Ravivarma, C. Satheeshkumar and P. Rajakumar, *Synlett*, **2014**, 25, 945–950.

96 S. Kavyani, S. Amjad-Iranagh and H. Modarress, *J. Phys. Chem. B*, **2014**, 118, 3257–3266.

97 A. D. Miller, *Curr. Med. Chem.*, **2003**, 10, 1195–1211.

98 P. L. Felgner, T. R. Gadek, M. Holm, R. Roman, H. W. Chan, M. Wenz, J. P. Northrop, G. M. Ringold and M. Danielsen, *Proc. Natl. Acad. Sci.*, **1987**, 84, 7413–7417.

99 R. I. Zhdanov, O. V. Podobed and V. V. Vlassov, *Bioelectrochemistry*, **2002**, 58, 53–64.

100 C. Lonez, M. Vandenbranden and J.-M. Ruysschaert, *Prog. Lipid Res.*, **2008**, 47, 340–347.

101 H. Deng and V. A. Bloomfield, *Biophys. J.*, **1999**, 77, 1556–1561.

102 B. I. Kankia, V. Buckin and V. A. Bloomfield, *Nucleic Acids Res.*, **2001**, 29, 2795–2801.

103 G. E. Plum, P. G. Arscott and V. A. Bloomfield, *Biopolymers*, **1990**, 30, 631–643.

104 S. He, P. G. Arscott and V. A. Bloomfield, *Biopolymers*, **2000**, 53, 329–341.

105 B. Ramakrishnan, C. Sekharudu, B. Pan and M. Sundaralingam, *Acta Crystallogr. D Biol. Crystallogr.*, **2003**, 59, 67–72.

106 X. Huang, X. Dong, X. Li, X. Meng, D. Zhang and C. Liu, *J. Inorg. Biochem.*, **2013**, 129, 102–111.

107 X. Dong, X. Wang, Y. He, Z. Yu, M. Lin, C. Zhang, J. Wang, Y. Song, Y. Zhang, Z. Liu, Y. Li and Z. Guo, *Chem. – Eur. J.*, **2010**, 16, 14181–14189.

108 B. Sun, J.-X. Guan, L. Xu, B.-L. Yu, L. Jiang, J.-F. Kou, L. Wang, X.-D. Ding, H. Chao and L.-N. Ji, *Inorg. Chem.*, **2009**, 48, 4637–4639.

109 G.-Y. Li, R.-L. Guan, L.-N. Ji and H. Chao, *Coord. Chem. Rev.*, **2014**, 281, 100–113.

110 J. Zheng, Z. Li, A. Wu, H. Zhou, H. Bai and Y. Song, *Biochem. Biophys. Res. Commun.*, **2002**, 299, 910–915.

111 J. Malina, M. J. Hannon and V. Brabec, *Chem. - Eur. J.*, **2015**, 21, 11189–11195.

112 J. Malina, N. P. Farrell and V. Brabec, *Angew. Chem. Int. Ed.*, **2014**, 53, 12812–12816.

113 A. Prisecaru, Z. Molphy, R. G. Kipping, E. J. Peterson, Y. Qu, A. Kellett and N. P. Farrell, *Nucleic Acids Res.*, **2014**, 42, 13474–13487.

114 S. Komeda, T. Moulaei, M. Chikuma, A. Odani, R. Kipping, N. P. Farrell and L. D. Williams, *Nucleic Acids Res.*, **2011**, 39, 325–336.

115 N. P. Farrell, *Chem Soc Rev*, **2015**, 44, 8773–8785.

Chapter II

C_3-Symmetric Opioid Scaffolds are pH-Responsive DNA Condensation Agents

This paper was accepted for publication in *Nucleic Acids Research*, 2017, DOI: 10.1093/nar/gkw1097. Referencing style is kept in publishing format and gel electrophoresis images are inverted for clarity.

Natasha McStay, Zara Molphy, Alan Coughlan, Attilio Cafolla, Vickie McKee, Nicholas Gathergood and Andrew Kellett.

My contribution to this paper was to design and synthesise a series of mono-substituted (C_1-symmetric), di-substituted (C_2-symmetric) and tri-substituted (C_3-symmetric) mesitylene-linked opioid scaffolds and conduct DNA condensation studies on them. Characterization of the opioids generated were conducted by me and including the AFM, turbidity, and condensation studies. The DNA binding studies were carried out in collaboration with my colleague Dr. Zara Molphy. Dr Molphy conducted the circular dichroism and thermal melting studies.

II. 1. Abstract

Herein we report the synthesis of tripodal C_3-symmetric opioid scaffolds as high-affinity condensation agents of duplex DNA. Condensation was achieved on both supercoiled and canonical B-DNA structures and identified by agarose electrophoresis, viscosity, turbidity, and atomic force microscopy (AFM) measurements. Structurally, the requirement of a *tris*-opioid scaffold for condensation is demonstrated as both di- (C_2-symmetric) and mono- substituted (C_1-symmetric) mesitylene-linked opioid derivatives poorly coordinate dsDNA. Condensation, observed by toroidal and globule AFM aggregation, arises from surface- binding ionic interactions between protonated, cationic, tertiary amine groups on the opioid skeleton and the phosphate nucleic acid backbone. Indeed, by converting the 6-hydroxyl group of C_3-morphine (**MC3**) to methoxy substituents in C_3-heterocodeine (**HC3**) and C_3-oripavine (**OC3**) molecules, dsDNA compaction is retained thus negating the possibility of phosphate hydroxyl surface-binding. Tripodal opioid condensation was identified as pH dependent and strongly influenced by ionic strength with further evidence of cationic amine-phosphate backbone coordination arising from thermal melting analysis and circular dichroism spectroscopy, with compaction also witnessed on synthetic dsDNA co-polymers poly[d(A-T)$_2$] and poly[d(G-C)$_2$]. On-chip microfluidic analysis of DNA condensed by C_3-agents provided concentration-dependent protection (inhibition) to site-selective excision by type II restriction enzymes: BamHI, HindIII, SalI, and EcoRI, but not to the endonuclease DNase I.

II. 2. Introduction

The search for new synthetic DNA recognition agents is an area of considerable research importance. These agents can be categorised, broadly, into two main areas: *i.*) those that covalently bind nucleic acids at electron rich sites on the nucleobase (1–3), and *ii.*) those that bind in non-covalent fashion through hydrogen (H)-bonding, ionic, or π-stacking interactions (4–6). Accordingly, non-covalent recognition scaffolds may be further classified to the area of DNA where recognition occurs thus giving rise to groove binders (7–9), intercalators (9–12) (including threading intercalators (13) and surface-binding compounds (14). Within this last category, surface interacting compounds have been designed, and compared, to naturally occurring protein binding domains containing, for example, cationic arginine (arginine fork (15)) or lysine (poly-*L*-lysine (16)) amino acid residues that

facilitate their complexation to nucleic acids. Indeed, a commonality between synthetic and naturally occurring surface binders is their ability to efficiently bind electron rich phosphate atoms located at the nucleic acid backbone, principally through H-bonding and electrostatic interactions. Furthermore, electrostatic binding by polycationic molecules can directly lead to a collapse in the B-DNA conformation with resultant condensation or aggregation of tertiary DNA helical structures (17). Condensation agents have, in-turn, found widespread utility in molecular biology as transfection agents capable of mediating cellular delivery of nucleic acids for ubiquitous therapeutic and bioprocessing applications (18). Thus, an important consideration in the development of new DNA condensation agents is their relative inertness toward chemical reactivity (*e.g.* artificial nuclease) or secondary interactions (*e.g.* intercalation) that may interrupt or block efficient transport and incorporation of target nucleic acids into mammalian cells.

While nucleic acid condensation can be achieved through mechanisms of neutral crowding, antisolvent precipitation and liposomal packaging (amongst others), significant attention focuses on the condensation properties of multivalent cationic compounds including cationic polymers. Although DNA condensation has been reviewed by Bloomfield (17) and others including theoretical descriptions into the dynamics of polymer collapse (19, 20), it is worth considering some examples of multivalent cations currently accessible to this field. Cationic charge density essential for the neutralisation of anionic phosphate charge and the reorganisation of water dipoles adjacent to DNA surfaces plays a critical role in driving condensation and the majority of cationic agents carry a formal charge of 3+ or higher. Prominent examples here include the naturally occurring polyamines spermine^{4+} and spermidine^{3+} that are abundantly found in living organisms and aid in the packaging of cellular DNA by lowering the free energy of transition required for condensation (21). Within the polyamine class, it was demonstrated that DNA collapse occurs once ~90% of phosphate charge neutralisation has occurred (22) and that polyamine structure, allied with charge, plays a role within condensation transitions (21). Polyamines of varying aliphatic linker length have recently been incorporated into substitution inert triplatinum(II) complexes (Triplatin) and these highly cationic agents are capable of aggregating nucleic acids (both RNA and DNA) through clamping interactions along the phosphate backbone and across the minor groove of DNA (23–25). Evidence of condensation by Triplatin agents was identified

by turbidity and AFM analysis with DNA (24), particularly poly[d(A-T)$_2$] (23), undergoing a B ⟶ ψ transition during the collapse. Another substitutionally inert complex cation, cobalt (III) hexammine $[Co(NH_3)_6]^{3+}$, has undergone extensive study for its ionic surface-binding, condensation and dehydration properties with DNA (26, 27). Although $[Co(NH_3)_6]^{3+}$ can also induce a B ⟶ ψ transitions in short oligonucleotide sequences, aggregation of long DNA polymers occurs without modification to the secondary B-DNA conformation (28). Furthermore, while the morphology of DNA condensates with $[Co(NH_3)_6]^{3+}$ are commonly toroidal in structure, non-toroidal (rod-like) structures are observed in the presence of alcohol solvents. A further example of metal complex-promoted DNA condensation was recently identified by *di*-Fe^{2+} supramolecular helicases; these 4+ cationic agents bind DNA non-covalently and are capable of inhibiting DNA-processing enzymes including RNA polymerase, DNA topoisomerase I, deoxyribonuclease I, along with a variety of restriction endonucleases (29). Polycations can also induce alternative changes in B-DNA configuration; a reversible B ⟶ A transition, regulated by dehydration, was recently evidenced in short G-C rich oligonucleotide sequences exposed to a poly(allylamine)-*graft*-dextran synthetic cationic polymer (16). Finally, although exceptions to the ≥3+ cationic valence requirement for DNA collapse are rare, both Mn^{2+} and the putrescine^{2+} cations are known to aggregate DNA but only at high (millimolar) concentration (30).

In this study we report the synthesis of a new class of DNA binding scaffold incorporating opioid derivatives. Opioids are naturally derived alkaloids from the opium poppy, *Papaver somniferum*, and serve as one of the major drug classes within pharmaceutical chemistry widely known for their potent analgesic properties (31). Morphine was the first opioid isolated from the poppy and is the most abundant opioid interacting with three principal opioid receptors located in the central nervous system (CNS): mu (μ, MOR), kappa (κ, KOR) and delta (δ, DOR). The interaction of opioids with CNS receptors has led toward the development of synthetic analogues (including heterocodeine, buprenorphine, and naltrexone) and to more heavily modified structures containing multiple opiate substituents. Morphine congeners can also be extracted from the poppy (*e.g.* codeine, thebaine and oripavine) and offer a range of bio-renewable derivatives to support proposed SAR studies. Our group has recently developed a high- throughput ethidium bromide displacement screen to identify potentially new DNA binding molecules (32) and, as such,

identified a synthetic C_3-symmetric morphine molecule (**MC3**), containing a mesitylene bridging ligand, as a lead compound that was subsequently found to induce DNA condensation at low micromolar concentration. Our motivation for developing heterocodeine (**HC3**) and oripavine (**OC3**) analogues stemmed from structural analysis of **MC3** that focused on the 6'-OH group in the morphine C ring as a possible hydrogen (H)-bonding site for phosphate coordination at the nucleic acid backbone. If this were the case, masking this H-bond through the introduction of methyl groups in the form of methoxy substituents present in heterocodeine (**H**) and oripavine (**O**) should render the DNA binding properties negligible. In addition, as oripavine is a natural product, and commercially available, a short and direct synthesis of the C_3-symmetry target was envisaged. Surprisingly however, enhanced EtBr displacement was observed for both **HC3** and **OC3** agents, thus implying only a limited role for 6'-OH phosphate interaction in the binding mechanism. Consequently, the DNA binding mode and condensation properties of this class of molecule were elucidated using an array of biophysical techniques including turbidity, viscosity, thermal melting, circular dichroism spectroscopy, electrophoresis and AFM analysis, and are reported herein.

II. 3. Materials and Methods

II. 3.1. Materials synthesis and characterisation

Chemicals and reagents were sourced from Sigma-Aldrich and were used without any further purification required. HPLC grade chloroform, methanol, and acetonitrile were used with no further purification. All other solvents were used as supplied. Morphine and oripavine were provided from Johnson Matthey MacFarlan Smith Ltd. Thin layer chromatography was performed on Fluka Silica gel (60 F254) coated on aluminium plates. The TLC plates were visualised using UV light. Davisil 60 Å silica gel was used for column chromatography. ^{1}H and ^{13}C NMR spectra were obtained on a Bruker AC 400 and 600 MHz NMR spectrometer. The pH was monitored by a Mettler Toledo InLab Expert Pro- ISM pH probe. Electrospray ionisation mass spectra (ESI-MS) were recorded using a Thermo Fisher Exactive Orbitrap mass spectrometer coupled to an Advion TriVersa Nanomate injection system with samples being prepared in 100% HPLC-grade acetonitrile prior to ESI-MS analysis. Circular dichroism spectrometry was conducted on an Applied Photophysics Chirascan plus qCD spectrometer with samples being prepared in acetonitrile.

Morphine-C_3 (MC3)

Morphine (0.573 g, 2.01 mmol) and potassium carbonate (1.110 g, 8.03 mmol) were suspended in ACN (30 ml) and heated to reflux. 2,4,6-*Tris*-(bromomethyl)-mesitylene (0.268 g, 0.66 mmol) was added in small aliquots to the reaction mixture and vigorously stirred overnight (18 h) under reflux conditions. After allowing the reaction mixture to cool to rt, the reaction solvent was removed by rotary evaporation and crude product dissolved in DCM (50 ml). The organic layer was washed with H_2O (40 ml) and the aqueous layer extracted with DCM (3 x 20 ml). All organic layers were combined, then washed with H_2O (3 x 20 ml) and with a saturated brine solution (20 ml). The organic layer was dried over magnesium sulfate, filtered and solvents removed by rotary evaporation. The crude product was purified by column chromatography (SiO_2, 95:1:1 to 92:8:1 CH_2Cl_2:MeOH:NH_4OH). The title compound **MC3** was isolated as a white solid in 50% yield (0.338 g, 0.33 mmol). mp. 187-189˚C. ^{1}H NMR (600 MHz, $CDCl_3$) δ: 6.80 (d, J = 8.2 Hz, 3H); 6.58 (d, J = 8.2 Hz, 3H); 5.69 (ddt, *J* = 9.9, 3.2, 1.4 Hz, 3H); 5.30 – 5.27 (m, 3H); 5.21 (d, *J* = 10.5 Hz, 3H); 5.05 (d, *J* = 10.4 Hz, 3H); 4.85 (dd, *J* = 6.5, 1.1 Hz, 3H); 4.17 – 4.13 (m, 3H); 3.35 (s, 3H); 3.05 (d, *J* = 18.7 Hz, 3H); 2.66 (s, 3H); 2.61 – 2.56 (m, 3H); 2.48 (s, 9H); 2.44 (s, 9H); 2.41 – 2.37 (m, 3H); 2.31 (dd, *J* = 18.7, 6.2 Hz, 3H); 2.05 (td, *J* = 12.4, 5.0 Hz, 3H); 1.88 (d, *J* = 11.3 Hz, 3H). ^{13}C NMR (151 MHz, $CDCl_3$) δ: 147.59, 141.43, 139.43, 133.41, 131.82, 131.44, 128.19, 119.61, 116.36, 91.27, 77.22, 77.00, 76.79, 67.32, 66.46, 58.93, 46.47, 43.09, 42.96, 40.81, 35.78, 20.64, 15.98. IR (ATR, cm^{-1}): 2907, 1632, 1602, 1492, 1443, 1247, 1200, 1157, 1118, 1099, 1034, 983, 940, 833, 784, 766, 731. ESI-MS: [**MC3**] 1012 m/z. $[\alpha]_D$ = − 85° (c = 0.154, $CHCl_3$, 589 nm, 25 ˚C).

Oripavine-C_3 (OC3)

A flask was charged with oripavine (0.595 g, 2.00 mmol), tetrabutylammonium hydroxide (40% aqueous solution, 18 ml) and DCM (6 ml) and stirred under nitrogen for 30 mins. A solution of 2,4,6-*tris*-(bromomethyl)-mesitylene (0.269 g, 0.66 mmol) in DCM (4 ml) was added and the biphasic reaction mixture was stirred for 6 h at room temperature (rt). The reaction solution was transferred into H_2O (150 ml) and washed with DCM (4 x 10 ml). Organic layers were combined and washed with aqueous NaOH solution (0.1 M, 2 x 20 ml) followed by d.H_2O (3 x 20 ml) then saturated brine solution (20 ml). The organic layer was dried over magnesium sulfate, filtered and solvents removed by rotary evaporation. The crude product was

purified by column chromatography (SiO_2, 95:1:1 to 92:8:1 CH_2Cl_2:MeOH:NH_4OH), The title compound **OC3** was isolated as a golden yellow solid in 47% yield (0.329 g, 0.31 mmol). mp 174-176˚C. ^{1}H NMR (600 MHz, $CDCl_3$) δ: 6.73 (d, *J* = 8.1 Hz, 3H); 6.58 (d, *J* = 8.1 Hz, 3H); 5.56 (d, *J* = 6.4 Hz, 3H); 5.28 (s, 3H); 5.25 (d, *J* = 10.7 Hz, 3H); 5.17 (d, *J* = 10.7 Hz, 3H); 5.03 (d, *J* = 6.4 Hz, 3H); 3.62 (d, *J* = 6.6 Hz, 3H); 3.59 (s, 9H); 3.32 (d, *J* = 18.0 Hz, 3H); 2.83 (td, *J* = 12.7, 3.3 Hz, 3H); 2.68 (dd, *J* = 18.1, 7.0 Hz, 3H); 2.63 (dd, *J* = 12.7, 4.6 Hz, 3H); 2.47 (s, 9H); 2.46 (s, 9H); 2.20 (td, *J* = 12.6, 5.1 Hz, 3H); 1.78 – 1.75 (m, 3H). ^{13}C NMR (151 MHz, $CDCl_3$) δ: 152.96, 146.07, 142.13, 139.65, 133.99, 132.59, 132.06, 128.73, 119.46, 117.48, 111.73, 96.09, 89.16, 89.11, 77.37, 77.16, 76.95, 67.74, 61.07, 55.04, 46.25, 46.16, 42.57, 37.11, 29.93, 16.02. IR (ATR, cm^{-1}): 2908, 1605, 1491, 1437, 1368, 1331, 1302, 1231, 1143, 1105, 1066, 1021, 987, 914, 867, 812, 767, 748, 698. ESI-MS: [**OC3**] + 1048 m/z. $[\alpha]_D$ = − 88° (c = 0.12, $CHCl_3$, 589 nm, 25 ˚C).

Heterocodeine (33, 34)

Reaction carried out on parallel synthesiser. Potassium hydride (4.421 g, 110.23 mmol) was washed with dry hexane in the reaction vessel under nitrogen flux and suspended in dry THF (150 ml) over ice (**Caution!** Dry potassium hydride is pyrophoric). A solution of morphine (2.862 g, 10.03 mmol) in THF (30 ml) was added slowly over 30 min to the reaction under a nitrogen atmosphere and the resulting solution was allowed to stir at rt for 16 h. Methyl iodide (1.710 g, 0.75 ml, 12.05 mmol) was added to the reaction slowly over 15 mins and reaction left stirring for 4 h. The reaction was quenched slowly with a mixture of THF/H_2O (10:1) at 0 ˚C. The solution was neutralised to pH 7.0 with 2 M HCl and volatiles were then removed by rotary evaporation. The pH was adjusted to 8.0 by the addition of 1M NaOH and the aqueous layer extracted with chloroform/isopropanol (3:1, 3 x 25 ml). The resulting organic layer was washed with H_2O (4 x 30 ml) and a final wash with saturated brine solution (20 ml). The organic layer was dried over magnesium sulfate, filtered and solvents removed by rotary evaporation. The crude product was purified by column chromatography (SiO_2, 95:1:1 to 92:8:1 CH_2Cl_2:MeOH:NH_4OH), heterocodeine was isolated as a white solid in 25% yield (756 mg, 2.53 mmol). ^{1}H NMR (600 MHz, $CDCl_3$,): δ 6.57 (d, *J* = 8.1 Hz, 1H); 6.41 (d, *J* = 8.1 Hz, 1H); 5.64 (ddt, *J* = 9.9, 3.2, 1.5 Hz, 1H); 5.26 (dt, *J* = 9.8, 2.7 Hz, 2H); 4.91 (dd, *J* = 5.8, 1.3 Hz, 1H); 3.72 (td, *J* = 5.5, 2.3 Hz, 1H); 3.45 (s, 3H); 3.32 (dd, *J* = 6.3, 3.2 Hz, 1H); 2.97 (d, *J* = 18.6 Hz,

1H); 2.63 – 2.49 (m, 2H); 2.43 – 2.31 (m, 4H); 2.23 (dd, *J* = 18.7, 6.4 Hz, 1H); 1.99 (td, *J* = 12.4, 5.1 Hz, 1H); 1.88 – 1.79 (m, 2H).

Heterocodeine-C_3 (HC3)

A flask was charged with heterocodeine (0.700 g, 2.34 mmol), tetrabutylammonium hydroxide (40% aqueous solution, 20 ml) and DCM (8 ml) and stirred under nitrogen for 30 mins. A solution of 2,4,6-*tris*-(bromomethyl)-mesitylene (0.269 g, 0.66 mmol) in DCM (4 ml) was added and the mixture was stirred for 6 h at rt. The reaction solution was transferred into d.H2O (150 ml) and washed with DCM (4 x 10 ml). Organic layers were combined and washed with aqueous NaOH solution (0.1 M, 2 x 20 ml) followed by H_2O (3 x 20 ml) then a saturated brine solution (20 ml). The organic layer was dried over magnesium sulfate, filtered and solvents removed by rotary evaporation. The crude product was purified by column chromatography (SiO_2, 95:1:1 to 92:8:1 CH_2Cl_2:MeOH:NH_4OH), **HC3** was isolated by column chromatography as a white solid in 13% yield (95 mg 0.09 mmol). mp. 164-166˚C. ^{1}H NMR (400 MHz, $CDCl_3$) δ: 6.73 (d, *J* = 8.1 Hz, 3H); 6.49 (d, *J* = 8.1 Hz, 3H); 5.71 (d, *J* = 9.9 Hz, 3H); 5.32 (dt, *J* = 10.0, 2.7 Hz, 3H); 5.27 – 5.16 (m, 6H); 5.00 (d, *J* = 5.1 Hz, 3H); 3.80 (dd, *J* = 5.4, 2.7 Hz, 3H); 3.51 (s, 9H); 3.36 (dd, *J* = 5.9, 3.1 Hz, 3H); 3.04 (d, *J* = 18.7 Hz, 3H); 2.69 – 2.65 (m, 3H); 2.61 – 2.56 (m, 3H); 2.52 (s, 9H); 2.44 (s, 9H); 2.40 (d, *J* = 3.4 Hz, 3H); 2.31 (dd, *J* = 18.7, 6.3 Hz, 3H); 2.04 (td, *J* = 12.4, 5.0 Hz, 3H); 1.93 (d, *J* = 11.0 Hz, 3H).^{13}C NMR (101 MHz, $CDCl_3$) δ: 148.88, 141.35, 139.66, 132.09, 131.46, 131.01, 128.56, 128.18, 119.02, 118.34, 89.14, 77.48, 77.36, 77.16, 76.84, 75.67, 68.01, 59.06, 56.92, 53.58, 46.68, 43.61, 43.26, 43.19, 41.23, 36.06, 29.82, 20.66, 16.10. IR (ATR, cm^{-1}): 2905, 2798, 1632, 1601, 1492, 1442, 1247, 1199,1104, 984, 941, 831, 787, 768, 727, 679. $[\alpha]_D = -185°$ (c = 0.08, $CHCl_3$, 589 nm, 25˚C).

II. 3.2. DNA binding experiments

Competitive Ethidium Bromide Displacement Assay

The DNA binding affinity of the tripodal series was determined over a five-hour time period using calf-thymus DNA (ctDNA, Ultra-Pure Invitrogen, 15633019) and synthetic alternating co-polymers poly[d(A-T)$_2$)] (Sigma Aldrich, P0883) and poly[d(G-C)$_2$] (Sigma Aldrich, P9389) by ethidium bromide fluorescence quenching in a similar manner to the high-throughput method previously reported by Kellett *et a.l (35)*. Each drug concentration was measured in triplicate, on at least two

separate occasions, and the apparent binding constants were calculated using K_{app} = K_b x 12.6/C_{50} where K_b = 8.80 × 106 M(bp)$^{-1}$ (K_{app} = apparent binding constant).

Viscosity studies

Experiments were conducted in a similar manner to the method reported previously using DV-II-Programmable Digital Viscometer equipped with Enhanced Brookfield UL Adapter at room temperature by gradually increasing the [compound/DNA] ratios from 0.02-0.20 (36).

Thermal Melting Studies

The thermal melting of DNA of varying %AT content was conducted using an Agilent Cary 100 dual beam spectrophotometer equipped with a 6 × 6 Peltier multicell system with temperature controller. The protocol was previously developed within the Kellett group and reported elsewhere (6, 7).

II. 3.3. DNA condensation studies (dsDNA)

Turbidity Investigation (ctDNA)

This method was adapted from the Brabec laboratory (24). Absorption spectra were initially measured at 260 nm in order to give a final absorbance of ~0.5 units and the concentration of ctDNA was determined using the extinction coefficient ε 260 = 12824 M(bp)$^{-1}$ cm^{-1}. The turbidity of the ctDNA solution was determined spectrophotometrically by monitoring the absorbance of DNA at both 350 nm and 260 nm at 25˚C using an Agilent Cary 100 dual beam spectrophotometer equipped with a 6×6 Peltier multicell system with temperature controller and stirring mechanism. In a final volume of 3 ml containing ~40 μM ctDNA, 1 mM PBS buffer (pH 7.0) and 25 mM NaCl, varying concentrations of **MC3**, **OC3** and **HC3** (2.5, 5, 7.5, 10, 12.5, 15, 20, 25, 30, 35, 45, 50, 65, 75, 80, 90, 100 μM) were titrated into quartz cuvettes. Between each aliquot, solutions were mixed thoroughly and allowed to incubate at 25 ˚C until the absorbance equilibrated and values obtained remained constant.

DNA condensation investigation (pUC19 scDNA)

The ability of the organic compounds to condense supercoiled plasmid DNA was determined using a method previously published by this laboratory with minor changes being made (23). Tripodal opiates were initially prepared in DMF and further diluted in 80 mM HEPES buffer (Fisher). Reactions were carried out according to the following general procedure: in a total volume of 20 µL using 80 mM HEPES buffer (pH 7.2) with 25 mM NaCl, 400 ng pUC19 (NEB, N3041) and varying concentrations of test compound (5, 10, 20 and 30 µM), samples were incubated at 37˚C for both 5 and 12 h. Reactions were quenched by adding 6× loading buffer (Fermentas) containing 10 mM Tris-HCl, 0.03% bromophenol blue, 0.03% xylene cyanole FF, 60% glycerol, 60 mM EDTA and samples were loaded onto an agarose gel (1.2%) containing 3 µL EtBr. Electrophoresis was completed at 60 V for 1 h in 1× TAE buffer.

DNA condensation investigation in the presence of non-covalently bound recognition elements (pUC19 scDNA)

This protocol was carried out as previously reported by this group with minor changes made (37). Briefly, 400 ng pUC19 was incubated with 25 mM NaCl, and 20 µM of either methyl green, netropsin or hexammine cobalt(III) chloride in 80 mM HEPES buffer (pH 7.2) for 30 min at 37 ˚C. Sample tubes were then vortexed and varying concentrations of test compound were added (5, 10, 20 and 30 µM). The reaction mixture was further incubated at 37 ˚C for 5 h. The reaction was then quenched and subjected to gel electrophoresis as previously described.

Investigation of DNase I inhibition by DNA condensation (pUC19 scDNA)

400 ng of pUC19 DNA was initially exposed to 75, 100, 200 and 300 µM of test compounds with 25 mM NaCl in a total volume of 20 µL using 80 mM HEPES buffer (pH 7.2) for 5 h at 37 ˚C. The condensed DNA was then treated with the endonuclease, DNase I (NEB, M0303S), for 10 min at 37 ˚C and heat inactivated at 75˚C for 10 min. Samples were then loaded onto an agarose gel (1.5%) containing 3 µL EtBr and electrophoresis was completed at 50 V for 40 min in 1× TAE buffer.

Circular Dichroism Spectrometry.

Opioid profiles (**MC3** and **OC3**) and opioid-DNA interactions were analysed using Starna quartz cuvettes in 10 mM PBS solution (pH 7.0) in the presence of 25 mM

NaCl. Salmon testes DNA (stDNA, Sigma Aldrich, D1626) was initially quantified using the extinction co-efficient ε260 = 12824 $M(bp)^{-1}$ cm^{-1} to give a working solution with final stDNA concentration of ~100 μM. The investigation was conducted in the range of 200-400 nm and measurements were recorded at a rate of 1 nm per second. 100 μM stDNA solution was incubated with **MC3**, **OC3** and control agent's hexammine cobalt (III) chloride and spermine at *r* = 0.1 (*r* being the ratio [drug] / [DNA]) over a 7 h period at 37 ˚C. The DNA free CD spectra for **MC3** and **OC3** are shown in supplementary A-2.

II. 3.4. DNA condensation studies (linear dsDNA)

PCR Primer Design

Primers were designed (Eurofins Genomics) such that it was possible to generate a 742 bp long sequence of linear dsDNA from the pUC19 vector encompassing the lacZα gene. The short nucleotide sequence was generated through PCR (35 cycles) with 1 ng pUC19 plasmid using 2× MyTaq Red Mix (Bioline) at an annealing temperature of 66 ˚C and the band generated was compared to a 50 bp DNA ladder (Invitrogen, 10416014).

Forward: `5'-TCGCGCGTTTCGGTGATGACGG-3'`

Reverse: `5'-CCGCTCGCCGCAGCCGAACG-3'`

DNA condensation investigation.

400 ng of the 742 bp transcript was then treated under identical conditions as described (5 h incubation at 5, 10, 20 and 30 μM) and samples were loaded onto an agarose gel (1.2%) containing EtBr. Electrophoresis was completed at 70 V for 40 min in 1× TAE buffer.

II. 3.5. Endonuclease enzyme Inhibition

Endonuclease Optimisation on linear DNA sequence

400 ng of linear dsDNA was treated with 1 μL of EcoRI (NEB, R0101S), BamHI (NEB, R0136S), SalI (NEB, R0138S) and HindIII (NEB, R0104S) respectively at 37 ˚C overnight to verify the presence of their recognition sites within the short 742 bp sequence. All enzymes induced double stranded nicks to this sequence as evidenced by agarose gel electrophoresis.

Microfluidic analysis of endonuclease inhibition assay using Agilent BioAnalyser DNA 1000 chip

This assay was conducted as previously described by the Kellett Group with small changes being made (23). 400 ng of the PCR fragment was pre-treated with 10, 25, 50, 100 and 200 μM of either **MC3, HC3** or **OC3**. Subsequent digestion experiments were performed by incubating drug treated and un-treated DNA with 1 μL of EcoRI, BamHI, SalI and HindIII overnight and heat deactivated as per NEB guidelines. The reactions of EcoRI, BamHI, SalI and HindIII, in the presence and absence of tripodal scaffolds, were then examined using the Agilent DNA 1000 microfluidic chip (Agilent 5067-1504) with data being collected on the Agilent Bioanalyser 2100 platform.

Atomic Force Microscopy

AFM was used to determine the morphology of the DNA condensates induced by morphine C_3 opiate to support the effects of condensation at low concentrations. AFM samples were prepared according to the following general procedure: in a total volume of 10 μL final concentrations of 3 ng/μL of pUC19 (NEB, N3041) or linearized pUC19, 5 mM MgCl, and varying concentrations of test compound, were incubated at 37˚C for 1 h. 10 μL of each sample was pipetted directly on to freshly cleaved mica and allowed to incubate for 5 min followed by rinsing with 500 μL of water. The samples were dried under compressed air for a period of 1 h. AFM examinations were performed in ambient air with a commercial microscope (Dimension 3100 controlled by a Nanoscope IIIa controller, Digital Instruments), in tapping-mode, using standard unmodified silicon cantilevers (BudgetSensors, Bulgaria) with a 40 N/m force constant. Topographic images are recorded at a scanning rate of 1–2 Hz, and a resonance frequency of about 300 kHz (nominal value). Images were processed using the WSxM software (38) to remove the background slope and normalise the z-scale across all images, no additional filtering was performed.

II. 3.7. Influence of pH and ionic strength on condensation

Influence of pH on condensation

Absorption spectra were initially measured at 260 nm in order to give a final absorbance of ~0.4 units and the concentration of ctDNA was determined using the extinction co-efficient ε_{260} = 12824 $M(bp)^{-1}$ cm^{-1}. The condensation aggregates of the ctDNA solution was determined spectrophotometrically by monitoring the absorbance of DNA at both 350 nm and 260 nm at 25 ˚C using an Agilent Cary 100

dual beam spectrophotometer equipped with a 6 × 6 Peltier multicell system with temperature controller. In a final volume of 5 mL containing ~30μM ctDNA, nuclease free water (pH 7) and 25 mM NaCl, containing 35 μM **OC3**, the pH of solution was adjusted with 1 M HCl and 1 M NaOH to basic and acidic conditions as required using a Mettler Toledo SevenExcellence™ pH meter equipped with a Mettler Toledo Inlab expert Pro-ISM pH probe. 100 μL aliquots were titrated into quartz cuvettes and between each pH adjustment the solution was mixed thoroughly and allowed to incubate at 25˚C until the absorbance equilibrated and values obtained remained constant.

DNA condensation in acidic and basic buffers

400 ng of pUC19 DNA was treated as previously stated with slight modifications (5 h incubation at 5, 10, 20, 30, and 50 μM). Samples were incubated in acidic and basic buffers at pH 4.0 and 8.0 respectively. Sodium acetate (NaOAc) and Tris buffers were prepared and adjusted with HCl and NaOH accordingly to achieve the desired pH. Samples were loaded onto an agarose gel (1.2%) containing 3 μL EtBr. Electrophoresis was completed at 70 V for 40 min in 1× TAE buffer.

II. 4. Results and Discussion

II. 4.1. Synthesis of opioid scaffolds

Morphine scaffolds **MC3**, **HC3**, and **OC3** were generated and their molecular structures are shown in Figure II-1. Treating 1 equivalent of 2,4,6-*tris*-(bromomethyl)-mesitylene with 3 equivalents of either morphine (**M**), heterocodeine (**H**) or oripavine (**O**) yielded the respective C_3-symmetric opioid compounds **MC3**, **HC3**, and **OC3**. These were isolated as yellow or white solids after purification by column chromatography. A satisfactory yield for both **MC3** (50%) and **OC3** (48%) was obtained, however **HC3** could only be isolated in a low yield (13%). Indeed, generation of the **HC3** opioid was restricted due to the poor synthetic conversion of morphine to heterocodeine with yields <25% (39), which leads to a low overall yield for **HC3** from morphine. C_1 and C_2 opiate analogues (**MC1**, **MC2**, **OC1** and **OC2**) were synthesised in a similar manner to the C_3 congeners using α^2- chloroisodurene (**MC1** and **OC1**) and 2,4-bis(chloromethyl)-1,3,5-trimethylbenzene (**MC2** and **OC2**), respectively, of each opioid derivative (supplemental A-7). The series of compounds for this study were all prepared in either a one or two-step synthesis and enable

rapid access to samples for evaluation in biological investigations. As part of this work, a green chemistry metric analysis (40) has been performed (Supplementary Section A-10) with the aim of identifying aspects of the synthesis that can be improved in future studies (41, 42). This will ensure that further efforts to improve the yield for the above reactions can be in tandem with the development of greener methodologies. All compounds were characterised by ^{1}H and ^{13}C nuclear magnetic resonance (NMR, Supplementary A-1) and attenuated total reflectance (ATR) Fourier transform infrared (FTIR) spectroscopies, and by electrospray ionisation mass spectrometry (ESI-MS). Solution-based NMR studies in deuterated chloroform were performed to elucidate whether all three opiate units were on the same face of the molecule (C_3) or whether rotation of one opiate 'arm' was rapidly occurring at room temperature. To test the latter, a temperature study was conducted. This confirmed a C_3-symmetric opioid compound was formed for each of the *tris* target compounds; a single set of peaks in the ^{1}H NMR was observed for the opioid substructure for **MC3**, **HC3** and **OC3** in both 1D and 2D NMR studies. As the probe temperature was decreased from 293 K to 243 K no changes in the proton NMR were detected, supporting the C_3 symmetry of the compounds as a stable configuration.

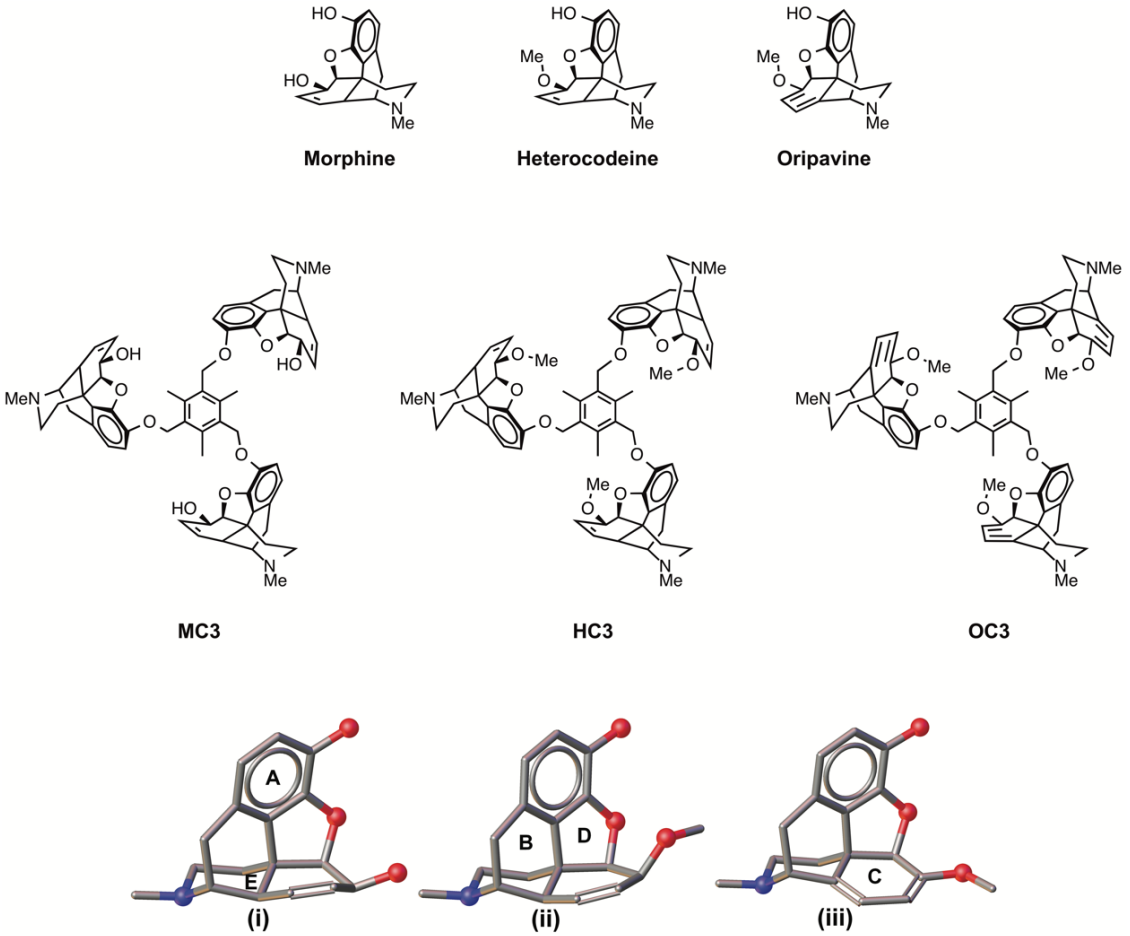

Figure II-1. Molecular structures of morphine, heterocodeine, and oripavine along with C_3-symmetic opioids molecules developed in this study: morphine (**MC3**), heterocodeine (**HC3**), and oripavine (**OC3**). Left to right, morphine, heterocodeine and oripavine scaffolds. Structures **(i)**, **(ii)** and **(iii)** show the geometries of each scaffold (morphine, heterocodeine and oripavine respectively), with labelled ring substituents A-E, modified from X-ray structures reported in the Cambridge Structural Database (CSD).

II. 4.2. Condensation of duplex DNA

C_3 opiate binding interactions with duplex DNA were first identified using a saturated ethidium bromide (EtBr) fluorescence quenching study with calf thymus DNA (ctDNA) (Figure II-2). In our initial high-throughput screen, which involved a series of novel opioid scaffolds, **MC3** was identified as a potentially new DNA binding molecule. Our motivation for developing **HC3** and **OC3** isomers stemmed from structural analysis on **MC3** that focused on the 6'-OH group in the morphine C ring as a possible H-bonding site for phosphate coordination. Since this group is masked by methylation in heterocodeine (**H**) and oripavine (**O**), we anticipated **HC3** and **OC3** analogues would have negligible DNA binding properties. Unexpectedly, however, enhanced EtBr displacement was observed (Table II-1), particularly on poly[d(G-

C)$_2$] and poly[d(A-T)$_2$] co-polymers with apparent binding constants (K_{app}) of ~106 M(bp^{-1}) and ~107 M(bp^{-1}), respectively.

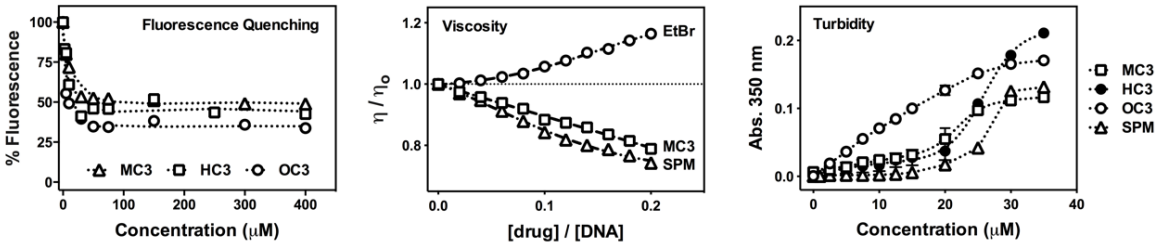

Figure II-2. Competitive fluorescence quenching of ethidium bromide bound to ctDNA by opioid drugs **MC3**, **HC3**, and **OC3**, viscosity properties of **MC3**, ethidium bromide (EtBr) and spermine (SPM) exposed to salmon testes dsDNA, and turbidity profiles of CT-DNA in the presence of titrated C_3 opioids and spermine. Data points being displayed as an average of triplicate measurement for fluorescence quenching and turbidity measurements.

Table II-1 Apparent binding constants of opioid C_3 compounds to dsDNA polymers.

	K_{app} M(bp^{-1})			ΔT_M °C (± S.D.)	
	Poly A-T (100% A-T)	CT-DNA (58% A-T)	Poly G-C (0% A-T)	Poly A-T (100% A-T)	Poly G-C (0% A-T)
Actinomycin D	N.D.	2.92 x 10^7	5.35 x 10^7	-0.32 ± 0.29	12.10 ± 0.95
Netropsin	5.75 x 10^7	2.5 x 10^6	N.D.	12.32 ± 0.79	2.83 ± 0.38
MC3	3.03 x 10^5	6.40 x 10^6	2.69 x 10^5	0.38 ± 0.71	2.63 ± 0.58
OC3	3.63 x 10^6	3.82 x 10^6	3.5 x 10^7	-0.17 ± 0.25	0.36 ± 0.17
HC3	9.1 x 10^6	7.84 x 10^6	1.15 x 10^7	0.73 ± 0.18	1.72 ± 0.61

To identify the significance of the C_3 opioid scaffold symmetry toward duplex DNA binding, **OC1**, **OC2**, **MC1** and **MC2** compounds were generated and tested using gel electrophoresis experiments (24, 35, 37). Condensation results, however, revealed negligible C_1 and C_2 activity (supplementary A-3) confirming the requirement of a tertiary opioid substituent to facilitate efficient nucleic acid coordination at low micromolar concentration. Thermal melting analysis on duplex polymers were then completed (Table II-1), and, unlike classic DNA binding agents of netropsin and actinomycin D (35), examined previously under identical conditions by this group, no significant stabilisation energies were identified for the *tris*-opiate compounds.

In order to probe the nature of DNA binding, viscosity studies with salmon testes DNA (ST-DNA) at varying drug load were evaluated (Figure II-2). Classical condensation behaviour by C_3 opioids was observed whereby all three agents exhibited identical, downward curving, hydrodynamic (η/ηo) values. As shown in Figure II-2, the profile of **MC3** is similar to the well-studied DNA compaction agent spermine (SPM), which was run as a control agent alongside the classical DNA intercalator EtBr. Since condensation of dsDNA can be monitored at 350 nm, a wavelength where nucleic acids do not normally absorb unless condensation/aggregation has occurred (24), UV-vis absorption spectrophotometry was employed to further characterise the condensation process. (Although turbidity of dsDNA can also be monitored at 260 nm, electronic absorption of C_3 opioids in this region precluded this measurement.) All three opioids exhibit concentration-dependent aggregation of dsDNA with binding isotherms of **MC3** and **HC3** being sigmoidal in nature and approximately similar in shape to spermine (Figure II-2). **OC3**, however, has a markedly different profile that increases almost linearly between 1– 25 μM before reaching a plateau beyond this titration point. Overall, and in comparison, to spermine, greater aggregation was observed for C_3 opioids tested up to 25 μM, beyond which, **OC3** and **MC3** scaffolds can be described as having the highest condensation effects in the series.

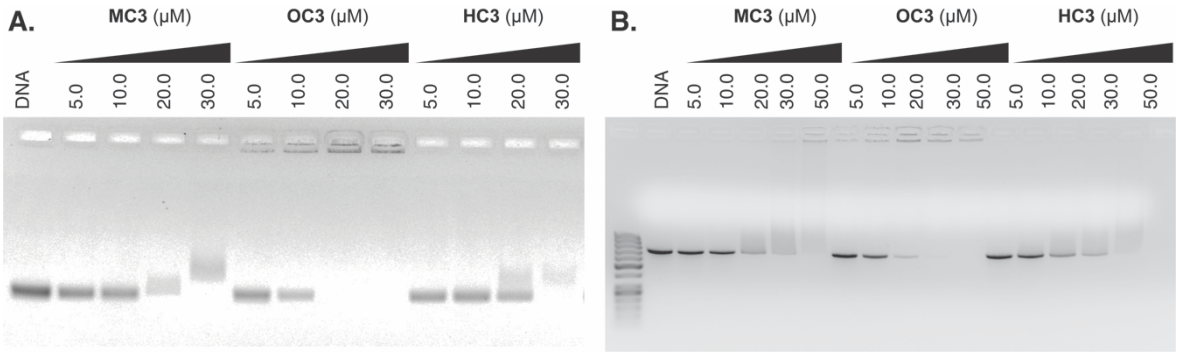

Figure II-3. A. Agarose gel electrophoresis of supercoiled (400 ng) and **B.** a 742 bp dsDNA fragment of pUC19 (400 ng) exposed to increasing concentrations of **MC3, OC3**, and **HC3**. Reactions were carried out in the presence of 25 mM NaCl for 5 h at 37˚C prior to electrophoretic analysis.

Since condensation by C_3-opioids had been established by viscosity and turbidity measurements, visualisation of DNA compaction was then followed by electrophoresis. Samples were titrated against both supercoiled pUC19 plasmid DNA and a 742 bp dsDNA fragment amplified from pUC19 encompassing the lacZα

gene, before incubation for 5 h prior to analysis by agarose gel electrophoresis (Figure II-3). All three opioid scaffolds were found to condense both supercoiled and linear dsDNA; **MC3** and **HC3** have similar profiles with the onset of aggregation at 20 μM, beyond which native DNA bands become fainter in appearance or disappear entirely from view, thus reflecting total condensation. **OC3**, however, exhibits improved condensation effects in comparison to morphine and heterocodeine scaffolds. Here, the initiation of aggregation can be visualised at 5 μM with the condensation process being completed at 20 μM and 30 μM on supercoiled plasmid and linear DNA, respectively. Indeed, on comparing the gels, it is evident that opioid-induced aggregation of supercoiled pUC19 (Figure II-3A) occurs more efficiently than for linear dsDNA (Figure II-3B).

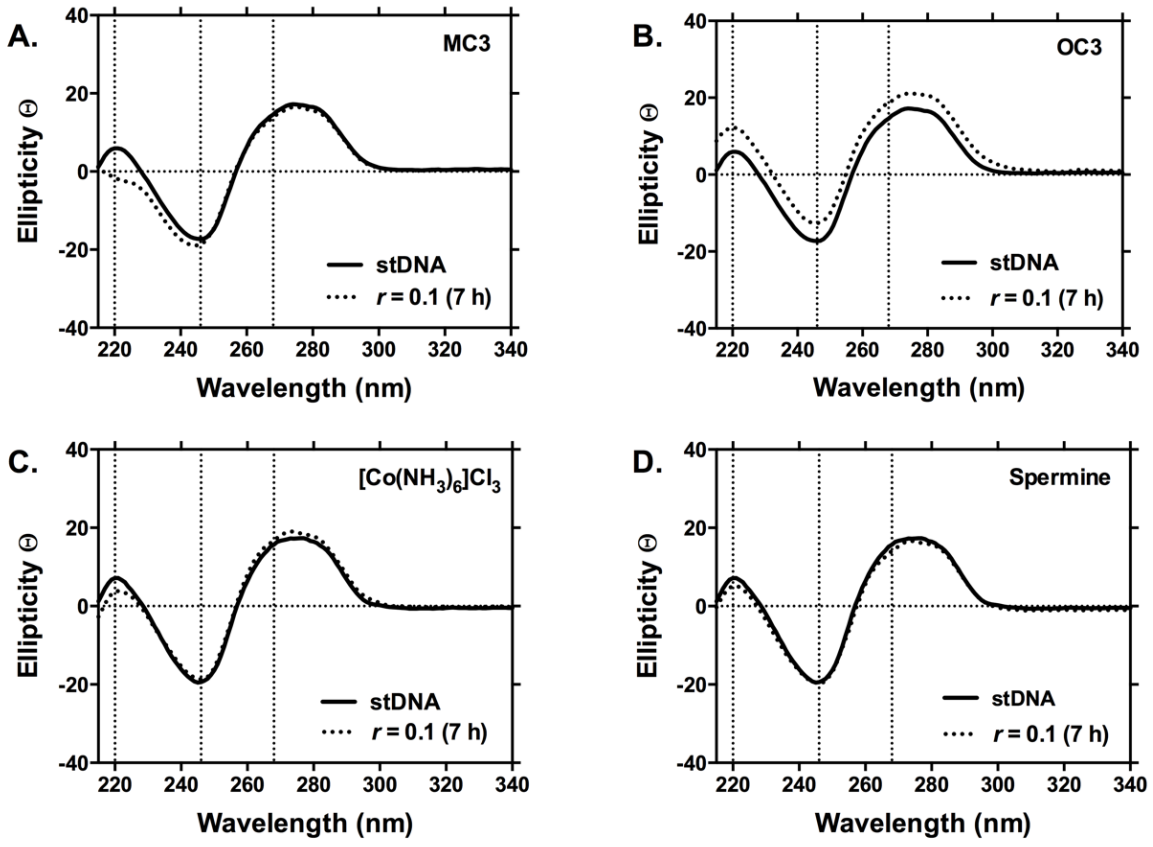

Figure II-4. Circular dichroism (CD) spectra of ST-DNA treated with **MC3**, **OC3** and electrostatic DNA binding controls hexammine cobalt (III) chloride and spermine over 7 h at *r* ([opioid] / [DNA]) values of 0.1.

To further probe the condensation mechanism, the interaction of C_3 opioids with pUC19 were examined in the presence of non-covalently bound recognition elements netropsin, which is well-characterised to bind within the minor groove (43), and methyl green an agent that binds at the major groove (44). In these experiments' plasmid DNA was pre-exposed to 20 μM of each recognition element prior to the introduction of opioid sample (5 – 50 μM). No differences were detected in the condensation process between the control (opioid + pUC19) and tested samples in any case, indicating interactions within the minor and major grooves are unlikely as prospective recognition sites for C_3 opioid binding (data not shown). Indeed, no evidence of minor or major groove binding, or of intercalation could be found in the circular dichroism (CD) spectra of **MC3** and **OC3** with ST-DNA (Figure II-4). It was further noted that no conformational change was induced upon opioid binding and condensation. Thus, the profiles for both C_3 scaffolds do not yield spectral shifts expected of classical DNA binding agents but, instead, are similar to surface-binding condensation agents spermine and $[Co(NH_3)_6]Cl_3$ (45) when tested with long DNA polymers. Finally, while the spectrum of **HC3** could not be examined owing to its limited solubility in CD accessible solvents, it is reasonable to assume the binding interaction should not deviate from that observed from **MC3** or **OC3**.

II. 4.3. Influence of pH and ionic strength on condensation

Since the biophysical evidence gathered on C_3 opioid-DNA binding points toward a surface-binding coordination mode, we considered the possibility of the tertiary amine within the morphine D (piperidine) ring as a possible cationic site responsible for H- bonding and/or electrostatic binding to the phosphate backbone. Indeed, this particular site is well recognised to undergo protonation prior to binding with specific amino acid residues within opioid receptor cavities (46). To examine this hypothesis, the condensation effects of supercoiled pUC19 were initially examined under sodium chloride titration on agarose electrophoresis. Here, 25 μM aliquots of **MC3**, **OC3**, and **HC3** were analysed with increasing NaCl ionic strength (25 – 1000 mM) with supercoiled pUC19 (Figure II-5A). At low salt concentrations (25 – 75 mM) the plasmid was condensed by all three opioids, however, in the presence of ≥100 mM NaCl, aggregation by **MC3** and **HC3** agents was inhibited as evidenced by the fraction of DNA migrating in supercoiled form. In contrast, **OC3** maintained its condensation effects up to 750 mM of titrated NaCl and only at the highest ionic strength examined, 1 M, could a fraction of native supercoiled pUC19 be identified.

These results indicate that condensation by C_3 morphine analogues are dependent on ionic charge, and that disruption of this interaction by the introduction of an ionic gradient can, at least partially, reverse DNA aggregation. Furthermore, it is worth highlighting that compaction by **MC3** and **HC3** is disrupted to the same degree by NaCl, while **OC3** is substantially more resistant to changes in ionic strength.

To further probe the involvement of quaternary amine cations in the condensation process, aggregation of pUC19 was then examined under acidic (pH 4.0) and basic (pH 9.0) buffered conditions. As anticipated, a clear enhancement of the condensation process at lower pH with sodium acetate buffer (Figure II-5B) was observed, while under basic conditions (Tris buffer) DNA aggregation was reduced (Figure II-5C). These results indicate that in an acidic environment, the piperidine opioid D ring becomes protonated and collapse of DNA proceeds at lower C_3 concentration. Indeed, on comparing Figure II-3A with Figure II-5 B and C it is clear that condensation in pH 4 buffered solution occurs with the highest efficiency across all three tested opioids, followed thereafter by condensates at pH 7.2 and then finally pH 9.0 where very little aggregation for both **MC3** and **HC3**. This analysis supports proposal that the amine group within the piperidine opioid ring is the protonation site responsible for condensation and, based on these condensation results, is highly probable the 3^+ polycationic state of the C_3 symmetric opioid scaffold is required to induce aggregation.

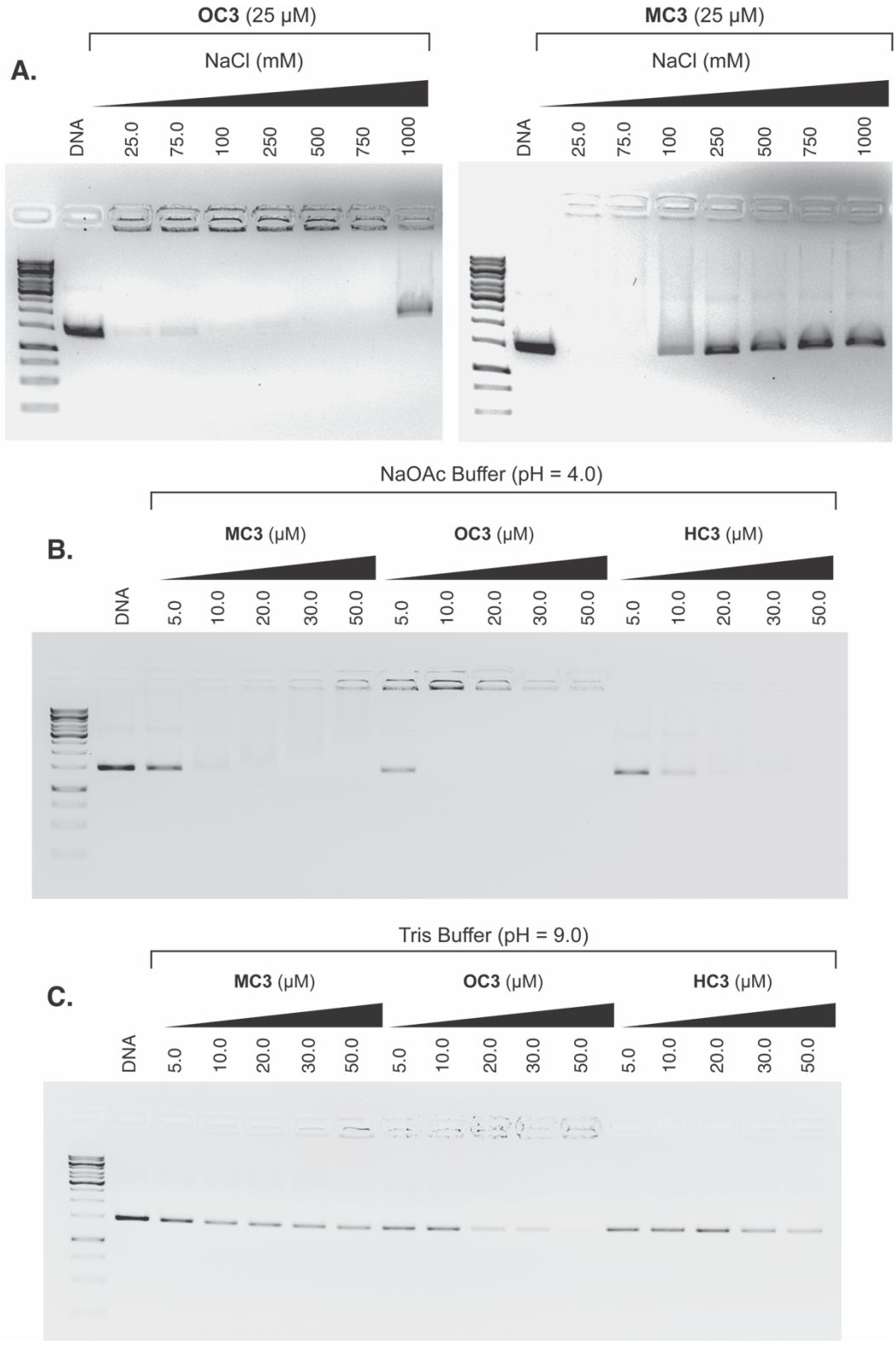

Figure II-5.(A.) Influence of ionic strength on pUC19 condensation (400 ng) by **OC3** and **MC3** (25 μM) opioid compounds. Condensation reactions on pUC19 (400 ng) by opioid compounds in **(B.)** acidic NaOAc buffer (80 mM, pH = 4.0), and **(C.)** basic Tris buffer (80 mM, pH = 9.0) in the presence of 25 mM NaCl.

II. 4.4. Atomic force microscopy (AFM)

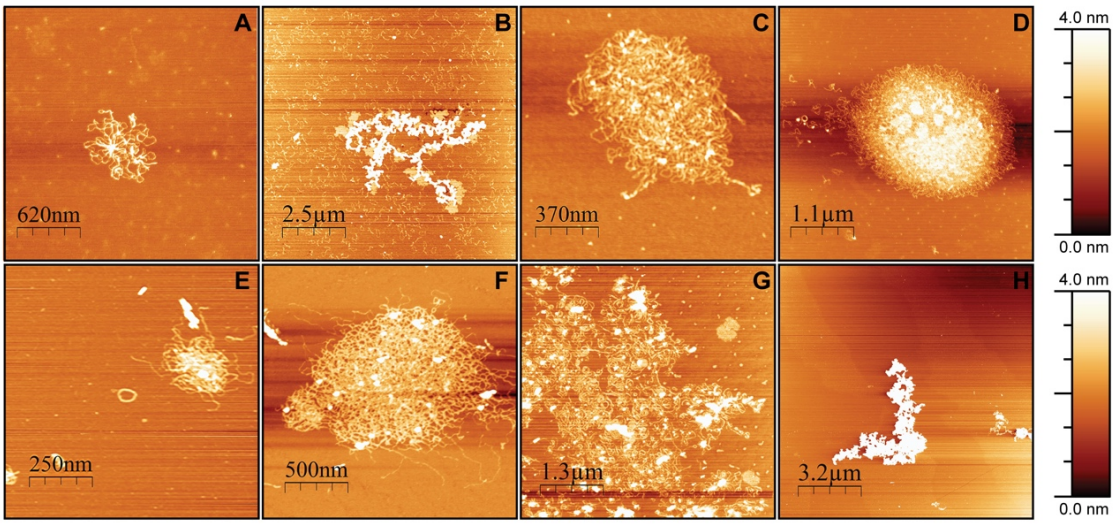

Figure II-6. AFM images of **MC3-**treated supercoiled and HindIII linearized pUC19 DNA; **A-D**: supercoiled pUC19 with 8, 9, 10, and 20 µM **MC3;** E-H: linear pUC19 with 5, 10, 20, and 50 µM **MC3**.

AFM imaging provides a direct tool for exploring the effects of ligand binding on DNA morphology(47, 48). Due to its nanoscale resolution there are numerous examples of AFM techniques used to determine the binding mode, affinity and site-exclusion number of DNA in the presence of suitable binding substrates. Recent AFM studies have characterised the binding modes of well-studied ligands such as doxorubicin, ethidium bromide and netropsin (49). Moreover, this technique can successfully probe morphological changes induced in closed circular plasmid and linear forms of DNA, along with RNA. In this work, AFM studies were performed with closed circular and HindIII linearized pUC19 in ambient air using a Tapping-Mode with unmodified silicon cantilevers at a 40 N/m force constant. Furthermore, we established that 5 mM of $MgCl_2$ was required for complete mica adhesion with no appreciable conformational changes to DNA morphology. **MC3** was selected as a representative compound in this series for AFM analysis. In the presence of 8 µM of **MC3**, supercoiled pUC19 exhibited small cluster formation where tight packing is present in the cluster centre with DNA strands extending from its midpoint (Figure II-6A). As the concentration of **MC3** increased to 9 µM, a sizeable increase in cluster formation was observed, however, unbound strands of DNA were evident at this point (Figure II-6B). A gradual increase in **MC3** concentration to 10 and 20 µM led to the near disappearance of unbound pUC19, leaving only large and tightly packed globules of ~800 nm and ~3.3 µm spherical dimension, respectively (Figure II-6 C and D). Data here supports our earlier gel electrophoresis analysis where 20 µM of **MC3**

was required to fully condense the supercoiled plasmid (see Figure II-3A). In the presence of linearized pUC19, a lower concentration of **MC3** (5 μM) initiated the onset of condensation (Figure II-6E) with both toroidal and cluster formation evident. Toroid condensates, however, were evident at low **MC3** concentration only with larger aggregates, >1 μm, appearing at 10 and 20 μM exposure with compact globules forming thereafter (50 μM). These results agree with our electrophoretic data on linear pUC19 (see Figure II-3B), where 50 μM of **MC3** was established to condense this sequence.

II. 4.5. Microfluidic analysis of endonuclease inhibition

The condensation effects of the opioid series on a 742 bp dsDNA fragment, amplified from the pUC19 vector encompassing the lacZα gene (supplemental A-6), and subsequent access by sequence-recognition type II restriction endonucleases were initially examined by gel electrophoresis. Results showed the inhibition of migration at ~20 μM of C_3 opioid exposure indicating condensation had occurred. An on-chip microfluidic assay using an Aglient 2100 Bioanalyzer was then employed (Figure II-7) to determine whether C_3-opoid induced condensation could block sequence-recognition by type II restriction enzymes BamHI, HindIII, SalI and EcoRI. These restriction enzymes were selected based on their single recognition site within our transcript with control experiments (supplemental A-5) establishing no direct interaction between restriction enzymes and C_3 opiates. A DNA 1000 microfluidic chip was employed in this study to detect and quantify excision fragments, resulting in the disappearance of the parent 742 bp band and the emergence of daughter fragments sized between 295 and 447 bp (Figure II-8A). Pre-incubation of the transcript with 50 μM of both **MC3** and **HC3** afforded little protection toward endonuclease accessibility (Figure II-8 B and C). An exception, however, was noted for BamHI activity to **HC3** exposed DNA; here, the parent fragment at 742 bp emerged with notable reduction in the excision fragment peak area at 325 and 417 bp. Interestingly, preincubation of the transcript with low micromolar loading of **OC3** (10 μM) was found to inhibit endonuclease accessibility by BamHI, SalI and EcoRI. Furthermore, in the case of the BamHI-treated transcript pre-exposed to **OC3**, almost complete protection of the oligo was observed. It was noted, however, that peak area of **OC3** exposed fragments were diminished in comparison to **MC3** and **HC3** experiments, most likely through the enhanced condensation effects of this agent. Finally, in a complimentary study using gel

electrophoresis, we identified that the non-specific endonuclease DNase I degraded all C_3-opioid plasmid pUC19 condensates with identical efficiency (data not shown).

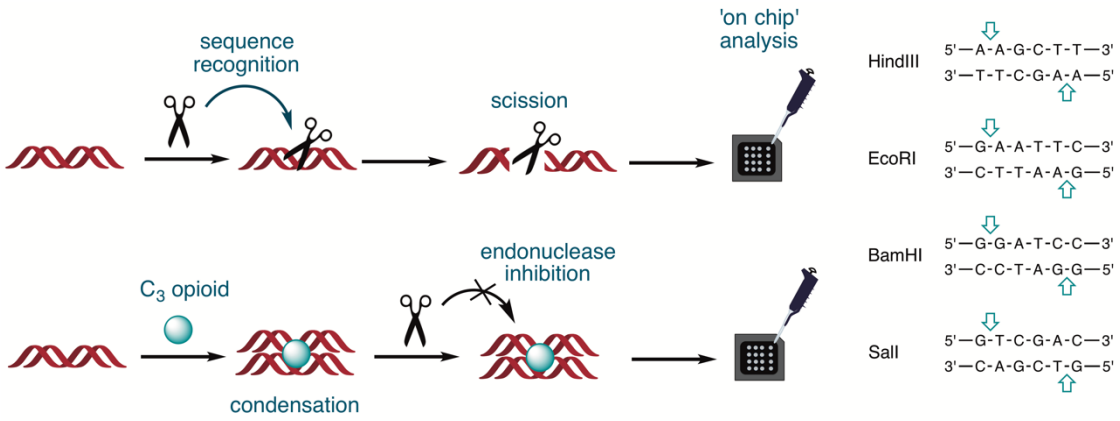

Figure II-7. Experimental design for the Bioanalyzer 2100 to identify site-specific endonuclease inhibition by opioid compounds, HindIII, EcoRI, BamHI, and SalI.

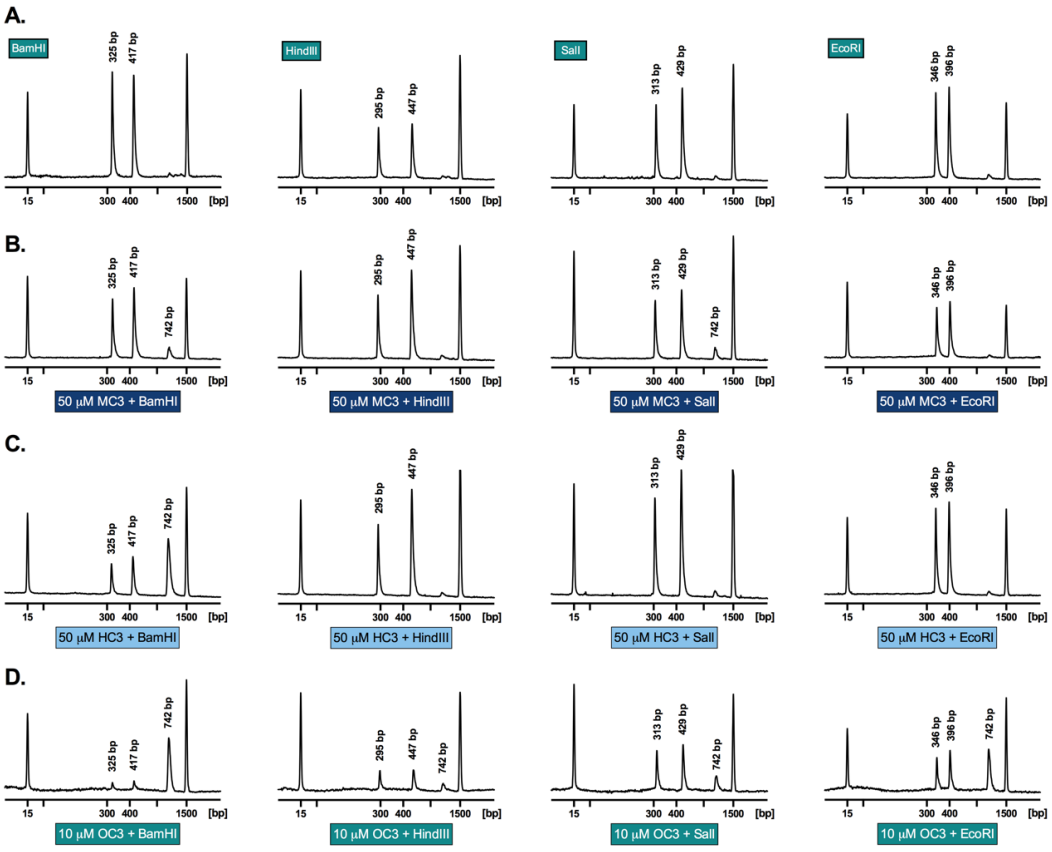

Figure II-8. A. Electrograms generated using the Bioanalyzer 2100 of 742 bp dsDNA fragment with treatment by endonuclease BamHI, HindIII, SalI, and EcoRI. Electrograms of the 742 bp fragment were pre- incubated for 5 h with either **MC3 (B), HC3 (C)**, and **OC3 (D)**, followed by exposure over night to the type II restriction endonuclease.

II. 5. Conclusions

To our knowledge opioid compounds have not previously been shown to interact with nucleic acids. This work may therefore open up new applications for these well-established analgesic compounds as semi-synthetic natural products that facilitate nucleic acid recognition. Target compounds were prepared via short synthetic routes, which in most cases involved a single step (*i.e.* from an opioid natural product and commercially available benzyl bromide derivative). The high-affinity DNA binding and condensation properties of this scaffold demonstrate a requirement for a tris-opiate, along with a polycationic charge of 3+, as the C_1 and C_2 opiate congeners showed negligible condensation effects by comparison. In this regard, this class of agent falls squarely in line with the majority of established DNA condensation agents where a ≥3+ cationic valence requirement for DNA collapse is generally required (22). Biophysical assays on duplex DNA polymers revealed no intercalative or major/minor groove residency, which led to the probing of C_3-opioids as potential electrostatic and/or H-bonding agents. Thus, our preliminary studies using C_3-morphine (**MC3**) focused on the possibility of the 6'-OH, located in the morphine C ring, as a possible surface binding moiety. Further, while physiological conditions promote interplay between morphine protonation (*kO*) and zwitterionic (*kN*) isomers (supplemental A-8), the 6'-OH does not engage in acid/base speciation and was therefore considered as a potential phosphate-interacting site (50, 51). To test this axiom, the development of C_3-heterocodeine (**HC3**) and C_3-oripavine (**OC3**) derivatives, where the 6'-OH site is masked by methoxy substituents, was undertaken. Biophysical studies, however, revealed comparable (**HC3**) and enhanced (**OC3**) high- affinity binding to DNA; these data, coupled with condensation properties observed at varying pH and ionic strength, implicate N-protonation of the piperidine (E) ring—a known cationic site that undergoes ionic bond formation with the opioid receptor (46) as the nucleation site responsible for nucleic acid coordination. A proposed model for DNA binding is shown in Figure II-9 where each opiate is protonated (and charged) at the piperidine ring that, in turn, surface binds the vicinal nucleic acid backbone. Based on this proposed model, the binding of C_3 opioids to other nucleic acid structures can be expected and preliminary experiments on the condensation of tRNA by **MC3** (supplemental A-9) evidences this. To corroborate the binding mode described in Figure II-9, methylation of each N-piperidine moiety in **MC3** was achieved (supplemental A-7) leading to isolation of the quateranized piperidium cation **MC3-NMe$_2$** as an iodide

salt. The condensation effects of **MC3-NMe$_2$** with pUC19, when directly compared to **MC3** (supplemental A-4), resulted in a significantly altered condensation profile. Thus, **MC3-NMe$_2$** did not aggregate DNA at any exposure value (1 – 30 μM) where **MC3** exhibited condensation and only at higher concentrations (>30 μM) was **MC3-NMe$_2$** condensation observed; we propose this interaction is electrostatic in nature and similar to **NMe$_2$**-quaternarized nucleic acid binding observed in the literature (52, 53). It is highly likely, therefore, that N-protonation of the *C$_3$* opioid scaffold is responsible for efficient condensation and that piperidinium phosphate hydrogen bonding interactions are required for these high-affinity interactions.

Further examination of *C$_3$* agents revealed i.) no conformational modification to long canonical DNA polymers, ii.) improved affinity toward aggregation of supercoiled plasmid versus linear DNA conformation, and iii.) an overall aggregation activity profile **OC3** >> **HC3** ≈ **MC3**. To derive some insight into the differences in binding between the oripavine compound and the morphine or heterocodeine analogues, we considered structural data for examples of each class taken from the CSD (54). Figure II-10 shows the cation of diacetylmorphine hydrogen chloride monohydrate (FAZDAM, CCDC 242245) and 3,6-dimethoxy-5,17-dimethyl-6,7,8,14-tetradehydro-4,5-epoxymorphinan (LOBGUG, CCDC 985664), for the purpose of comparison a proton has been added to the amine at the calculated position in the latter case. The increased unsaturation in the oripavine means that the “C” ring is flattened relative to the morphine or codeine systems and that one of the hydrogen atoms in an axial position relative to the amine proton is lost. As a consequence, the amine site is clearly less sterically crowded in the oripavine system and this might be expected to make interaction with the DNA phosphate backbone easier. There are also electronic changes in the π system of ring C, which may influence both the pKa of the amine and electronic aspects of bonding.

The condensation process at neutral pH, studied by AFM analysis with **MC3**, identified toroidal formation of pUC19 at low compound loading, while higher loading promoted tightly packed globule formation in both closed circular and linear DNA structures. The combined effect of high binding constants and condensation of the C$_3$-opioid class was then considered in terms of interrupting protein-DNA recognition (23). Since condensation agents have found widespread utility as transfection agents or carriers of nucleic acids (55, 56) protection of this “cargo” to endonuclease

degradation is of considerable importance. While DNase I mediated complete transcript degradation from all three C_3-opioid carriers, type II restriction endonucleases inhibition for **HC3** (50 μM) and **OC3** (10 μM) was witnessed at the G-G excision region of BamHI, while **OC3** (10 μM) further protected the G-A excision region of EcoRI. In summary, this work has revealed the discovery of a new high-affinity DNA binding scaffold capable of mediating condensation ostensibly through electrostatic and H-bonding interactions with the phosphate backbone. Our attention now turns to further explore the condensation effects of RNA and alternative DNA structures by these molecules and for their ability to successfully deliver gene vectors.

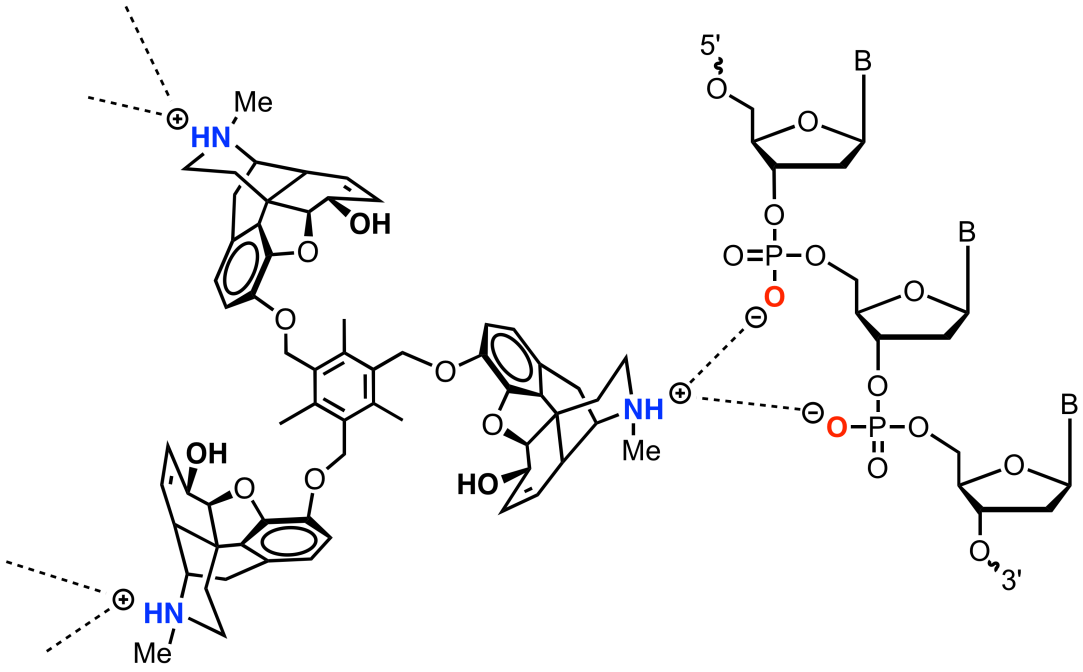

Figure II-9. Proposed ionic binding by the *C_3* opioid scaffold to the nucleic acid phosphate backbone.

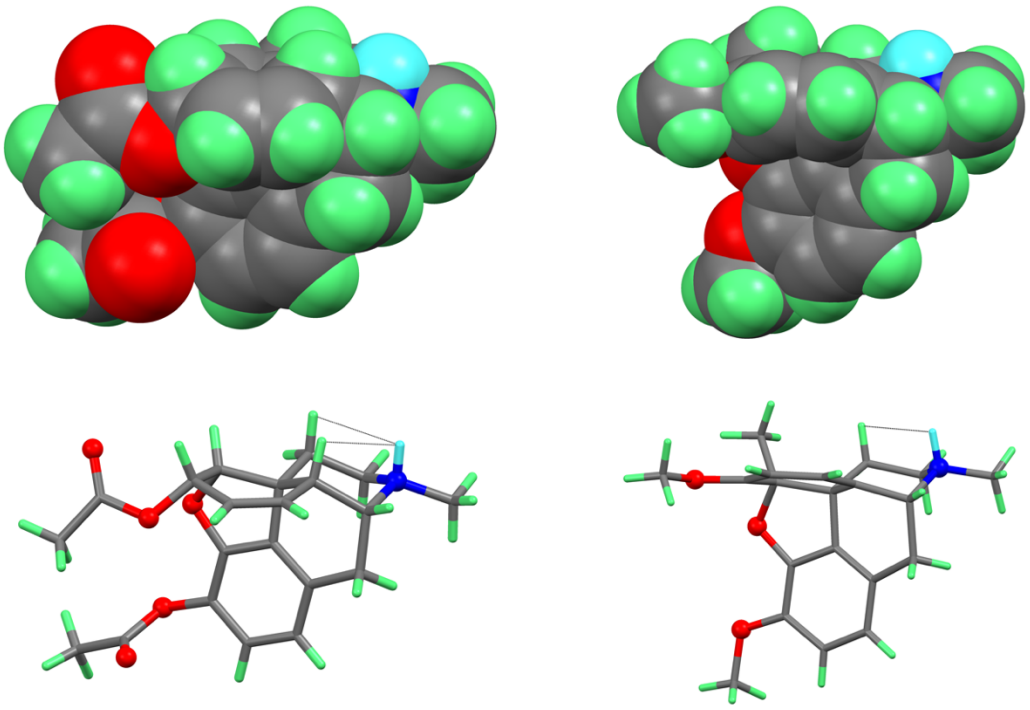

Figure II-10. Structures of protonated diacetylmorphine (FAZDAM left) and protonated 3,6-dimethoxy-5,17-dimethyl-6,7,8,14-tetradehydro-4,5-epoxymorphinan (LOBGUG right) redrawn from the CSD data (the amine proton has been added to the structure at a calculated position for LOBGUG). The amine proton (highlighted in cyan) is more exposed in the oripavine. Dashed lines show the interactions with neighbouring axial protons.

To the best of our knowledge the C_3-opioid scaffolds developed within our lab remain the only opioid compounds to display nucleic acid condensation, along with the recently developed **CC3** scaffold discussed in Chapter III (57). C_3-symmetric molecules for biological or biomolecular-related investigations such as targeting amino acids (58) and DNA (59) are very rare. Sun *et al*. (60) reported a propeller-like molecule with three terminal amino side groups found to be a selective nucleic acid binder towards telo21 G-quadruplex DNA when compared to single and double stranded DNA. In the interest to further gene delivery applications recent advances in synthetic condensing agents have incorporated chromophores to include an on-off switch as DNA becomes compacted (61). Compact DNA structures with redox-responsive donor-acceptor moieties are attractive for biosensor and drug delivery applications. The ongoing developments with CRISPR/Cas9 (62) has led to a surge of new synthetic non-viral vector discovery for improved gene delivery platforms (63, 64). Gene delivery remains the rate limiting step for the enhancement of Gene therapy and continued efforts are of great importance.

II. 6. References

1. Kelland, L. (2007) The resurgence of platinum-based cancer chemotherapy. *Nature Reviews Cancer*, **7**, 573–584.
2. Takahara, P.M., Rosenzweig, A. C., Frederick, C. A. and Lippard, S. J. (1995) Crystal structure of double-stranded DNA containing the major adduct of the anticancer drug cisplatin. *Nature*, **377**, 649–652.
3. Pieper, R.O., Futscher, B. W. and Erickson, L.C. (1989) Transcription-terminating lesions induced by bifunctional alkylating agents in vitro. *Carcinogenesis*, **10**, 1307–1314.
4. Strekowski, L. and Wilson, B. (2007) Noncovalent interactions with DNA: An overview. *Mutation Research/Fundamental and Molecular Mechanisms of Mutagenesis*, **623**, 3–13.
5. Niyazi, H., Hall, J. P., O'Sullivan, K., Winter, G., Sorensen, T., Kelly, J.M. and Cardin, C.J. (2012) Crystal structures of Λ-[Ru(phen)2dppz]2+ with oligonucleotides containing TA/TA and AT/AT steps show two intercalation modes. *Nature Chemistry*, **4**, 621–628.
6. Hurley, L. H. (2002) DNA and its associated processes as targets for cancer therapy. *Nature Reviews Cancer*, **2**, 188–200.
7. Cai, X., Gray, P. J. and Von Hoff, D. D. (2009) DNA minor groove binders: Back in the groove. *Cancer Treatment Reviews*, **35**, 437–450.
8. Hamilton, P. L. and Arya, D. P. (2012) Natural product DNA major groove binders. *Nat. Prod. Rep.*, **29**, 134–143.
9. Bailly, C., Hénichart, J.-P., Colson, P. and Houssier, C. (1992) Drug—DNA sequence-dependent interactions analysed by electric linear dichroism. *J. Mol. Recognit.*, **5**, 155–171.
10. Tuite, E. and Nordén, B. (1995) Intercalative interactions of ethidium dyes with triplex structures. *Bioorganic & Medicinal Chemistry*, **3**, 701–711.
11. Erkkila, K.E., Odom, D.T. and Barton, J.K. (1999) Recognition and Reaction of Metallointercalators with DNA. *Chemical Reviews*, **99**, 2777–2796.
12. Liu, H.-K. and Sadler, P.J. (2011) Metal Complexes as DNA Intercalators. *Accounts of Chemical Research*, **44**, 349–359.
13. Hopcroft, N.H., Brogden, A.L., Searcey, M. and Cardin, C.J. (2006) X-ray crystallographic study of DNA duplex cross-linking: simultaneous binding to two d(CGTACG)2 molecules by a bis(9-aminoacridine-4-carboxamide) derivative. *Nucleic Acids Research*, **34**, 6663–6672.

14. Farrell, N.P. (2015) Multi-platinum anti-cancer agents. Substitution-inert compounds for tumor selectivity and new targets. *Chem. Soc. Rev.*, **44**, 8773–8785.
15. Calnan, B.J., Tidor, B., Biancalana, S., Hudson, D., Frankel, A.D. and others (1991) Arginine-mediated RNA recognition: the arginine fork. *Science*, **252**, 1167–1171.
16. Yamaguchi, N., Zouzumi, Y., Shimada, N., Nakano, S., Sugimoto, N., Maruyama, A. and Miyoshi, D. (2016) A reversible B–A transition of DNA duplexes induced by synthetic cationic copolymers. *Chem. Commun.*, **52**, 7446–7449.
17. Bloomfield, V.A. (1996) DNA condensation. *Current opinion in structural biology*, **6**, 334–341.
18. Teif, V.B. and Bohinc, K. (2011) Condensed DNA: Condensing the concepts. *Progress in Biophysics and Molecular Biology*, **105**, 208–222.
19. Bloomfield, V.A. (1997) DNA condensation by multivalent cations. *Biopolymers*, **44**, 269–282.
20. Grosberg, A.Y. and Kuznetsov, D.V. (1992) Quantitative theory of the globule-to-coil transition. 1. Link density distribution in a globule and its radius of gyration. *Macromolecules*, **25**, 1970–1979.
21. Vijayanathan, V., Thomas, T., Shirahata, A. and Thomas, T.J. (2001) DNA Condensation by Polyamines: A Laser Light Scattering Study of Structural Effects. *Biochemistry*, **40**, 13644–13651.
22. Wilson, R.W. and Bloomfield, V.A. (1979) Counterion-induced condensation of deoxyribonucleic acid. A light-scattering study. *Biochemistry*, **18**, 2192–2196.
23. Prisecaru, A., Molphy, Z., Kipping, R.G., Peterson, E.J., Qu, Y., Kellett, A. and Farrell, N.P. (2014) The phosphate clamp: sequence selective nucleic acid binding profiles and conformational induction of endonuclease inhibition by cationic Triplatin complexes. *Nucleic Acids Research*, **42**, 13474–13487.
24. Malina, J., Farrell, N.P. and Brabec, V. (2014) DNA Condensing Effects and Sequence Selectivity of DNA Binding of Antitumor Noncovalent Polynuclear Platinum Complexes. *Inorganic Chemistry*, **53**, 1662–1671.
25. Malina, J., Farrell, N.P. and Brabec, V. (2014) Substitution-Inert Trinuclear Platinum Complexes Efficiently Condense/Aggregate Nucleic Acids and

Inhibit Enzymatic Activity. *Angewandte Chemie International Edition*, **53**, 12812–12816.

26. Plum, G.E., Arscott, P.G. and Bloomfield, V.A. (1990) Condensation of DNA by trivalent cations. 2. Effects of cation structure. *Biopolymers*, **30**, 631–643.
27. He, S., Arscott, P.G. and Bloomfield, V.A. (2000) Condensation of DNA by multivalent cations: Experimental studies of condensation kinetics. *Biopolymers*, **53**, 329–341.
28. Kankia, B.I., Buckin, V. and Bloomfield, V.A. (2001) Hexamminecobalt (III)-induced condensation of calf thymus DNA: circular dichroism and hydration measurements. *Nucleic acids research*, **29**, 2795–2801.
29. Malina, J., Hannon, M.J. and Brabec, V. (2015) Iron(II) Supramolecular Helicates Condense Plasmid DNA and Inhibit Vital DNA-Related Enzymatic Activities. *Chemistry A European Journal*, **21**, 11189–11195.
30. Andrushchenko, V., van de Sande, H. and Wieser, H. (2003) DNA interaction with Mn2+ ions at elevated temperatures: VCD evidence of DNA aggregation. *Biopolymers*, **69**, 529–545.
31. Vallejo, R., Barkin, R. L. and Wang, V.C. (2011) Pharmacology of Opioids in the Treatment of Chronic Pain Syndromes. *Pain Physician*, **14**, 343–360.
32. Prisecaru, A., McKee, V., Howe, O., Rochford, G., McCann, M., Colleran, J., Pour, M., Barron, N., Gathergood, N. and Kellett, A. (2013) Regulating Bioactivity of Cu^{2+} Bis-1,10-phenanthroline Artificial Metallonucleases with Sterically Functionalized Pendant Carboxylates. *Journal of Medicinal Chemistry*, **56**, 8599–8615.
33. Barber, R.B. and Rapoport, H. (1975) Synthesis of Thebaine and Oripavine from Codeine and Morphine. *Journal of Medicinal Chemistry*, **18**, 1076–1077.
34. Rapoport, H and Barber, R.B. (1977) Method of producing thebaine from codeine and oripavine from morphine. (US4045440 A).
35. Molphy, Z., Prisecaru, A., Slator, C., Barron, N., McCann, M., Colleran, J., Chandran, D., Gathergood, N. and Kellett, A. (2014) Copper Phenanthrene Oxidative Chemical Nucleases. *Inorganic Chemistry*, **53**, 5392–5404.
36. McCann, M., McGinley, J., Ni, K., O'Connor, M., Kavanagh, K., McKee, V., Colleran, J., Devereux, M., Gathergood, N., Barron, N., Prisecaru, A., and Kellett, A. (2013) A new phenanthroline–oxazine ligand: synthesis, coordination chemistry and atypical DNA binding interaction. *Chemical Communications*, **49**, 2341-2343.

37. Molphy, Z., Slator, C., Chatgilialoglu, C. and Kellett, A. (2015) DNA oxidation profiles of copper phenanthrene chemical nucleases. *Frontiers in Chemistry*, **3**, 1–9.
38. Horcas, I., Fernández, R., Gómez-Rodríguez, J.M., Colchero, J., Gómez-Herrero, J. and Baro, A.M. (2007) WSXM : A software for scanning probe microscopy and a tool for nanotechnology. *Review of Scientific Instruments*, **78**, 013705.
39. W. Cunningham, C., N. Thatcher, L. and Coop, A. (2006) Methylation of Non-acidic Alcohols of Alkaloids with TMS-diazomethane: Conversion of Codeine to Codeine-6-methyl Ether. *HETEROCYCLES*, **68**, 837.
40. McElroy, C.R., Constantinou, A., Jones, L.C., Summerton, L. and Clark, J.H. (2015) Towards a holistic approach to metrics for the 21st century pharmaceutical industry. *Green Chem.*, **17**, 3111–3121.
41. Gore, R.G., Myles, L., Spulak, M., Beadham, I., Garcia, T.M., Connon, S.J. and Gathergood, N. (2013) A new generation of aprotic yet Brønsted acidic imidazolium salts: effect of ester/amide groups in the C-2, C-4 and C-5 on antimicrobial toxicity and biodegradation. *Green Chemistry*, **15**, 2747-2760.
42. Jordan, A., Haiß, A., Spulak, M., Karpichev, Y., Kümmerer, K. and Gathergood, N. (2016) Synthesis of a series of amino acid derived ionic liquids and tertiary amines: green chemistry metrics including microbial toxicity and preliminary biodegradation data analysis. *Green Chem.*, **18**, 4374–4392.
43. Neidle, S. (2001) DNA minor-groove recognition by small molecules (up to 2000). *Natural Product Reports*, **18**, 291–309.
44. Kim, S.K. and Nordén, B. (1993) Methyl green: a DNA major-groove binding drug. *FEBS letters*, **315**, 61–64.
45. Arscott, P.G., Li, A.-Z. and Bloomfield, V.A. (1990) Condensation of DNA by trivalent cations. 1. Effects of DNA length and topology on the size and shape of condensed particles. *Biopolymers*, **30**, 619–630.
46. McFadyen, I.J., Houshyar, H., Liu-Chen, L.-Y., Woods, J.H. and Traynor, J.R. (2000) The steroid 17α-acetoxy-6-dimethylaminomethyl-21-fluoro-3-ethoxy-pregna-3, 5-dien-20-one (SC17599) is a selective μ-opioid agonist: Implications for the μ-opioid pharmacophore. *Molecular pharmacology*, **58**, 669–676.

47. Hansma, H.G., Golan, R., Hsieh, W., Lollo, C.P., Mullen-Ley, P. and Kwoh, D. (1998) DNA condensation for gene therapy as monitored by atomic force microscopy. *Nucleic Acids Research*, **26**, 2481–2487.
48. Zhou, T., Llizo, A., Wang, C., Xu, G. and Yang, Y. (2013) Nanostructure-induced DNA condensation. *Nanoscale*, **5**, 8288.
49. Cassina, V., Seruggia, D., Beretta, G.L., Salerno, D., Brogioli, D., Manzini, S., Zunino, F. and Mantegazza, F. (2011) Atomic force microscopy study of DNA conformation in the presence of drugs. *European Biophysics Journal*, **40**, 59–68.
50. Mazák, K. and Noszál, B. (2012) Lipophilicity of morphine microspecies and their contribution to the lipophilicity profile. *European Journal of Pharmaceutical Sciences*, **45**, 205–210.
51. Mazák, K., Hosztafi, S., Rácz, Á. and Noszál, B. (2009) Structural and physicochemical profiling of morphine and related compounds of therapeutic interest. *Mini reviews in medicinal chemistry*, **9**, 984–995.
52. Jin, C., Qiu, H., Han, L., Shu, M. and Che, S. (2009) DNA transcription into diverse porous silicas by a co-structure directing route: chiral, ring and ordered nanochannel arrays. *Chemical Communications*, 3407–3409.
53. Squire, C.J., Clark, G.R. and Denny, W.A. (1997) Minor groove binding of a bis-quaternary ammonium compound: the crystal structure of SN 7167 bound to d $(CGCGAATTCGCG)_2$. *Nucleic acids research*, **25**, 4072–4078.
54. Groom, C.R. and Allen, F.H. (2014) The Cambridge Structural Database in Retrospect and Prospect. *Angewandte Chemie International Edition*, **53**, 662–671.
55. Volcke, C., Pirotton, S., Grandfils, C., Humbert, C., Thiry, P.A., Ydens, I., Dubois, P. and Raes, M. (2006) Influence of DNA condensation state on transfection efficiency in DNA/polymer complexes: An AFM and DLS comparative study. *Journal of Biotechnology*, **125**, 11–21.
56. Dunlap, D.D., Maggi, A., Soria, M.R. and Monaco, L. (1997) Nanoscopic structure of DNA condensed for gene delivery. *Nucleic acids research*, **25**, 3095–3101.
57. McStay, N., Reilly, A. M., Gathergood, N. and Kellett, A. (2018) Efficient DNA Condensation by a C_3-Symmetric Codeine Scaffold. *ChemPlusChem*, **81**, 38-42.

58. Kotha, S. and Shah, V. R. (2008) Synthesis of C_3-symmetric and C_4-symmetric amino acid derivatives via Suzuki–Miyaura cross-coupling reaction. *Amino Acids*, **35**, 83–88.
59. Bertrand, H., Granzhan, A., Monchaud, D., Saettel, N., Guillot, R., Clifford, S., Guédin, A., Mergny, J. L. and Teulade-Fichou, M. P. (2011) Recognition of G-Quadruplex DNA by Triangular Star-Shaped Compounds: With or Without Side Chains? *Chem. Eur. J.*, **17**, 4529–4539.
60. Sun, N., Li, D., Hou, J., Long, W., Guo, Q., Lu, Y., Zhang, K., Yuan, W. and Wong, W.-L. (2018) A propeller-like small molecule as a novel G-quadruplex DNA binder: The study of fluorescent sensing property and preferential interactions with human telo21 structure. *Chem. Biol. Drug Des.*, 10.1111/cbdd.13394.
61. Mondal, J.H., Pramanik, B., Shinde, M.N., Khurana, R., Barooah, N., Bhasikuttan,A.C., Das,D. and Mohanty,J. (2018) DNA-Induced Novel Optical Features of Ethyl Viologen-Tethered Perylenediimide Triad. *J. Phys. Chem. C*, **122**, 18061–18069.
62. Xia,A.-L., He,Q.-F., Wang,J.-C., Zhu,J., Sha,Y.-Q., Sun,B. and Lu,X.-J. (2019) Applications and advances of CRISPR-Cas9 in cancer immunotherapy. *J. Med. Genet.*, **56**, 4–9.
63. Givens, B.E., Naguib, Y.W., Geary, S.M., Devor, E.J. and Salem, A.K. (2018) Nanoparticle-Based Delivery of CRISPR/Cas9 Genome-Editing Therapeutics. *AAPS J.*, **20**, 108.
64. Luther, D.C., Lee, Y.W., Nagaraj, H., Scaletti, F. and Rotello, V.M. (2018) Delivery approaches for CRISPR/Cas9 therapeutics in vivo: advances and challenges. *Expert Opin. Drug Deliv.*, **15**, 905–913.

Chapter III

Efficient DNA Condensation by a C_3-Symmetric Codeine Scaffold

This paper was accepted for publication in *ChemPlusChem*, 2019, DOI: cplu.201800480. Referencing style is kept in publishing format and gel electrophoresis images are inverted for clarity.

Natasha McStay, Anthony Reilly, Nicholas Gathergood and Andrew Kellett.

My contribution to this paper was to design and synthesise a series of codeine opioid scaffolds and conduct condensation studies on them. I completed the synthesis of the described compounds, including the full characterisation, AFM, turbidity, DLS and condensation studies. The computational studies were carried out in collaboration with Dr Anthony Reilly.

III. 1. Abstract

A novel tripodal codeine scaffold (**CC3**) was rationally designed using computational methods as a DNA condensing alkaloid. Separation of the piperidine nitrogen atoms in **CC3** is considerably larger at 14.36 Å than previously reported tripodal opioids allowing for enhanced aggregation of larger DNA plasmids (>4,000 bp). The scaffold undergoes protonation at physiological pH that allows for controlled compaction and release of nucleic acids. Condensation is inhibited under basic conditions and nucleic acid release can be achieved by modulating the ionic strength. Zeta potential experiments indicate stabilised DNA particles at low alkaloid loading with AFM measurements showing particles sizes with a height of 103 nm and diameter of 350 nm. Since condensation is a prerequisite for the cellular uptake of DNA, this new class of alkaloid represents a novel nucleic acid condensation agent with potential gene therapy applications.

III. 2. Introduction

The development of novel strategies for the treatment of human disease is a vital research goal and major progress is now being witnessed in the form of gene therapy.[1] Gene therapy models routinely use adeno-associated viruses (AVVs) as the most effective form of nucleic acid delivery *in vivo*.[2],[3] Developing therapies based on this methodology, however, are accompanied with major drawbacks and concerns from a clinical standpoint.[4] AAVs have small packing sizes and multiple viruses are generally required to deliver the payload to target cells which enhances carcinogenicity and immunogenicity.[5],[6] New methods are therefore required to establish viable non-viral transportation systems for the progression of gene therapy.[7] Synthetic non-viral vectors offer a number of advantages over viral systems such as improved safety, lack of immunogenicity, and ease of large-scale production.[8] Since they are amenable to engineering, these systems allow for flexibility with regard to the size of the gene being administered and can offer improved targeting effects with the ultimate aim of delivering more copies of genomic material to the requisite cell.[8–11]

This work focuses on the non-analgesic use of opioids as a bio-renewable resource capable of packaging DNA. While opioids are predominantly used for their potent analgesic properties, serving as one of the major drug classes within the

pharmaceutical industry,[12],[13] specific architectures were recently identified to have DNA binding properties.[14] In that study, we identified morphine (**MC3**), oripavine (**OC3**) and heterocodeine (**HC3**) C_3-opioids could condense DNA. It was postulated that nucleic acid aggregation arises from ionic bridging between the cationic piperidine ring on the opioid skeleton and the negatively charged phosphate backbone. From a structural perspective, however, all three C_3-opioids (**MC3**, **OC3**, and **HC3**) were linked to the mesitylene core by the phenolic hydroxyl group (*cf.* **HC3** Figure III-1) but subtle structural changes in the oripavine opioid (Appendix C-1) delivered enhanced DNA recognition and condensation properties.

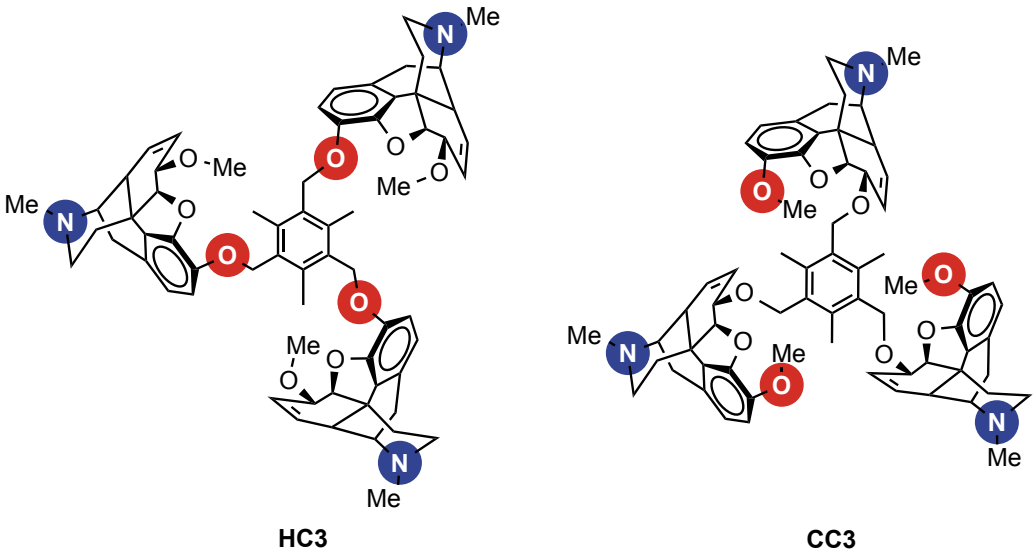

Figure III-1. Molecular structures of symmetric opioids: C_3-heterocodeine (**HC3**) and C_3-codeine (**CC3**).

III. 3. Results and Discussion

An important question that now arises is the structural variability within this class of material for the assembly of new DNA condensing scaffolds. Here, we report the development of a C_3-symmetric codeine derivative linked through the allylic hydroxyl group to offer a new orientation for the C_3-opioid. Codeine (**C**) was chosen as an ideal candidate and was compared using computational methods to its inverse analogue heterocodeine (**H**). Prior work suggested trivalent opioids adopt a C_3 conformation in solution[14] and to better understand their structure, analysis with informatics-based conformation generation and *ab initio* optimisation were used to establish the molecular geometry of C_3-heterocodeine (**HC3**) and C_3-codeine (**CC3**) molecules (Figure III-1 and Appendix C-2). The lowest energy C_3 conformers found

for **HC3** and **CC3** are shown in Figure III-2A where there is a clear difference in both the placement and orientation of the codeine groups with respect to heterocodeine. In **HC3** the separation of the nitrogen atoms is ~9.77 Å, whereas in **CC3**, the separation is considerably larger at 14.36 Å and this effect is clearly visible when both structures are overlapped (Figure III-2B). There are two additional C_3 conformers within 8 kJ/mol of the lowest-energy C_3 conformer of **HC3** and they similarly place the nitrogen atoms within each piperidine substituent 9.6–9.8 Å apart. The next lowest-energy conformer for **CC3** is *ca*. 17 kJ/mol higher in energy and is therefore unlikely to be encountered in solution. Since the architectural change imposed by codeine promotes a significant structural change compared with **HC3**, the C_3 substituted codeine molecule (**CC3**) was synthesised along with C_1 and C_2 codeine derivatives for analysis as novel DNA condensing agents.

CC3 was generated by treating 1 equivalent of 2,4,6-*tris*-(bromomethyl)-mesitylene with 3 equivalents of codeine and the resulting compound was synthesised as a beige solid after purification by column chromatography. Although a low yield for **CC3** was obtained (15%), it is slightly higher than the equivalent **HC3** opioid (13%, overall yield from morphine) and significantly easier to prepare requiring just one reaction step. **CC1** and **CC2** opiate analogues were accessed using α-2-chloroisodurene (**CC1**) and 2,4-*bis*-(chloromethyl)-1,3,5-trimethylbenzene (**CC2**). All three compounds were characterized by ^{1}H and ^{13}C nuclear magnetic resonance (NMR), attenuated total reflectance (ATR) Fourier transform infrared (FTIR) spectroscopies, elemental analysis and electron spray ionisation mass spectrometry (ESI-MS) (Appendix C-4). The symmetry of the C_3-codeine molecule was investigated by variable temperature NMR measurements and compared to earlier conformational analysis. These solution-based ^{1}H NMR studies were conducted in deuterated chloroform where the temperature probe was adjusted from 293 K to 233 K (Figure III-2C, Appendix C-5). Since molecular rearrangements can rapidly occur at room temperature, probing non-equivalent nuclear environments using this method may provide additional information regarding the solution structure.[15],[16]

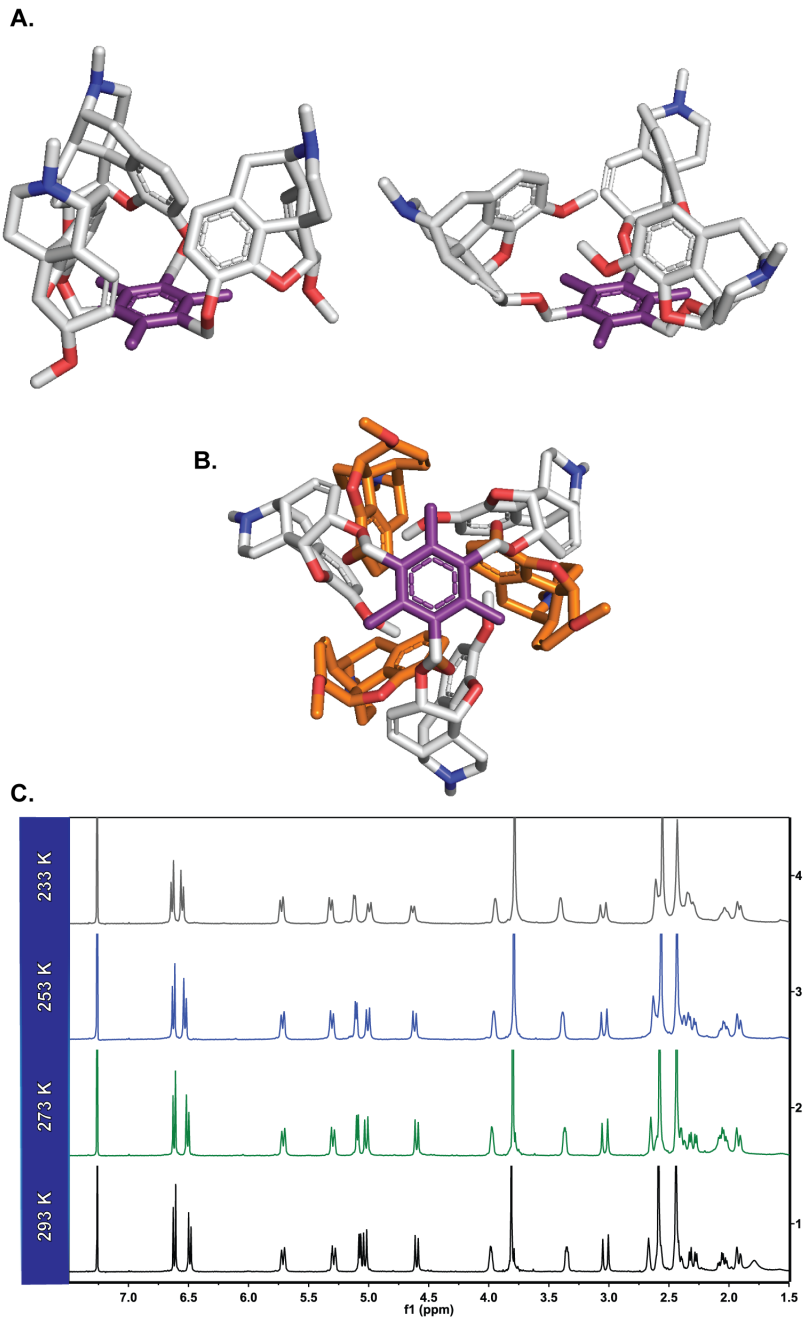

Figure III-2. A. lowest-energy C_3 conformers found for heterocodeine **HC3** and codeine **CC3**; **B.** overlay of the two (**HC3** coloured orange and H atoms omitted for clarity) Colour key: mesitylene (purple), O (red) and N (blue); **C.** Variable temperature ^{1}H NMR profile of **CC3** in $CDCl_3$ at decreasing temperatures.

Thus, lowering the temperature of the probe allows the exchange to slow on the NMR timescale which can allow a break in the time-averaged symmetry.[17] As the temperature decreased, the ^{1}H NMR for **CC3** showed no observable symmetry changes confirming the C_3-symmetric opioid compound is favoured where each codeine moiety is co-planar within the scaffold. To identify DNA condensation effects of this class, gel electrophoresis experiments with plasmid DNA were

undertaken. Limited DNA condensation was found for both **CC1** and **CC2,** were the onset of condensation for **CC2** was observed at 250 μM (Figure III-3A and B). At neutral pH, **CC3** initiated condensation of pUC19 (2,686 bp) at 30 μM with complete condensation achieved at 50 μM (Figure III-3C). Interestingly, when incubated with a larger plasmid pBR322 (4,361 bp) the onset of condensation was visualised at 10 μM and complete condensation reached at 30 μM (Figure III-3D).

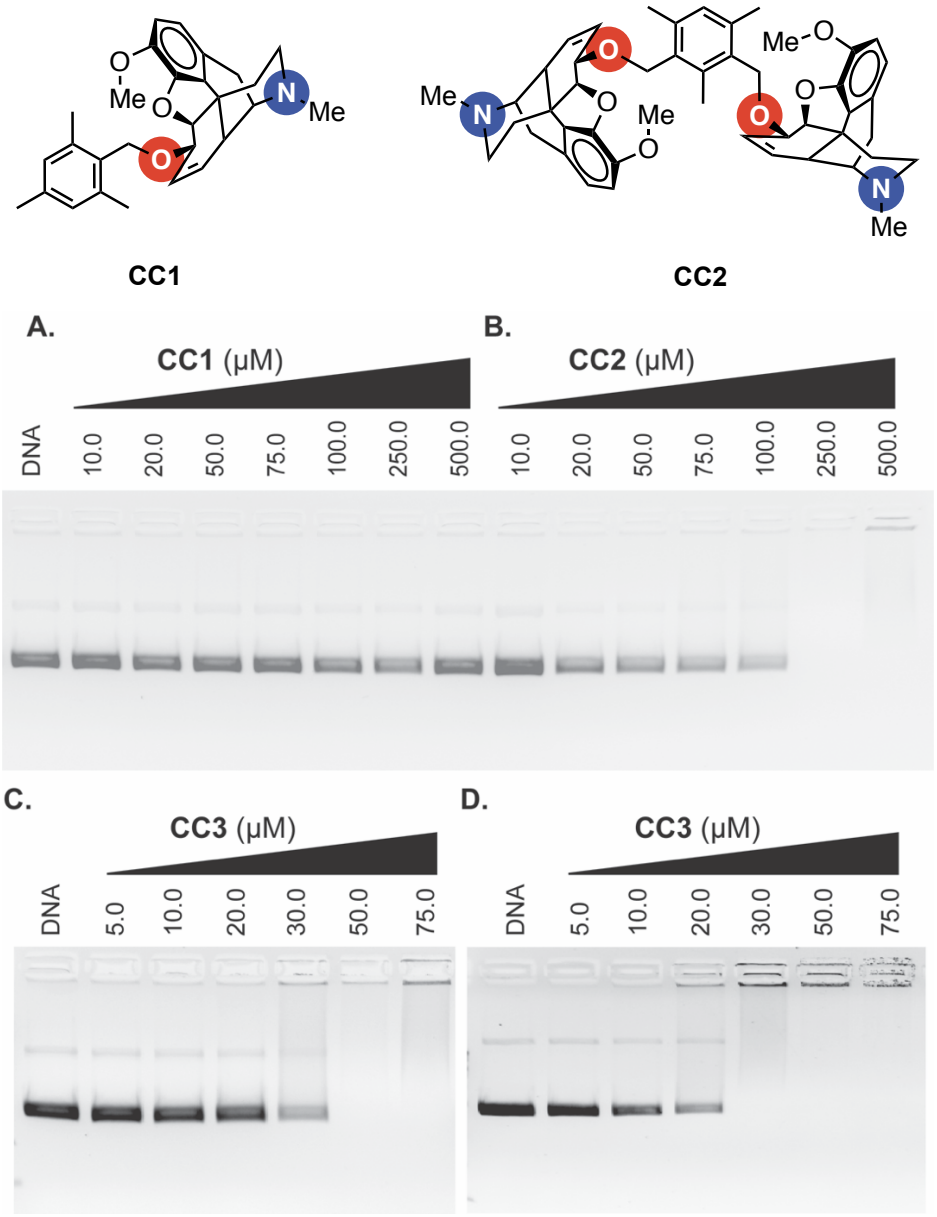

Figure III-3. Molecular structures of symmetric opioids: **CC1** and **CC2**; Agarose gel electrophoresis of supercoiled dsDNA pUC19 (400 ng) exposed to increasing concentrations of **A. CC1** and **B. CC2.** Agarose gel electrophoresis of supercoiled dsDNA pUC19 (**C**) and pBR322 (**D**) (400 ng) exposed to increasing concentrations of **CC3**. Reactions were carried out in the presence of 25 mM NaCl for 5 h at 37 ˚C prior to electrophoretic analysis.

The requirement for the *tris*-scaffold to compact DNA likely arises since cationic charge density plays a critical role in DNA aggregation where the majority of cationic condensation agents carry a 3+ or higher charge to fully collapse the helical backbone.[18],[19] The condensation effect of **CC3** appears dependent on ionic strength where the release of bound plasmid DNA was identified by increasing salt (NaCl) concentrations (Figure III-4A). Significantly, pH was found to strongly influence the condensation effects of **CC3** where an acidic environment (pH 4.0) increases condensation effects while under basic conditions (pH 9.0) condensation was almost completely inhibited (Figure III-4B and C).

DNA condensation was next characterised using viscosity, turbidity, zeta potentials, and average hydrodynamic size with results compared to the natural DNA condensing agent spermine (SPM). Since DNA condensation is routinely studied with naturally occurring spermidine (3+) and spermine (4+), along with inorganic cations such as cobalt(III) hexammine $[Co(NH_3)_6]^{3+}$, the use of SPM[20] in this analysis served as an important control. Viscosity studies were conducted with salmon testes DNA (stDNA)[21] exposed to increasing concentrations of C_3-opioid and controls of SPM and ethidium bromide (EtBr) (Figure III-4). Both **CC3** and SPM exhibit comparable viscosity profiles with downward curving hydrodynamic values (η/η_o) while EtBr displayed classical intercalative behaviour. Turbidity was then measured at both 260 nm (control) and 350 nm using calf thymus DNA (ctDNA) as insoluble aggregates formed by condensed DNA can be measured at this longer wavelength.[22,23] **CC3** showed an exponential increase in turbidity starting at 10 μM and reached a plateau at 30 μM. In contrast, SPM did not begin to influence turbidity measurements until *ca*. 20 μM of the agent was present in solution (Figure III-4). Given this interesting result, and coupled with earlier observations of pH-dependent aggregation, dynamic light scattering (DLS) was selected to probe the condensation interface in greater detail.

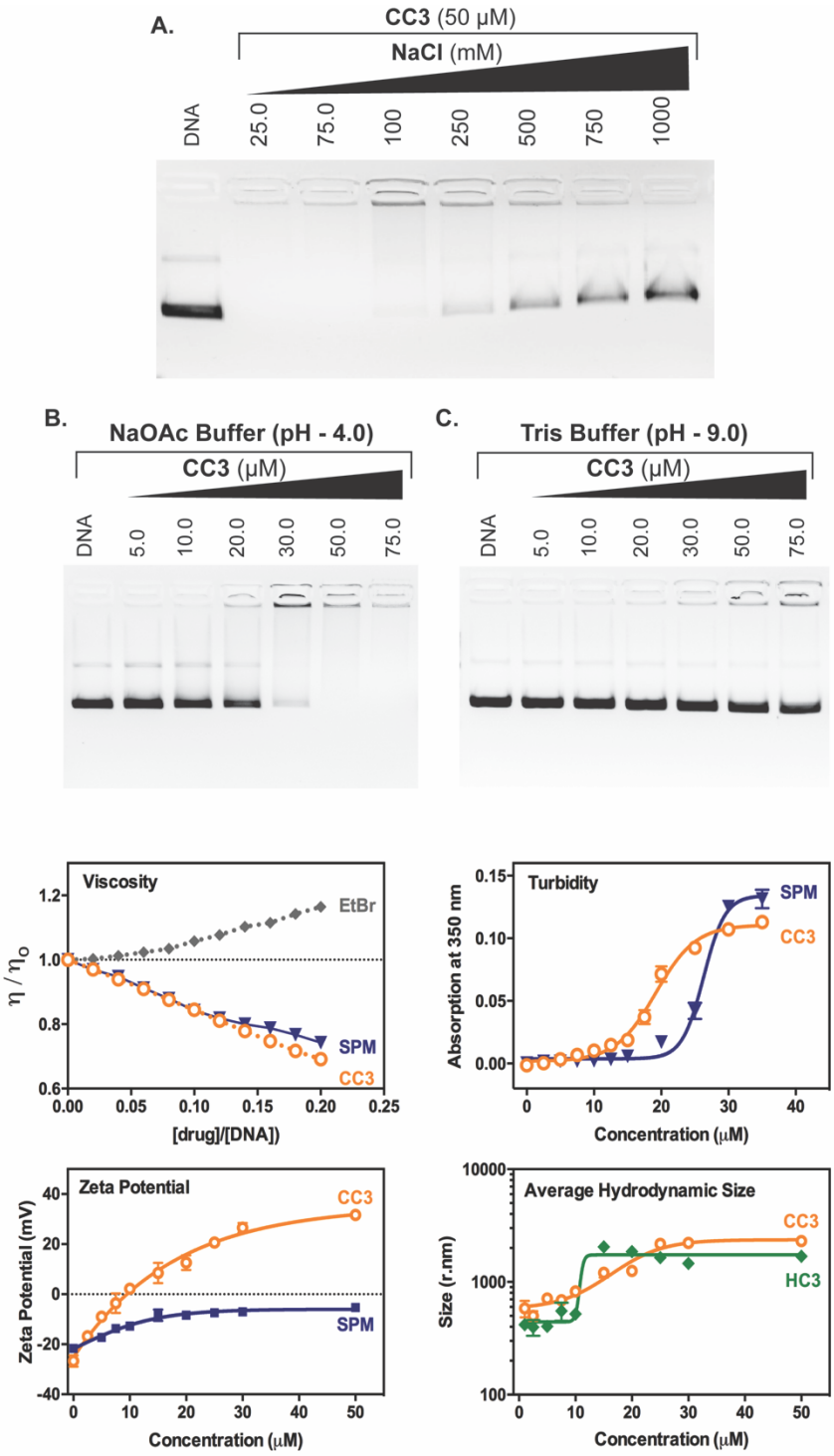

Figure III-4. A. Influence of ionic strength on pUC19 condensation (400 ng) by **CC3** (50 μM). Condensation reactions on pUC19 (400 ng) by **CC3** in (**B**) acidic NaOAc buffer (80 mM, pH = 4.0), and (**C**) basic Tris buffer (80 mM, pH = 9.0) in the presence of 25 mM NaCl. Viscosity properties of **CC3**, ethidium bromide (EtBr) and spermine (SPM) exposed to salmon testes dsDNA, and turbidity profiles of ctDNA in the presence of titrated **CC3** and SPM. Zeta potential of supercoiled dsDNA pUC19 (1 mg/L) exposed to increasing concentrations of **CC3**, and SPM. Reactions were carried out in the presence of 10 mM NaOAc buffer (pH 4) for 1 h at 25 ˚C prior to zeta potential measurements. Average hydrodynamic radius of supercoiled dsDNA pUC19 (0.4 mg/L) exposed to increasing concentrations of **CC3**, and **HC3**. Reactions were carried out PBS buffer (10 mM, pH 7.2) for 1 h at 25 ˚C prior to DLS analysis.

Surface charge and hydrodynamic size measurements were studied at increasing drug loadings by DLS (Figure III-4). The zeta potential (ξ-potential) measurements were conducted in an acidic pH buffer (10 mM NaOAc, pH 4.0) to ensure full protonation of **CC3** and samples were incubated with plasmid DNA (pUC19, 1 μg/ml) for 1 h prior to each measurement. The ξ-potential of **CC3** indicates a stable positive charge in the absence of DNA (30 mV). In the presence of titrated **CC3**, however, ξ-potential values changed from negative (-26.7 mV, DNA alone) through neutral (10 μM **CC3**) to positively charged particles, which indicates cationic condensation in excellent agreement with gel electrophoresis and turbidity results. Interestingly, the ξ-potentials for DNA/SPM remain negative under the same tested concentration range, an effect previously reported by Hays *et al*.[24] To probe this phenomenon further, low concentrations of **CC3** (below 10 μM) were identified to have an average particle size in the range 300-700 nm, while beyond this concentration larger particles were observed up to a maximum of 2 μm. The most striking observation is the steep inflection point of **HC3** over a small sample range (10-15 μM) which contrasts with a much broader distribution of **CC3** (10-30 μM). An important aspect in the characterisation of nucleic acid transport vectors is the hydrodynamic size of aggregates formed. The characterisation of **CC3** aggregates is in marked contrast to SPM where the average size initially decreases to 100 nm and gradually increases at concentrations of 50 μM and above (Appendix C-8).

Atomic Force Microscopy (AFM) was used to study the morphological changes induced by **CC3** in both pUC19 and pBR322 plasmid DNA vectors. In the presence of **CC3** (8 μM), pUC19 exhibited small cluster formation of varying sizes with free DNA visible in the surrounding area (Figure III-5A). A moderate increase in concentration resulted in larger cluster formation with tight packing present at the aggregate centre (Figure III-5B-D). In the presence of the larger pBR322 plasmid, similar behaviour was identified at lower drug loading (6 μM) where small clusters are abundant. Higher concentrations of **CC3** (≥12 μM), however, give rise to larger tightly aggregated DNA. An interesting feature of this codeine scaffold is the presence of large particles *ca*. 100 nm in height (Figure III-5G-I). This particle is tightly packed with no observable free plasmid in the surrounding area and has highly desirable dimensions for transport through biological barriers with a height of 103nm and diameter of ~350 nm. Particle size plays a significant role in the

efficiency of cellular uptake and in determining gene transfection efficacy.[25] Free plasmid DNA is imaged along with each sample to ensure sample preparation techniques does not interfere with the morphological changes induced by C_3-opioids.

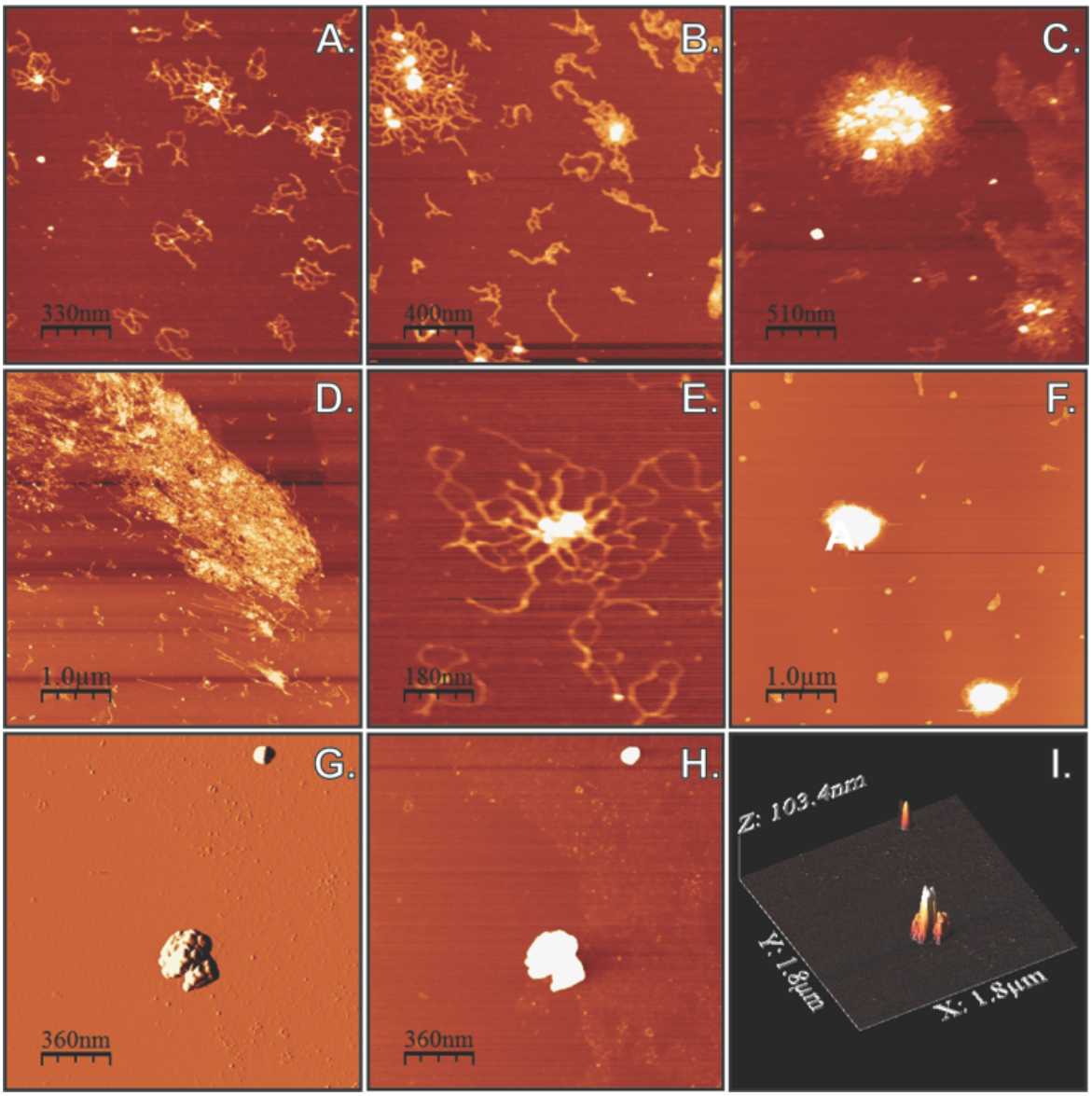

Figure III-5. Atomic force microscopy (AFM) images of **CC3**-treated supercoiled pUC19 (**A**–**D**, **G**-**I**) and pBR322 DNA (**E–F**). Supercoiled pUC19 with 8, 10, 15, 20 µM (**A**–**D**), and 16 µM **CC3** (**G** phase, **H** height, **I** 3D height); pBR322 with 6, and 12 µM **CC3** (**E-F**). (z-scale set to 5 nm, A-H).

While internalization of DNA/Ligand particles with diameters of between 50 and 100 nm is a relatively rapid process, particles up to 500 nm have shown good cell membrane transport[26,27] but an upper size limit of ≥1 µm is generally accepted.[28] In contrast to previously reported **MC3** (which has a similar molecular structure to

HC3), AFM studies conducted with plasmid DNA (pUC19) identified large DNA aggregates ≥1 μM with visible free plasmid in the surrounding surface area.[14] **CC3**, on the other hand, produces tightly packed particles that may offer improved transfection efficacy and protection from endonuclease activity.

To investigate the effects of long-range coiling, which can significantly impact viscosity[29] and in turn aggregation, a short 12 bp duplex was examined to probe the mechanism of aggregation further. Long-range coiling occurs when a ligand induces supercoiling effects downfield from the site of binding;[29,30] by examining the condensation of sheared DNA or small oligomers this form of aggregation can be ruled out. As shown in Figure III-6, it appears likely that both **CC3** and **HC3** are capable of aggregating short nucleic acid fragments and so long-range coiling effects can be discounted within their aggregation mechanism.

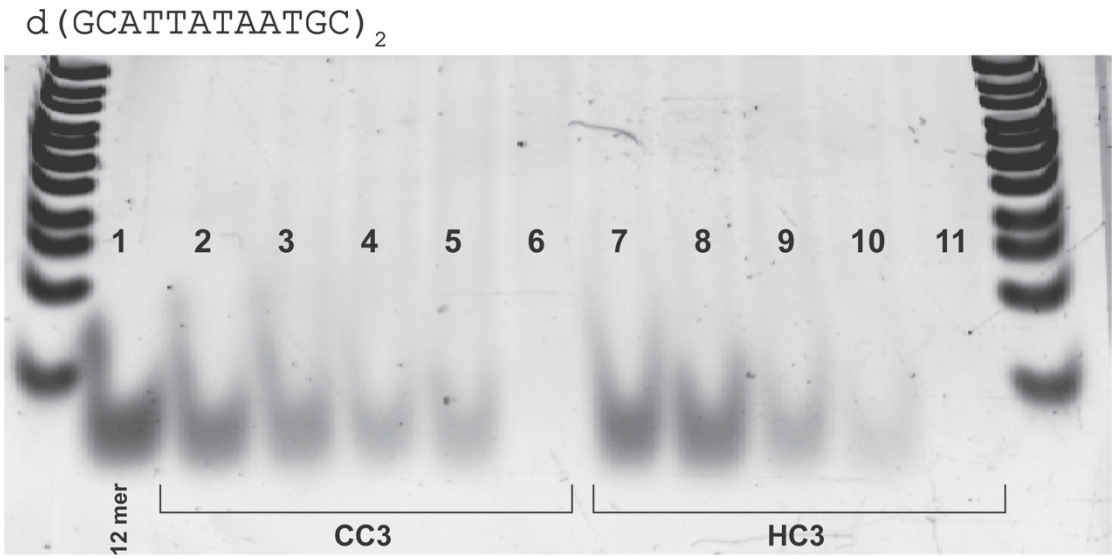

Figure III-6. Polyacrylamide gel electrophoresis of a short 12 mer (50 ng) exposed to increasing concentrations of **CC3** and **HC3**. Lane 1, 12 mer; lane (2-6, 7-11) drug concentration (30, 50, 75, 100, 250 μM). Reaction was carried out in the presence of 25 mM NaCl for 15 h at 37 ˚C prior to electrophoretic analysis on a 20% TBE Page gel, run in 1x TBE buffer at 70 V for 150 min. Ultra-low range DNA ladder (Invitrogen™) on either side. Gel stained with 1x SYBR Gold in TBE.

III. 4. Conclusion

In summary a codeine C_3-opioid DNA condensing scaffold (**CC3**) was rationally designed through informatics-based conformation generation and ab initio geometry optimisation. Variable temperature ^{1}H NMR spectroscopy indicates a symmetrical C_3-opioid which correlates to computational analysis where the scaffold retains a C_3 solution symmetry. Nucleic acid condensation by **CC3** is enhanced under acidic conditions supporting the requirement of 3+ charge for DNA aggregation identified through gel electrophoresis assays. A broad dynamic range was revealed by DLS and turbidity assays highlighted an ability to control particle size formation for the packaging of DNA vectors. This analysis was supported by AFM measurements where favourable parameters to facilitate cell membrane transport were identified. Long-range coiling effects were excluded by examining condensation effects on a short DNA fragment (12 bp) by gel electrophoresis. Efforts are now underway to establish the transfection efficiency of this novel opioid scaffold.

III. 5. References

[1] D. J. Segal, J. F. Meckler, *Annu. Rev. Genomics Hum. Genet.* **2013**, *14*, 135–158.

[2] F. A. Ran, L. Cong, W. X. Yan, D. A. Scott, J. S. Gootenberg, A. J. Kriz, B. Zetsche, O. Shalem, X. Wu, K. S. Makarova, et al., *Nature* **2015**, *520*, 186–191.

[3] M. F. Naso, B. Tomkowicz, W. L. Perry, W. R. Strohl, *Biodrugs* **2017**, *31*, 317–334.

[4] M. A. Kotterman, T. W. Chalberg, D. V. Schaffer, *Annu. Rev. Biomed. Eng.* **2015**, *17*, 63–89.

[5] S. Lin, B. T. Staahl, R. K. Alla, J. A. Doudna, *eLife* **2014**, *3*, 1–13.

[6] C. E. Thomas, A. Ehrhardt, M. A. Kay, *Nat. Rev. Genet.* **2003**, *4*, 346–358.

[7] T. Bentin, in *DNA-Target. Mol. Ther. Agents* (Ed.: M.J. Waring), Royal Society of Chemistry, **2018**, pp. 391–407.

[8] H. Yin, R. L. Kanasty, A. A. Eltoukhy, A. J. Vegas, J. R. Dorkin, D. G. Anderson, *Nat. Rev. Genet.* **2014**, *15*, 541–555.

[9] I. Slivac, D. Guay, M. Mangion, J. Champeil, B. Gaillet, *Expert Opin. Biol. Ther.* **2017**, *17*, 105–118.

[10] T. J. Thomas, H. A. Tajmir-Riahi, T. Thomas, *Amino Acids* **2016**, *48*, 2423–2431.

[11] Z. Zawada, A. Tatar, P. Mocilac, M. Buděšínský, T. Kraus, *Angew. Chem. Int. Ed.* **2018**, *57*, 9891–9895.

[12] M. P. Center, *Pain Physician* **2011**, *14*, E343–E360.

[13] A. N. Nafziger, R. L. Barkin, *J. Clin. Pharmacol.* **2018**, *58*, 1111–1122.

[14] N. McStay, Z. Molphy, A. Coughlan, A. Cafolla, V. McKee, N. Gathergood, A. Kellett, *Nucleic Acids Res.* **2017**, *45*, 527–540.

[15] R. Cramer, *J. Am. Chem. Soc.* **1964**, *86*, 217–222.

[16] M. W. Gillick-Healy, E. V. Jennings, H. Müller-Bunz, Y. Ortin, K. Nikitin, D. G. Gilheany, *Chem. – Eur. J.* **2017**, *23*, 2332–2339.

[17] M. J. McGlinchey, *Symmetry* **2014**, *6*, 622–654.

[18] R. W. Wilson, V. A. Bloomfield, *Biochemistry* **1979**, *18*, 2192–2196.

[19] G. S. Manning, *Q. Rev. Biophys.* **1978**, *11*, 179–246.

[20] J. Pelta, F. Livolant, J.-L. Sikorav, *J. Biol. Chem.* **1996**, *271*, 5656–5662.

[21] A. Prisecaru, Z. Molphy, R. G. Kipping, E. J. Peterson, Y. Qu, A. Kellett, N. P. Farrell, *Nucleic Acids Res.* **2014**, *42*, 13474–13487.

[22] M. Zaman, S. K. Chaturvedi, N. Zaidi, A. Qadeer, T. I. Chandel, S. Nusrat, P. Alam, R. H. Khan, *RSC Adv.* **2016**, *6*, 37591–37599.

[23] J. Malina, N. P. Farrell, V. Brabec, *Angew. Chem. Int. Ed.* **2014**, *53*, 12812–12816.

[24] M. E. Hays, Christopher M. Jewell, Y. Kondo, D. M. Lynn, N. L. Abbott, *Biophys. J.* **2007**, *93*, 4414–4424.

[25] J.-Y. Cherng, P. van de Wetering, H. Talsma, D. J. A. Crommelin, W. E. Hennink, *Pharm. Res.* **1996**, *13*, 1038–1042.

[26] J. Rejman, V. Oberle, I. S. Zuhorn, D. Hoekstra, *Biochem. J.* **2004**, *377*, 159–169.

[27] L. Liu, H. Zhang, X. Meng, J. Yin, D. Li, C. Liu, Biomaterials **2010**, 31, 1380–1391.

[28] M. Ogris, P. Steinlein, M. Kursa, K. Mechtler, R. Kircheis, E. Wagner, *Gene Ther.* **1998**, *5*, 1425–1433.

[29] L. S. Lerman, *J. Mol. Biol.* **1961**, *3*, 18-IN14.

[30] O. V. Bocharova, L. Breydo, V. V. Salnikov, I. V. Baskakov, *Biochemistry* **2005**, *44*, 6776–6787.

Chapter IV

The Development of Non-Opioid C_3-Symmetric Scaffolds as Condensation Agents

This chapter details the development of non-opioid compounds including the synthesis and characterisation of novel compounds. This work is anticipated to be published. Referencing style is Royal Society of Chemistry.

Dr Paul Kelly, NIBRT/National Institute for Bioprocessing Research and Training, conducted cell culture experiments detailed in section IV.2. and Prof Kieran Nolan, School of Chemical Sciences, Dublin City University, donated five imidazole compounds detailed in section IV.3.

IV. 1. Introduction

Work presented so far has highlighted key characteristics for the condensation of dsDNA through the protonated form of a novel series of tripodal opioids. These novel C_3-opioids are the first of our knowledge of opioid derivatives capable of binding and condensing DNA fully at low concentrations and exhibiting pH and ionic strength control. This surprising result has encouraged new non-analgesic applications for these trivalent opioids in the field of gene therapy, more specifically as transfection agents. Transfection agents can be broadly classified into two areas (i) viral and (ii) non-viral agents. Synthetic non-viral vectors offer a number of advantages over viral systems such as improved safety, lack of immunogenicity, low frequency of integration and ease of large-scale production.[1] These systems allow for flexibility with regards to the therapeutic size of the gene, and targeting administration ultimately leading to more copies of genomic material being transported to cell. Non-viral agents can then be further classified by the key attributes present in the system such as (i) lipid based vectors, (ii) polymeric vectors, (iii) dendrimer-based vectors, (iv) cationic vectors, and (v) nanoparticles.[2] For the purpose of this work our focus was drawn towards cationic non-viral vectors as a key category to induce sufficient DNA condensation and protection for the purpose of gene delivery.

IV. 2. Cytotoxicity of OC3 in CHO cells

The Chinese hamster ovary (CHO) cell is the dominant mammalian cell line used in the biopharmaceutical industry for the production of complex recombinant therapeutic proteins. These cells have become a favourite expression platform due to the long history of regulatory approval, genetic plasticity, and ability to grow in suspension culture and to ability to transfer human-like post-translational modifications (PTMs) to the final protein product.[3] One major contributor to generating a high producing CHO cell line is for the stable integration of a gene of interest (GOI) into an area of the genome that is highly transcriptionally active and stable over ~100 generations. Unstable genomic locations can ultimately lead to transgene silencing which ultimately means the loss of the integrated gene leading to a drop-in productivity over time.

Several methods have and are being employed to ensure that genetic material containing the therapeutic protein for manufacturing are inserted into genetic hotspots within the genome or the payload of gene copy number per genome is high.[4] The sophisticated CRISPR-Cas genome editing tool can be used to target a transgene into particular locations,[5] however, given the poor annotation and sequence information of CHO, this method is limited to characterised genomic locations. Stable transgene integration is random and occurs at a very low frequency hence the requirement for high initial transfection efficiency and the necessity of an extensive cell line development process. To overcome these issues non-viral vectors have been exploited for the transfection of genomic material into the host cell.[1] These systems allow for flexibility with regards to the therapeutic size of the gene, and targeting administration ultimately leading to more copies of genomic material being transported to cell, significantly accelerating cell line development programmes in the biopharmaceutical industry. As previously identified, tripodal opioids have now been shown to condense and protect dsDNA fragments and thus has the potential to mediate transfection.[3] Prior to examining the transfection capability of these opioids it is necessary to establish the degree of cytotoxicity towards the parent cell line to ensure the degree of transfection out weights the degree of toxicity, a common bottleneck when developing transfection agents.

To determine the toxicity of the tripodal opioids towards the parent cell line, CHO-K1 (ATCC® CCL-61™), **OC3** was chosen as a representative C_3-opioid from series due its potent onset of nucleic acid condensation.[3] Typical cell culture techniques employed for the transfection processes require large concentrations of plasmid vector, upwards of 1-5 μg, depending on the cell type and size of plasmid. Previously we have shown that **OC3** can fully condense 400 ng of plasmid DNA at concentrations up to 10 μM. It was anticipated that higher concentrations of the C_3-opioid would be required to fully condense larger concentrations of plasmid (1 μg) and two concentrations of 25 μM and 50 μM drug loading was chosen for initial cytotoxicity screening.

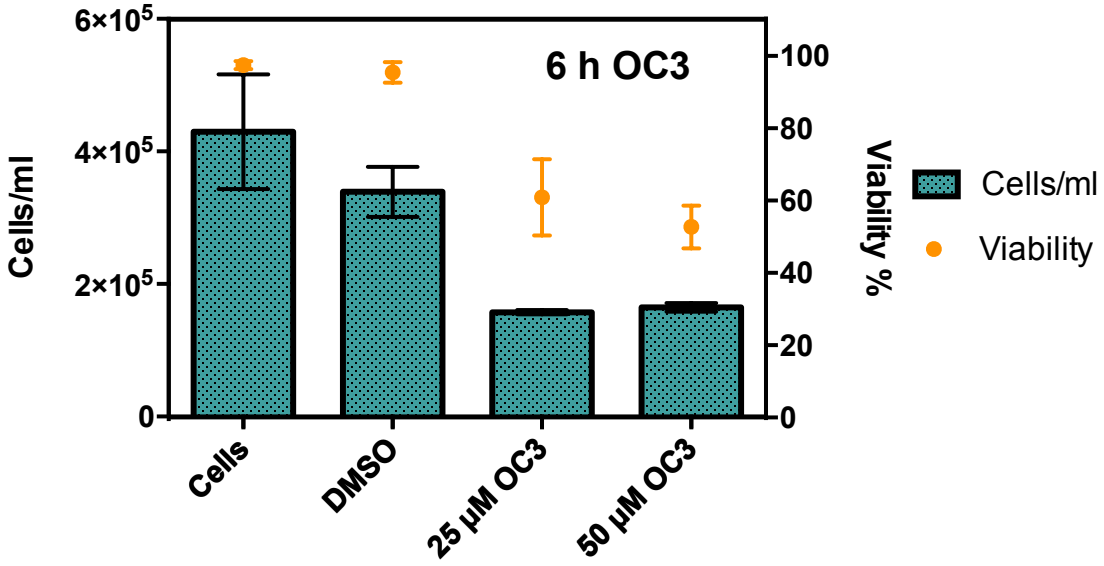

Figure IV-1. Cell growth (Cells/mL) and viability (%) in the presence of **OC3** at 25 µM and 50 µM over 6 h in CHO-K1 (ATCC® CCL-61™).

Initial stocks of C_3-opioid were prepared in DMSO and further diluted in HEPES buffer (80 mM, pH 7.2). Screening was conducted in biological triplicates under the growth conditions described (Appendix D-1) and monitored for cell growth (Cells/ml) and viability (%) using the ViaCount™ viability stain (Millipore, UK) on a Guava 5HT benchtop cytometer at 6 and 24 h (Figure IV-1 and Figure IV-2). Initial counts at 6 h highlighted a decrease in both cell growth and viability of both concentrations tested of **OC3**, Figure IV-1. This result highlights the onset of cytotoxicity where the two concentrations analysed seem to have similar cytotoxicity profiles at the six-hour time point. This is a general observation and a full concentration range would be required to determine the drug/dose response curve to CHO-K1 cell line and determine the IC_{50} concentration.

Cell viability holds strong at 60% after both the 6 and 24 h time points addressed for **OC3**. However, cell growth has reduced compared to the controls observed for 24 h (Figure IV-2), control cells measured at 6.6 x10^5 cells/ml and **OC3** at both 25 and 50 µM was measured at 2.1 x 10^5 cells/ml. These preliminary results suggest cytotoxicity towards CHO-K1 cell line under these experimental conditions. Although these results highlight initial toxicity of the novel C_3-opioid **OC3**, these compounds are the first opioid based nucleic acid condensation agents and further screening

will allow for a better understanding of this class of alkaloid for the purposes of developing a novel transfection agent.

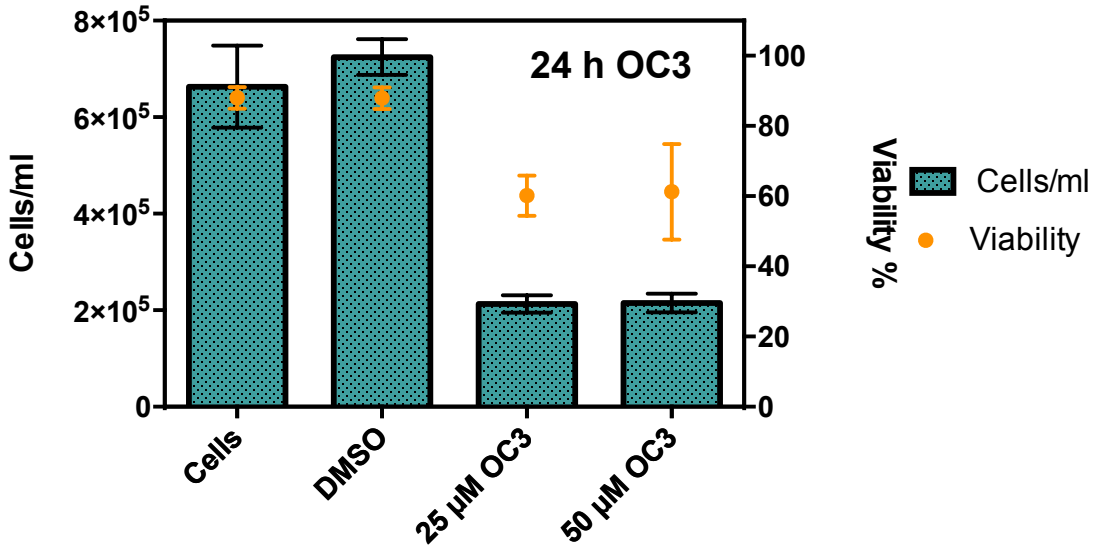

Figure IV-2. Cell growth (Cells/mL) and viability (%) in the presence of **OC3** at 25 µM and 50 µM over 24 h in CHO-K1 (ATCC® CCL-61™).

IV. 3. Imidazolium Salts as Potential DNA Condensation Agents

To explore the potential of non-opioid based condensation agents, imidazolium salts were investigated as alternative scaffolds. Imidazole rings have been employed to modify polymers to allow for fast endosomal escape via a "proton sponge" effect[6] and the constant charge on the imidazolium ring allows for improved DNA-binding and aggregation. For example, Allen *et al.* prepared imidazolium-based copolymers via functionalized 1-vinylimidazole homopolymers with hydroxyl functionalized alkyl chains, and then investigated the degree of quaternization, DNA binding, cytotoxicity, and *in vitro* transfection efficiency.[7] However as Li *et al.* pointed out, the degree of DNA-binding increased as the degree of quaternization but had a negative effect on transfection due from a competition between the buffering capacity and DNA binding affinity to the imidazole and imidazolium moieties.[8] The development of a polycationic vector requires well-designed functions for the purpose of versatility, solubility, and efficient transfection. These functions can be achieved through the incorporation of an imidazole ring. Allen *et al.* continued this research further and prepared the imidazolium-based copolymers functionalized with folic acid to target cancer cells as receptor-mediated gene delivery therapeutics.[9] This work incorporated a series of varying polyamine chain lengths linked to folic acid conjugated onto imidazolium copolymers and showed significant influence on the

overall transfection efficiency of these DNA delivery vehicles. Overall, this body of work demonstrated that imidazole rings have great potential for the development of versatile and biocompatible transfection agents.

Five imidazole samples, labelled **NAM1-5**, were kindly donated by Prof Kieran Nolan's research group (Dublin City University) for the purpose of nucleic acid screening. These compounds were examined as a starting point into developing novel non-opioid scaffolds that preserve the core mesitylene ring and C_3-symmetry. These compounds retain a constant 3+ charge and have varying chiral substituent groups leading from the 1,3-imidazole bound to the core mesitylene ring. Cationic charge density plays a critical role in DNA aggregation where the majority of cationic condensation agents carry a 3+ or higher charge to fully collapse the helical backbone of DNA,[10,11] which suggests that these imidazole compounds have the capacity to condense DNA. The imidazole ring is a planar 5-membered ring that is classified as aromatic due to the presence of the sextet of π-electrons. The positive charge can be located on either of the two nitrogen atoms and contributes to the imidazole ring being highly water-soluble, a current issue with the tripodal opioids. The charged nature of these compounds could offer an increased condensation effect compared to the C_3-opioids where protonation of the piperidine ring occurs at physiological pH. These compounds have previously been developed for applications for the enantioselective discrimination of enantiomers, however have not yet been investigated for possible DNA-binding interactions.

IV. 3.1. Characterisation of imidazole salts

The homochiral imidazoles shown (Figure IV-3) have three varying chiral substituents, which consist of naphthylmethyl, apopinane, and a phenyl group. We would expect similar binding properties of sample **NAM1** and **NAM3** due to the simple aromatic nature of the chiral groups bound to the mesitylene ring, however the reduced crowding of the chiral apopinane bound to the imidazole ring on **NAM2** may offer an increased surface area for binding to occur, similar to what was observed for the oripavine C_3 compound.

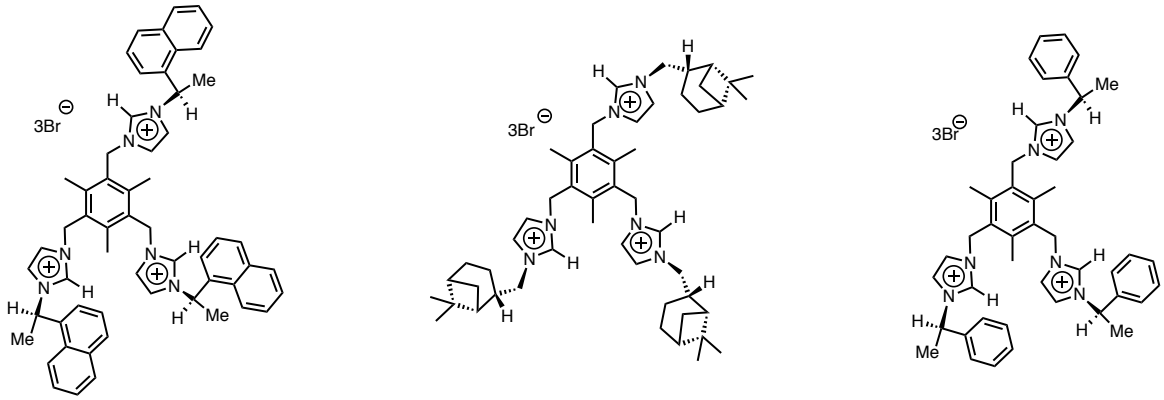

Figure IV-3. Imidazolium Salts, **NAM1**, **NAM2**, and **NAM3**

The homochiral imidazole samples **NAM4** and **NAM5** (Figure IV-4) have two different chiral groups consisting of a simple butyl group and cyclohexyl group. The compounds shown were previously reported[12,13] and were re-characterised by electro-spray ionisation mass spectra (ESI-MS) and ^{1}H NMR. The proton NMR spectra of all five compounds were in accordance with the literature provided and agreed with the expected spectra (Appendix D-2). The spectra obtained corresponded to the structures shown.

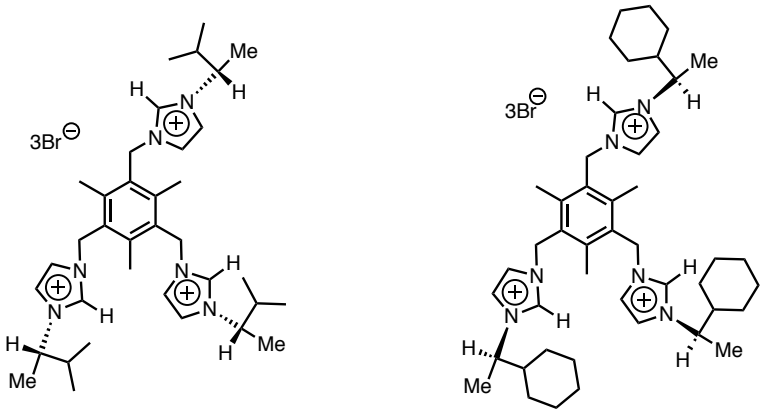

Figure IV-4. Imidazolium salts; **NAM4**, and **NAM5.**

IV. 3.2. Nucleic acid screening

The ability of the imidazole compounds to condense supercoiled plasmid DNA was determined using a method previously developed.[14] Imidazole stock samples were prepared in DMF and further diluted in 80 mM HEPES buffer (Fisher) prior to reactions. Initial screening was conducted at drug high loading (500 μM) over 2.5 h and 5 h incubation times to determine DNA interactions (Figure IV-5). Two imidazole scaffolds were identified as potential condensation agents, **NAM1** and **NAM2**. Fully condensed supercoiled plasmid (pUC19) was shown after 2.5 h, while samples

NAM3 and **NAM5** exhibited a reduction in fluorescence compared to the control lane, these scaffolds were unable to fully condense after 5 h. **NAM4** showed no change compared to the control DNA present highlighting that this compound had no affinity towards nucleic acid condensation.

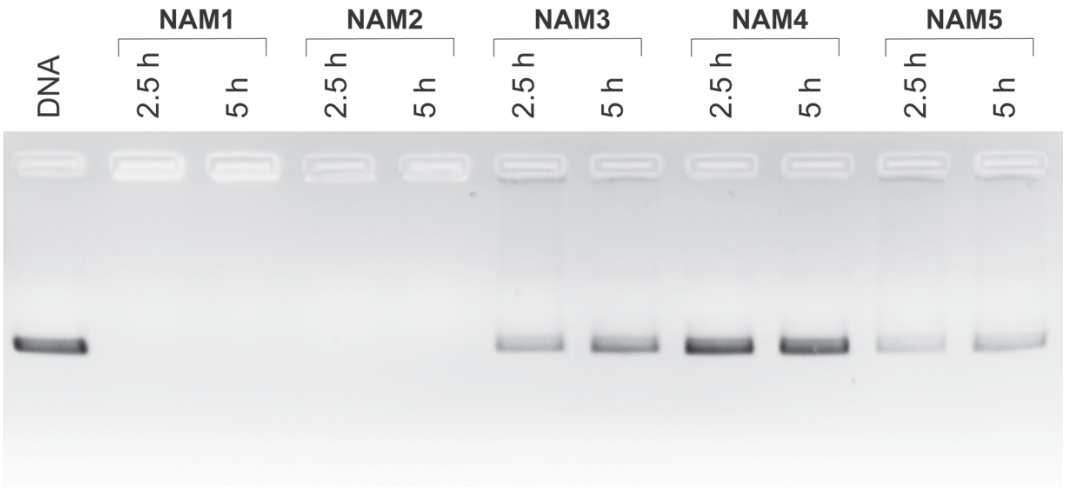

Figure IV-5. Agarose gel electrophoresis of supercoiled dsDNA (400 ng) exposed to 500 μM concentration of **NAM1**, **NAM2**, **NAM3**, **NAM4**, and **NAM5**. Reactions were carried out in the presence of 25 mM NaCl over 2.5 h and 5 h at 37˚C prior to electrophoretic analysis.

To further probe the condensation ability of **NAM1**, a full concentration range (5-500 μM) was conducted over both 2.5 h and 5 h incubation times to determine the concentration at which DNA fully aggregates. The onset of condensation can be observed at 20 μM, where the native DNA bands become fainter in appearance and fully disappear at 100 μM, reflecting total condensation. It can be seen from clearly that this sample can fully condense supercoiled dsDNA at 100 μM at 2.5 h (Figure IV-6 A) and at 75 μM at 5 h (Figure IV-6 B).

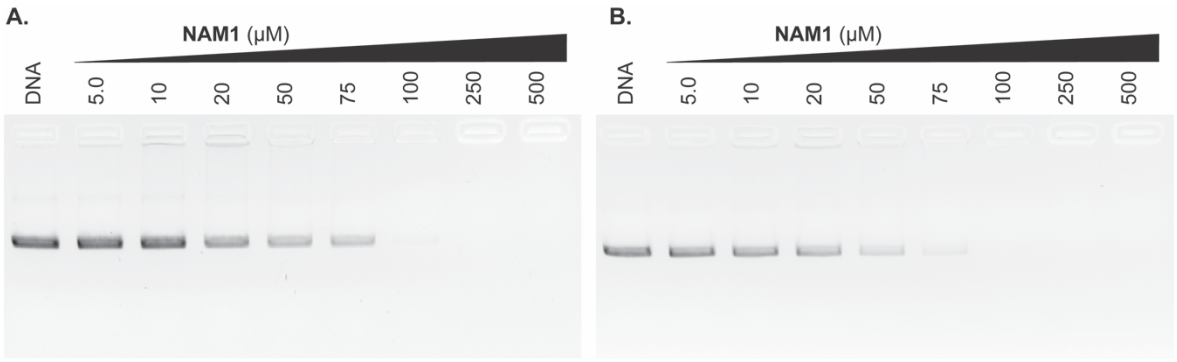

Figure IV-6. Agarose gel electrophoresis of supercoiled dsDNA (400 ng) exposed to increasing concentrations of **NAM1**. Reactions were carried out in the presence of 25 mM NaCl over 2.5 h (**A**) and 5 h (**B**) at 37 ˚C prior to electrophoretic analysis.

The condensation ability of **NAM2** was investigated under the similar conditions described for **NAM1**. Unfortunately, this compound did not display a potent onset of condensation at low drug loading. **NAM2** showed the onset of condensation at 250 μM drug loading and completely condensed at 500 μM, Figure IV-7.

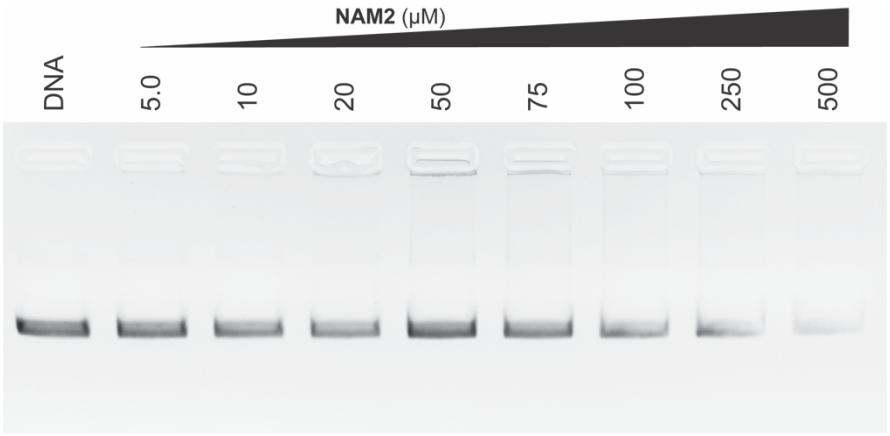

Figure IV-7. Agarose gel electrophoresis of supercoiled dsDNA (400 ng) exposed to increasing concentrations of **NAM2**. Reactions were carried out in the presence of 25 mM NaCl over 2.5 h at 37˚C prior to electrophoretic analysis.

To summarise, five imidazole C_3-scaffolds were characterised by ^{1}H NMR spectroscopy and ESI-MS to determine sample purity for nucleic acid screening. Through DNA condensation investigations with supercoiled plasmid (pUC19) it was identified that **NAM1** was capable of fully condensing DNA at 75 μM over 5 h, while **NAM2** fully condensed DNA at 500 μM over 2.5 h incubation. The onset of condensation was observed for **NAM3** and **NAM5** at 500 μM, however full condensation was not observed. **NAM 4** showed no onset of condensation at 500 μM. These results highlight that a non-opioid C_3-scaffolds are proficient DNA condensation agents and now opens the path for the development of new scaffolds.

An imidazolium core is an important structural unit in medicinal chemistry and numerous drug molecules containing this moiety are currently used in varying treatments; it is the essential core in a number of ionic liquids and natural products like histidine and nucleic acid bases further highlighting its importance. However it is important to note that there are several methods for the preparation of this imidazole core such as: Debus;[15] Walach;[16] and Van Leusen[17] methods however these methods suffer from drawbacks including low regioselectivity, low yields, and poor functional group tolerance. Although continued reports of improved protocols are emerging they are far from perfect.[18] For the purpose of drug discovery, a more

reliable and robust method can be achieved through the use of click chemistry. Herein we aim to exploit the highly developed copper(I) catalysed click reaction to generate a large library of tripodal systems for the tailored targeting of DNA condensation agents.

IV. 4. Click Chemistry

In the quest to develop new pharmaceutical agents quickly and efficiently has been an on-going expedition sought after by chemists for generations. Ideally, these reactions would offer high producing yields, reproducibility, versatility and more importantly with reduced purification requirements. In this regard, Sharpless and Meldal[19] independently discovered the copper(I)-catalyzed variation of the classical Huisgen 1,3-dipolar (azide-alkyne) cycloaddition. In his landmark review in 2001, Sharpless defined click chemistry as a group of reactions that "*must be modular, wide in scope, give very high yields, generate only inoffensive by products that can be removed by non-chromatographic methods, and be stereospecific (but not necessarily enantioselective).*"[20] The Huisgen 1,3-dipolar (azide-alkyne) cycloaddition was developed in 1963[21,22] and required long reaction times with intense heating, often leading to a mixture of isomers. Since the introduction of this new click reaction the concept has experienced rapid popularity across a number of applications in pharmaceutical sciences[23] such as: drug discovery,[24] biochemistry,[25] chemical sensors,[26,27] and polymer chemistry.[28]

In a further refinement of click chemistry, Sharpless states that a click reaction must include simple reaction conditions, the process must be insensitive to oxygen and water, must use readily available starting materials or reagents and incorporate either solvent free conditions or in aqueous media. Where purification is required it must be by non-chromatographic methods and products should be simply isolated through crystallization or through distillation procedures.[20] Click chemistry itself refers to a group of powerful linking reactions that are simple to perform; to date there are four major classifications of click reactions that have been identified, highlighted in Table IV-1.

Table IV-1. Major classifications of click reactions.

Click reaction	Examples
Cycloaddition	1,3-dipolar cycloadditions, hetero-Diels-Alder cycloadditions
Nucleophile ring-openings	Opening of strained heterocylic electrophiles such as aziridines, epoxides, and cyclic sulfates
Carbonyl chemistry of the non-aldol type	Formation of ureas, hydrazones, and oxime ethers.
Additions to carbon-carbon multiple bonds	Epxoidations and nitrosyl halide additions.

Among the four major classifications, cycloadditions, particularly the copper(I)-catalysed azide alkyne cycloaddition (CuAAC) reaction of azides and terminal alkynes for the formation of 1,2,3-triazoles, are the most widely used. This metal-catalysed reaction established a substantial improvement of the classical Huisgen-type thermal 1,3-dipolar cycloaddition, which affords mixtures of 1,4- and 1,5-disubstituted triazoles that required long reaction times and substantial heating. It has been highly documented that this regioselective triazole synthesis has served as a powerful ligation tool in the formation of new chemicals for numerous applications.[23] Through copper(I) catalysis this reaction exclusively forms 1,4-substituted products, making it regiospecific whereas, interestingly the ruthenium(II) catalysis of this reaction only forms the 1,5-triazole compared to the classical means were mixtures are observed (Scheme IV-1). Recent articles have shown alternative metals for the catalysis of a 1,3-dipolar cycloaddition, such as a silver complex reported by McNulty *et al*.[29,30] however they highlight that silver salts alone are not able to catalyse the reaction proving copper to be the most versatile and robust choice. The CuAAC reaction typically does not require temperature elevation but can be performed over a wide range of temperatures (0–160 ˚C), and in a variety of solvents (including water). This reaction proceeds almost 10^7 times faster than the un-catalysed version, and purification commonly consists of product filtration.[24]

Copper-free click chemistry promoted by ring-strain has also been shown (Scheme IV-1) and was first published in 1961 by Wittig et al.[31] In this paper it was reported that the reaction between the cyclic alkyne cyclooctyne reacts violently when combined neat with phenyl azide, forming a triazole product by 1,3-dipolar cycloaddition. This ultrafast reaction can be explained by the ring-strain in the

cyclooctyne molecule and release of the ring-strain drives the fast reaction. The advantage of ring-strained click chemistry is the absence of copper for reactions carried out *in vivo.* It was first applied as click reaction in biological systems by Bertozzi *et al*. who noted that the presence of a Cu(I) catalyst promotes cell toxicity making it undesirable for *in vivo* click chemistry.[32] Bertozzi[33–35] and Boons *et al*.[36] reported even greater reaction rates when electron-withdrawing groups were placed on the cyclooctyne ring. In recent years there has been an influx of commercially available probes for *in vitro* click chemistry applications that incorporate ring-strained cyclooctynes.

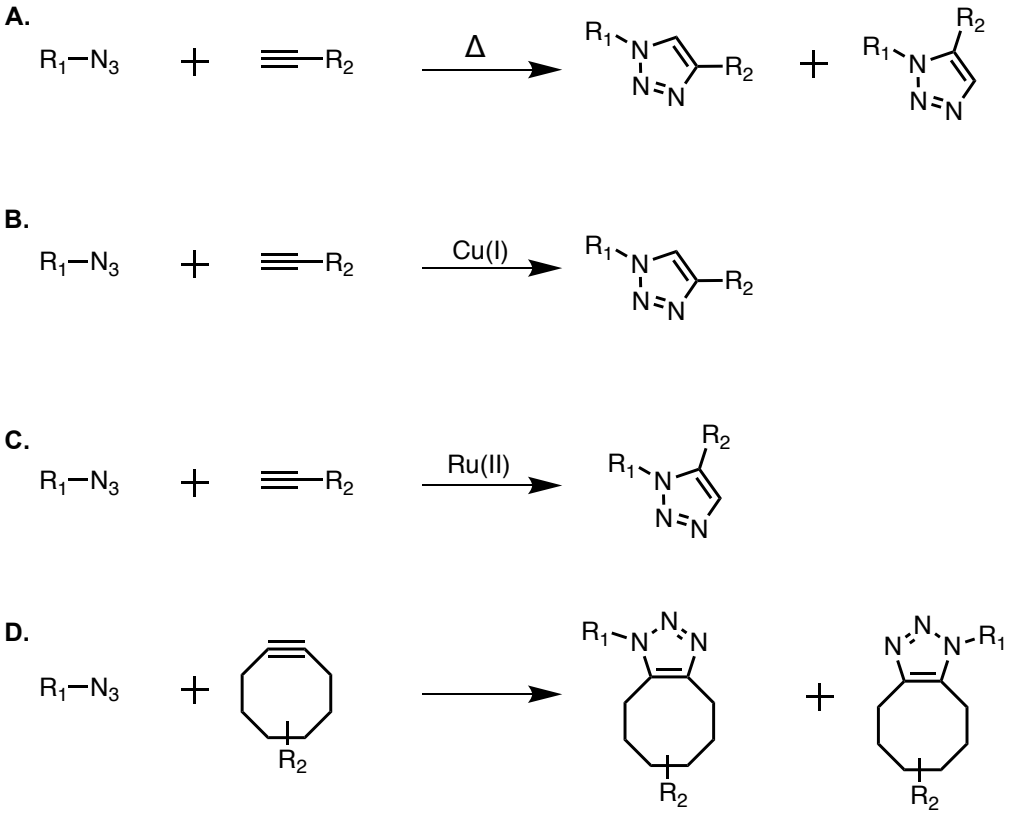

Scheme IV-1. Schematic representation of the four variations of a click reaction between an azide and alkyne functional groups. **A**. Thermal Huisgen cycloaddition; **B.** copper(I) catalysed click reaction; **C.** ruthenium(II) catalysed click reaction; **D.** ring-strained click reaction.

Azide and alkyne functional groups are known to be some of the most energetic sets in organic chemistry but separately are also the least reactive as they are essentially inert functional groups to most biological and organic conditions including oxygen, water and the general conditions used in synthetic organic chemistry and more importantly they are easy functional groups to introduce. The

triazole ring is not a naturally occurring ring structure formed in nature but solely synthetic, however they have become attractive connecting units because they are stable to metabolic degradation and are capable of hydrogen bonding, which can be favourable in the binding of bio-molecular targets and improved solubility. They are rigid and reliable linking units that cannot be hydrolytically cleaved and are almost impossible to oxidise or reduce unlike related aromatic heterocycles.[37]

There are a number of reported methods for the preparation of the active copper(I) species for the CuAAC reaction, one of the most common techniques is to reduce copper(II) salts such as copper(II) sulfate ($CuSO_4$), in situ to its copper(I) form, and this is predominately performed by the addition of a reducing agent in excess such as sodium ascorbate (Na-*L*-ascorbate), which is typically in excess. This technique allows reactions to be carried out in an oxygenated environment and in aqueous conditions. A major disadvantage of this method is that the reducing agent could reduce the copper(I) species to its copper(0) form, however this can be easily controlled through stoichiometrically controlled ratios of the reducing agent or the addition of a copper stabilizing agent.[20] An alternative method for the preparation of the active catalyst is to directly add a copper(I) salt, such as copper(I) bromide (CuBr), and copper(I) iodide (CuI). A major drawback of this approach is that they must be performed in an deoxygenated environment, organic solvent, and often in the presence of excess base such as DIPEA or 2,6-lutidine.[38]

In a short period click chemistry has had a dramatic and diverse impact in the area of drug discovery and development. Indeed, the versatility of CuAAC seems endless, offering new targets to be prepared through fewer reaction steps and through limited purification required. This project was aimed at exploiting the well documented CuAAC reaction for the preparation of a library of C_3-symmetric polyamine scaffolds for the applications of nucleic acid condensation. These scaffolds incorporate three “clickable” sites and will be further referred to as “Tri-Click” scaffolds, shown in Scheme IV-2. The synthetic aim for the preparation of this library included using commercially available reactive handles containing either azide or alkyne functional groups, and keeping the reaction steps to a minimum when possible. The ability to prepare novel scaffolds quickly for screening purposes was an important aspect of this work.

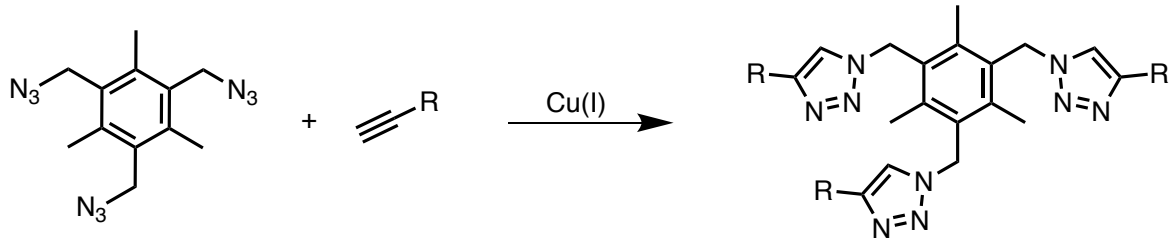

Scheme IV-2. Schematic representation for the preparation of the Tri-Click scaffolds through CuAAC reaction. The R represents terminal modifications.

IV. 4.1. Establishment of an azide containing mesitylene core unit and click reactions

In concept with the theme of the work described so far, a tripodal core structure was incorporated through the generation of 1,3,5-*tris*(azidomethyl)-2,4,6-trimethylbenzene (triazide) as the starting point in the generation of a library of polyamine scaffolds produced through CuAAC chemistry. The triazide compound was prepared from 2,4,6-*tris*(bromomethyl)mesitylene in DMF in the presence of excess sodium azide as shown in Scheme IV-3.[39] The reaction was performed at 0˚C while sodium azide was added in portions controlled slow additions and allowed to warm to rt and stir under ambient conditions. The product was extracted using EtOAc and recrystallized from Hex:EtOAc to afford a white crystalline solid. Precautions should be taken in the preparation and storage of this compound, azides

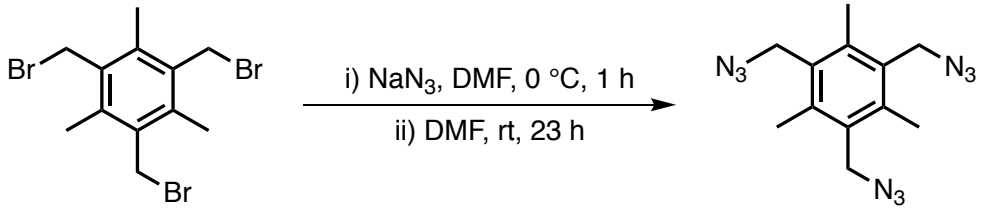

Scheme IV-3. Reaction scheme for the generation of triazide compound.[39]

Reactions were performed with two alkynes, 4-bromo-1-butyne and 2-methyl-3-butyn-2-ol, both selected due to their commercial availability and also to act as controls within the nucleic acid condensation screen. It was envisioned that these two products would act as standards to study the interactions of the triazole rings towards nucleic acid binding and act as a comparison for the amine containing scaffolds, along with finding the optimum conditions for the preparation of a Tri-Click product.

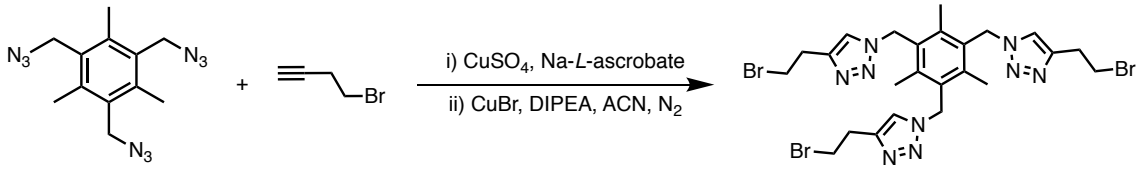

Scheme IV-4. Reaction conditions attempted for the click reaction with 4-bromo-1-butyne. i) $CuSO_4$ (1-5%), Na-*L*-ascorbate (5-10%) 25 ˚C and ii) CuBr (1-5%), DIPEA (5-10%), ACN, N_2, 25 ˚C.

Previously reports have shown, that catalytic amounts of $CuSO_4$, usually between 1-5% mole loading, and Na *L*-ascorbate (5-10 % mole loading) was required to efficiently click an alkyne functional group with an azide affording the 1,3-triazole ring. This systematic approach was attempted for the click reactions with the triazide starting material to determine an appropriate copper-loading ratio in an appropriate solvent system, Scheme IV-4. The reactions attempted with 4-bromobutyne are described in Table IV-2. From this table it can be summarised that $CuSO_4$ in the presence of Na-*L*-ascorbate resulted in no product formation. The result of these reactions leads us to believe that $CuSO_4$ was not reducing to the copper(I) oxidation state and to eliminate this possibility, CuBr was substituted as shown in reaction NS114 and NS115 resulting in the formation of the product in high yield of 85%. The reaction conditions required an inert atmosphere in the presence of CuBr; when an excess of CuBr was present (as in NS115) the reaction was complete over 24 h as compared to NS114 were a reaction time of 72 h was required for the complete conversion of the target compound. The long reaction time was believed to be due to the three “click” sites on the triazide, along with the insolubility of CuBr. From the results, CuBr was an ideal copper(I) catalyst for the click reactions with the triazide parent scaffold. Although these conditions require the use of inert atmosphere, organic solvent, and the presence of a base, the isolation and yield of the desired product make these conditions more attractive. The reaction was further optimised by addressing the solvent choice for catalytic loading of $CuSO_4$ which lead to the formation of the desired product in high yield (85%). The final conditions are outlined in Appendix D-3, briefly the azide and alkyne reagents were dissolved in a solvent mixture of THF/H_2O (1:1) and $CuSO_4$ (1%) was added in the presence of reducing agent Na L-adsorbate (5%).

Table IV-2. Reaction conditions of triazide and 4-bromo-butyne click reaction.

Reaction	Conditions	Success
NS110	To a solution of triazide (1 mmol) and 4-bromo-butyne (3 mmol) in THF/H_2O (1:1, 10 ml), $CuSO_4$ (1%) and Na-*L*-ascorbate (5%) was added, the reaction was carried out at 25˚C, 24 h.	✗
NS112	To a solution of triazide (1 mmol) and 4-bromo-butyne (3 mmol) in *t*-BuOH/H_2O (1:1, 10 ml), in the presence of $CuSO_4$ (1%) and Na-*L*-ascorbate (5%), reaction was carried out at 25˚C 72 h.	✗
NS113	To a solution of triazide (1 mmol) and 4-bromo-butyne (3 mmol) in THF/H_2O (1:1, 25 ml), in the presence of $CuSO_4$ (5%) and Na-*L*-ascorbate (10%) reaction stirred at 25˚C, 24 h.	✗
NS114	To a solution of triazide (1 mmol) and 4-bromo-butyne (3 mmol) in ACN (10 ml), CuBr (1%) and DIPEA (5%) was added under inert atmosphere (N_2) at 25˚C, 72 h.	✓
NS115	To a solution of triazide (1 mmol) and 4-bromo-butyne (3 mmol) in ACN (25 ml) in the presence of DIPEA (10%), CuBr (5%) was added under inert atmosphere (N_2) stirring at 25˚C, 18 h.	✓

For the preparation of Tri-Click scaffold incorporating the 2-methyl-3-butyn-2-ol, the synthesis was greatly simplified just requiring catalytic loading of $CuSO_4$ (1%) and Na-*L*-ascorbate (10%), Scheme IV-5. The product was isolated as a precipitate from the reaction in good yield (71%). This reaction was reproducible and highlighted from the onset that this reaction fits within Sharpless's required traits for a desirable click reaction.

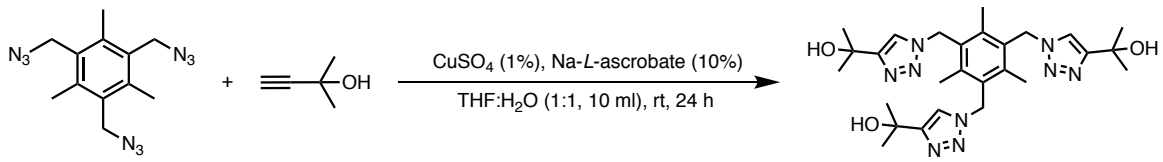

Scheme IV-5. Reaction conditions for the preparation of Tri-Click 2-methyl-3-butyne-2-ol.

Following from the success of the click reactions from the triazide scaffold, a series of amine containing alkyne handles was established to mimic the piperidine ring on the opioid scaffold. The series of alkyne handles are highlighted in Figure IV-8 varying from a simple propargylamine to that of an aromatic ethynylaniline series. In each series there is a primary, secondary and tertiary amine present in the alkyne

handles to allow for a structure activity relationship study for nucleic acid binding and condensation properties.

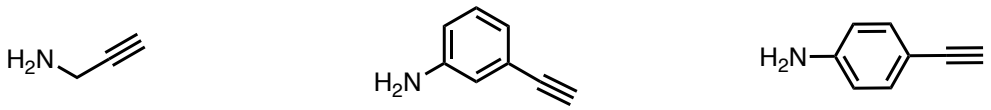

Propargylamine 3-Ethynylaniline 4-Ethynylaniline

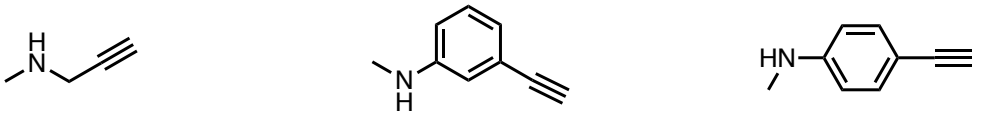

N-Methylpropargylamine 3-Ethynyl-*N*-methylaniline 4-Ethynyl-*N*-methylaniline

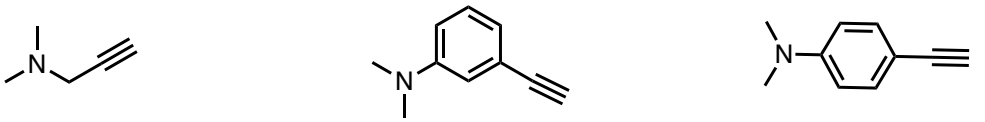

N,N-Dimethylpropargylamine 3-Ethynyl-*N,N*-dimethylaniline 4-Ethynyl-*N,N*-dimethylaniline

Figure IV-8. Molecular structures of alkyne amine compounds selected for click chemistry reaction.

From the target alkyne handles shown Figure IV-8, a small library of 9 compounds was envisioned to be prepared through the use of click chemistry with the triazide parent structure. In the cases of the alkyne handles that are not commercially available, these alkyne handles were easily prepared and will be discussed as such. The main aim of generating these Tri-Click compounds was to make them in the minimum required steps, quickly, efficiently and with little to no purification through copper(I) catalysed click chemistry.

IV. 4.2. Development of the Tri-Click propargylamine series

The first series developed via click chemistry was the propargylamine series, consisting of propargylamine, a primary amine, *N*-methylpropargylamine, a secondary amine, and *N,N*-dimethylpropargylamine, a tertiary amine. The three alkyne handles are commercially available through Merck and are shown in Figure IV-9.

Propargylamine *N*-Methylpropargylamine *N,N*-Dimethylpropargylamine

Figure IV-9. Propargylamine Alkyne handles.

The reaction conditions attempted for the formation of the propargylamine click product are summarised in Table IV-3. Initially no click product could be formed directly from propargylamine with the triazide scaffold. A series of reactions conditions were attempted including the typical reaction conditions using $CuSO_4$ and a reducing agent, Na-*L*-ascorbate. Following from this, CuBr was substituted as the copper(I) source to promote the formation of the desired click product. The reactions involving propargylamine did not yield any product and to study this further a click reaction was attempted using *N,N*-dimethylpropargylamine as seen in Scheme IV-6.

Table IV-3. Reaction conditions for the triazide and propargylamine click reaction.

Reaction	Conditions	Success
NS124	To a solution of triazide (1 mmol) and propargylamine (3 mmol) in THF/H_2O (1:1, 10 ml), in the presence of $CuSO_4$ (1%) and Na-*L*-ascorbate (5%) at rt, 24 h.	✗
NS126	To a solution of triazide (1 mmol) and propargylamine (3 mmol) in THF/H_2O (1:1, 10 ml), in the presence of $CuSO_4$ (5%) and Na-L-ascorbate (10%) at 40˚C, 24 h.	✗
NS135	To a solution of triazide (1 mmol) and propargylamine (3 mmol) in ACN (10 ml), in the presence of $CuSO_4$ (10%) and Na-*L*-ascorbate (20%) under nitrogen at rt, 72 h.	✗
NS137	To a solution of triazide (1 mmol) and propargylamine (3 mmol) in ACN (25 ml), CuBr (1 mmol) was added under nitrogen at rt, 48 h.	✗
NS141	To a solution of triazide (0.7 mmol) and propargylamine (2.1 mmol) in ACN (20 ml), CuBr (1.2 mmol) was added under nitrogen at reflux, 120 h.	✗
NS146	To a solution of triazide (1mmol) and CuBr (1 mmol) in ACN (20 ml) propargylamine (3.1 mmol) was added as a solution in ACN (5 ml) over 30 min, reaction carried under nitrogen at rt, 48 h.	✗

The reaction conditions used for the click reaction of *N*-methylpropargylamine and *N,N*-dimethylpropargylamine were CuBr in the presence of DIPEA over 72 h in a solution of acetonitrile (ACN), Scheme IV-6. The reaction between *N,N*-dimethylpropargylamine and the triazide compound afforded the desired click product on first attempt which suggested perhaps a primary and secondary amine could be interfering with the copper source, where a tertiary amine cannot. However, although a secondary amine would be expected to offer enough shielding from the copper(I) catalyst in the case of *N*-methylpropargylamine, a methyl group may not be a large enough blocking group to displace any unwanted reaction/coordination between the amine and the copper(I) catalyst. To test this hypothesis, amine protection chemistry was utilised to understand the reactivity of a primary amine under click chemistry conditions.

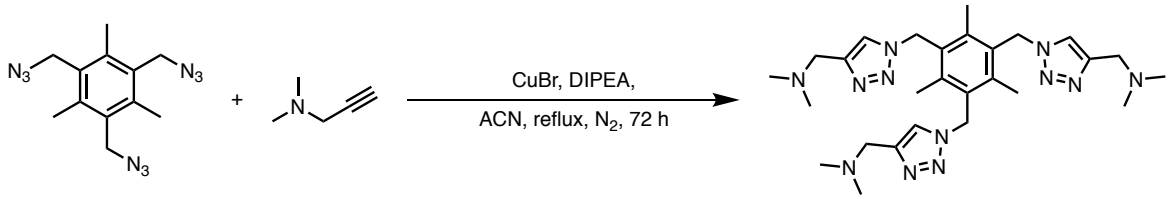

Scheme IV-6. Reaction conditions for the preparation of Tri-Click *N,N*-dimethylpropargylamine.

Common amine protecting groups include tert-butyl carbamate groups (Boc), fluorenylmethyloxycarbonyl chloride (FMOC) groups and phthalimide groups. For the purpose of this project the Boc protecting group was chosen due to its stability in basic conditions simplicity of use and ease of displacement. The formation of the Boc-protected amine can be prepared in both aqueous and anhydrous conditions in the presence or absence of a base. The reaction mechanism of the Boc-protected product of propargylamine is highlighted in Scheme IV-7. The amine attacks a carbonyl site on the di-tert-butyl-dicarbonate compound and tert-butyl carbonate is formed as a leaving group. Tert-butyl carbonate picks up a proton from the now protonated amine resulting in the final Boc-protected amine. Side products of this reaction include tert-butyl bicarbonate, which is further broken down to CO_2 and tert-butanol. Boc-protected amines can be cleaved under anhydrous acidic conditions with common reagents such as HCl and trifluoroacetic acid (TFA).

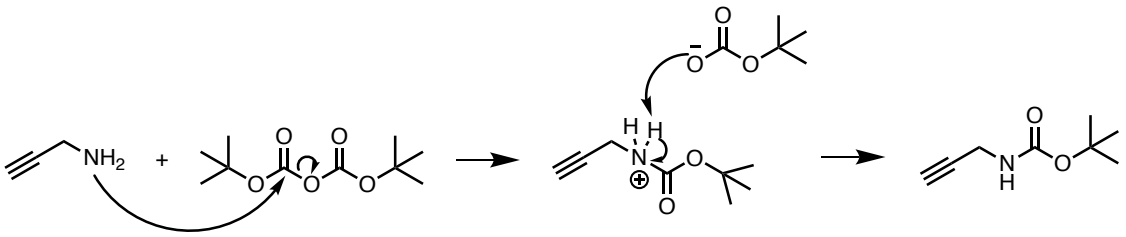

Scheme IV-7. Mechanism of Boc-protection of propargylamine.

For the Boc-protection of propargylamine and *N*-methyl-propargylamine, the amine was stirred in DCM over ice while the tert-butyl-dicarbonate was added dropwise.[40,41] The formation of the Boc-amine products were monitored steadily by TLC and the resulting solution was concentrated to afford the crude sample which was purified by column chromatography. Boc-propargylamine and Boc-*N*-methypropargylamine products were used in a click reaction with the triazide compound to afford the desired click products shown in Scheme IV-8. The final click products were purified through column chromatography a white and yellow solid for the Boc-propargylamine and Boc-*N*-methylpropargylamine respectfully, in moderate yields.

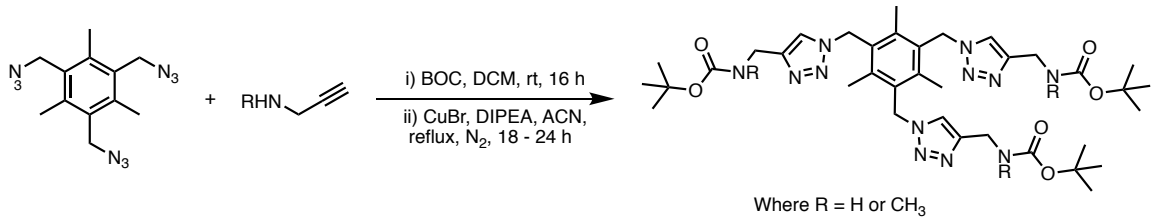

Scheme IV-8. Reaction conditions for the preparation of Boc-ligands (i) and click reaction with Boc-propargylamine and Boc-*N*-methylpropargylamine (ii), where R represents either H or CH_3 for propargylamine and *N*-methylpropargylamine.

Attempts to remove the Boc-protecting groups for each product resulted in loss of product or degradation of the final product, as seen by ^{1}H NMR spectra. Boc removal was carried out using anhydrous HCl (4 M in dioxane) and TFA in DCM at varying equivalents to no avail. Keeping in mind of the scope of this project a multistep reaction procedure was less than ideal and the use of catalytic copper loading was revisited under alternative conditions. The solvent mixture was changed from THF to tert-butanol (*t*-BuOH) a more polar protic solvent used in the first click reactions reported by Sharpless.[20] The preparation of Tri-Click propargylamine and *N*-methylpropargylamine products was achieved through careful reaction conditions outlined in Appendix D-3. In brief, Tri-Click propargylamine was successfully synthesised in a solvent mixture of degassed *t*-BuOH/H_2O (1:1) with Na-*L*-ascorbate

(5%) and $CuSO_4$ (1%) under a nitrogen atmosphere at room temperature, Scheme IV-9. A high yield of 84% was achieved and the product was fully characterised. The Tri-Click *N*-methylpropargylamine product was prepared in the same manner detailed in the appendix (D-3).

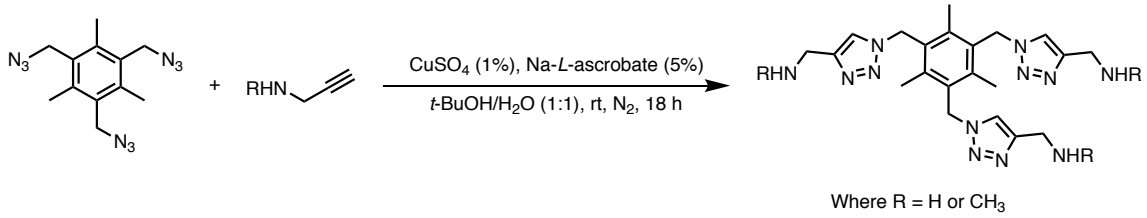

Scheme IV-9. Reaction conditions for the preparation of Tri-Click propargylamine and *N*-methylpropargylamine. Where R represents either H or CH_3.

IV. 4.3. Development of the Tri-Click 3-ethynylaniline series

The 3-ethynylaniline series was targeted as shown in Figure IV-10, similar to that of the propargylamine series that was previously discussed the primary and secondary amines interfered with the copper(I) catalyst and did not afford the desired Tri-Click product, however the tertiary amine was successfully synthesized with no protection chemistry required as shown in Scheme IV-10. Ideally, click reactions can be performed in aqueous conditions without the need for protection groups, however this only applies to products that are water soluble, and since the ethynylaniline reagents were not water soluble, an organic solvent had to be used to fully dissolve them which required amine protection chemistry to avoid unwanted side reactions. As the 3-ethynyl-*N*-methylaniline, and 3-ethynyl-*N,N*-dimethylaniline reagents were not commercially available at the time they were prepared from the starting material 3-ethynylaniline (Appendix D-3).

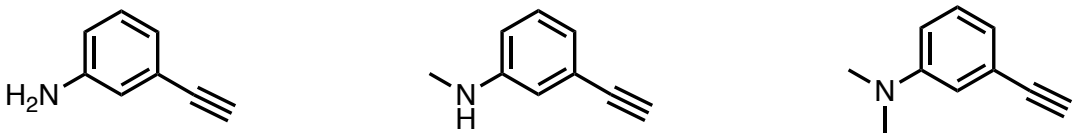

3-ethynylaniline 3-ethynyl-*N*-methylaniline 3-ethynyl-*N,N*-dimethylaniline

Figure IV-10. 3-Ethynylaniline series: 3-ethynylaniline, 3-ethynyl-*N*-methylaniline, and 3-ethynyl-*N,N*-dimethylaniline.

The starting material 3-ethynylanline was commercially available and from this starting material the 3-ethynyl-*N,N*-dimethylaniline alkyne linker was prepared in the presence of excess caesium carbonate stirring at rt with the addition of excess

methylating agent, iodomethane.[42] The product was easily isolated through column chromatography in moderate yields of ~30%. Attempts were made to improve the yield by substituting an alternative base in the place of caesium carbonate; potassium carbonate and potassium hydroxide were attempted and in both cases no improvement in yield was achieved.

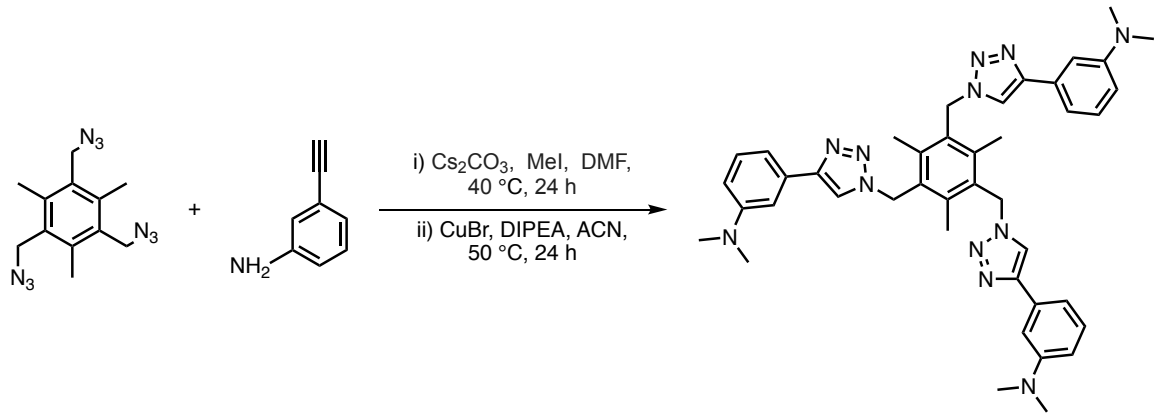

Scheme IV-10. Reaction scheme for the preparation of the Tri-Click scaffold with 3-3-ethynyl-*N,N*-dimethylaniline.

Boc was used as a protecting group for the preparation of Boc-3-ethynylaniline and Boc-methyl-3-ethynylaniline. The Boc-3-ethynylaniline ligand was obtained in high yield (94%) and purified through column chromatography to afford a colourless liquid. This product was successively used in a click reaction with the triazide scaffold after a period of 48 h at 50 ˚C, Scheme IV-11. For the preparation of the Boc-methyl-3-ethynlaniline compound a stronger base was used to deprotonate the protected amine, method adapted from similar work.[43,44] Through the presence of 3 molar equivalents of sodium hydride and excess iodomethane the methylated Boc-3-ethynylaniline was successfully prepared, however careful column chromatography was required to successfully remove any unreacted Boc-3-ethynylaniline. This product was successively used in a click reaction with the triazide scaffold to afford the click product. The removal of the Boc protecting group was easily achieved through the use of excess TFA (16 molar equivalents) in DCM, highlighted Scheme IV-11. The deprotected products were isolated through a flash column and dried under reduced pressure to afford two beige solids (Appendix D-3). However, the Tri-Click methyl-3-ethynylaniline product is hygroscopic and required storage under argon.

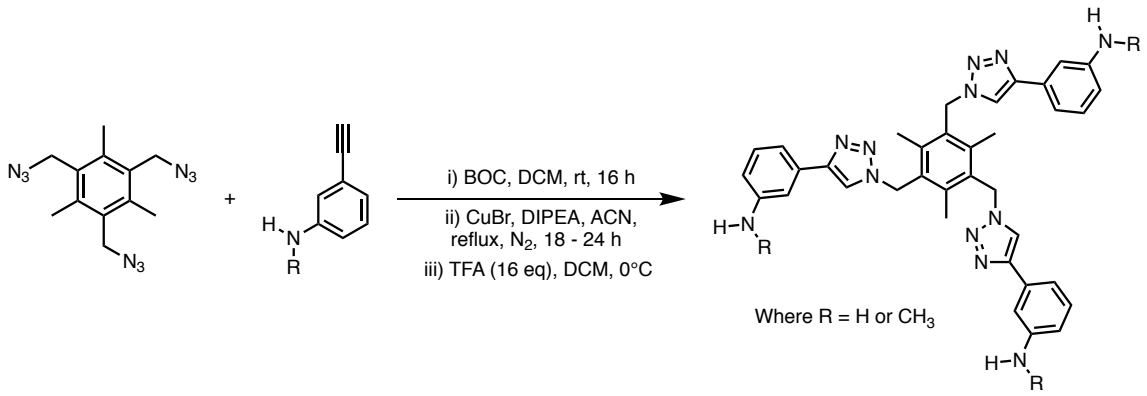

Scheme IV-11. Reaction scheme for the preparation of the Tri-Click 3-ethynylaniline and 3-ethynyl-*N*-methylaniline scaffolds. Where R represents either H or CH_3.

IV. 4.4. Development of the Tri-Click 4-ethynylaniline series

To establish a complete structural activity relationship for the ethynylaniline series an aromatic ring with a para substituted amine functional group with a primary, secondary and tertiary amine were designed as alkyne reactive handles for the preparation of Tri-Click products with the core triazide scaffold. The 4-ethynylaniline series was targeted as shown in Figure IV-11.

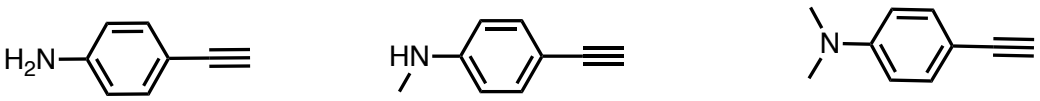

4-ethynylaniline | 4-ethynyl-*N*-methylaniline | 4-ethynyl-*N,N*-dimethylaniline

Figure IV-11. Para-ethynylaniline series: 4-ethynylaniline, 4-ethynyl-*N*-methylaniline, and 4-ethynyl-*N,N*-dimethhylaniline

The starting material 4-ethynylaniline was commercially available (Merck) and from this starting material the 4-ethynyl-*N,N*-dimethylaniline alkyne linker was prepared under the same reaction conditions used for the preparation of 3-ethynyl-*N,N*-dimethylaniline compound. This product was successfully clicked to the triazide parent scaffold as previously described, Scheme IV-12. However, in parallel to current findings the unprotected 4-ethynylaniline-alkyne handle did not form the desired click product, and Boc protection was used to mask the primary amine from unwanted side reactions.

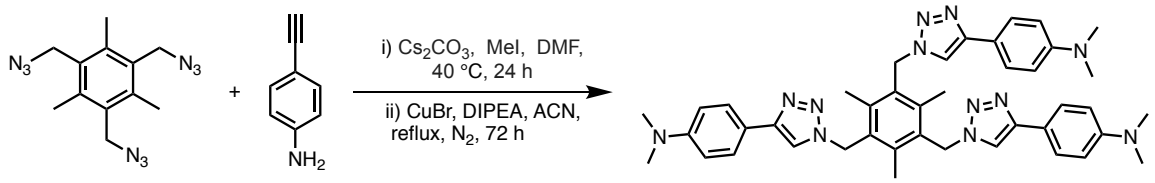

Scheme IV-12. Reaction conditions for the preparation of Tri-click scaffold with 4-ethynyl-*N,N*-dimethylaniline.

For the preparation of 4-ethynyl-*N*-methylaniline, 4-ethynylaniline was first Boc-protected. The Boc-protection of 4-ethynylaniline was carried out as per literature procedures,[45] and was isolated as a white solid. The reaction conditions are outlined in Scheme IV-13. The first attempt as the subsequent methylation reaction for the preparation of this alkyne handle recovered the desired product by 50% through ^{1}H NMR spectroscopy, however the attempted purification of this product from the starting material proved troublesome. Literature procedures highlighted this product was purified by column chromatography on an elution system of Hex:EtOAc (varying ratios). This was attempted using a gradient system with increasing ratios of ethyl acetate to hexane to allow for a clean separation. Unfortunately, this was unsuccessful and constant co-elution of the product with this solvent system prevailed. The reaction was repeated using an increased ratio of sodium hydride (4 equivalents) and longer reaction time to try achieving higher conversion to the methylated derivative. This was successfully achieved and a 70% conversion was observed through ^{1}H NMR spectroscopy, again this product could not be cleanly separated from the starting Boc-aniline using standard chromatography methods, alternative purification methods were attempted such as recrystallisation. A final attempt at fully converting this product was achieved with the highest conversion rate of 80% achieved, however after several attempts at purification this product was not separated from the starting material and it was deemed not feasible to continue to the next step in the synthesis.

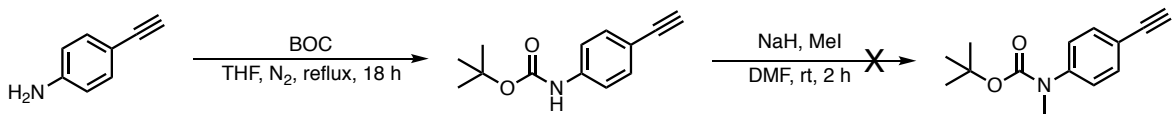

Scheme IV-13. Reaction scheme for the attempted preparation of Boc-4-ethynyl-N-methylaniline

Due to the success of the Boc-protected amine containing alkyne handles this method was adapted to incorporate a Boc-protected para-ethynylaniline alkyne for the preparation of the final click product. Unfortunately, all attempts at producing a copper(I) catalyst click product proved unsuccessful, Scheme IV-14. A series of reaction conditions were attempted and the key few are highlighted in Table IV-4.

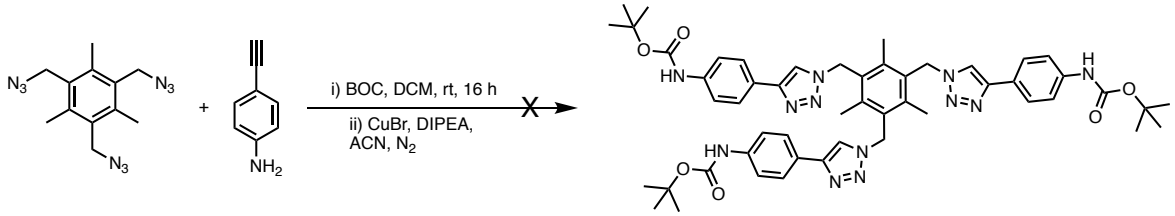

Scheme IV-14. Attempted synthesis of Tri-Click scaffold with boc-4-ethynylaniline.

Reaction conditions included CuBr as the copper(I) source in the click reaction with the triazide parent scaffold, all reactions were carried out in dry degassed acetonitrile. The first attempt recovered only starting materials and no click product; longer reaction times were then attempted at both room temperature and elevated temperature with no success. This was unusual given that the 3-ethynylaniline series were successfully prepared using these established conditions. $CuSO_4$ was then attempted in the presence of excess Na-*L*-ascorbate to reduce the copper(II) to its copper(I) oxidation state *in situ*, however this approach failed.

Products containing similar functional groups/structures to 4-ethynylaniline have been prepared using click chemistry methods, typically $CuSO_4$ was used as the copper(I) source achieving moderate yields[46,47] and using CuI with the presence of an additive.[48] Similarly 4-ethynylaniline has been used in a click reaction through microwave assisted synthesis.[49] However this alkyne handle is more predominantly used in Sonogashira cross-coupling reactions[50] and precursors for an alkyne handle used in a CuAAC reaction.[51] Nonetheless it is important to highlight that in all these cases only one clickable sight on the parent azide compound was present. Similar conditions were attempted using the triazide compound to no success.

Table IV-4. Reaction conditions attempted with boc-4-ethynylaniline.

Reaction	Conditions	Success
NS152	To a solution of triazide (1 mmol), DIPEA (1 mmol) and CuBr (1 mmol) in ACN (25 ml), Boc-4-ethynylaniline (3.1 mmol) was added as a solution in ACN (5 ml). The reaction was carried out under nitrogen at rt, 24 h.	✗
NS162	To a solution of triazide (1 mmol), DIPEA (1 mmol) and CuBr (1 mmol) in ACN (25 ml), Boc-4-ethynylaniline (3.1 mmol) was added as a solution in ACN (5 ml) over 10 min. The reaction was carried out under nitrogen at 50˚C, 24 h.	✗
NS186	To a solution of triazide (1 mmol), DIPEA (1 mmol) and CuBr (1 mmol) in ACN (25 ml), Boc-4-ethynylaniline (3.1 mmol) was added as a solution in ACN (5 ml) over 15 min. The reaction was carried out under nitrogen at rt, 144 h.	✗
NS188	To a solution of triazide (0.7 mmol), Na-*L*-ascorbate (20%), $CuSO_4$ (10%), THF/H_2O (1:1, 10 ml). Boc-4-ethynylaniline (2.2 mmol) was added and reaction left to stir at rt, 16 h.	✗
NS190	To a solution of triazide (1 mmol), DIPEA (1 mmol) and CuBr (1 mmol) in degassed ACN (25 ml), Boc-4-ethynylaniline (3.1 mmol) was added as a solution in ACN (5 ml) over 10 min. The reaction was carried out under argon at 50˚C, 72 h.	✗
NS199	To a solution of triazide (1 mmol), DIPEA (1 mmol) and CuBr (1 mmol) in degassed ACN (15 ml), Boc-4-ethynylaniline (3.1 mmol) was added as a solution in ACN (5 ml). The reaction was carried out under nitrogen at reflux, 24 h.	✗
NS202	To a solution of triazide (1 mmol) and Boc-4-ethynylaniline (3.1 mmol) in THF/H_2O (1:1, 10 ml), in the presence of $CuSO_4$ (5%) and Na-*L*-ascorbate (10%) at 30˚C, 48 h.	✗
NS204	To a solution of triazide (0.7 mmol) and boc-4-ethynylaniline (2.17 mmol) in *t*-BuOH/H_2O (1:1, 10 ml), in the presence of $CuSO_4$ (1%) and Na-*L*-ascorbate (10%) at 50˚C, 24 h.	✗
NS210	To a solution of triazide (1 mmol), TEA (1 mmol) and CuI (1 mmol) in dry DMF (20 ml) a solution of Boc-4-ethynylaniline was added slowly over 20 min in a solution of DMF (5 ml), reaction was carried out under nitrogen at rt, 24 h.	✗

The inability to form the Tri-Click scaffold may also be due to the deactivating resonance structure of 4-ethynylaniline shown in Scheme IV-15. Hergenrother proposed this deactivating resonance structure when attempting to prepare *N*-(4-ethynylphenyl)phthalimide by applying the same conditions used to prepare the *N*-(3-ethynylphenyl)phthalimide derivative.[52] He later developed a new method for the preparation of the phthalimide derivative successfully, however this deactivating resonance structure may be the reason for the Tri-Click product being unable to form.

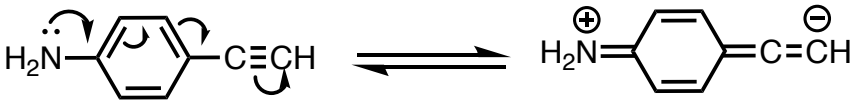

Scheme IV-15. Proposed resonance structure of 4-Ethynylaniline.[53]

To further probe this theory, *N*-(4-ethynylphenyl)phthalimide was prepared as per outlined[52] with one minor alteration, acetonitrile was substituted in the place of dimethylacetamide (DMAC) for the solvent system. The phthalimide protecting group was envisioned to offer more protection against the resonance structure than previously pursued Boc-protected adduct and can be easily removed by a reducing agent such as hydrazine hydrate. Reactions were attempted using catalytic loading of $CuSO_4$ and molar equivalents of CuBr in the presence of a base under inert conditions, Scheme IV-16. Through ^1H NMR monitoring these reactions did not proceed and no Tri-Click product was obtained.

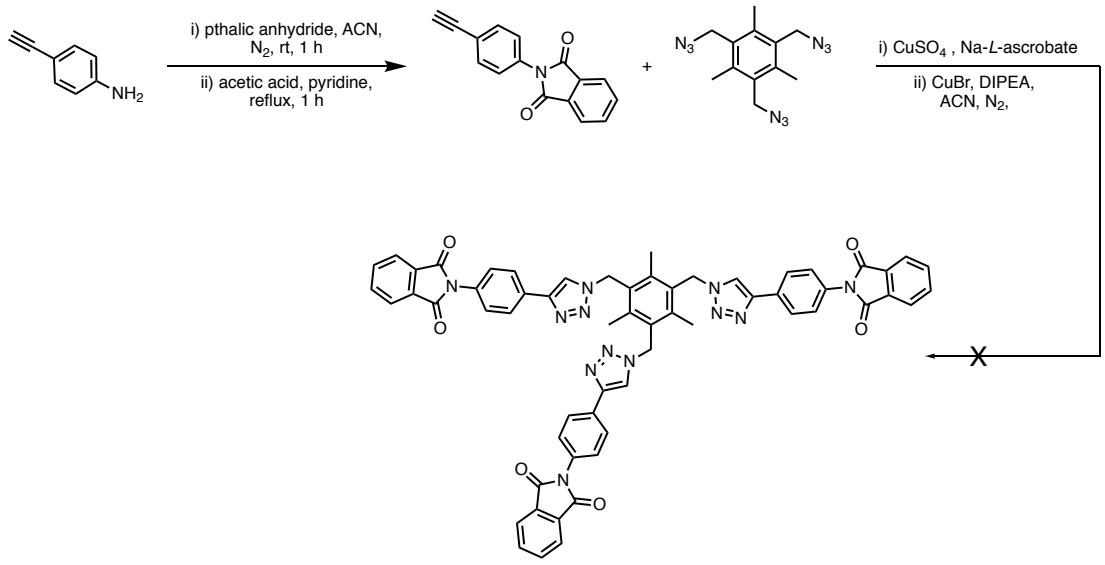

Scheme IV-16. Reaction conditions for the preparation of *N*-(4-ethynylphenyl)phthalimide, and attempted synthesis of the Tri-Click scaffold.

To further the study of the 4-ethynylaniline, 4-(2-propynyloxy) aniline was identified as a possible solution to the resonance issues suspected with the 4-ethynylaniline products. This alkyne was commercially available and it also suited the project aims to use diverse commercially available amine containing reactive handles. The reaction pathway is outlined as per Scheme IV-17 where the alkyne was first Boc-protected prior to reacting with the triazide scaffold, attempts were also made with the free amine scaffold prior however no product formed. Unfortunately, all attempts made did not result in the desired product. Catalytic loading of $CuSO_4$ was attempted and no product formed. Reaction conditions with CuBr, DIPEA, and dry ACN under nitrogen conditions were attempted also. TLC and ^1H NMR monitoring of this reaction showed only starting materials present and indicated that no triazole rings had formed.

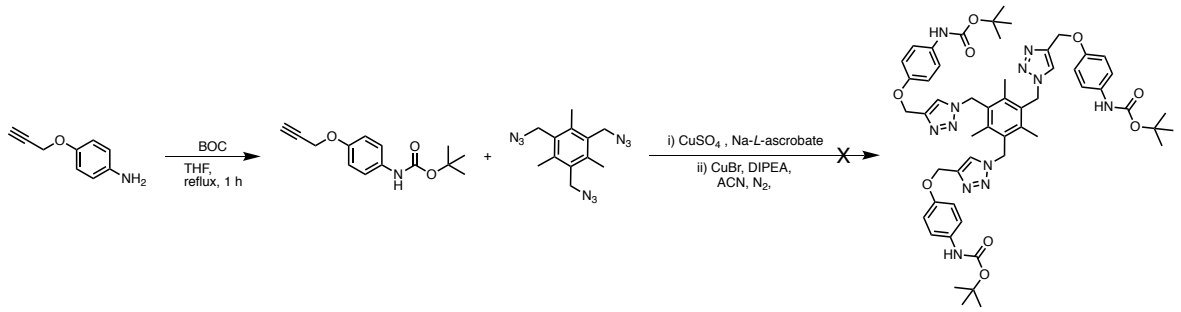

Scheme IV-17. Reaction pathway for attempted synthesis of the Tri-Click product of 4-(2-propynyloxy)aniline.

To examine the hypothesis that the presence of three click sites that in hindering the final step of the para- substituted aniline alkyne handles, the preparations of the mono-azide and di-azide derivatives of the triazide parent scaffold was carried out. The 2,4,6-trimethylbenzyl azide (mono-azide) were generated from α^2-chloroisodurene stirring at an elevated temperature of 65˚C with 3 equivalents of sodium azide to form the mono-azide compound as per literature methods.[53,54] The reaction conditions attempted for the click reaction with the mono-azide compound and Boc-protected anilines are highlighted in Scheme IV-18. Literature standard procedures for classical CuAAC reactions were first attempted with catalytic proportions of $CuSO_4$ (1-5%) with excess Na-*L*-ascorbate (10-20%) in a mixture of aqueous and organic solvent (THF/*t*-BuOH) but these resulted in no product formation. Alternative copper(I) sources such as CuBr and CuI were then attempted without success.

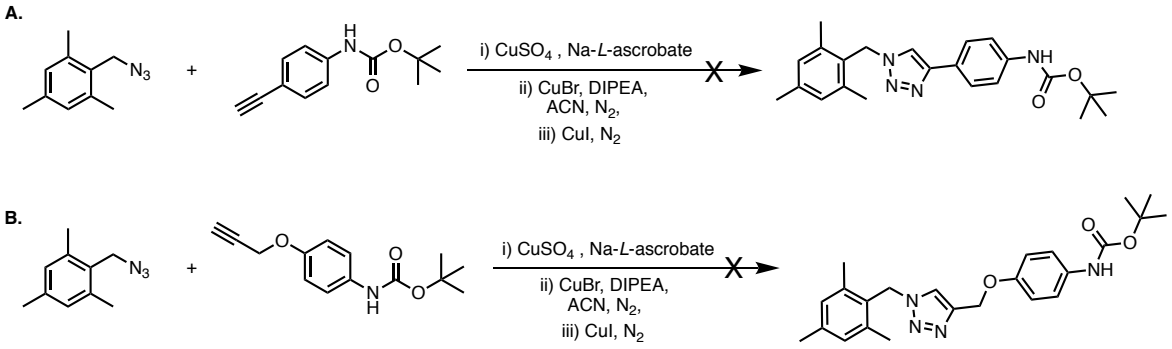

Scheme IV-18. Attempted synthesis of mono-azide with (**A**) Boc-4-ethynylaniline and (**B**) Boc-4-(2-propynyloxy) aniline.

1,3-*bis*(azidomethyl)-2,4,6-trimethyl benzene (di-azide) was prepared in similar manner to the mono-azide compound, stirring at an elevated temperature of 60-70˚C with excess sodium azide until complete substitution of the halogen was achieved using starting material 2,4-*bis*(chloromethyl)-1,3,5-trimethylbenzene.[53,55] The reaction scheme for the di-azide and Boc-protected anilines is outlined in Scheme IV-19. Several reaction conditions were attempted for each aniline starting material and no product was recovered. Through ^{1}H NMR spectroscopy the reaction appears to show the formation of up to one triazole ring, however the quantification by NMR was low and the product could not be easily isolated following reaction workup.

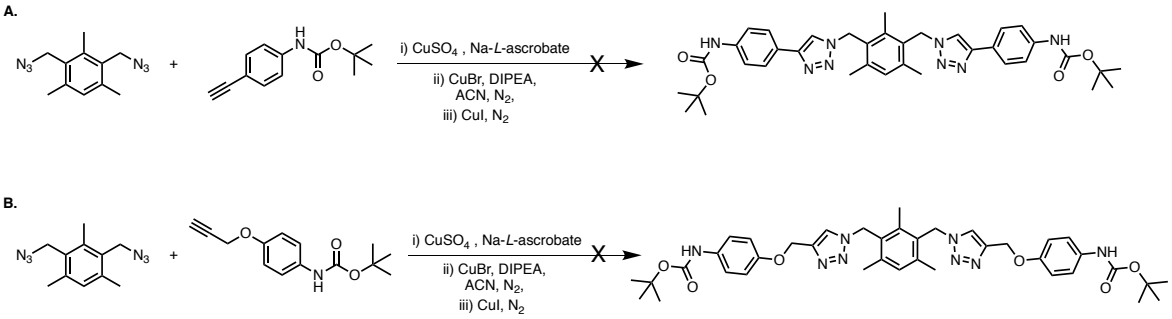

Scheme IV-19. Attempted synthesis of di-azide with (**A**) boc-4-ethynylaniline and (**B**) Boc-4-(2-propynyloxy) aniline.

In a final attempt to prepare a para-substituted ethynylaniline Tri-Click scaffold, 1-ethynyl-4-nitrobenzene was employed. The synthesis of the Tri-Click scaffold is outlined in Scheme IV-20, where catalytic loading of $CuSO_4$ (1%) resulted in the precipitation of the desired scaffold as a pink solid in high yield, 93%. Nitrobenzene can be easily converted to phenylamine using a mixture of tin and concentration HCl, the mixture was typically refluxed for up to 1 h to allow for the full conversion

into phenylammonium ions, which can be neutralised using sodium hydroxide. When this approached was attempted degradation of the triazole ring was identified by ^{1}H NMR. The conditions required to reduce the nitro group proved excessively harsh for the triazole rings present and sodium borohydride was then attempted as per literature procedures[56] but unfortunately product degradation was also observed. Lastly, catalytic hydrogenation with palladium on carbon (Pd/C) was attempted. This reaction was attempted using 10% Pd/C with constant hydrogen bubbling through the system over a prolonged period. The reaction was monitored by TLC and ^{1}H NMR, reduction of the nitro groups were successful however over reduction was observed resulting in the opening of the triazole ring. Although attempted reduction of the nitro Tri-Click product was deemed unsuccessful, the nitro-product was included for nucleic acid screening.

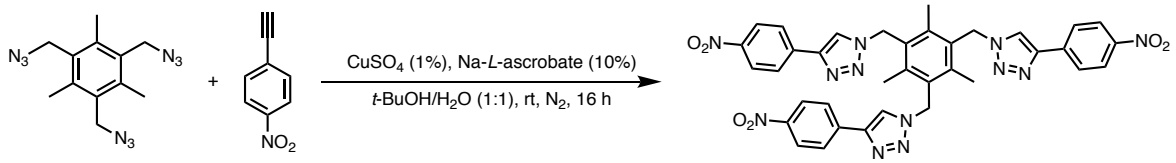

Scheme IV-20. Reactions conditions for the preparation of the Tri-Click 1-ethynyl-4-nitrobenzene scaffold.

IV. 4.5. Development of polyamine controls

As a series of Tri-Click products have been targeted as potential lead compounds, it was important to consider compounds without triazole substituents that will allow a clear comparison to related polyamine structures. For this purpose, three polyamines were selected and are shown in Figure IV-12. Each structure retains the mesitylene core with varying polyamine chains, the simplest of them being 3,5-*tris*(aminomethyl)-2,4,6-trimethyl benzene (Tri-amine), which has the potential to have a 3+ charge in solution. The other two polyamine controls, on the other hand, have the potential to have up to 6+ charge in solution.

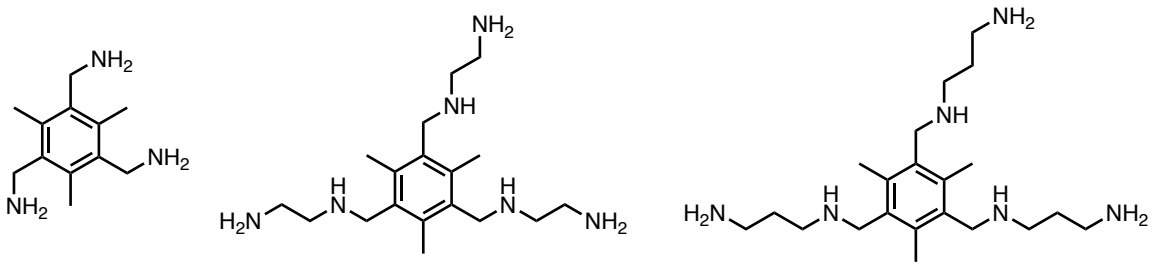

Figure IV-12. Molecular structures of control polyamines. **Left**: 1, 3, 5-tris(aminomethyl)-2, 4, 6-trimethyl benzene (Tri-amine); **Centre:** N^1,$N^{1'}$,$N^{1''}$-((2,4,6-trimethylbenzene-1,3,5-triyl) tris(methylene)) tris(ethane-1,2-diamine); **Right***:* N^1,$N^{1'}$,$N^{1''}$-((2,4,6-trimethylbenzene-1,3,5-triyl)tris(methylene)) tris(propane-1,3-diamine).

All three control compounds were previously reported in the literature and were prepared according to reported procedures. The preparation of the tri-amine scaffold was carried out as per literature procedures from the triazide starting material previously generated.[39,57,58] For the preparation of N^1,$N^{1'}$,$N^{1''}$-((2,4,6-trimethylbenzene-1,3,5-triyl) *tris*(methylene)) *tris*(ethane-1,2-diamine) and N^1,$N^{1'}$,$N^{1''}$-((2,4,6-trimethylbenzene-1,3,5-triyl)*tris*(methylene)) *tris*(propane-1,3-diamine) slight modifications to the literature procedure were carried out.[59] Apart from the preparation of the triamine scaffold, the preparation of these scaffolds heavily relies on the complete conversion of the product and volatile starting diamine reagents for a means of purification. The conditions used for this type of S_N2 reaction would not transfer as easily to a wider range of ligands and thus would require significant reaction optimisation.

IV. 5. Conclusion

Preliminary results identified cytotoxicity towards the CHO-K1 mammalian cell line by the C_3-opioid **OC3**. While this cytotoxic response was not desirable, further development and screening of related compounds may facilitate the discovery of biocompatible C_3 analogues. Non-opioid scaffolds **NAM1** and **NAM2** bearing an imidazole linking chain from the mesitylene core were identified as nucleic acid binding agents, inducing condensation at moderate concentrations of 75 μM (**NAM1**). These results highlighted that DNA condensation can occur through non-opioid C_3 scaffolds and a library of Tri-Click scaffolds was developed.

The CuAAC reaction was exploited in the preparation of novel C_3-Tri-Click scaffolds for the development of new class of DNA condensing agents. These systems were modelled from the previously developed C_3-opioid scaffolds resulting in a simplified polyamine structure. In total, ten Tri-Click scaffolds were prepared, including primary, secondary, and tertiary terminal amines along with a bromo, hydroxyl and nitro end terminal end group. The majority of the reagents and starting materials were commercially available and only moderate modifications were required prior to the final click reaction. Where we experienced difficulties at first with the classical means of generating the copper(I) ions required through the reduction of $CuSO_4$ *in situ*, the alternative method of a direct copper(I) source such as CuBr was found to be a suitable reaction condition yielding moderate to high yields.

The synthesis of a 4-ethynylaniline Tri-Click scaffold was challenging and attempts with Boc and phthalimide protection yielded no success. An alternative ligand 4-(2-propynyloxy) aniline was also unable to undergo formation to a Tri-Click product. The attempted synthesis of mono and di-azide mesitylene cores did not shed any light to why a para substituted scaffold results in limited reactivity. A nitro-benzene scaffold was successfully synthesised, however, and followed desirable click reaction conditions described by Sharpless. Here, catalytic loading of $CuSO_4$ (1%) was used and the product was easily isolated as a pink precipitate in high yield (93%). Although attempted reduction of the nitro Tri-Click product was unsuccessful, the nitro-product was included for nucleic acid screening.

Finally, to allow for a direct comparison, three C_3-polyamines were prepared for nucleic acid screening. Each structure retains the mesitylene core with varying polyamine chains with the simplest of them being 3,5-*tris*(aminomethyl)-2,4,6-trimethyl benzene (Tri-amine), which has the potential to become a 3+ solution cation. The other polyamine controls have the potential to have up to 6+ charge in solution.

IV. 6. References

1 A. G. Schätzlein, *J. Biomed. Biotechnol.*, **2003**, 2, 149–158.

2 M. A. Mintzer and E. E. Simanek, *Chem. Rev.*, **2009**, 109, 259–302.

3 N. McStay, Z. Molphy, A. Coughlan, A. Cafolla, V. Mckee, N. Gathergood and A. Kellett, *Nucleic Acids Res.*, **2017**, 45, 527–540.

4 T. Inao, Y. Kawabe, T. Yamashiro, Y. Kameyama, X. Wang, A. Ito and M. Kamihira, *J. Biosci. Bioeng.*, **2015**, 120, 99–106.

5 J. S. Lee, T. B. Kallehauge, L. E. Pedersen and H. F. Kildegaard, *Sci. Rep.*, **2015**, 5, 1–11.

6 X. Cai, Y. Li, D. Yue, Q. Yi, S. Li, D. Shi and Z. Gu, *J Mater Chem B*, **2015**, 3, 1507–1517.

7 M. H. Allen, M. D. Green, H. K. Getaneh, K. M. Miller and T. E. Long, *Biomacromolecules*, **2011**, 12, 2243–2250.

8 J. Li, J. Zhao, J. Gao, J. Liang, W. Wu and L. Liang, *New J. Chem.*, **2016**, 40, 7222–7228.

9 M. H. Allen, K. N. Day, S. T. Hemp and T. E. Long, *Macromol. Chem. Phys.*, **2013**, 214, 797–805.

10 V. A. Bloomfield, *Curr. Opin. Struct. Biol.*, **1996**, 6, 334–341.

11 G. S. Manning, *Q. Rev. Biophys.*, **1978**, 11, 179–246.

12 N. Alhashimy, D. J. Brougham, J. Howarth, A. Farrell, B. Quilty and K. Nolan, *Tetrahedron Lett.*, **2007**, 48, 125–128.

13 J. Howarth and N. A. Al-Hashimy, *Tetrahedron Lett.*, **2001**, 42, 5777–5779.

14 A. Prisecaru, Z. Molphy, R. G. Kipping, E. J. Peterson, Y. Qu, A. Kellett and N. P. Farrell, *Nucleic Acids Res.*, **2014**, 42, 13474–13487.

15 H. Debus, *Ann. Chem. Pharm.*, **1858**, 107, 199–208.

16 T. Benincori, E. Brenna and F. Sannicolo, *J. Chem. Soc. Perkin 1*, **1993**, 675.

17 J. Wildeman, O. H. Oldenziel and A. M. Van Leusen, *J. Org. Chem.*, **1977**, 42, 1153–1159.

18 E. Vessally, S. Soleimani-Amiri, A. Hosseinian, L. Edjlali and A. Bekhradnia, *RSC Adv*, **2017**, 7, 7079–7091.

19 C. W. Tornøe, C. Christensen and M. Meldal, *J. Org. Chem.*, **2002**, 67, 3057–3064.

20 H. C. Kolb, M. G. Finn and K. B. Sharpless, *Angew. Chem. Int. Ed.*, 2001, 40, 2004–2021.

21 R. Huisgen, *Angew. Chem. Int. Ed. Engl.*, **1963**, 2, 633–645.

22 R. Huisgen, *Angew. Chem. Int. Ed. Engl.*, **1963**, 2, 565–598.

23 C. D. Hein, X.-M. Liu and D. Wang, *Pharm. Res.*, **2008**, 25, 2216–30.

24 H. C. Kolb and K. B. Sharpless, *Drug Discov. Today*, **2003**, 8, 1128–1137.

25 W. Xi, S. Pattanayak, C. Wang, B. Fairbanks, T. Gong, J. Wagner, C. J. Kloxin and C. N. Bowman, *Angew. Chem. Int. Ed.*, **2015**, 54, 14462–14467.

26 Y. H. Lau, P. J. Rutledge, M. Watkinson and M. H. Todd, *Chem. Soc. Rev.*, **2011**, 40, 2848–66.

27 Q. Xie, X. Weng, L. Lu, Z. Lin, X. Xu and C. Fu, *Biosens. Bioelectron.*, **2016,** 77, 46–50.

28 R. Duncan, *Nat. Rev. Drug Discov.*, **2003**, 2, 347–360.

29 J. McNulty, K. Keskar and R. Vemula, *Chem. Eur. J.*, **2011**, 17, 14727–14730.

30 J. McNulty and K. Keskar, *Eur. J. Org. Chem.*, **2012**, 5462–5470.

31 G. Wittig and A. Krebs, *Chem. Ber.*, **1961**, 94, 3260–3275.

32 N. J. Agard, J. A. Prescher and C. R. Bertozzi, *J. Am. Chem. Soc.*, **2004**, 126, 15046–15047.

33 J. A. Codelli, J. M. Baskin, N. J. Agard and C. R. Bertozzi, *J. Am. Chem. Soc.*, **2008**, 130, 11486–11493.

34 J. C. Jewett and C. R. Bertozzi, *Chem. Soc. Rev.*, **2010**, 39, 1272.

35 E. M. Sletten and C. R. Bertozzi, *Acc. Chem. Res.*, **2011**, 44, 666–676.

36 X. Ning, J. Guo, M. A. Wolfert and G.-J. Boons, *Angew. Chem. Int. Ed.*, 2008, **47**, 2253–2255.

37 S. G. Agalave, S. R. Maujan and V. S. Pore, *Chem. - Asian J.*, **2011**, 6, 2696–2718.

38 V. V. Rostovtsev, L. G. Green, V. V. Fokin and K. B. Sharpless, *Angew. Chem. Int. Ed Engl.*, **2002,** 41, 2596–2599.

39 J. L. Nallasivam and R. A. Fernandes, *Eur. J. Org. Chem.*, **2015**, 2012–2022.

40 H. Chachignon, N. Scalacci, E. Petricci and D. Castagnolo, *J. Org. Chem.*, **2015**, 80, 5287–5295.

41 B. M. Partridge, S. P. Thomas and V. K. Aggarwal, *Tetrahedron*, **2011**, 67, 10082–10088.

42 N. H. Nguyen, J. W. Apriletti, J. D. Baxter and T. S. Scanlan, *J. Am. Chem. Soc.*, **2005**, 127, 4599–4608.

43 M. J. Deetz, C. C. Forbes, M. Jonas, J. P. Malerich, B. D. Smith and O. Wiest, *J. Org. Chem.*, **2002**, 67, 3949–3952.

44 A. Paul, J. Einsiedel, R. Waibel, F. W. Heinemann, K. Meyer and P. Gmeiner, *Tetrahedron*, **2009**, 65, 6156–6168.

45 L. Fomina, J. G. Sánchez, J. A. Olivares, F. L. S. Cuppo, L. E. Sansores and R. Salcedo, *J. Mol. Struct.*, **2014**, 1074, 534–541.

46 M. M. D. Cominetti, S. A. Goffin, E. Raffel, K. D. Turner, J. C. Ramoutar, M. A. O'Connell, L. A. Howell and M. Searcey, *Bioorg. Med. Chem. Lett.*, **2015**, 25, 4878–4880.

47 R. Neelarapu, D. L. Holzle, S. Velaparthi, H. Bai, M. Brunsteiner, S. Y. Blond and P. A. Petukhov, *J. Med. Chem*., **2011**, 54, 4350–4364.

48 K. Tanaka, C. Kageyama and K. Fukase, *Tetrahedron Lett.*, **2007**, 48, 6475–6479.

49 J. I. Sarmiento-sánchez, A. Ochoa-terán and I. A Rivero, *Arkivoc*, **2011**, 177–188.

50 P. Jagadesan, T. Whittemore, T. Beirl, C. Turro and P. L. McGrier, *Chem. - Eur. J.*, **2017**, 23, 917–925.

51 S. Stahlová, J. Sedláček, J. Svoboda, M. Polášek and J. Zedník, *Aust. J. Chem.*, **2015**, 68, 1237–1248.

52 P. M. Hergenrother, *J. Heterocycl. Chem.*, **1980**, 17, 5–10.

53 C. Wu, E. R. Decker, N. Blok, H. Bui, Q. Chen, B. Raju, A. R. Bourgoyne, V. Knowles, R. J. Biediger, R. V. Market, S. Lin, B. Dupré, T. P. Kogan, G. W. Holland, T. A. Brock and R. A. F. Dixon, *J. Med. Chem.*, **1999**, 42, 4485–4499.

54 Y. Bai, X. Feng, H. Xing, Y. Xu, B. K. Kim, N. Baig, T. Zhou, A. A. Gewirth, Y. Lu, E. Oldfield and S. C. Zimmerman, *J. Am. Chem. Soc.*, **2016**, 138, 11077–11080.

55 J. R. Thomas, X. Liu and P. J. Hergenrother, *J. Am. Chem. Soc.*, **2005**, 127, 12434–12435.

56 S. Piña, D. M. Cedillo, C. Tamez, N. Izquierdo, J. G. Parsons and J. J. Gutierrez, *Tetrahedron Lett.*, **2014**, 55, 5468–5470.

57 N. De Rycke, F. Couty and O. R. P. David, *Tetrahedron Lett.*, **2012**, 53, 462–466.

58 J. N. Moorthy and S. Saha, *Eur. J. Org. Chem.*, **2010**, 6359–6365.

59 M. Sawicki, D. Lecerclé, G. Grillon, B. Le Gall, A.-L. Sérandour, J.-L. Poncy, T. Bailly, R. Burgada, M. Lecouvey, V. Challeix, A. Leydier, S. Pellet-

Rostaing, E. Ansoborlo and F. Taran, *Eur. J. Med. Chem.*, **2008**, 43, 2768–2777.

Chapter V

DNA Recognition by Novel C_3-Symmetric "Tri-Click" Scaffolds

This chapter details the DNA recognition screening and profiling of compounds generated from Chapter IV. This chapter is anticipated to be published along with the detailed synthesis described in Chapter IV. Referencing style is Royal Society of Chemistry.

V. 1. Introduction

Gene therapy has gained sustainable attention in the fight against prominent diseases and cancers, however, significant barriers exist in the effective delivery of nucleic acid targets. Gene therapy relies on a method of delivery that is efficient, non-toxic, specific and high-throughput; yet delivery options are limited. Viral vectors are the prevailing method of choice for on-going clinical trials, with an average of up to 70% usage.[1] Although they are a popular option, they come with serious risks including, inflammation, carcinogenesis, immunogenicity, limited DNA packaging and difficult reproducible vector production.[2,3] The FDA recently approved the first gene therapy in the U.S. to treat patients with a rare form of inherited vision loss, voretigene neparvovecrzyl under the trade name Luxturna.[4,5] This therapy is transported via an altered adeno-associated virus that can cause mild immune response highlighting the need for an improved delivery system with little to no side effects.[6] Thus, there is a need to develop new non-viral vectors.[7] For the purpose of this project our focus is on polyamine-based cationic vectors. Numerous natural and synthetic polyamines have been used and developed as vectors for gene therapy. Natural occurring polyamines include proteins such as histones and amino polysaccharides such as chitosan. Synthetic analogues include peptides such as poly-*L*-lysine, poly-*L*-ornithine and polyamines such as polyethylenimine (PEI), where both linear and dendritic derivatives have shown efficient gene delivery.[8] Although these compounds offer promising results they still suffer from low efficiency and in some cases their toxicity profile overshadows their transfection abilities.

1,2,3-Triazole based heterocycles have attractive linking groups for the generation of numerous medicinal scaffolds for applications as anti-HIV, anticancer, antibacterial, and antimicrobial, to name but a few.[9] 1,2,3-Triazoles are stable towards hydrolysis, oxidative/reductive conditions, and enzymatic degradation. They participate in hydrogen bonding which can aid in solubility properties. There are only a limited number of triazole-based compounds reported to condense DNA. For example, Yue *et al*. reported coumarin containing scaffolds prepared through a CuAAC reaction that showed effective DNA condensation.[10]

Our interest focuses on polyamine-DNA interactions towards condensation of nucleic acids for gene delivery due to their chemical diversity and immense potential

for functionalization.[11] Polyamines are positively charged organic cations under physiologic ionic and pH conditions and thus interact with negatively charged macromolecules such as DNA and RNA causing a collapse of the phosphodiester backbone resulting in nanoparticles of nucleic acid/polyamine constructs.[12] Through incorporation of a triazole ring via CuAAC chemistry we aim to improve solubility and reduce toxicity while maintaining a high nitrogen content.[10]

V. 2. Tri-Click Screening

A series of 8 Tri-Click compounds were generated by CuAAC reaction to form tripodal amine containing scaffolds. These compounds contain either primary, secondary, or tertiary polyamine reactive handles that will allow protonation at physiological pH with a charge of up to 3+ in solution—the charge required to induce the collapse the helical backbone of DNA. The structures of these Tri-Click products are detailed in Figure V-1. The Tri-Click propargylamine series (**TC1-3**) is the simplest of the series containing a simple amine handle in a 1,4-disubstitued triazole linked to the core mesitylene ring by one carbon spacer between each functional group. **TC1** is by far the simplest scaffold of the entire series with three primary amines, whereas **TC3** contains three tertiary amines which could be directly compared to our previous C_3-opioid series also containing tertiary amines. The Tri-Click ethynylaniline series (**TC4-7**) provides a rigid reactive amine handle with increased distance to the centre core which in turn could offer additional comparisons to that of the C_3-opioid series. **TC8** is the only nitro-containing compound present in the Tri-Click series. This compound is anticipated to act as a neutral, non-cationic nucleic acid agent.[13]

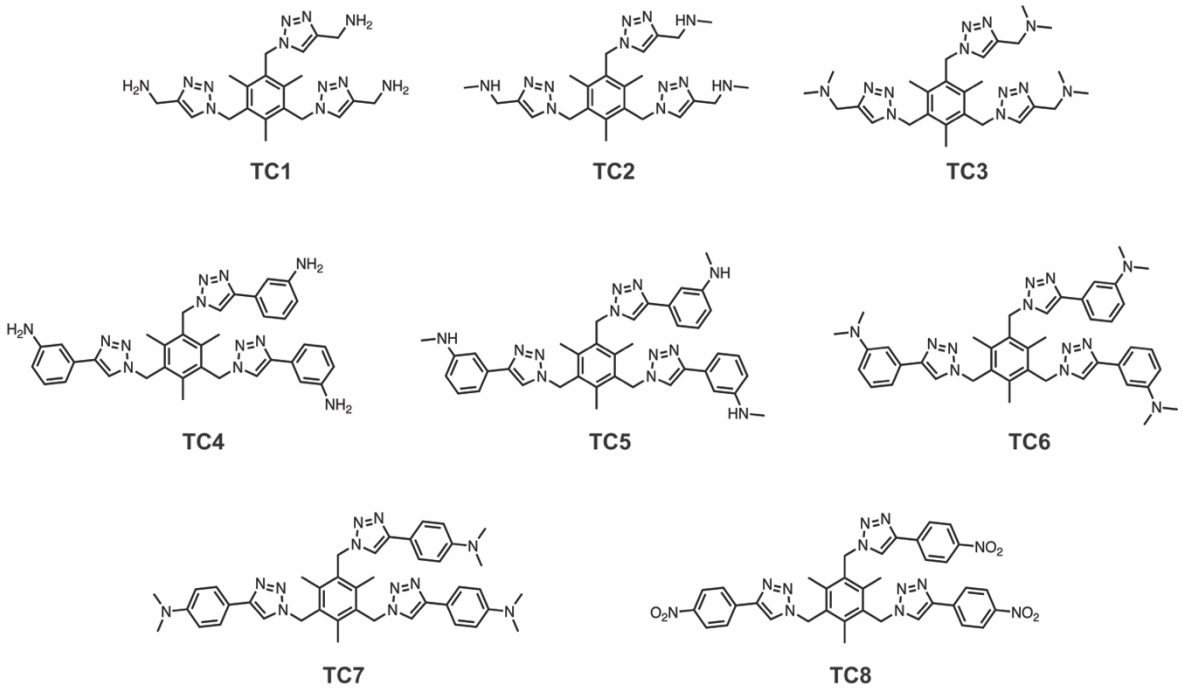

Figure V-1. Molecular structures of Tri-Click Series **TC1-8**.

It was advantageous to prepare similar Tri-Click scaffolds that did not contain a reactive amine handle to ensure the triazole ring does not have secondary interactions when tested. Ideally the triazole ring should be a neutral analogue in the series that will offer improved solubility properties as shown in the literature.[14] Two controls were generated, **TC9** and **TC10** (Figure V-2), where neither contains any additional nitrogen atoms except those of the triazole ring but rather a bromine and hydroxyl group. It was also important for a full structure activity relationship profile to prepare the most simplified tripodal amine and analogues of such. For this purpose, 1,3,5-*tris*(aminomethyl)-2,4,6-trimethyl benzene (tri-amine, **T1**) was prepared. Similarly, **TC2** and **TC3** were prepared, however these compounds have the capability to retain up to a 6+ charge in solution (Figure V-2).

Typically, compounds are screened in the group by our high-through put ethidium bromide displacement assay.[15,16] This assay can provide in-depth analysis on the ability of a compound to bind with DNA, however, the assay lacks the ability to recognise direct nucleic acid condensation. Due to this limitation, gel electrophoresis was employed as an efficient screening method for the visualisation and quantification of any nucleic acid condensation.

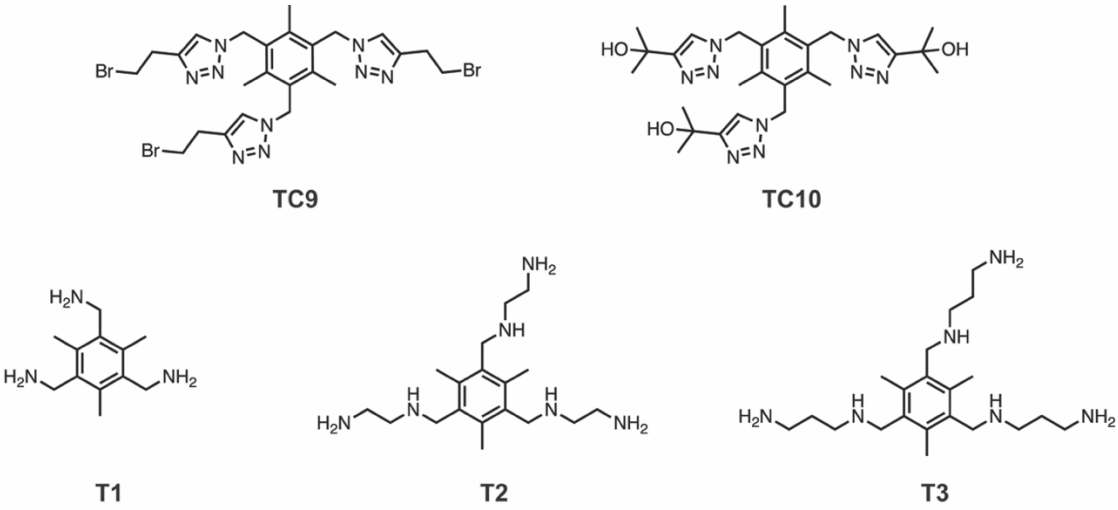

Figure V-2. Molecular structures of Tri-Click control compounds, **TC9-10** and **T1-3**.

V. 2.1. pUC19 condensation

TC1 was selected as an ideal starting point in the screening of the Tri-Click library; since this scaffold is the simplest of the reactive amine handles, testing this compound offered some insight into the activity profile of this new class of DNA recognition agents. **TC1** was titrated against supercoiled pUC19 plasmid DNA encompassing the lacZα gene, before incubation for 90 min prior to analysis by agarose gel electrophoresis, Figure V-3. Reactions were carried out in both neutral (HEPES buffer, 80 mM, pH 7.2) and acidic conditions (NaOAc, 80 mM, pH 4.0) to ensure complete protonation of the amine scaffold while retaining intact supercoiled plasmid. Carrying out reactions in extreme acidic environments could induce unwanted DNA damage and thus the pH was maintained at 4.0. For example, under low pH (<2.0) both RNA and DNA hydrolyse resulting in the phosphodiester back bone breaking, however in high pH (>11.0) RNA under goes hydrolyses, while DNA will denature but the phosphodiester backbone remains intact.[17] **TC1** was found to condense supercoiled DNA where the onset of aggregation occurs at 5 μM, beyond which native DNA bands become fainter in appearance or disappear entirely from view thus reflecting total condensation at 500 μM in both gels at pH 7.2 and pH 4.0, Figure V-3. Although the appearance of condensation occurs at a low concentration the concentration required to fully condense DNA does not compare to the more potent opioid series. The C_3-opioids were capable of inducing complete condensation at 10 μM. There was no significant improvement in the aggregation profile of **TC1** under acidic condition at the incubation times tested.

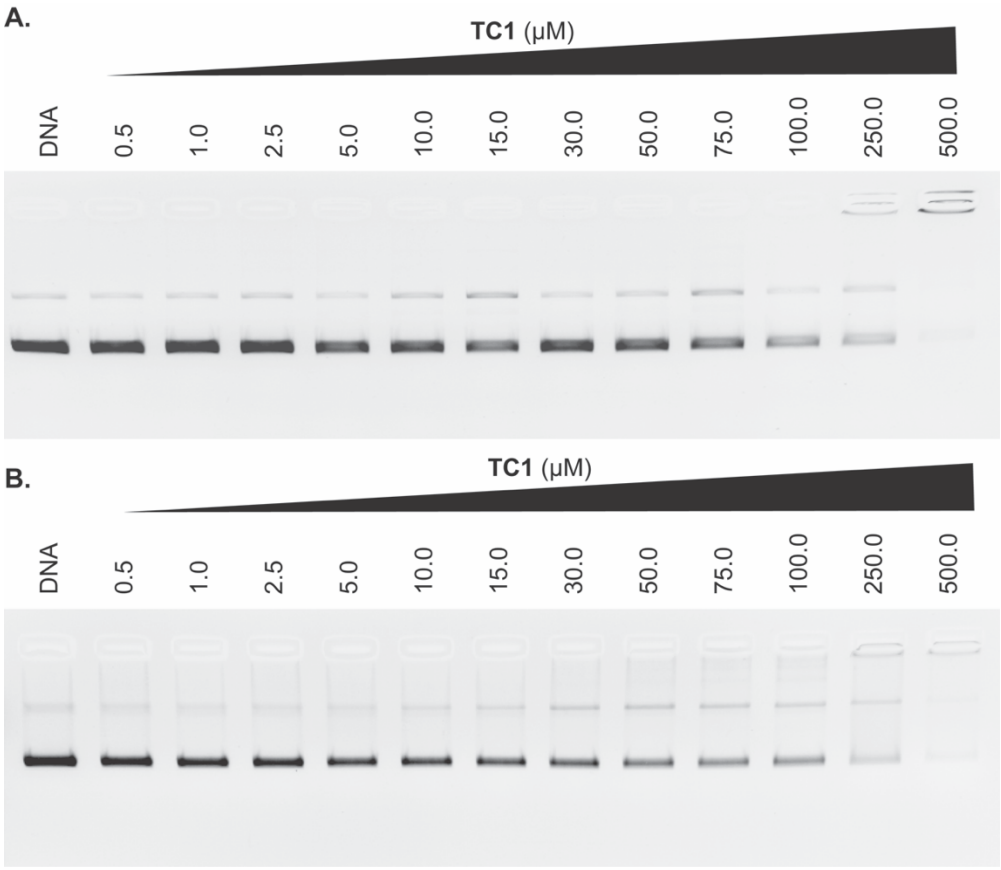

Figure V-3. Agarose gel electrophoresis of supercoiled (400 ng) pUC19 exposed to increasing concentrations of **TC1** prepared in **A.** neutral HEPES buffer (80 mM, pH 7.2) and **B.** acidic buffer (NaOAc 80 mM, pH 4.0). Reactions were carried out in the presence of 25 mM NaCl for 90 mins at 37˚C prior to electrophoretic analysis. Reactions were quenched by adding 6x loading buffer (Fermentas) containing 10 mM Tris-HCl, 0.03% bromophenol blue, 0.03% xylene cyanole FF, 60% glycerol, 60 mM EDTA and samples were loaded onto an agarose gel (1.2%) containing 4 μl EtBr. Electrophoresis was completed at 70 V for 1 h in 1x TAE buffer.

TC2-**TC8** were screened at fixed concentrations of 100 and 500 μM under the same conditions as per **TC1**. Gel electrophoresis of the remaining Tri-Click samples under neutral pH (7.2) highlighted both **TC6** and **TC7** to have low condensation properties as shown by the electrophoretic banding pattern, however these compounds were not able to fully condense the plasmid DNA at test concentrations. Concentrations of drug loading above 500 μM was deemed undesirable for future work. **TC8** induced DNA damage by causing a single strand break which renders the supercoiled plasmid (form I) into its open circular/nicked form (form II), Figure V-4A. Surprisingly, the results of the gel electrophoresis under acidic pH (4.0), Figure V-4B, highlights Tri-Click compounds **TC2**, **TC4**, and **TC5** along with **TC8** are capable of inducing single strand breaks after 90 min incubation with plasmid DNA. This

potentially opens a new avenue for the Tri-Click series, the development of small molecules capable of nucleic acid cleavage is of considerable research interest for applications as biotechnological tools and nucleic-acid targeting therapeutics. Nucleic acid polymers are stable towards hydrolysis under physiological conditions and thus generating agents to efficiently target and cleave DNA has been an ongoing battle. Classical examples of chemical nucleases include 1,10-phenanthroline-copper complexes reported by Sigman,[18] however macrocyclic polyamines are also capable of nucleic acid cleavage.[19]

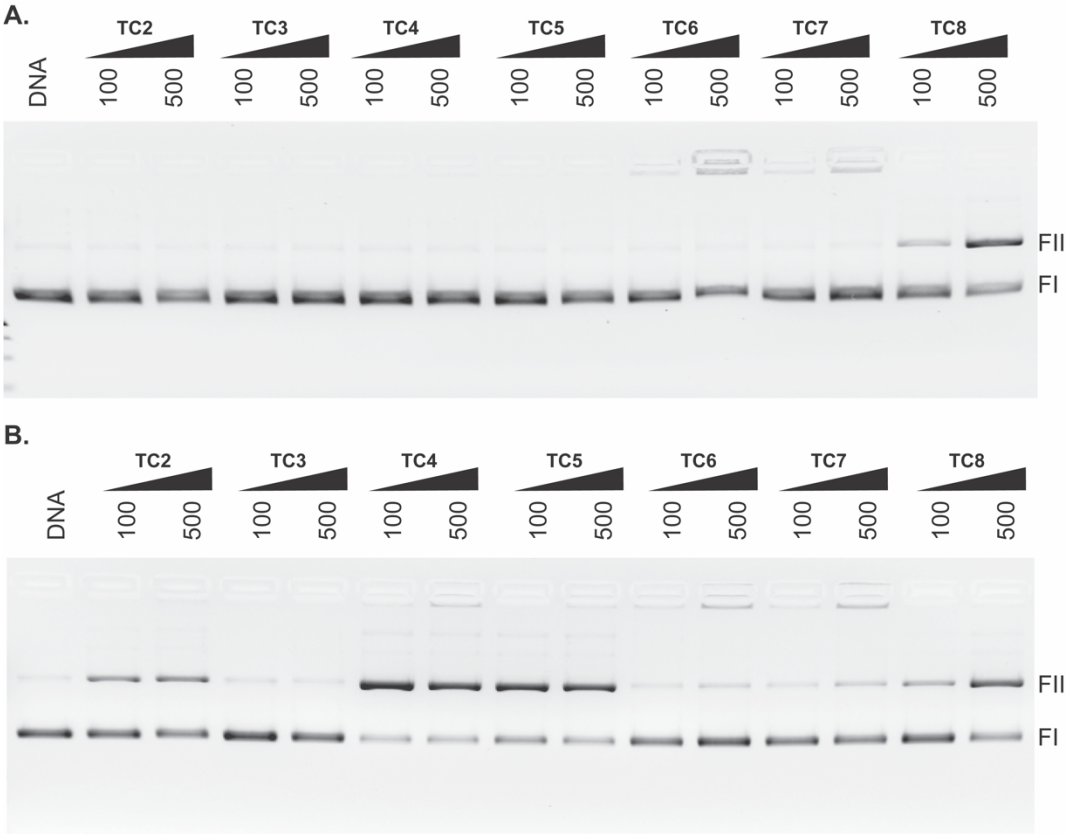

Figure V-4. Agarose gel electrophoresis of supercoiled (400 ng) pUC19 exposed to Tri-Click samples (**TC2-8**) at concentrations of 100 and 500 μM prepared in **A.** HEPES buffer (80 mM, pH 7.2) and **B.** acidic buffer (NaOAc 80 mM, pH 4.0). Reactions were carried out in the presence of 25 mM NaCl for 90 mins at 37 ˚C prior to electrophoretic analysis as described previously.

The control compounds **TC9**, **TC10** and **T1-3** were incubated with pUC19 plasmid for 90 min at pH 7.0, where both Tri-Click compounds **TC9** and **TC10** are unable to induce any condensation and show no signs of DNA damage under experimental conditions tested (Figure V-5A-B). Tripodal polyamines **T1-3** have considerable condensation properties (Figure V-5A) where **T1** shows condensation at 500 μM,

however complete condensation is not shown were visible supercoiled DNA remains. **T2** and **T3** both have the potential to retain a 6+ charge under physiological pH and as expected have extensive nucleic acid condensation properties. No visible bands are present for **T3** at test concentrations, whereas a faint presence of supercoiled DNA is shown for **T2** at 100 μM. These compounds were previously synthesised and reported as precursors for the preparation of a series of bisphosphonate sequestering agents.[20]

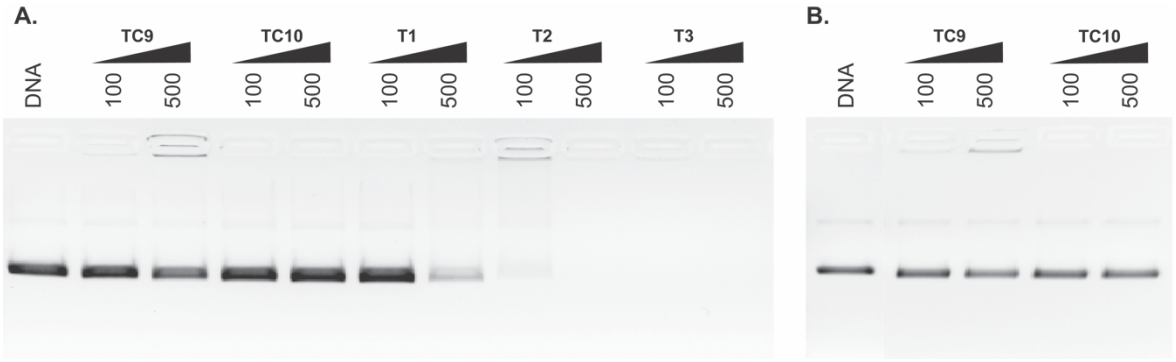

Figure V-5. Agarose gel electrophoresis of supercoiled (400 ng) pUC19 exposed to Tri-Click samples (**TC9, TC10**) and controls (**T1-3**) at concentrations of 100 and 500 μM prepared in **A**. HEPES buffer (80 mM, pH 7.2) and **B.** acidic buffer (NaOAc 80 mM, pH 4.0). Reactions were carried out in the presence of 25 mM NaCl for 90 mins at 37 ˚C prior to electrophoretic analysis as described previously.

V. 2.2. Influence of pH

We have previously shown after 90 mins incubation at 37 ˚C, that these compounds induce single strand nicking, however some intact supercoiled DNA remains. We postulated that over a prolonged period these compounds could induce clustered DNA damaging effects. The degree of DNA damage was studied further under acidic conditions for **TC1**, **TC2**, **TC4**, **TC5**, and **TC8** over three time points between 6-24 h. The Tri-Click scaffolds were incubated with supercoiled DNA at concentrations of 25, 50, and 100 μM, gel electrophoresis results are shown in Figure V-6. At 6 h, Figure V-6A, a visible increase in the formation of form II DNA is present for the amine containing scaffolds, however supercoiled DNA is still present in faint bands. After 12 h, Figure V-6B, almost all supercoiled DNA is converted into its open circular form except for compound **TC8**, the nitro-Tri-Click scaffold. The appearance of linearized DNA (FIII) is evident for **TC4** at 12 h and is prominent for

TC1, **TC2**, and **TC5** at 24 h. Whilst this new series did not show condensation properties as anticipated, it has shown chemical nuclease properties.

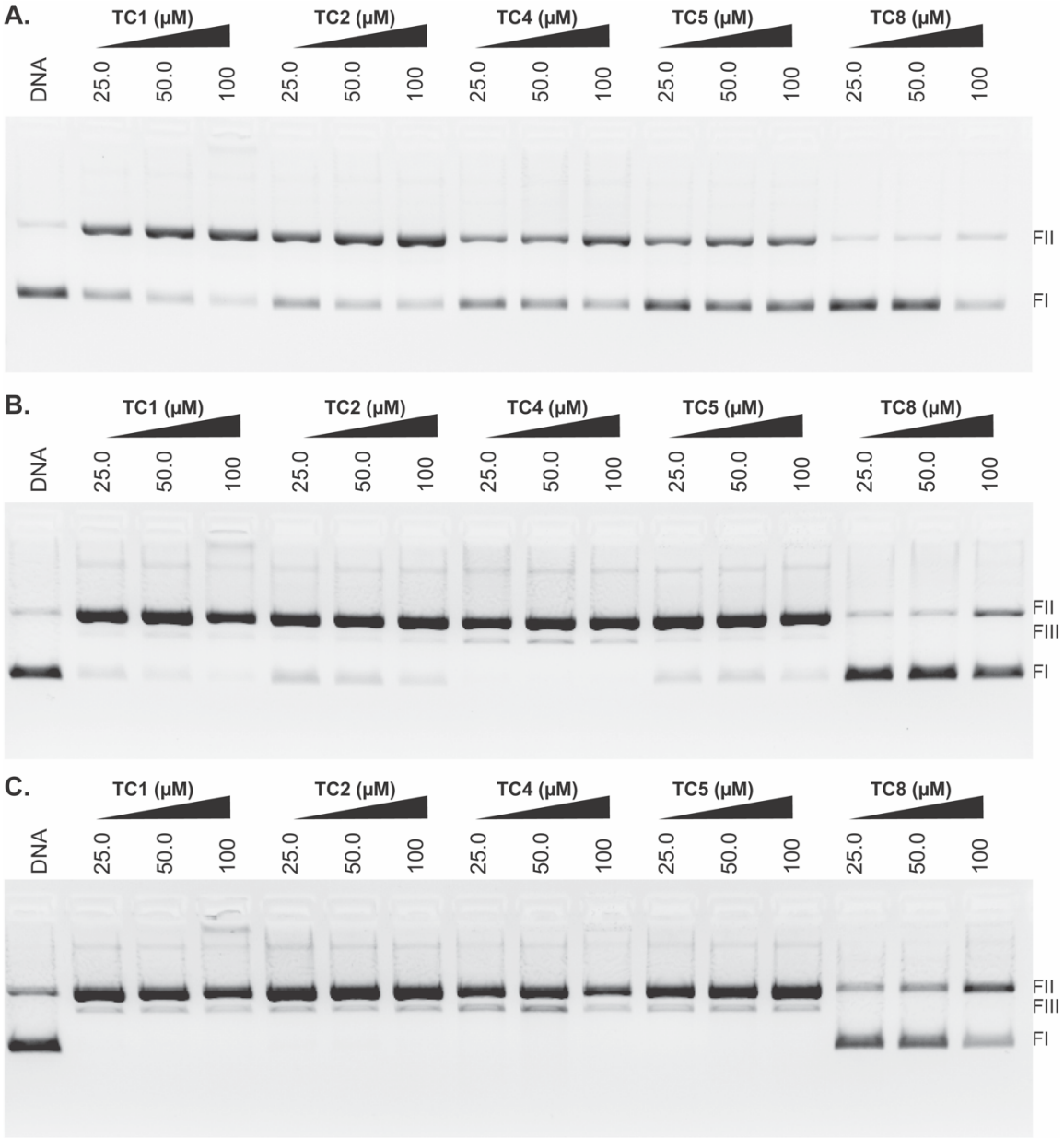

Figure V-6. Agarose gel electrophoresis of supercoiled (400 ng) pUC19 exposed to Tri-Click samples (**TC1**, **TC2**, **TC4**, **TC5**, and **TC8**) at fixed concentrations of 25, 50 and 100 μM, prepared in acidic buffer (NaOAc 80 mM, pH 4.0). Reactions were carried out in the presence of 25 mM NaCl for **A.** 6 h, **B.** 12 h and **C.** 24 h at 37˚C prior to electrophoretic analysis as described previously.

The full library of Tri-Click scaffolds (**TC1-8**) was examined to ensure a complete profile was obtained over acidic, neutral and basic conditions after 24 h. Each compound was incubated with plasmid DNA at test concentrations of 100 μM. Under acidic pH (4.0), Figure V-7A, **TC1**, **TC2**, and **TC4** show complete conversion to open circular DNA with a faint presence of linear DNA, while the remaining compounds have converted up to 50% of the supercoiled plasmid into its open circular form. Some nucleic acid condensation is present for **TC1**, **TC6** and **TC7** by the electrophoretic banding pattern. Under neutral conditions, Figure V-7B, **TC1** and **TC8** are the only compounds to show nicking properties and under basic conditions (pH 9.0) where the amines are in their free base form, no DNA damage is evident and no condensation is observed, Figure V-7C. Thus, the amines must be in their protonated form to induce DNA damage. Interestingly the Tri-Click compounds containing a primary or secondary amine have the most potent DNA cleavage properties compared to those containing a tertiary amine group.

Aside from well-studied DNA damaging agents such as the ene-dienes, organic compounds containing simple amine groups are not generally associated with DNA cleavage. However, Li *et al*. reported on a metal free nuclease based on a poly(aspartic acid)-polyamine conjugate capable of double-strand cleavage.[21] They postulated a possible mechanism for the process of DNA double-strand cleavage by their polyamine compound, where the protonated polyamine contributes to the formation of a bis-amine cation/phosphate anion pair, which is connected via hydrogen bonds and electrostatic interactions. The phosphate backone of DNA can then be attacked by a free nucleophilic group.[21] A similar mechanism was proposed by Sheng *et al.*[22] where DNA cleavage involving a 1,4,7-triazacyclononane derivative with guanidinium and hydroxyethyl side arms was identified. The guanidinium group recognizes and binds to the anionic phosphodiester back bone through hydrogen bonding and electrostatic interactions.[23] While these examples provide potential clues as to how the Tri-Click series behave in an acidic environment with DNA, more work would be required to probe this in detail.

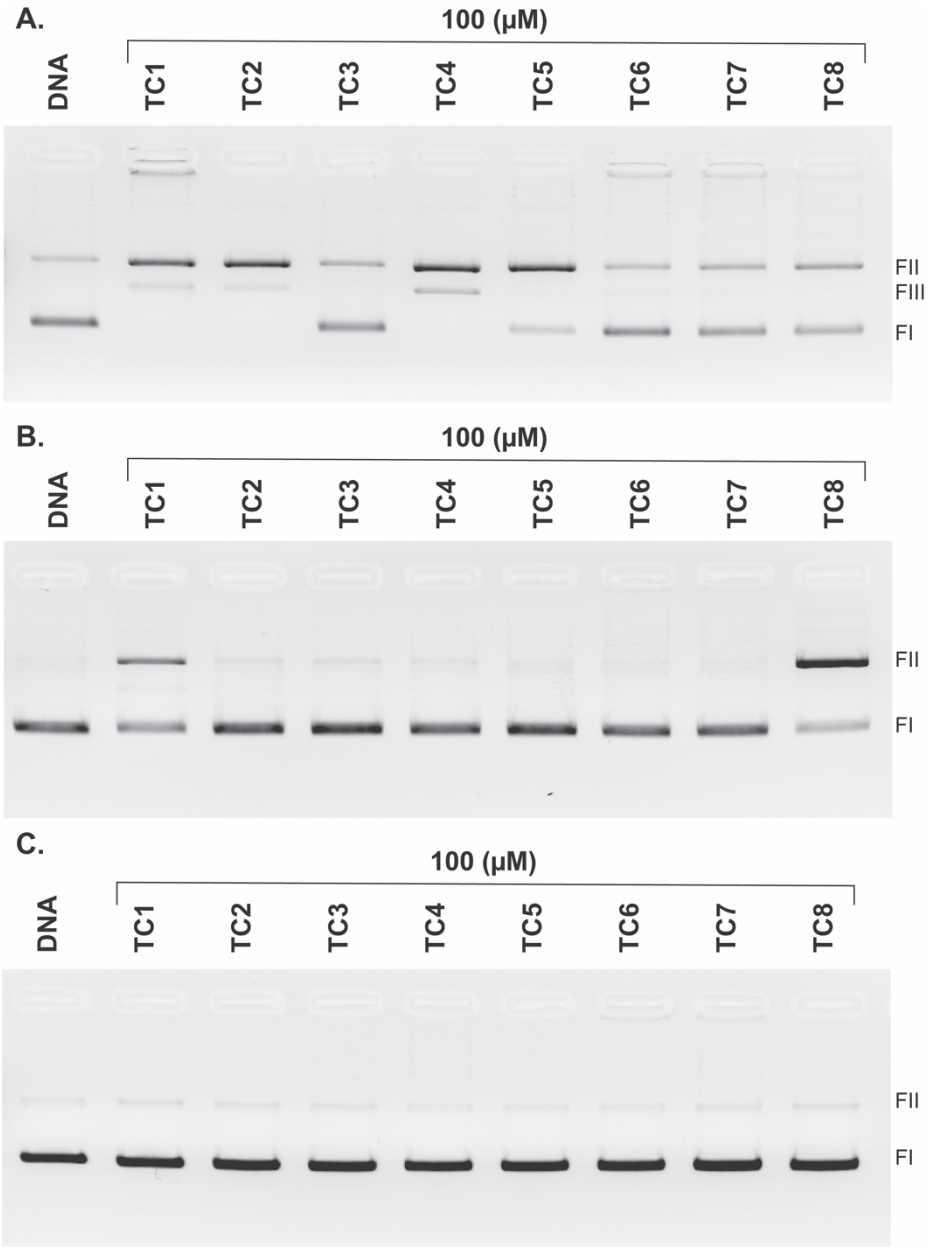

Figure V-7. Agarose gel electrophoresis of supercoiled (400 ng) pUC19 exposed to Tri-Click samples (**TC1-8**) at 100 μM. Reactions were carried out in **A.** Acidic NaOAc buffer (80 mM, pH = 4.0), **B.** neutral HEPES buffer (80 mM, pH = 7.2), and **C.** basic Tris buffer (80 mM, pH = 9.0) in the presence of 25 mM NaCl for 24 h at 37ºC prior to electrophoretic analysis as described previously.

To summarise results so far, the Tri-Click scaffolds were screened for nucleic acid recognition with the anticipation of DNA aggregation properties. These novel scaffolds, however, are capable of inducing DNA damage, in particular DNA cleavage in the absence of metal ions. DNA cleavage is prevalent for scaffolds containing either a primary (**TC1, TC4)** or secondary (**TC2, TC5**) amine reactive handle and is enhanced under acidic conditions when this handle is in its protonated form, however activity is completely inhibited under basic conditions (pH 9.0).

V. 2.3. Analysis in the presence of selected metal ions

The development of artificial nucleases is of great importance and significant work is ongoing within the group for the development of copper(II)[24–28] (direct) and manganese(II)[29] (indirect) based nucleases. As this series has already shown nuclease activity in the absence of metal ions, it was desirable to determine if any co-metal ion interactions could enhance activity. Thus, the Tri-Click scaffolds **TC1-8** were pre-incubated with copper(II), manganese(II) and zinc(II) to identify if any increase in cleavage occurred. Each scaffold was incubated with three molar equivalents of the metal ion for 30 min prior to the exposure to plasmid DNA. We hypothesised that up to three metal centres could coordinate to each of the three reactive amine handles extending from the mesitylene core. Copper(II), manganese(II), and zinc(II) (300 μM), and Tri-Click compounds (100 μM) were titrated against pUC19 plasmid in both neutral (pH 7.2, Figure V-8A) and acidic (pH 4.0, Figure V-8B) buffers for 90 min prior to gel electrophoresis methods. Controls included untreated plasmid and copper(II) treated DNA to ensure activity was not a result of reactive oxygen species (ROS) formed from the metal salt in solution.[30] Reactions were quenched with 6x loading buffer (Fermentas) containing 60 mM EDTA prior to gel electrophoresis procedure.

Interestingly, **TC1**-Cu(II) was the only copper compound from the entire Tri-Click library to induce DNA cleavage without the presence of a reducing agent. While we have shown that the Tri-Click library has DNA damaging properties, **TC1** has enhanced damaging effects in the presence of copper. This compound resembles a bidentate ligand, such as ethylenediamine, as there are two donor nitrogen atoms free to bind to copper(II) on each of the three sides of the mesitylene ring. **TC2**, however, only varies by the difference of one methyl group on the nitrogen atom and shows no DNA cleavage properties. The methyl group present may be orientated in such a way that is blocking the interaction to the copper(II) centre rendering the ligand unable to bind. Under acidic conditions there was no increase in activity found when co-incubated with a copper(II) salt, this may be due to the amines being in their protonated form which inhibits binding to the metal centre, Figure V-8B. The results with Mn(II) and Zn(II) showed no observable DNA cleavage or damage, Figure V-8C-D.

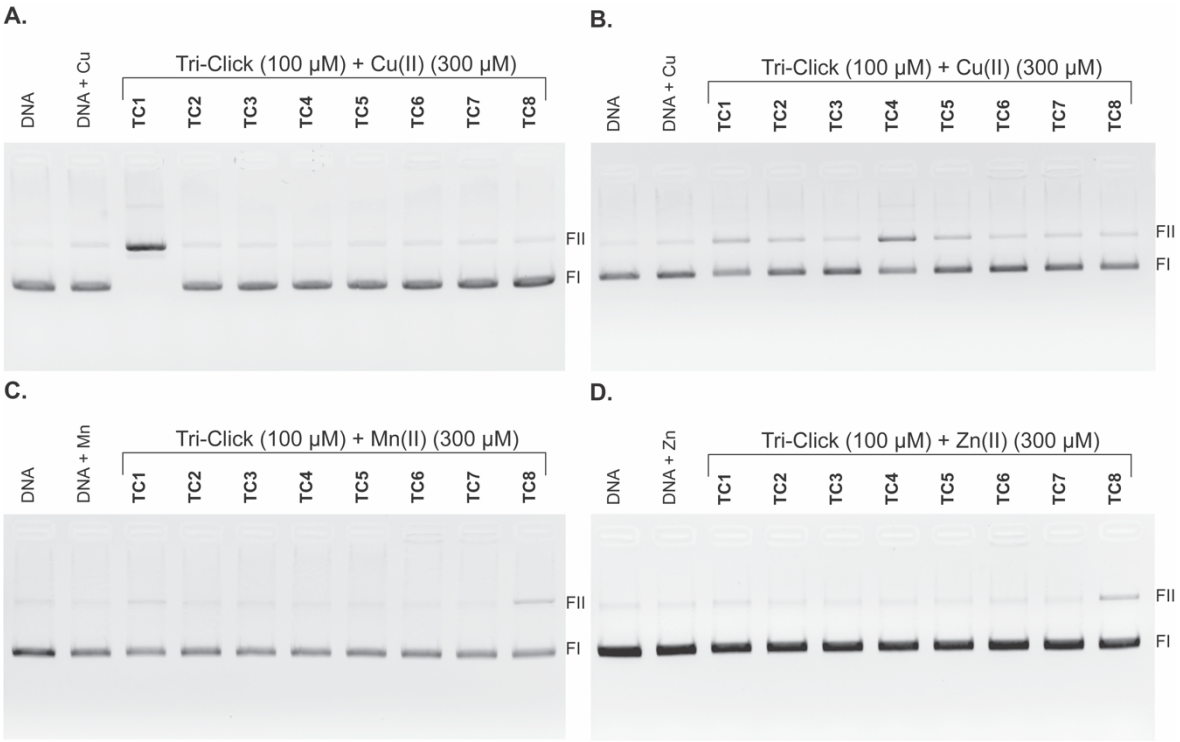

Figure V-8. Agarose gel electrophoresis of supercoiled (400 ng) pUC19 exposed to Tri-Click compounds at 100 μM in the presence of three equivalents of metal ions. Tri-Click samples were pre-incubated with 300 μM Cu(II) for 30 minutes before reactions were carried out in **A.** HEPES buffer (80 mM, pH = 7.2) and **B.** acidic NaOAc buffer (80 mM, pH = 4.2). Tri-Click samples were pre-incubated with 300 μM of Mn(II) and Zn(II) (**C-D**) for 30 minutes before reactions were carried out in HEPES buffer (80 mM, pH = 7.2) in the presence of 25 mM NaCl for 90 mins at 37 ºC prior to electrophoretic analysis. Reactions were quenched by adding 6x loading buffer (Fermentas) containing 10 mM Tris-HCl, 0.03% bromophenol blue, 0.03% xylene cyanole FF, 60% glycerol, 60 mM EDTA

V. 3. TC1 – Cu(II) complex

TC1 is the only compound that shows cleavage activity in the presence of copper(II) ions from the series of Tri-Click scaffolds and so the complex was examined in greater detail. Firstly, it was important to determine the correct ratio of ligand to metal and this was achieved by measuring the *d-d* transitions of the copper(II) complex in solution by UV-Vis spectroscopy, where the ratio of ligand was kept constant as the molar ratio of copper(II) salt was increased from 1 to 3, Figure V-9. The complex was allowed to equilibrate for 30 min at 37 ºC prior to measuring the absorbance. The UV-Vis spectra of **TC1** (2 mM) and Cu(II) nitrate (12 mM) alone was also recorded for direct comparison. At ratios of 1:1 the *d-d* transitions of the complex are evident at 591 nm, Figure V-9. The complex has shown to be fully coordinated to three copper(II) centres which is evident from the bathochromic shift

of 590 nm at ratios of 1:3 (**TC1**:Cu(II)). Ratios above 1:3 for the ligand:copper(II) complex were studied and are shown in Appendix E (E-3, Figure E1). Simple molecular modelling of the ligand using MolView software shown in Figure V-9. Here, it can be clearly seen that up to three copper(II) centres could bind to each of the three side arms extending from the mesitylene core, where the free terminal amine and the nitrogen present in the triazole ring could bind to copper(II).

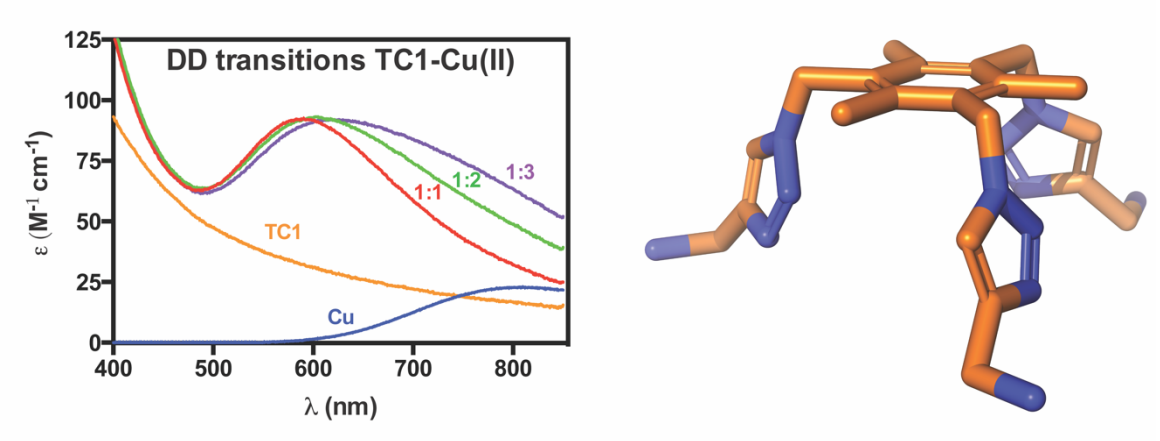

Figure V-9. UV Scans of **TC1**-Cu(II) complex at ratios of 1:1-3, where the concentration of **TC1** is kept constant (2 mM) and the concentration of Cu(II) nitrate is varied from 2 mM up to 6 mM. The absorbance recorded were divided by the concentration and data were plotted against the extinction coefficient ε (M^{-1} cm^{-1}). Samples were incubated for 30 mins and each sample measured three times. **TC1** stock was prepared in DMF and diluted to its final concentration in H_2O, the percentage of DMF in water was < 5%, all copper(II) samples were prepared in H_2O. Molecular model of **TC1** ligand.

V. 3.1. DNA damage

The DNA cleavage potential of **TC1**-Cu(II) complex was determined by gel electrophoresis where supercoiled plasmid DNA (Form I) can be separated from nicked (Form II) and linear (Form III) forms that are indicative of single and double strand breaks, respectively. In all experiments conducted, the complex was formed *in situ* in a 1:3 ratio of **TC1**:Cu(II) for 30 mins prior exposure to plasmid DNA. The concentration required to induce DNA cleavage was determined using 90 min and 6 h timepoints under physiological conditions (pH 7.2, 37 ˚C) in the absence of added reductant. The results shown in Figure V-10 indicate that copper(II) alone (tested at the highest loading) does not induce DNA damage, however in the presence of **TC1** the onset of cleavage is shown at 5 μM and completely converts supercoiled DNA (FI) into its open circular form (FII) by 30 μM after 90 min, Figure

V-10A. Extending the incubation time to 6 h showed this complex is capable of nicking plasmid DNA at concentrations as low as 5 μM, Figure V-10B. Interestingly, **TC1**-Cu(II) did not mediate double strand breaks (FIII) even at elevated concentrations up to 100 μM.

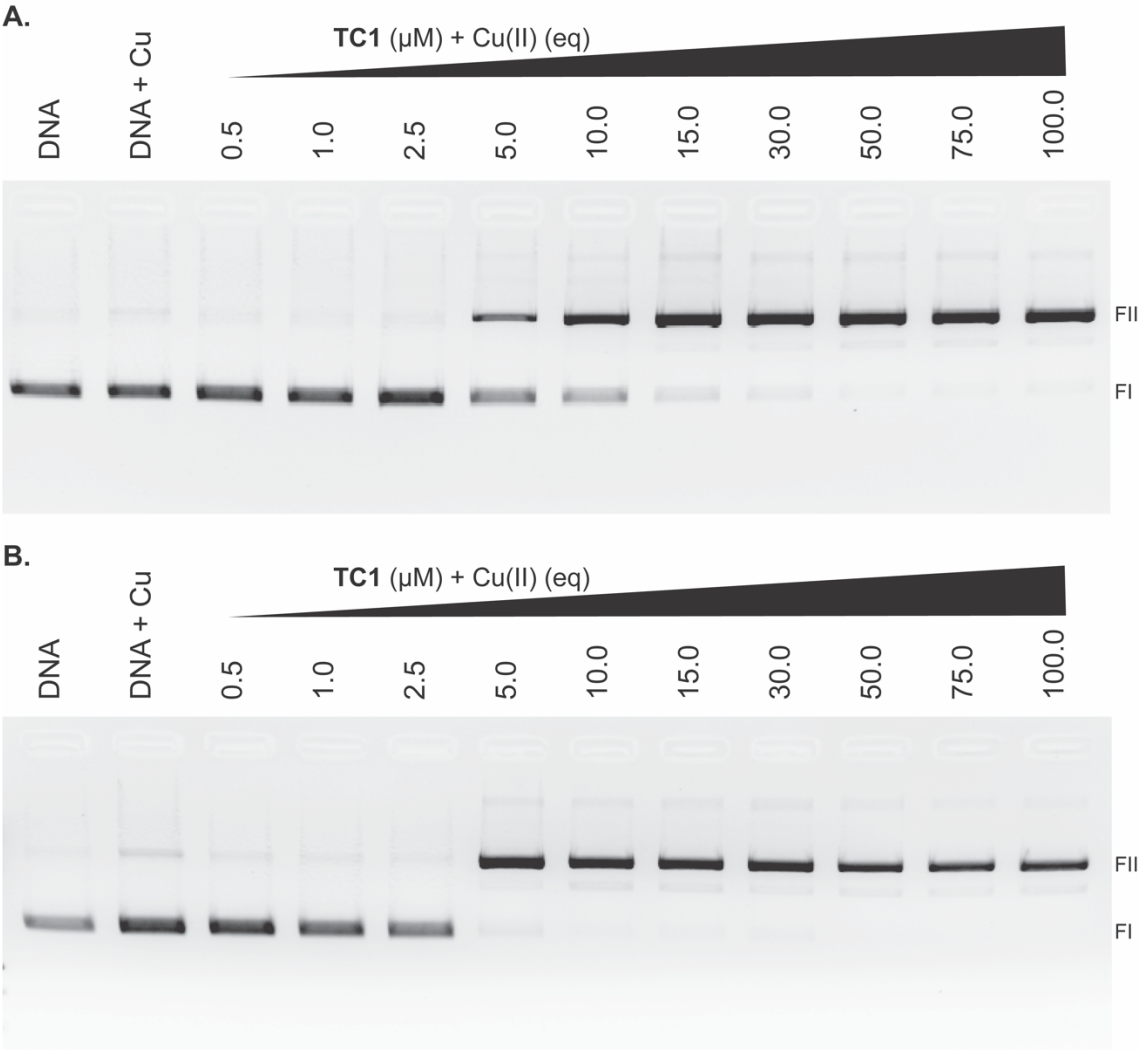

Figure V-10. Agarose gel electrophoresis of supercoiled (400 ng) pUC19 exposed to increasing concentrations of **TC1** with 3 equivalents of copper(II) nitrate. **TC1** and Cu(II) were pre-incubated for 30 mins at 37 ˚C prior to the addition of the DNA solution. Reactions were carried out in neutral HEPES buffer (80 mM, pH = 7.2) at (**A.**) 90 mins and (**B.**) 6 h, in the presence of 25 mM NaCl at 37 ˚C prior to electrophoretic analysis. Reactions were quenched by adding 6x loading buffer (Fermentas) containing 10 mM Tris-HCl, 0.03% bromophenol blue, 0.03% xylene cyanole FF, 60% glycerol, 60 mM EDTA.

In the absence of reductant the **TC1**-Cu(II) complex induces single strand cleavage up to 6 h and to identify if the complex could induce double strand breaks, the **TC1**-Cu(II) complex was exposed to plasmid DNA over a prolonged period (24 h) in the absence of reductant. To determine whether double-strand breaks result from random coincidence of single-strand breaks or whether they occur as an independent event, band densitometry experiments was employed to quantify the different forms of DNA damage. A similar approach was used to study the cleavage potential of bleomycin to show that double strand breaks are not a result of coincidences between random breaks in the complimentary strand.[31,32] Over a period of 24 h **TC1**-Cu(II) was exposed to supercoiled DNA (400 ng) at a fixed concentration of 25 μM (**TC1**-Cu(II) complex). Control experiments were conducted in parallel using untreated DNA and copper(II) exposed DNA to ensure the presence of the metal salt did not induce any damage over the same experimental conditions, Figure V-11A. Each reaction was carried out in triplicate using ethidium bromide (EtBr) as the fluorescent dye which was used to visualise and quantify DNA. EtBr is unaffected by the differences in base composition and as little as 1-5 ng of DNA can be estimated by this reporter. EtBr, however, is known to bind plasmid conformations (i.e. FI, FII, and FIII) differently. Open circular and linear forms of binds to the same amount of the fluorescent dye.[33] A correction factor of 1.47 used for scDNA (Form I) taking into account the weaker interaction of Ethidium Bromide to scDNA compared to nicked and linear DNA.[34,35] It is evident from the gel that the formation of nicked DNA (Form II, Figure V-11B) occurs after 30 mins exposure and little to no supercoiled DNA is present up to 12 h. After 24 h of exposure double strand breaks were detected, however, these were present to a limited extent (5.5%) Figure V-11C.

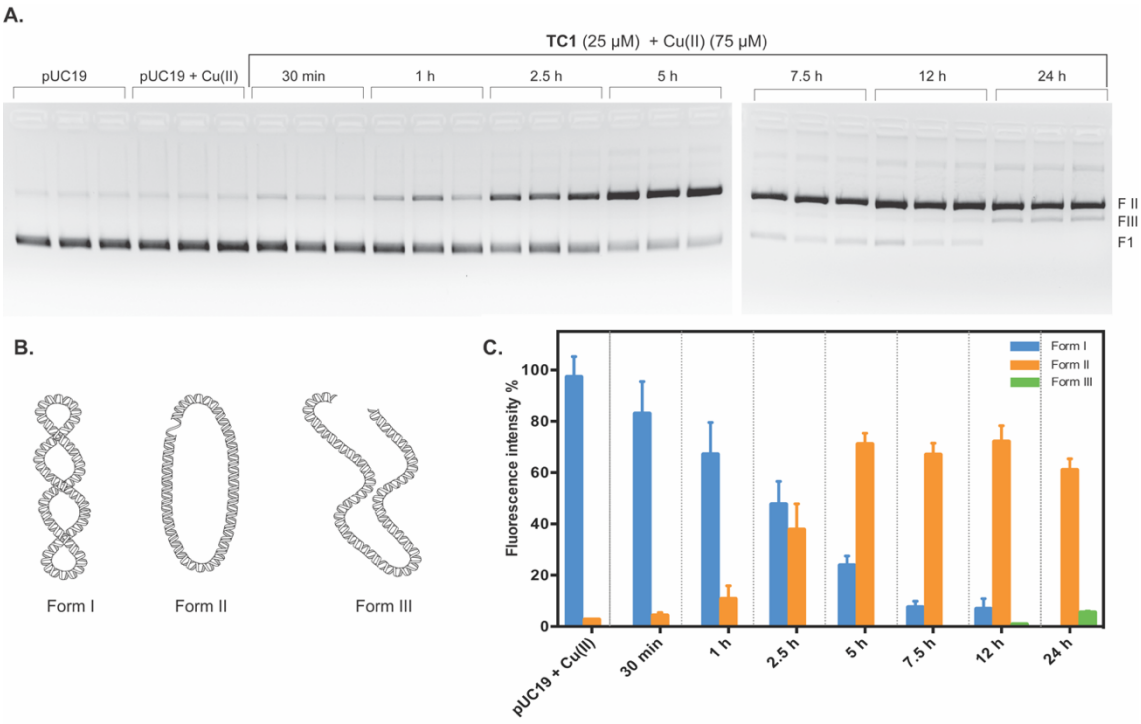

Figure V-11. Band densitometry of supercoiled pUC19 was quantified using the Image J software package. **A.** Agarose gel electrophoresis of supercoiled (400 ng) pUC19 exposed to **TC1**-Cu(II) (25 μM). Reactions were carried out in triplicate in neutral HEPES buffer (80 mM, pH = 7.2) in the presence of 25 mM NaCl at 37 ºC for 30 mins, 1, 2.5, 5, 7.5, 12, and 24 h incubation times prior to electrophoretic analysis. Reactions were quenched by adding 6x loading buffer (Fermentas) containing 10 mM Tris-HCl, 0.03% bromophenol blue, 0.03% xylene cyanole FF, 60% glycerol, 60 mM EDTA and samples were loaded onto an agarose gel (1.2%) containing 4 μl EtBr. Electrophoresis was completed at 70 V for 90 mins in 1x TAE buffer. B. Graphical representation of the three main forms of plasmid DNA, supercoiled (form I), nicked/open circular (form II), and linear DNA (form III). **C.** Bar chart of quantified nucleic acids with respect to control (pUC19 + Cu(II)). A correction factor of 1.47 used for scDNA (Form I) taking into account the weak interaction of Ethidium Bromide to scDNA compared to nicked and linear DNA.[34,35]

V. 3.2. DNA Damage in the presence of reductant

Intracellular generation of reactive oxygen species (ROS) via reduction of copper ($Cu^{2+} \rightarrow Cu^{+}$) has been assumed as the major mechanism underlying the anticancer activity of copper(II) complexes.[30,36] With this in mind, the degree of DNA cleavage by **TC1**-Cu(II) was examined in the presence of exogenous reductant. The influence of biologically relevant reductants (mercaptopropionic acid, glutathione, and ascorbic acid) can impact the anti-cancer properties of copper(II) complexes. 3-

Mercaptopropionic acid, a thiol containing reducing agent is a common additive used alongside copper(II) complexes,[37,38] however the cleavage of supercoiled plasmid by the **TC1**-Cu(II) complex in the presence of 3-mercaptopropionic acid (MPA) at a 100-fold molar excess relative to the complex, did not show any apparent DNA cleavage (data not shown). The complex was found to be cleavage inactive in the presence of this reductant a phenomenon previously reported in the literature.[39] The interaction of superhelical pUC19 with **TC1**-Cu(II) complex was then studied with the addition of sodium L-ascorbate (Na-L-ascorbate) as a reductant using standard agarose gel electrophoresis. Na-L-ascorbate is commonly used as a reductant for copper(II) complexes to catalyse oxidative DNA cleavage.[16,25] Reactions were carried over a range of complex concentrations (0.25 – 10 μM) under physiological pH at 30 min prior to electrophoretic analysis. The complex induced single and double strand breaks which was evident by the presence of nicked (Form I) and linear (Form II) tertiary conformations at 2.5 μM, Figure V-12.

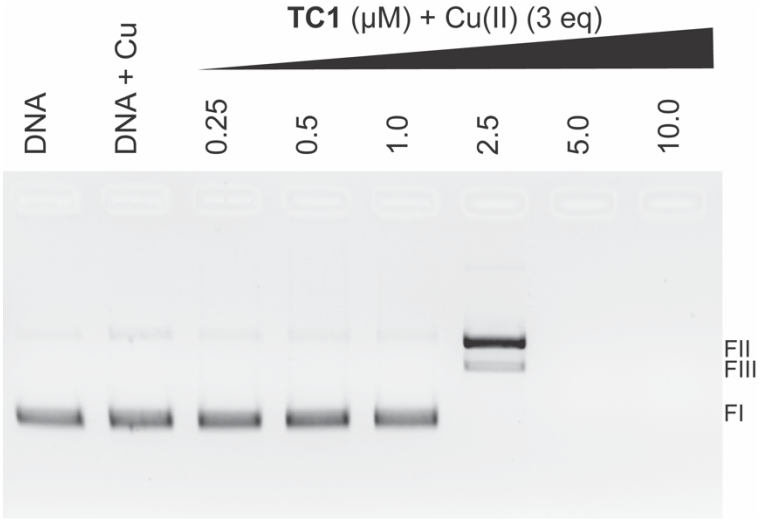

Figure V-12. Agarose gel electrophoresis of supercoiled (400 ng) pUC19 exposed to increasing concentrations of **TC1** with 3 equivalents of Cu(II) in the presence of reductant (Na-*L*-ascorbate, 1 mM). **TC1** and Cu(II) were pre-incubated for 30 mins at 37 ºC prior to the addition of the DNA solution. Reactions were carried out in neutral HEPES buffer (80 mM, pH = 7.2) in the presence of 25 mM NaCl at 37 ºC for 30 mins prior to electrophoretic analysis. Reactions were quenched by adding 6x loading buffer (Fermentas) containing 10 mM Tris-HCl, 0.03% bromophenol blue, 0.03% xylene cyanole FF, 60% glycerol, 60 mM EDTA.

V. 3.3. Atomic force microscopy (AFM) analysis

AFM imaging allows for a direct visual tool for exploring the effects of ligand binding on DNA morphology.[40] It was important to highlight that the conditions optimised to carry out AFM analysis of supercoiled plasmid (pUC19) can be greatly impacted by the ionic strength of the buffered solution. As shown in Figure V-13A, supercoiled plasmid was prepared in AFM buffer (Tris-HCl, 40 mM, pH 7.2) containing EDTA (80 mM) and magnesium chloride ($MgCl_2$) (10 mM). Plasmids are shown as tightly supercoiled structures with some natural unwinding observed in the upper right-hand corner of the image, however, there is a reduced presence of DNA on the mica surface under these conditions. When the buffer was substituted to a $MgCl_2$ solution (5 mM), plasmid DNA had a greater adherence to the mica surface under the same plasmid DNA concentration (3 ng/μL), although more plasmid unwinding was observed (Figure V-13B-C).

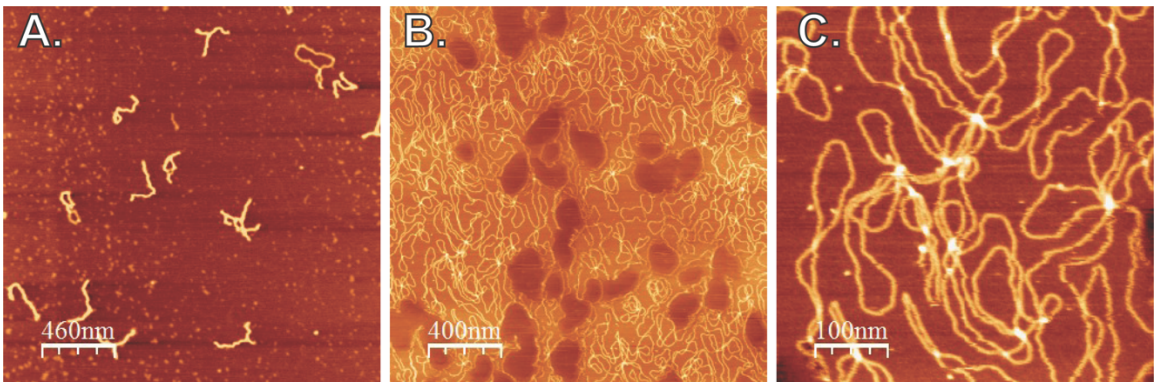

Figure V-13. Atomic force microscopy (AFM) images of supercoiled pUC19 (3 ng/μL) treated in AFM buffer (**A**) and nuclease free H_2O (**B** and **C**).

Through gel electrophoresis we have shown that copper complex **TC1**-Cu(II) is capable of mediating the transformation of supercoiled plasmid to open circular and linear forms. To study this conformational change in more detail, AFM measurements were undertaken with pUC19 and **TC1**-Cu(II). In the presence of excessive reductant, DNA is predominantly in its supercoiled state however, 500 nm of **TC1**-Cu(II) initiated single strand breaks that are visualised in Figure V-14A. Points where ligand-DNA binding occur are shown as increases in the height profile of circular structures Figure V-14A-B. An increase in complex concentration (1 μM**)** renders plasmid DNA predominantly in its open circular form, Figure V-14B, and complete degradation of the plasmid DNA was reached at 7.5-10 μM, Figure V-14C-D. Evidence here strongly supports oxidative damage to pUC19 induced by the **TC1**-Cu(II) Complex.

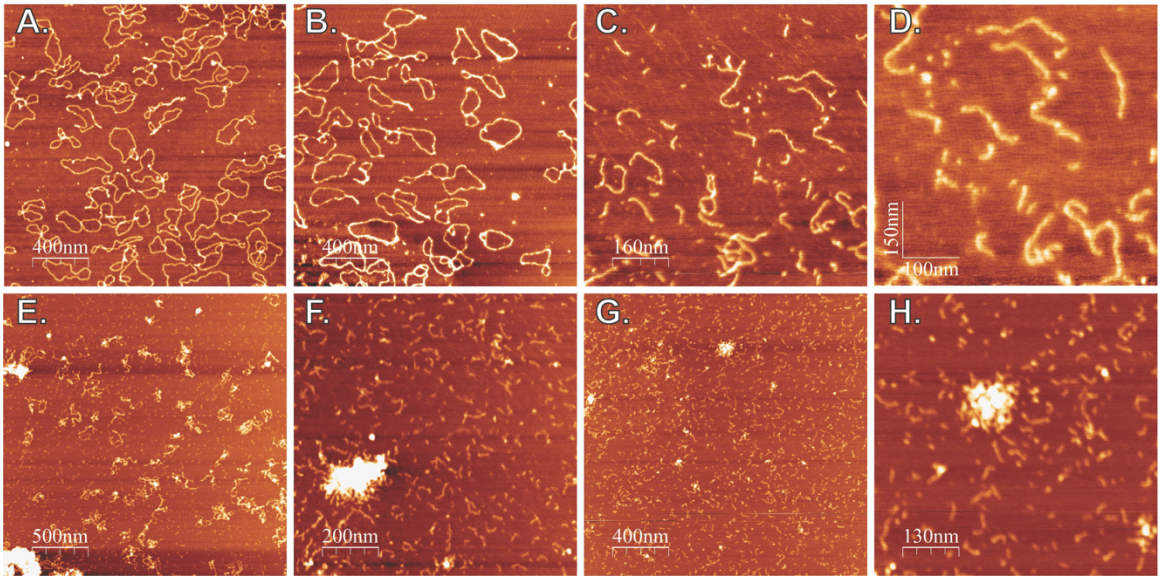

Figure V-14. Atomic force microscopy (AFM) images of **TC1**-Cu(II) treated supercoiled pUC19 (3ng/μL) in the presence of reductant (**A-D)** and absence of reductant (**E-H**) at concentrations of (0.5, 1.0, 7.5, and 10 μM) and (5, 10 and 30 μM) respectfully.

DNA damage was also visualised in the absence of reductant at low concentrations of the complex (Figure V-14E, 5 μM). Small compact clusters of fragmented DNA were intermediately observed when AFM analysis was being carried out. These small particles are evident in Figure V-14F-G. On closer inspection of the cluster present in Figure V-14G it can be clearly seen that small fragmented DNA is surrounding the compact particle (Figure V-14H). These compacted DNA fragments could not be visualised through gel electrophoresis due to their small size, however AFM analysis has highlighted moderate condensation. The compaction of fragmented DNA may be due to the cationic charge of the complex. When the ligand binds to three copper(II) ions, the complex carries a 6+ charge which could give rise to nucleic acid condensation.

V. 3.4. Insight into DNA cleavage mechanism

The ability of copper(I) to mediate free radical species has been exploited by many research groups by preparing copper(II) co-ordinated complexes which are capable of inducing DNA damage and cellular toxicity. Workers in this group have successfully probed ROS formation including superoxide ($O_2^{\bullet -}$), hydrogen peroxide (H_2O_2), hydroxyl radical ($^{\bullet}OH$), metal-oxo and metal-hydroxo species as critical components to the oxidative DNA damaging profile of a number of copper(II) complexes.[16,25,27,29] In order to examine the mechanism by which the Tri-Click compound interact and cleaves supercoiled DNA, the presence of specific ROS

were probed using radical-specific scavengers and stabilizers outlined in Figure V-15. This method was adapted from previously reported procedure published by this group.[25] Scavengers were firstly confirmed to have no impact on pUC19 conformation prior to experiments (data not shown). Treatment of supercoiled pUC19 (FI) with **TC1**-Cu(II) in the presence of exogenous reductant resulted in single strand nicking to open circular DNA (FII, lane 2-3) at 0.5 and 1.0 μM. **TC1**-Cu(II) in the presence of exogenous reductant induced double strand cleavage (linear, FIII, lane 4) at 2.5 μM exposure, and complete DNA degradation at 5 μM (lane 5). Control experiments are in excellent agreement with those observed in Figure V-12 (lanes 3-6). As shown in Figure V-15A, the results suggest superoxide ($O_2^{\bullet -}$) is the most prevalent radical species involved in the cleavage mechanism as pre-incubation with 4,5-dihydroxy-1,3-benzenedisulfonic acid (tiron) significantly inhibited activity. The presence of the hydroxyl radical ($^{\bullet}OH$) scavenger, DMSO, also inhibited cleavage activity, but activity was impeded to a lower extent when compared directly with tiron. The presence of the hydrogen peroxide (H_2O_2) scavenger, KI, was also found to inhibit chemical nuclease activity of the tested complex. The role of singlet oxygen ($^1O_2$) was next examined utilizing sodium azide (NaN_3) as a scavenger and D_2O as a $^1O_2$ stabilizer. Nuclease activity was only slightly inhibited by NaN_3, while a marginal change in activity relative to the control was observed in D_2O thus suggesting a limited role in DNA oxidation by $^1O_2$.

To probe ROS involved in mediating DNA damage further, ROS specific scavengers have been studied and include; *D*-mannitol, *L*-methionine, and *N,N*′-dimethylthiourea (DMTU).[41] These scavengers were employed to probe the role of the hydroxyl radical ($^{\bullet}OH$), hydrogen peroxide (H_2O_2), hypochlorous acid (HOCl) or a combination thereof. The results of these scavengers are shown in Figure V-15B. In these experiments, the delayed onset of nicked plasmid (FII) and the inhibition of linearized DNA were evident. Results suggest that H_2O_2 is the most prevalent radical species involved in the cleavage mechanism as DMTU inhibits the complete transformation of supercoiled DNA to nicked open circular DNA which agrees with KI as a H_2O_2 scavenger. Hydroxyl radial ($^{\bullet}OH$) scavenging agent *D*-mannitol had no influence on DNA cleavage, shown by the complete degradation of plasmid DNA at drug loading of 4 μM. Finally, *L*-methionine inhibited the formation of linearized DNA which could be attributed to its ability to scavenge H_2O_2.The trapping experiments used here are designed to capture the hydroxyl radical, hydrogen peroxide,

superoxide, and hypochlorite show that this novel complex does not exactly follow classical Fenton-type or Haber-Weiss processes but instead generates superoxide and hydrogen peroxide. This suggests that DNA damage is possibly mediated through a superoxide dismutase (SOD) type pathway which should be further examined.

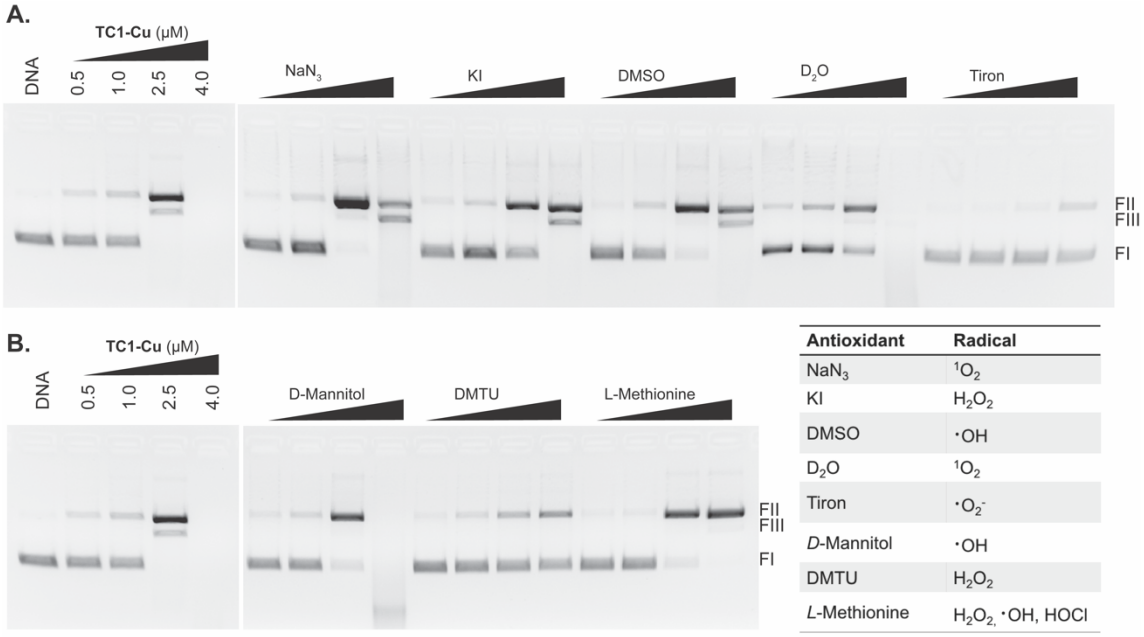

Antioxidant	Radical
NaN_3	$^1O_2$
KI	H_2O_2
DMSO	·OH
D_2O	$^1O_2$
Tiron	$·O_2^-$
D-Mannitol	·OH
DMTU	H_2O_2
L-Methionine	H_2O_2, ·OH, HOCl

Figure V-15. DNA cleavage reactions in the presences of ROS-specific scavengers. Supercoiled pUC19 (400 ng) was incubated for 30 min at 37˚C with complex concentrations of 0.5, 1, 2.5, and 4 μM in the presence of 25 mM NaCl and 1 mM Na-*L*-Ascorbate in 80 mM HEPES. Lane 1: DNA only. Lanes 2−5: 0.5, 1.0, 2.5, 4.0 μM **TC1**-Cu(II). **A.** Lanes 6−9: + 10 mM NaN_3. Lanes 10−13: + 10 mM KI. Lanes 14−17: + 10% DMSO. Lanes 18−21: + 77% D_2O. Lanes 22-25: + 10 mM tiron. **B.** Lanes 6−9: + 10 mM *D*-mannitol. Lanes 10−13: + 10 mM DMTU. Lanes 14−17: + 10 mM *L*-methionine.

In order to examine the oxidative damage mechanism in greater detail, DNA repair enzymes which can recognize specific nucleoside modifications typically associated with oxidative damage were employed. This method was adapted from Fantoni *et al.*[41] with slight modifications. Cleavage experiments were designed to identify the mechanism of oxidative damage via gel electrophoresis. Repair proteins that have specific lesion recognition are known as glycoylase and can incise DNA, removing the base and generating abasic sites (AB). Glycoylases and several repair endonucleases also recognise AP (apurine / apyrimidine) sites and mediate strand nicking adjacent to the base-free lesion. Specific lesions acted upon by repair

enzymes in this assay are listed in Figure V-16A and include: formamidopyrimidine [fapy]-DNA glycosylase (Fpg)[42–44] and endonuclease (Endo) III[44,45] that are bifunctional glycosylases with associated AP lyase activity; both Endo IV[46] and Endo V[47–50] that nick DNA at AB sites *via* endonuclease activity; and human alkyladenine (alkyl purine) glycosylase (hAAG)[51,52] that possess base modified recognition properties. It was shown that the enzymes alone in the presence of DNA did not induce any DNA damage which is shown in Figure V-16B. Control experiments involving hydroxyl radical ($^{\bullet}OH$) generated from a Cu^{2+}/H_2O_2 Fenton system were examined for comparison. Reactions conditions were optimised where the Fenton system (Figure V-16C, lanes 2-4) initiated cleavage of supercoiled plasmid to its nicked (FII) and linearized forms (FIII), prior to the addition of the repair enzymes. There was inhibition of DNA damage in the presence of Fpg and EndoIII which supports the formation of oxidised purine and pyrimidine bases by the hydroxyl radical formed from the Fenton system (Figure V-16C, lanes 5-10). Limited change was found in the presence of other DNA repair enzymes, EndoIV, EndoV, and hAAG (Figure V-16C, lanes 11-19).

Reaction conditions for **TC1**-Cu(II) (2.5 – 7.5 μM) were optimized to initiate cleavage of supercoiled pUC19 to all three forms of plasmid DNA by gel electrophoresis (Figure V-16D, lanes 2–4, 60 min). Controls taken after 30 min of continuous exposure of **TC1**-Cu(II) to pUC19 DNA were also examined as a reference point prior to the addition of repair enzyme (Appendix E-4, Figure E2). In the presence of all repair enzymes, the formation of linear DNA was inhibited. In the presence of Fpg and EndoIII, however, a significant reduction in the formation of nicked DNA, along with protection of intact plasmid DNA was observed. These results overlap somewhat with Fenton's reagent and strongly support the role of hydrogen peroxide and the hydroxyl radical—identified in earlier scavenger experiments—within the cleavage process of **TC1**-Cu(II).

A.

Endonuclease				
FpG	EndoIII	EndoIV	EndoV	hAAG
Oxidised Pu	Oxidised Py	AB sites	Deoxyinosine	Deoxyinosine
AP sites	Ap Sites		AB sites	Alkylated Pu
8-oxo-purines	Urea		Urea	3-Me-A
FaPy-G	5,6-Dihydroxy-T		Mismatches	7-Me-G
Me-FaPy-G	T-glycol		Flaps	1, N6-enthoA
FaPy-A	5-OH-5-Me-dHyd		Pseudo Y-structures	Hypoxanthine
5-OH-C	U-glycol			
5-OH-U				

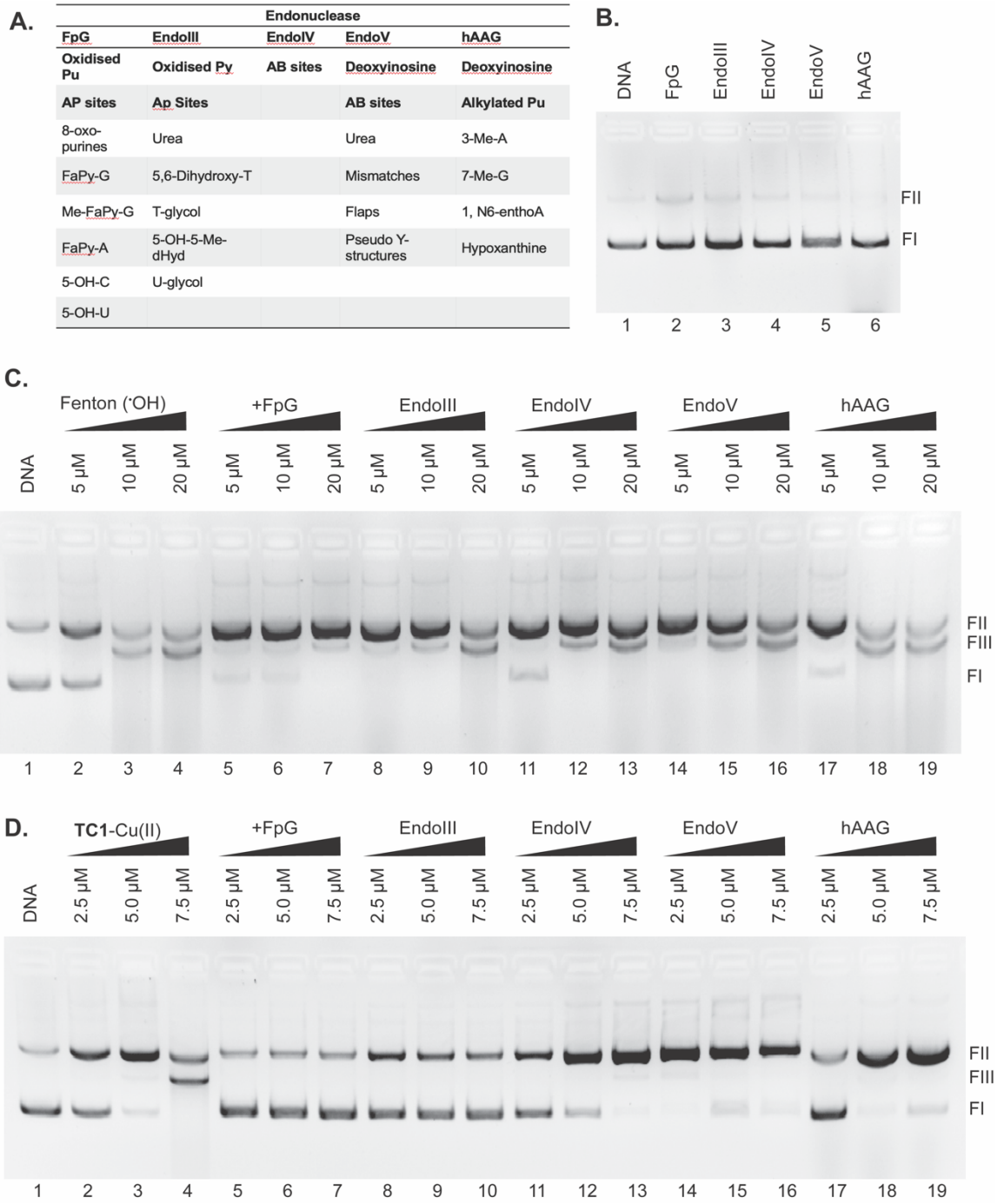

Figure V-16. A. Table highlighting base lesion recognised or excised by respective repair enzymes. Abbreviations are as follows: A = adenine, G = guanine, T= thymine, C = cytosine, U = uracil, Pu = purines (A and G), Py = pyrimidines (C, T and U), Me = methyl, OH = hydroxy, H = hydro, dH = dihydro, FaPy = formamidopyrimidine, dHyd = deoxyhydanton, Me-Tar-U = methyltartronylurea, dI = deoxyinosine, dU = deoxyuracil. **B.** pUC19 only controls in the presence of repair enzymes, FpG, EndoIII, EndoIV, EndoV, and hAAG. **C.** Hydroxyl radical generated from Cu^{2+}/H_2O_2 Fenton-system (5, 10, and 20 µM; lanes 2-4) in the presence of 1 mM Na-*L*-ascorbate and repair enzymes Fpg (lanes 5-7), Endo III (lanes 8-10), Endo IV (lanes 11-13), EndoV (lanes 14-16), and hAAG (lanes 17-19). **D. TC1**-Cu(II) (2.5, 5, and 7.5 µM; lanes 2-4) in the presence of 1 mM Na-*L*-ascorbate and repair enzymes

Fpg (lanes 5-7), Endo III (lanes 8-10), Endo IV (lanes 11-13), EndoV (lanes 14-16), and hAAG (lanes 17-19).

V. 4. Conclusions

A new library of terminal polyamine C_3-scaffolds was prepared using the copper-catalysed azide-alkyne cycloaddition reaction. This new series, called "Tri-Click", was developed as potential non-viral vectors for gene delivery. Control Tri-Click scaffolds containing either a bromine or hydroxyl terminal group showed no condensation properties suggesting the triazole ring is inert towards DNA binding under physiological conditions. The solubility of Tri-Click compounds was greatly improved compared to C_3-opioids scaffolds but evidence of nucleic acid damage was also identified. Scaffolds containing primary or secondary terminal amines displayed the most significant DNA damaging effects under acidic pH (4.0) while terminal amines had reduced cleavage properties and activity was inhibited under basic conditions.

A single scaffold was identified to bind to copper(II) to form a copper(II) complex in situ, **TC1**-Cu(II), which was capable of enhanced DNA cleavage properties compared to the ligand alone. In the absence of reductant this complex was capable of inducing single strand breaks at low drug loading (5 μM), however when a reducing agent was introduced the cleavage potential increased forming double strand breaks. The cleavage potential was examined through AFM which allowed for the visualisation of supercoiled plasmid to open circular and linear forms, and finally fragmented nucleic acid strands. This DNA damage mechanism was then probed using a variety of biophysical methods with specific trapping agents for reactive oxygen species (ROS) indicating single stranded DNA breaks mediated by copper-catalysed free radicals. The complex was shown to promote the formation of superoxide and hydrogen peroxide radicals.

Although these compounds did not mediate efficient DNA condensation as anticipated, the DNA damage mediated by the **TC1**-Cu(II) complex in the absence of reductant, and its acceleration in the presence of ascorbate, is a significant discovery that may lead to new therapeutic and gene-directed applications for this agent.

V. 5. References

1 M. A. Kotterman, T. W. Chalberg and D. V. Schaffer, *Annu. Rev. Biomed. Eng.*, **2015**, 17, 63–89.

2 C. E. Thomas, A. Ehrhardt and M. A. Kay, *Nat. Rev. Genet.*, **2003**, 4, 346–358.

3 L. Li, Z.-Y. He, X.-W. Wei, G.-P. Gao and Y.-Q. Wei, *Hum. Gene Ther.*, **2015**, 26, 452–462.

4 M. F. Dias, K. Joo, J. A. Kemp, S. L. Fialho, A. da Silva Cunha, S. J. Woo and Y. J. Kwon, *Prog. Retin. Eye Res.*, **2018**, 63, 107-131.

5 Office of the Commissioner, Press Announcements - FDA approves novel gene therapy to treat patients with a rare form of inherited vision loss, https://www.fda.gov/NewsEvents/Newsroom/PressAnnouncements/ucm589467.htm, (accessed 11 January 2018).

6 N. Chirmule, K. J. Propert, S. A. Magosin, Y. Qian, R. Qian and J. M. Wilson, *Gene Ther.*, **1999**, 6, 1574.

7 M. Ramamoorth and A. Narvekar, *J. Clin. Diagn. Res.*, **2015**, 9, GE01–GE06.

8 M. Thomas and A. M. Klibanov, *Appl. Microbiol. Biotechnol.*, **2003**, 62, 27–34.

9 P. Yue, Y. Zhang, Z.-F. Guo, A.-C. Cao, Z.-L. Lu and Y.-G. Zhai, *Org Biomol Chem*, **2015**, 13, 4494–4505.

10 D. Dheer, V. Singh and R. Shankar, *Bioorganic Chem.*, **2017**, 71, 30–54.

11 H. Yin, R. L. Kanasty, A. A. Eltoukhy, A. J. Vegas, J. R. Dorkin and D. G. Anderson, *Nat. Rev. Genet.*, **2014**, 15, 541–555.

12 T. J. Thomas, H. A. Tajmir-Riahi and T. Thomas, *Amino Acids*, **2016**, 48, 2423–2431.

13 A. I. Khalaf, C. Bourdin, D. Breen, G. Donoghue, F. J. Scott, C. J. Suckling, D. MacMillan, C. Clements, K. Fox and D. A. T. Sekibo, *Eur. J. Med. Chem.*, **2012**, 56, 39–47.

14 S. G. Agalave, S. R. Maujan and V. S. Pore, *Chem. - Asian J.*, **2011**, 6, 2696–2718.

15 A. Prisecaru, Z. Molphy, R. G. Kipping, E. J. Peterson, Y. Qu, A. Kellett and N. P. Farrell, *Nucleic Acids Res.*, **2014**, 42, 13474–13487.

16 Z. Molphy, A. Prisecaru, C. Slator, N. Barron, M. McCann, J. Colleran, D. Chandran, N. Gathergood and A. Kellett, *Inorg. Chem.*, **2014**, 53, 5392–5404.

17 M. Ageno, E. Dore and C. Frontali, *Biophys. J.*, **1969**, 9, 1281–1311.

18 D. S. Sigman, A. Mazumder and D. M. Perrin, *Chem. Rev.*, **1993**, 93, 2295–2316.

19 X. Yu and J. Zhang , in *Macrocyclic Polyamines*, Wiley-Blackwell, **2017**, pp. 45–81.

20 M. Sawicki, D. Lecerclé, G. Grillon, B. Le Gall, A.-L. Sérandour, J.-L. Poncy, T. Bailly, R. Burgada, M. Lecouvey, V. Challeix, A. Leydier, S. Pellet-Rostaing, E. Ansoborlo and F. Taran, *Eur. J. Med. Chem.*, **2008**, 43, 2768–2777.

21 C. Li, F. Zhao, Y. Huang, X. Liu, Y. Liu, R. Qiao and Y. Zhao, *Bioconjug. Chem.*, **2012**, 23, 1832–1837.

22 X. Sheng, X.-M. Lu, J.-J. Zhang, Y.-T. Chen, G.-Y. Lu, Y. Shao, F. Liu and Q. Xu, *J. Org. Chem.*, **2007**, 72, 1799–1802.

23 K. A. Schug and W. Lindner, *Chem. Rev.*, **2005**, 105, 67–114.

24 A. Prisecaru, M. Devereux, N. Barron, M. McCann, J. Colleran, A. Casey, V. McKee and A. Kellett, *Chem. Commun.*, **2012**, 48, 6906.

25 Z. Molphy, C. Slator, C. Chatgilialoglu and A. Kellett, *Front. Chem.*, **2015**, 3, 1-9.

26 G. Rochford, Z. Molphy, N. Browne, C. Surlis, M. Devereux, M. McCann, A. Kellett, O. Howe and K. Kavanagh, *J. Inorg. Biochem.*, **2018**, DOI:10.1016/j.jinorgbio.2018.05.020.

27 C. Slator, Z. Molphy, V. McKee, C. Long, T. Brown and A. Kellett, *Nucleic Acids Res.*, **2018**, 46, 2733–2750.

28 Z. Molphy, D. Montagner, S. S. Bhat, C. Slator, C. Long, A. Erxleben and A. Kellett, *Nucleic Acids Res.*, **2018**, DOI:10.1093/nar/gky806.

29 C. Slator, Z. Molphy, V. McKee and A. Kellett, *Redox Biol.*, **2017**, 12, 150–161.

30 S. J. Stohs and D. Bagchi, *Free Radic. Biol. Med.*, **1995**, 18, 321–336.

31 R. S. Lloyd, C. W. Haidle and D. L. Robberson, *Biochemistry*, **1978**, 17, 1890–1896.

32 L. F. Povirk, W. Wübter, W. Köhnlein and F. Hutchinson, *Nucleic Acids Res.*, **1977**, 4, 3573–3580.

33 Z. Topcu, *Acta Biochim. Pol.*, **2000**, 47, 835–839.

34 Y. Zhao, J. Zhu, W. He, Z. Yang, Y. Zhu, Y. Li, J. Zhang and Z. Guo, *Chem. – Eur. J.*, **2006**, 12, 6621–6629.

35 Y. Jin and J. A. Cowan, *J. Am. Chem. Soc.*, **2005**, 127, 8408–8415.

36 C. R. Kowol, P. Heffeter, W. Miklos, L. Gille, R. Trondl, L. Cappellacci, W. Berger and B. K. Keppler, *JBIC J. Biol. Inorg. Chem.*, **2012**, 17, 409–423.

37 Y. Zhao, J. Zhu, W. He, Z. Yang, Y. Zhu, Y. Li, J. Zhang and Z. Guo, *Chem. Eur. J.*, **2006,** 12, 6621–6629.

38 S. Dhar, M. Nethaji and A. R. Chakravarty, *Dalton Trans.*, 2004, 4180.

39 P. K. Sasmal, A. K. Patra and A. R. Chakravarty, *J. Inorg. Biochem.*, **2008,** 102, 1463–1472.

40 V. Cassina, D. Seruggia, G. L. Beretta, D. Salerno, D. Brogioli, S. Manzini, F. Zunino and F. Mantegazza, *Eur. Biophys. J.*, **2011**, 40, 59–68.

41 N. Z. Fantoni, Z. Molphy, C. Slator, G. Menounou, G. Toniolo, G. Mitrikas, V. McKee, C. Chatgilialoglu and A. Kellett, *Chem. Eur. J.*, **2018**, DOI:10.1002/chem.201804084.

42 J. Tchou and A. P. Grollman, *J. Biol. Chem.*, **1995**, 270, 11671–11677.

43 J. Tchou, V. Bodepudi, S. Shibutani, I. Antoshechkin, J. Miller, A. P. Grollman and F. Johnson, *J. Biol. Chem.*, **1994**, 269, 15318–15324.

44 Z. Hatahet, Y. W. Kow, A. A. Purmal, R. P. Cunningham and S. S. Wallace, *J. Biol. Chem.*, **1994**, 269, 18814–18820.

45 M. Dizdaroglu, J. Laval and S. Boiteux, *Biochemistry*, **1993**, 32, 12105–12111.

46 J. D. Levin, A. W. Johnson and B. Demple, *J. Biol. Chem.*, **1988**, 263, 8066–8071.

47 M. Yao, Z. Hatahet, R. J. Melamede and Y. W. Kow, *J. Biol. Chem.*, **1994**, 269, 16260–16268.

48 M. Yao and Y. W. Kow, *J. Biol. Chem.*, **1994**, 269, 31390–31396.

49 M. Yao and Y. W. Kow, *J. Biol. Chem.*, **1996**, 271, 30672–30676.

50 M. Yao and Y. W. Kow, *J. Biol. Chem.*, **1997**, **272**, 30774–30779.

51 C. W. Abner, A. Y. Lau, T. Ellenberger and L. B. Bloom, *J. Biol. Chem.*, **2001**, 276, 13379–13387.

52 G. Dianov and T. Lindahl, *Nucleic Acids Res.*, **1991**, 19, 3829–3833.

53 P. M. Keane, J. P. Hall, F. E. Poynton, B. C. Poulsen, S. P. Gurung, I. P. Clark, I. V. Sazanovich, M. Towrie, T. Gunnlaugsson, S. J. Quinn, C. J. Cardin and J. M. Kelly, *Chem. - Eur. J.*, **2017**, 23, 10344–10351.

54 J. Cadet and J. R. Wagner, *Cold Spring Harb. Perspect. Biol.*, **2013**, 5 (2) 1-20.

Thesis Conclusions and Future Work

This work focused on the design and synthesis of new molecular scaffolds with a major focus on the use of synthetic tripodal C_3-symmetric opioid scaffolds as efficient condensation agents of DNA. Morphine, codeine, heterocodeine, and oripavine C_3-opioids were generated and showed comparable condensation capabilities. Condensation was achieved on both superhelical and linear dsDNA conformations and identified by agarose electrophoresis, viscosity, turbidity, dynamic light scattering (DLS) and atomic force microscopy (AFM) measurements. Tripodal opioid aggregation was identified as pH dependent and strongly influenced by ionic strength with further evidence of cationic amine-phosphate backbone coordination. Preliminary toxicity screening of the C_3-oripavine opioid with a selected a Chinese hamster ovary (CHO) cell line indicated poor tolerance and from these results the second aim of this project to generate non-opioid DNA condensing agents unfolded.

Five imidazole C_3-scaffolds were screened for nucleic acid activity as alternatives to the opioid series. Two compounds, **NAM1** and **NAM2**, highlighted the onset of nucleic acid condensation at high drug loading of upwards of 100 μM for **NAM1** and 500 μM for **NAM2**. Although these compounds are capable of inducing DNA compaction, they require high drug loading when compared to opioid scaffolds we reported, where **OC3** inducing complete condensation at low concentrations of 5 μM. The concentrations required to induce condensation was unsuitable for further investigations and an alternative synthetic approach for the preparation of new compounds was undertaken.

A new library of terminal polyamine C_3-scaffolds was prepared using the copper-catalysed azide-alkyne cycloaddition reaction. This new series, called “Tri-Click”, was developed as potential non-viral vectors for gene delivery and modelled from the C_3-opioid scaffold. Simplifying the scaffold into the most basic form of a C_3-polyamines resulted in nucleic acid damage induced by the Tri-Click scaffolds rather than condensation. The rigid structure of the opioid backbone allows for electrostatic binding where the simplified scaffolds favours damaging properties. Advanced nucleic acid damage was identified when **TC1** interacts with copper(II) *in situ*. This

DNA damage mechanism was then probed using a variety of biophysical methods with specific trapping agents for reactive oxygen species (ROS) indicating single stranded DNA breaks mediated by copper-catalysed free radicals.

As a continuation of this work new scaffolds for the development of novel C_3-symmertric scaffolds for DNA condensation could be developed along with linear variations. The preparation of new ligands prepared through CuAAC reactions capable of binding to copper(II) is an interesting field of research that could be developed further.

Appendix A

Supporting information accompanying Chapter II, C_3-Symmetric Opioid Scaffolds are pH-Responsive DNA Condensation Agents. Referencing style is kept in publishing format.

A-1: NMR spectroscopy

MC3 spectra:

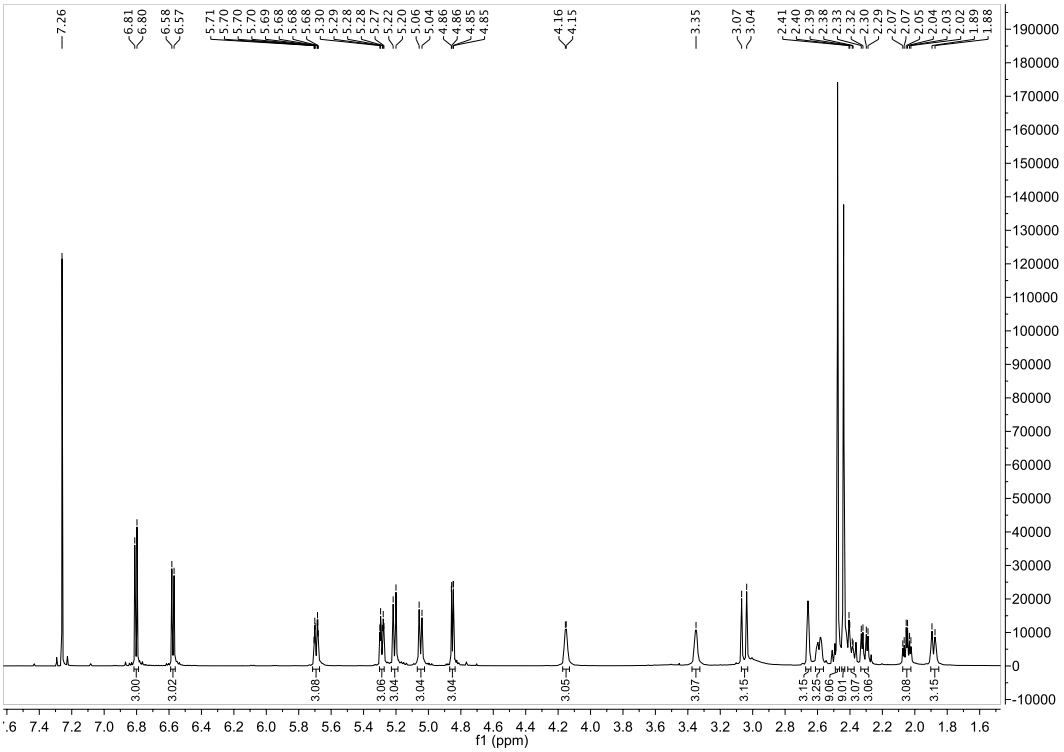

Figure A-1. ^{1}H NMR spectra for **MC3**.

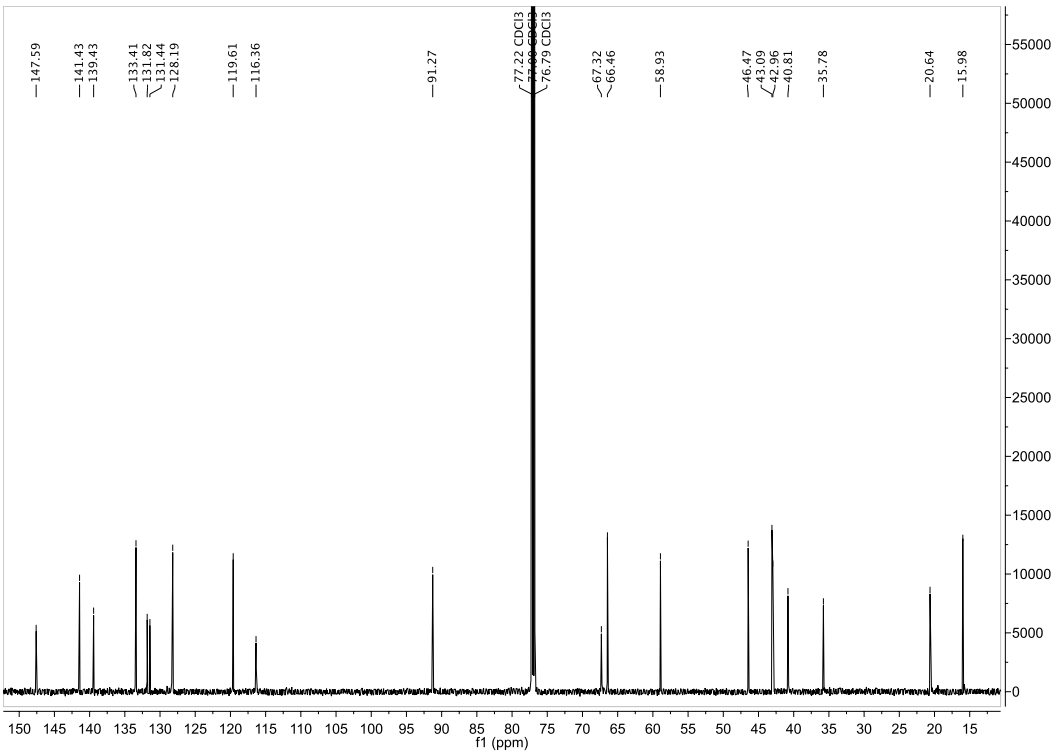

Figure A-2. ^{13}C NMR spectra for **MC3.**

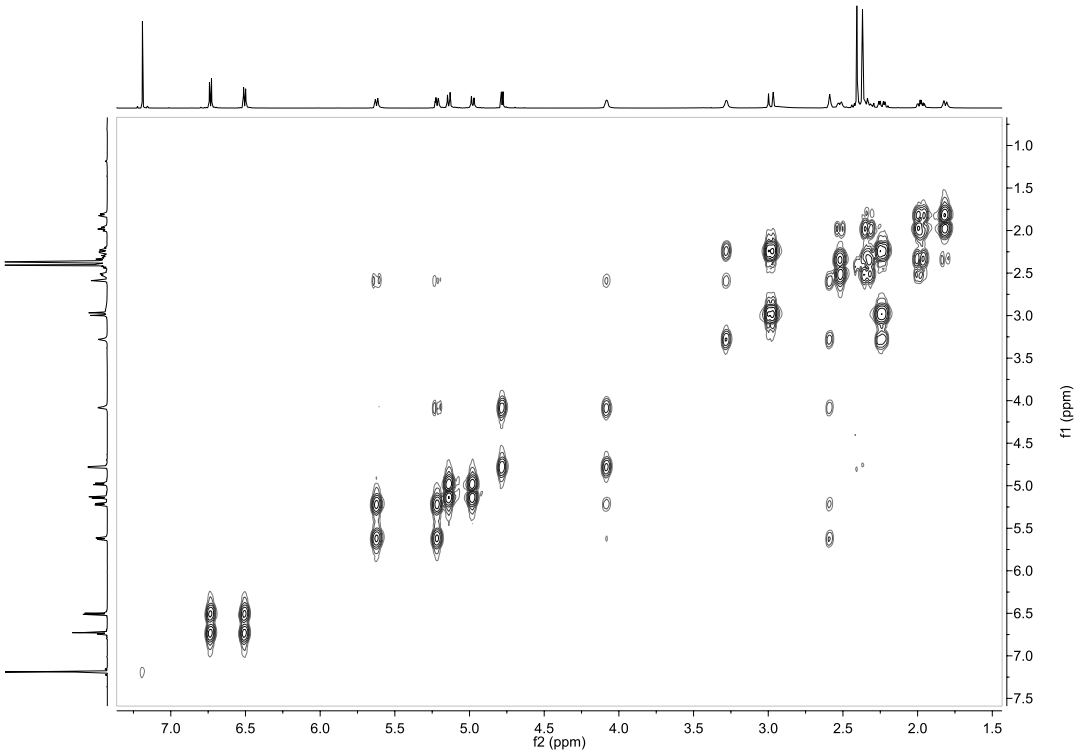

Figure A-3. COSY NMR spectra for **MC3.**

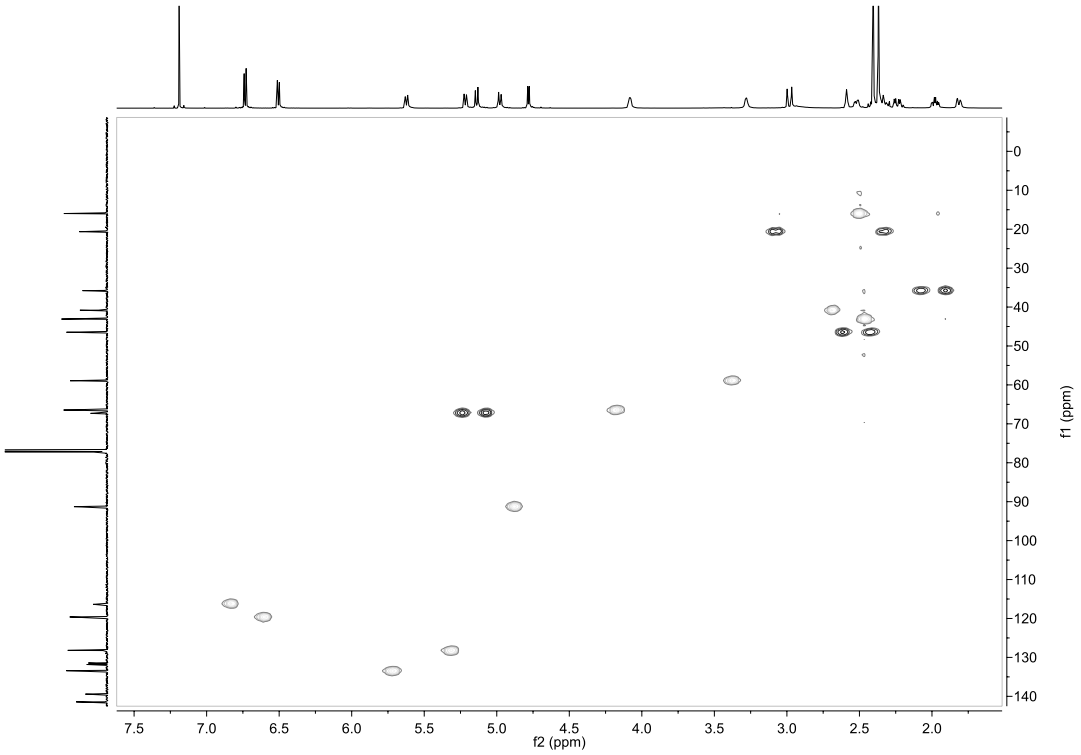

Figure A-4. HSQC NMR spectra for **MC3**.

OC3 Spectra:

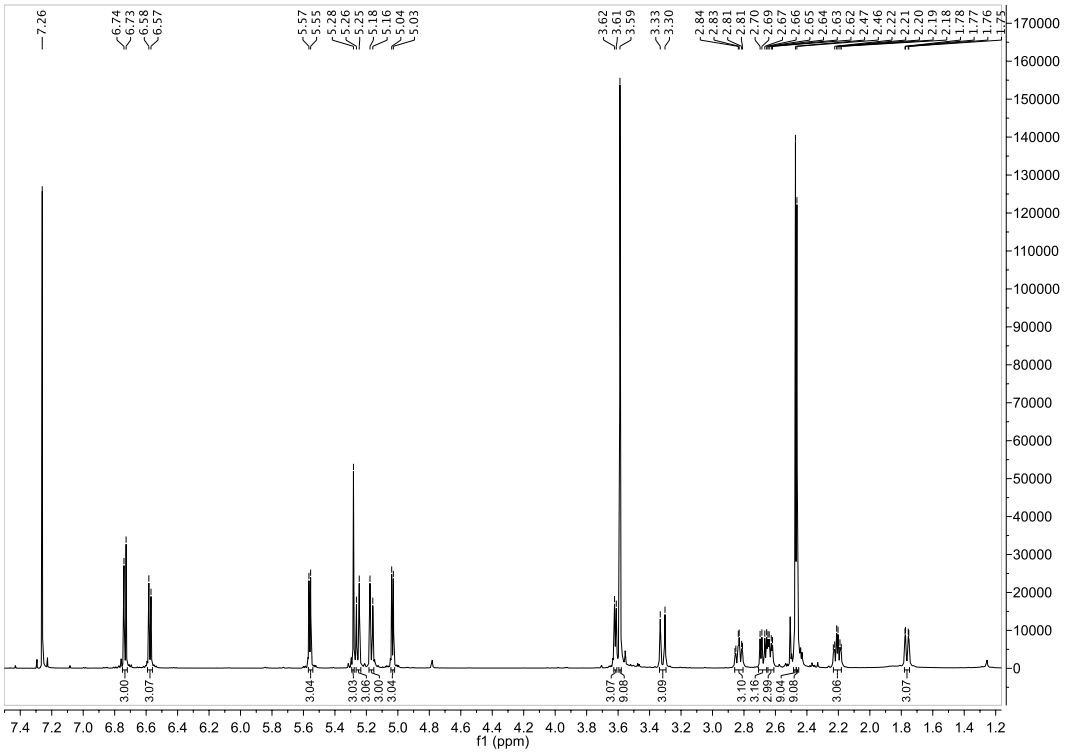

Figure A-5. ^{1}H NMR spectra for **OC3**.

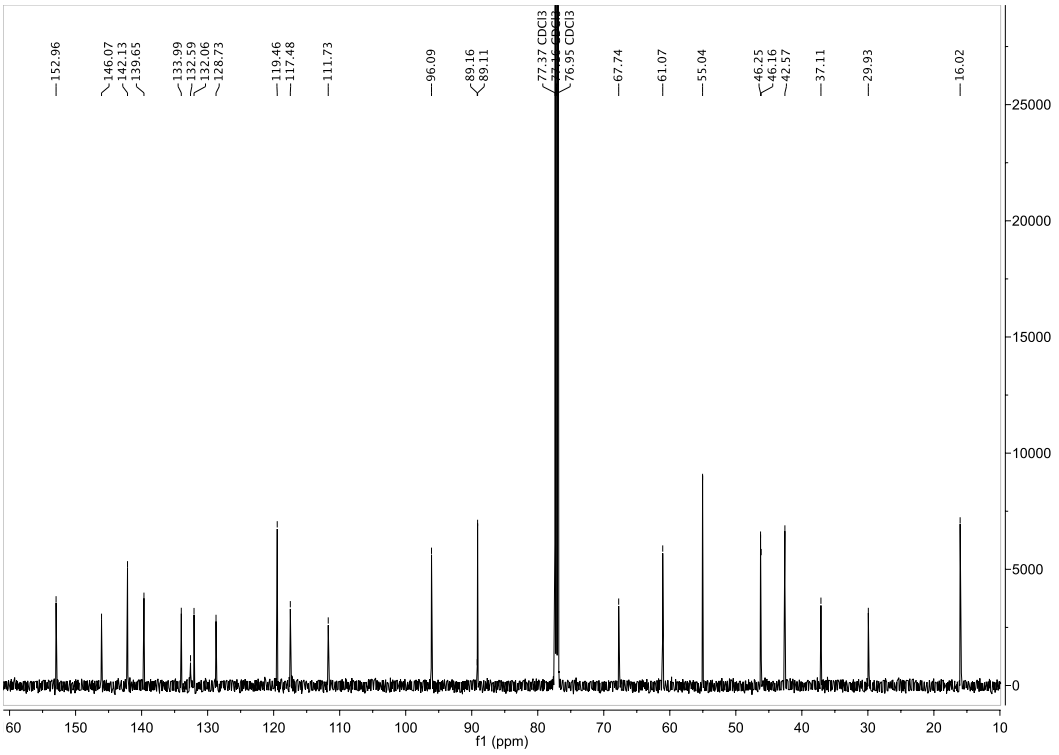

Figure A-6. ^{13}C NMR spectra for **OC3.**

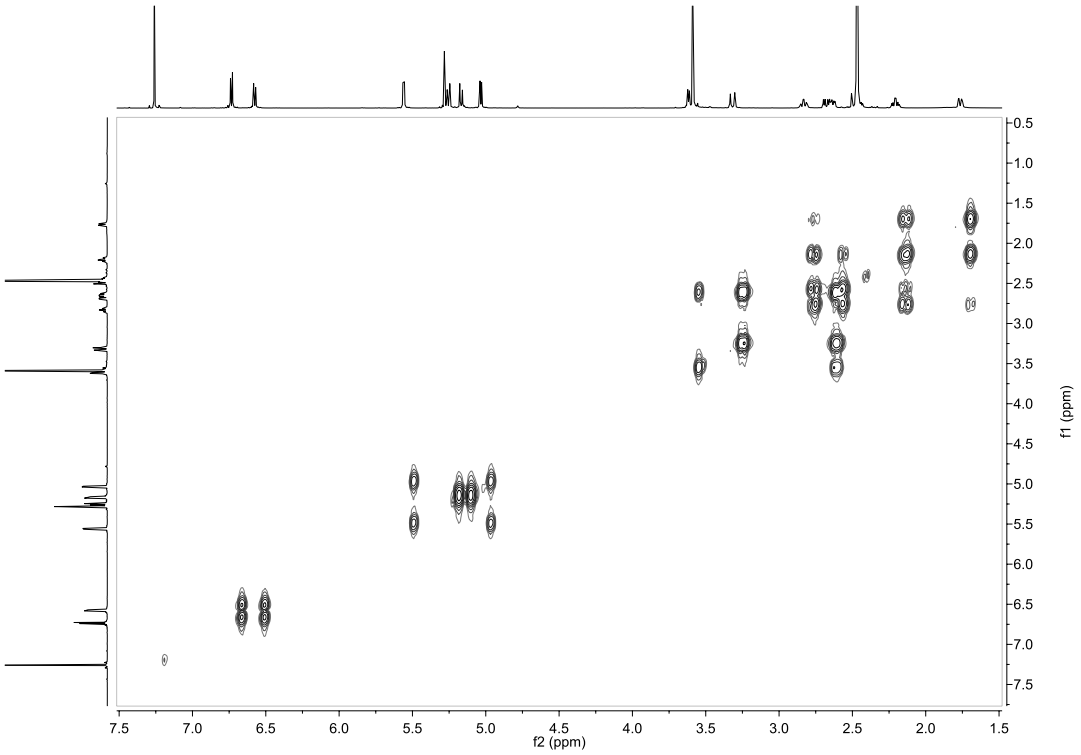

Figure A-7. COSY NMR spectra for **OC3.**

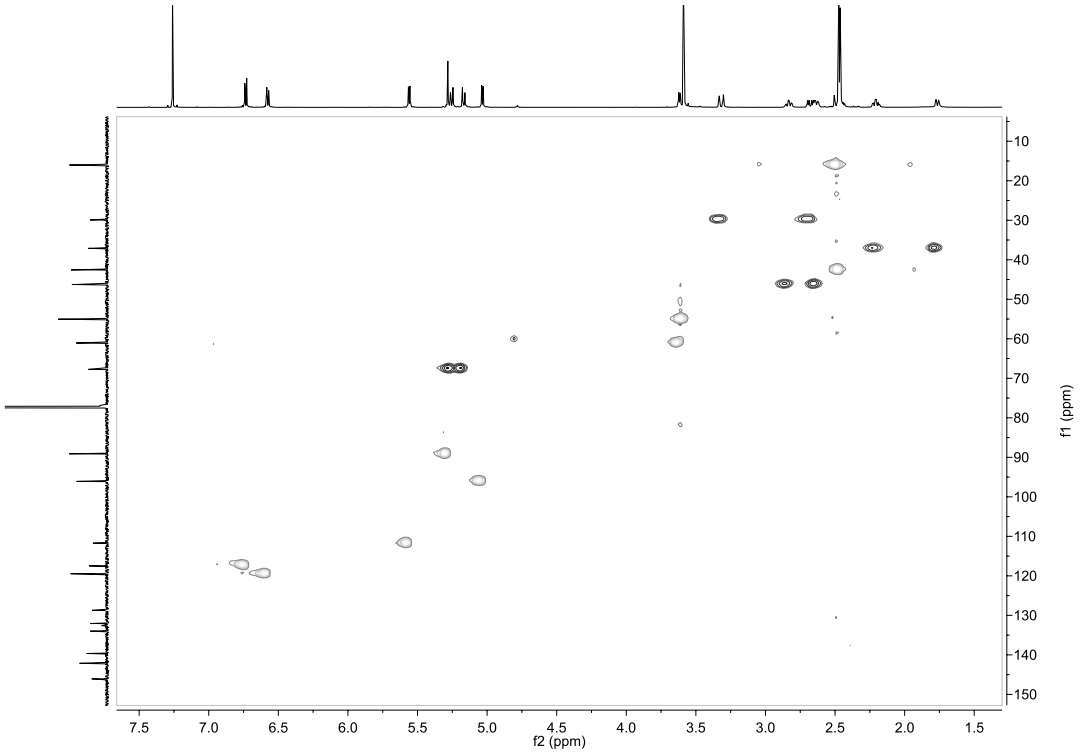

Figure A-8. HSQC NMR spectra for **OC3.**

HC3 Spectra:

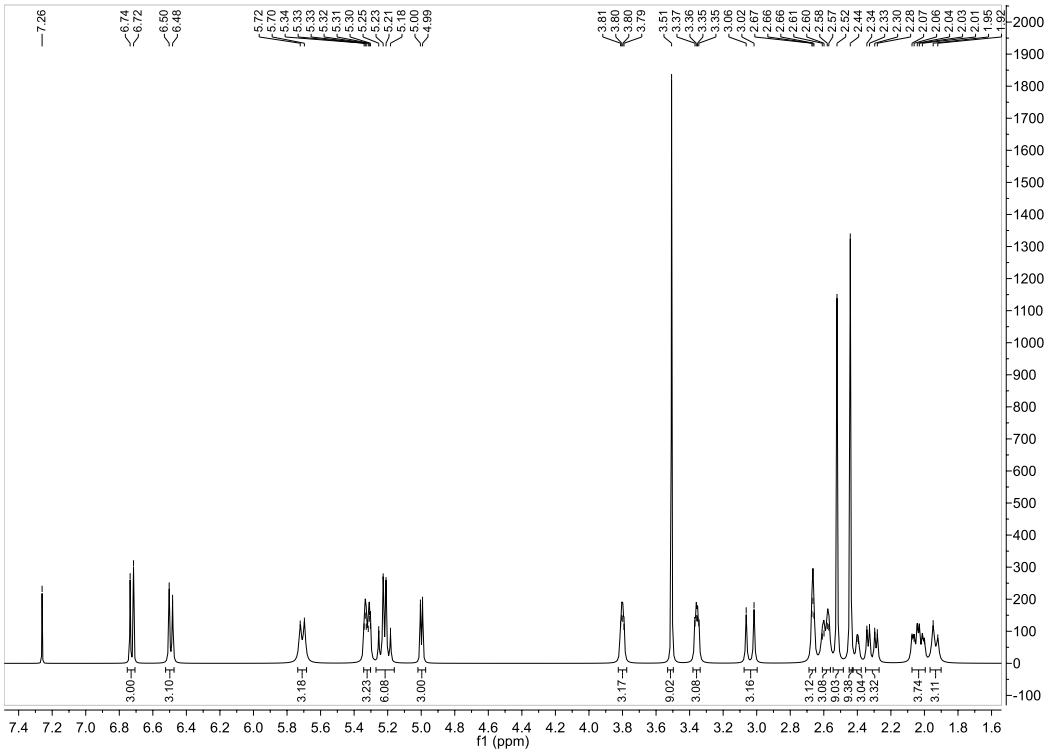

Figure A-9. ^{1}H NMR spectra for **HC3.**

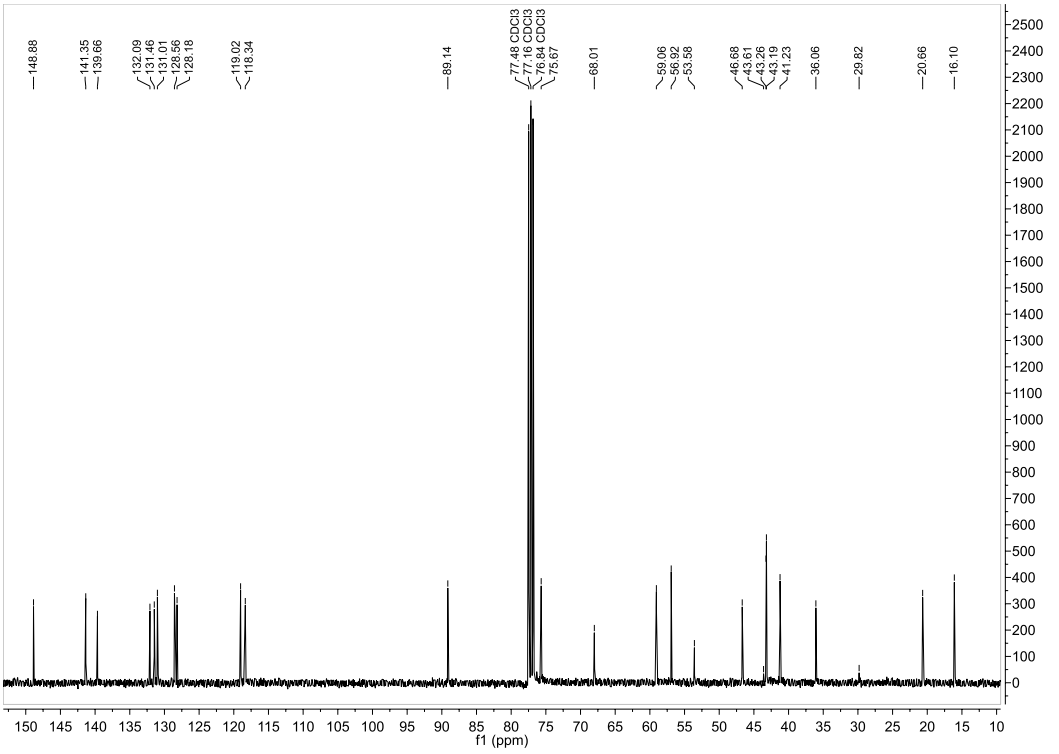

Figure A-10. ^{13}C NMR spectra for **HC3.**

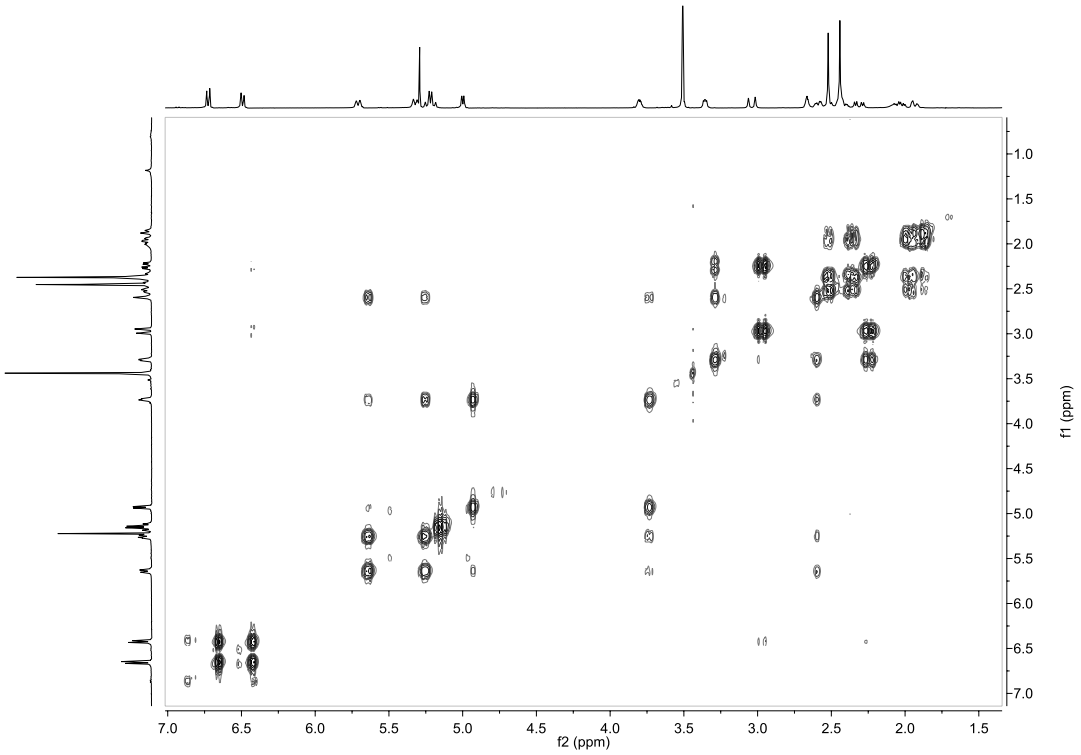

Figure A-11. COSY NMR spectra for **HC3.**

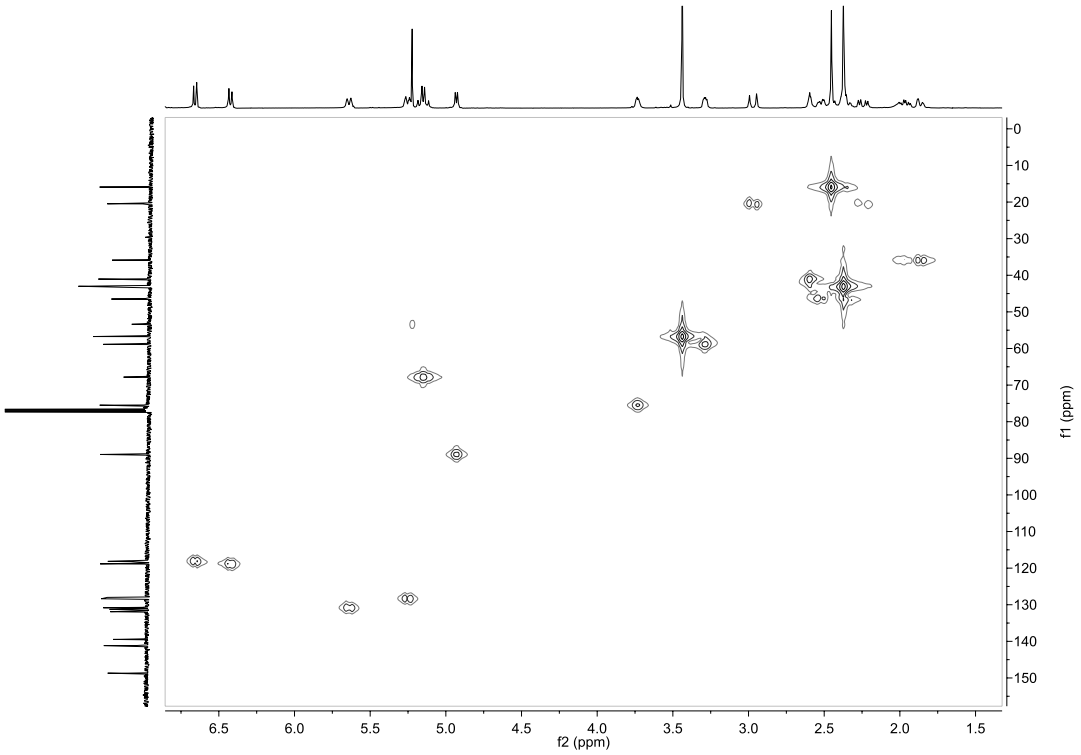

Figure A-12. HSQC NMR spectra for **HC3.**

A-2: Circular dichroism spectra

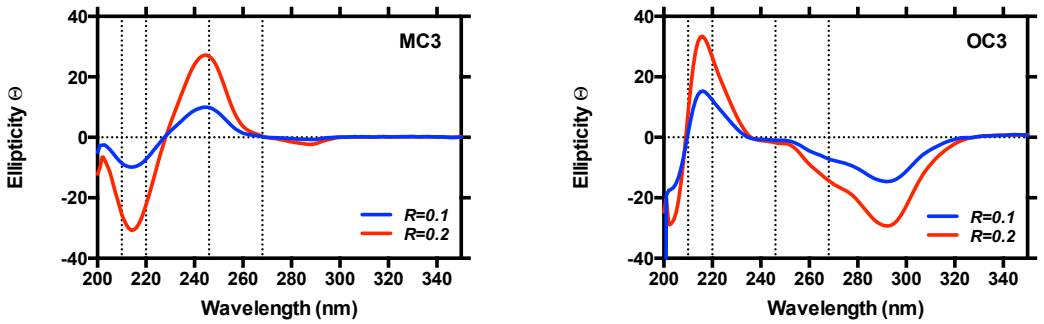

Figure A-13. CD spectra of opioid scaffolds **MC3** and **OC3** in the absence of stDNA at 10 μM and 20 μM loading (at equivalent concentrations to the *r* values of 0.1 and 0.2, respectively).

A-3: Gel electrophoresis with C_1 and C_2 derivatives

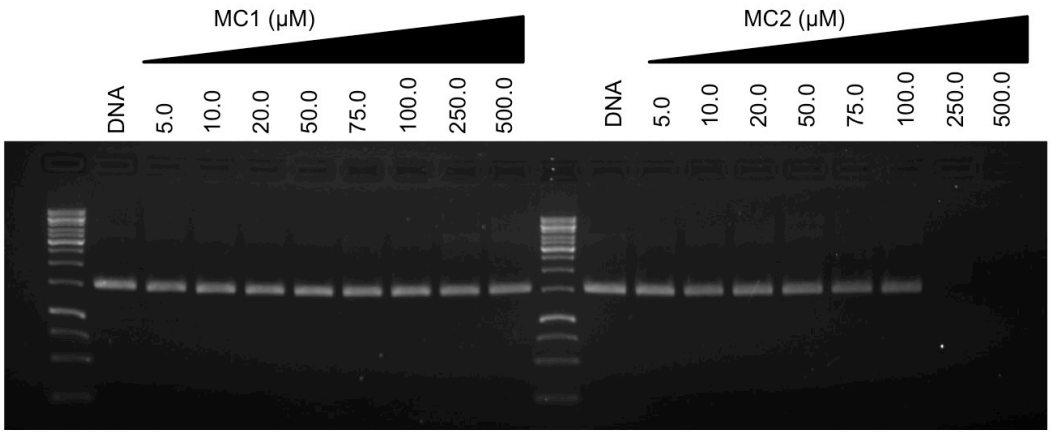

Figure A-14. Agarose gel electrophoresis of supercoiled (400 ng) exposed to increasing concentrations of **MC1**, and **MC2**. Reactions were carried out in the presence of 25 mM NaCl for 5 h at 37˚C prior to electrophoretic analysis.

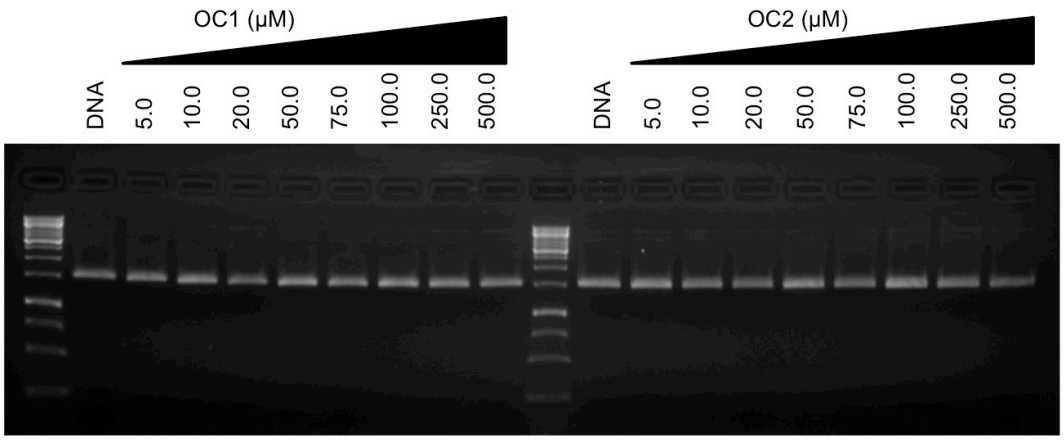

Figure A-15. Agarose gel electrophoresis of supercoiled (400 ng) exposed to increasing concentrations of OC1, and OC2. Reactions were carried out in the presence of 25 mM NaCl for 5 h at 37˚C prior to electrophoretic analysis.

A-4: Gel electrophoresis experiments with MC3 and -NMe_2 derivatives

Both **MC3** and the **MC3–NMe_2** derivative were initially prepared in DMF and further diluted in 80 mM HEPES buffer (Fisher). Reactions were carried out according to the following general procedure: in a total volume of 20 μl using 80 mM HEPES buffer (pH 7.2) with 25 mM NaCl, 400 ng pUC19 (NEB, N3041) and varying concentrations of test compound (5, 10, 20 and 30 μM), were incubated at 37˚C for 5 h. Reaction mixtures were subjected to gel electrophoresis as previously stated.

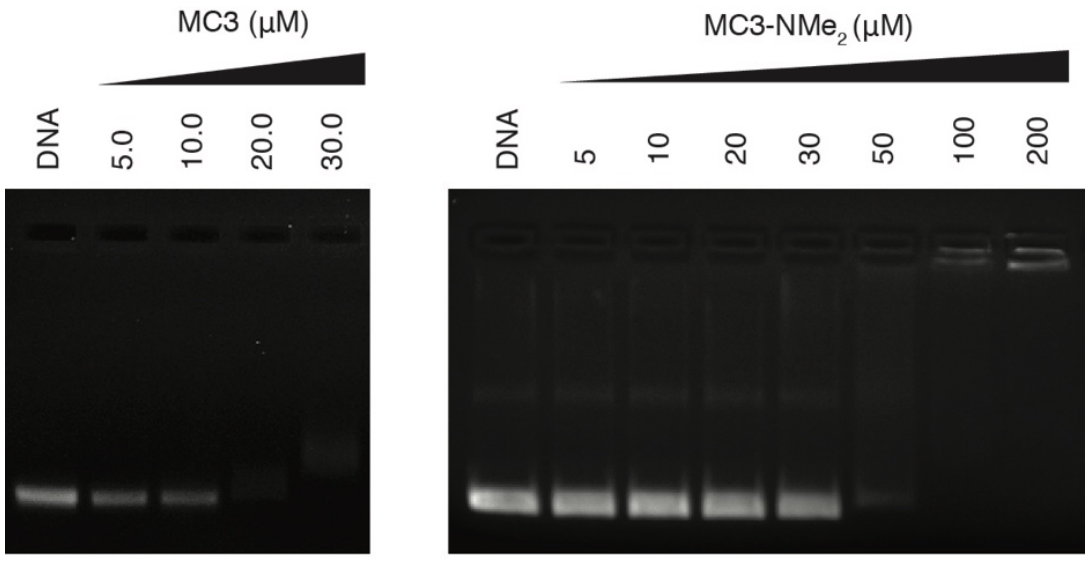

Figure A-16. Agarose gel electrophoresis of supercoiled (400 ng) exposed to increasing concentrations of **MC3** and **MC3-NMe_2**. Reactions were carried out in the presence of 25 mM NaCl for 5 h at 37˚C prior to electrophoretic analysis.

A-5: Restriction enzyme interactions with MC3 and -NMe_2 derivatives

Restriction enzymes HindIII, EcoRI, SalI and BamHI (1 µl) were combined with 30 µM of either MC3 or MC3-NMe_2 derivatives in a final volume of 20 µl using 80 mM HEPES buffer (pH 7.2) and incubated for 2 h at 37˚C. 400 ng of pUC19 was then added to each reaction mixture and incubated for 1 hr 30 minutes at 37˚C and subjected to gel electrophoresis as previously described.

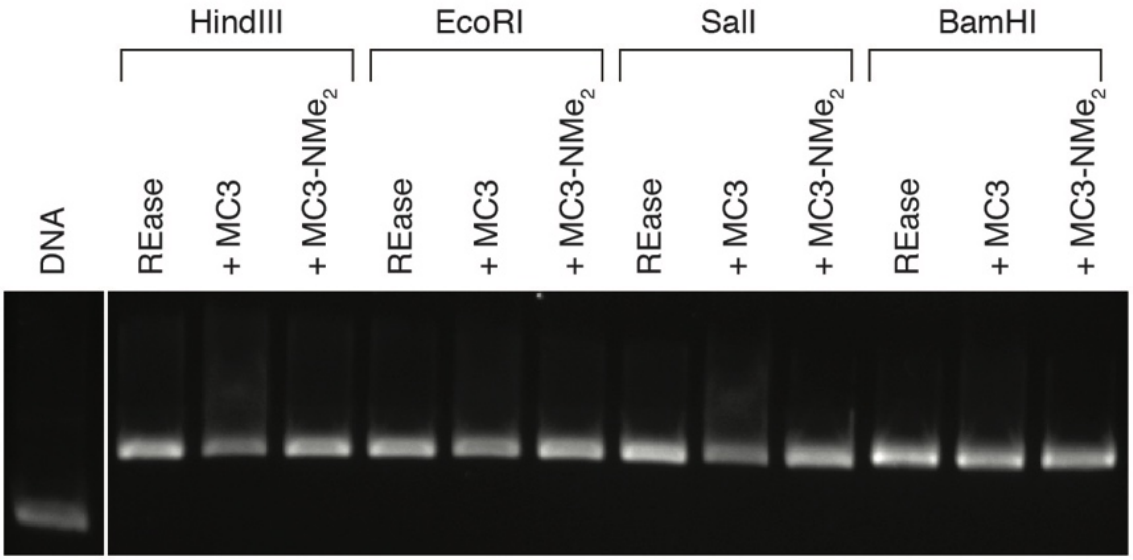

Figure A-17. Agarose gel electrophoresis of selected restriction enzymes pre-treated with 30 µM of either **MC3** or **MC3-NMe_2** prior to the addition of 400 ng supercoiled pUC19.

A-6: Bioanalyzer restriction map

TCGCGCGTTTCGGTGATGACGGTGAAAACCTCTGACACATGCAGCTCCCGGAGACGGTCA
CAGCTTGTCTGTAAGCGGATGCCGGGAGCAGACAAGCCCGTCAGGGCGCGTCAGCGGGTG
TTGGCGGGTGTCGGGGCTGGCTTAACTATGCGGCATCAGAGCAGATTGTACTGAGAGTGC
ACCATATGCGGTGTGAAATACCGCACAGATGCGTAAGGAGAAAATACCGCATCAGGCGCC
ATTCGCCATTCAGGCTGCGCAACTGTTGGGAAGGGCGATCGGTGCGGGCCTCTTCGCTAT
TACGCCAGCTGGCGAAAGGGGGATGTGCTGCAAGGCGATTAAGTTGGGTAACGCCAGGGT
TTTCCCAGTCACGACGTTGTAAAACGACGGCCAGTGAATTCGAGCTCGGTACCCGGGGAT
CCTCTAGAGTCGACCTGCAGGCATGCAAGCTTGGCGTAATCATGGTCATAGCTGTTTCCT
GTGTGAAATTGTTATCCGCTCACAATTCCACACAACATACGAGCCGGAAGCATAAAGTGT
AAAGCCTGGGGTGCCTAATGAGTGAGCTAACTCACATTAATTGCGTTGCGCTCACTGCCC
GCTTTCCAGTCGGGAAACCTGTCGTGCCAGCTGCATTAATGAATCGGCCAACGCGCGGGG
AGAGGCGGTTTGCGTATTGGGCGCTCTTCCGCTTCCTCGCTCACTGACTCGCTGCGCTCG
GTCGTTCGGCTGCGGCGAGCGG

A-7: Synthesis of C_1 and C_2 derivatives

Morphine-C_1 (**MC1**)

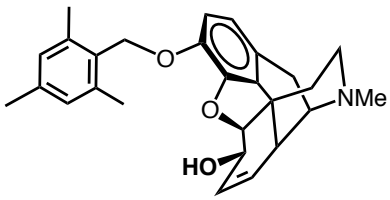

Morphine (0.579 g, 2.03 mmol) and potassium carbonate (1.122 g, 8.12 mmol) were suspended in acetonitrile (30 ml) and heated to reflux. α^2-Chloroisodurene (0.337 g, 2.00 mmol) was added in small aliquots to the reaction mixture and vigorously stirred overnight (18 h) under reflux conditions. After allowing the reaction mixture to cool to rt, the reaction solvent was removed by rotary evaporation and crude product dissolved in DCM (50 ml). The organic layer was washed with d.H_2O (40 ml) and the aqueous layer extracted with DCM (3 x 20 ml). All organic layers were combined, then washed with d.H_2O (3 x 20 ml) and with a saturated NaCl solution (20 ml). The organic layer was dried over magnesium sulfate, filtered and solvents removed by rotary evaporation. The crude product was purified by column chromatography (SiO_2, 95:1:1 to 92:8:1 CH_2Cl_2:MeOH:NH_4OH). The title compound **MC1** was isolated as a white solid in 73% (0.609 g, 1.46 mmol). mp. 225-226 ˚C. ^{1}H NMR (600 MHz, $CDCl_3$) δ: 6.87 (s, 2H), 6.79 (d, *J* = 8.1 Hz, 1H), 6.57 (d, *J* = 8.1 Hz, 1H), 5.67 (ddt, *J* = 9.9, 3.1, 1.8 Hz, 1H), 5.31 – 5.28 (m, 1H), 5.15 (d, *J* = 10.3 Hz, 1H), 4.99 (d, *J* = 10.3 Hz, 1H), 4.86 (dd, *J* = 6.6, 1.2 Hz, 1H), 4.15 (s, 1H), 3.35 (dd, *J* = 6.1, 3.2 Hz, 1H), 3.06 (d, *J* = 18.6 Hz, 1H), 2.77 (s, 1H), 2.66 (p, *J* = 2.7 Hz, 1H), 2.59 (dd, *J* = 12.2, 4.1 Hz, 1H), 2.44 (s, 3H), 2.44 – 2.39 (m, 1H), 2.37 (s, 6H), 2.33 – 2.29 (m, 1H), 2.27 (s, 3H), 2.06 (td, *J* = 12.5, 5.1 Hz, 1H), 1.90 – 1.87 (m, 1H). ^{13}C NMR (151 MHz, $CDCl_3$) δ: 147.65, 141.57, 138.13, 138.09, 133.38, 131.40, 130.23, 128.99, 128.24, 128.18, 119.63, 116.79, 91.16, 77.47, 77.20, 77.12, 76.99, 76.78, 67.00, 66.35, 58.93, 46.48, 43.11, 42.90, 40.81, 35.83, 20.99, 20.61, 19.52. IR (ATR, cm^{-1}): 2928, 2789, 1634, 1500, 1485, 1447, 1380, 1271, 1249, 1152, 1113, 1058, 1037, 1008, 934, 855, 833, 817, 792, 781, 756, 719, 701, 671. $[\alpha]_D$ = − 70 ° (c = 0.152, $CHCl_3$, 589 nm, 25 ˚C)

Morphine-C_2 (**MC2**)

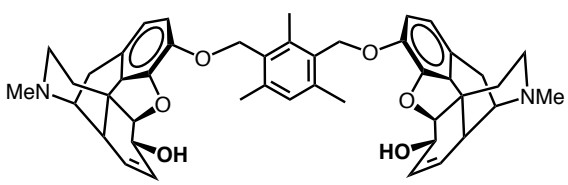

Morphine (0.536 g, 1.88 mmol) and potassium carbonate (1.038 g, 7.51 mmol) were suspended in acetonitrile (30 ml) and heated to reflux. 2,4,-Bis(chloromethyl)-1,3,5-trimethylbenzene (0.204 g, 0.94 mmol) was added in small

aliquots to the reaction mixture and vigorously stirred overnight (18 h) under reflux conditions. After allowing the reaction mixture to cool to rt, the reaction solvent was removed by rotary evaporation and crude product dissolved in DCM (50 ml). The organic layer was washed with d.H_2O (40 ml) and the aqueous layer extracted with DCM (3 x 20 ml). All organic layers were combined, then washed with d.H_2O (3 x 20 ml) and with a saturated NaCl solution (20 ml). The organic layer was dried over magnesium sulfate, filtered and solvents removed by rotary evaporation. The crude product was purified by column chromatography (SiO_2, 95:1:1 to 92:8:1 CH_2Cl_2:MeOH:NH_4OH). The title compound **MC2** was isolated as a white solid in 35% yield (0.235 g, 0.33 mmol). mp. 144-146 ˚C. ^{1}H NMR (600 MHz, $CDCl_3$) δ: 6.92 (s, 1H), 6.80 (d, *J* = 8.1 Hz, 2H), 6.58 (d, *J* = 8.1 Hz, 2H), 5.68 (ddt, *J* = 9.9, 3.1, 1.4 Hz, 2H), 5.30 – 5.27 (m, 2H), 5.18 (d, *J* = 10.3 Hz, 2H), 5.02 (d, J = 10.4 Hz, 2H), 4.86 (dd, J = 6.5, 1.1 Hz, 2H), 4.17 – 4.12 (m, 2H), 3.36 (dd, *J* = 5.4, 2.9 Hz, 2H), 3.05 (d, *J* = 18.7 Hz, 2H), 2.91 (s, 2H), 2.69 – 2.65 (m, 2H), 2.61 (dd, *J* = 12.0, 4.1 Hz, 2H), 2.46 (d, *J* = 5.4 Hz, 9H), 2.41 (dd, *J* = 12.6, 3.1 Hz, 2H), 2.37 (s, 6H), 2.34 – 2.29 (m, 2H), 2.06 (td, *J* = 12.5, 5.0 Hz, 2H), 1.91 – 1.87 (m, 2H). ^{13}C NMR (151 MHz, $CDCl_3$) δ: 147.58, 141.48, 138.95, 138.45, 133.39, 131.40, 131.33, 130.20, 128.09, 119.59, 116.55, 91.15, 77.16, 76.95, 76.74, 67.15, 66.34, 58.91, 46.44, 43.02, 42.86, 40.70, 35.70, 20.61, 19.74, 15.34. IR (ATR, cm^{-1}): 2907, 1633, 1602,1493, 1443, 1374, 1349, 1273, 1248, 1200, 1175, 1157, 1118, 1099, 1034, 983, 940, 833, 784, 766, 730. $[\alpha]_D$ = − 78° (c = 0.155, $CHCl_3$, 589 nm, 25 ˚C)

Oripavine-C_1 (**OC1**)

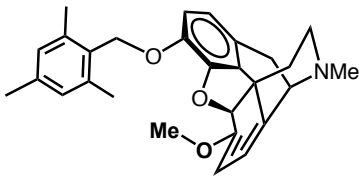

A flask was charged with oripavine (0.654 g, 2.19 mmol), tetrabutylammonium hydroxide (40% aqueous solution, 18 ml) and CH_2Cl_2 (8 ml) and stirred under nitrogen for 30 mins. A solution of α^2-chloroisodurene (0.371 g, 2.20 mmol) in CH_2Cl_2 (4 ml) was added and the biphasic reaction mixture was stirred for 6 h at rt. The reaction solution was transferred into d.H_2O (150 ml) and washed with DCM (4 x 10 ml). Organic layers were combined and washed with aqueous sodium hydroxide solution (0.1 M, 2 x 20 ml) followed by d.H_2O (3 x 20 ml) then saturated brine solution (20 ml). The organic layer was dried over magnesium sulfate, filtered and solvents removed by rotary evaporation. The crude product was purified by column chromatography (SiO_2, 95:1:1 to 92:8:1 CH_2Cl_2:MeOH:NH_4OH), The title compound **OC1** was isolated as a white solid in in 54% (0.511 g, 1.19

mmol). mp. 74-76˚C. ^{1}H NMR (600 MHz, $CDCl_3$) δ: 6.86 (s, 2H), 6.73 (d, *J* = 8.1 Hz, 1H), 6.58 (d, *J* = 8.1 Hz, 1H), 5.57 (d, *J* = 6.4 Hz, 1H), 5.29 (s, 1H), 5.19 (d, *J* = 10.4 Hz, 1H), 5.10 (d, *J* = 10.4 Hz, 1H), 5.04 (d, *J* = 6.4 Hz, 1H), 3.63 (d, *J* = 6.7 Hz, 1H), 3.60 (s, 3H), 3.33 (d, *J* = 18.0 Hz, 1H), 2.84 (td, *J* = 12.7, 3.5 Hz, 1H), 2.69 (dd, *J* = 18.2, 7.2 Hz, 1H), 2.65 (dd, *J* = 12.9, 5.0 Hz, 1H), 2.47 (s, 3H), 2.38 (s, 6H), 2.27 (s, 3H), 2.22 (td, *J* = 12.6, 5.0 Hz, 1H), 1.77 (dd, *J* = 12.5, 2.0 Hz, 2H). ^{13}C NMR (151 MHz, $CDCl_3$) δ: 153.12, 146.24, 142.42, 138.62, 138.18, 134.14, 132.74, 130.90, 129.23, 128.87, 119.62, 117.48, 111.97, 96.30, 89.30, 77.58, 77.37, 77.16, 67.20, 61.27, 55.20, 46.43, 46.36, 42.73, 37.26, 30.16, 30.04, 21.34, 19.84. IR (ATR, cm^{-1}): 2912, 1602, 1493, 1473, 1369, 1331, 1278, 1232, 1144, 1022, 985, 868, 817, 768, 704. $[\alpha]_D$ = − 124° (c = 0.154, $CHCl_3$, 589nm, 25 ˚C)

Oripavine-C_2 (**OC2**)

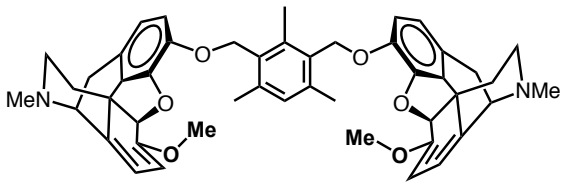

A flask was charged with oripavine (0.612 g, 2.05 mmol), tetrabutylammonium hydroxide (40% aqueous solution, 18 ml) and CH_2Cl_2 (6 ml) and stirred under nitrogen for 30 mins. A solution of 2,4-Bis(chloromethyl)-1,3,5-trimethylbenzene (0.224 g, 1.03 mmol) in CH_2Cl_2 (4 ml) was added and the biphasic reaction mixture was stirred for 6 h at rt. The reaction solution was transferred into d.H_2O (150 ml) and washed with DCM (4 x 10 ml). Organic layers were combined and washed with aqueous sodium hydroxide solution (0.1 M, 2 x 20 ml) followed by d.H_2O (3 x 20 ml) then saturated brine solution (20 ml). The organic layer was dried over magnesium sulfate, filtered and solvents removed by rotary evaporation. The crude product was purified by column chromatography (SiO_2, 95:1:1 to 92:8:1 CH_2Cl_2:MeOH:NH_4OH), The title compound **OC2** was isolated as a white solid in 30% yield (0.172 g, 0.23 mmol). ^{1}H NMR (600 MHz, $CDCl_3$) δ: 6.88 (s, 1H), 6.74 (d, *J* = 8.1 Hz, 2H), 6.58 (d, *J* = 8.1 Hz, 2H), 5.56 (d, *J* = 6.4 Hz, 2H), 5.29 (s, 2H), 5.23 (d, *J* = 10.5 Hz, 2H), 5.13 (d, *J* = 10.5 Hz, 2H), 5.03 (d, *J* = 6.4 Hz, 2H), 3.62 (d, *J* = 6.8 Hz, 2H), 3.59 (s, 6H), 3.32 (d, *J* = 18.0 Hz, 2H), 2.83 (td, *J* = 12.7, 3.4 Hz, 2H), 2.68 (dd, *J* = 18.2, 7.1 Hz, 2H), 2.63 (dd, *J* = 12.8, 4.8 Hz, 2H), 2.47 (d, *J* = 5.1 Hz, 9H), 2.37 (s, 6H), 2.21 (td, *J* = 12.6, 5.1 Hz, 2H), 1.76 (dd, *J* = 12.5, 2.0 Hz, 2H). ^{13}C NMR (151 MHz, $CDCl_3$) δ: 153.02, 146.19, 142.28, 139.50, 138.66, 134.11, 132.78, 131.93, 130.30, 128.87, 119.55, 117.53, 111.79, 96.24, 89.24, 77.58, 77.37, 77.16, 67.53, 61.17, 55.13, 46.37, 46.29, 42.71, 37.26, 30.04, 20.03, 15.57. IR (ATR, cm^{-1}): 2909, 1605, 1491,

1436, 1369, 1367, 1232, 1143, 1021, 983, 867, 816, 746. $[\alpha]_D$ = − 106° (c = 0.156, $CHCl_3$, 589 nm, 25 ˚C)

N-Methyl Morphine-C_3 (**MC3-NMe$_2$**)

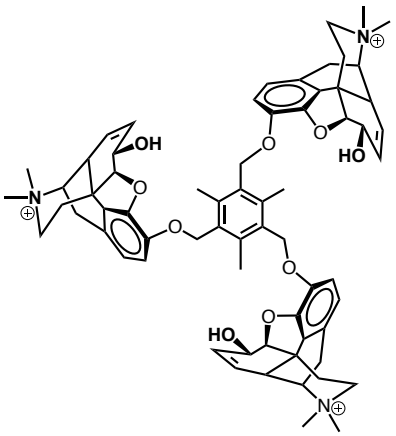

A flask was charged with **MC3** (100 mg, 0.098 mmol) and dissolved in hot EtOH (5 ml), MeI (100 µL, 1.60 mmol) was added and heated under reflux conditions for 18 h. The solution was allowed to cool and the precipitate collected by vacuum filtration. The product was twice recrystallized from MeOH. The title compound **MC3-NMe$_2$** was isolated as a yellow solid in 14% yield (20 mg, 0.013 mmol). mp. 264-265˚C. ^{1}H NMR (600 MHz, CD_3CN) δ: 6.92 (d, *J* = 8.2 Hz, 3H), 6.66 (d, *J* = 8.2 Hz, 3H), 5.75 (d, *J* = 10.0 Hz, 3H), 5.32 (dt, *J* = 10.0, 2.6 Hz, 3H), 5.23 (d, *J* = 10.9 Hz, 3H), 5.16 (d, *J* = 10.9 Hz, 3H), 4.98 (dd, *J* = 6.5, 1.0 Hz, 3H), 4.36-4.31 (m, 3H), 4.03-3.99 (m, 3H), 3.48 (d, *J* = 20.5 Hz, 3H), 3.40 (s, 3H), 3.36 – 3.30 (m, 15H), 3.25 (s, 9H), 3.20 (td, *J* = 13.4, 3.7 Hz, 3H), 2.90 (dd, *J* = 20.5, 6.0 Hz, 3H), 2.59 – 2.53 (m, 3H), 2.44 (s, 9H). IR (ATR, cm^{-1}): 2944, 1632, 1607, 1494, 1448, 1250, 1186, 1163, 1119, 1037, 1014, 985, 944, 849, 782, 757.

MC1 spectra:

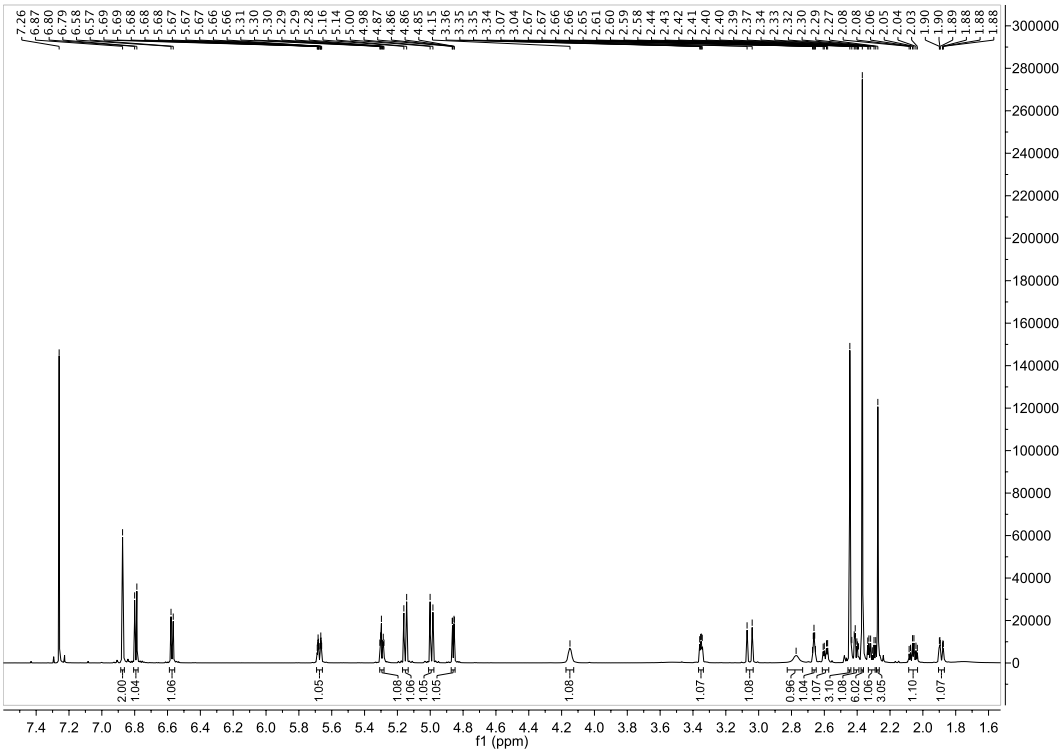

Figure A-18. ^{1}H NMR spectra for **MC1.**

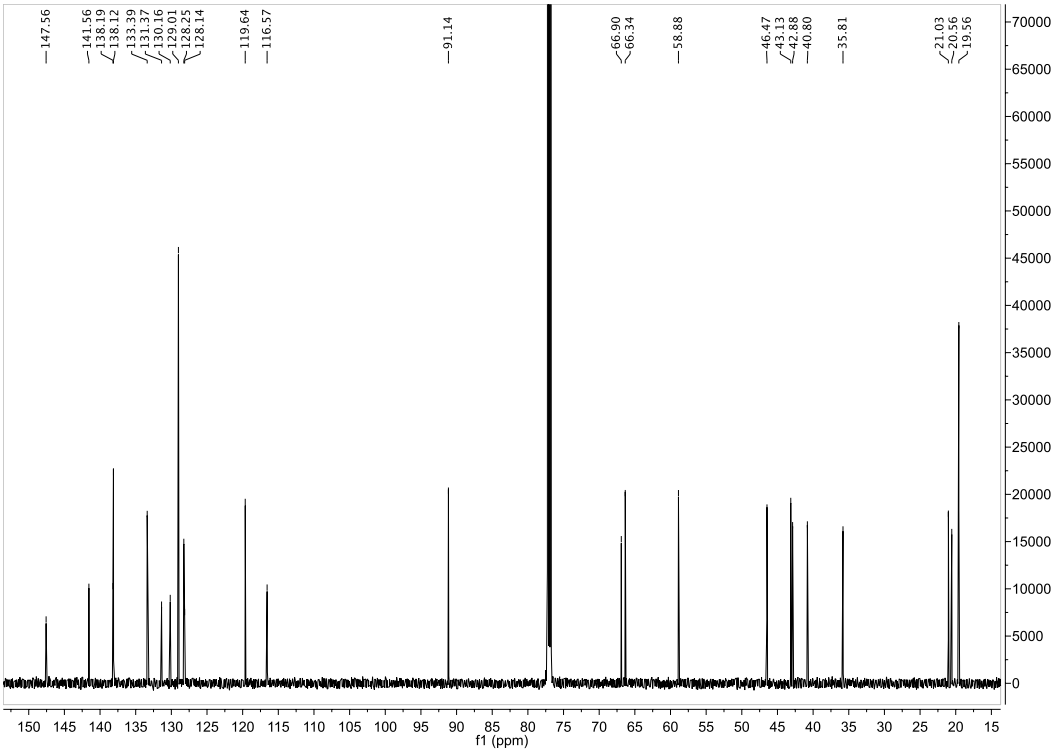

Figure A-19. ^{13}C NMR spectra for **MC1.**

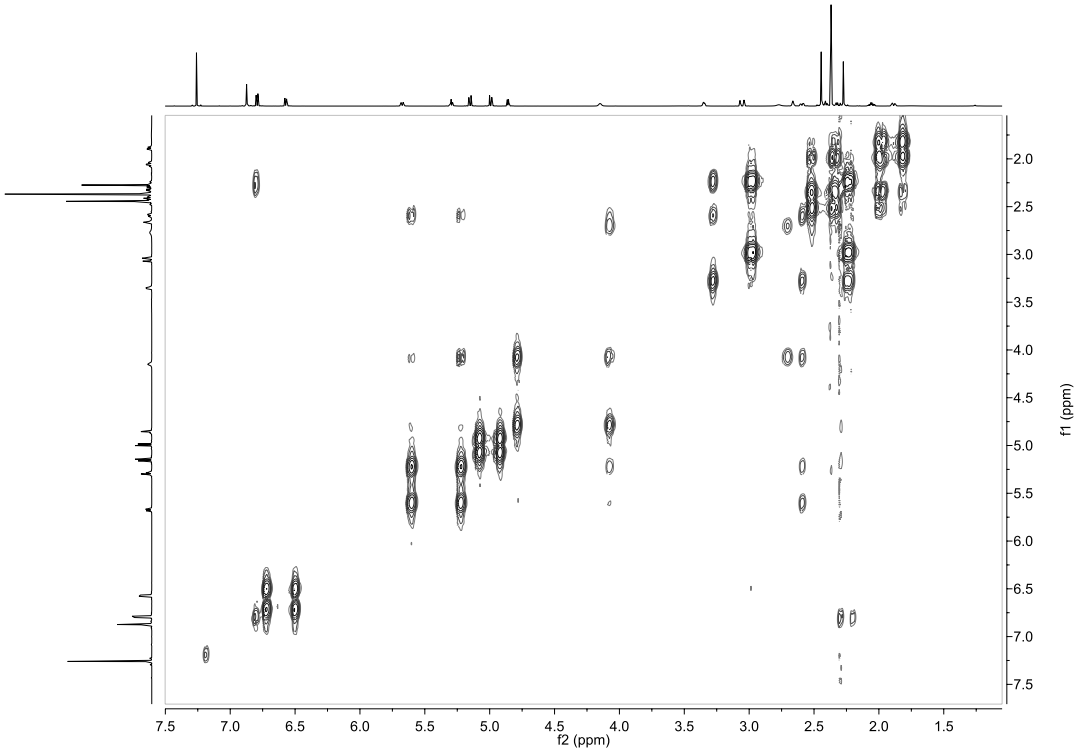

Figure A-20. COSY NMR spectra for **MC1.**

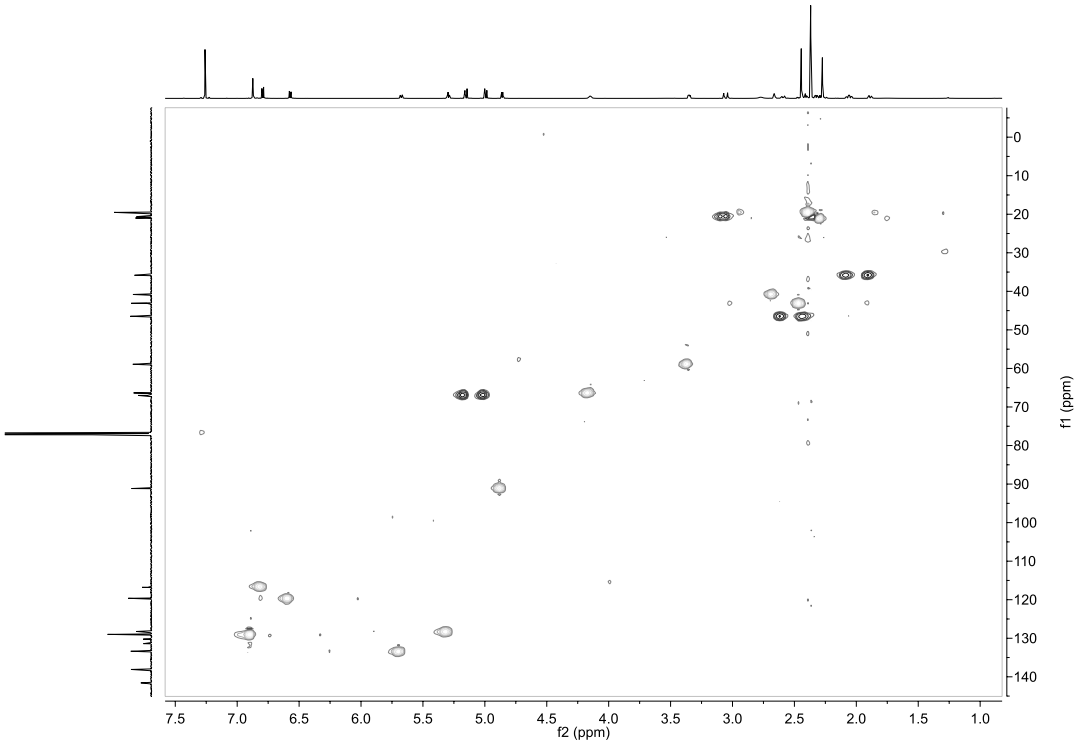

Figure A-21. HSQC NMR spectra for **MC1.**

MC2 spectra:

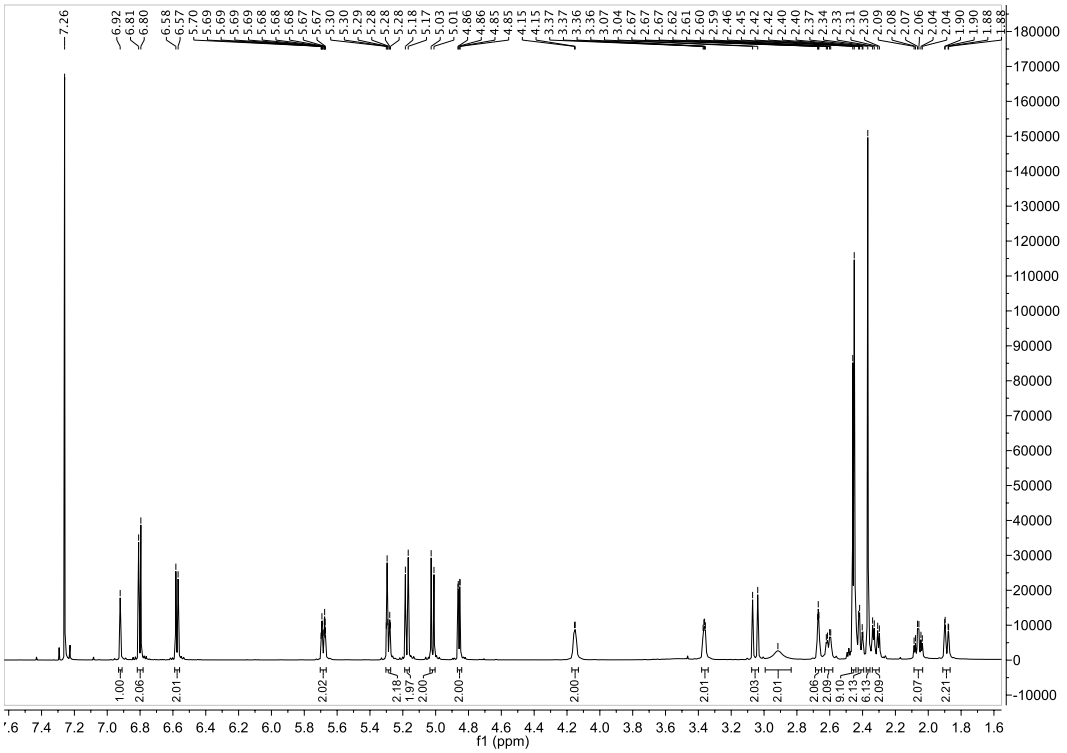

Figure A-22. ^{1}H NMR spectra for **MC2.**

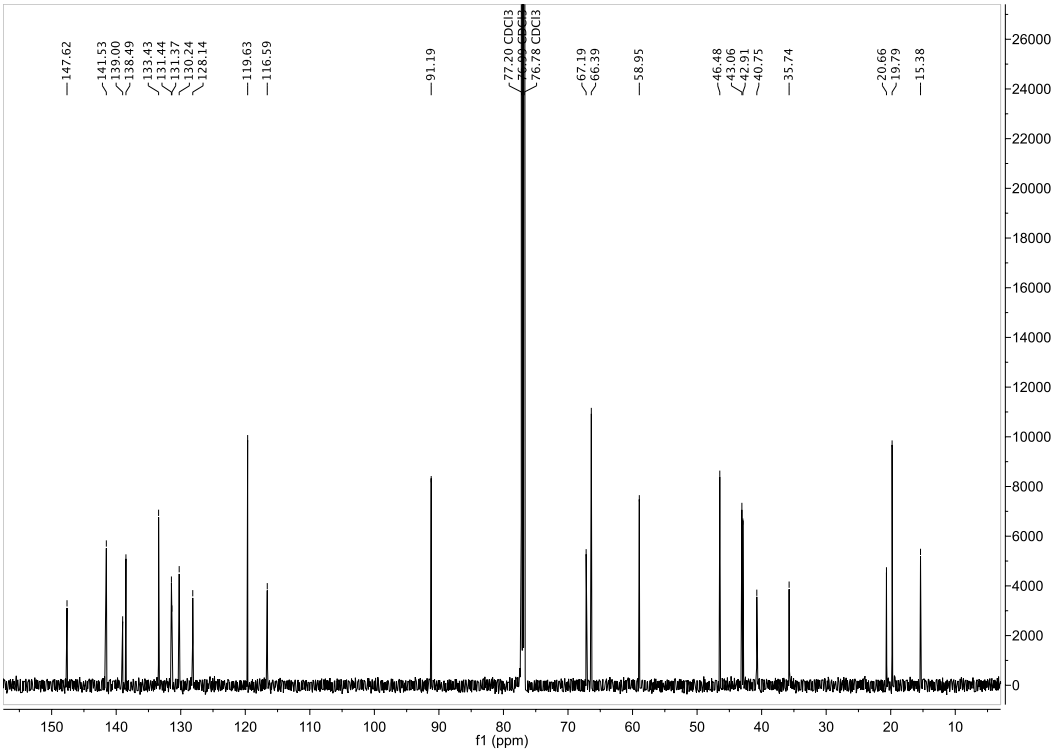

Figure A-23. ^{13}C NMR spectra for **MC2.**

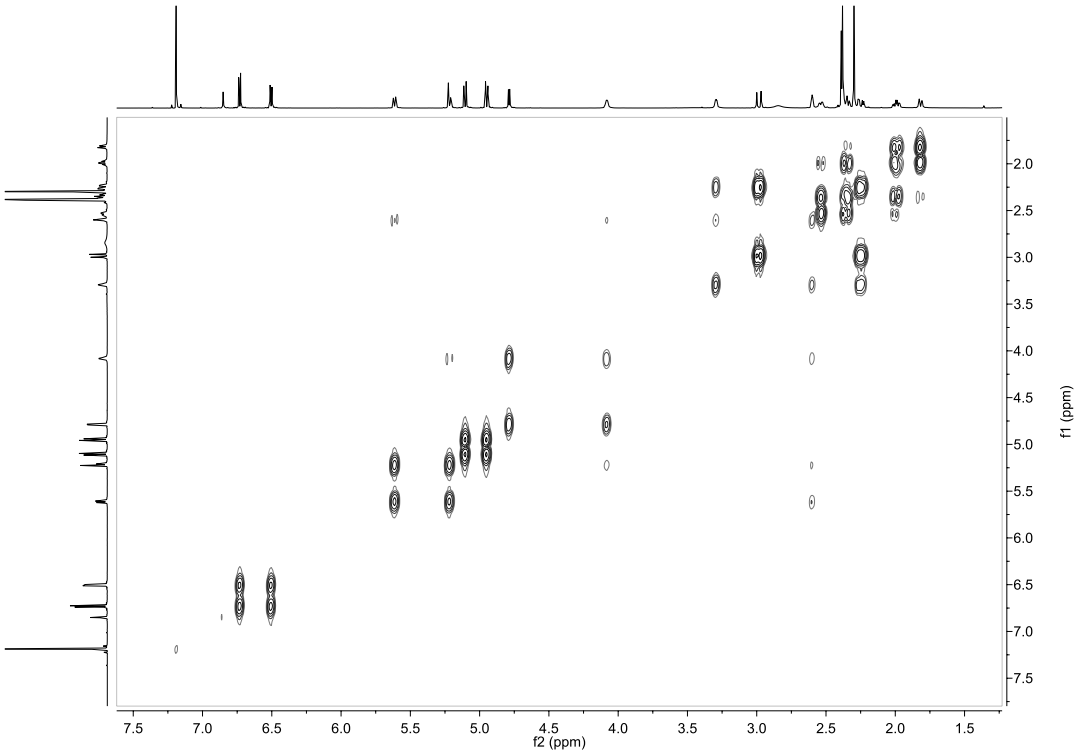

Figure A-24. COSY NMR spectra for **MC2.**

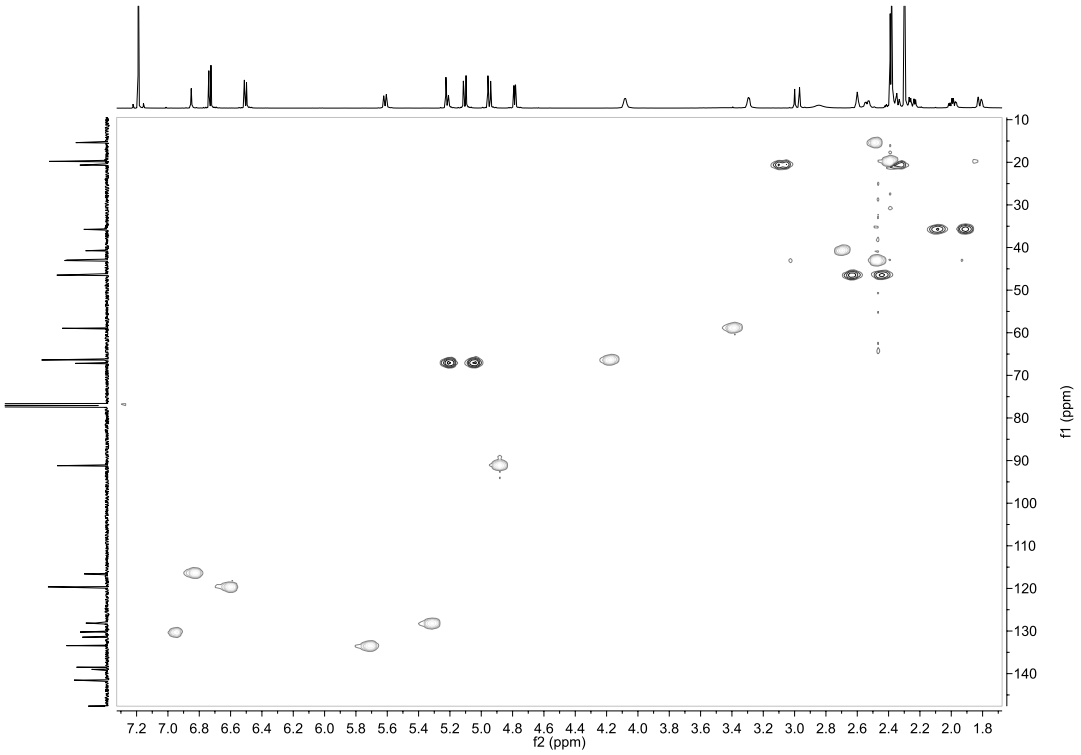

Figure A-25. HMQC NMR spectra for **MC2.**

OC1 Spectra:

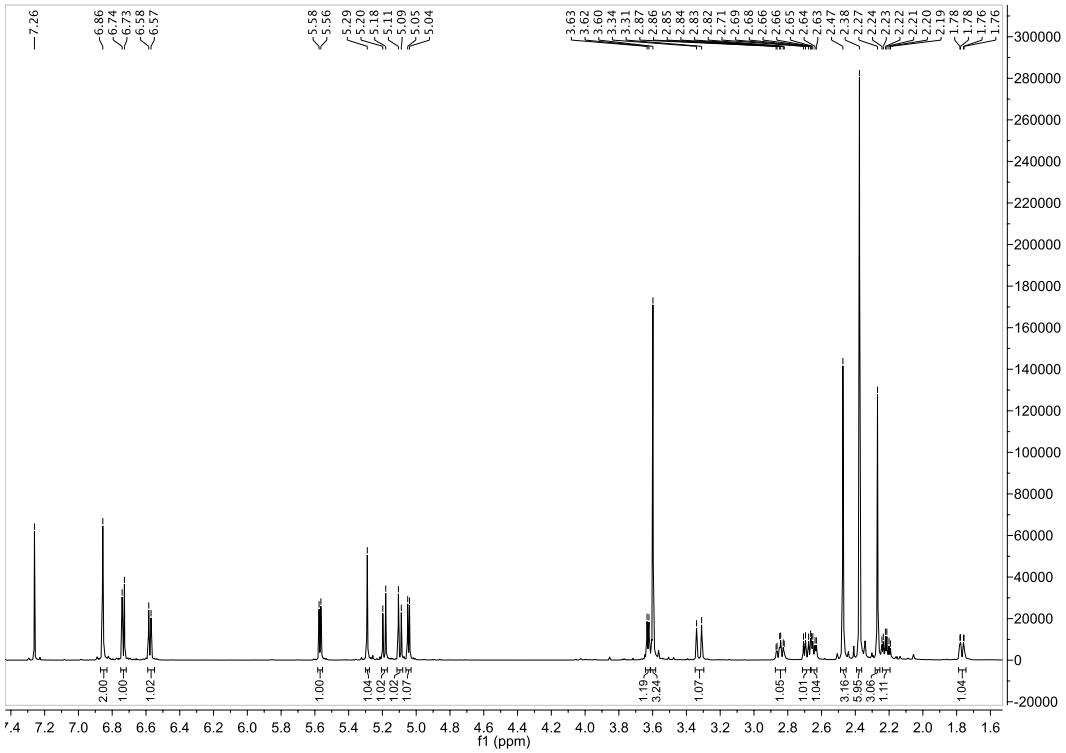

Figure A-26. ^{1}H NMR spectra for **OC1**.

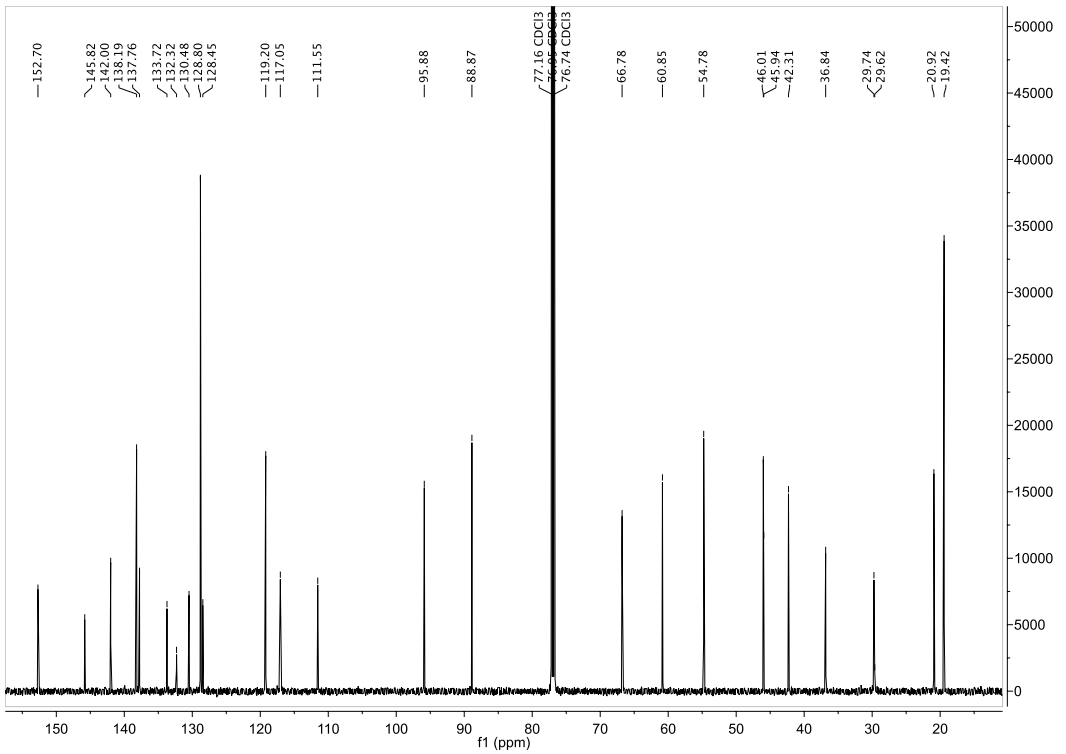

Figure A-27. ^{13}C NMR spectra for **OC1**.

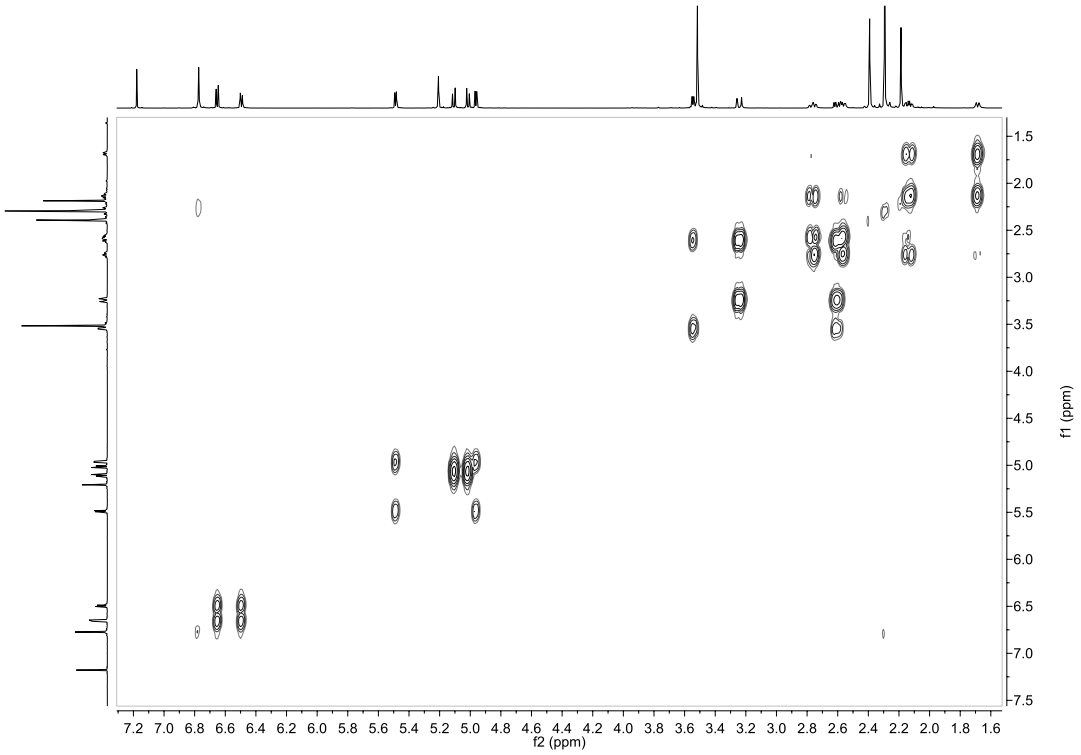

Figure A-28. COSY NMR spectra for **OC1**.

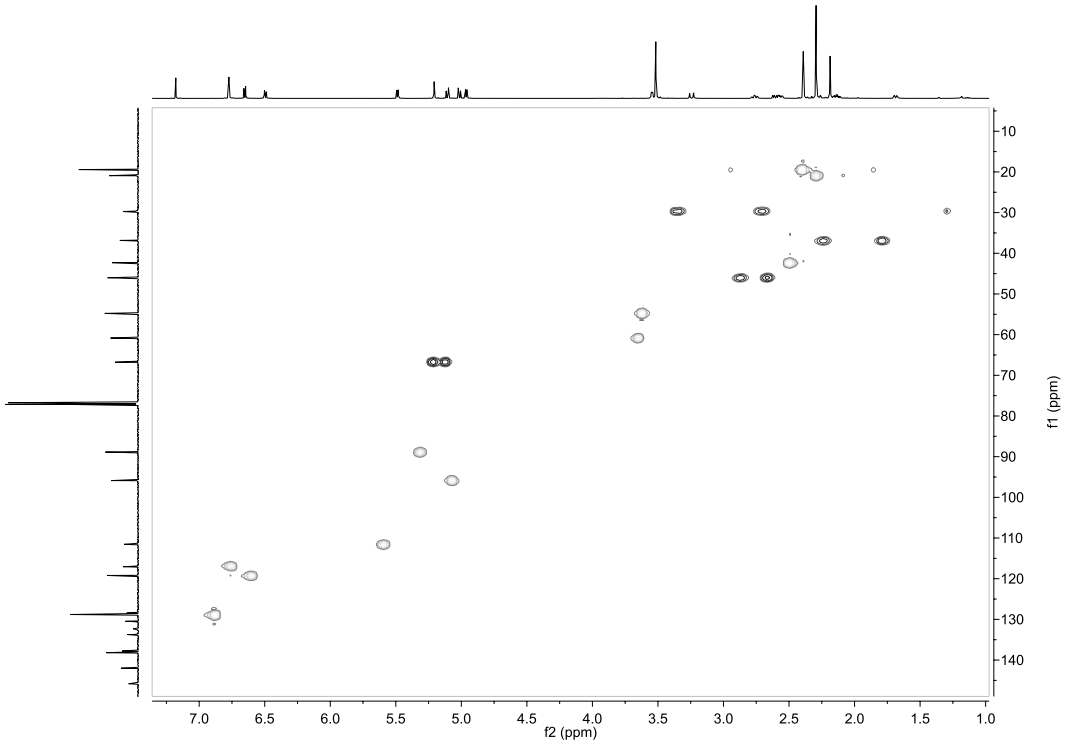

Figure A-29. HMQC NMR spectra for **OC1**.

OC2 spectra:

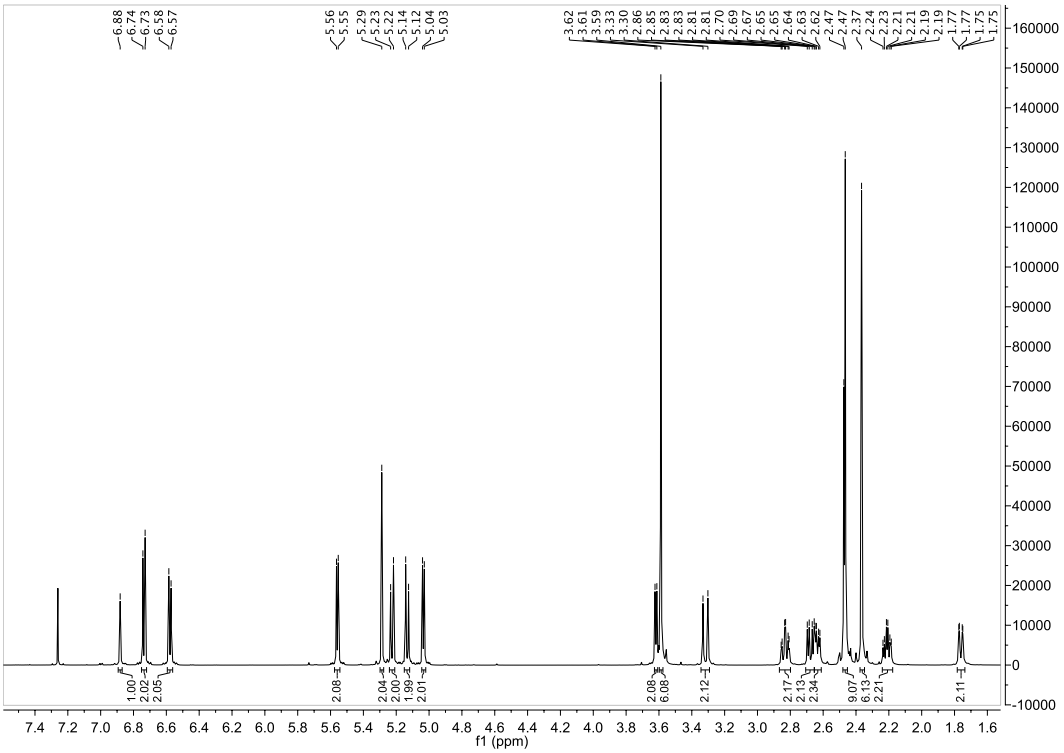

Figure A-30. ^{1}H NMR spectra for **OC2**.

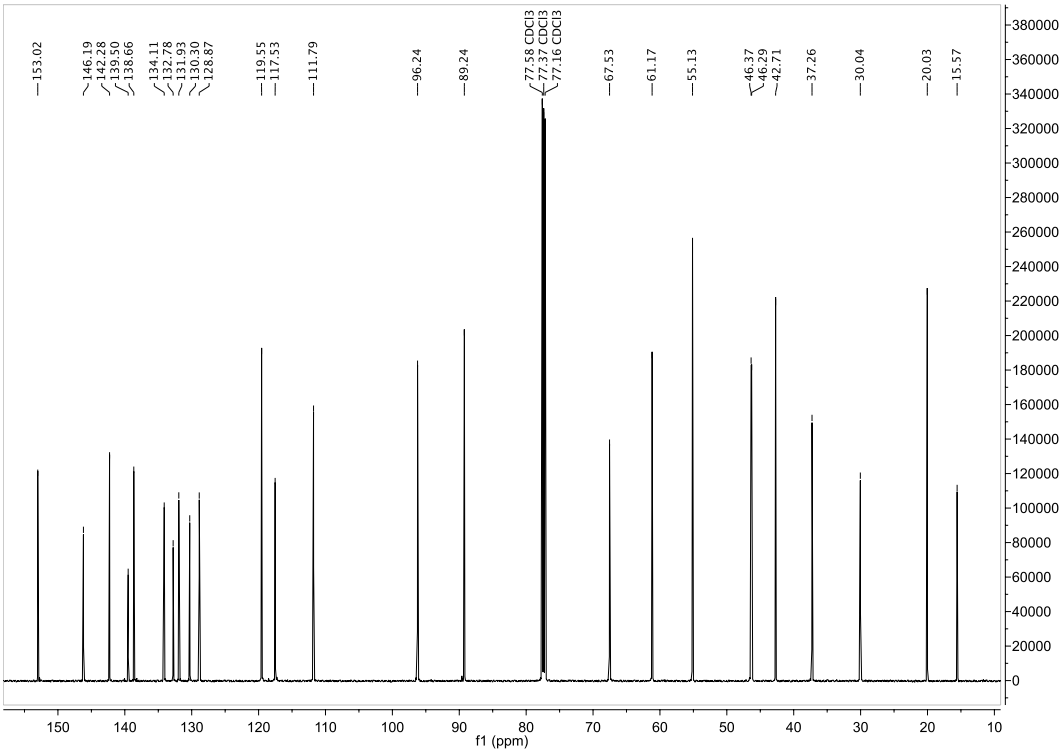

Figure A-31. ^{13}C NMR spectra for **OC2**.

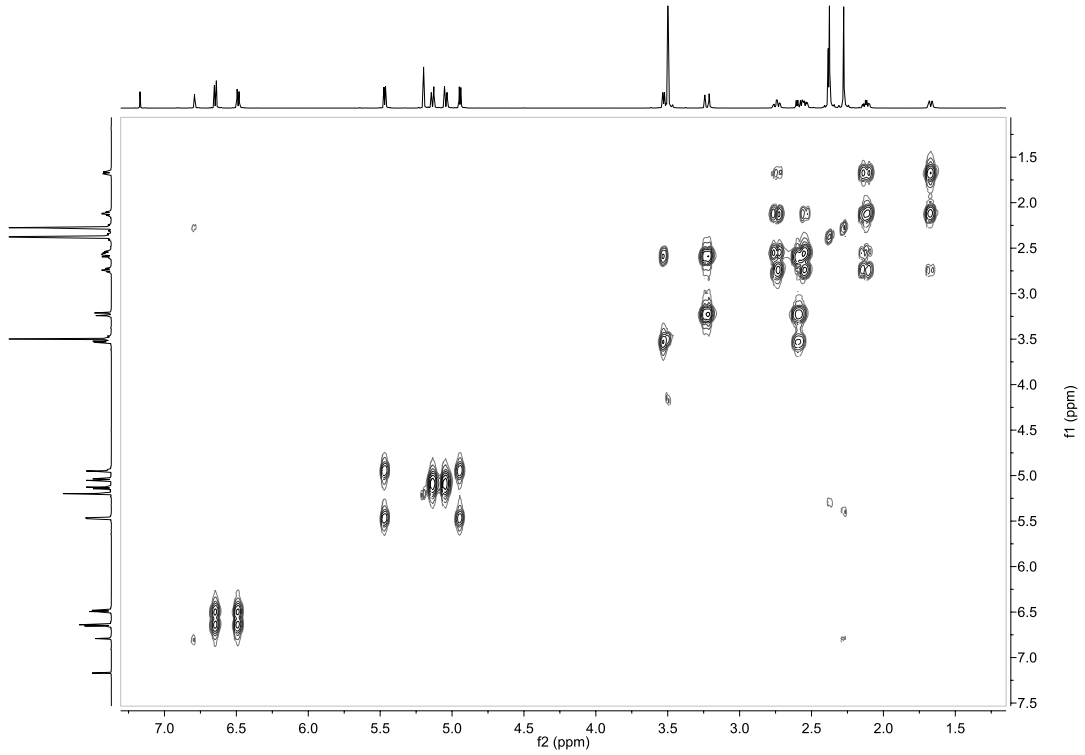

Figure A-32. COSY NMR spectra for **OC2**.

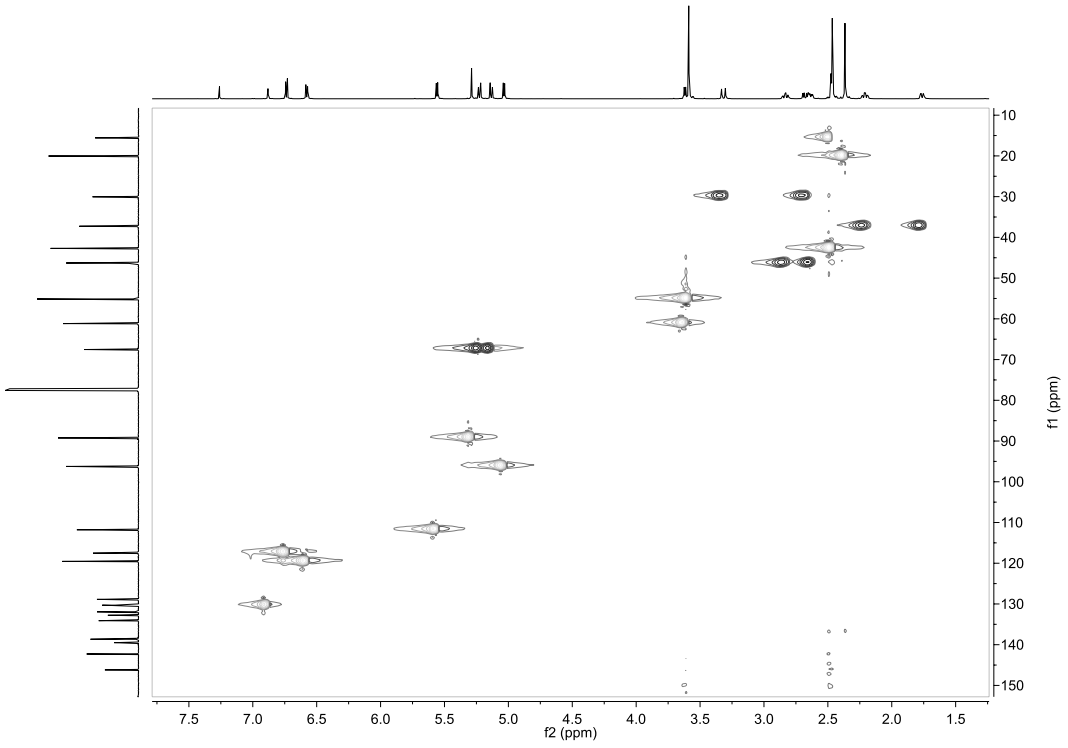

Figure A-33. HMQC NMR spectra for **OC2**.

MC3-NMe$_2$ spectra:

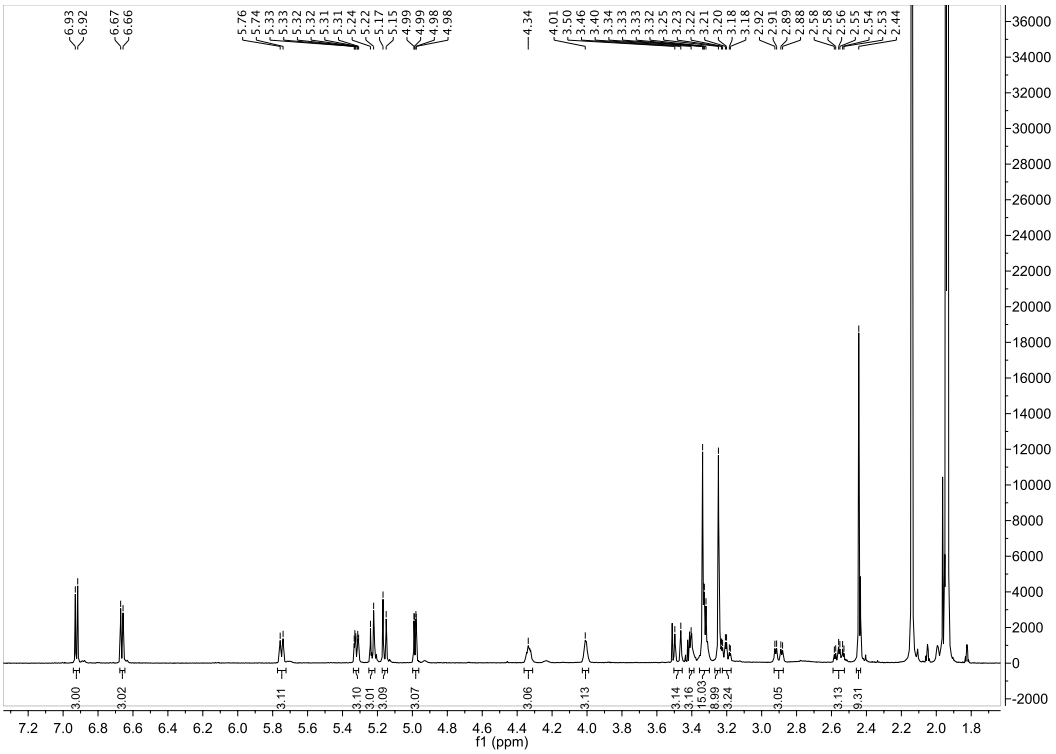

Figure A-34. ^{1}H NMR spectra for **MC3-NMe$_2$**.

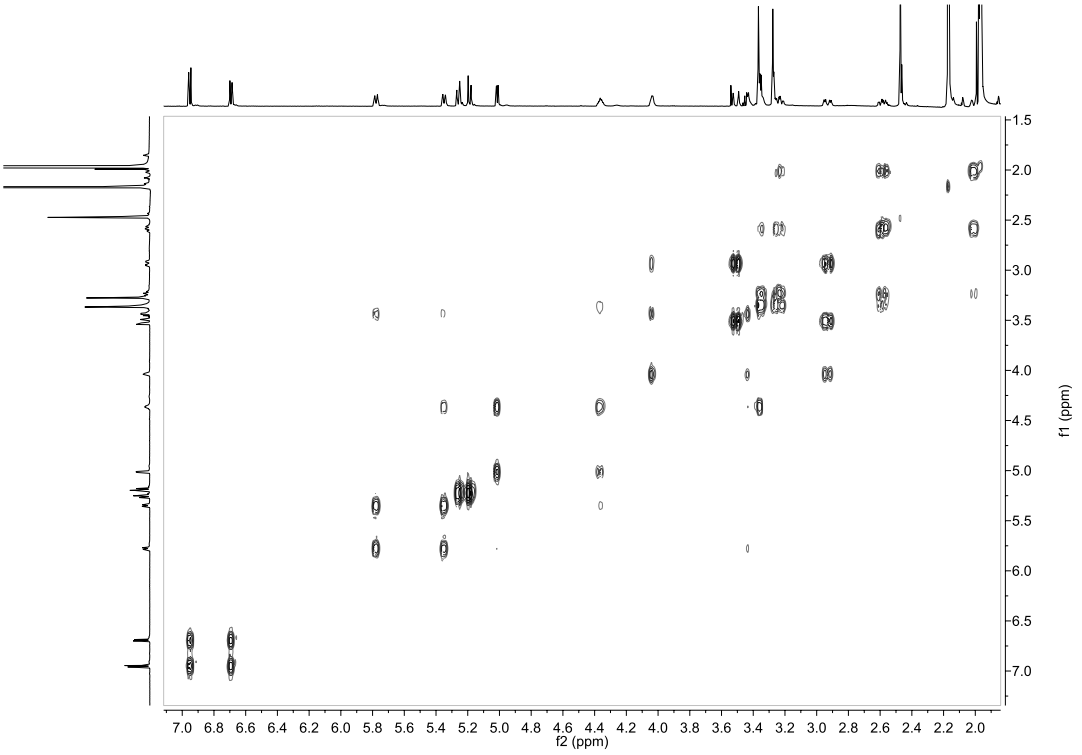

Figure A-35. COSY NMR spectra for **MC3-NMe$_2$**.

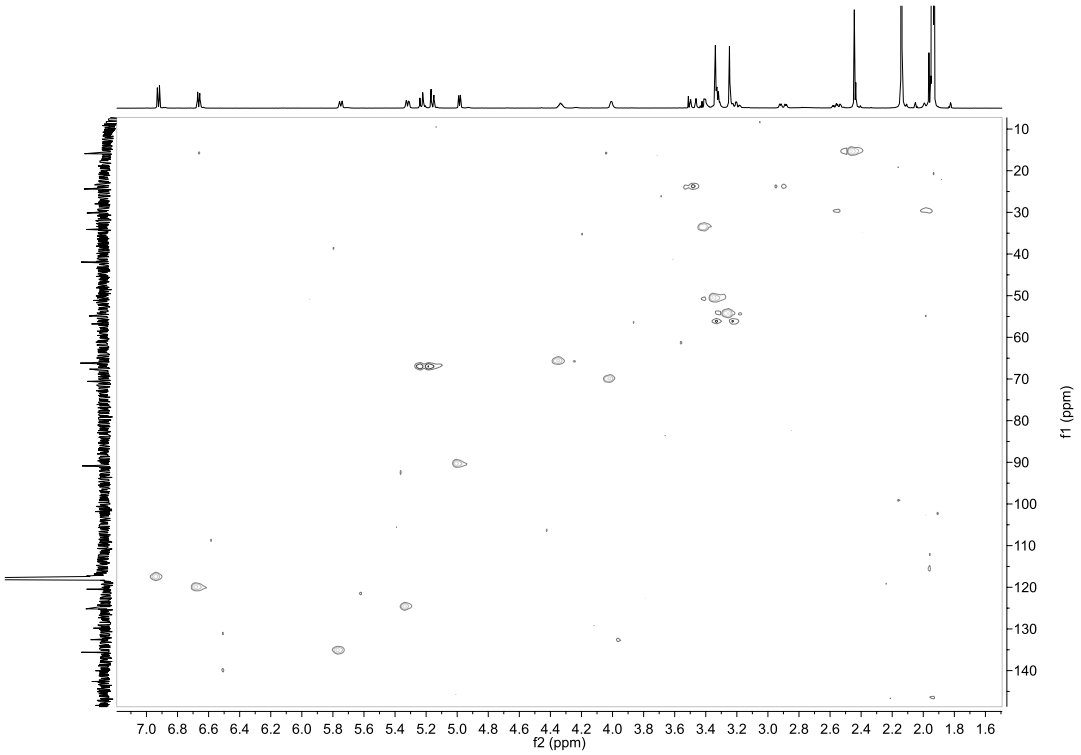

Figure A-36. HSQC NMR spectra for **MC3-NMe$_2$**.

A-8: Morphine isomerization

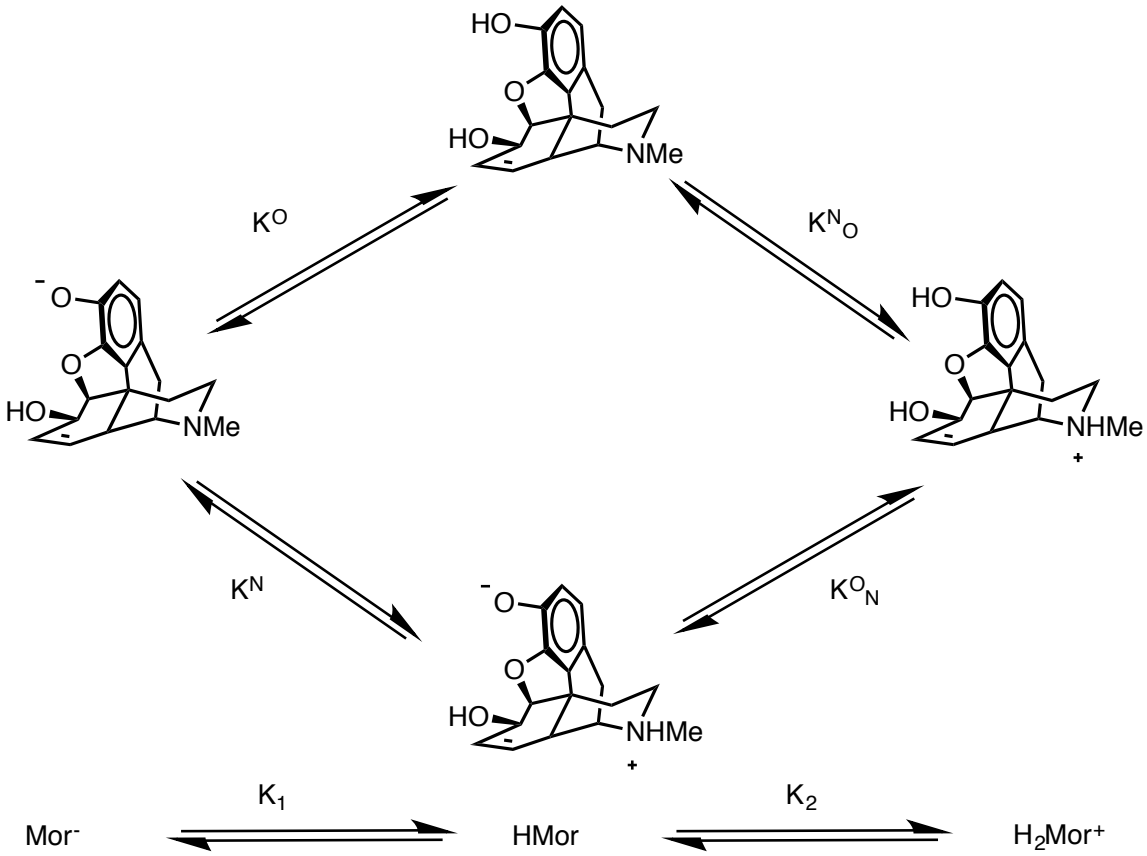

Scheme A-1. Interplay between morphine protonation (k^O) and zwitterionic (k^N) isomers under physiological conditions.

A-9: Gel electrophoresis with yeast tRNA

In a total volume of 20 µL using 80 mM HEPES buffer (pH 7.2) with 25 mM NaCl, 400 ng yeast tRNA (ε_{260} = 9,250 M^{-1} cm^{-1}) (AM7119, Invitrogen) was titrated against **MC3** (0.5 – 50.0 µM). Samples were incubated at 37˚C for 5 h, quenched by adding 6 × loading buffer (Fermentas) containing 10 mM Tris-HCl, 0.03 % bromophenol blue, 0.03 % xylene cyanole FF, 60 % glycerol, 60 mM EDTA and loaded onto an agarose gel (1.2 %) containing 3 µL EtBr. Electrophoresis was completed at 60 V for 1 h in 1 × TAE buffer.

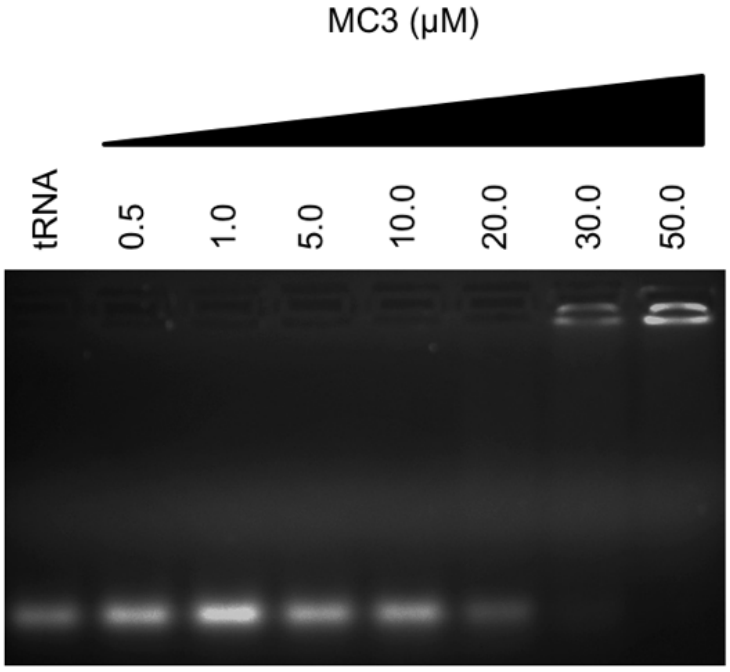

Figure A-37. Agarose gel electrophoresis of yeast tRNA (400 ng) exposed to increasing concentrations of **MC3**. Reactions were carried out in the presence of 25 mM NaCl for 5 h at 37 ˚C prior to electrophoretic analysis.

A-10: Green chemistry metrics

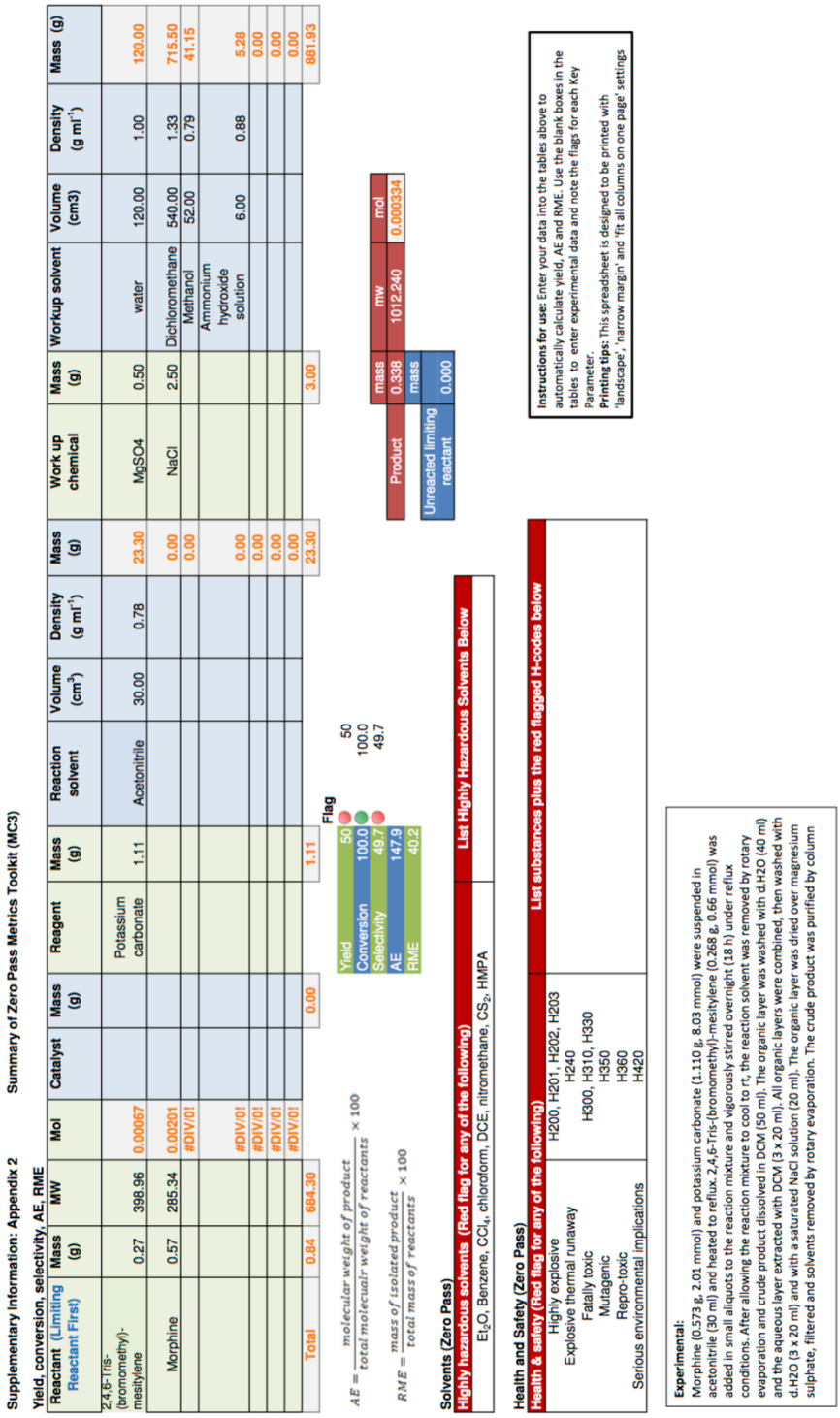

Figure A-38. Zero pass metric **MC3**.

Figure A-39. First pass metric **MC3.**

Supplementary Information: Appendix 2 **Summary of First Pass Metrics Toolkit (MC3)**

Yield, AE, RME, MI/PMI and OE

Reactant (Limiting Reactant First)	Mass (g)	MW	Mol	Catalyst	Mass (g)	Reagent	Mass (g)	Reaction solvent	Volume (cm^3)	Density ($g\ ml^{-1}$)	Mass (g)	Work up chemical	Mass (g)	Workup solvent	Volume (cm3)	Density ($g\ ml^{-1}$)	Mass (g)
2,4,6-Tris-(bromomethyl)-mesitylene	0.27	398.96	0.00067			Potassium carbonate	1.11	Acetonitrile	30.00	0.78	23.40	MgSO4	0.50	water	120.00	1.00	120.00
Morphine	0.57	285.34	0.00201								0.00	NaCl	2.50	Dichloromethane	540.00	1.33	715.50
			#DIV/0!								0.00			Methanol	52.00	0.79	41.15
			#DIV/0!								0.00			Ammonium hydroxide solution	6.00	0.88	5.28
			#DIV/0!								0.00						0.00
			#DIV/0!								0.00						0.00
Total	0.84	684.30			0.00		1.11				23.40		3.00				881.93

$$RME = \frac{mass\ of\ isolated\ product}{total\ mass\ of\ reactants} \times 100$$

$$AE = \frac{molecular\ weight\ of\ product}{total\ molecualr\ weight\ of\ reactants} \times 100$$

$$mass\ intensity = \frac{total\ mass\ in\ a\ process\ or\ process\ step}{mass\ of\ product}$$

$$OE = \frac{RME}{AE} \times 100$$

		Flag
Yield	50	50
Conversion	100.0	100.0
Selectivity	49.7	49.7
AE	147.9	
RME	40.2	OE 27.2
PMI total	2693.1	
PMI Reaction	75.0	
PMI reactants, reagents, catlyst	5.8	
PMI reaction solvents	69.2	
PMI Workup	2618.1	
PMI Workup chemical	8.9	
PMI workup solvents	2609.3	

	Mass	MW	Mol
Product	0.338	1012.240	0.00033
	mass		
Unreacted limiting reactant	0.00		

Experimental:
Morphine (0.573 g, 2.01 mmol) and potassium carbonate (1.110 g, 8.03 mmol) were suspended in acetonitrile (30 ml) and heated to reflux. 2,4,6-Tris-(bromomethyl)-mesitylene (0.268 g, 0.66 mmol) was added in small aliquots to the reaction mixture and vigorously stirred overnight (18 h) under reflux conditions. After allowing the reaction mixture to cool to rt, the reaction solvent was removed by rotary evaporation and crude product dissolved in DCM (50 ml). The organic layer was washed with d.H2O (40 ml) and the aqueous layer extracted with DCM (3 x 20 ml). All organic layers were combined, then washed with d.H2O (3 x 20 ml) and with a saturated NaCl solution (20 ml). The organic layer was dried over magnesium sulphate, filtered and solvents removed by rotary evaporation. The crude product was purified by column chromatography (SiO2, 95:1:1 to 92:8:1 CH2Cl2:MeOH:NH4OH). The title compound MC3 was isolated as a white solid in 50 % yield (0.338 g, 0.33 mmol).

Solvents (First Pass)

		List solvents below
Preferred solvents	**water,** EtOH, nBuOH, AcOipr, AcOnBu, PhOMe, MeOH, tBuOH, BnOH, ethylene glycol, acetone, MEK, MIBK, **AcOEt,** sulfolane	Water, MeOH
Problematic solvents: (acceptable only if substitution does not offer advantages)	DMSO, cyclohexanone, DMPU, AcOH, Ac2O, Acetonitrile, AcOMe, THF, heptane, Me-cyclohexane, toluene, xylene, MTBE, **cyclohexane**, chlorobenzene, formic acid, pyridine, Me-THF	Acetonitrile
Hazardous solvents: These solvents have significant health and/or safety concerns.	dioxane, pentane, TEA, diisopropyl ether, DME, DCM, DMF, DMA, NMP, methoxyethanol, hexane	DCM
Highly hazardous solvents: The solvents which are agreed not to be used, even in screening	Et_2O, Benzene, CCl_4, chloroform, DCE, nitromethane, CS_2, HMPA	

Instructions for use: Enter your data into the tables above to automatically calculate yield, AE, RME, MI/PMI and OE.
Use the blank boxes in the tables to enter experimental data and note the flags for each Key Parameter.
Printing tips: This spreadsheet is designed to be printed with 'landscape', 'narrow margin' and 'fit all columns on one page' settings

Catalyst/enzyme (First Pass)

		Tick
Catalyst or enzyme used, **or** reaction takes place without **any** catalyst/reagents.	Green Flag	
Use of stoichiometric quantities of reagents	Amber Flag	
Use of reagents in excess	Red Flag	✓

		Tick
Facile recovery of catalyst/enzyme	Green Flag	
catalyst/enzyme not recovered	Amber Flag	

Figure A-40. First pass metric **MC3** continued.

Figure A-41. Zero pass metric **OC3**.

Supplementary Information: Appendix 2 **Summary of Zero Pass Metrics Toolkit (OC3)**

Yield, conversion, selectivity, AE, RME

Reactant (Limiting Reactant First)	Mass (g)	MW	Mol	Catalyst	Mass (g)	Reagent	Mass (g)	Reaction solvent	Volume (cm^3)	Density (g ml^{-1})	Mass (g)	Work up chemical	Mass (g)	Workup solvent	Volume (cm3)	Density (g ml^{-1})	Mass (g)
2,4,6-Tris-(bromomethyl)-mesitylene	0.27	398.96	0.00067			tetrabutyl-ammonium hydroxide	7.27	water	18.00	1.00	18.00	MgSO4	0.50	water	120.00	1.00	120.00
Oripavine	0.60	297.35	0.00200					DCM	10.00	1.33	13.30	NaCl	2.50	dichloromethane	440.00	1.33	583.00
			#DIV/0!								0.00	NaOH	0.16	Methanol	55.00	0.79	43.52
			#DIV/0!								0.00			Ammonium hydroxide solution	5.00	0.88	4.40
			#DIV/0!								0.00						0.00
			#DIV/0!								0.00						0.00
			#DIV/0!								0.00						0.00
Total	0.86	696.31			0.00		7.27				31.30		3.16				750.92

$$AE = \frac{molecular\ weight\ of\ product}{total\ molecualr\ weight\ of\ reactants} \times 100$$

$$RME = \frac{mass\ of\ isolated\ product}{total\ mass\ of\ reactants} \times 100$$

		Flag	
Yield	47	🔴	47
Conversion	100.0	🟢	100.0
Selectivity	46.5	🔴	46.5
AE	150.5		
RME	38.1		

	mass	mw	mol
Product	0.329	1048.290	0.000314
	mass		
Unreacted limiting reactant	0.000		

Solvents (Zero Pass)

Highly hazardous solvents (Red flag for any of the following)	List Highly Hazardous Solvents Below
Et_2O, Benzene, CCl_4, chloroform, DCE, nitromethane, CS_2, HMPA	

Health and Safety (Zero Pass)

Health & safety (Red flag for any of the following)		List substances plus the red flagged H-codes below
Highly explosive	H200, H201, H202, H203	
Explosive thermal runaway	H240	
Fatally toxic	H300, H310, H330	
Mutagenic	H350	
Repro-toxic	H360	
Serious environmental implications	H420	

Instructions for use: Enter your data into the tables above to automatically calculate yield, AE and RME. Use the blank boxes in the tables to enter experimental data and note the flags for each Key Parameter.
Printing tips: This spreadsheet is designed to be printed with 'landscape', 'narrow margin' and 'fit all columns on one page' settings

Experimental:
A flask was charged with oripavine (0.595 g, 2.00 mmol), tetrabutylammonium hydroxide (40% aqueous solution, 18 ml) and CH2Cl2 (6 ml) and stirred under nitrogen for 30 mins. A solution of 2,4,6-tris-(bromomethyl)-mesitylene (0.269 g, 0.66 mmol) in CH2Cl2 (4 ml) was added and the biphasic reaction mixture was stirred for 6 h at rt. The reaction solution was transferred into d.H2O (150 ml) and washed with DCM (4 x 10 ml). Organic layers were combined and washed with aqueous sodium hydroxide solution (0.1 M, 2 x 20 ml) followed by d.H2O (3 x 20 ml) then saturated brine solution (20 ml). The organic layer was dried over magnesium sulphate, filtered and solvents removed by rotary evaporation. The crude product was purified by column chromatography (SiO2, 95:1:1 to 92:8:1 CH2Cl2:MeOH:NH4OH), The title compound OC3 was isolated as a golden yellow solid in 47 % yield (0.329 g, 0.31 mmol).

Figure A-42. First pass metric **OC3.**

Supplementary Information: Appendix 2 **Summary of First Pass Metrics Toolkit (OC3)**

Yield, AE, RME, MI/PMI and OE

Reactant (Limiting Reactant First)	Mass (g)	MW	Mol	Catalyst	Mass (g)	Reagent	Mass (g)	Reaction solvent	Volume (cm^3)	Density ($g\ ml^{-1}$)	Mass (g)	Work up chemical	Mass (g)	Workup solvent	Volume (cm3)	Density ($g\ ml^{-1}$)	Mass (g)
2,4,6-Tris-(bromomethyl)-mesitylene	0.27	398.96	0.00067			Tetrabutyl-ammonium Hydroxide solution	7.27	water	18.00	1.00	18.00	MgSO4	0.50	water	120.00	1.00	120.00
Oripavine	0.60	297.35	0.00200					DCM	10.00	1.33	13.30	NaCl	2.50	dichloromethane	440.00	1.33	583.00
			#DIV/0!								0.00	NaOH	0.16	Methanol	55.00	0.79	43.52
			#DIV/0!								0.00			Ammonium hydroxide solution	5.00	0.88	4.40
			#DIV/0!								0.00						0.00
			#DIV/0!								0.00						0.00
Total	0.86	696.31			0.00		7.27				31.30		3.16				750.92

$$RME = \frac{mass\ of\ isolated\ product}{total\ mass\ of\ reactants} \times 100$$

$$AE = \frac{molecular\ weight\ of\ product}{total\ molecualr\ weight\ of\ reactants} \times 100$$

$$mass\ intensity = \frac{total\ mass\ in\ a\ process\ or\ process\ step}{mass\ of\ product}$$

$$OE = \frac{RME}{AE} \times 100$$

		Flag
Yield	47	47
Conversion	100.0	100.0
Selectivity	46.5	46.5
AE	150.5	
RME	38.1	OE 25.3
PMI total	2411.9	
PMI Reaction	119.9	
PMI reactants, reagents, catlyst	24.7	
PMI reaction solvents	95.1	
PMI Workup	2292.0	
PMI Workup chemical	9.6	
PMI workup solvents	2282.4	

	Mass	MW	Mol
Product	0.329	1048.290	0.00031
	mass		
Unreacted limiting reactant	0.00		

Experimental:
A flask was charged with oripavine (0.595 g, 2.00 mmol), tetrabutylammonium hydroxide (40% aqueous solution, 18 ml) and CH2Cl2 (6 ml) and stirred under nitrogen for 30 mins. A solution of 2,4,6-tris-(bromomethyl)-mesitylene (0.269 g, 0.66 mmol) in CH2Cl2 (4 ml) was added and the biphasic reaction mixture was stirred for 6 h at rt. The reaction solution was transferred into d.H2O (150 ml) and washed with DCM (4 x 10 ml). Organic layers were combined and washed with aqueous sodium hydroxide solution (0.1 M, 2 x 20 ml) followed by d.H2O (3 x 20 ml) then saturated brine solution (20 ml). The organic layer was dried over magnesium sulphate, filtered and solvents removed by rotary evaporation. The crude product was purified by column chromatography (SiO2, 95:1:1 to 92:8:1 CH2Cl2:MeOH:NH4OH), The title compound OC3 was isolated as a golden yellow solid in 48 % yield (0.329 g, 0.31 mmol).

Solvents (First Pass)		List solvents below
Preferred solvents	**water,** EtOH, nBuOH, AcOipr, AcOnBu, PhOMe, MeOH, tBuOH, BnOH, ethylene glycol, acetone, MEK, MIBK, **AcOEt,** sulfolane	Water, MeOH
Problematic solvents: (acceptable only if substitution does not offer advantages)	DMSO, cyclohexanone, DMPU, AcOH, Ac2O, Acetonitrile, AcOMe, THF, heptane, Me-cyclohexane, toluene, xylene, MTBE, **cyclohexane**, chlorobenzene, formic acid, pyridine, Me-THF	
Hazardous solvents: These solvents have significant health and/or safety concerns.	dioxane, pentane, TEA, diisopropyl ether, DME, DCM, DMF, DMA, NMP, methoxyethanol, hexane	DCM
Highly hazardous solvents: The solvents which are agreed not to be used, even in screening	Et_2O, Benzene, CCl_4, chloroform, DCE, nitromethane, CS_2, HMPA	

Instructions for use: Enter your data into the tables above to automatically calculate yield, AE, RME, MI/PMI and OE.
Use the blank boxes in the tables to enter experimental data and note the flags for each Key Parameter.
Printing tips: This spreadsheet is designed to be printed with 'landscape', 'narrow margin' and 'fit all columns on one page' settings

Catalyst/enzyme (First Pass)		Tick
Catalyst or enzyme used, **or** reaction takes place without **any** catalyst/reagents.	Green Flag	
Use of stoichiometric quantities of reagents	Amber Flag	
Use of reagents in excess	Red Flag	✓

		Tick
Facile recovery of catalyst/enzyme	Green Flag	
catalyst/enzyme not recovered	Amber Flag	

Figure A-43. First pass metric **OC3** continued.

Figure A-44. Zero pass metric heterocodeine.

Supplementary Information: Appendix 2 **Summary of Zero Pass Metrics Toolkit (Heterocodeine)**

Yield, conversion, selectivity, AE, RME

Reactant (Limiting Reactant First)	Mass (g)	MW	Mol	Catalyst	Mass (g)	Reagent	Mass (g)	Reaction solvent	Volume (cm^3)	Density ($g\ ml^{-1}$)	Mass (g)	Work up chemical	Mass (g)	Workup solvent	Volume (cm3)	Density ($g\ ml^{-1}$)	Mass (g)
Morphine	0.57	285.34	0.0020			Potassium Hydride	0.84	THF	30.00	0.89	26.67	MgSO4	0.50	water	250.00	1.00	250.00
methyl Iodide	0.34	141.94	0.0024								0.00	NaCl	2.50	dichloromethane	640.00	1.33	848.00
			#DIV/0!								0.00	NaOH	0.40	Methanol	50.00	0.79	39.57
			#DIV/0!								0.00	HCl	1.97	Ammonium hydroxide solution	8.00	0.88	7.04
			#DIV/0!								0.00			Chloroform	60.00	1.49	89.40
			#DIV/0!								0.00			Isopropanol	20.00	0.79	15.72
			#DIV/0!								0.00						0.00
Total	0.91	427.28			0.00		0.84				26.67		5.37				1249.73

$$AE = \frac{molecular\ weight\ of\ product}{total\ molecualr\ weight\ of\ reactants} \times 100$$

$$RME = \frac{mass\ of\ isolated\ product}{total\ mass\ of\ reactants} \times 100$$

		Flag
Yield	25	25
Conversion	100.0	100.0
Selectivity	25.2	25.2
AE	70.1	
RME	16.5	

	mass	mw	mol
Product	0.151	299.360	0.00050
	mass		
Unreacted limiting reactant	0.000		

Solvents (Zero Pass)

Highly hazardous solvents (Red flag for any of the following)	List Highly Hazardous Solvents Below
Et_2O, Benzene, CCl_4, chloroform, DCE, nitromethane, CS_2, HMPA	

Health and Safety (Zero Pass)

Health & safety (Red flag for any of the following)		List substances plus the red flagged H-codes below
Highly explosive	H200, H201, H202, H203	
Explosive thermal runaway	H240	
Fatally toxic	H300, H310, H330	
Mutagenic	H350	
Repro-toxic	H360	
Serious environmental implications	H420	

Instructions for use: Enter your data into the tables above to automatically calculate yield, AE and RME. Use the blank boxes in the tables to enter experimental data and note the flags for each Key Parameter.
Printing tips: This spreadsheet is designed to be printed with 'landscape', 'narrow margin' and 'fit all columns on one page' settings

Experimental:
Reaction carried out on parallel synthesiser in 5 flasks. Potassium hydride (4.421 g, 110.23 mmol) was prepared in the reaction vessel under nitrogen flux and washed with dry hexane, suspended in dry THF (150 ml) over ice. A solution of morphine (2.862 g, 10.03 mmol) in THF (30 ml) was added slowly over 30 min to the reaction under a nitrogen atmosphere and the resulting solution was allowed to stir at room temperature for 16 h. Methyl Iodide (1.710 g, 0.75 ml, 12.05 mmol) was added to the reaction slowly over 15 mins and reaction left stirring for 4 h. The reaction was quenched with a mixture of 10:1 THF/H2O over ice. The solution was neutralised to pH 7 using 2 M HCl and volatiles removed by rotary evaporation. pH adjusted to 8 using 1M NaOH and extracted with chloroform/isopropanol (3:1, 3 x 25 ml). The resulting organic layer was washed with H2O (4 x 30 ml) and final wash with saturated brine solution (20 ml). The organic layer was dried over magnesium sulphate, filtered and solvents removed by rotary evaporation. The crude product was purified by column chromatography (SiO2, 95:1:1 to 92:8:1 CH2Cl2:MeOH:NH4OH), heterocodeine was isolated as a white solid in 756 mg (2.53 mmol, 25 % yield).

Figure A-45. First pass metric heterocodeine

Supplementary Information: Appendix 2 **Summary of First Pass Metrics Toolkit (Heterocodeine)**

Yield, AE, RME, MI/PMI and OE

Reactant (Limiting Reactant First)	Mass (g)	MW	Mol	Catalyst	Mass (g)	Reagent	Mass (g)	Reaction solvent	Volume (cm^3)	Density ($g\ ml^{-1}$)	Mass (g)	Work up chemical	Mass (g)	Workup solvent	Volume (cm3)	Density ($g\ ml^{-1}$)	Mass (g)
Morphine	0.57	285.34	0.0020			Potassium Hydride	0.84	THF	30.00	0.89	26.67	MgSO4	0.50	water	250.00	1.00	250.00
methyl Iodide	0.34	141.94	0.0024								0.00	NaCl	2.50	dichloromethane	640.00	1.33	848.00
			#DIV/0!								0.00			Methanol	50.00	0.79	39.57
			#DIV/0!								0.00	NaOH	0.40	Ammonium hydroxide solution	8.00	0.88	7.04
			#DIV/0!								0.00			Isopropanol	20.00	0.79	15.72
			#DIV/0!								0.00						0.00
Total	0.91	427.28			0.00		0.84				26.67		3.40				1160.33

$$RME = \frac{mass\ of\ isolated\ product}{total\ mass\ of\ reactants} \times 100$$

$$AE = \frac{molecular\ weight\ of\ product}{total\ molecualr\ weight\ of\ reactants} \times 100$$

$$mass\ intensity = \frac{total\ mass\ in\ a\ process\ or\ process\ step}{mass\ of\ product}$$

$$OE = \frac{RME}{AE} \times 100$$

		Flag
Yield	25	25
Conversion	100.0	100.0
Selectivity	25.2	25.2
AE	70.1	
RME	16.5	OE 23.6
PMI total	7895.0	
PMI Reaction	188.3	
PMI reactants, reagents, catlyst	11.6	
PMI reaction solvents	176.6	
PMI Workup	7706.8	
PMI Workup chemical	22.5	
PMI workup solvents	7684.3	

	Mass	MW	Mol
Product	0.151	299.360	0.00050
	mass		
Unreacted limiting reactant	0.00		

Experimental:
Reaction carried out on parallel synthesiser in 5 flasks. Potassium hydride (4.421 g, 110.23 mmol) was prepared in the reaction vessel under nitrogen flux and washed with dry hexane, suspended in dry THF (150 ml) over ice. A solution of morphine (2.862 g, 10.03 mmol) in THF (30 ml) was added slowly over 30 min to the reaction under a nitrogen atmosphere and the resulting solution was allowed to stir at room temperature for 16 h. Methyl Iodide (1.710 g, 0.75 ml, 12.05 mmol) was added to the reaction slowly over 15 mins and reaction left stirring for 4 h. The reaction was quenched with a mixture of 10:1 THF/H2O over ice. The solution was neutralised to pH 7 using 2 M HCl and volatiles removed by rotary evaporation. pH adjusted to 8 using 1M NaOH and extracted with chloroform/isopropanol (3:1, 3 x 25 ml). The resulting organic layer was washed with H2O (4 x 30 ml) and final wash with saturated brine solution (20 ml). The organic layer was dried over magnesium sulphate, filtered and solvents removed by rotary evaporation. The crude product was purified by column chromatography (SiO_2, 95:1:1 to 92:8:1 CH2Cl2:MeOH:NH4OH), heterocodeine was isolated as a white solid in 756 mg (2.53 mmol, 25 % yield).

Solvents (First Pass)

		List solvents below
Preferred solvents	**water,** EtOH, nBuOH, AcOipr, AcOnBu, PhOMe, MeOH, tBuOH, BnOH, ethylene glycol, acetone, MEK, MIBK, **AcOEt,** sulfolane	Water, MeOH
Problematic solvents: (acceptable only if substitution does not offer advantages)	DMSO, cyclohexanone, DMPU, AcOH, Ac2O, Acetonitrile, AcOMe, THF, heptane, Me-cyclohexane, toluene, xylene, MTBE, **cyclohexane**, chlorobenzene, formic acid, pyridine, Me-THF	THF
Hazardous solvents: These solvents have significant health and/or safety concerns.	dioxane, pentane, TEA, diisopropyl ether, DME, DCM, DMF, DMA, NMP, methoxyethanol, hexane	DCM
Highly hazardous solvents: The solvents which are agreed not to be used, even in screening	Et_2O, Benzene, CCl_4, chloroform, DCE, nitromethane, CS_2, HMPA	Chloroform

Instructions for use: Enter your data into the tables above to automatically calculate yield, AE, RME, MI/PMI and OE.
Use the blank boxes in the tables to enter experimental data and note the flags for each Key Parameter.
Printing tips: This spreadsheet is designed to be printed with 'landscape', 'narrow margin' and 'fit all columns on one page' settings

Catalyst/enzyme (First Pass)		Tick
Catalyst or enzyme used, **or** reaction takes place without **any** catalyst/reagents.	Green Flag	
Use of stoichiometric quantities of reagents	Amber Flag	
Use of reagents in excess	Red Flag	✓

		Tick
Facile recovery of catalyst/enzyme	Green Flag	
catalyst/enzyme not recovered	Amber Flag	

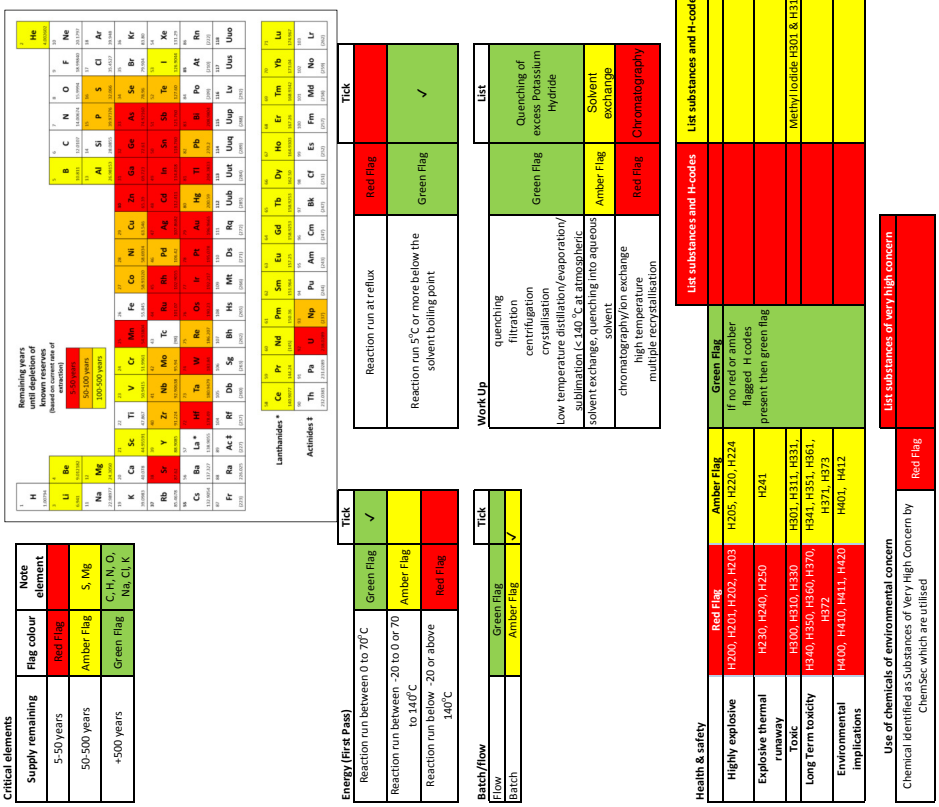

Figure A-46. First pass metric heterocodeine continued.

Figure A-47. Zero pass **HC3**.

Supplementary Information: Appendix 2 **Summary of Zero Pass Metrics Toolkit (HC3)**

Yield, conversion, selectivity, AE, RME

Reactant (Limiting Reactant First)	Mass (g)	MW	Mol	Catalyst	Mass (g)	Reagent	Mass (g)	Reaction solvent	Volume (cm^3)	Density (g ml^{-1})	Mass (g)	Work up chemical	Mass (g)	Workup solvent	Volume (cm3)	Density (g ml^{-1})	Mass (g)
2,4,6-Tris-(bromomethyl)-mesitylene	0.27	398.96	0.0007			Potassium Hydride	0.84	water	20.00	1.00	20.00	MgSO4	0.50	water	200.00	1.00	200.00
Heterocodeine	0.70	299.36	0.0023					DCM	12.00	1.33	15.96	NaCl	2.50	dichloromethane	500.00	1.33	662.50
			#DIV/0!								0.00	NaOH	0.16	Methanol	40.00	0.79	31.65
			#DIV/0!								0.00			Ammonium hydroxide solution	5.00	0.88	4.40
			#DIV/0!								0.00						0.00
			#DIV/0!								0.00						0.00
			#DIV/0!								0.00						0.00
Total	0.97	698.32			0.00		0.84				35.96		3.16				898.55

$$AE = \frac{molecular\ weight\ of\ product}{total\ molecualr\ weight\ of\ reactants} \times 100$$

$$RME = \frac{mass\ of\ isolated\ product}{total\ mass\ of\ reactants} \times 100$$

		Flag	
Yield	13		13
Conversion	100.0		100.0
Selectivity	13.4		13.4
AE	150.7		
RME	9.8		

	mass	mw	mol
Product	0.095	1052.340	9E-05
	mass		
Unreacted limiting reactant	0.000		

Solvents (Zero Pass)

Highly hazardous solvents (Red flag for any of the following)	List Highly Hazardous Solvents Below
Et_2O, Benzene, CCl_4, chloroform, DCE, nitromethane, CS_2, HMPA	

Health and Safety (Zero Pass)

Health & safety (Red flag for any of the following)		List substances plus the red flagged H-codes below
Highly explosive	H200, H201, H202, H203	
Explosive thermal runaway	H240	
Fatally toxic	H300, H310, H330	
Mutagenic	H350	
Repro-toxic	H360	
Serious environmental implications	H420	

Instructions for use: Enter your data into the tables above to automatically calculate yield, AE and RME. Use the blank boxes in the tables to enter experimental data and note the flags for each Key Parameter.
Printing tips: This spreadsheet is designed to be printed with 'landscape', 'narrow margin' and 'fit all columns on one page' settings

Experimental:
A flask was charged with heterocodeine (0.700 g, 2.34 mmol), tetrabutylammonium hydroxide (40% aqueous solution, 20 ml) and CH2Cl2 (8 ml) and stirred under nitrogen for 30 mins. A solution of 2,4,6-tris-(bromomethyl)-mesitylene (0.269 g, 0.66 mmol) in CH2Cl2 (4 ml) was added and the mixture was stirred for 6 h at rt. The reaction solution was transferred into d.H2O (150 ml) and washed with DCM (4 x 10 ml). Organic layers were combined and washed with aqueous sodium hydroxide solution (0.1 M, 2 x 20 ml) followed by d.H2O (3 x 20 ml) then saturated brine solution (20 ml). The organic layer was dried over magnesium sulphate, filtered and solvents removed by rotary evaporation. The crude product was purified by column chromatography (SiO2, 95:1:1 to 92:8:1 CH2Cl2:MeOH:NH4OH), HC3 was isolated by column

Figure A-48. First pass metric **HC3.**

Supplementary Information: Appendix 2 **Summary of First Pass Metrics Toolkit (HC3)**

Yield, AE, RME, MI/PMI and OE

Reactant (Limiting Reactant First)	Mass (g)	MW	Mol	Catalyst	Mass (g)	Reagent	Mass (g)	Reaction solvent	Volume (cm^3)	Density ($g\,ml^{-1}$)	Mass (g)	Work up chemical	Mass (g)	Workup solvent	Volume (cm3)	Density ($g\,ml^{-1}$)	Mass (g)
2,4,6-Tris-(bromomethyl)-	0.27	398.96	0.0007			Tetrabutyl-ammonium Hydroxide solution	8.36	water	20.00	1.00	20.00	MgSO4	0.50	water	200.00	1.00	200.00
Heterocodeine	0.70	299.36	0.0023					DCM	12.00	1.33	15.96	NaCl	2.50	dichloromethane	500.00	1.33	662.50
			#DIV/0!								0.00	NaOH	0.16	Methanol	40.00	0.79	31.65
			#DIV/0!								0.00			Ammonium hydroxide solution	5.00	0.88	4.40
			#DIV/0!								0.00						0.00
			#DIV/0!								0.00						0.00
			#DIV/0!								0.00						0.00
Total	0.97	698.32			0.00		8.36				35.96		3.16				898.55

$$RME = \frac{mass\ of\ isolated\ product}{total\ mass\ of\ reactants} \times 100$$

$$AE = \frac{molecular\ weight\ of\ product}{total\ molecualr\ weight\ of\ reactants} \times 100$$

$$mass\ intensity = \frac{total\ mass\ in\ a\ process\ or\ process\ step}{mass\ of\ product}$$

$$OE = \frac{RME}{AE} \times 100$$

		Flag
Yield	13	13
Conversion	100.0	100.0
Selectivity	13.4	13.4
AE	151.0	
RME	9.8	OE 6.5
PMI total	9968.4	
PMI Reaction	476.7	
PMI reactants, reagents, catlyst	98.2	
PMI reaction solvents	378.5	
PMI Workup	9491.7	
PMI Workup chemical	33.3	
PMI workup solvents	9458.4	

	Mass	MW	Mol
Product	0.095	1054.340	0.000090
	mass		
Unreacted limiting reactant	0.00		

Experimental:
A flask was charged with heterocodeine (0.700 g, 2.34 mmol), tetrabutylammonium hydroxide (40% aqueous solution, 20 ml) and CH_2Cl_2 (8 ml) and stirred under nitrogen for 30 mins. A solution of 2,4,6-tris-(bromomethyl)-mesitylene (0.269 g, 0.66 mmol) in CH_2Cl_2 (4 ml) was added and the mixture was stirred for 6 h at rt. The reaction solution was transferred into d.H_2O (150 ml) and washed with DCM (4 x 10 ml). Organic layers were combined and washed with aqueous sodium hydroxide solution (0.1 M, 2 x 20 ml) followed by d.H_2O (3 x 20 ml) then saturated brine solution (20 ml). The organic layer was dried over magnesium sulphate, filtered and solvents removed by rotary evaporation. The crude product was purified by column chromatography (SiO_2, 95:1:1 to 92:8:1 CH_2Cl_2:MeOH:NH_4OH), HC3 was isolated by column chromatography as a white solid in 13 % yield (95 mg 0.09 mmol).

Solvents (First Pass)		List solvents below
Preferred solvents	**water,** EtOH, nBuOH, AcOipr, AcOnBu, PhOMe, MeOH, tBuOH, BnOH, ethylene glycol, acetone, MEK, MIBK, **AcOEt,** sulfolane	Water, MeOH
Problematic solvents: (acceptable only if substitution does not offer advantages)	DMSO, cyclohexanone, DMPU, AcOH, Ac2O, Acetonitrile, AcOMe, THF, heptane, Me-cyclohexane, toluene, xylene, MTBE, **cyclohexane**, chlorobenzene, formic acid, pyridine, Me-THF	
Hazardous solvents: These solvents have significant health and/or safety concerns.	dioxane, pentane, TEA, diisopropyl ether, DME, DCM, DMF, DMA, NMP, methoxyethanol, hexane	DCM
Highly hazardous solvents: The solvents which are agreed not to be used, even in screening	Et_2O, Benzene, CCl_4, chloroform, DCE, nitromethane, CS_2, HMPA	

Instructions for use: Enter your data into the tables above to automatically calculate yield, AE, RME, MI/PMI and OE.
Use the blank boxes in the tables to enter experimental data and note the flags for each Key Parameter.
Printing tips: This spreadsheet is designed to be printed with 'landscape', 'narrow margin' and 'fit all columns on one page' settings

Catalyst/enzyme (First Pass)		Tick
Catalyst or enzyme used, **or** reaction takes place without **any** catalyst/reagents.	Green Flag	
Use of stoichiometric quantities of reagents	Amber Flag	
Use of reagents in excess	Red Flag	✓

		Tick
Facile recovery of catalyst/enzyme	Green Flag	
catalyst/enzyme not recovered	Amber Flag	

Figure A-49. First pass metric **HC3.**

Appendix B

Opioid Architectures as New DNA Binding Molecules

This conference paper was published in Symmetry: Culture and Science, 2017, 28, 195-198. This work was presented at Symmetry Festival 2016, Vienna University of Technology, 18-22nd July.

Natasha McStay, Zara Molphy, Nicholas Gathergood and Andrew Kellett. Opioid Architectures as New DNA Binding Molecules.

B-1. Abstract

Herein we report the discovery of C_3-symmetric opioid architectures as efficient DNA binding molecules. To our knowledge these agents are the first opioid-based structures with nucleic acid recognition properties. These architectures may now pave the way toward the development of a new class of semi-synthetic DNA binding molecule with potential applications in gene delivery.

B-2. Introduction

The discovery of new synthetic DNA recognition agents is an area of considerable research interest. These agents can be categorised, broadly, into two main areas: i.) those that covalently bind nucleic acids at electron rich sites on the nucleobase,[1] and ii.) those that coordinate in non-covalent fashion through hydrogen(H)-bonding, ionic, or π-stacking interactions.[2] Non-covalent binders may be further classified according to the area of DNA where recognition occurs thus giving rise to groove binders,[3] intercalators,[4] and surface-binding compounds.[5] The quest to discover new materials that non-covalently interact with DNA carries tremendous application to the areas of human health and biomedical diagnostics. Indeed, non-covalent DNA binding agents have already found widespread utility as antitumoral agents,[6] as probes for the fluorescent labelling and detection of nucleic acids,[7] and as condensation agents[8] that efficiently package nucleic acids for gene delivery (transfection) to mammalian cells. Recently, this group have established high-throughput DNA screening methodologies to identify potentially new nucleic acid binding molecules.[9] As part of this screen, we have identified C_3 symmetric opioid architectures as novel architectures that efficiently complex dsDNA through ionic surface-driven interactions that result in efficient nucleic acid condensation arising from the collapse in the regular B-DNA structure.

B-3. C_3 opioid DNA binding interactions

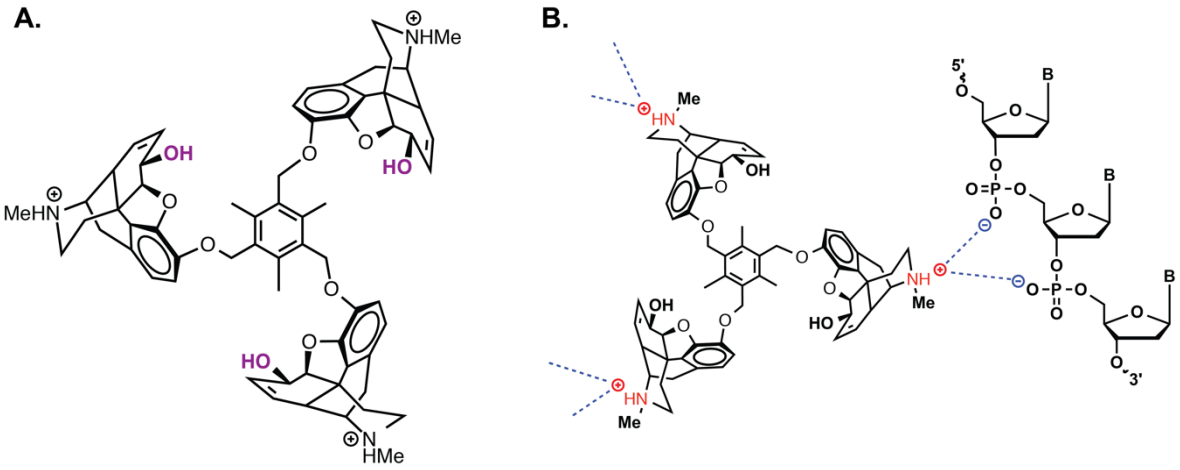

Figure B-1. A. Molecular structure of **MC3** in the cationic form. **B.** Proposed DNA binding mode by **MC3** whereby the protonated tertiary amine group electrostatically binds to the phosphate nucleic acid surface.

Using a high-throughput DNA binding screen based on ethidium bromide fluorescence quenching, a series of novel opioid scaffolds were examined. The C3 symmetric tris-morphine scaffold (**MC3**, Figure B-1A) was identified as a potentially new DNA binding molecule. Our initial thoughts on the potential binding mode focused on the 6'-OH group in the morphine C ring as a possible hydrogen(H)-bonding site for phosphate oxygen coordination at the nucleic acid backbone. To examine this hypothesis, we then masked this H-bond through the introduction of methyl groups in the form of methoxy substituents present in heterocodeine (H) and oripavine (O) by developing synthetic methods for isolating trivalent C_3-heterocodeine (**HC3**) and C_3-oripavine (**OC3**) analogues. To our surprise, however, ethidium bromide displacement was enhanced for these modified opioid architectures with the overall series yielding apparent DNA binding constants (K_{app}) between ~105 M(bp^{-1}) to ~107 M(bp^{-1}) across a variety of double stranded DNA polymers. To further probe the nature of the binding interaction from this class, a range of biophysical and spectroscopic assays were conducted including viscosity, thermal melting, turbidity, circular dichroism, electrophoresis, and atomic force microscopy (AFM). From this analysis we identified a possible new surface-driven nucleic acid binding mode associated between the protonated amine group within the opioid D ring, and phosphate oxygen group along the nucleic acid backbone (Figure B-1B). Thus, these novel C_3 architectures efficiently complex dsDNA

through ionic surface-driven interactions and result in the condensation/aggregation of the tertiary double stranded helical structure. We hypothesise this condensation process arises from the collapse in regular B-DNA structure through opioid H-bonding interruption.

B-4. Summary

In conclusion, this abstract presents a summary of our recent findings on the DNA binding properties of new C_3 symmetric opioid structures. These architectures are first to our knowledge where the opioid class has demonstrated effective DNA binding affinity and may now open up an exciting new semi-synthetic frontier for nucleic acid research. One final note of interests is the unique surface-driven interaction afforded by these architectures; this binding mode results in the efficient condensation of DNA and may therefore lead to potential application in the future delivery of gene vectors or antisense therapeutics.

B-5. References

1 D. Fu, J. A. Calvo and L. D. Samson, *Nat Rev Cancer*, 2012, **12**, 104–120.

2 L. Strekowski and B. Wilson, *Mutation Research/Fundamental and Molecular Mechanisms of Mutagenesis*, 2007, **623**, 3–13.

3 M. C. Vega, I. García Sáez, J. Aymamí, R. Eritja, G. A. Van der Marel, J. H. Van Boom, A. Rich and M. Coll, *Eur. J. Biochem.*, 1994, **222**, 721–726.

4 Z. Molphy, A. Prisecaru, C. Slator, N. Barron, M. McCann, J. Colleran, D. Chandran, N. Gathergood and A. Kellett, *Inorganic Chemistry*, 2014, **53**, 5392–5404.

5 B. I. Kankia, V. Buckin and V. A. Bloomfield, *Nucleic acids research*, 2001, **29**, 2795–2801.

6 P. A. Marks and R. Breslow, *Nature Biotechnology*, 2007, **25**, 84–90.

7 N. Spink, D. G. Brown, J. V. Skelly and S. Neidle, *Nucleic Acids Res*, 1994, **22**, 1607–1612.

8 J. Malina, N. P. Farrell and V. Brabec, *Angewandte Chemie International Edition*, 2014, **53**, 12812–12816.

9 M. McCann, J. McGinley, K. Ni, M. O'Connor, K. Kavanagh, V. McKee, J. Colleran, M. Devereux, N. Gathergood, N. Barron, A. Prisecaru and A. Kellett, *Chemical Communications*, 2013, **49**, 2341.

Appendix C

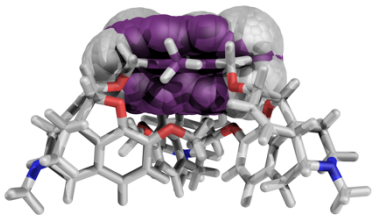

No pain and all gain! A novel codeine molecule (**CC3**) is reported to have excellent DNA condensation properties. Aggregation can be controlled by modulating pH and release triggered by changing the ionic strength. AFM measurements of **CC3**-compacted plasmid DNA (2686 bp) show gene delivery particles sizes of *ca*. 100 nm

Supporting information accompanying Chapter III, Efficient DNA Condensation by a C_3-Symmetric Codeine Scaffold. Referencing style is kept in publishing format.

C-1: Tripodal Opioids – MC3 and OC3

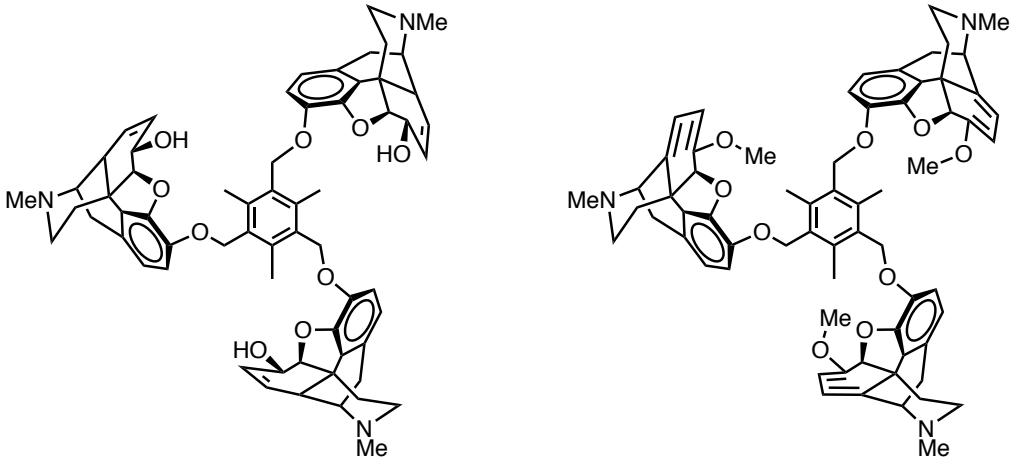

MC3 **OC3**

Figure C-1. Molecular structures of tripodal opioids **MC3** and **OC3**

C-2: Conformational Analysis of codeine and heterocodeine molecules

The starting point for this analysis was to generate potential conformations of the mono-codeine molecules **CC1** and **HC1** (Fig. C-2) using the *CSD Conformer Generator* (CSD GC).[1] This tool uses information on the conformational preferences of molecules in the Cambridge Structural Database[2] (CSD) to provide likely values for dihedrals, valance angles and bonds in a molecule. The initial three-dimensional (3-D) conformations used as input to the CSD GC were obtained by converting the two-dimensional chemical diagrams to 3-D structures using *PerkinElmer Chem3D*® (version 16.0) and optimising using the MM2 force field.[3] Using the default parameters for the CSD GC, just over 100 putative conformations were generated for each molecule.

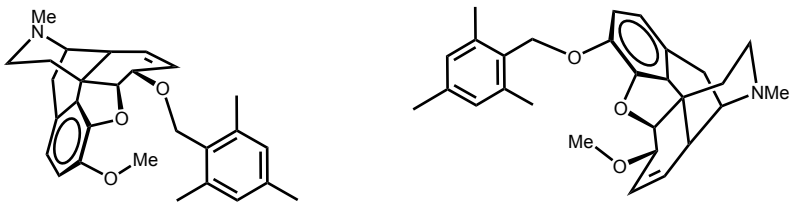

CC1 **HC1**

Figure C-2. Molecular structures of mono-codeine molecules **CC1** and **HC1**

The two sets of conformations were then optimised using the HF-3c semi-empirical method[4] and clustered and then re-optimised at the PBE-D3(BJ)/def2-SVP level of theory,[5–8] with all calculations being performed using *ORCA* 4.0.1.[9] After both optimisations the resulting conformers were clustered using the *CSD Python API*[2] to remove duplicate conformers, based on any two conformers having an energy difference of less than 0.5 kJ/mol and a root mean squared deviation of less than 0.1 Å. This procedure produced 20 unique conformers for **CC1** and 15 for **HC1**. In both cases, only a few kJ/mol separate the lowest-energy conformations.Two procedures were used to generate conformers of **HC3** and **CC3**. The first was to apply the same procedure applied above for **HC1** and **CC1**. However, the CSD GC cannot, at present, enforce symmetry and the flexibility of the three independent codeine groups leads to many 1000s of putative conformations. To make the search tractable, the top 250 conformations (in terms of the CSD GC's probability score) were carried forward to optimisation with HF-3c and PBE-D3(BJ)/def2-SVP.

The vast majority of the resulting conformers do not feature any rotational symmetry, including the lowest-energy conformers found using this procedure for both **HC3** and **CC3**, which feature significant differences between the conformations of the codeine groups. The lack of symmetry in the lowest-energy conformations does not match with the prior experimental observation of a single C_3 conformation in solution for **HC3** and the experimental work presented here for **CC3**. However, the third lowest-energy conformer (11.9 kJ/mol higher) for **CC3** does have C_3 symmetry. However, the calculations performed here represent energy differences at 0 K *in vacuo*, neglecting any solvent effects or finite-temperature contributions, while calculations with higher-level functionals and basis sets might alter the ordering of the conformations. To illustrate this, the free-energy difference between the lowest-energy conformation and the C_3 conformation at room temperature was calculated from the harmonic vibrational frequencies of the two molecules, halving the energy difference to 4.8 kJ/mol. Separately performing single-point calculations with PBE0-D3(BJ)/def2-SVP[10] level of theory reduces the gap to 8.3 kJ/mol, while a single-point calculation with the SMD solvent model[11] also closes the underlying PBE-D3(BJ)/def2-SVP gap to 6.2 kJ/mol. The combination of these effects and full optimisations, which is beyond the scope of the present search for *plausible* conformations, could readily lead to the C_3 conformer being found in solution. It is also worth noting that when the five lowest-energy conformers for **CC3** are tri-

protonated and re-optimised at the PBE-D3(BJ)/def2-SVP level of theory, the C_3conformer becomes the lowest-energy conformer by over 25 kJ/mol, most likely as it maximises the separation of the positively charged nitrogen atoms.

As very few C_3 conformers were found for either molecule in the full CSD GC searches, most likely due to the complexity of the conformational landscape of the molecules, the second approach used to generate conformations was to manually map the codeine groups in each of the **CC1** and **HC1** conformers so that all three codeines adopted the same relative conformation to the phenyl ring. This procedure led to a number of unrealistic conformations with clashes and overlap of the codeine groups but still produced 12 and 15 C_3 conformers for **HC3** and **CC3**, respectively. The lowest-energy conformer found in this fashion for **CC3**, matches the low-energy C_3 **CC3** conformer found using the full non-symmetry restricted search, while the lowest-energy **HC3** conformer found in this fashion is lower in energy than any of the conformers generated using the full unrestricted search. This suggests that the conformers generated are representative of C_3 conformers of the two molecules and of the likely conformers adopted by them in solution.

C-3: Synthesis – CC1, CC2, CC3

Chemicals and reagents were sourced from Sigma-Aldrich and were used without any further purification required. HPLC grade chloroform, methanol, and acetonitrile were used with no further purification. All other solvents were used as supplied unless otherwise stated. Codeine was provided from Johnson Matthey MacFarlan Smith Ltd. Thin layer chromatography was performed on Fluka Silica gel (60 F254) coated on aluminium plates. The TLC plates were visualised using UV light. Davisil 60 Å silica gel was used for column chromatography. ^{1}H and ^{13}C NMR spectra were obtained on a Bruker AC 600 MHz NMR spectrometer. The pH was monitored by a Mettler Toledo InLab Expert Pro-ISM pH probe. IR spectrometry was conducted on a FT-IR Perkin Elmer spectrum two spectrometer. Microanalytical data were reported by the Microanalytical Laboratory, University College Dublin, Ireland. Electrospray ionization mass spectra (ESI-MS) were recorded using a Thermo Fisher Ex- active Orbitrap mass spectrometer coupled to an Advion TriVersa Nanomate injection system with samples being prepared in 100% HPLC-grade acetonitrile prior to ESI- MS analysis.

Codeine-C1 (CC1)

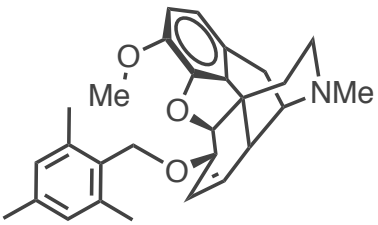

Codeine (0.900 g, 3.01 mmol), potassium hydroxide (KOH) (2.021 g, 36.02 mmol), and potassium iodide (KI) (0.100 g, 0.60 mmol) were suspended in ACN (30 ml) and heated to reflux. α^2-Chloroisodurene (0.506 g, 3.00 mmol) was added in small aliquots to the reaction mixture and vigorously stirred overnight (18 h) under reflux conditions. After allowing the reaction mixture to cool to rt, the reaction solvent was removed by rotary evaporation and crude product dissolved in DCM (50 ml). The organic layer was washed with d.H_2O (40 ml) and the aqueous layer extracted with DCM (3 x 20 ml). All organic layers were combined, then washed with d.H_2O (3 x 20 ml) and with a saturated brine solution (20 ml). The organic layer was dried over magnesium sulfate, filtered and solvents removed by rotary evaporation. The crude product was purified by column chromatography (SiO_2, 98:1:1 to 91:8:1 CH_2Cl_2:MeOH:NH_4OH). The title compound **CC1** was isolated as a yellow solid in 34% yield (0.350 g, 1.023 mmol). Mp 129-130 ˚C.^{1}H NMR (600 MHz, $CDCl_3$) δ: 6.85 (s, 2H), 6.62 (d, *J* = 8.1 Hz, 1H), 6.49 (d, *J* = 8.2 Hz, 1H), 5.71 (dddd, *J* = 9.9, 3.2, 2.0, 1.3 Hz, 1H), 5.29 (dt, *J* = 9.9, 2.8 Hz, 1H), 5.05 (dd, *J* = 6.0, 1.3 Hz, 1H), 4.96 (d, *J* = 10.2 Hz, 1H), 4.53 (d, *J* = 10.1 Hz, 1H), 3.96 (ddt, *J* = 5.8, 3.2, 2.3 Hz, 1H), 3.81 (s, 3H), 3.35 (dd, *J* = 6.2, 3.3 Hz, 1H), 3.03 (d, *J* = 18.5 Hz, 1H), 2.66 (t, *J* = 2.8 Hz, 1H), 2.59 (dd, *J* = 11.9, 3.9 Hz 1H), 2.44 (d, *J* = 4.3 Hz, 9H), 2.43 – 2.38 (m, 1H), 2.30 (dd, *J* = 18.7, 6.4 Hz, 1H), 2.26 (s, 3H), 2.05 (td, *J* = 12.5, 5.1 Hz, 1H), 1.92 (ddd, *J* = 12.6, 3.7, 1.7 Hz, 1H). ^{13}C NMR (151 MHz, $CDCl_3$) δ: 147.77, 142.24, 138.21, 137.62, 131.43, 131.22, 130.90, 128.90, 128.31, 127.03, 118.70, 113.67, 89.71, 73.85, 65.13, 59.00, 56.65, 46.57, 43.47, 43.12, 41.17, 36.10, 21.00, 20.45, 19.59. Anal. Cal. for $C_{28}H_{33}NO_3$: C, 77.93; H, 7.71; N, 3.35. %Found: C, 77.66; H, 7.94; N, 3.06. IR (ATR, cm^{-1}): 2895, 2900, 1605, 1502, 1446, 1374, 1280, 1198, 1142, 113, 1092, 1079, 1049, 1020, 977, 939, 841, 826, 777, 745, 709, 668, 641, 622. ESI-MS: [**CC1**]$^+$ 433 m/z. $[\alpha]_D$ = 203˚ (c = 0.076, $CHCl_3$, 589 nm, 25 ˚C).

Codeine-C2 (CC2)

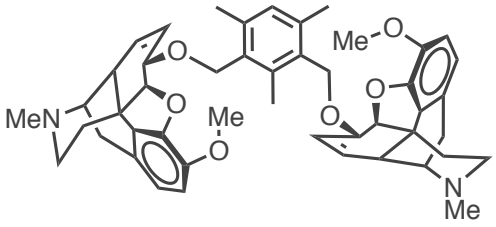

Codeine (0.908 g, 3.03 mmol), potassium hydroxide (2.032 g, 36.22 mmol), and potassium iodide (0.106 g, 0.64 mmol) were suspended in ACN (30 ml) and heated to reflux. 2,4,-Bis(chloromethyl)-1,3,5-trimethylbenzene (0.325 g, 1.50 mmol) was added in small aliquots to the reaction mixture and vigorously stirred overnight (18 h) under reflux conditions. After allowing the reaction mixture to cool to rt, the reaction solvent was removed by rotary evaporation and crude product dissolved in DCM (50 ml). The organic layer was washed with d.H_2O (40 ml) and the aqueous layer extracted with DCM (3 x 20 ml). All organic layers were combined, then washed with d.H_2O (3 x 20 ml) and with a saturated brine solution (20 ml). The organic layer was dried over magnesium sulfate, filtered and solvents removed by rotary evaporation. The crude product was purified by column chromatography (SiO_2, 98:1:1 to 91:8:1 CH_2Cl_2:MeOH:NH_4OH). The title compound **CC2** was isolated as a cream solid in 19% yield (0.210 g, 0.28 mmol). Mp 120-121 ˚C. ^{1}H NMR (600 MHz, $CDCl_3$) δ: 6.89 (s, 1H), 6.61 (d, *J* = 8.1 Hz, 2H), 6.49 (d, *J* = 8.1 Hz, 2H), 5.71 (dddd, *J* = 9.9, 3.2, 2.0, 1.3 Hz, 2H), 5.29 (dt, *J* = 9.9, 2.6 Hz, 2H), 5.06 (dd, *J* = 6.0, 1.3 Hz, 2H), 4.99 (d, *J* = 10.3 Hz, 2H), 4.57 (d, *J* = 10.3 Hz, 2H), 3.96 (ddt, *J* = 5.7, 3.1, 2.3 Hz, 2H), 3.81 (s, 6H), 3.35 (dd, *J* = 6.2, 3.3 Hz, 2H), 3.03 (d, *J* = 18.5 Hz, 2H), 2.69 – 2.64 (m, 2H), 2.58 (dd, *J* = 12.2, 4.1 Hz, 2H), 2.56 (d, *J* = 2.8 Hz, 3H), 2.44 (d, *J* = 2.2 Hz, 12H), 2.42 – 2.38 (m, 2H), 2.30 (dd, *J* = 18.3, 5.9 Hz, 2H), 2.05 (td, *J* = 12.4, 5.1 Hz, 2H), 1.92 (ddd, *J* = 12.6, 3.7, 1.7 Hz, 2H).^{13}C NMR (151 MHz, $CDCl_3$) δ: 147.80, 142.23, 139.06, 138.11, 132.32, 131.45, 130.94, 130.08, 128.31, 127.09, 118.69, 113.84, 89.70, 73.82, 65.51, 58.99, 56.76, 46.57, 43.47, 43.13, 41.17, 36.10, 20.46, 19.84, 15.33. Anal. Cal. for $C_{47}H_{54}N_2O_6$: C, 75.98; H, 7.33; N, 3.77. %Found: C, 75.01; H, 7.25; N, 3.74. IR (ATR, cm^{-1}): 2897, 2899, 1601, 1451, 1440, 1269, 1244, 1193, 1108, 1088, 1072, 1043, 1009, 971, 941, 778, 787, 752, 648. ESI-MS: [**CC2**]$^{+2}$ 373 m/z. $[\alpha]_D$ = 241˚ (c = 0.132, $CHCl_3$, 589 nm, 25 ˚C).

Codeine-C3 (CC3)

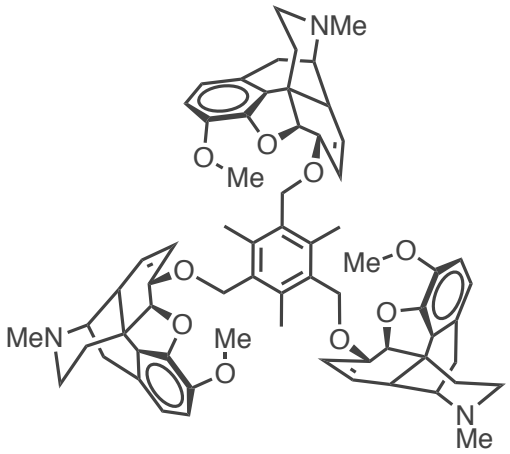

Sodium hydride (4 eq) was washed with dry hexane and suspended in dry THF (20 ml) over ice in the reaction vessel under nitrogen flux. (**Caution!** Dry sodium hydride is pyrophoric). A solution of codeine (0.600 g, 2.00 mmol) in THF (10 ml) was added slowly over 30 min to the reaction under a nitrogen atmosphere and the resulting solution was allowed to stir at rt for 2 h. 2,4,6-trisbromomethyl mesitylene (0.527 g, 1.32 mmol) was added to the reaction slowly over 10 mins and reaction left stirring for 12 h. The reaction was quenched slowly with H_2O at 0 ˚C. The solution was diluted with H_2O (50 ml) and solvents removed by rotary evaporation. Aqueous layer extracted with chloroform:2-propanol (3:1, 3 x 40 ml) The organic layers were combined and further washed with H_2O (3 x 30 ml) and finally with brine. The organic layer was dried over magnesium sulfate, filtered and solvents removed by rotary evaporation. The product was purified by column chromatography (SiO_2, 98:1:1 to 91:8:1 CH_2Cl_2:MeOH:NH_4OH). The title compound **CC3** was isolated as a white solid in 15.1% yield (0.210 g, 0.199 mmol). Mp 160-162 ˚C. ^{1}H NMR (600 MHz, $CDCl_3$) δ: 6.62 (d, *J* = 8.2 Hz, 3H), 6.49 (d, *J* = 8.1 Hz, 3H), 5.71 (ddt, *J* = 9.9, 3.1, 2.0 Hz, 3H), 5.29 (dt, *J* = 9.9, 2.9 Hz, 3H), 5.07 (dd, *J* = 5.9, 1.3 Hz, 3H), 5.03 (d, *J* = 10.5 Hz, 3H), 4.60 (d, *J* = 10.5 Hz, 3H), 3.98 (ddt, *J* = 5.8, 3.1, 2.2 Hz, 3H), 3.81 (s, 9H), 3.35 (dd, *J* = 6.2, 3.3 Hz, 3H), 3.03 (d, *J* = 18.6 Hz, 3H), 2.68 – 2.65 (m, 3H), 2.59 (s, 12H), 2.44 (s, 9H), 2.41 (dd, *J* = 12.2, 3.5 Hz, 3H), 2.30 (dd, *J* = 18.7, 6.3 Hz, 3H), 2.05 (td, *J* = 12.5, 5.1 Hz, 3H), 1.94 – 1.90 (m, 3H).^{13}C NMR (151 MHz, $CDCl_3$) δ: 147.84, 142.25, 139.05, 132.59, 131.49, 130.98, 128.29, 127.13, 118.69, 114.06, 89.71, 73.86, 65.87, 59.00, 56.91, 46.58, 43.47, 43.14, 41.14, 36.07, 20.49, 15.90. Anal. Cal. for $C_{66}H_{75}N_3O_9$: C, 75.19; H, 7.17; N, 3.99. %Found: C, 73.15; H, 6.98; N, 3.88. IR (ATR, cm^{-1}): 2905, 2900, 2834, 2792, 1630, 1598, 1449, 1440, 1372, 1346, 1325, 1274, 1240, 1198, 1147, 115, 1094, 1076, 1047, 1016, 980, 937, 831, 782, 749, 667, 642. ESI-MS: [**CC3**]$^{+2}$ 526 m/z. $[\alpha]_D$ = 248˚ (c = 0.162, $CHCl_3$, 589 nm, 25 ˚C).

C-4: NMR spectroscopy

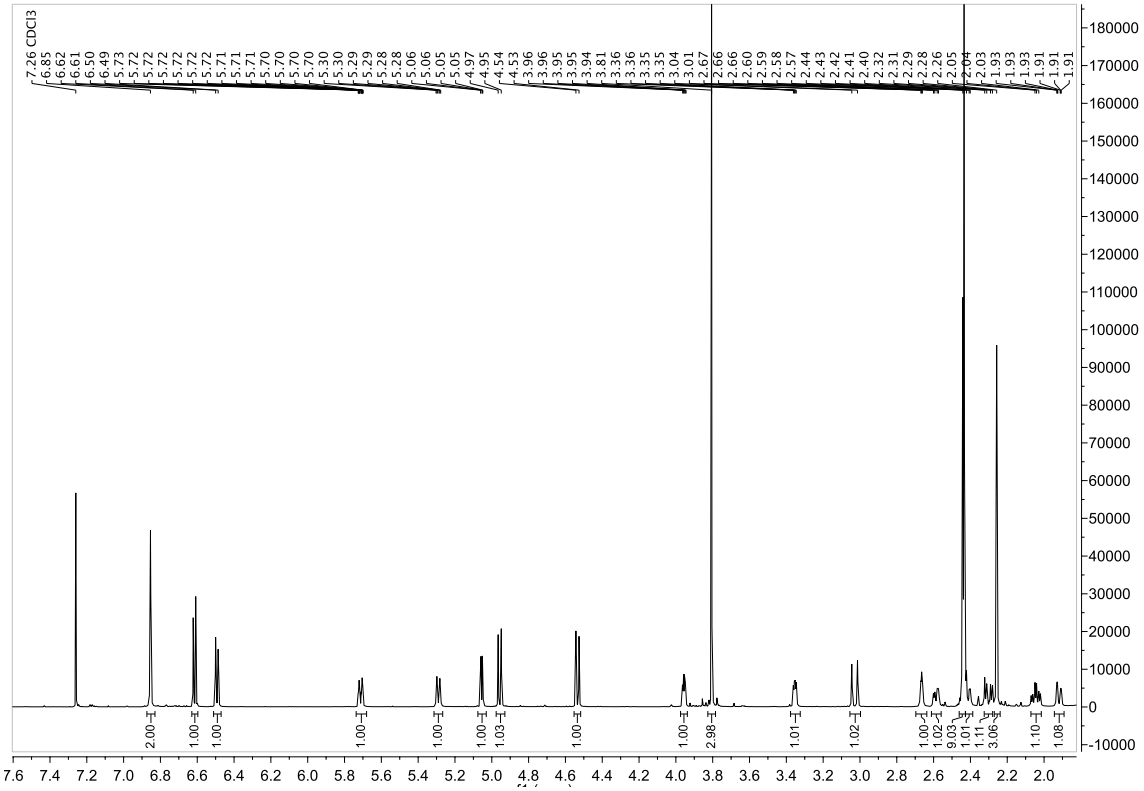

Figure C-3. ^{1}H NMR spectra for **CC1.**

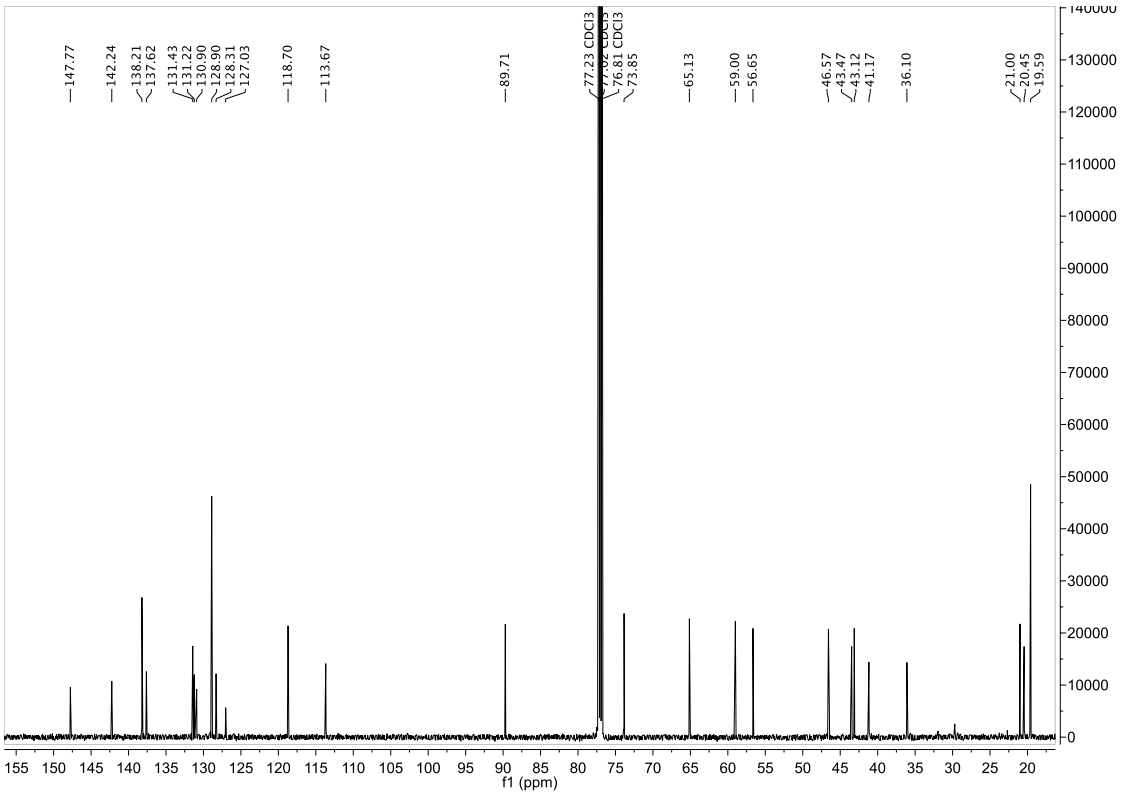

Figure C-4. ^{13}C NMR spectra for **CC1**.

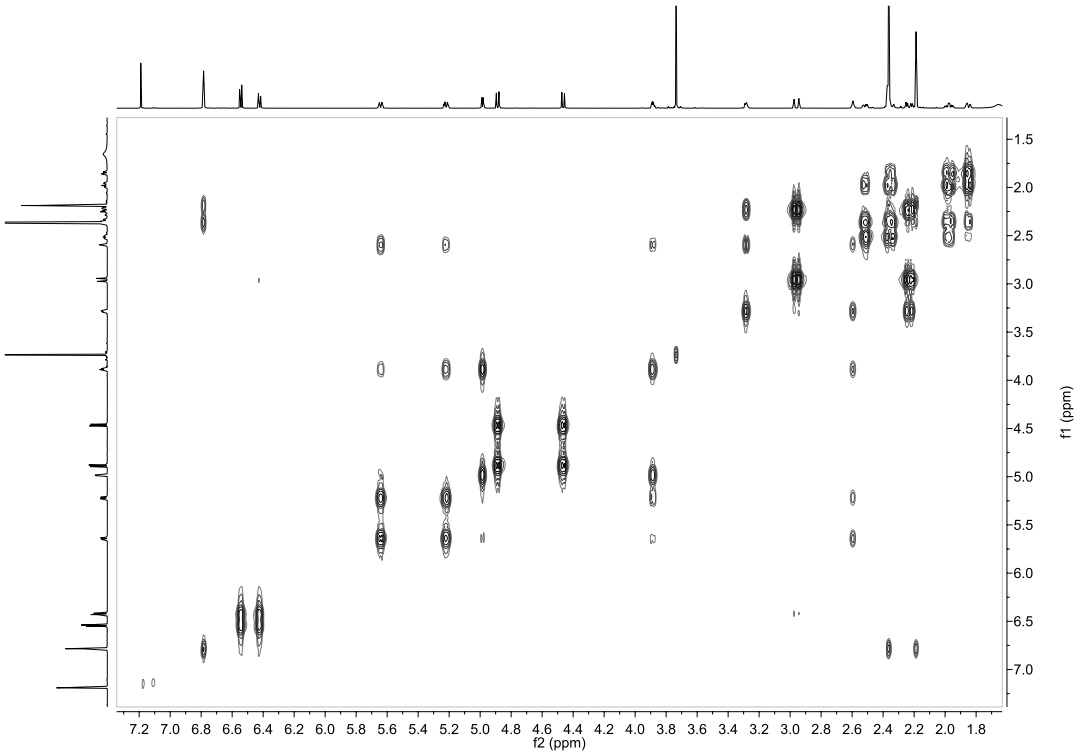

Figure C-5. COSY NMR spectra for **CC1.**

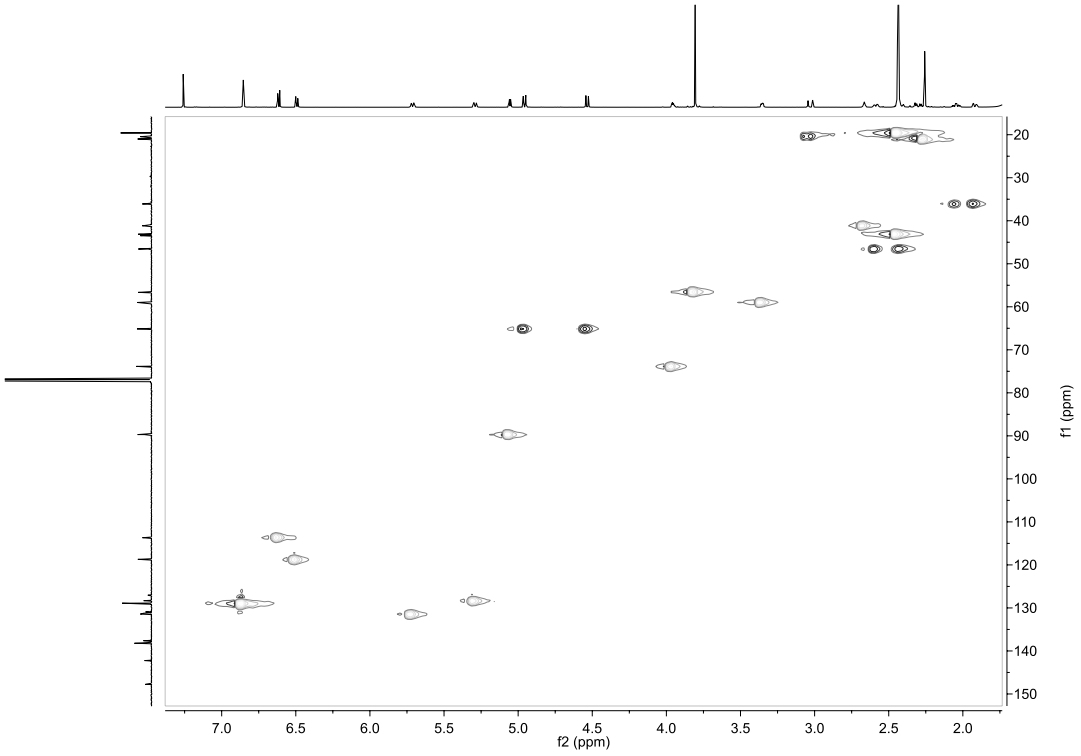

Figure C-6. HSQC NMR spectra for **CC1.**

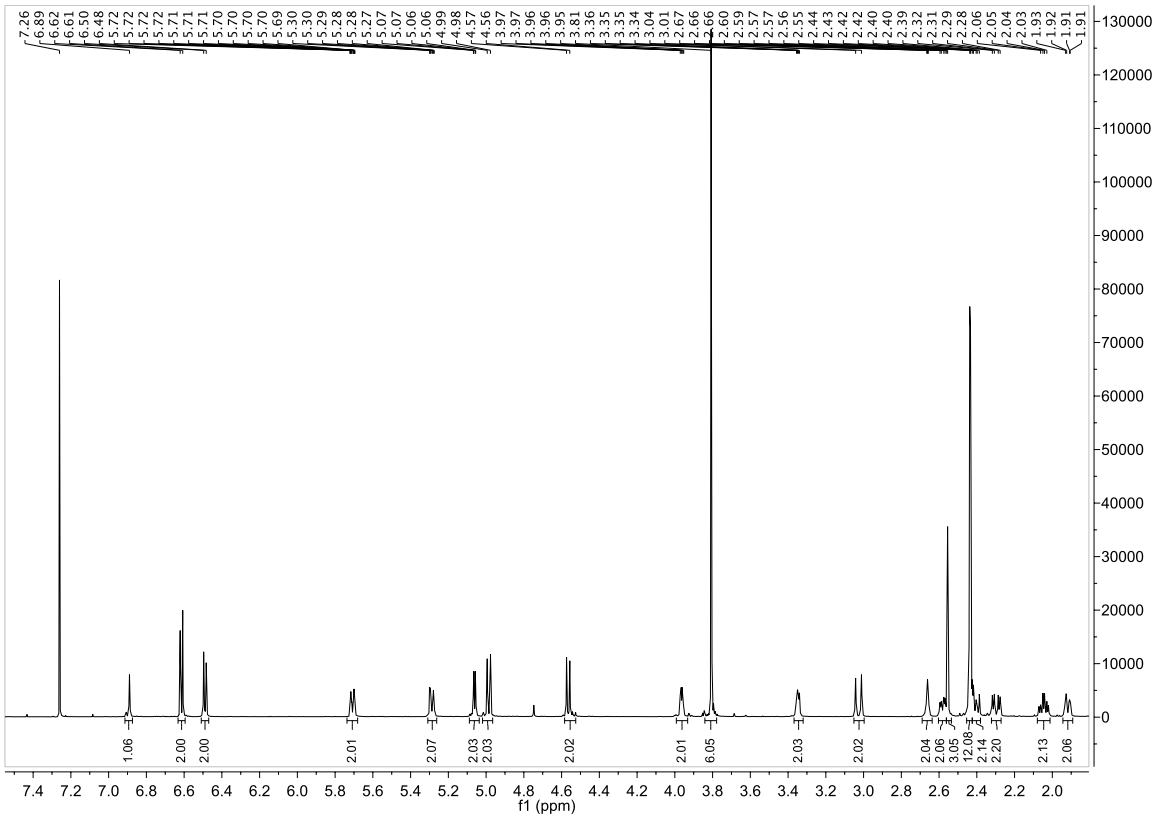

Figure C-7. ^{1}H NMR spectra for **CC2.**

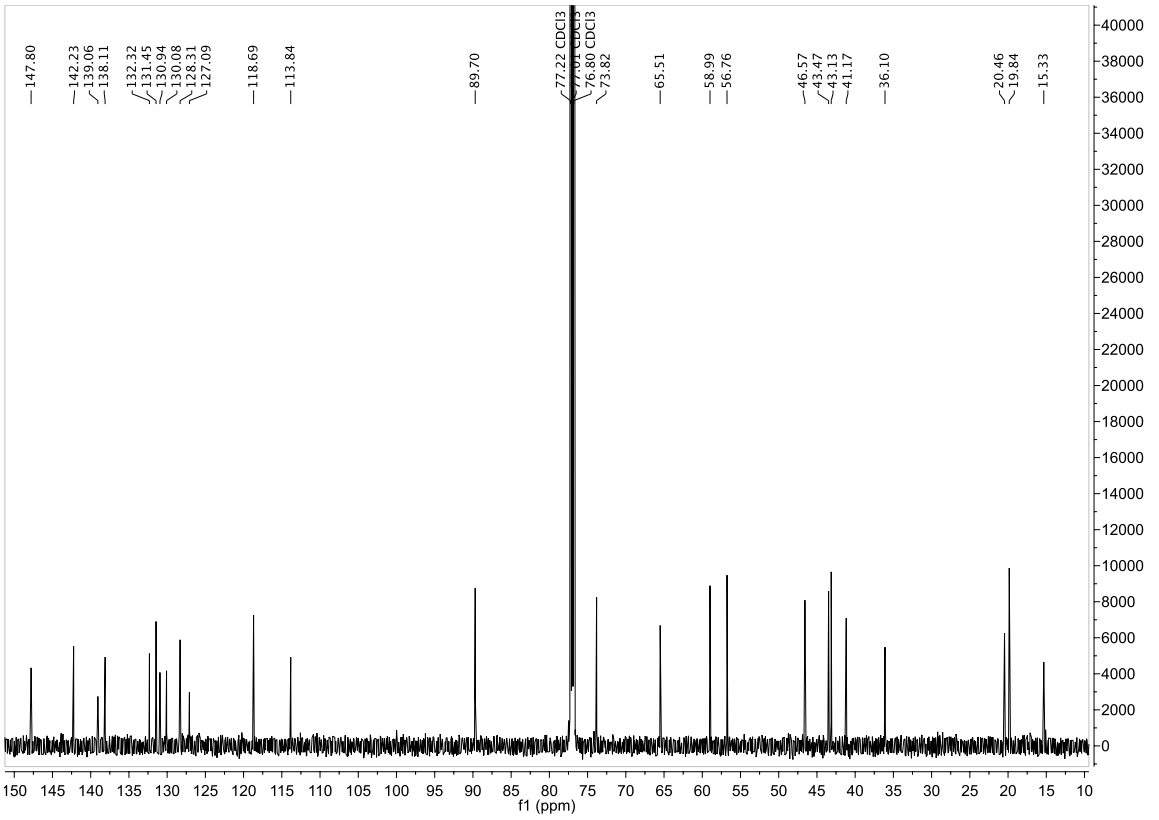

Figure C-8. ^{13}C NMR spectra for **CC2.**

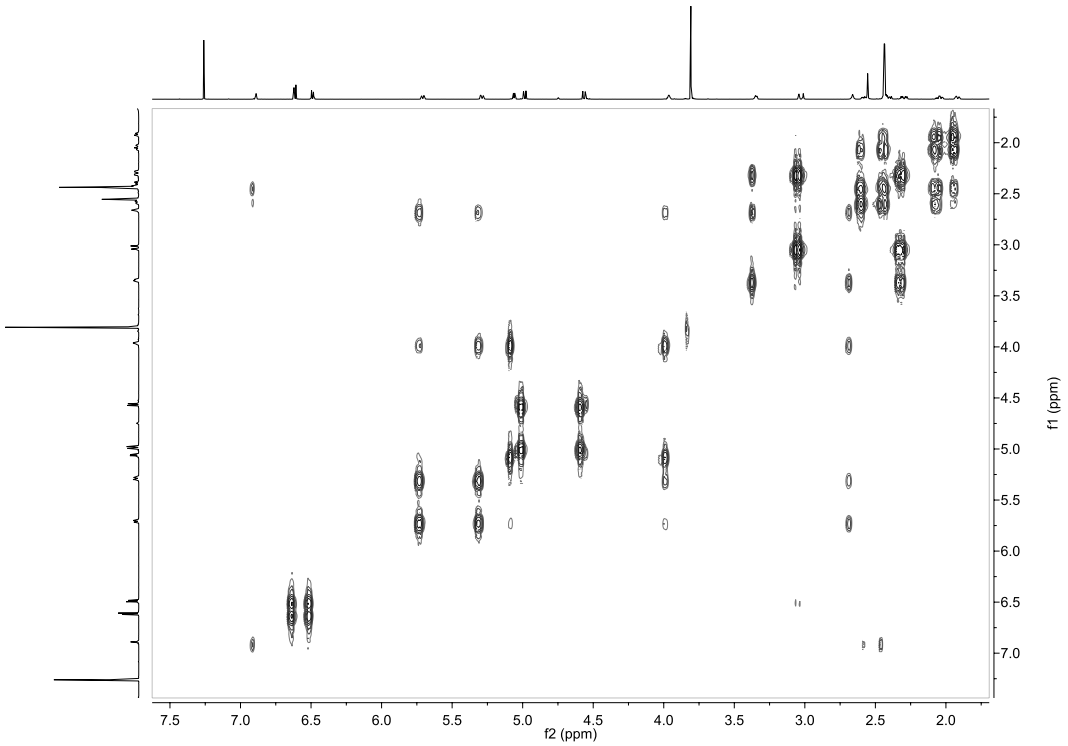

Figure C-9. COSY NMR spectra for **CC2.**

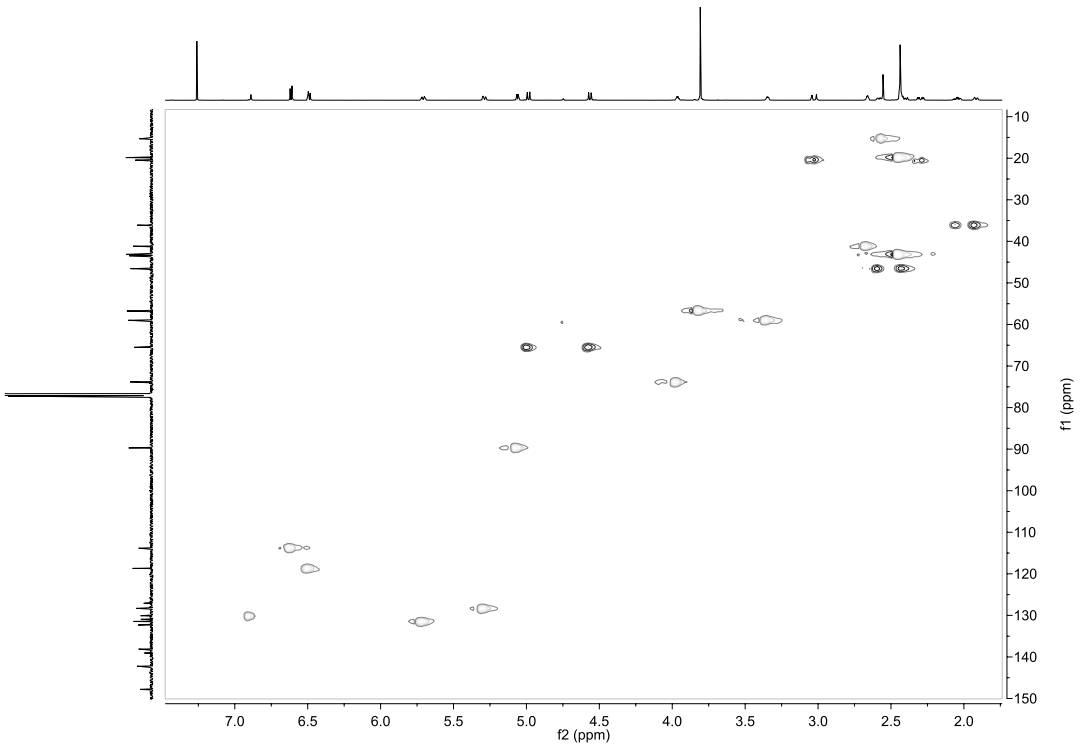

Figure C-10. HSQC NMR spectra for **CC2.**

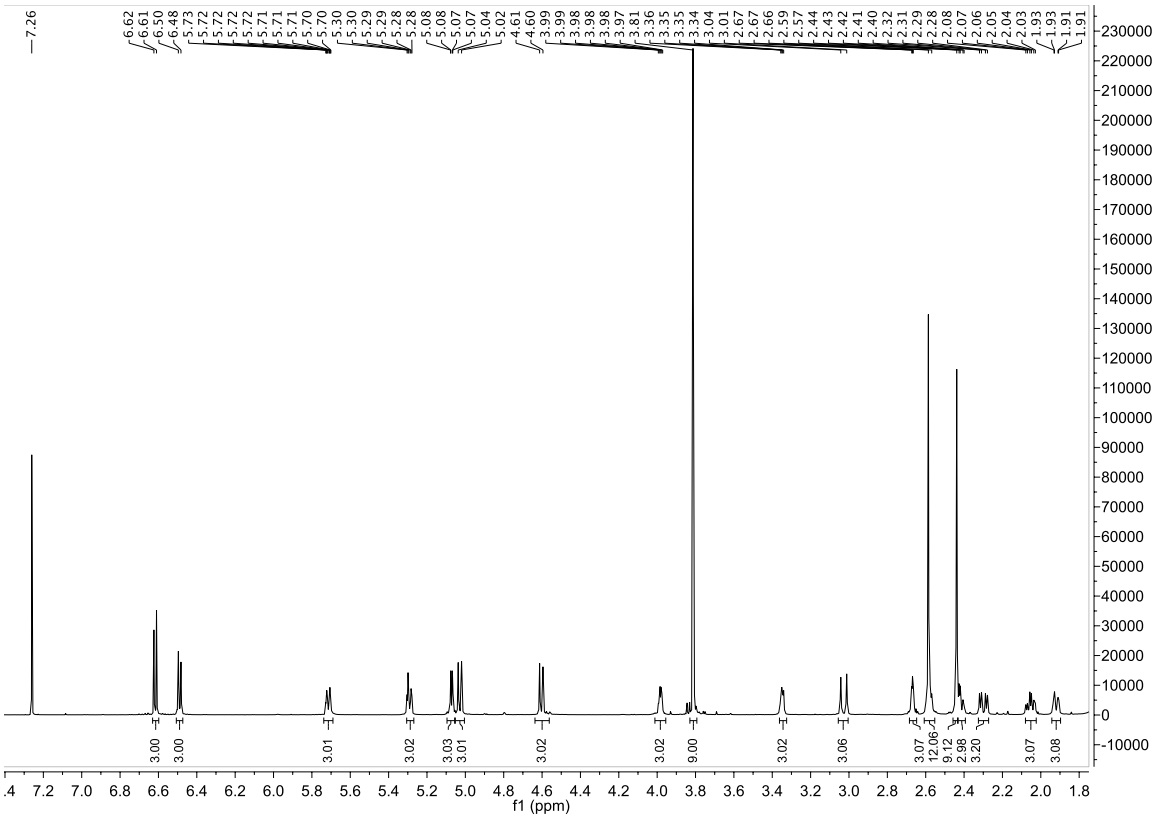

Figure C-11. ^{1}H NMR spectra for **CC3.**

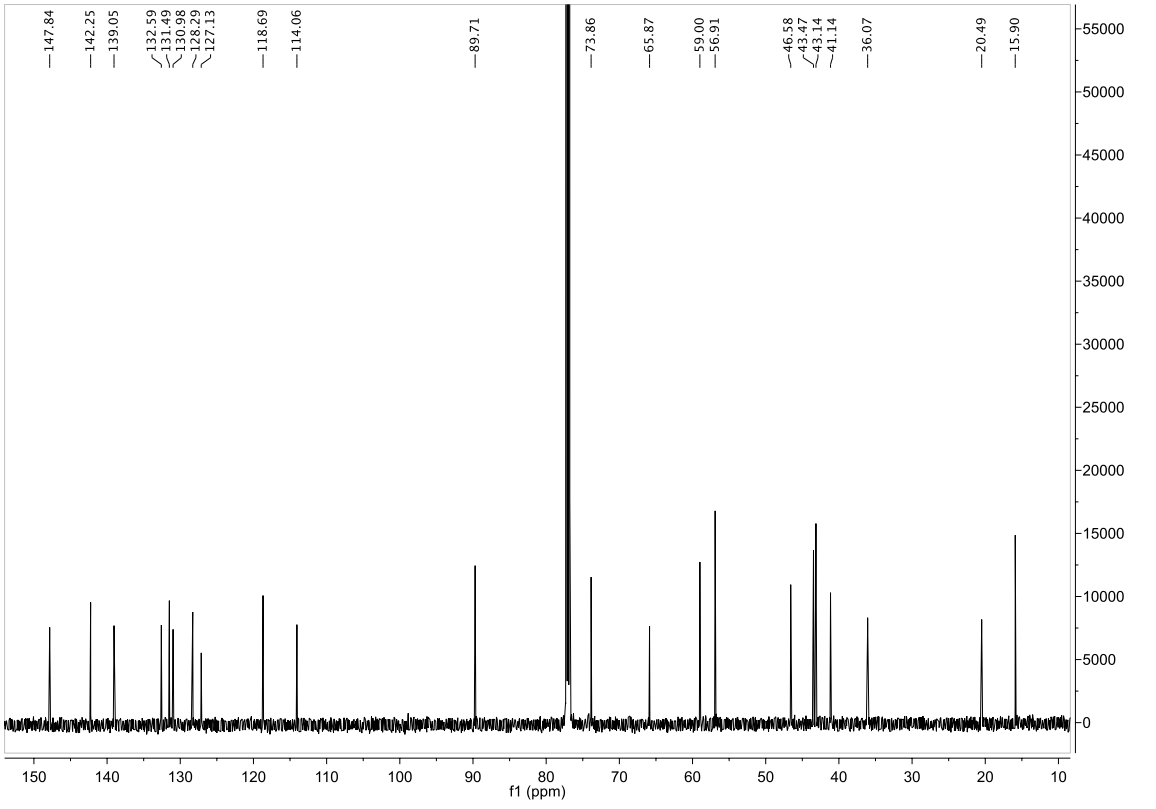

Figure C-12. ^{13}C NMR spectra for **CC3.**

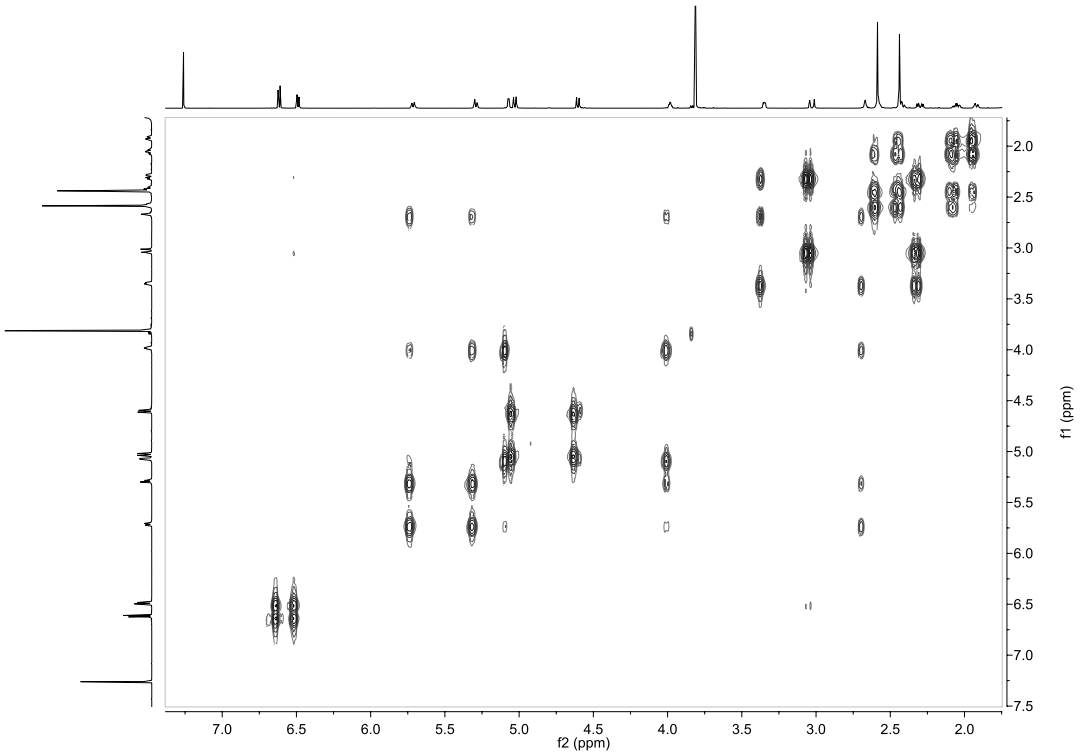

Figure C-13. COSY NMR spectra for **CC3.**

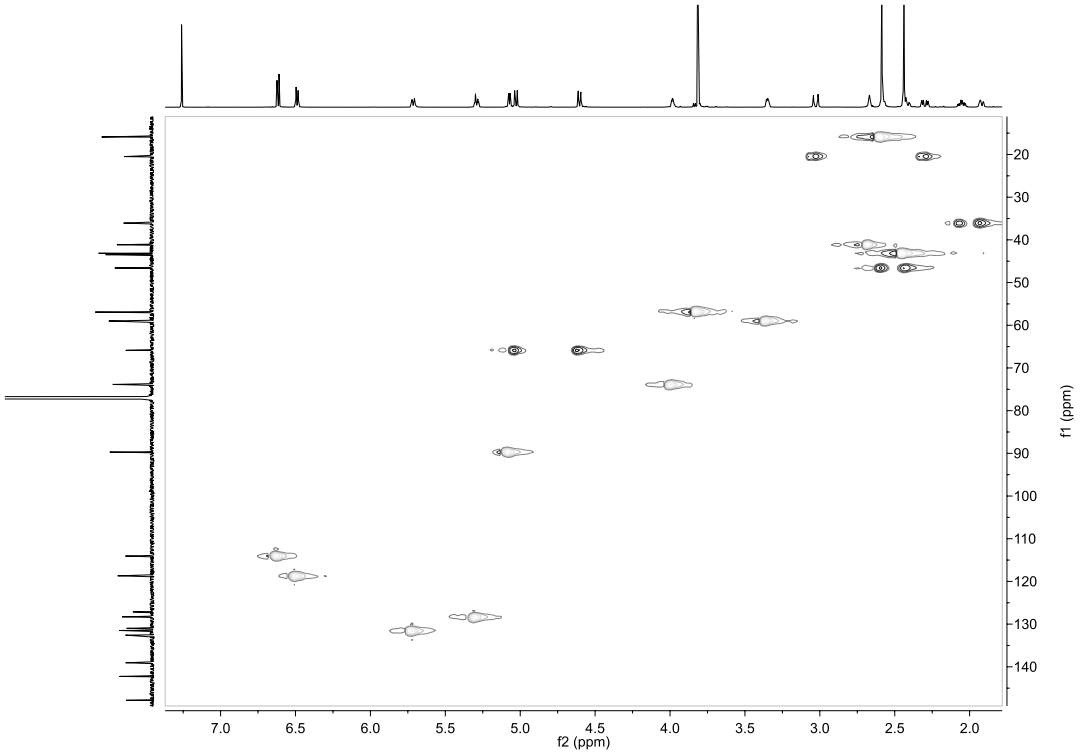

Figure C-14. HSQC NMR spectra for **CC3.**

C-5: Variable Temperature ^{1}H NMR study of HC3

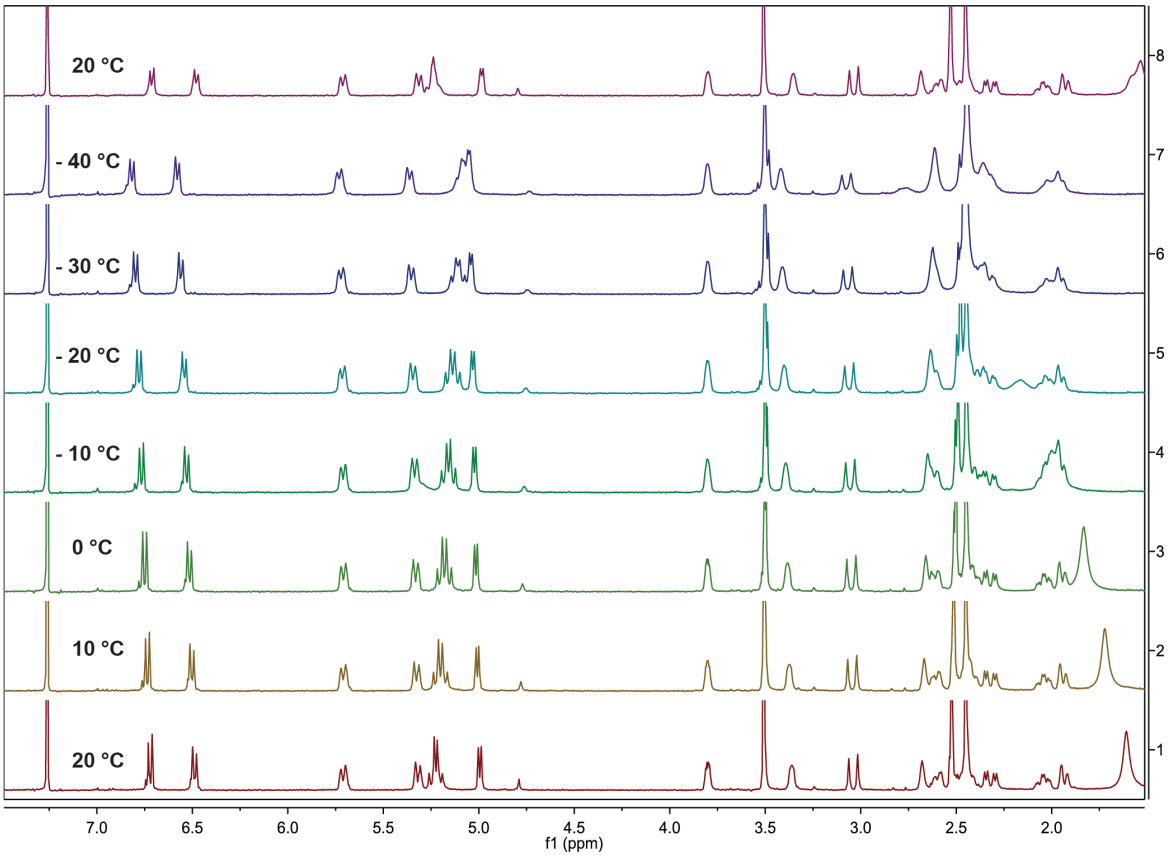

Figure C-15. ^{1}H NMR spectra for **HC3** in $CDCl_3$ starting at 20 ˚C gradually reducing by 10 ˚C intervals to - 40 ˚C and returning to 20 ˚C.

C-6: Dynamic Light scattering – Size and Zeta Potential measurements

Average hydrodynamic size

The size of plasmid dsDNA (pUC19) condensates were characterized by means of DLS measurements using a Malvern Nano ZS instrument with a thermostatic sample chamber and He−Ne laser operating at a wavelength of 633 nm. All measurements were detected at 25 ˚C at a backscattering angle of 173˚ to the incident beam, in disposable low volume cuvettes (40 μL, Malvern ZEN0040). Briefly, plasmid DNA (pUC19, 0.4 mg/L) was initially exposed to increasing concentrations of test compound in a total volume of 40 μL using 10 mM PBS buffer (pH7.2) for 1 h at 25 ˚C. All buffers were filtered through 0.4 μm type GS Millipore filters before use. An average of 6 measurements were taken for each sample and the average hydrodynamic radius was provided by the software itself. The software used cumulant algorithm to calculate the distribution and averages.

Zeta Potential

Zeta potential measurements were performed by a Zetasizer Nano ZS spectrometer in a disposable (Malvern DTS1070) zeta cell. The DNA concentrations in all the samples for Zeta potential measurements were held constant (pUC19 1 ug/ml) whereas the concentration of each test compound was varied. Zeta potential was carried out in NaOAc buffer (10 mM, pH 4.0), DNA /compound mix was prepared in a volume of 50 μL incubated for 1 h at 25 ˚C prior to being diluted to the final volume of 1 mL with the same buffer. The zeta potential values were calculated by the Smoluchowski approximation of Henry's equation.

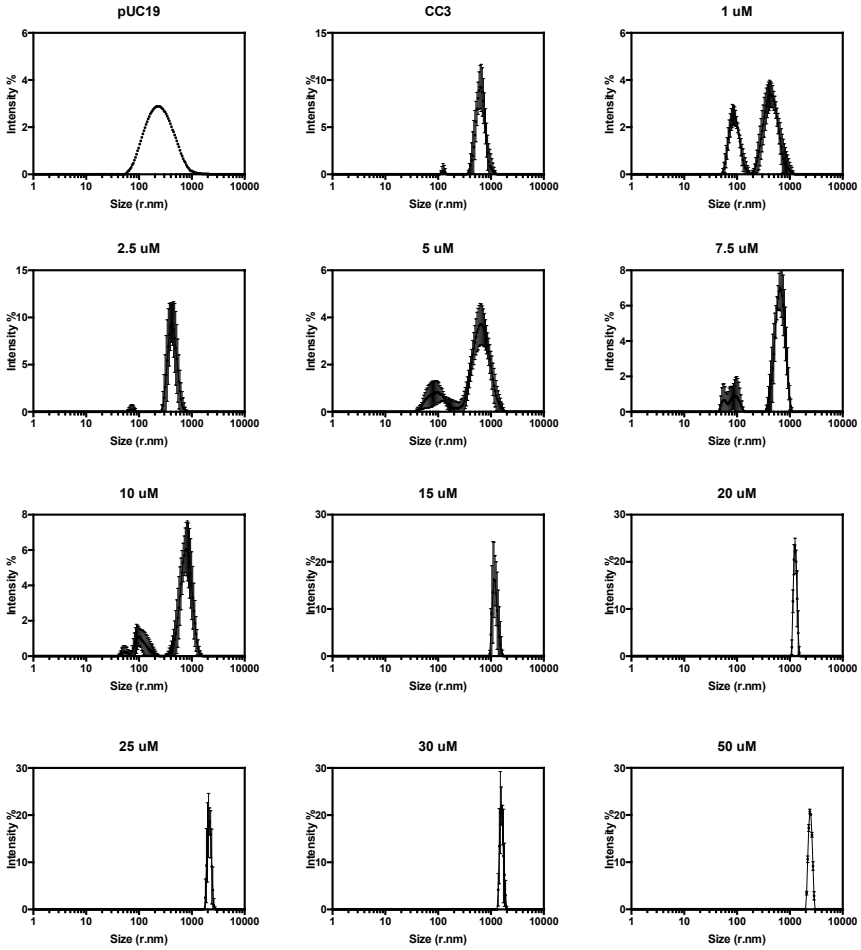

Figure C-16. The distributions of the intensity of light scattered by DNA/**CC3** aggregates at increasing opioid concentrations.

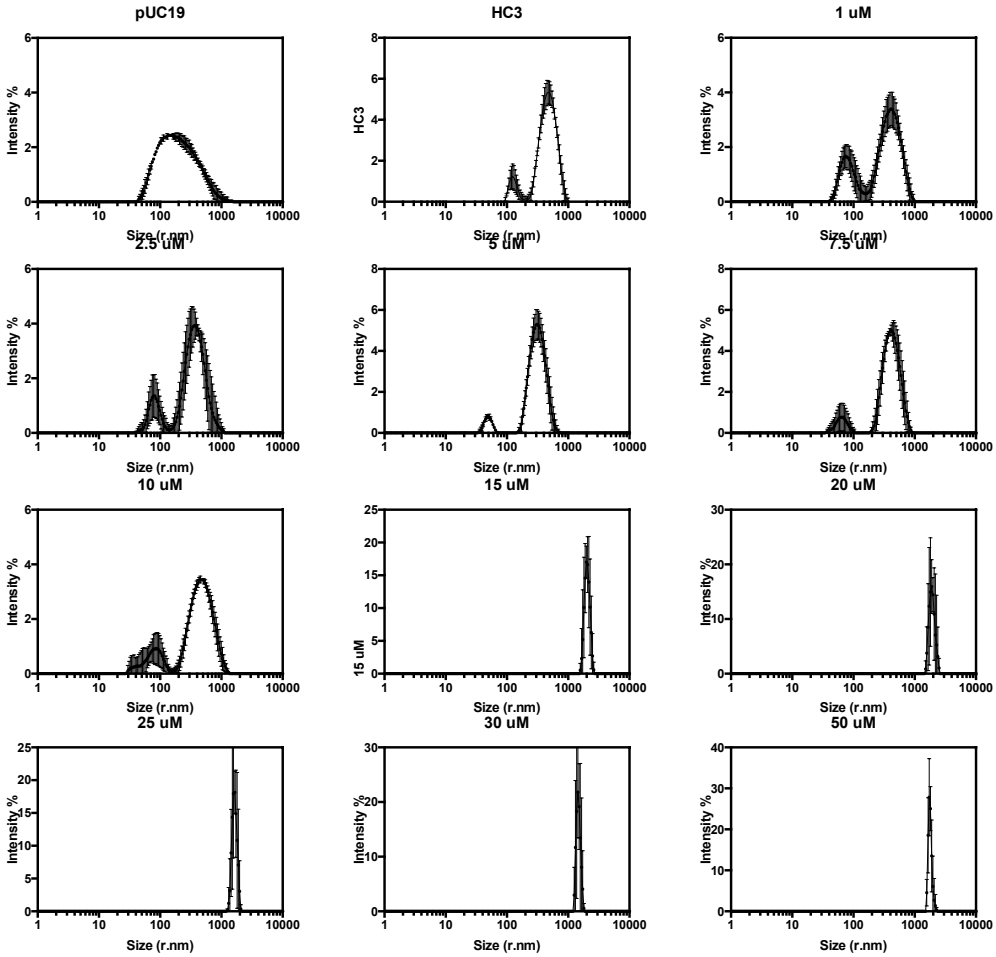

Figure C-17. The distributions of the intensity of light scattered by DNA/**HC3** aggregates at increasing opioid concentrations.

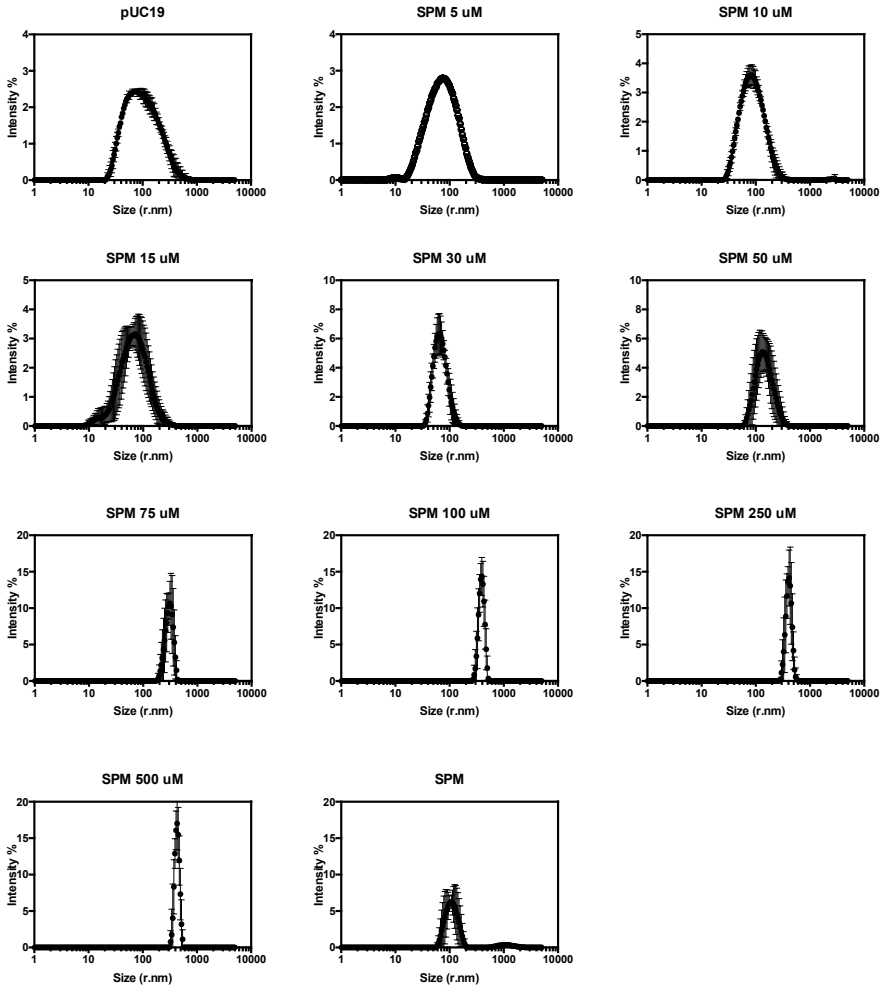

Figure C-18. The distributions of the intensity of light scattered by DNA/SPM aggregates at increasing opioid concentrations.

C-7: References

[1] J. C. Cole, O. Korb, P. McCabe, M. G. Read, R. Taylor, *J. Chem. Inf. Model.* **2018**, *58*, 615–629.

[2] C. R. Groom, I. J. Bruno, M. P. Lightfoot, S. C. Ward, *Acta Cryst B* **2016**, *72*, 171–179.

[3] N. L. Allinger, *J. Am. Chem. Soc.* **1977**, *99*, 8127–8134.

[4] R. Sure, S. Grimme, *J. Comput. Chem.* **2013**, *34*, 1672–1685.

[5] J. P. Perdew, K. Burke, M. Ernzerhof, *Phys Rev Lett* **1996**, *77*, 3865–3868.

[6] S. Grimme, J. Antony, S. Ehrlich, H. Krieg, *J Chem Phys* **2010**, *132*, 154104.

[7] F. Weigend, R. Ahlrichs, *Phys. Chem. Chem. Phys.* **2005**, *7*, 3297.

[8] S. Grimme, S. Ehrlich, L. Goerigk, *J. Comput. Chem.* **2011**, *32*, 1456–1465.

[9] F. Neese, *Wiley Interdiscip. Rev. Comput. Mol. Sci.* **2012**, *2*, 73–78.

[10] C. Adamo, V. Barone, *J Chem Phys* **1999**, *110*, 6158–6170.

[11] A. V. Marenich, C. J. Cramer, D. G. Truhlar, *J. Phys. Chem. B* **2009**, *113*, 6378–6396.

Appendix D

Supporting information accompanying Chapter IV, The Development of Non-Opioid C_3-Symmetric Scaffolds as Condensation Agents.

D-1: Cytotoxicity of OC3 in CHO-K1

A parental Chinese hamster ovary (CHO) cell line, CHO-K1 (ATCC® CCL-61™), was cultured in serum-free media (SFM), CHO-S-SFMII (Biosciences, 12052-098), supplemented with 2% v/v polyvinyl alcohol (PVA) as an anti-clumping agent. Routine stock maintenance was performed in a 50 mL tube with filtered top containing 5 mL working volume of media sub-cultured during exponential growth (3-4 days) at a seeding density of $2x10^5$ cells/mL. Suspension culture was performed in an orbital shaking incubator (Kuhner, UK) at 170 rpm, at 37˚C under 5% CO_2. Cytotoxicity assays were carried out using an **OC3** stock at a concentration of 35 mM in DMSO. This was further diluted 1:34 in HEPES buffer and further in SFM growth media to the final working concentration of 25 and 50 µM. DMSO only was diluted to the same factor (1:688) as the highest **OC3** concentration and used as a vehicle control to account for toxicity of DMSO alone. Samples were set up in biological triplicates under the growth conditions described and monitored for cell growth (Cells/mL) and viability (%) using the ViaCount™ viability stain (Millipore, UK) on a Guava 5HT benchtop cytometer

D-2: Imidazolium compound characterisation and nucleic acid screening

Characterisation of Imidazolium compounds

Spectral characterisation was carried out on the samples provided prior to nucleic acid screening and compared to reported literature.[1,2] Sample were examined in the same previously reported deuterated solvent for ease of ^1H NMR comparison. ESI mass spectra were recorded on a microspray LC-MS Bruker micrOTOF-Q II. Samples for ESI-MS were prepared in 100% HPLC-grade acetonitrile prior to analysis. It has been demonstrated that the imidazolium based tripodal compounds have considerable affinity for halide anions in polar solvent through electrostatic interactions and C—H—X" hydrogen bonds. It has been reported the complexation of the halide anion occurs via hydrogen bonding, where the association constants were calculated to be 75,000-72,00 M^{-1} and association constants decrease in the order $Cl^- > Br^- > I^-$.[1,2] Thus, ESI-MS spectra observed show bromine complexation and fits were carried out using mMass software (version 5.5.0).[3]

NAM1

Reported Spectra: ^{1}H NMR (CD_3CN) δ (ppm): 9.69 (s, 3H, NCHN), overlapping 7.91-8.03 (m, 15H, (Ar-H), (NCHCH)), 7.79 (s, 3H, NCHCH), 7.58 (m, 9H, Ar-H), 6.16 (q, 3H, *J* = 6.8 Hz, CH), 5.60 (s, 6 H, CH_2), 2.29 (s, 9H, CH_3), 1.95 (d, 9H, *J* = 6 Hz, CH_3).

Found Spectra: ^{1}H NMR (400 MHz, CD_3CN) δ: 10.07 (s, 3H), 8.02 (d, *J* = 1.9 Hz, 3H), 7.89 – 7.81 (m, 10H), 7.74 (t, *J* = 1.9 Hz, 3H), 7.61 – 7.46 (m, 14H), 6.36 (q, *J* = 7.1 Hz, 3H), 5.50 (s, 6H), 2.27 (s, 10H), 2.17 (s, 14H).

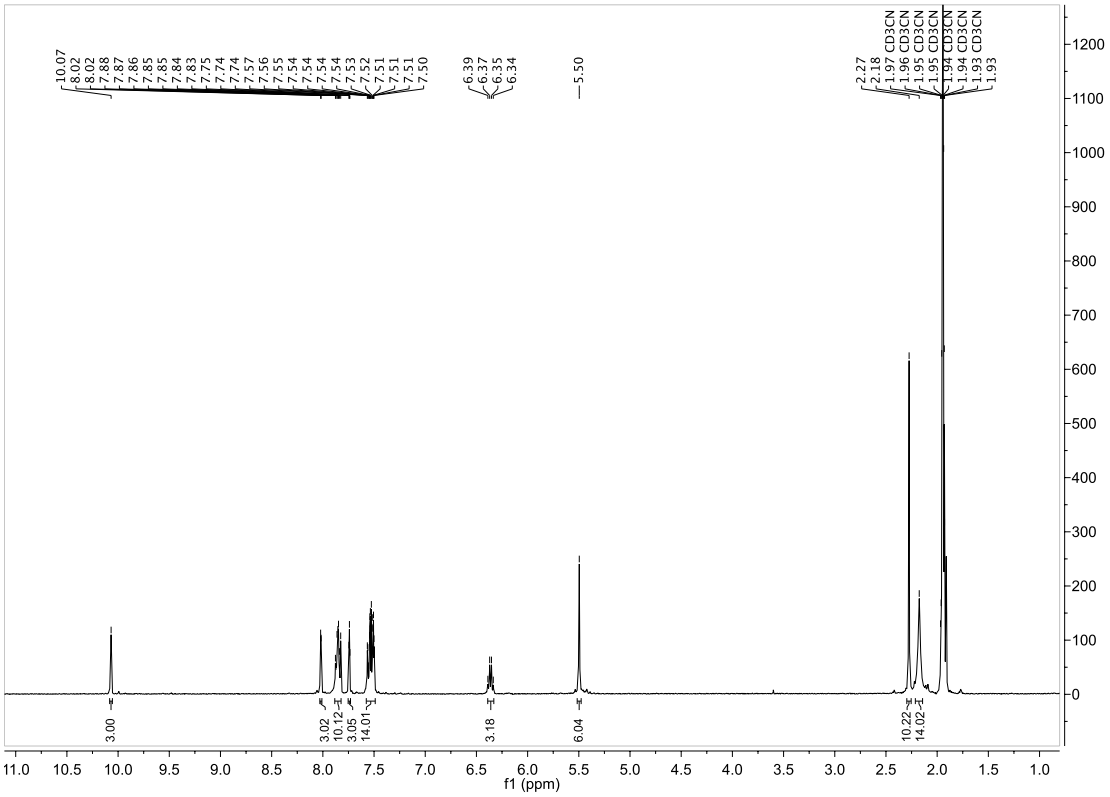

Figure D-1. ^{1}H NMR spectra for **NAM1**.

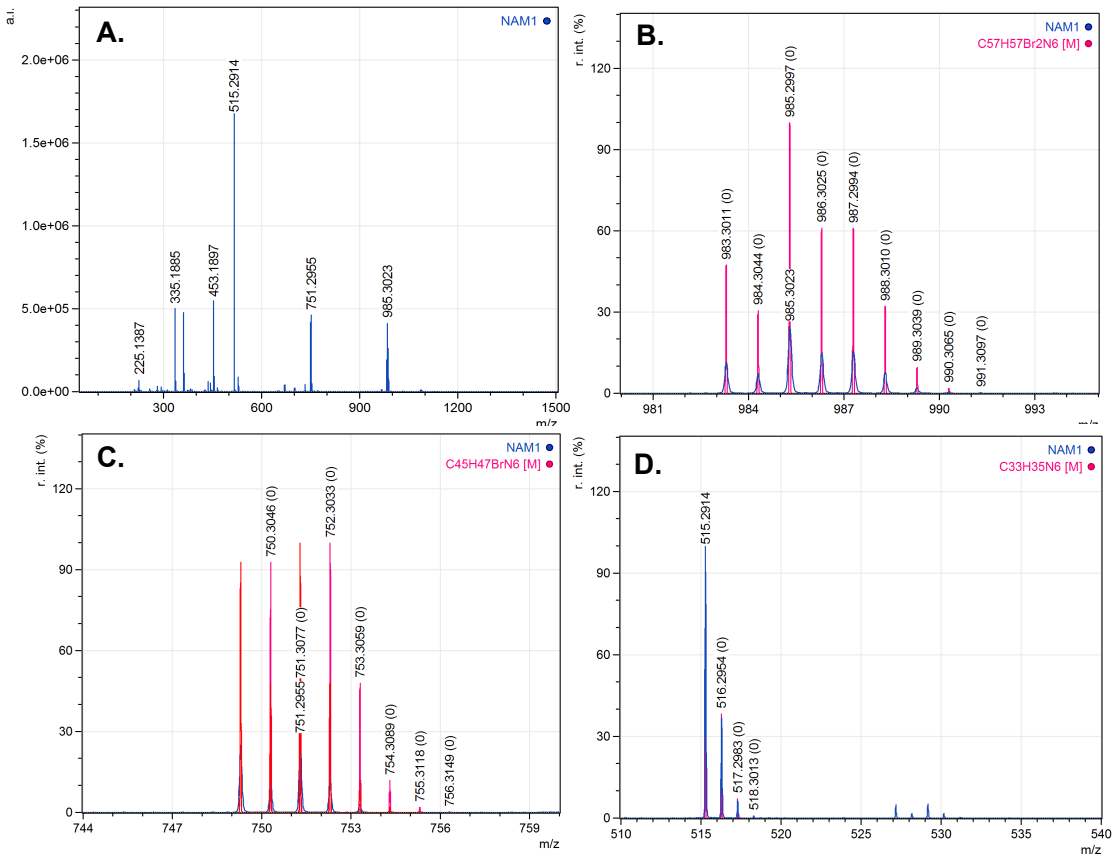

Figure D-2. Mass Spec of **NAM1**. **A.** Full spectra, **B**. fit 1, **C**. fit 2, and **D**. Fit 3

NAM2

Reported Spectra: ^{1}H NMR (CD_3CN) δ (ppm): 10.09 (s, 3H, NCHN), 8.44 (s, 3H, NCHCH), 7.21 (d, 3H, *J* =6.8 Hz, NCHCH), 5.75 (s, 6 H, CH_2), 4.29 (m, 3H, CH), 4.12 (m, 3H, CH), 2.44 (m, 3H, CH), 2.26 (s, 9H, CH_3), overlapping 1.75-1.87 (m, 15H, CH_2CH_2CH), 1.46 (m, 3H, CH), 1.11 (s, 9H, CH_3), 1.01 (s, 9H, CH_3), 0.83 (d, 3H, 7=9.6 Hz, CH).

Found Spectra: ^{1}H NMR (400 MHz, CD_3CN) δ: 9.96 (s, 3H), 7.71 (t, *J* = 1.7 Hz, 3H), 7.46 (t, *J* = 1.7 Hz, 3H), 5.46 (s, 6H), 4.32 (dd, *J* = 13.2, 9.0 Hz, 3H), 4.16 (dd, *J* = 13.2, 6.7 Hz, 3H), 2.52 (p, *J* = 7.7, 7.1 Hz, 3H), 2.42 – 2.32 (m, 4H), 2.22 (s, 10H), 2.18 (s, 9H), 1.92 – 1.70 (m, 15H), 1.67 – 1.52 (m, 3H), 1.17 (s, 9H), 1.09 (s, 9H), 0.89 (d, J = 9.6 Hz, 3H).

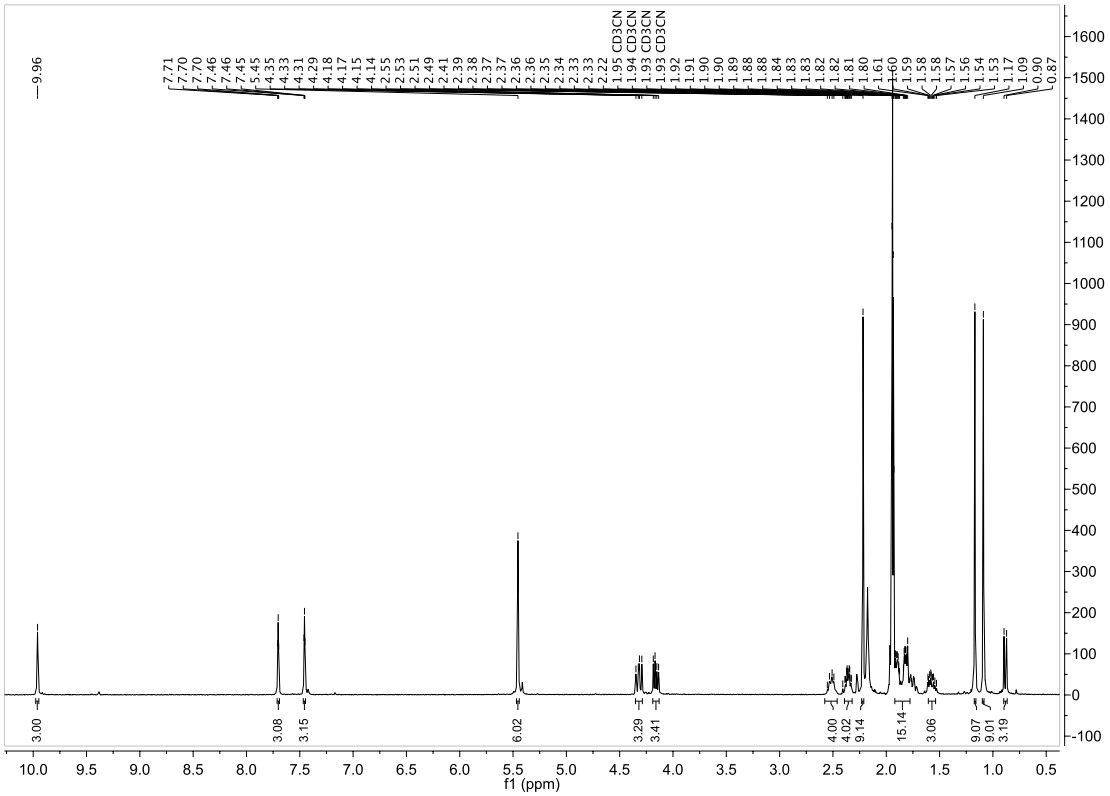

Figure D-3. ^{1}H NMR spectra for **NAM2**.

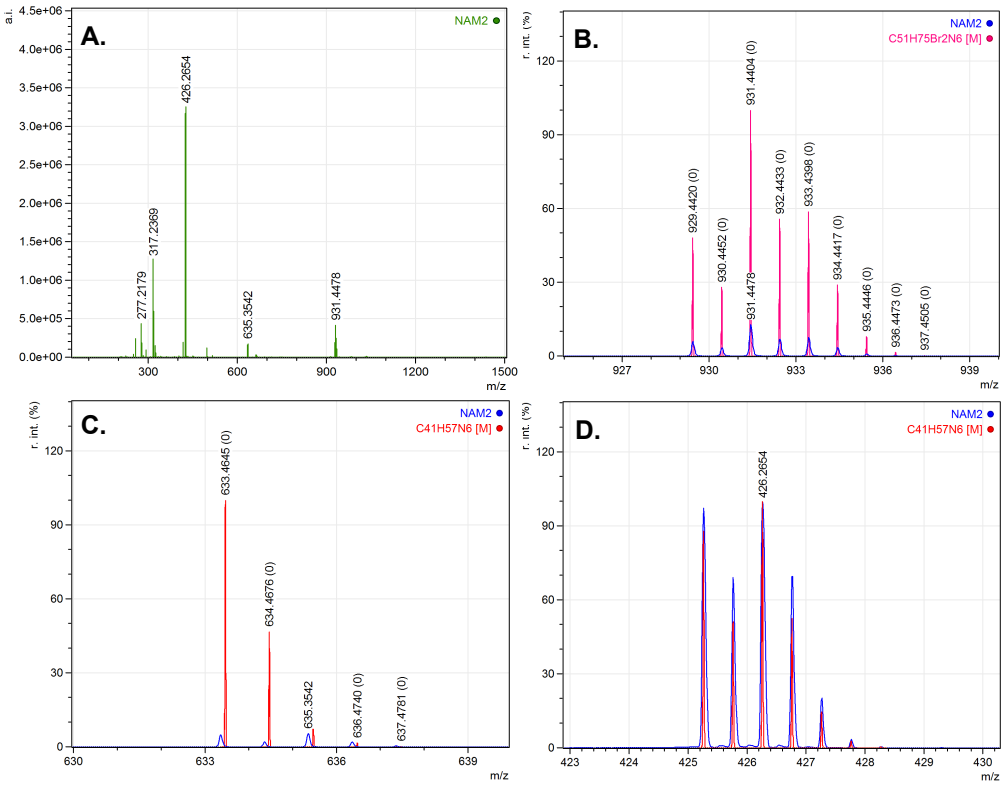

Figure D-4. Mass Spec of **NAM2**. **A.** Full spectra, **B.** fit 1, **C.** fit 2, and **D.** Fit 3.

NAM3

Reported Spectra: ^{1}H NMR (CD_3CN) δ (ppm): 10.21 (s, 3H, NCHN), 8.31 (s, 3H, NCHCH), 7.25 (m, 15H, Ar-H), 7.06 (s, 3H, NCHCH), 6.03 (q, H, *J* = 7.2 Hz, CH), 5.75 (q, 6 H, *J* = 8 Hz, CH2), 2.25 (s, 9H, CH3), 1.82 (d, 9H, *J* = 12 Hz, CH3).

Found Spectra: ^{1}H NMR (400 MHz, CD_3CN) δ: 10.00 (s, 3H), 7.76 (s, 3H), 7.50 (dt, *J* = 4.8, 2.6 Hz, 9H), 7.37 (dd, *J* = 5.1, 2.0 Hz, 9H),), 6.24 (q, *J* = 7.1 Hz, 3H), 5.50 (s, 6H), 2.25 (s, 9H), 1.87 (d, *J* = 7.1 Hz, 9H).

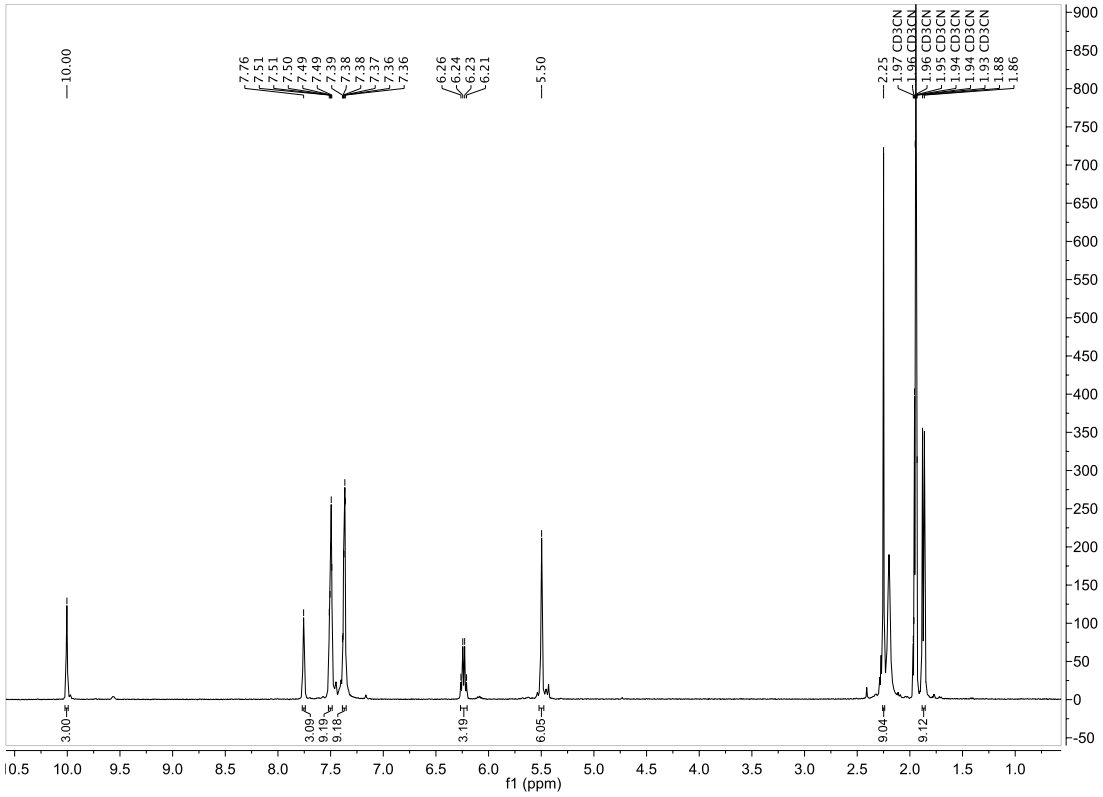

Figure D-5. ^{1}H NMR spectra for **NAM3.**

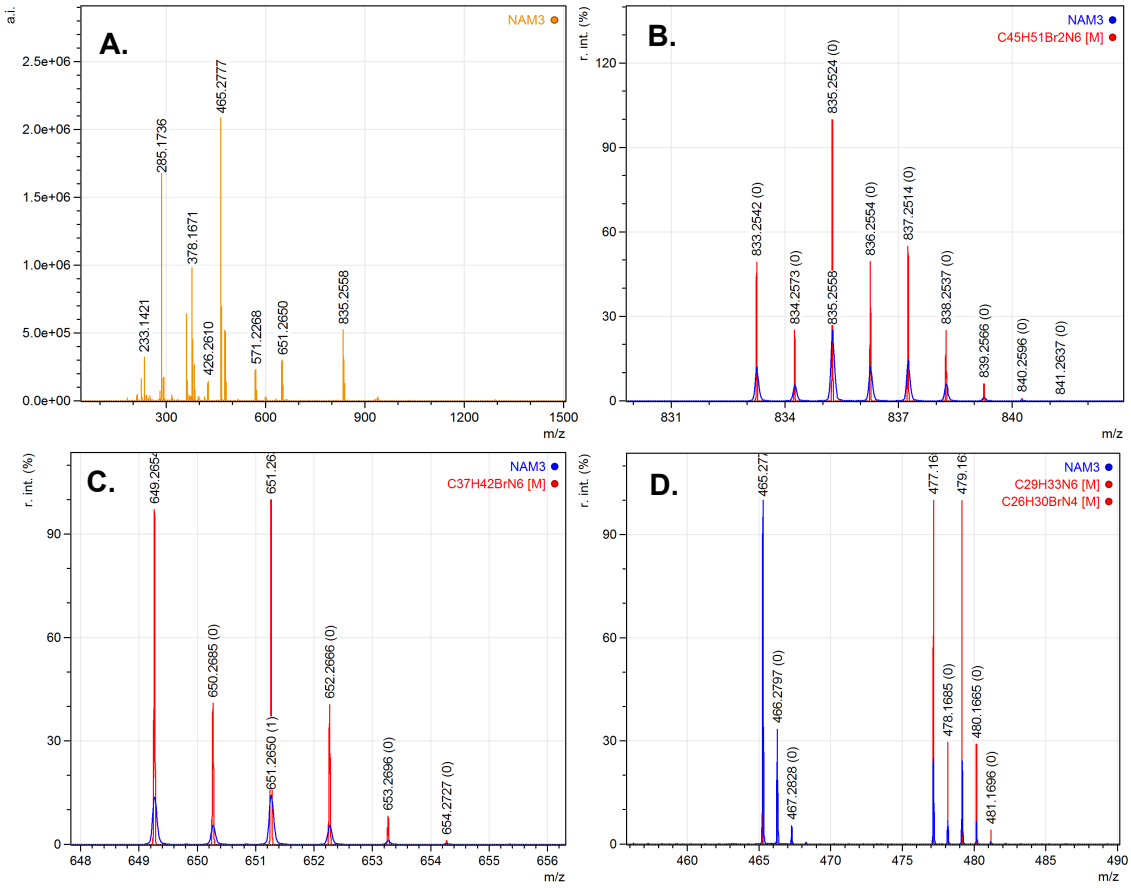

Figure D-6. Mass Spec of **NAM3**. **A.** Full spectra, **B.** fit 1, **C.** fit 2, and **D.** Fit 3.

NAM4

Reported Spectra: ^{1}H NMR (CD_3CN) δ (ppm): 10.09 (s, 3H, NCHN), 8.57 (s, 3H, NCHCH), 7.46 (s, 3H, NCHCH), 5.85 (q, 6 H, *J* = 8.4 Hz, CH_2), 4.70 (q, 3H, *J* = 7.6 Hz, CH), 2.33 (s, 9H, CH_3), 2.00 (q, 3H, *J* = 7.2 Hz, CH), 1.52 (d, 34, *J* = 6.8 Hz, CH_3), 0.95 (d, 9H, *J* = 6.4 Hz, CH_3), 0.71 (d, 9H, *J* = 6.4 Hz, CH_3),

Found Spectra: ^{1}H NMR (400 MHz, CD_3CN) δ: 9.90 (s, 3H), 7.74 (d, *J* = 2.0 Hz, 3H), 7.50 (t, *J* = 1.8 Hz, 3H), 5.46 (s, 6H), 4.67 (dt, *J* = 8.6, 6.8 Hz, 3H), 2.22 (s, 9H), 2.03 (ddd, J = 13.3, 6.7, 1.7 Hz, 3H), 1.47 (d, *J* = 6.9 Hz, 9H), 0.94 (dd, *J* = 6.7, 2.1 Hz, 9H), 0.67 (d, *J* = 6.7 Hz, 9H).

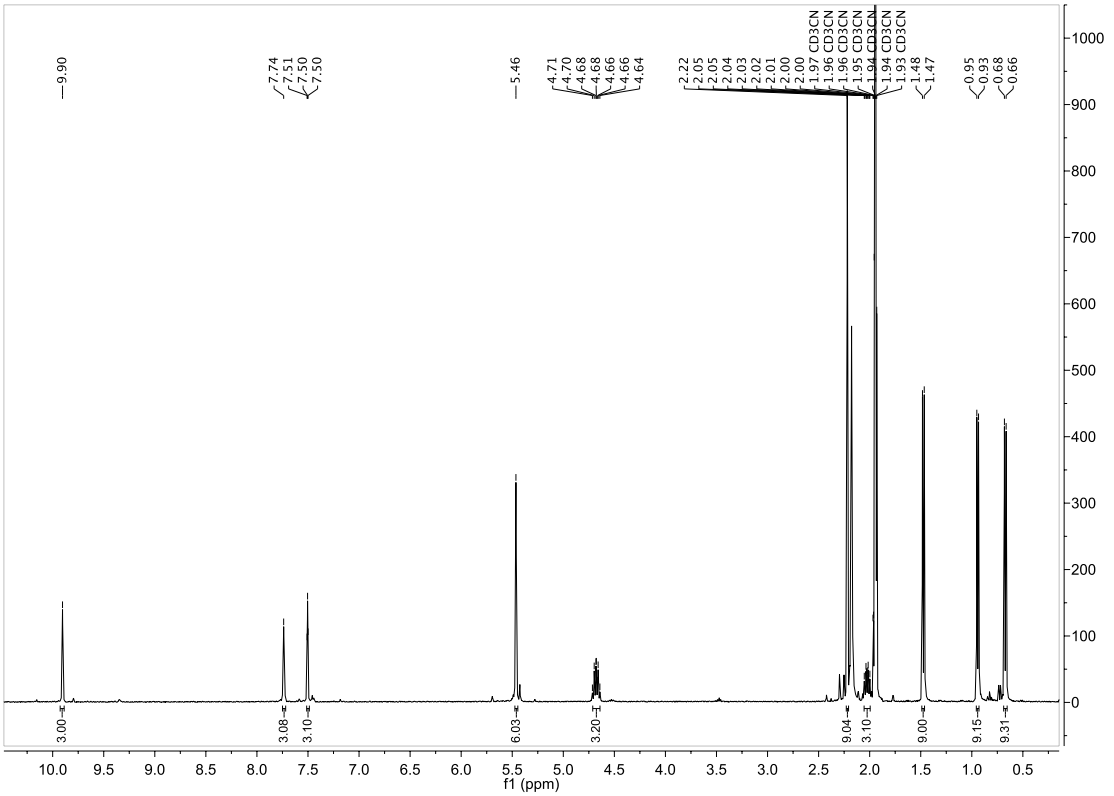

Figure D-7. ^{1}H NMR spectra for **NAM4**.

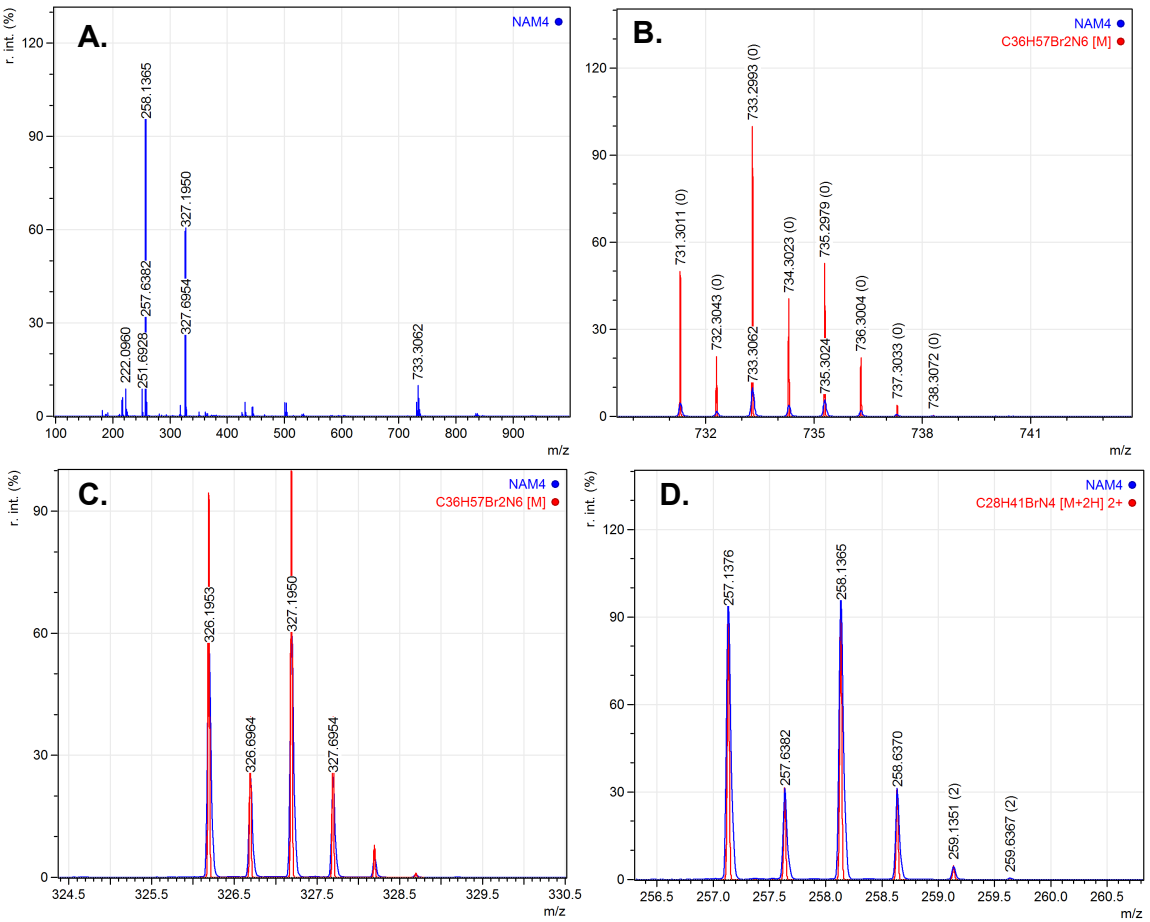

Figure D-8. Mass Spec of **NAM4**. **A.** Full spectra, **B**. fit 1, **C.** fit 2, and **D**. Fit 3.

NAM5

Reported Spectra: ^{1}H NMR (CD_3CN) δ (ppm): 10.05 (s, 3H, NCHN). 8.52 (s, 3H, NCHCH), 7.26 (s, 3H, NCHCH), 5.81 (d, 6H, *J* = 5.6 Hz, CH_2), 4.67 (m, 3H, CH), 2.30 (s, 9H, CH_3), overlapping 1.48-1.77 (m, 15H, hexyl-CH), 1.45 (d, 9H, *J* = 6.8 Hz, CH_3), overlapping 0.88-1.19 (m, 18H, hexyl-CH).

Found Spectra: ^{1}H NMR (400 MHz, CD_3CN) δ: 9.87 (s, 3H), 7.82 (t, *J* = 1.9 Hz, 3H), 7.51 (t, *J* = 1.8 Hz, 3H), 5.50 (s, 6H), 4.73 (dq, *J* = 8.8, 6.9 Hz, 3H), 2.23 (s, 9H), 1.81 (d, *J* = 12.9 Hz, 3H), 1.72 (tt, *J* = 9.2, 6.7, 3.1 Hz, 6H), 1.60 (d, *J* = 8.1 Hz, 6H), 1.45 (d, *J* = 7.0 Hz, 9H), 1.23 (d, *J* = 12.7 Hz, 3H), 1.14 – 1.07 (m, 9H), 0.99 – 0.90 (m, 6H).

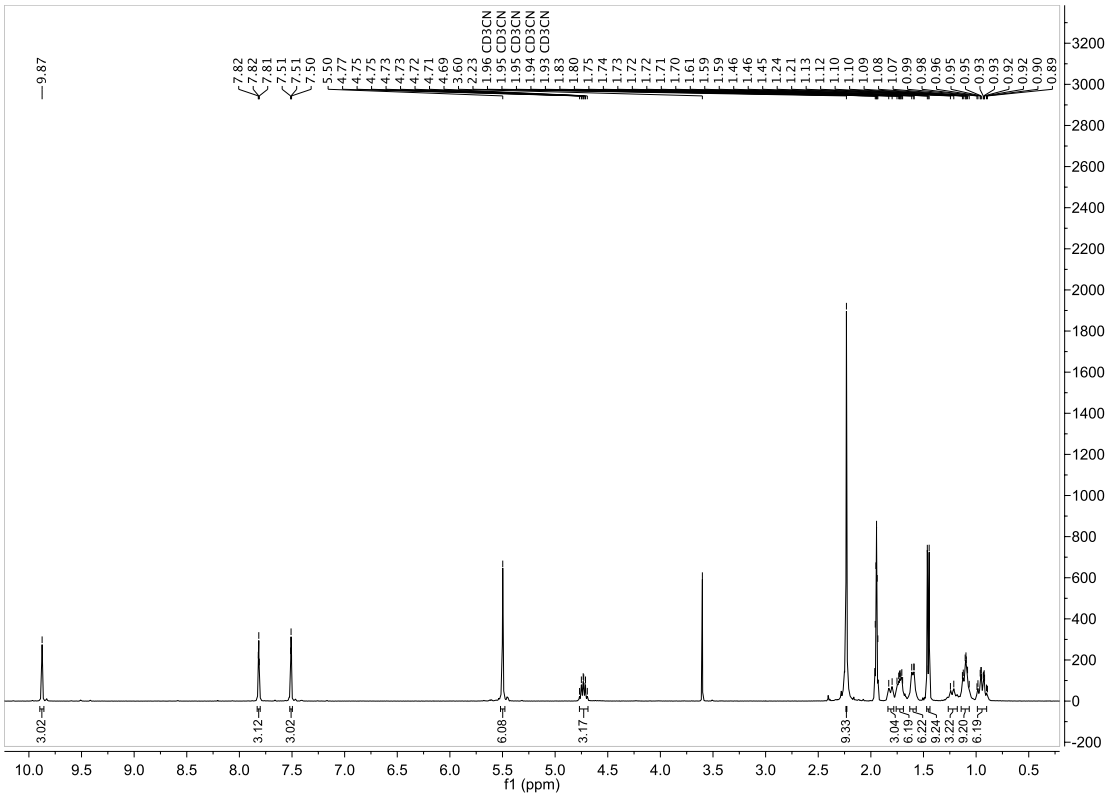

Figure D-9. ^{1}H NMR spectra for **NAM5.**

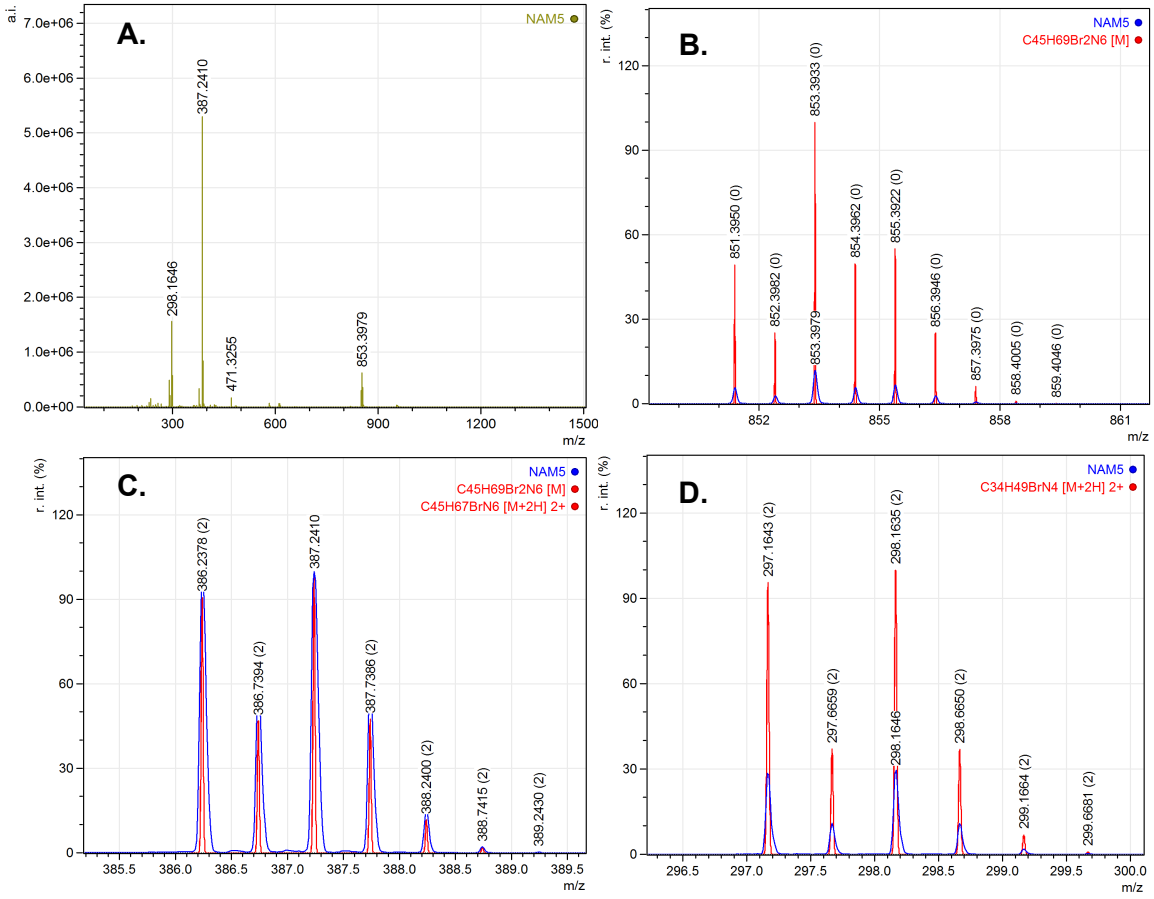

Figure D-10. Mass Spec of **NAM5**. **A.** Full spectra, **B.** fit 1, **C.** fit 2, and **D.** Fit 3.

DNA condensation investigation (pUC19 scDNA).

The ability of the organic compounds to condense supercoiled plasmid DNA was determined using a method previously published by this research group with minor changes being made.[4] Reactions were carried out according to the following general procedure: in a total volume of 20 µL using 80 mM HEPES buffer (pH 7.2) with 25 mM NaCl, 400 ng pUC19 (NEB, N3041) and varying concentrations of test compound (5, 10, 20, 50, 75, 100, 250, and 500 µM), samples were incubated at 37˚C for 2.5 h and 5 h respectfully. Reactions were quenched by adding 6 × loading buffer (Fermentas) containing 10 mM Tris-HCl, 0.03% bromophenol blue, 0.03% xylene cyanole FF, 60% glycerol, 60 mM EDTA and samples were loaded onto an agarose gel (1.2%) containing 4 µL EtBr. Electrophoresis was completed at 60 V for 1 h in 1 × TAE buffer.

D-3: Ligand preparations and CuAAC reactions

Materials and Methods

Chemicals and reagents were sourced from Sigma-Aldrich and Tokyo Chemical Industry (TCI) and were used without any further purification. HPLC grade chloroform, methanol, and acetonitrile were used with no further purification. All other solvents were used as supplied. Thin layer chromatography was performed on Fluka Silica gel (60 F254) coated on aluminium plates. The TLC plates were visualised using UV light. Davisil 60 Å silica gel was used for column chromatography. ^{1}H and ^{13}C NMR spectra were obtained on a Bruker AC 400 MHz and 600 MHz NMR spectrometer. Electrospray ionisation mass spectra (ESI-MS) were recorded using a Thermo Fisher Exactive Orbitrap mass spectrometer coupled to an Advion TriVersa Nanomate injection system with samples being prepared in 100% HPLC-grade acetonitrile or methanol prior to ESI-MS analysis. All novel compounds were characterised by melting point (MP) (when appropriate), nuclear magnetic resonance (NMR) spectroscopy, attenuated total reflectance (ATR) Fourier transform infrared (FTIR) spectroscopy, and electron spray ionisation mass spectrometry (ESI-MS).

Caution! Sodium azide is acutely toxic and is an explosion hazard. Refer to organic azide stability prior to the preparation of any azido compounds. The total number of nitrogen atoms in a final organic azide should not exceed that of carbon. Organic azides with C/N ratio of <1 should never be isolated. It may be synthesized if the azide is a transient intermediate species AND the limiting reagent in the reaction mixture AND is limited to a maximum quantity of 1 gram. Each azido compound should be individually evaluated.

Ligand preparation:

1,3,5-tris(azidomethyl)-2,4,6-trimethylbenzene (triazide)

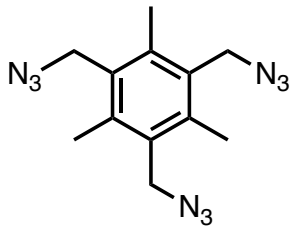

The synthesis of 1,3,5-*tris*(azidomethyl)-2,4,6-trimethylbenzene was carried out as per literature with slight modifications.[5] To a solution of 2,4,6-*tris*-(bromomethyl)-

mesitylene (1.025 g, 2.56 mmol) in DMF (25 ml), sodium azide (1.00 g, 15.38 mmol) was added in portions over ice over a period of 20 minutes. (**Caution!** Sodium azide is acutely toxic and is an explosion hazard. Refer to organic azide stability prior to the preparation of any azido compounds). The reaction was stirred on ice for 1 h prior to stirring at rt for 23 h. The reaction was quenched with 8 ml of H_2O, and the solution extracted with EtOAc (3 x 20 ml). The combined organic phase was washed with H_2O (5 x 5 ml) and the organic layer dried over magnesium sulfate, filtered and solvents removed by rotary evaporation. The sample was recrystallized from a solvent system of hex:EtOAc (5:1) to afford the triazide (0.677 g, 2.37 mmol, 93%) as a white crystalline solid. ^{1}H NMR (600 MHz, $CDCl_3$) δ: 4.50 (s, 6H), 2.46 (s, 9H).^{13}C NMR (151 MHz, $CDCl_3$) δ: 138.15, 130.88, 77.27, 77.06, 76.85, 48.94, 16.50. ^{1}H and ^{13}C NMR in agreement with literature data.[4] IR (ATR, cm^{-1}): 2901, 2085, 1678, 1572, 1449, 1232, 1072, 859, 698, 640, 552.

1,3-bis(azidomethyl)-2,4,6-trimethylbenzene (di-azide)

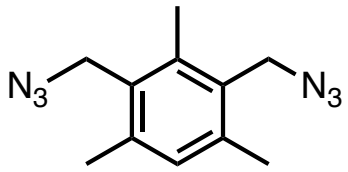

The synthesis of 1,3-bis(azidomethyl)-2,4,6-trimethylbenzene was carried out as per literature procedures with slight modifications.[6,7] To a solution of 2,4,-*bis*(chloromethyl)-1,3,5-trimethylbenzene (1.003 g, 4.62 mmol) in DMF (25 ml), sodium azide (0.923 g, 14.20 mmol) was added in portions over ice over a period of 20 minutes. The reaction was allowed to warm to rt for 1 h and then heated to 60 ˚C for 23 h. The reaction was quenched with 20 ml of H_2O, and the solution extracted with EtOAc (3 x 20 ml). The combined organic phase was washed with H_2O (5 x 5 ml) and the organic layer dried over magnesium sulfate, filtered and solvents removed by rotary evaporation. The sample was recrystallized from a solvent system of hex:EtOAc (5:1) to afford the di-azide (0.911 g, 3.96 mmol, 85.6%) as a white crystalline solid.^{1}H NMR (400 MHz, $CDCl_3$) δ: 6.98 (s, 1H), 4.43 (s, 4H), 2.42 (s, 3H), 2.38 (s, 6H). ^{1}H NMR in agreement with literature data. IR (ATR, cm^{-1}): 2981, 2957, 2926, 2086, 1448, 1241, 1208, 858, 826, 671, 557, 481.

2,4,6-trimethylbenzyl azide (mono-azide)

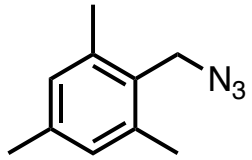

The synthesis of 2,4,6-trimethylbenzyl azide was carried out as per literature procedures with slight modifications.[8] To a solution of α^2-chloroisodurene (1.022 g, 6.05 mmol) in DMF (25 ml), sodium azide (1.201 g, 18.14 mmol) was added in portions over ice over a period of 20 minutes. The reaction was allowed to warm to rt for 1 h and then heated to 60 ˚C for 23 h. The reaction was quenched with 20 ml of H_2O, and the solution extracted with EtOAc (3 x 20 ml). The combined organic phase was washed with H_2O (5 x 5 ml) and the organic layer dried over magnesium sulfate, filtered and solvents removed by rotary evaporation. The product was isolated as a viscous oil (0.670 g, 3.82 mmol, 62%). ^{1}H NMR (400 MHz, $CDCl_3$) δ: 6.93 (s, 2H), 4.41 (s, 2H), 2.39 (s, 6H), 2.31 (s, 3H). ^{1}H NMR in agreement with literature data.[7] IR (ATR, cm^{-1}): 2918, 2863, 2086, 1614, 1447, 1378, 1337, 1244, 1206, 1031, 850, 793, 670, 566, 485

3-Ethynyl-*N, N*-dimethylaniline

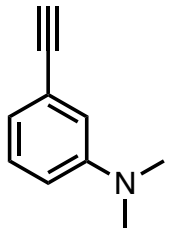

Product was prepared according to literature procedures with slight modifications.[9] To a solution of 3-ethynylaniline (1.034 g, 8.83 mmol) and cesium carbonate (8.306 g, 25.5 mmol) in dry DMF (50 ml) under nitrogen, methyl iodide was added drop wise over 15 min (1.700 ml, 26.0 mmol). The reaction was heated to 40˚C for 24 h. The reaction was monitored by TLC (Hex:EtOAc). From the complete conversion by TLC, the reaction was cooled and diluted with H_2O (100ml) and extracted with EtOAc (3 x 30 ml). The organic layers were combined and washed with H_2O (3 x 10 ml) and finally with brine solution. The organic layer was dried over $MgSO_4$ and reduced to dryness. Product was purified by column chromatography (SiO_2, Hex:EtOAc, 9:1) as a yellow liquid (383 mg, 2.64 mmol, 30%).^{1}H NMR (400 MHz, $CDCl_3$) δ: 7.22 – 7.16 (m, 1H), 6.90 – 6.84 (m, 2H), 6.74 (ddd, *J* = 8.4, 2.6, 1.0 Hz, 1H), 3.03 (s, 1H), 2.95 (s, 6H). The ^{1}H NMR spectra agreed with literature data.[10]

4-Ethynyl-*N, N*-dimethylaniline

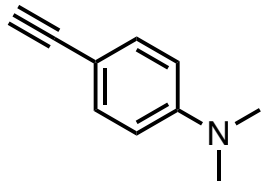

Product was prepared according to literature procedures with slight modifications.[9] To a solution of 4-ethynylaniline (1.003 g, 8.56 mmol) and cesium carbonate (8.345 g, 25.6 mmol) in dry DMF (50 ml) under nitrogen, methyl iodide was added drop wise over 15 min (1.600 ml, 26.0 mmol). The reaction was heated to 40˚C for 24 h. The reaction was monitored by TLC (Hex:EtOAc). From the complete conversion by TLC, the reaction was cooled and diluted with H_2O (100ml) and extracted with EtOAc (3 x 30 ml). The organic layers were combined and washed with H_2O (3 x 10 ml) and finally with brine solution. The organic layer was dried over $MgSO_4$ and reduced to dryness. Product was purified by column chromatography (SiO_2, Hex:EtOAc, 9:1) as a colourless liquid (383 mg, 2.64 mmol, 31%). ^{1}H NMR (400 MHz, $CDCl_3$) δ: 7.39 (dt, 2H), 6.65 (dt, 2H), 3.00 (s, 7H). The ^{1}H NMR spectra was in agreement with literature data.[9]

Boc-Protection

***N*-Boc-propargylamine**

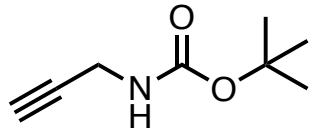

The compound was prepared according to literature procedures with slight modifications.[11] To a solution of propargylamine (0.86 g, 1.00 ml, 15.61mmol) in DCM (20 ml), di-tert-butyl dicarbonate (3.57 g, 3.76 ml, 16.36 mmol) in DCM (5 ml) was added dropwise over ice. Reaction was allowed to warm to rt and stirred for 1 hour. Reaction monitored by TLC. Solvent was reduced under pressure and the resulting material was purified by column chromatography (SiO_2, Hex:EtOAc, 9:1) to yield the boc-protected product as a colourless liquid, which was used as such without further purification (1.892 g, 12.16 mmol, 78%). ^{1}H NMR (400 MHz, $CDCl_3$) δ: 4.93 (br s, 1H), 3.90 (br s, 2H), 2.21 (t, J = 2.5 Hz, 1H), 1.43 (s, 9H). The ^{1}H NMR spectra was in agreement with literature data.[11]

***N*-Boc-methylpropargylamine**

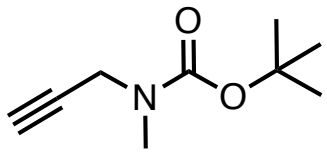

The compound was prepared according to literature procedures with slight modifications.[11] To a solution of *N*-methyl propargylamine (500 µL, 5.93 mmol) in DCM (14 ml), di-tert-butyl dicarbonate (1.42 g, 6.52 mmol) in DCM (5 ml) was added drop wise over ice. Reaction was allowed to warm to rt and stirred for 16 h. Reaction monitored by TLC. Solvent was reduced under pressure and the resulting crude material was purified by column chromatography (SiO_2, Hex:EtOAc, 9:1) to yield the boc-protected product as a colourless liquid (0.833 g, 4.92 mmol, 83%). ^{1}H NMR (400 MHz, $CDCl_3$) δ: 4.03 (s, 2H), 2.89 (s, 3H), 2.21 (t, *J* = 2.4 Hz, 1H), 1.51 (s, 1H), 1.45 (s, 9H). The ^{1}H NMR spectra was in agreement with literature data.[11]

***N*-Boc-4-ethynylaniline**

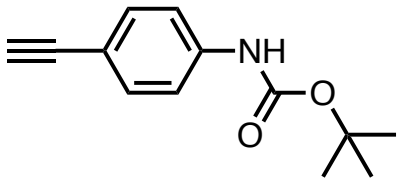

The compound was prepared according to literature procedures.[12,13] To a solution of 4-ethynylaniline (5 mmol) in dry THF (20 ml), di-tert-butyl dicarbonate (15 mmol) was added dropwise. Reaction was refluxed under nitrogen for 18 h. Monitored by TLC (Hex:EtOAc 9:1) until the complete conversion of product was observed. The reaction was allowed to cool to rt and solvent removed under reduced pressure. Crude yellow oil was subjected to column chromatography (SiO_2, Hex:EtOAc, 9.5:0.5 – 9:1) to yield the pure product as a colourless liquid in high yield (0.98 g, 4.51 mmol, 90% yield). ^{1}H NMR (400 MHz, $CDCl_3$) δ: 7.47 – 7.31 (m, 4H), 6.64 (s, 1H), 3.04 (s, 1H), 1.53 (s, 9H). The ^{1}H NMR spectra was in agreement with literature data.[13]

***N*-Boc-3-ethynylaniline**

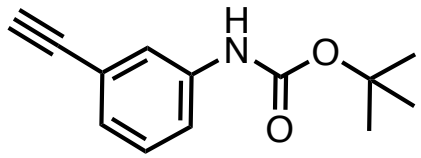

The compound was prepared according to literature procedure.[14] To a solution of 3-ethynylaniline (5.040 g, 43.02 mmol) in dry THF (80 ml), di-tert-butyl-dicarbonate (10.112 g, 46.33 mmol) in THF (10 ml) was added dropwise. Reaction was refluxed for 18 h. Reaction monitored by TLC. Solvent was reduced under pressure and the resulting material was purified by column chromatography (Hex:EtOAc) to yield the product as a colourless liquid. (8.786 g, 40.44 mmol, 94% yield) ^{1}H NMR (600 MHz, $CDCl_3$) δ: 7.37 (d, *J* = 7.3 Hz, 1H), 7.24 (t, *J* = 7.8 Hz, 1H), 7.17 (dt, *J* = 7.6, 1.3 Hz, 1H), 6.58 (s, 1H), 3.06 (s, 1H), 1.53 (s, 9H). The ^{1}H NMR spectra was in agreement with literature data.[15]

Boc-4-(2-propynyloxy)aniline

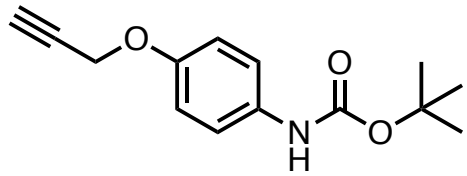

To a solution of 4-(2-propynyloxy) aniline (0.500 g, 3.397 mmol) in dry THF (2ml), di-tert-butyl-dicarbonate (1.112 g, 5.096 mmol) in THF (4 ml) was added dropwise. Reaction was refluxed for 1 h. Reaction monitored by TLC. Solvent was reduced under pressure and the resulting crude material was purified by column chromatography (Hex:EtOAc) to yield the desired product as a white solid (0.825 g, 3.336 mmol, 98% yield). ^{1}H NMR (400 MHz, $CDCl_3$) δ: 7.55 – 7.49 (m, 2H), 7.19 – 7.13 (m, 2H), 6.62 (br s, 1H), 4.90 (d, *J* = 2.4 Hz, 2H), 2.74 (t, *J* = 2.4 Hz, 1H), 1.75 (s, 9H). The ^{1}H NMR spectra was in agreement with literature data.[16]

***N*-(4-ethynylphenyl)phthalimide**

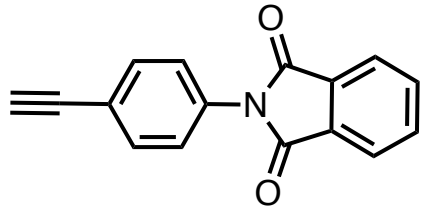

The compound was prepared according to literature procedure with slight modifications.[17] Under schlenk line techniques, 4-ethynylaniline (0.850 g, 7.26

mmol) was added to an oven dried two neck round bottom flask equipped with phthalic anhydride (1.083 g, 7.31 mmol). Dry ACN (15 ml) was added and the solution was allowed to stir under nitrogen at rt for 1 h. The resulting solution was then added dropwise to a refluxing solution of acetic acid (15 ml) and pyridine (1 ml). The reaction was allowed to reflux for 1 h and monitored by TLC. While the solution was hot it was added to water (250 ml, 0˚C) with constant stirring. The solution was agitated until no further precipitate formed. The yellow precipitate was collected by vacuum filtration and recrystallized from ethanol to yield the target compound as soft beige needles (0.752 g, 3.04 mmol, 42%). ^{1}H NMR (600 MHz, $CDCl_3$) δ: 7.96 (dd, *J* = 5.4, 3.0 Hz, 2H), 7.81 (dd, *J* = 5.5, 3.0 Hz, 2H), 7.62 (d, *J* = 8.7 Hz, 2H), 7.48 – 7.44 (m, 2H), 3.13 (s, 1H). The ^{1}H NMR spectra was in agreement with literature data.[18]

***N*-Methyl-boc-3-ethynylaniline**

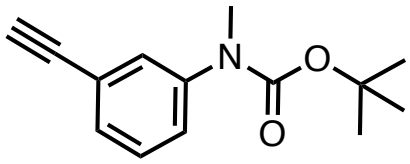

The target ligand was prepared by previously reported methods with slight modifications.[19] Sodium hydride (3 eq, 14.8 mmol) was prepared in the reaction vessel under nitrogen flux and washed with dry hexane, suspended in dry DMF (40 ml) over ice. A solution of boc-3-ethynylaniline (1.038 g, 4.93 mmol) in DMF (10 ml) was added slowly over 30 min to the reaction under a nitrogen atmosphere and the resulting solution was allowed to stir at rt for 2 h. Methyl Iodide (1.54 ml, 5 eq, 24.7 mmol) was added to the reaction slowly over 5 min and reaction left stirring for 4 h. The reaction was quenched slowly with H_2O at 0˚C. The solution was diluted with H_2O (50 ml) and extracted with EtOAc (4 x 30 ml). The organic layers were combined and further washed with H_2O (5 x 10 ml) and finally with brine. The organic layer was dried over magnesium sulfate, filtered and solvents removed by rotary evaporation. The crude product was purified by column chromatography (SiO_2, 9.5:0.5 Hex:EtOAc) as an off white solid. (850 mg, 3.68 mmol, 74.6%) ^{1}H NMR (400 MHz, $CDCl_3$) δ: 7.38 (q, *J* = 1.4 Hz, 1H), 7.31 – 7.26 (m, 3H), 3.27 (s, 3H), 3.09 (s, 1H), 1.47 (s, 9H). The ^{1}H NMR spectra was in agreement with literature data.[19]

Click Chemistry:

Tri-click - 4-bromo-1, butyne

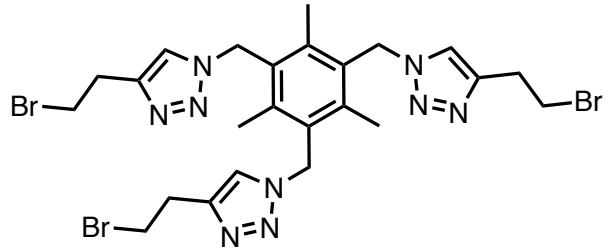

To a solution of triazide (0.100 g, 0.35 mmol) in 10 ml THF:H_2O (1:1), sodium ascorbate (5%) was added followed by copper(II) sulfate (1%) under a nitrogen atmosphere. To this solution 4-bromo-1, butyne (0.1 ml, 1.05 mmol) was added. The reaction was allowed to stir at rt for 24 h, a white precipitate was observed after 8 h. On the completion of the reaction, the white precipitate was collected by vacuum filtration and washed with diethyl ether to afford the title compound as a white solid (0.239 g, 0.35 mmol, 85%). MP: decomposed at 269 ˚C. ^{1}H NMR (400 MHz, $CDCl_3$) δ: 7.10 (s, 3H), 5.58 (s, 6H), 3.56 (t, *J* = 6.7 Hz, 6H), 3.17 (t, *J* = 6.7 Hz, 6H), 2.35 (s, 9H). ^{13}C NMR (151 MHz, $CDCl_3$) δ: 144.91, 139.70, 130.71, 121.10, 77.24, 77.03, 76.82, 48.93, 31.81, 29.31, 29.28, 16.67, 16.63. Anal. Cal. for $C_{24}H_{30}Br_3N_9$: C, 42.13; H, 4.42; N, 18.42; Br, 35.03. %Found: C, 42.41; H, 4.38; N, 18.50; Br, 34.65. IR (ATR, cm^{-1}): 3065, 1558, 1441, 1259, 1216, 1147, 1046, 925, 880, 812, 667, 553. ESI-MS m/z: $[M+H]^+$ Cald for $C_{24}H_{31}Br_3N_9^+$: 682.0247; found 682.0212. $[M+2H]^{+2}$ Cald for $C_{24}H_{32}Br_3N_9^{2+}$: 341.5160; found 341.5153.

Tri-click 2-methyl-3-butyne-2-ol

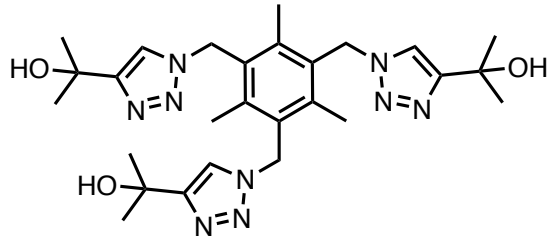

To a solution of triazide (0.430 g, 1.5 mmol) in THF:H_2O (1:1, 15 ml), sodium ascorbate (10%, 0.45 mmol) was added followed by copper(II) sulfate (1%, 0.045 mmol) under a nitrogen atmosphere. To this solution 2-methyl-3-butyne-2-ol (0.382 g, 0.44 ml, 4.52 mmol) was added drop-wise. The reaction was stirred at 25˚C for 24 h. The resulting precipitate was isolated by vacuum filtration and washed with cold EDTA (0.1 M, 3 x 10 ml) and ice-cold water (3 x 10 ml). A white solid was recovered in good yield, (570 mg, 1.06 mmol, 71%). MP: 274-275 ˚C. ^{1}H NMR (600

MHz, $(CD_3)_2SO$) δ: 7.65 (s, 3H), 5.66 (s, 6H), 5.08 (s, 3H), 2.44 (s, 9H), 1.42 (s, 18H). ^{13}C NMR (151 MHz, $(CD_3)_2SO$) δ: 156.19, 139.61, 131.48, 120.44, 67.56, 48.67, 31.18, 16.87. Anal. Cal. for $C_{27}H_{39}N_9O_3$: C, 60.32; H, 7.31; N, 23.45. %Found: C, 58.62; H, 7.26; N, 21.71. IR (ATR, cm^{-1}): 3057, 1368, 1216, 1175, 1058, 955, 857,827, 806, 714. ESI-MS m/z: $[M+Na]^+$ Cald for $C_{27}H_{39}N_9O_3Na^+$: 560.3074; found 560.3060.

Tri-click boc-propargylamine

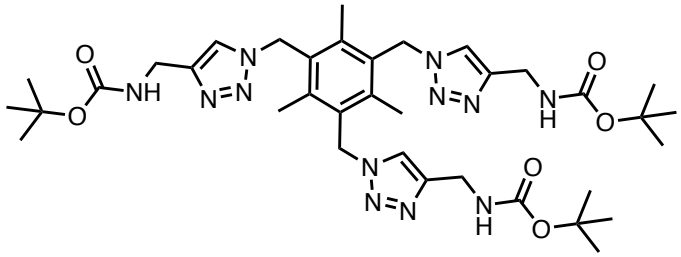

To a solution of Triazide (0.286 1.00 mmol) in degassed ACN (20 ml), CuBr (0.145 g, 1.00 mmol) was added slowly under nitrogen atmosphere. The solution was stirred for 15 minutes and boc-propargylamine (0.490 g, 3.16 mmol) was added dropwise as a solution in ACN (5 ml) to the reaction. The reaction was refluxed for 24 h, untill the complete conversion was observed by TLC. The reaction was allowed to cool and ACN removed by reduced pressure. The resulting crude was suspended in 0.1M EDTA solution (pH 8) and heated to reflux for 1 h. The solution was allowed to cool and extracted with DCM (3 x 50 ml). The organic layers were combined and washed with H_2O (3 x 30 ml) and brine. The organic solution was dried over $MgSO_4$ and reduced to dryness. The crude product was column purified (SiO_4 DCM:MeOH, 9:1) resulting in the title product as a white solid (0.520 g, 0.69 mmol, 69%) ^1H NMR (400 MHz, $CDCl_3$) δ: 7.26 (d, *J* = 18.2 Hz, 3H), 5.65 (s, 6H), 4.35 (d, *J* = 6.0 Hz, 6H), 2.40 (s, 9H), 1.41 (s, 27H). The removal of the protecting group was attempted using trifluoroacetic acid (TFA) and attempting HCl (4 M, in dioxane); both attempts resulted in either the degradation or loss through aqueous work up. Direct synthesis was achieved without the need for amine protection detailed below.

Tri-Click propargylamine

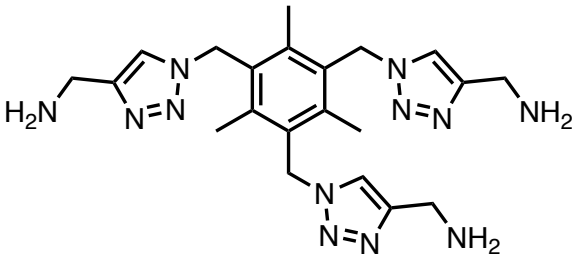

To a solution of triazide (0.214 g, 0.75 mmol) in degassed *t*-BuOH:H_2O (1:1, 6 ml), propargylamine (147 μl, 2.29 mmol) and sodium ascorbate (5%, 0.15 mmol) was added and stirred under a nitrogen atmosphere for 15 minutes, prior to the addition of a solution of copper(II) sulfate (1%, 0.03 mmol) in *t*-BuOH:H_2O (1:1, 2 ml) which was added dropwise over 10 min. The reaction was stirred at 25˚C for 18 h. The solvent was reduced to 3 ml under a stream of nitrogen and cooled on ice. The resulting precipitate was collected by vacuum filtration and washed with ice cold EDTA (0.1 M, 3 x 8 ml) and ice-cold diethyl ether (3 x 10 ml). A yellow solid was recovered in good yield, (284 mg, 0.63 mmol, 84.1%). MP: 119-120 ˚C. ^{1}H NMR (600 MHz, D_2O) δ: 7.66 (s, 3H), 5.64 (s, 6H), 3.77 (s, 6H), 2.21 (s, 9H). ^{13}C NMR (151 MHz, D_2O) δ: 148.32, 140.12, 130.00, 122.69, 49.03, 35.46, 15.51. IR (ATR, cm^{-1}): 3124, 2982, 1666, 1603, 1442, 1381, 1328, 1215, 1120, 1046, 949, 802. ESI-MS m/z: $[M+H]^+$ Cald for $C_{21}H_{31}N_{12}^+$: 451.56 ; found 451.6.

Tri-click boc-*N* -methylpropargylamine

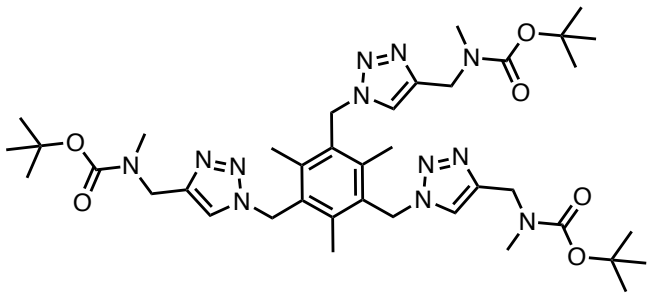

To a solution of Triazide (0.286 1.00 mmol) and DIPEA (0.174 ml, 1.00 mmol) in degassed ACN (20 ml), CuBr (0.144 g, 1.00 mmol) was added slowly under nitrogen atmosphere. The solution was stirred for 15 minutes and boc-*N*-methylpropargylamine (0.524g, 3.10 mmol) was added dropwise as a solution in ACN (5 ml) to the reaction. The reaction was refluxed for 18 h, until the complete conversion was observed by TLC. The reaction was allowed to cool and ACN removed by reduced pressure. The resulting crude was suspended in 0.1M EDTA solution (pH 8) and heated to reflux for 1 h. The solution was allowed to cool and

extracted with DCM (3 x 50 ml). The organic layers were combined and washed with H_2O (3 x 30 ml) and brine. The organic solution was dried over $MgSO_4$ and reduced to dryness. The crude product was column purified (SiO_4 DCM:MeOH, 9:1) resulting in the title product as an orange solid (0.682 g, 0.86 mmol, 86%).^{1}H NMR (400 MHz, $CDCl_3$) δ: 5.63 (s, 6H), 4.44 (s, 6H), 2.91 (s, 9H), 2.42 (s, 9H), 1.43 (s, 28H). The removal of the protecting group was attempted using trifluoroacetic acid (TFA) and HCl (4 M, in dioxane); both attempts resulted in either the degradation or loss through aqueous work up. Direct synthesis was achieved without the need for amine protection detailed below.

Tri-Click *N*-methyl propargylamine

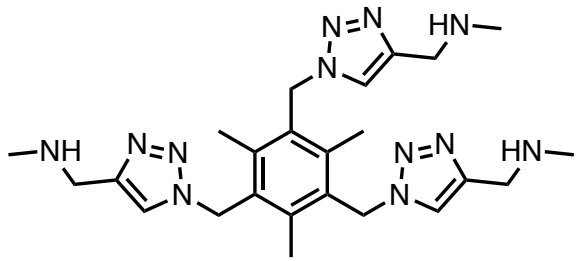

To a solution of triazide (0.430 g, 1.5 mmol) in degassed *t*-BuOH:H_2O (1:1, 8 ml), *N*-methyl propargylamine (380 μl, 4.52 mmol) and sodium ascorbate (10%, 0.45 mmol) was added and stirred under a nitrogen atmosphere for 15 minutes, prior to the addition of a solution of copper(II) sulfate (1%, 0.045 mmol) in *t*-BuOH:H_2O (1:1, 2 ml) which was added dropwise over 10 min. The reaction was stirred at 25˚C for 18 h. The solvent was removed under reduced pressure and the product was suspended in 0.1 M EDTA solution (pH 8) and extracted with DCM (3 x 50 ml). The organic layers were combined and washed with ice cold H_2O (3 x 20 ml) and brine (3 x 30 ml). The organic solution was dried over $MgSO_4$ and solvent removed under reduced pressure. A white solid was recovered (0.548 g, 1.13 mmol, 74%). MP: 197-199 ˚C. ^{1}H NMR (600 MHz, $CDCl_3$) δ: 7.24 (s, 3H), 5.63 (s, 6H), 3.82 (s, 6H), 2.44 (s, 9H), 2.38 (s, 9H).^{13}C NMR (151 MHz, $CDCl_3$) δ: 146.83, 139.73, 130.66, 120.91, 48.88, 46.84, 36.16, 16.57. IR (ATR, cm^{-1}): 3066, 2981, 1634, 1550, 1447, 1380, 1331, 1261, 1207, 1131, 1047, 811. ESI-MS m/z: $[M+H]^+$ Cald for $C_{24}H_{36}N_{12}^+$: 493.33; found 493.2.

Tri-click *N,N*-dimethylprop-2-yne-1-amine

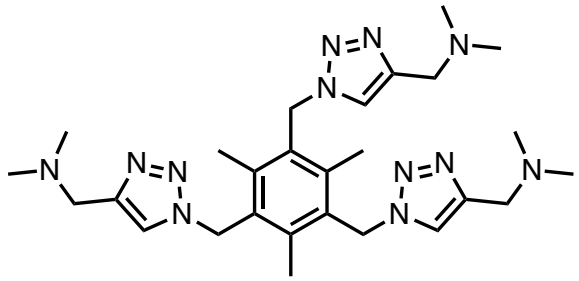

To a solution of Triazide (0.286 1.00 mmol) and DIPEA (0.174 ml, 1.00 mmol) in degassed ACN (20 ml), CuBr (0.144 g, 1.00 mmol) was added slowly under nitrogen atmosphere. The solution was stirred for 15 minutes and *N,N*-dimethylprop-2-yne-1-amine (0.340 ml, 3.16 mmol) was added dropwise as a solution in ACN (5 ml) to the reaction. The reaction was refluxed for 72 h, until the complete conversion was observed by TLC. The reaction was allowed to cool and ACN removed by reduced pressure. The resulting mixture was suspended in 0.1 M EDTA solution (pH 8) and heated to reflux for 1 h. The solution was allowed to cool and extracted with DCM (3 x 50 ml). The organic layers were combined and washed with H_2O (3 x 20 ml) and brine (3 x 30 ml). The organic solution was dried over $MgSO_4$ and solvent removed under reduced pressure. The resulting product was column purified (SiO_4 DCM:MeOH, 9:1) and the title product was isolated as an orange solid (338 mg, 0.63 mmol, 63%). MP: 227-229 ˚C. ^{1}H NMR (600 MHz, $(CD_3)_2SO$) δ: 7.75 (s, 3H), 5.67 (s, 6H), 3.43 (s, 6H), 2.39 (s, 9H), 2.09 (s, 18H). ^{13}C NMR (151 MHz, $(CD_3)_2SO$) δ: 144.10, 139.56, 131.42, 123.66, 54.02, 48.75, 45.04, 16.71. Anal. Cal. for $C_{27}H_{42}N_{12}$: C, 60.65; H, 7.92; N, 31.43. %Found: C 59.34, H 7.72, N 30.45. IR (ATR, cm^{-1}): 3111, 3070, 2977, 2939, 2814, 2762, 1455, 1380, 1336, 1297, 1255, 1213, 1174, 1135, 1037, 1016, 840, 812, 798, 704. ESI-MS m/z: $[M]^+$ Cald for $C_{27}H_{42}N_{12}$: 534.72; found 535.3.

Tri-click boc-3-ethynylaniline

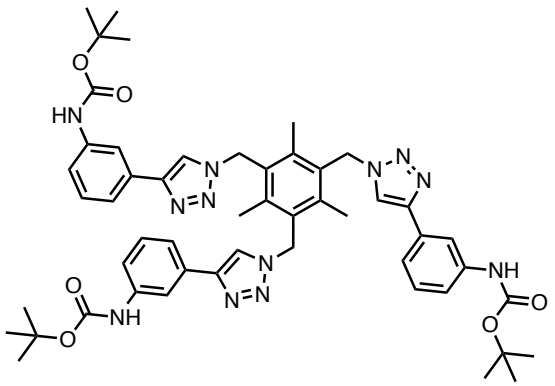

To a solution of Triazide (0.285 1.00 mmol) and DIPEA (0.174 ml, 1.00 mmol) in degassed ACN (20 ml), CuBr (0.144 g, 1.00 mmol) was added slowly under nitrogen atmosphere. The solution was stirred for 15 minutes and boc-3-ethynylaniline (0.679 g, 3.13 mmol) was added dropwise as a solution in ACN (5 ml) to the reaction. The reaction was refluxed for 50˚C for 48 h, until the complete conversion was observed by TLC. The reaction was allowed to cool and ACN removed by reduced pressure. The resulting crude material was suspended in 0.1 M EDTA solution (pH 8) and heated to reflux for 1 h. The solution was allowed to cool and extracted with DCM (3 x 50 ml). The organic layers were combined and washed with H_2O (3 x 30 ml) and brine. The organic solution was dried over $MgSO_4$ and reduced to dryness. The crude product was column purified (SiO_4 DCM:MeOH, 9:1) resulting in the title product as cream solid (505 mg, 0.538 mmol, 54%). ^{1}H NMR (400 MHz, $CDCl_3$) δ: 7.77 (s, 3H), 7.57 (s, 3H), 7.51 (dd, *J* = 7.6, 1.4 Hz, 3H), 7.41 – 7.37 (m, 3H), 7.31 (t, *J* = 7.9 Hz, 3H), 6.80 (s, 3H), 5.74 (s, 6H), 2.49 (s, 9H), 1.52 (s, 27H). Amine deprotection detailed below.

Tri-click 3-ethynylaniline

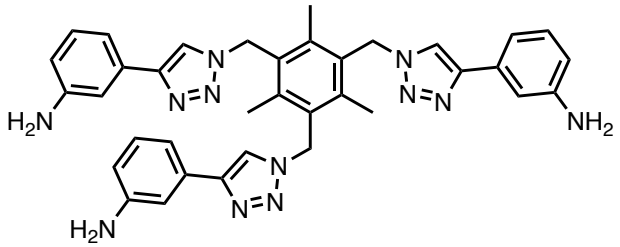

The procedure was adapted from the literature.[19] To a solution of Tri-click boc-3-ethynylaniline (0.505 mg, 0.539 mmol) in DCM (10 ml) TFA (0.615 μl, 8 mmol) was added slowly over ice. The solution was allowed to stir over ice and monitored by TLC to ensure complete removal of Boc group. The solvent and excess TFA were removed under a stream of nitrogen, residue was dissolved in HCl(aq) (1.0 M, 10 ml) and washed with DCM (3 × 20 ml). DCM (20 ml) and water (20 ml) was added to the aqueous fraction and the pH was adjusted to 8 with NaOH (1 M) while stirring. The organic fraction was collected, and the aqueous layer was extracted with DCM (2 × 10 ml). The combined organic fractions were dried ($MgSO_4$) and filtered, and the solvent was removed under reduced pressure. The resulting product was column purified (SiO_4 DCM:MeOH, 9:1) to afford a white solid (0.295 g, 0.464 mmol, 86%). MP: 228-230 ˚C. ^{1}H NMR (600 MHz, $(CD_3)_2SO$) δ: 8.24 (s, 3H), 7.12 (t, *J* = 2.0 Hz, 3H), 7.06 (t, *J* = 7.8 Hz, 3H), 6.97 (dt, *J* = 7.5, 1.2 Hz, 3H), 6.54 (ddd, *J* =

8.0, 2.4, 1.1 Hz, 3H), 5.74 (s, 6H), 3.35 (s br, 6H), 2.48 (s, 9H). ^{13}C NMR (151 MHz, $(CD_3)_2SO$) δ: 157.87, 157.66, 148.37, 146.77, 139.40, 131.11, 130.81, 129.27, 120.62, 113.88, 113.57, 110.82, 48.59, 16.42.IR (ATR, cm^{-1}): 3347, 1674, 1611, 1589, 1430, 1182, 1123, 1045, 836, 802, 782, 722, 691. ESI-MS m/z: $[M+H]^+$ Cald for $C_{36}H_{37}N_{12}^+$: 637.3259; found 637.3241.

Tri-click boc-3-ethynyl-methyl-aniline

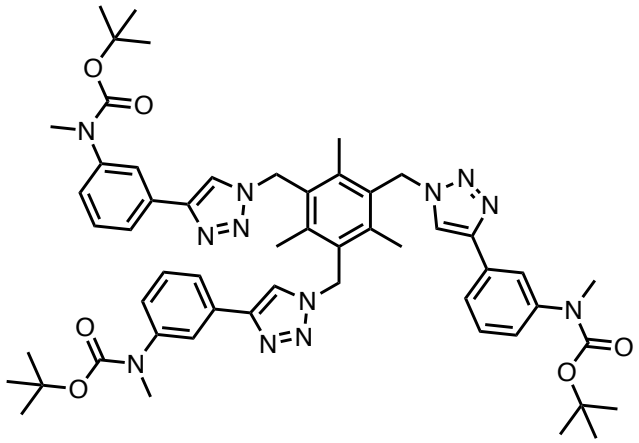

To a solution of Triazide (0.286 1.00 mmol) and DIPEA (0.174 ml, 1.00 mmol) in degassed ACN (20 ml), CuBr (0.144 g, 1.00 mmol) was added slowly under nitrogen atmosphere. The solution was stirred for 15 minutes and boc-3-ethynyl-methyl-aniline (0.718 g, 3.11 mmol) was added dropwise as a solution in ACN (5 ml) to the reaction. The reaction was refluxed for 18 h, until the complete conversion was observed by TLC. The reaction was allowed to cool and ACN removed by reduced pressure. The resulting crude was suspended in 0.1M EDTA solution (pH 8) and heated to reflux for 1 h. The solution was allowed to cool and extracted with DCM (3 x 50 ml). The organic layers were combined and washed with H_2O (3 x 30 ml) and brine. The organic solution was dried over $MgSO_4$ and reduced to dryness. The crude product was column purified (SiO_4 DCM:MeOH, 9:1) resulting in the title product as white solid (866 mg, 0.88 mmol, 88%). ^{1}H NMR (400 MHz, $CDCl_3$) δ: 7.74 (t, *J* = 1.9 Hz, 3H), 7.55 (d, *J* = 10.4 Hz, 6H), 7.35 (t, *J* = 7.8 Hz, 3H), 7.22 (ddd, *J* = 8.0, 2.3, 1.1 Hz, 3H), 5.75 (s, 6H), 3.29 (s, 9H), 2.54 (s, 9H), 1.47 (d, *J* = 2.8 Hz, 27H). Amine deprotection procedure detailed below.

Tri-click -3-ethynyl-methyl-aniline

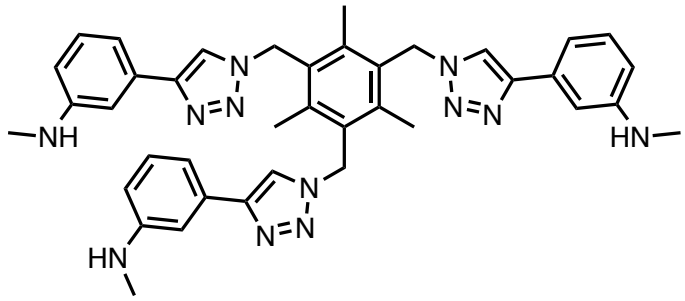

The removal of the protecting group was carried out as per the procedure detailed for the deprotection of Tri-Click 3-ethynylaniline. Briefly, to a solution of Tri-Click boc-3-ethynyl-methyl-aniline (0.850 g, 0.87 mmol mmol) in DCM (15 ml) TFA (1 ml, 13.05 mmol) was added slowly over ice. The solution was allowed to stir over ice and monitored by TLC to ensure complete removal of Boc group. No alterations were made to the workup as detailed previously. The resulting product was column purified (SiO_4 DCM:MeOH, 9:1). Solvent was removed under reduced pressure and foamed with THF to afford an extremely hygroscopic white solid (0.366 g, 0.539 mmol, 62%). Product is stored under argon. ^{1}H NMR (600 MHz, $(CD_3)_2SO$) δ: 8.31 (s, 3H), 7.17 – 7.13 (m, 6H), 7.08 (dt, *J* = 7.6, 1.3 Hz, 3H), 6.59 (ddd, *J* = 8.0, 2.4, 1.0 Hz, 3H), 5.75 (s, 6H), 2.73 (s, 9H), 2.49 (s, 9H). ^{13}C NMR (151 MHz, $(CD_3)_2SO$) δ: 146.81, 139.50, 131.32, 130.87, 129.40, 120.87, 119.79, 117.83, 115.86, 114.22, 113.89, 112.54, 109.16, 48.63, 30.42, 16.50, 1.17. IR (ATR, cm^{-1}): 3112, 1670, 1435, 1177, 1123, 837, 7800, 722, 710, 599, 518. ESI-MS m/z: $[M+H]^+$ Cald for $C_{39}H_{43}N_{12}^+$: 679.3728; found 679.3710.

Tri-click 3-ethynyl-*N*, *N*-dimethylaniline

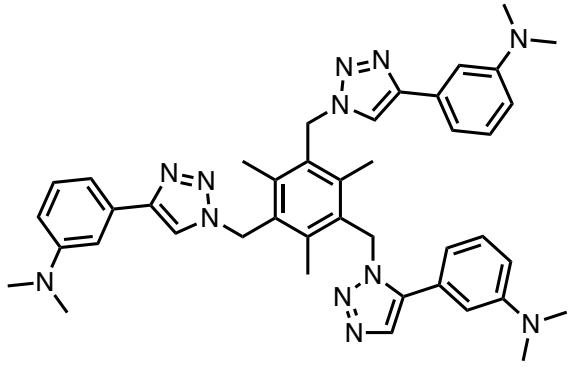

To a solution of Triazide (0.286 1.00 mmol) and DIPEA (0.174 ml, 1.00 mmol) in degassed ACN (20 ml), CuBr (0.144 g, 1.00 mmol) was added slowly under nitrogen atmosphere. The solution was stirred for 15 minutes and 3-ethynyl-*N*,*N*-dimethylaniline (0.450 g, 3.09 mmol) was added dropwise as a solution in ACN (5

ml) to the reaction. The reaction was heated to 50˚C under nitrogen for 24 h, until the complete conversion was observed by TLC. The reaction was allowed to cool and ACN removed by reduced pressure. The resulting crude was suspended in 0.1M EDTA solution (pH 8) and heated to reflux for 1 h. The solution was allowed to cool and extracted with DCM (3 x 50 ml). The organic layers were combined and washed with H_2O (3 x 30 ml) and brine. The organic solution was dried over $MgSO_4$ and reduced to dryness. The crude product was column purified (SiO_4 DCM:MeOH, 9:1) resulting in the title product as beige powder (399 mg, 0.52 mmol, 52.4%). MP: 259-260 ˚C. ^{1}H NMR (600 MHz, $CDCl_3$) δ: 7.46 (s, 3H), 7.29 (dd, *J* = 2.7, 1.5 Hz, 3H), 7.21 (t, *J* = 8.2 Hz, 3H), 6.95 (ddd, *J* = 7.5, 1.5, 0.9 Hz, 3H), 6.69 (ddd, *J* = 8.4, 2.7, 0.9 Hz, 3H), 5.71 (s, 6H), 2.98 (s, 18H), 2.51 (s, 9H). ^{13}C NMR (151 MHz, $CDCl_3$) δ: 151.13, 148.74, 139.96, 131.00, 130.98, 129.58, 118.98, 114.19, 112.69, 109.75, 49.21, 40.78, 16.96. IR (ATR, cm^{-1}): 1605, 1582, 1497, 1442, 1350, 1223, 1182, 1042, 986, 857, 780, 692, 461. Anal. Cal. for $C_{42}H_{48}N_{12}$: C, 69.97; H, 6.71; N, 23.31. %Found: C, 69.30; H, 6.66; N, 22.70. ESI-MS m/z: $[M+H]^+$ Cald for $C_{42}H_{49}N_{12}^+$: 721.4198; found 721.4178.

Tri-click 4-ethynyl-*N*, *N*-dimethylaniline

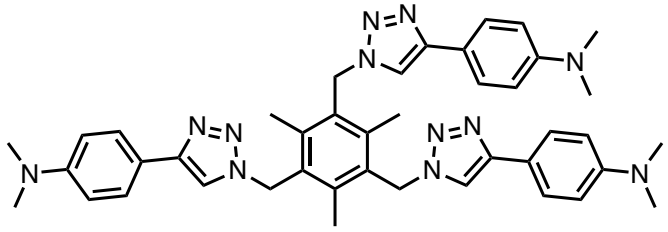

To a solution of Triazide (0.286 1.00 mmol) and DIPEA (0.174 ml, 1.00 mmol) in degassed ACN (20 ml), CuBr (0.144 g, 1.00 mmol) was added slowly under nitrogen atmosphere. The solution was stirred for 15 minutes and 4-ethynyl-*N*,*N*-dimethylaniline (0.454 g, 3.13 mmol) was added dropwise as a solution in ACN (5 ml) to the reaction. The reaction was refluxed for 72 h, until the complete conversion was observed by TLC. The reaction was allowed to cool and ACN removed by reduced pressure. The resulting crude was suspended in 0.1M EDTA solution (pH 8) and heated to reflux for 1 h. The solution was allowed to cool and extracted with DCM (3 x 50 ml). The organic layers were combined and washed with H_2O (3 x 30 ml) and brine. The organic solution was dried over $MgSO_4$ and reduced to dryness. The crude product was column purified (SiO_4 DCM:MeOH, 9:1) resulting in the title product as a cream solid (249 mg, 0.345 mmol, 35%). MP: 284-286 ˚C. ^{1}H NMR

(600 MHz, $(CD_3)_2SO$) δ: 8.09 (s, 3H), 7.63 (d, *J* = 8.8 Hz, 6H), 6.71 (d, *J* = 8.9 Hz, 6H), 5.73 (s, 6H), 2.91 (s, 18H), 2.47 (s, 9H).^{13}C NMR (151 MHz, $(CD_3)_2SO$) δ: 150.41, 147.27, 139.75, 131.35, 126.58, 119.39, 119.02, 112.66, 49.00, 16.84. ATR-IR (cm^{-1}): 2851, 1619,1559, 1443,1348, 1220, 1170, 1040, 947, 812, 695, 533. ESI-MS m/z: $[M+H]^+$ Cald for $C_{42}H_{49}N_{12}^+$: 721.4198; found 721.4179.

Tri-Click 1-ethynyl-4-nitrobenzene

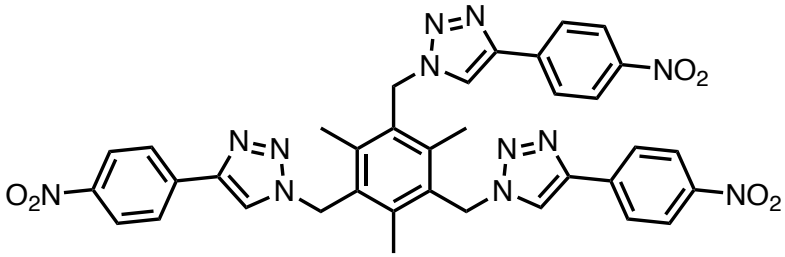

To a solution of triazide (0.286 g, 1.0 mmol) in *t*-BuOH:H_2O (1:1, 14 ml), 1-ethynyl-4-nitrobenzene (0.450 g, 3.0 mmol) was added in small aliquots. To this yellow solution sodium ascorbate (10%, 0.30 mmol) was added followed by copper(II) sulfate (1%, 0.03 mmol) under a nitrogen atmosphere after which the colour of the solution changed to orange. The reaction was stirred at rt and monitored by TLC until the complete conversion was observed (16 h). The resulting red precipitate was collected by vacuum filtration and washed with cold EDTA (0.1 M, 3 x 10 ml) and cold diethyl ether (3 x 10 ml). A red solid was recovered in good yield, (0.674 g, 0.927 mmol, 92.7%). MP - decomposed at 280 ˚C. ^{1}H NMR (600 MHz, $(CD_3)_2SO$) δ: 8.66 (s, 1H), 8.28 (s, 2H), 8.13 (s, 2H), 5.84 (s, 2H), methyl peak hidden under deuterated solvent peak - confirmed by HSQC NMR. ^{13}C NMR (151 MHz, $(CD_3)_2SO$) δ: 147.02, 144.81, 140.20, 137.50, 131.11, 126.45, 124.74, 123.58, 49.37, 16.96. ATR-IR (cm^{-1}): 2981, 1607, 1515, 1452, 1337, 1224, 1112, 1047, 976, 852, 756, 710, 691. ESI-MS m/z: $[M+H]^+$ Cald for $C_{36}H_{31}N_{12}O_6^+$: 727.2484; found 727.2459.

Polyamine controls:

1, 3, 5-tris(aminomethyl)-2, 4, 6-trimethyl benzene (Tri-amine)

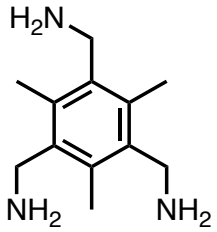

1, 3, 5-tris(aminomethyl)-2, 4, 6-trimethyl benzene was prepared as per literature procedures from 1,3,5-tris(azidomethyl)-2,4,6-trimethylbenzene (triazide).[5,21,22] To a solution of triazide (1.00 g, 2.1 mmol) in absolute EtOH (40 ml)was added Pd/C (10% w/w, 100 mg), and the reaction mixture was stirred under a H_2 balloon for 6 h. It was then filtered through a small pad of celite, which was rinsed with EtOAc (3 x 15 ml). The filtrate was concentrated to afford tri-amine (1.186 g, quant.) as a white solid. MP 149-150 ˚C. ^{1}H NMR (600 MHz, $CDCl_3$) δ: 3.95 (s, 6H), 2.48 (s, 9H). ^{13}C NMR (151 MHz, $CDCl_3$) δ: 138.13, 133.48, 40.84, 15.42. The melting point and ^{1}H NMR spectra was in agreement with literature data.[5,23] ATR-IR (cm^{-1}): 3342, 2958, 2903, 2218, 1568, 1448, 1379, 1298, 1050, 861,620. ESI-MS m/z: $[M+H]^+$ Cald for $C_{12}H_{22}N_3^+$: 208.1808; found 208.1804.

***N*^{1}, *N*$^{1'}$, *N*$^{1''}$-((2,4,6-trimethylbenzene-1,3,5-triyl)tris(methylene)) tris(ethane-1,2-diamine) (NS234)**

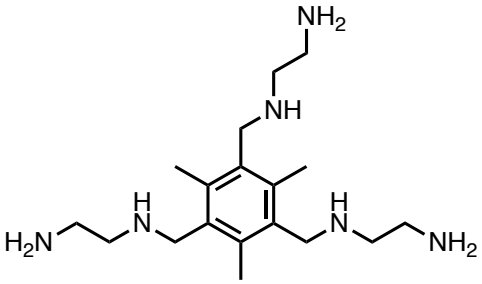

The target amine scaffold was prepared by previously reported methods with slight modifications.[24] To a solution of 2,4,6-*tris*-(bromomethyl)-mesitylene (1.200 g, 3.0 mmol) in dry THF (50 ml) ethylenediamine (8.04 ml, 120 mmol) was added. The resulting solution was stirred at 25 ˚C until the complete conversion was observed by ^{1}H NMR (24 h). Solvent and excess diamine were removed under reduced pressure. The resulting oil was solubilized in MeOH (30 ml) and KOH (0.340 g, 6 mmol) was added and the inorganic salts were precipitated by the addition of diethyl ether and removed my filtration. The solvent was removed under reduced pressure and product dried under schlenk line. The resulting amine scaffold was identified as a thick oil (0.673 g, 1.99 mmol, 66.7%). ^{1}H NMR (600 MHz, $CDCl_3$) δ: 3.76 (s, 6H),

2.84 – 2.75 (m, 12H), 2.42 (s, 9H). ^{13}C NMR (151 MHz, $CDCl_3$) δ: 135.03, 135.00, 52.84, 48.47, 41.68, 15.48. The ^{1}H NMR spectra was in agreement with literature data.[24] ATR-IR (cm^{-1}): 3266, 2852, 1651, 1568, 1450, 1338, 1105, 1030, 814, 747. ESI-MS m/z: $[M+H]^+$ Cald for $C_{18}H_{37}N_6^+$: 337.3074; found 337.3063.

N^1, $N^{1'}$, $N^{1''}$-((2,4,6-trimethylbenzene-1,3,5-triyl)tris(methylene)) tris(propane-1,3-diamine) (NS235)

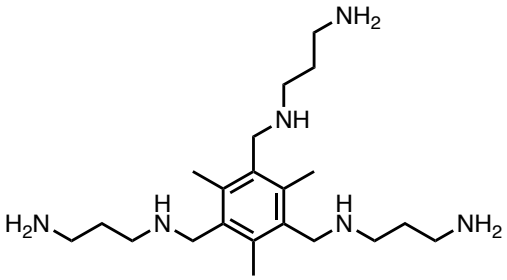

The target amine scaffold was prepared by previously reported methods with slight modifications.[24] To a solution of 2,4,6-*tris*-(bromomethyl)-mesitylene (1.200 g, 3.0 mmol) in dry THF (50 ml) 1, 3-diaminopropane (10.02 ml, 120 mmol) was added. The resulting solution was stirred at 25 ˚C until the complete conversion was observed by ^{1}H NMR (24 h). Solvent and excess diamine were removed under reduced pressure. The resulting oil was solubilized in MeOH (30 ml) and KOH (0.505 g, 9 mmol) was added and the inorganic salts were precipitated by the addition of diethyl ether and removed my filtration. The solvent was removed under reduced pressure and product dried under schlenk line. The resulting amine scaffold was identified as a thick oil (1.003 g, 2.65 mmol, 88.3%). ^{1}H NMR (600 MHz, CD_3OD) δ: 3.86 (s, 6H), 2.98 (t, *J* = 7.1 Hz, 6H), 2.89 (t, *J* = 7.0 Hz, 6H), 2.46 (s, 9H), 1.87 (p, *J* = 7.0 Hz, 6H). ^{13}C NMR (151 MHz, CD_3OD) δ: 137.15, 135.46, 40.56, 29.53, 16.46.The ^{1}H NMR spectra was in agreement with literature data.[24] ATR-IR (cm^{-1}): 3256, 2922, 2856, 1567, 1452, 1377, 1327, 1103, 1026, 969, 815, 752.
ESI-MS m/z: $[M+H]^+$ Cald for $C_{21}H_{43}N_6^+$: 379.3544; found 379.3542. $[M+2H]^{+2}$ Cald for $C_{21}H_{43}N_6^{+2}$: 190.1808; found 190.1811. $[M+3H]^{+3}$ Cald for $C_{21}H_{43}N_6^{+3}$ Cald 127.1230; found 127.1236.

D-4: NMR Spectroscopy

Ligand ^{1}H NMR spectra:

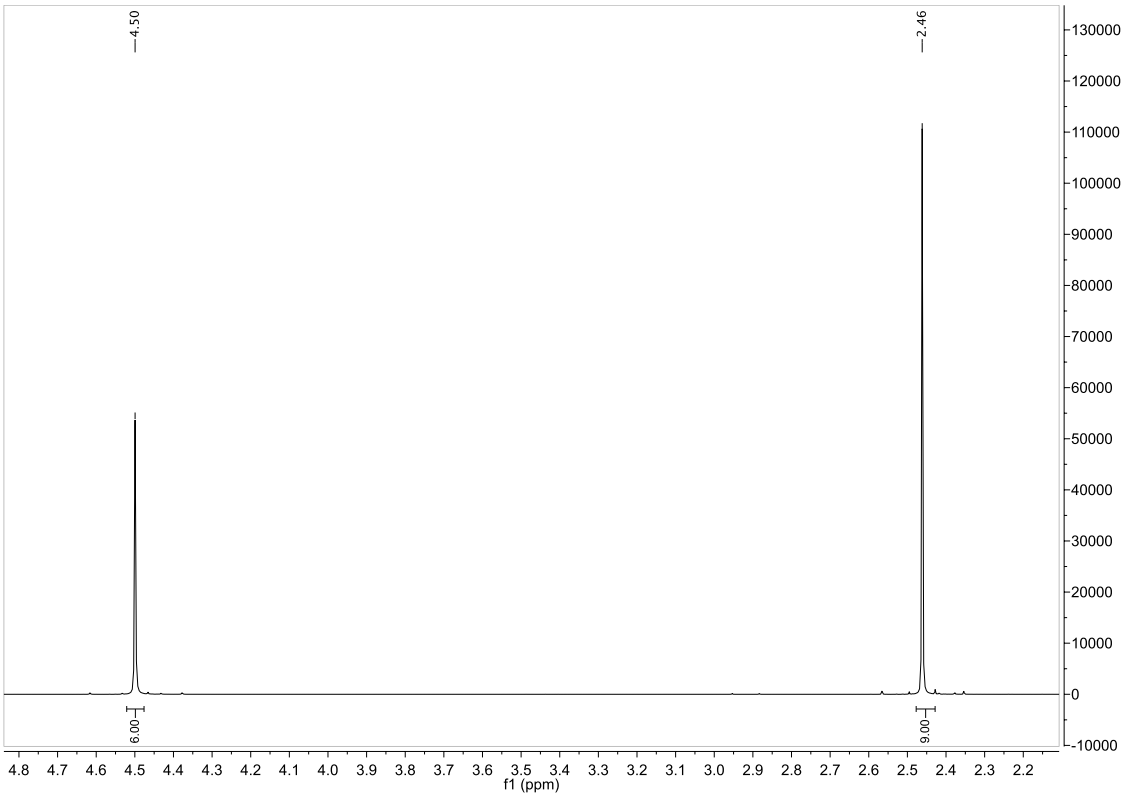

Figure D-11. ^{1}H NMR spectra for triazide.

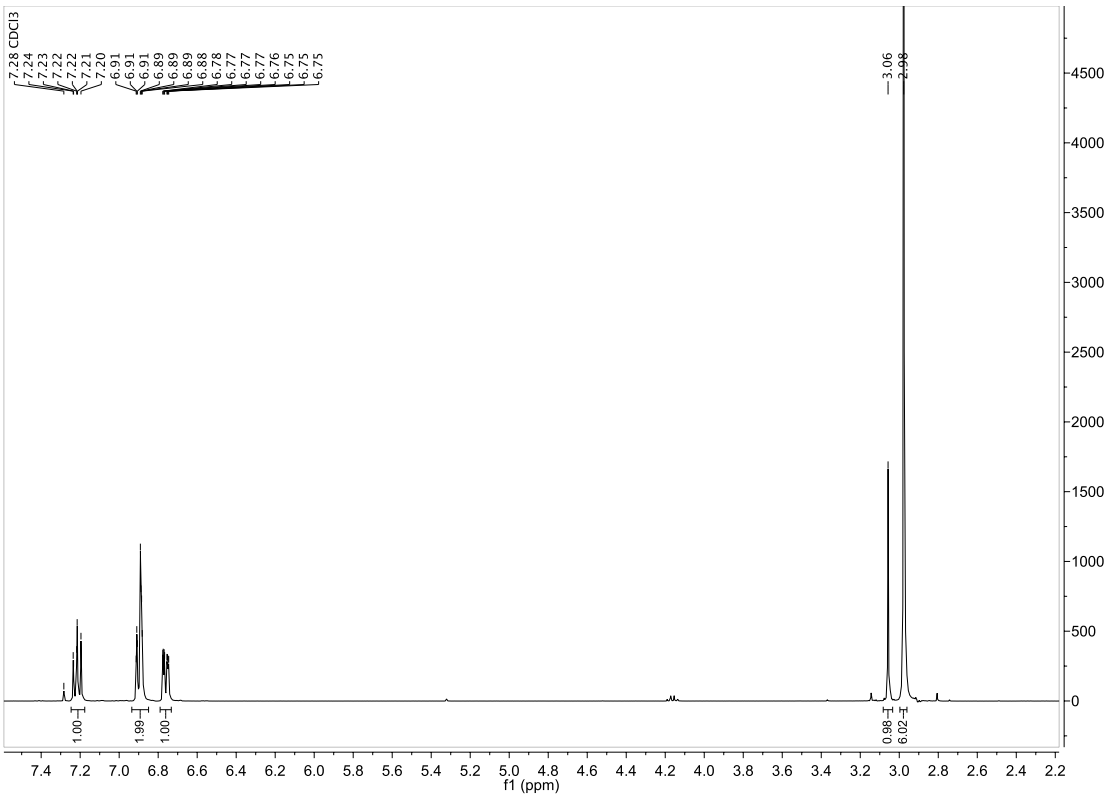

Figure D-12. ^{1}H NMR spectra for 3-ethynyl-*N,N*-dimethylaniline.

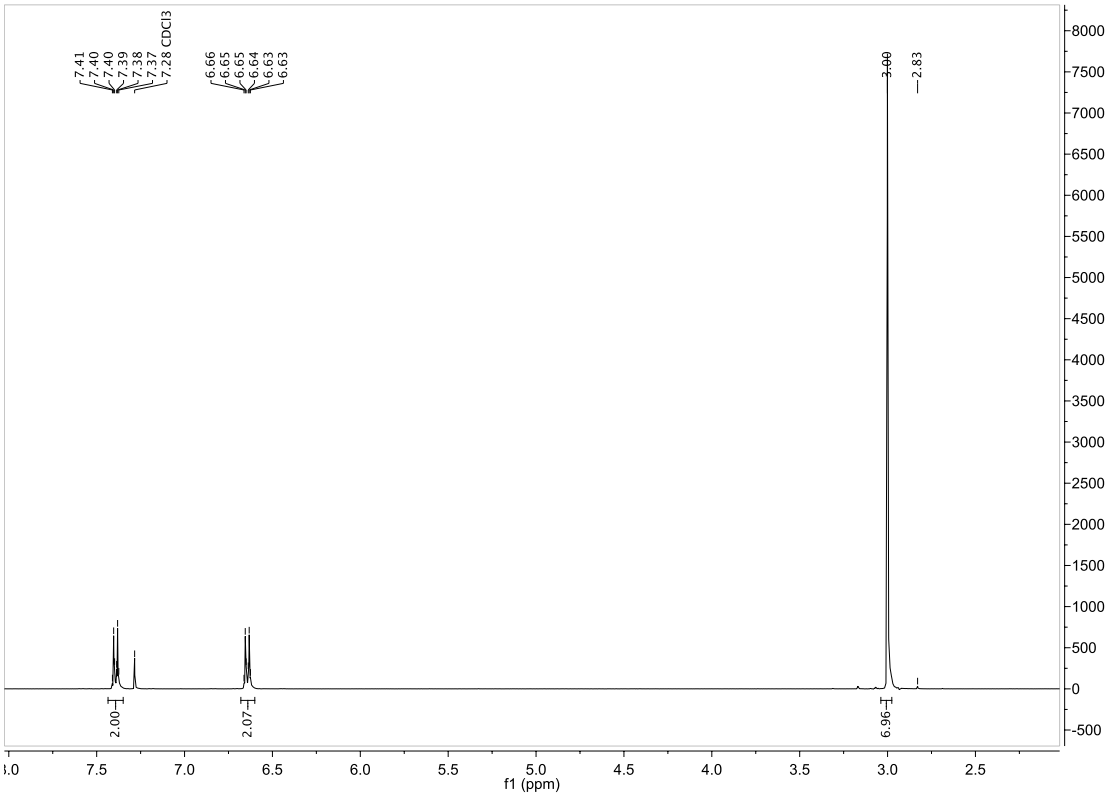

Figure D-13. ^{1}H NMR spectra for 4-ethynyl-*N,N*-dimethylaniline.

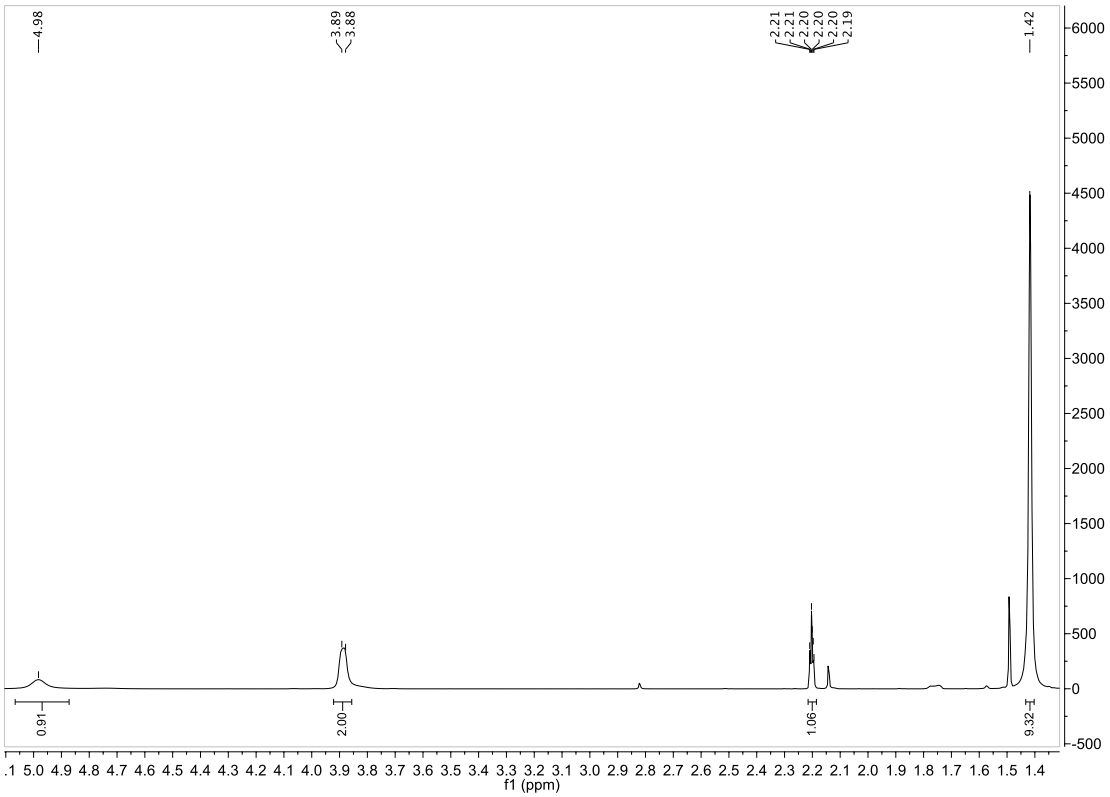

Figure D-14. ^{1}H NMR spectra for *N*-boc-propargylamine.

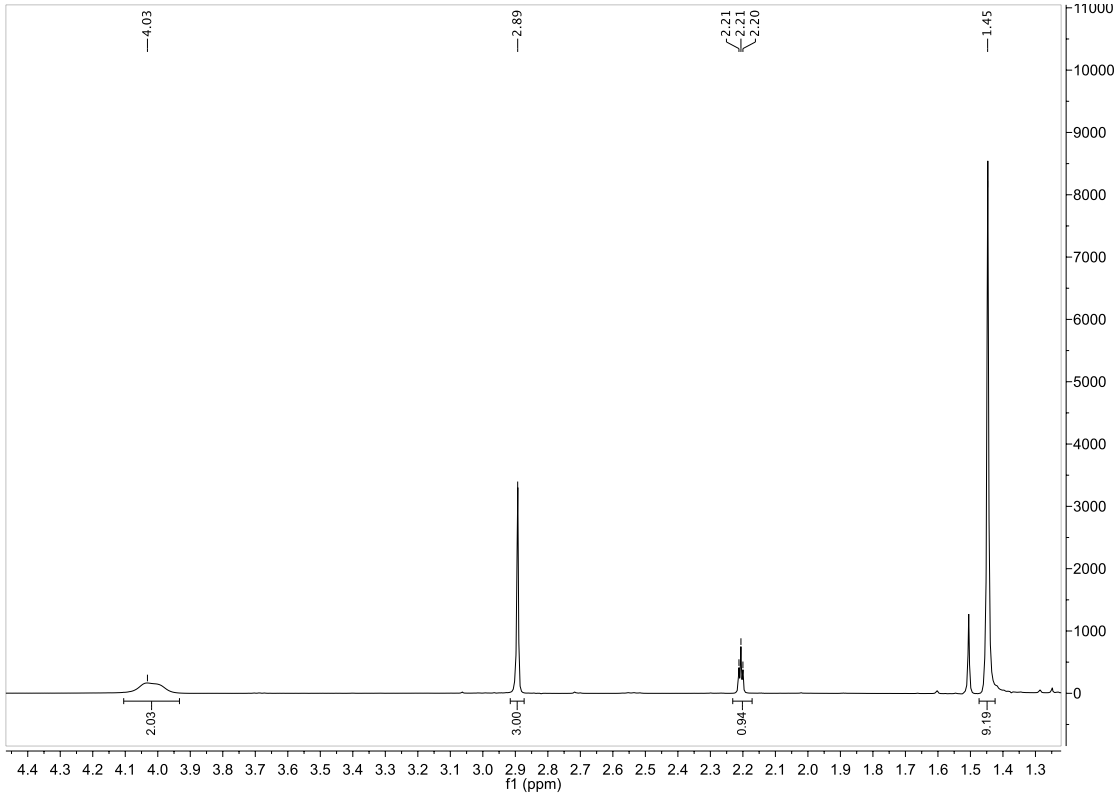

Figure D-15. ^{1}H NMR spectra for *N*-boc-methyl propargylamine.

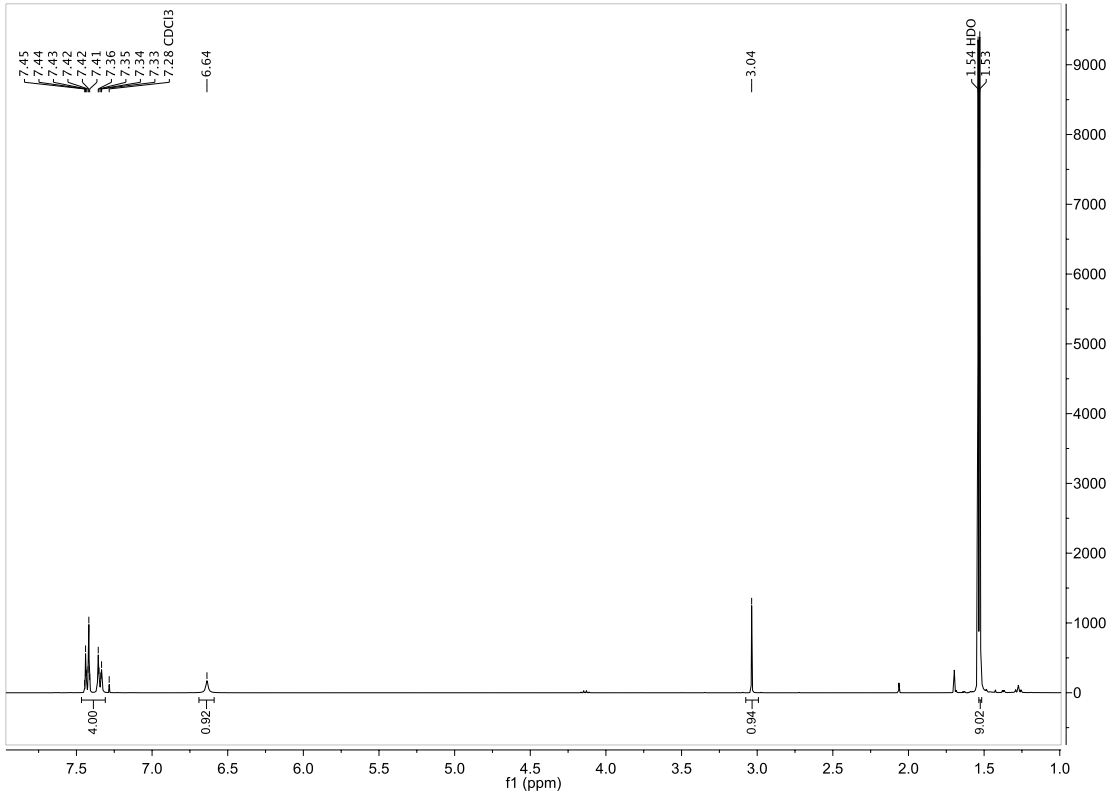

Figure D-16. ^{1}H NMR spectra for *N*-boc-4-ethynylaniline.

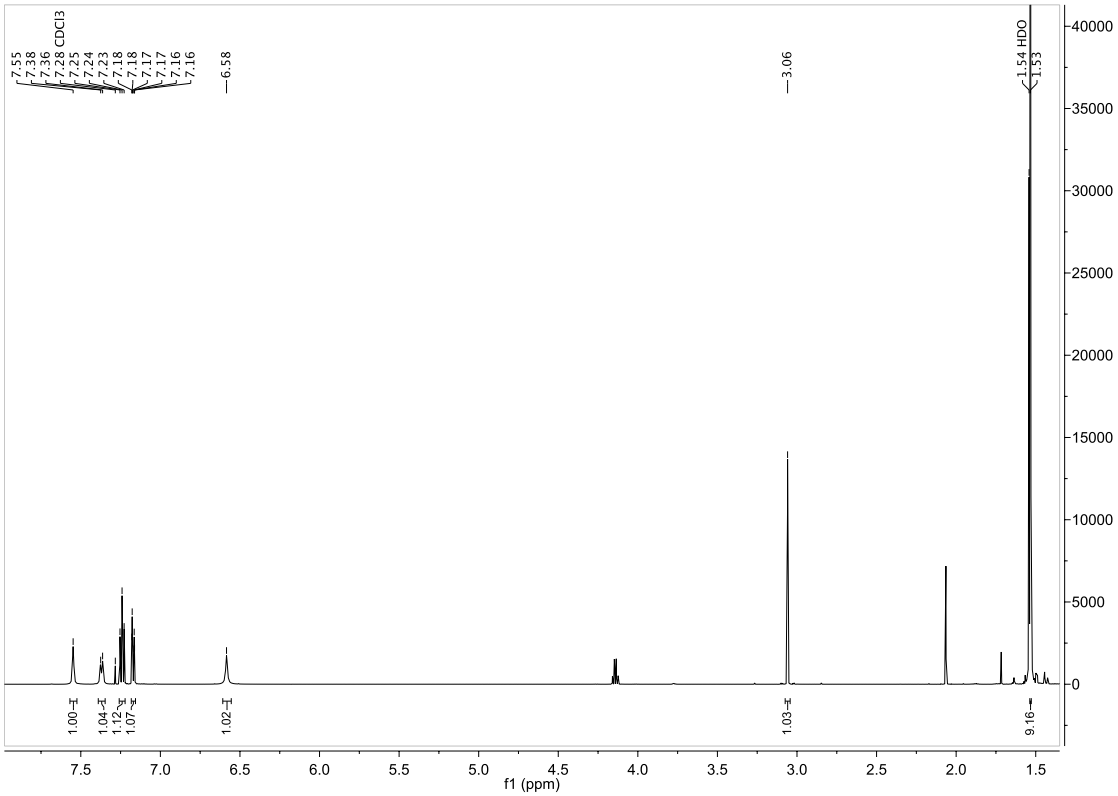

Figure D-17. ^{1}H NMR spectra for *N*-boc-3-ethynylaniline.

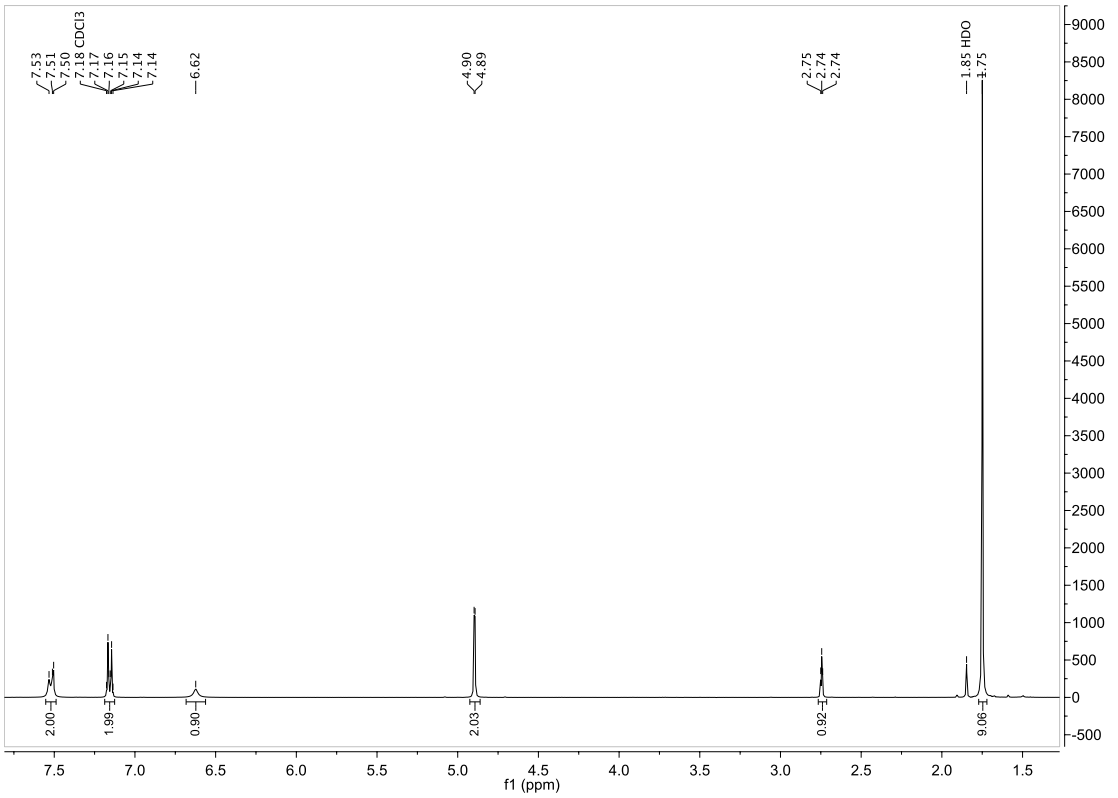

Figure D-18. ^{1}H NMR spectra for boc-4-(2-propynyloxy)aniline

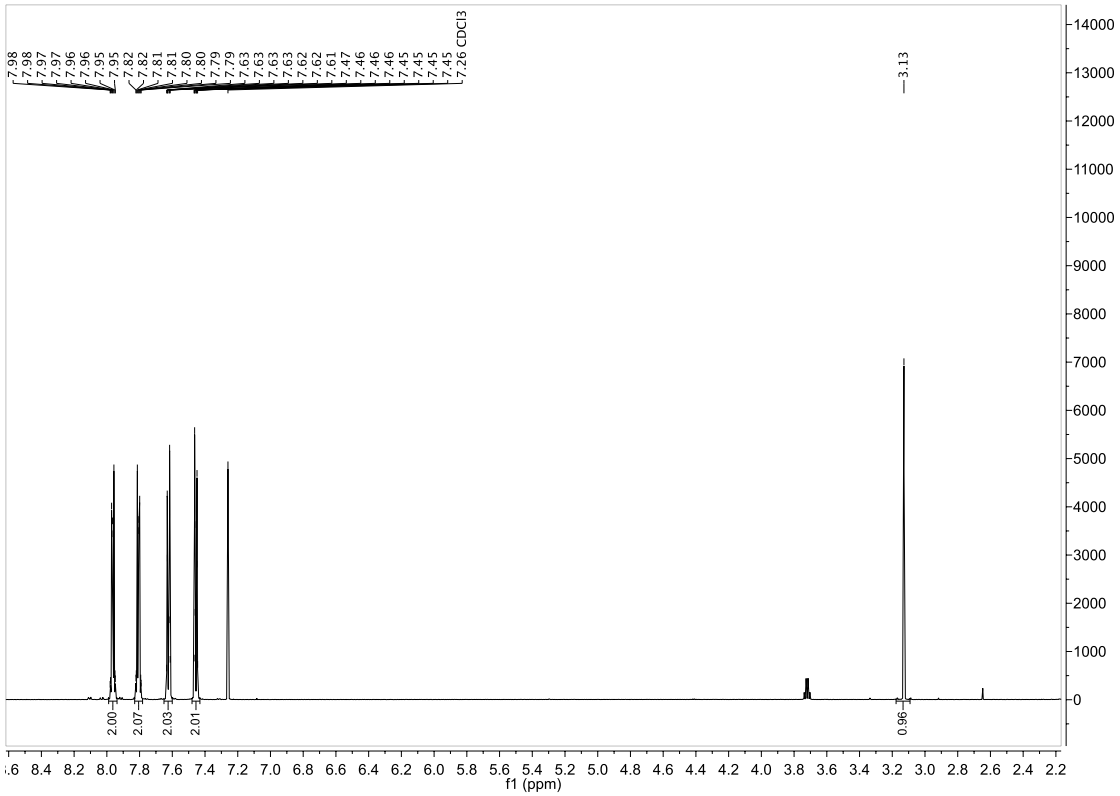

Figure D-19. ^{1}H NMR spectra for *N*-(4-ethynylphenyl) phthalimide.

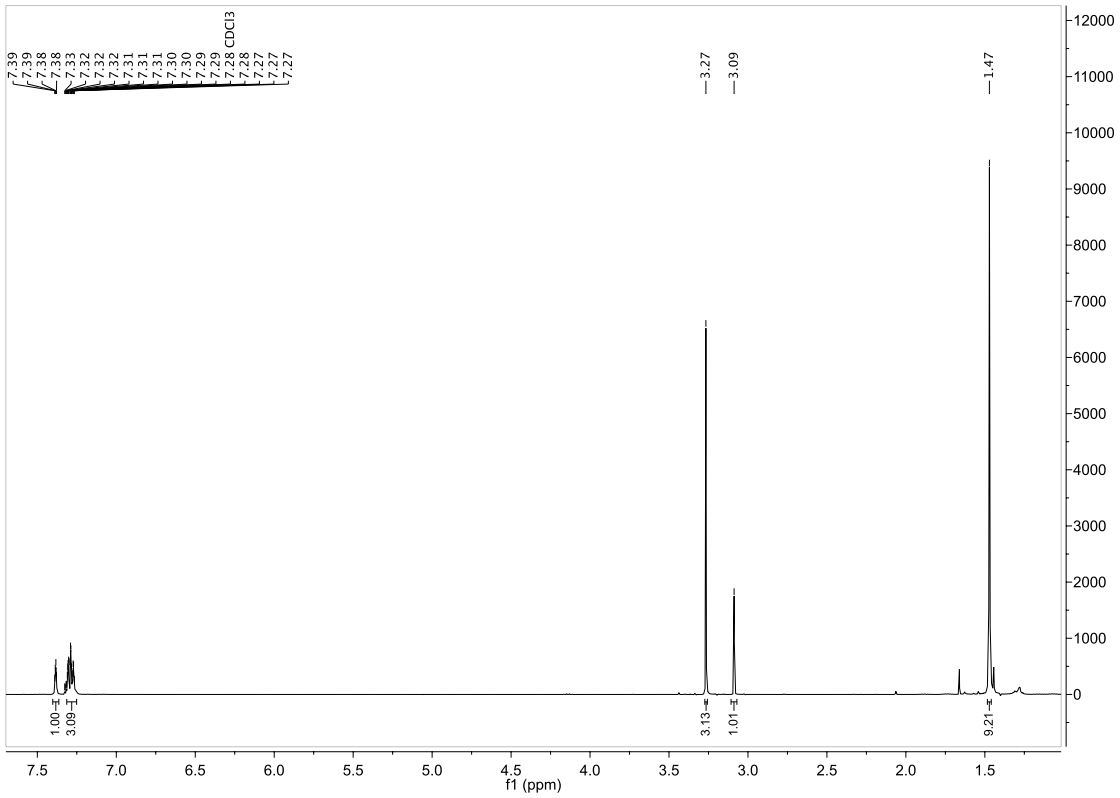

Figure D-20. ^{1}H NMR spectra for *N*-methyl-boc-3-ethynylaniline.

Tri-Click compound NMR spectra:

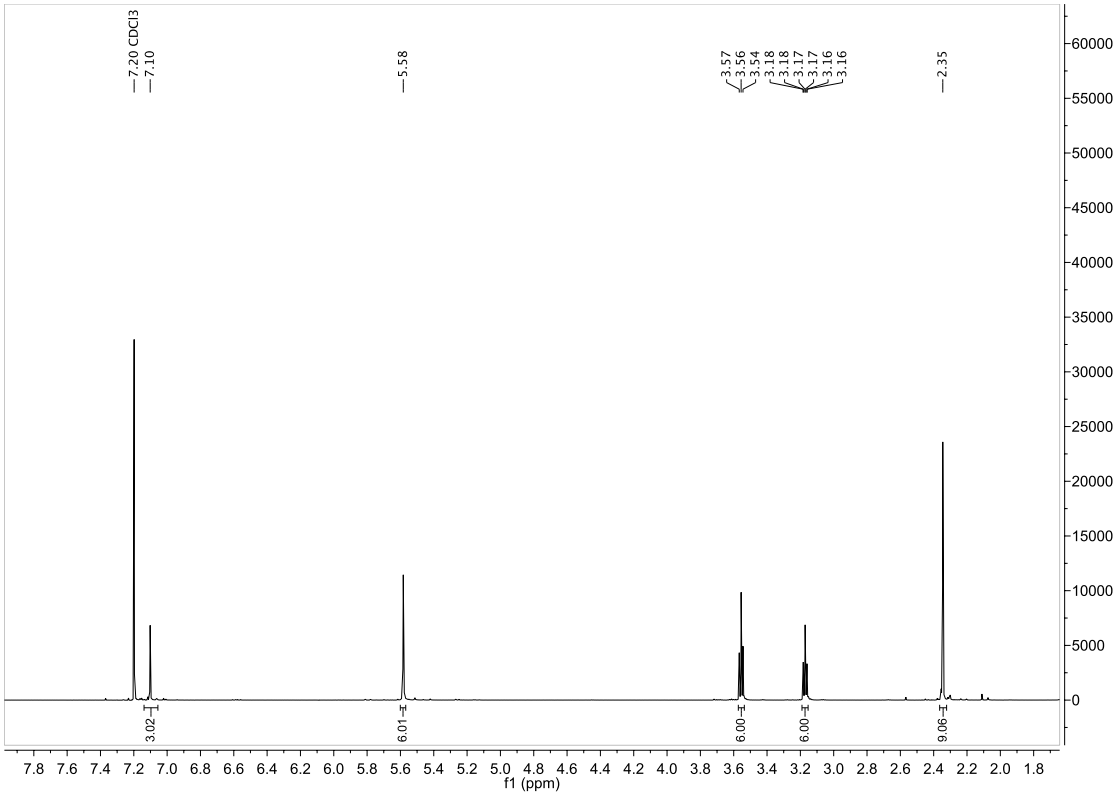

Figure D-21. ^{1}H NMR spectra for Tri-Click 4-bromo-1-butyne.

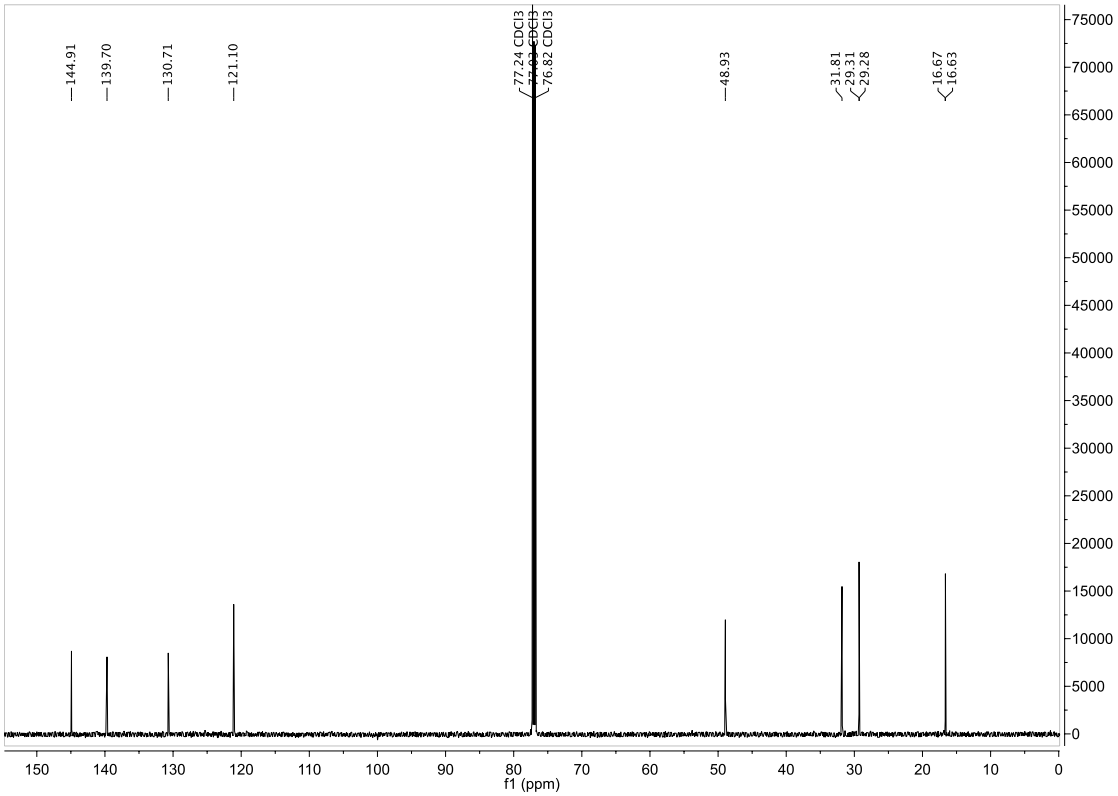

Figure D-22. ^{13}C NMR spectra for Tri-Click 4-bromo-1-butyne.

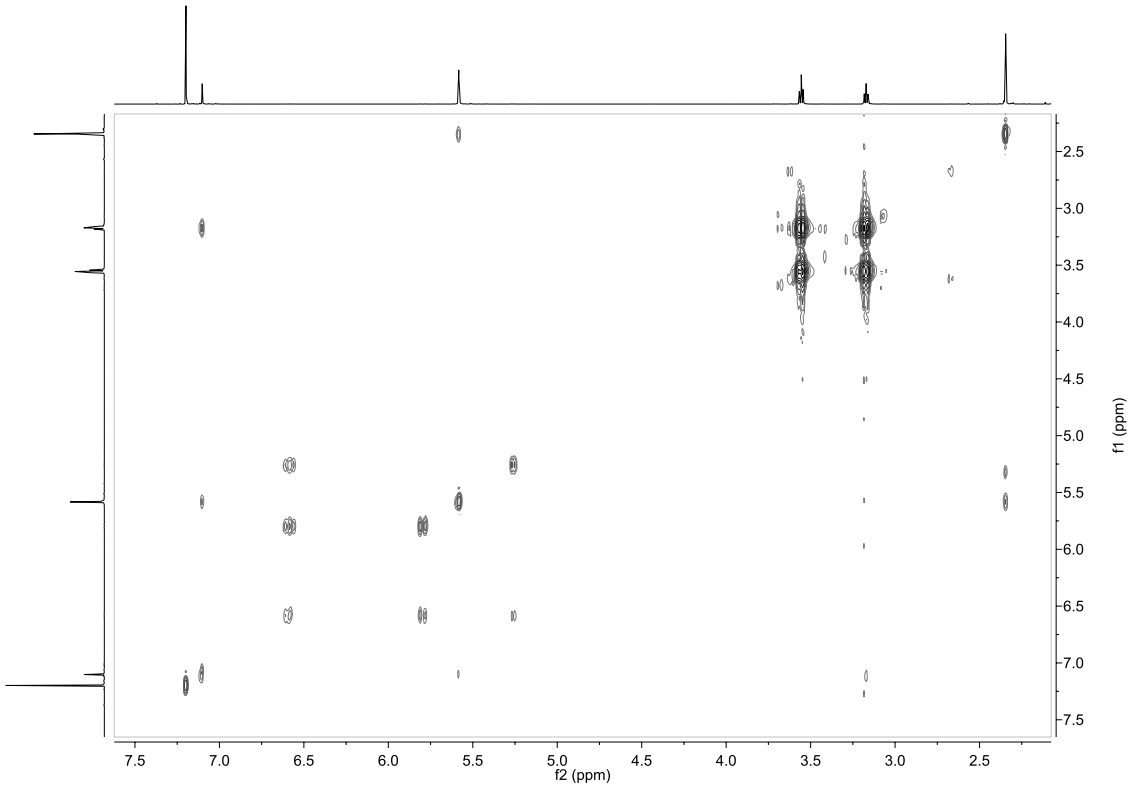

Figure D-23. COSY NMR spectra for Tri-Click-4-bromo-1-butyne.

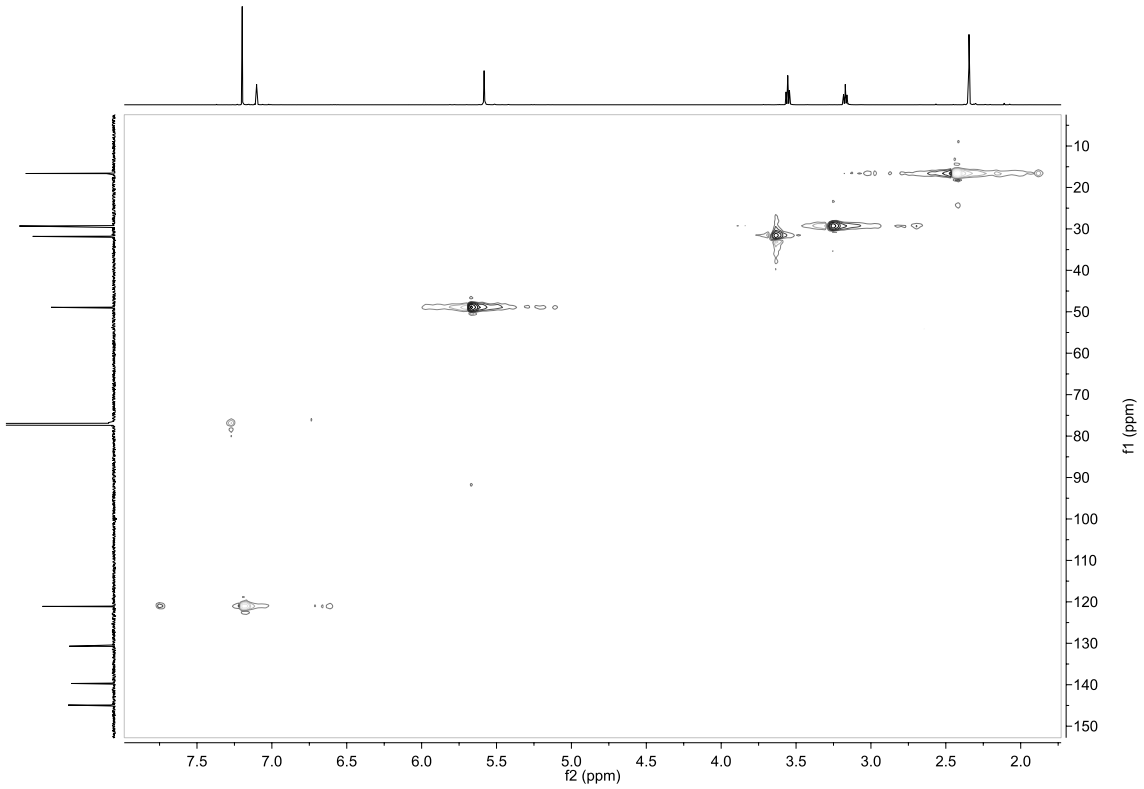

Figure D-24. HSQC NMR spectra for Tri-Click-4-bromo-1-butyne.

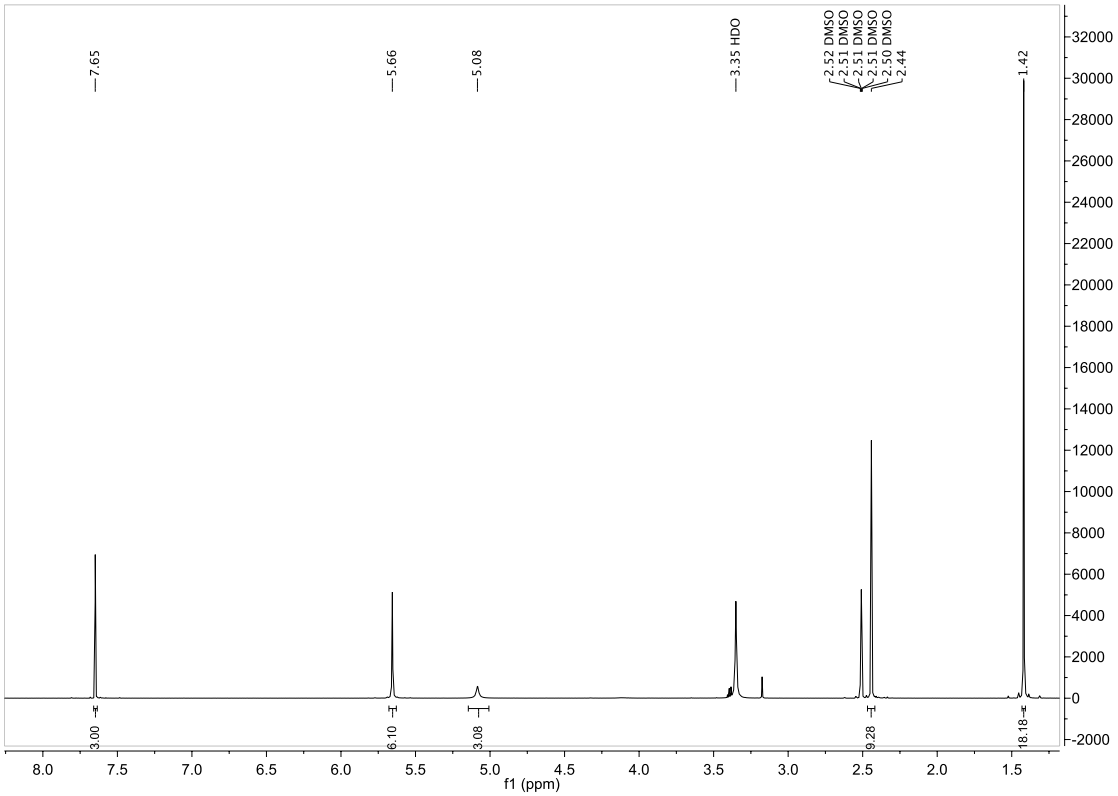

Figure D-25. ^{1}H NMR spectra for Tri-Click-2-methyl-3-butyne-2-ol.

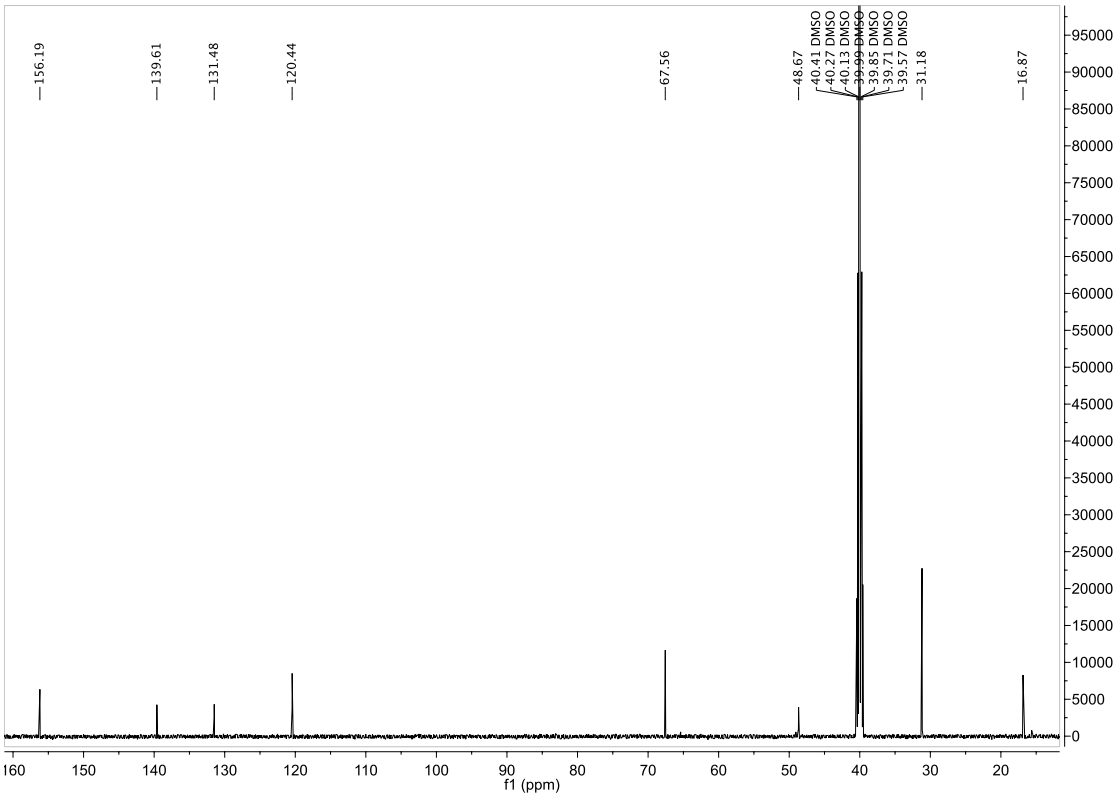

Figure D-26. ^{13}C NMR spectra for Tri-Click-2-methyl-3-butyne-2-ol.

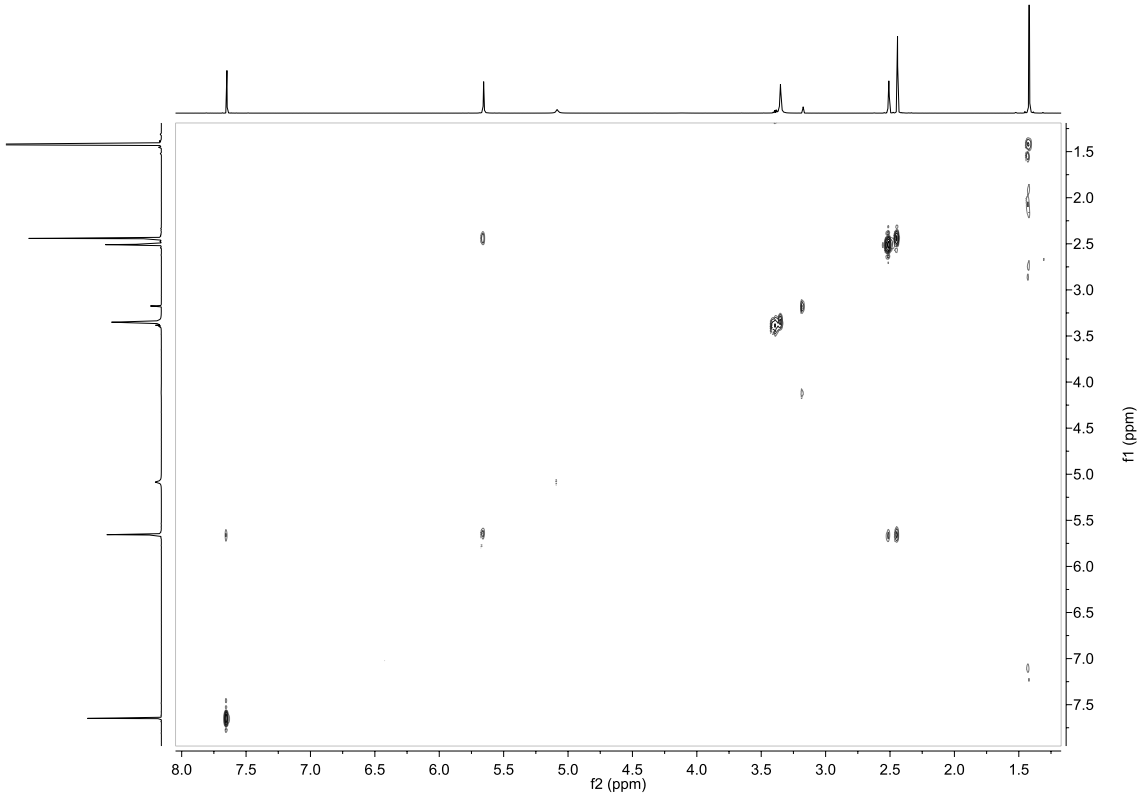

Figure D-27. COSY NMR spectra for Tri-Click 2-methyl-3-butyne-2-ol.

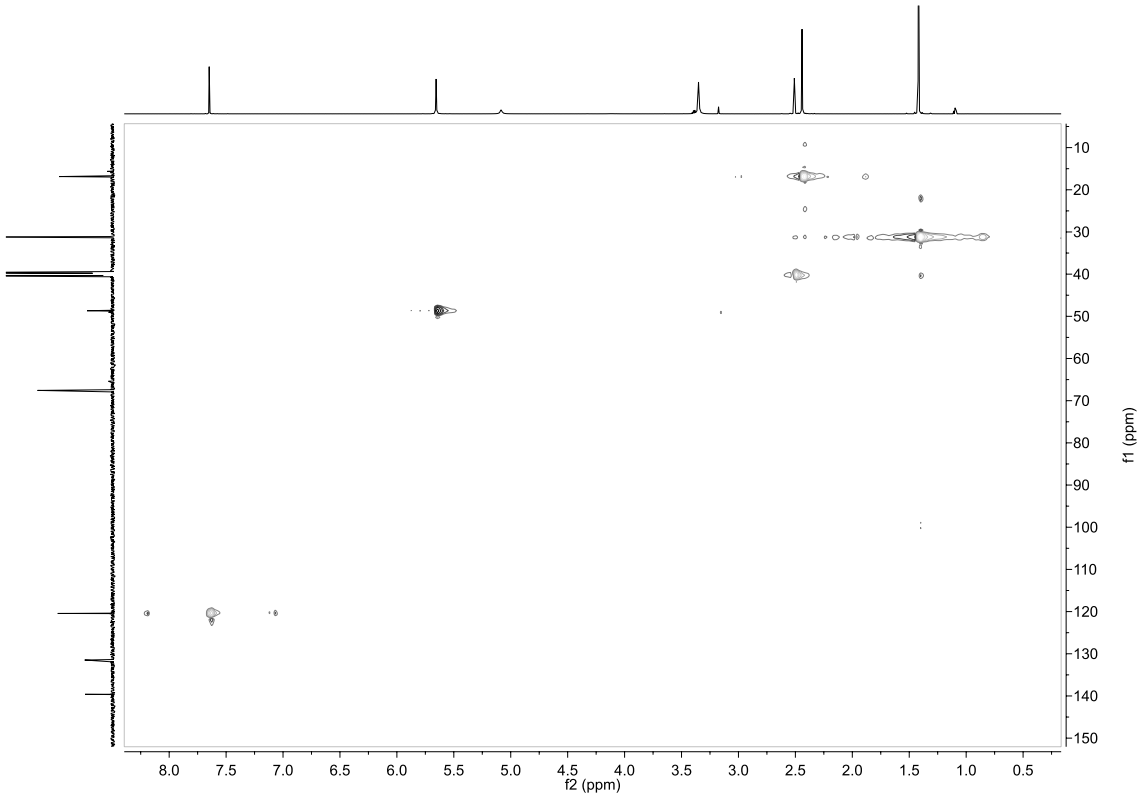

Figure D-28. HSQC NMR spectra for Tri-Click 2-methyl-3-butyne-2-ol.

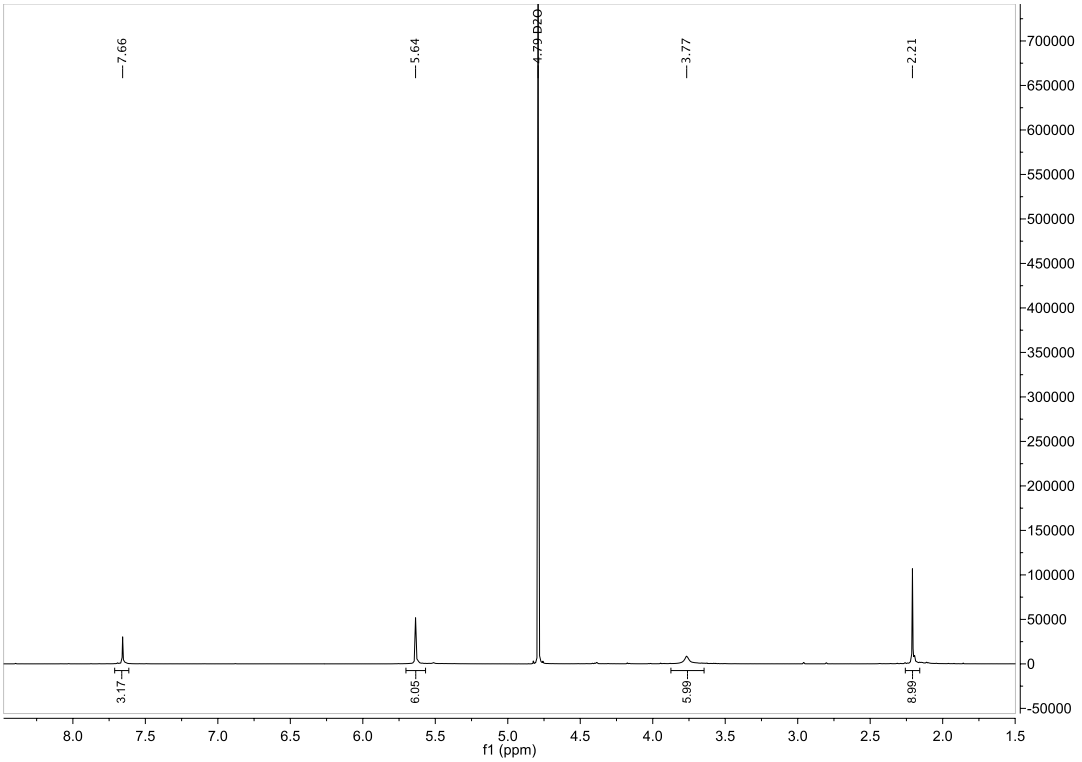

Figure D-29. ^{1}H NMR spectra for Tri-Click propargylamine.

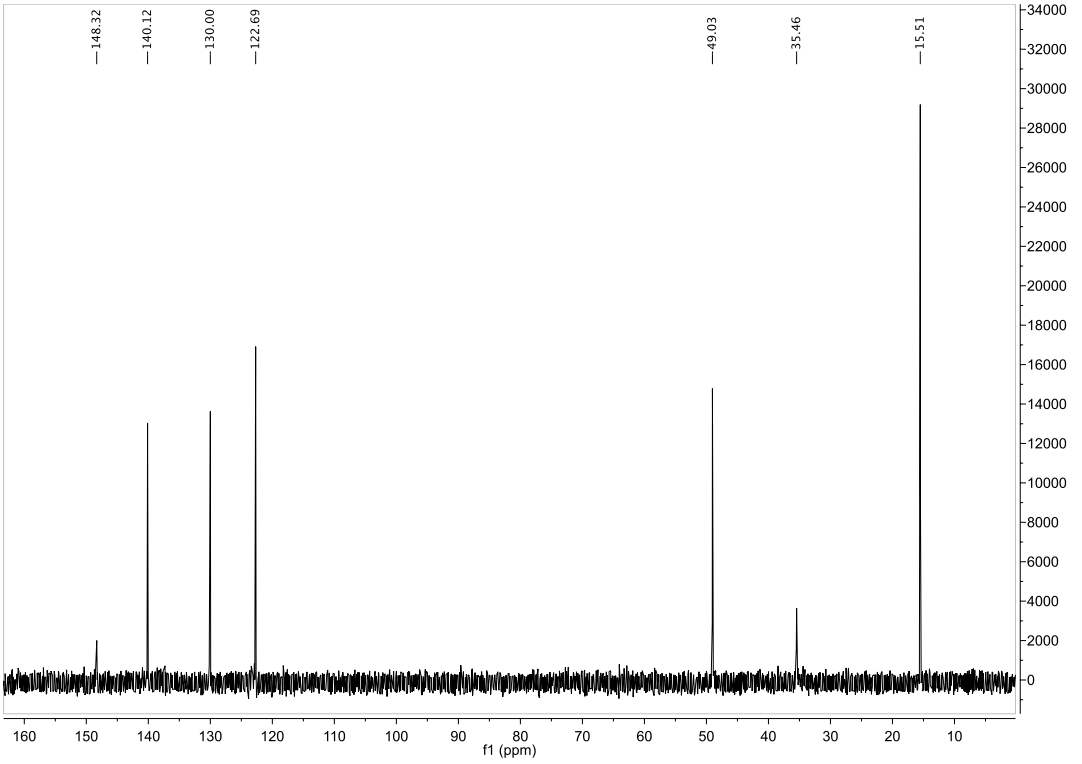

Figure D-30. ^{13}C NMR spectra for Tri-Click propargylamine.

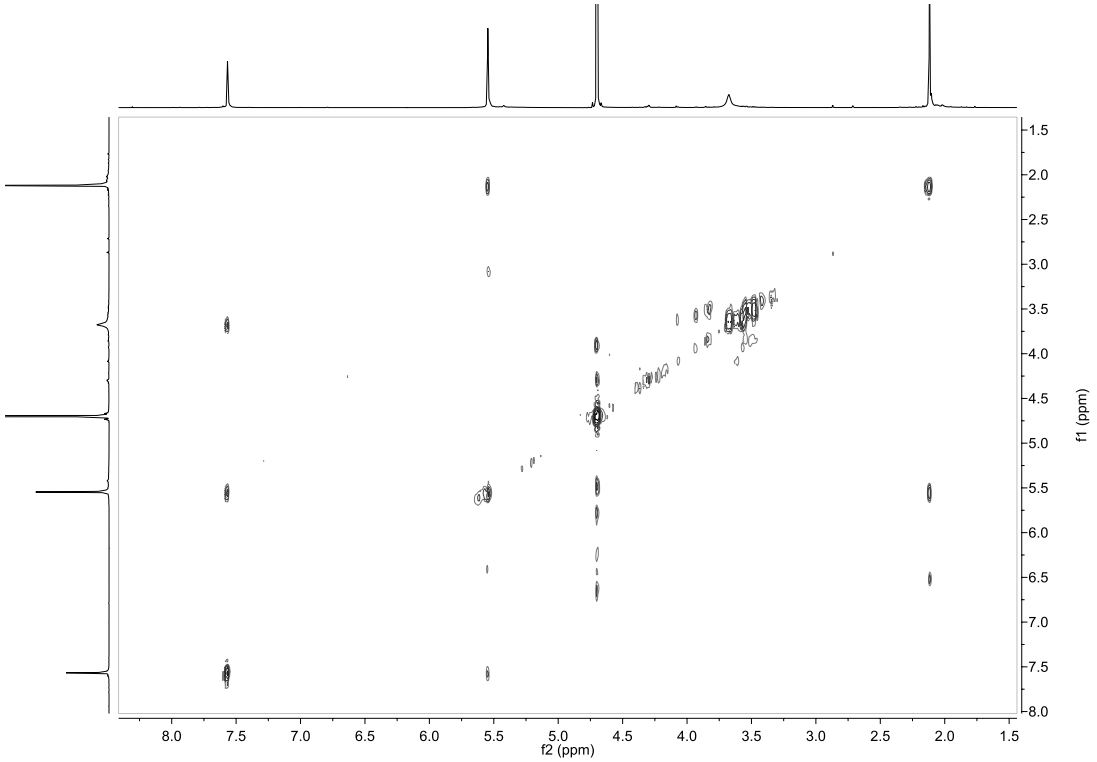

Figure D-31. COSY NMR spectra for Tri-Click propargylamine.

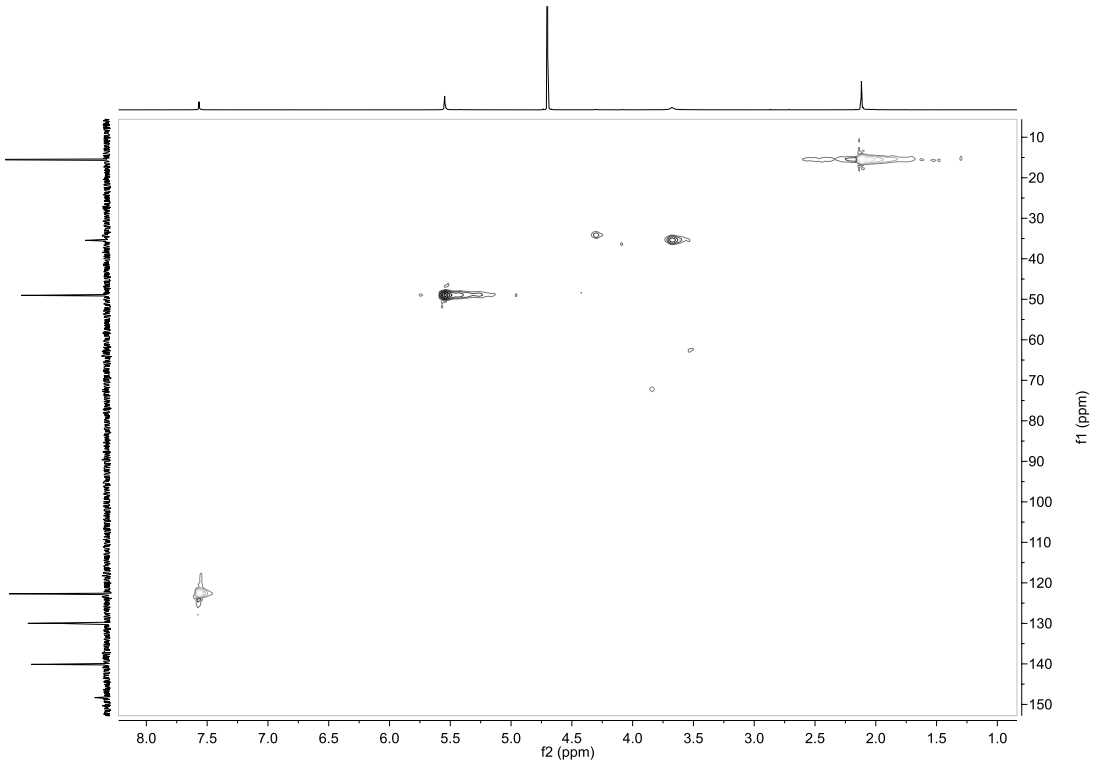

Figure D-32. HSQC NMR spectra for Tri-Click propargylamine.

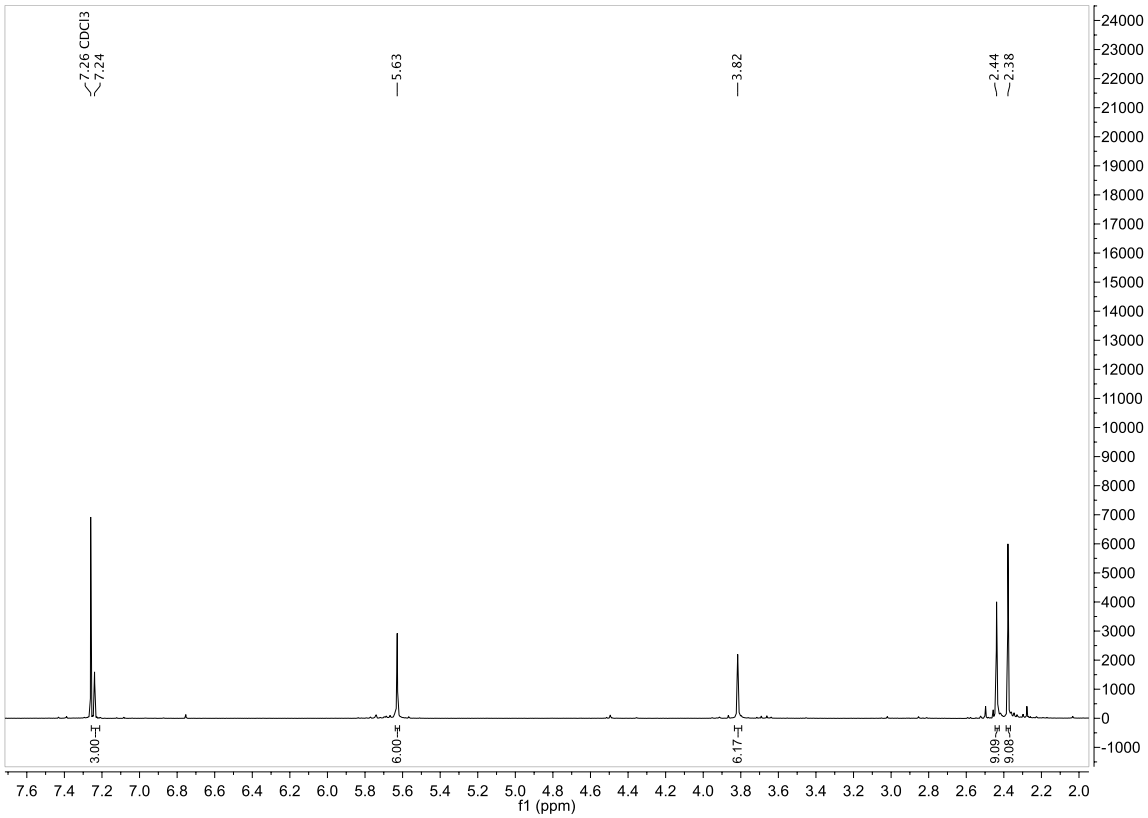

Figure D-33. ^{1}H NMR spectra for Tri-Click *N*-methyl propargylamine.

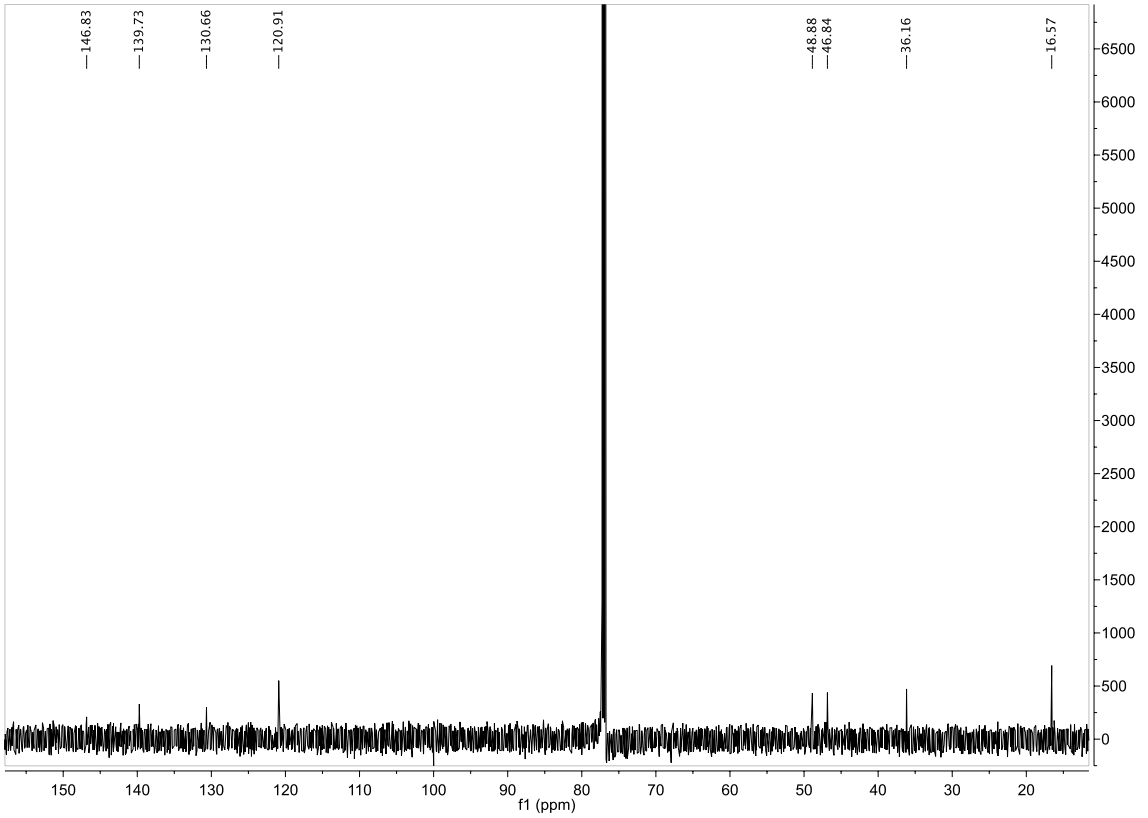

Figure D-34. ^{13}C NMR spectra for Tri-Click *N*-methyl propargylamine.

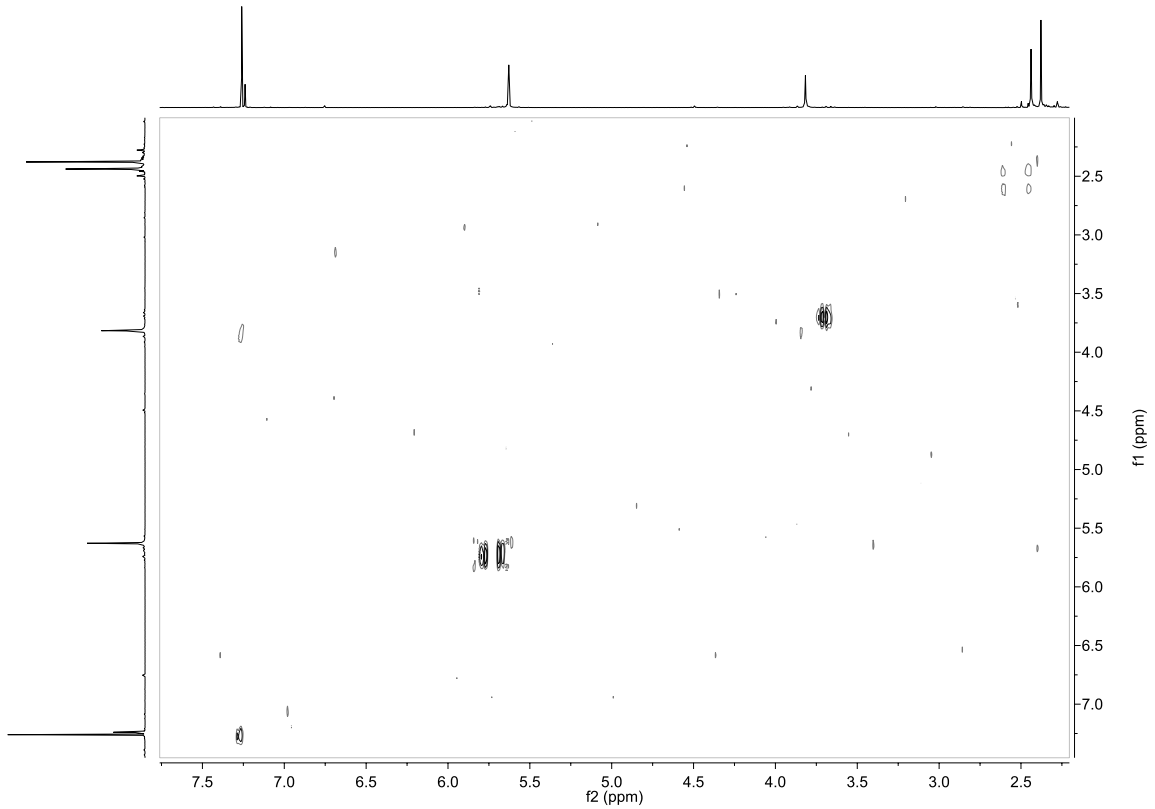

Figure D-35. COSY NMR spectra for Tri-Click *N*-methyl propargylamine.

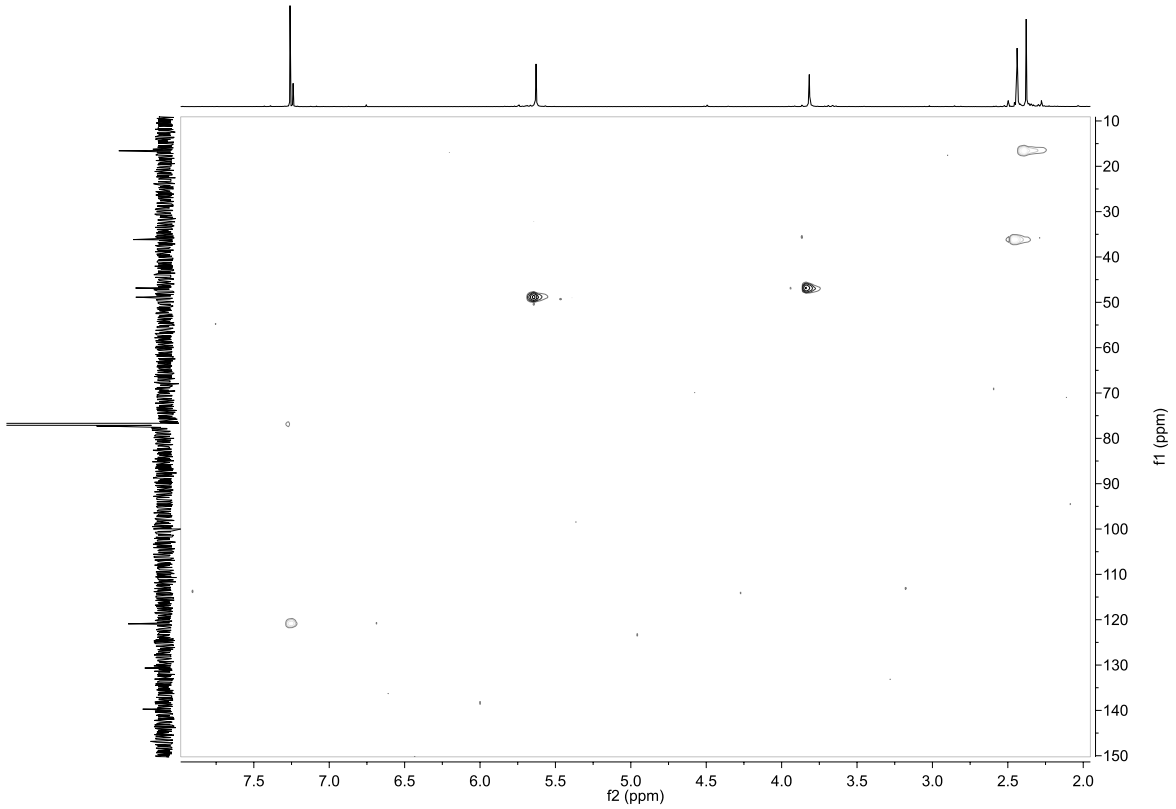

Figure D-36. HSQC NMR spectra for Tri-Click *N*-methyl propargylamine.

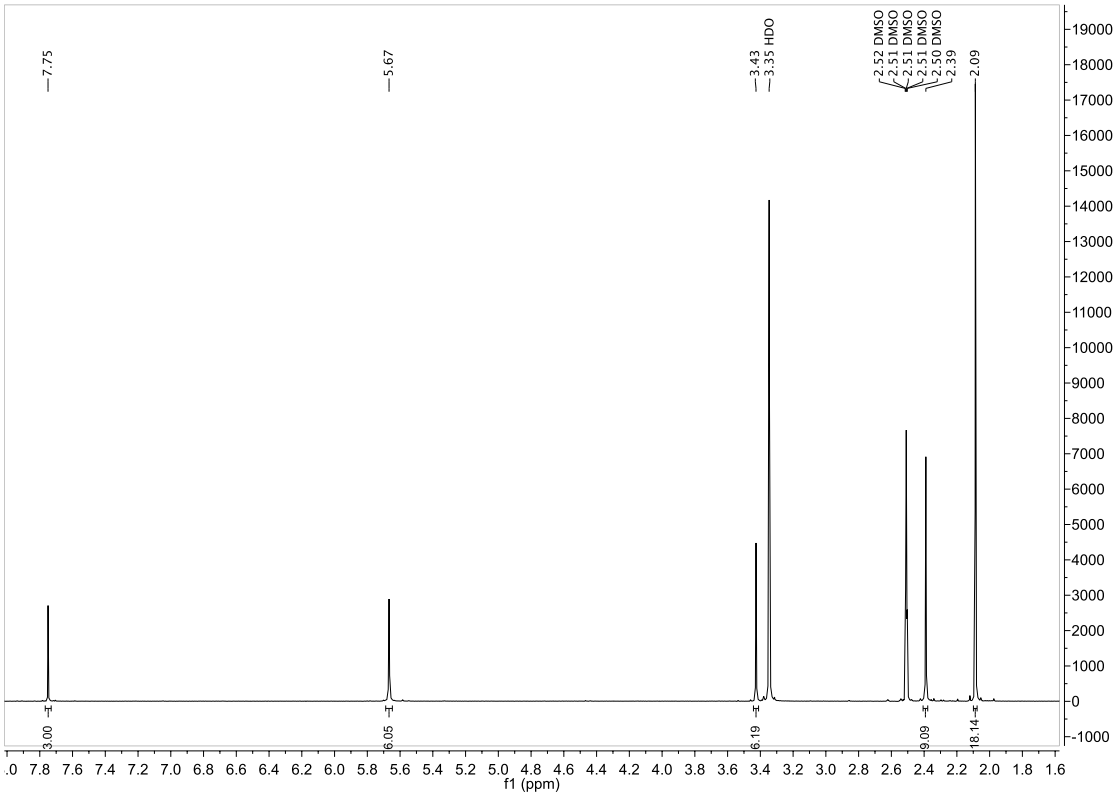

Figure D-37. ^{1}H NMR spectra for Tri-Click *N,N*-dimethylprop-2-yne-1-amine.

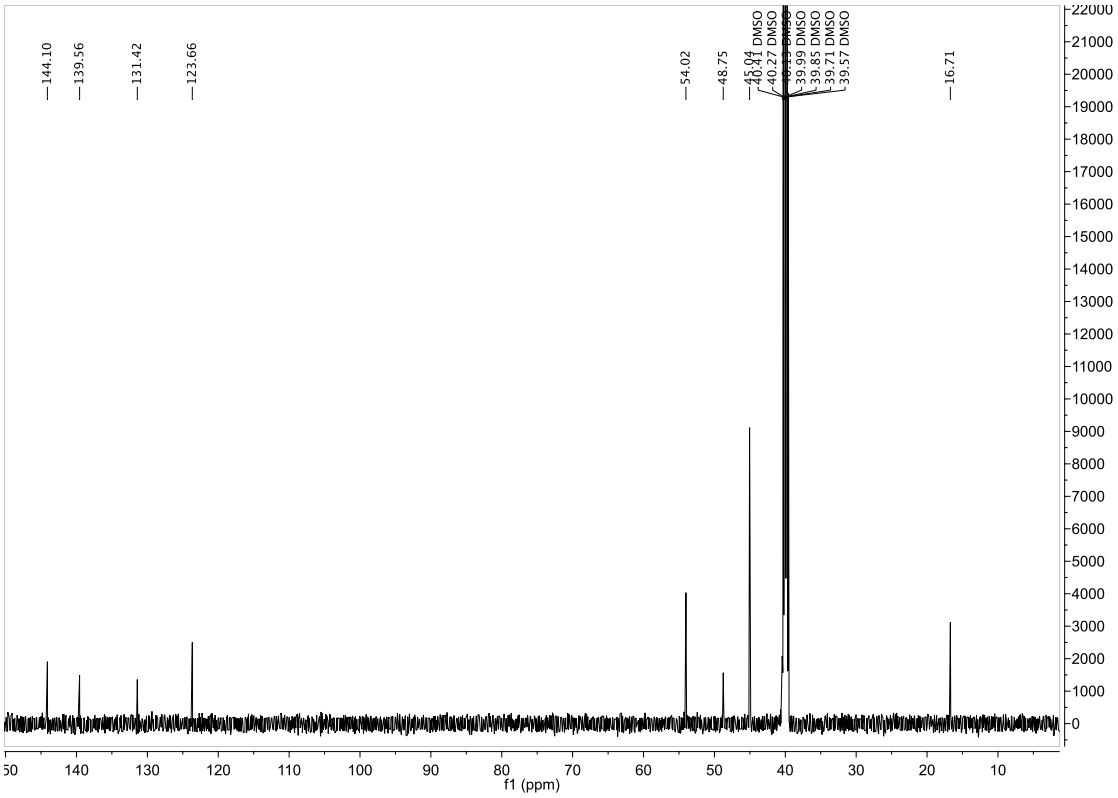

Figure D-38. ^{13}C NMR spectra for Tri-Click *N,N*-dimethylprop-2-yne-1-amine.

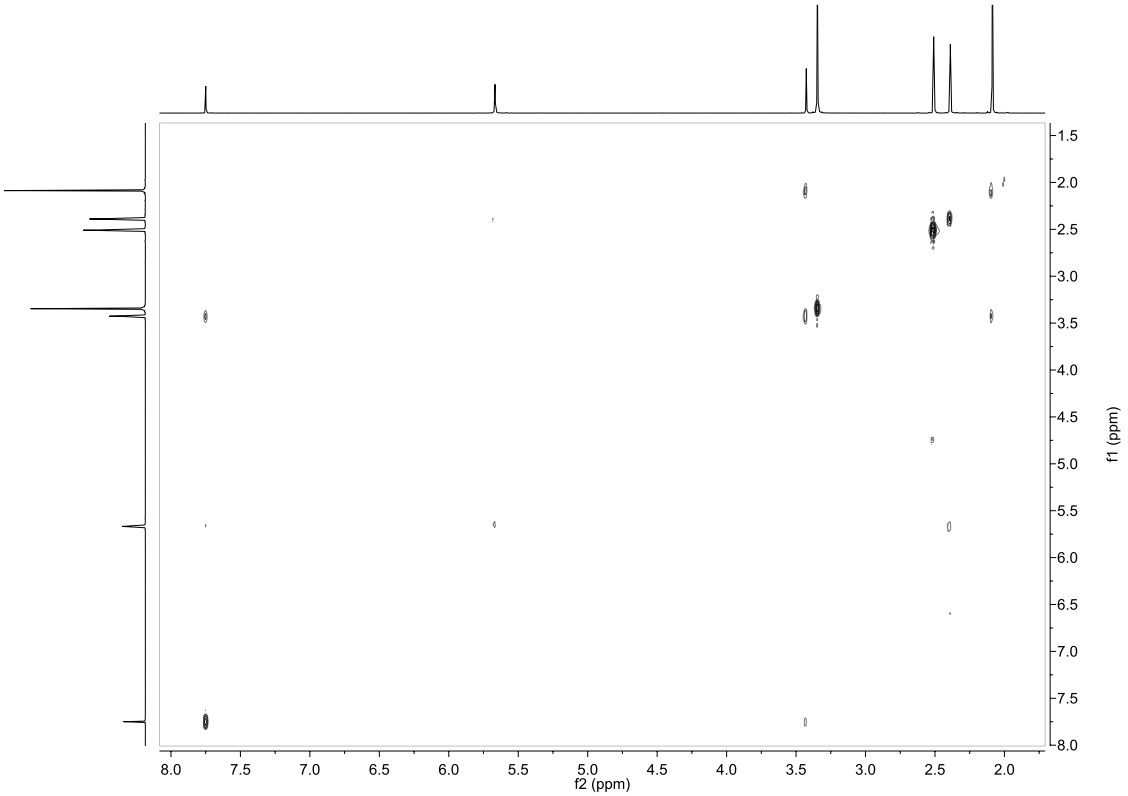

Figure D-39. COSY NMR spectra for Tri-Click *N,N*-dimethylprop-2-yne-1-amine.

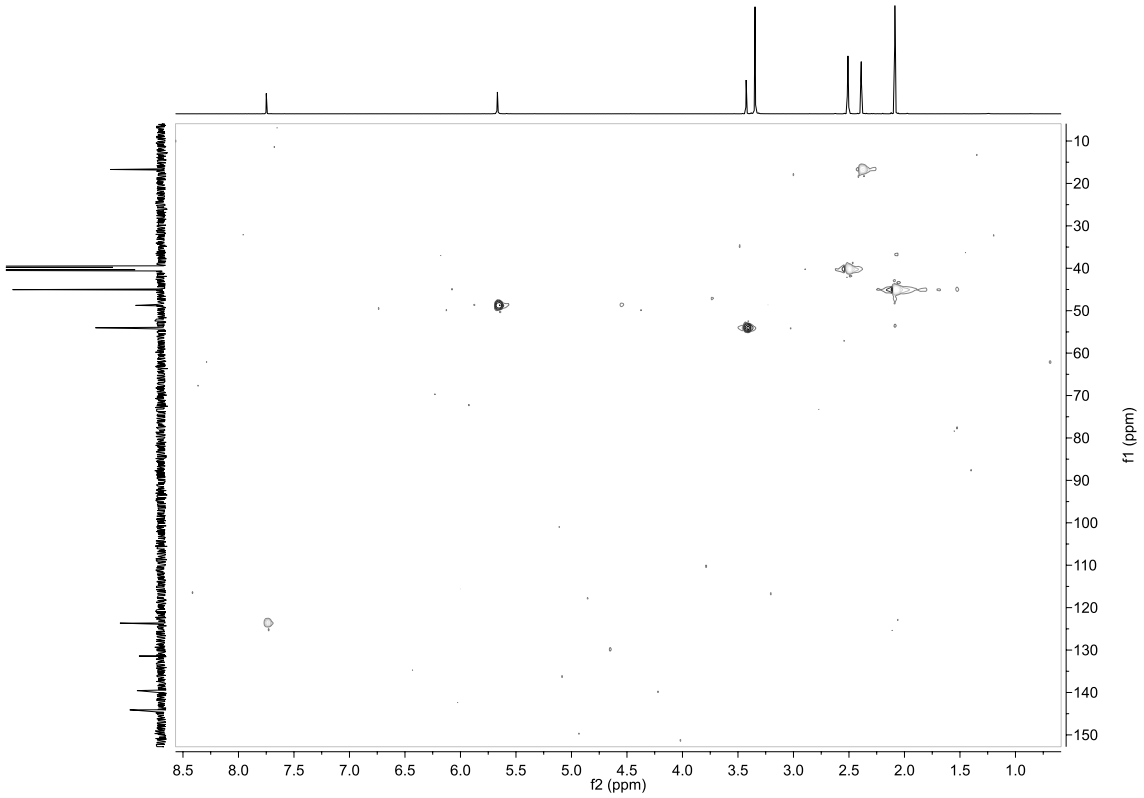

Figure D-40. HSQC NMR spectra for Tri-Click *N,N*-dimethylprop-2-yne-1-amine.

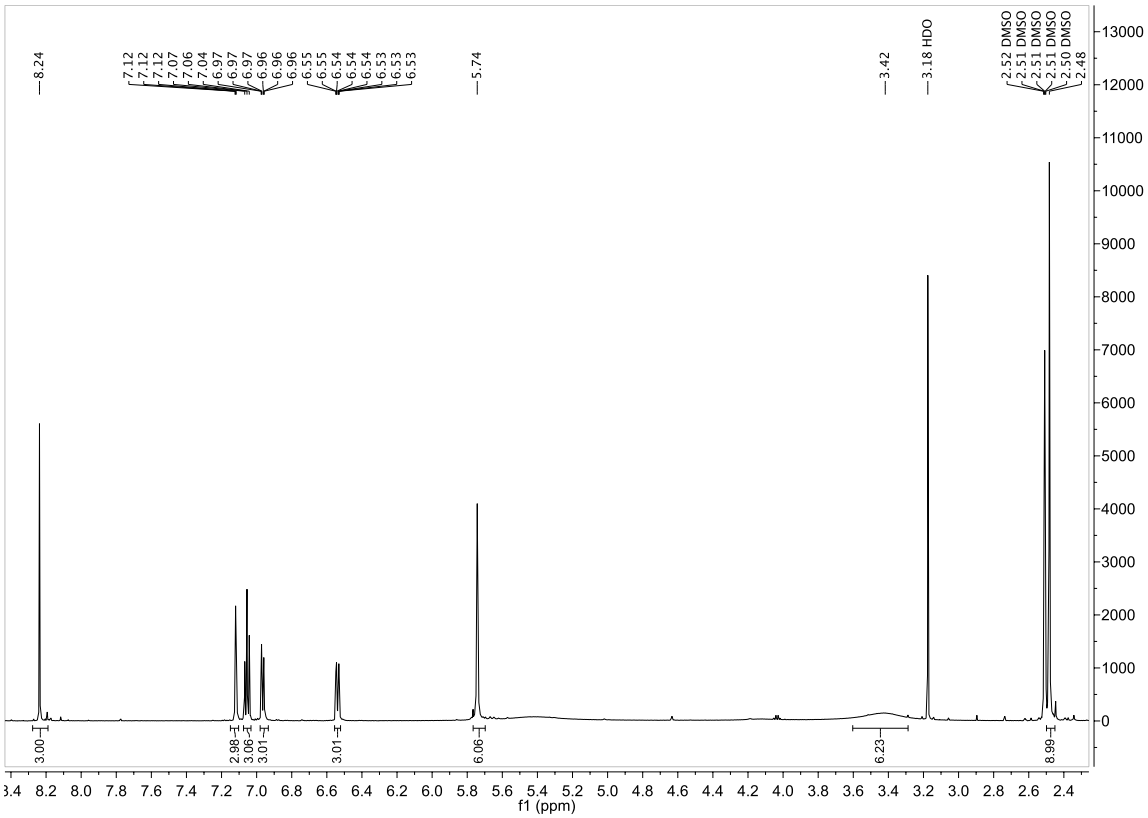

Figure D-41. ^{1}H NMR spectra for Tri-Click 3-ethynyl aniline.

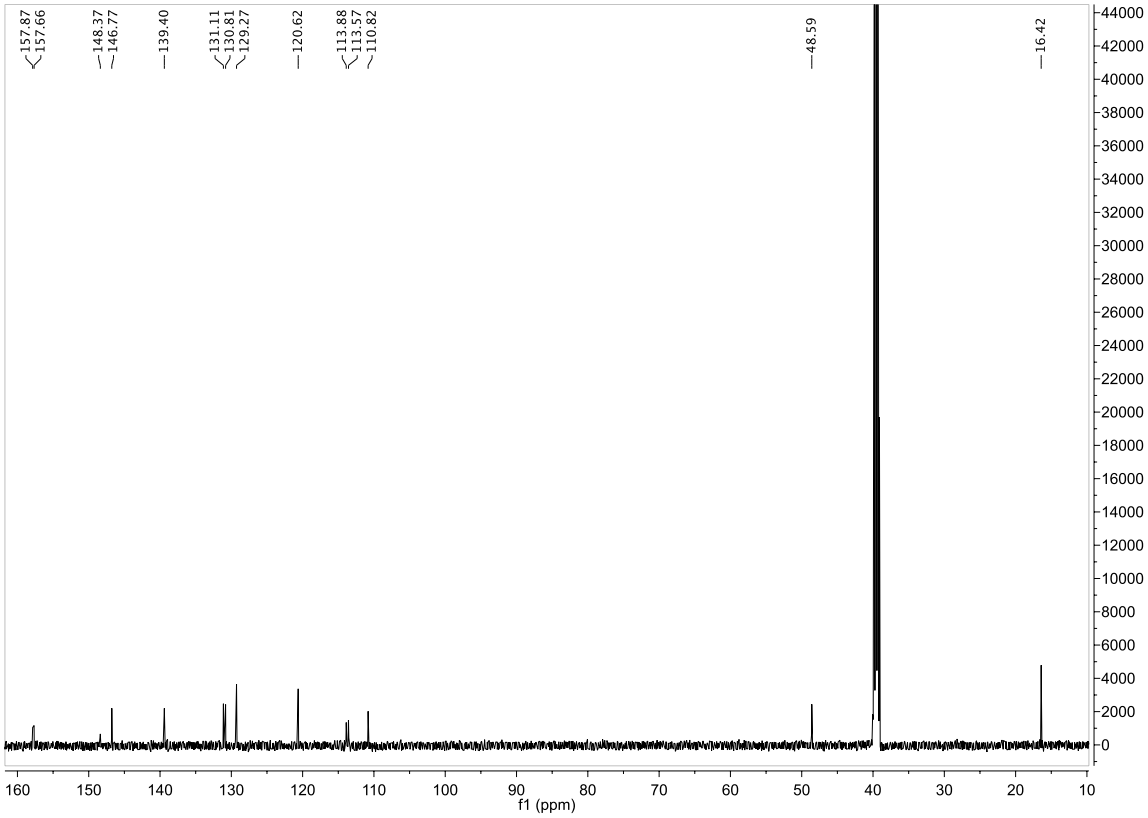

Figure D-42. ^{13}C NMR spectra for Tri-Click 3-ethynyl aniline.

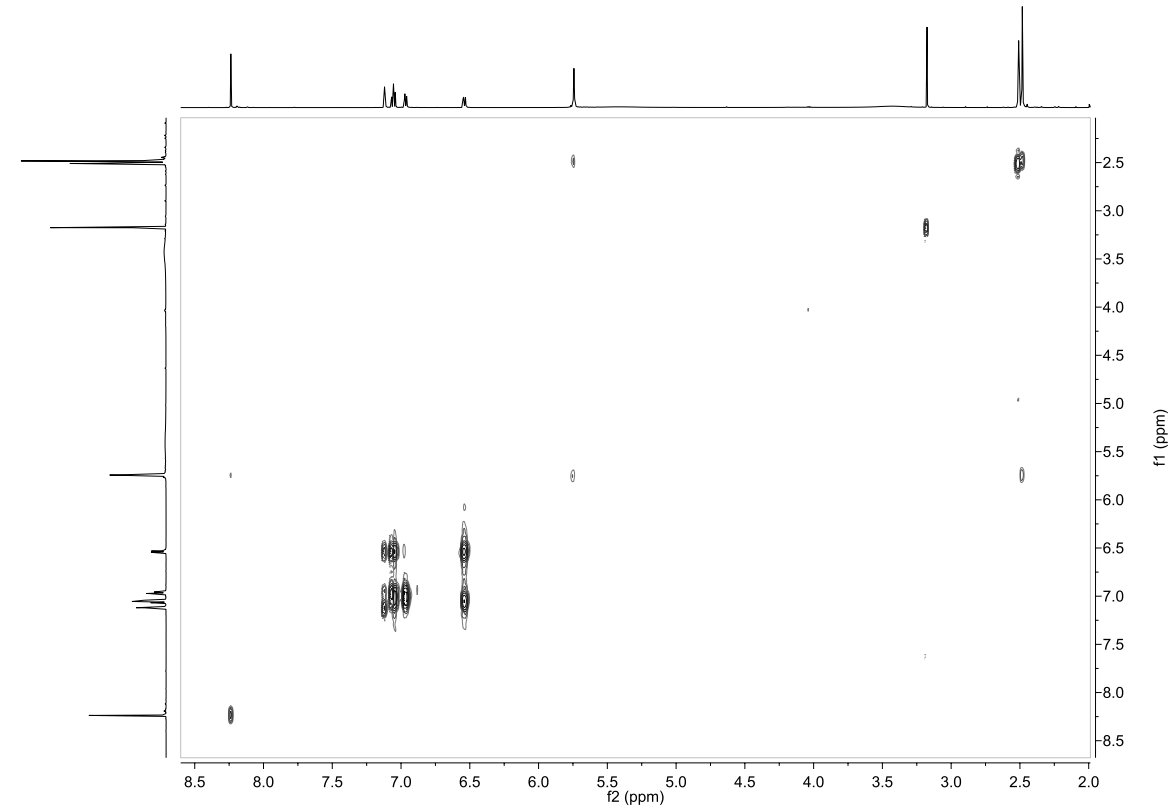

Figure D-43. Cosy NMR spectra for Tri-Click 3-ethynyl aniline.

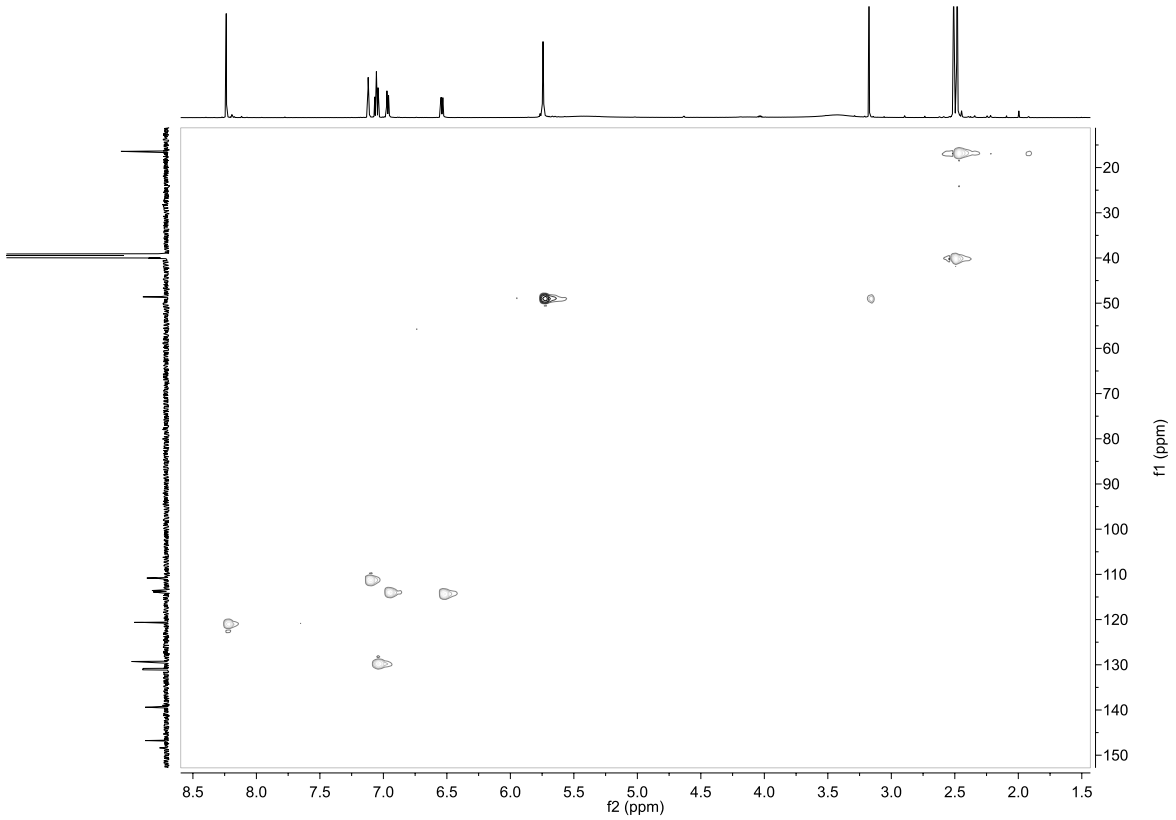

Figure D-44. HSQC NMR spectra for Tri-Click 3-ethynyl aniline.

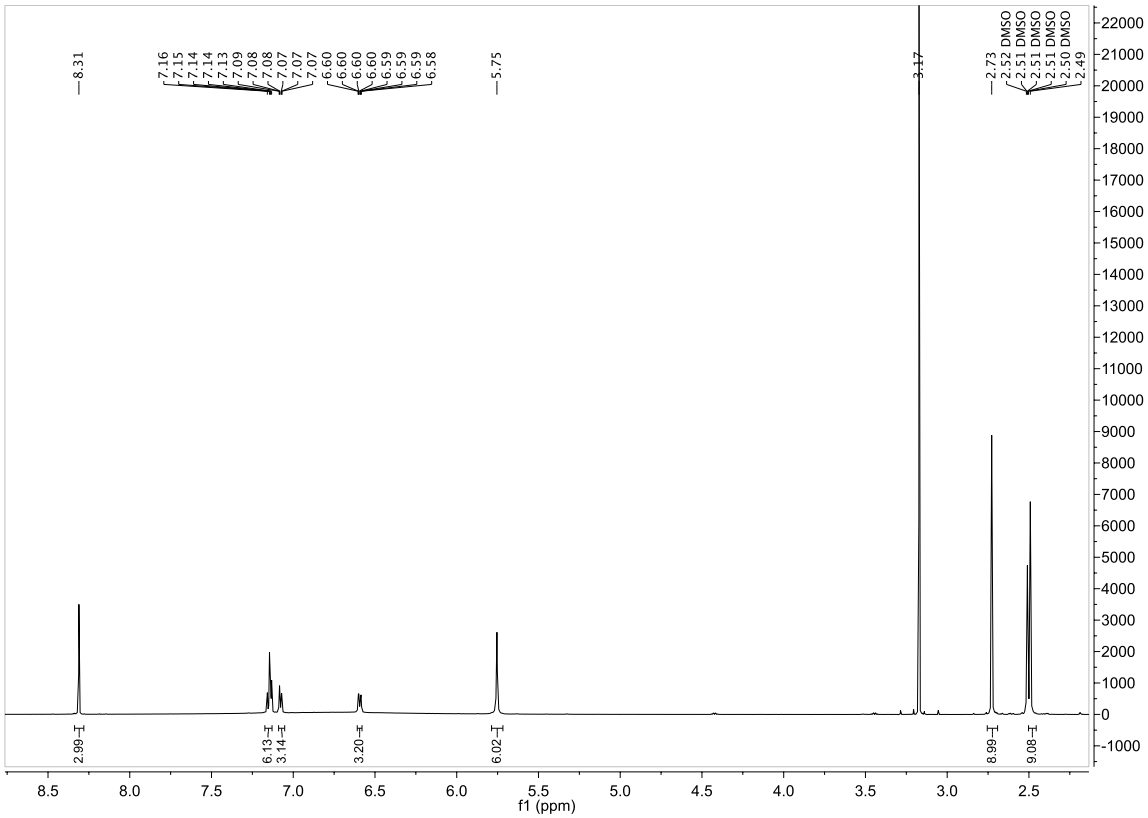

Figure D-45. ^{1}H NMR spectra of Tri-Click 3-ethynyl-methyl-aniline.

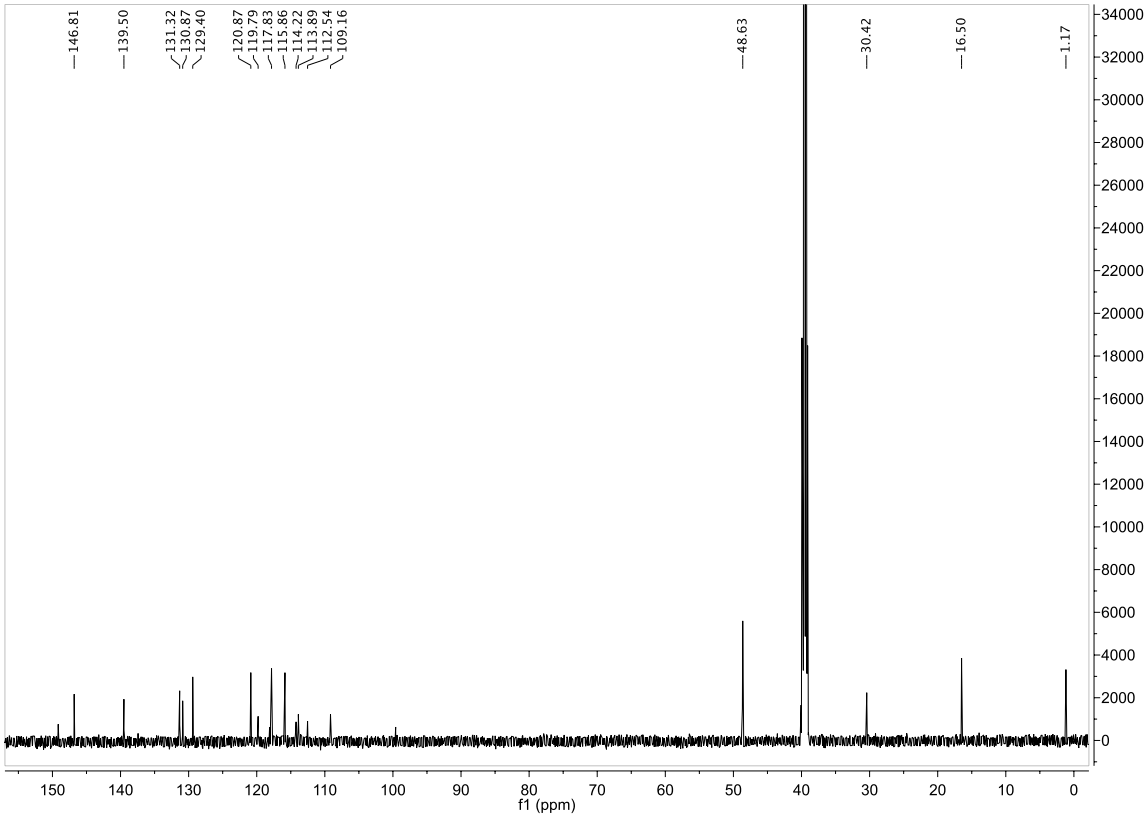

Figure D-46. ^{13}C NMR spectra of Tri-Click 3-ethynyl-methyl-aniline.

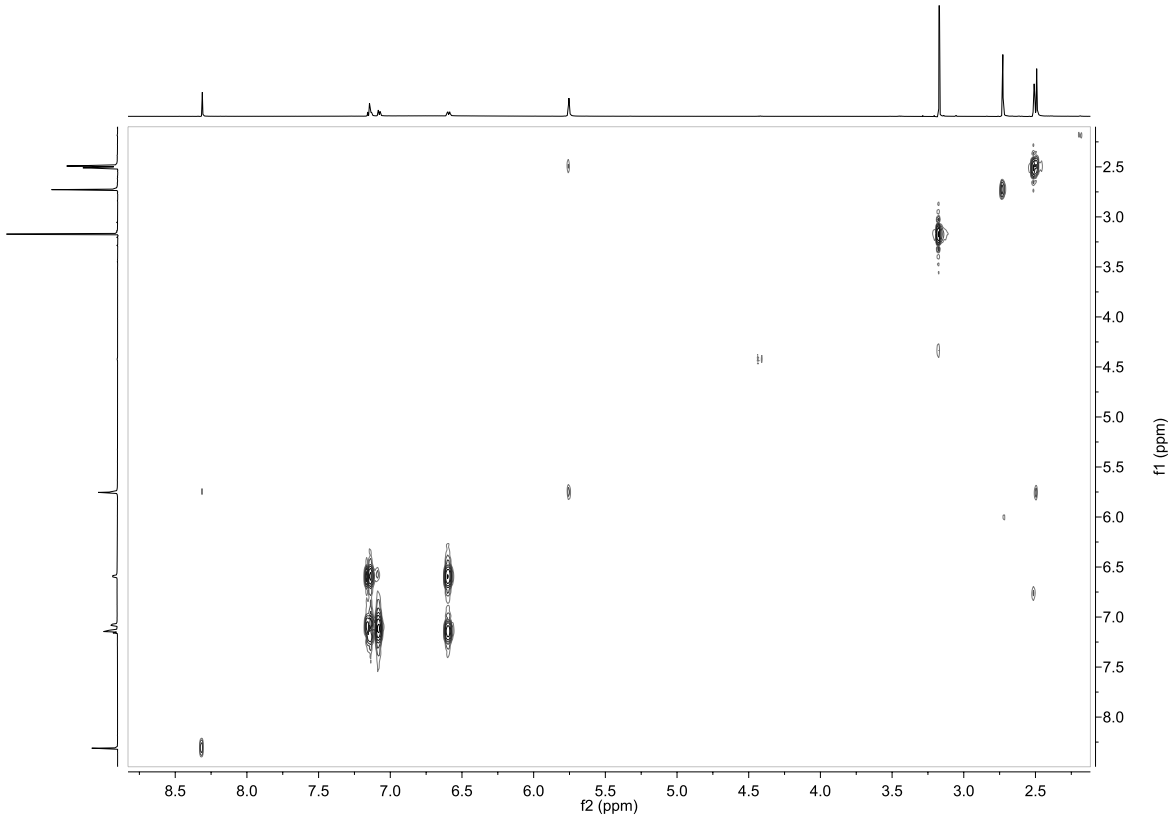

Figure D-47. COSY NMR spectra of Tri-Click 3-ethynyl-methyl-aniline.

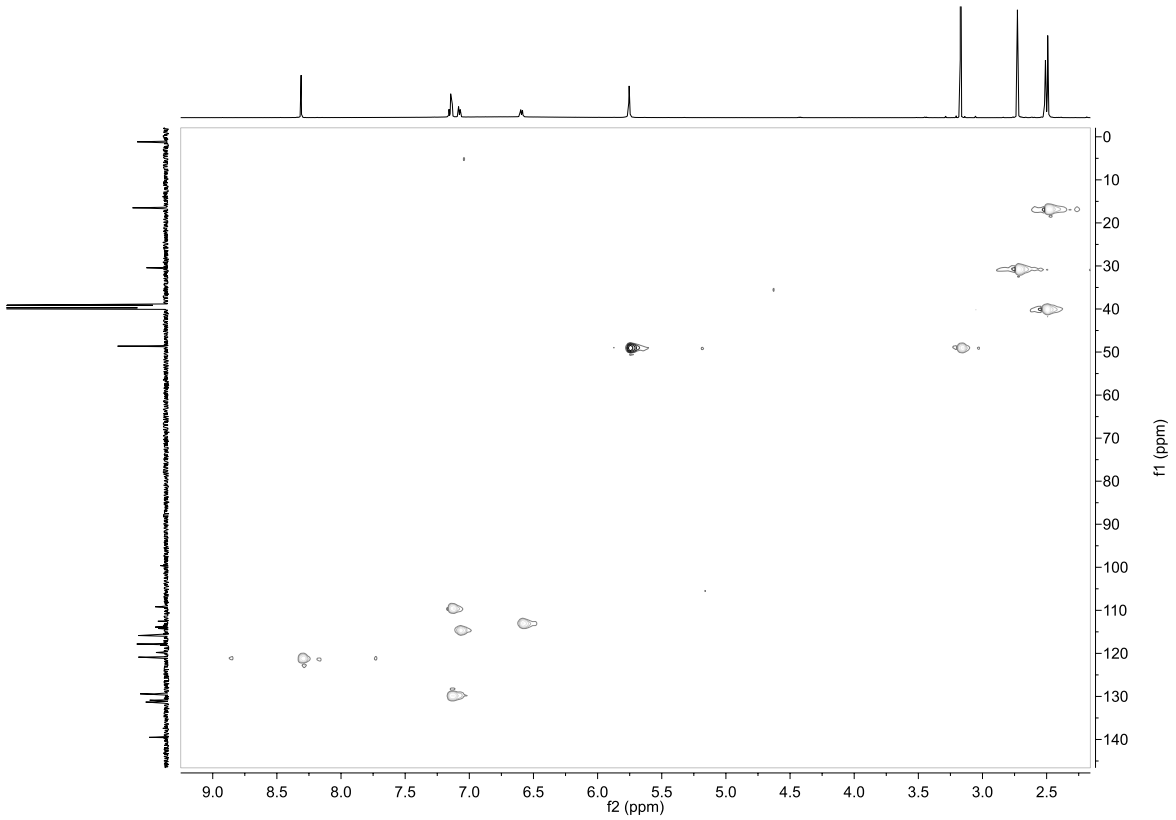

Figure D-48. HSQC NMR spectra of Tri-Click 3-ethynyl-methyl-aniline.

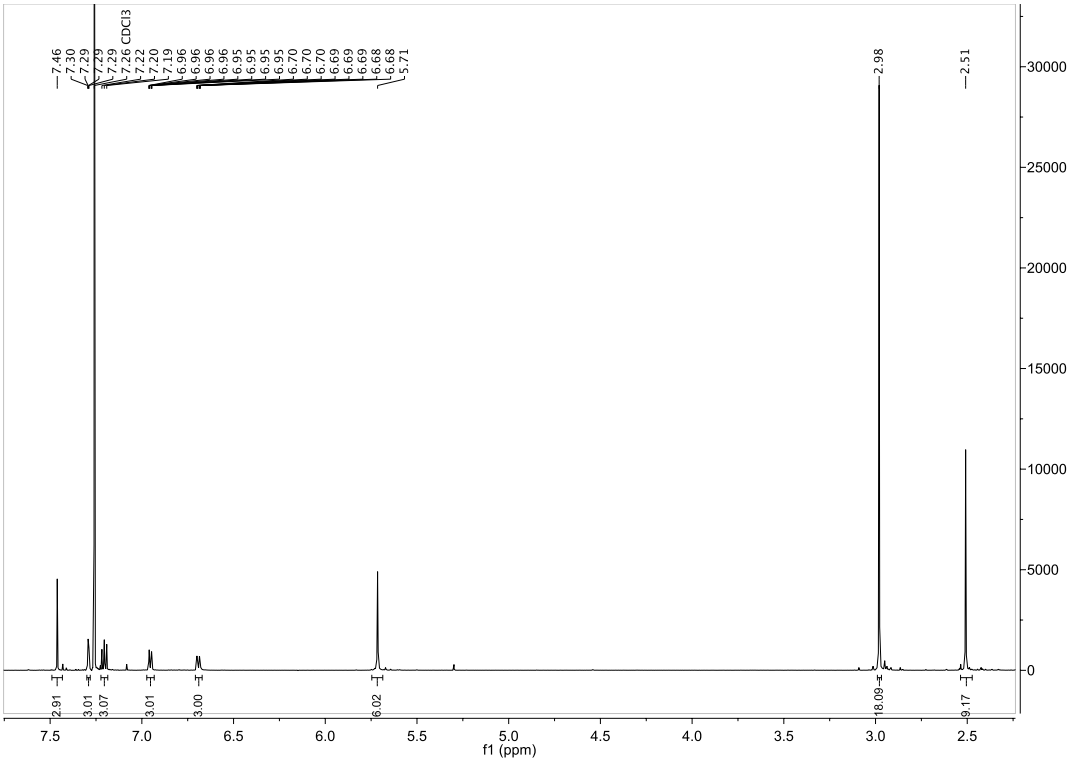

Figure D-49. [1]H NMR spectra for Tri-Click 3-ethynyl-*N,N*- dimethylaniline.

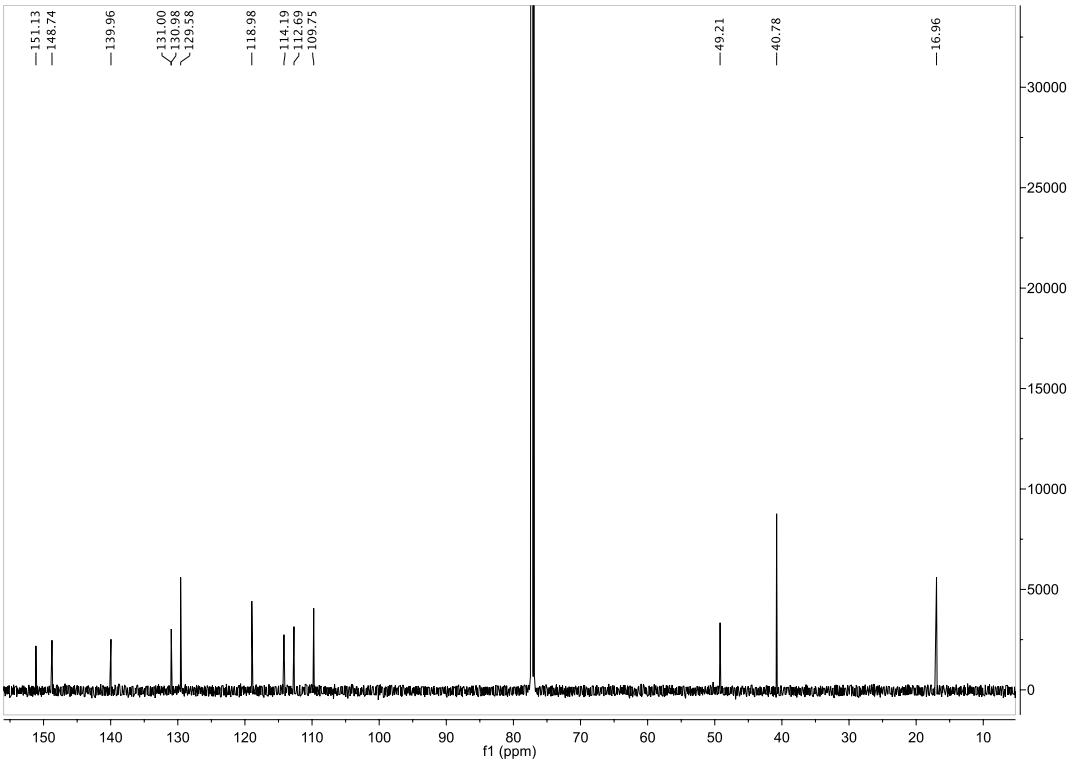

Figure D-50. [13]C NMR spectra for Tri-Click 3-ethynyl-*N,N*- dimethylaniline.

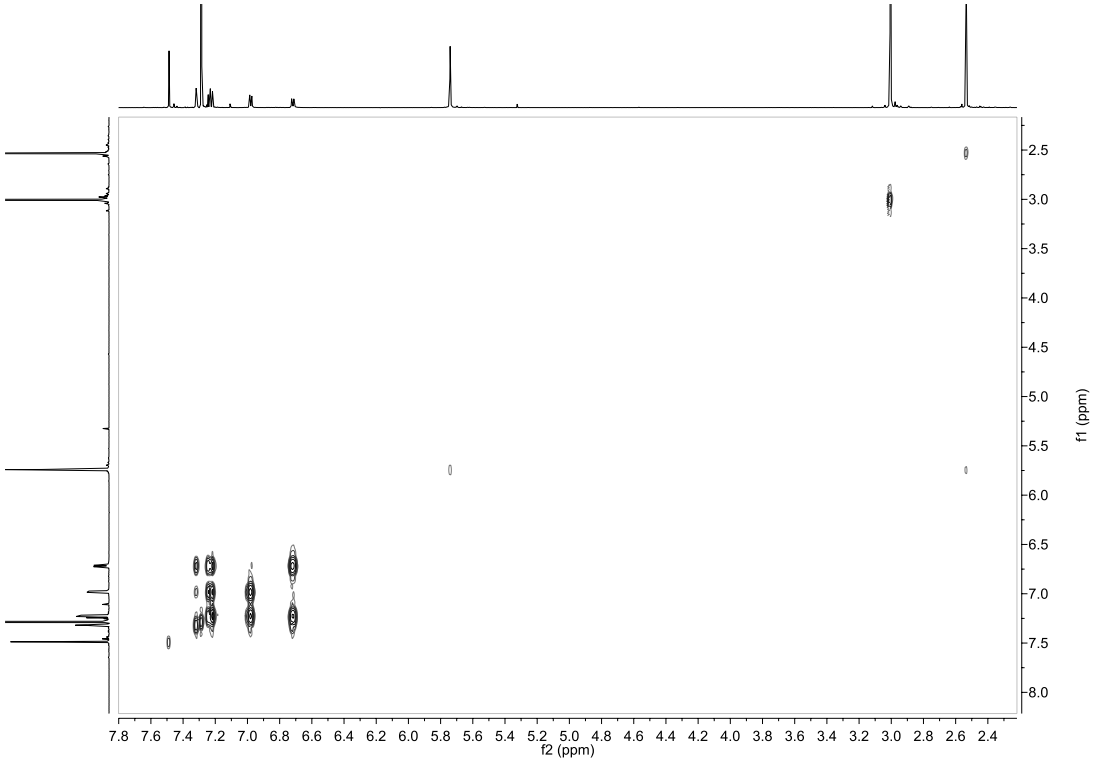

Figure D-51. COSY NMR spectra for Tri-Click 3-ethynyl-*N,N*- dimethylaniline.

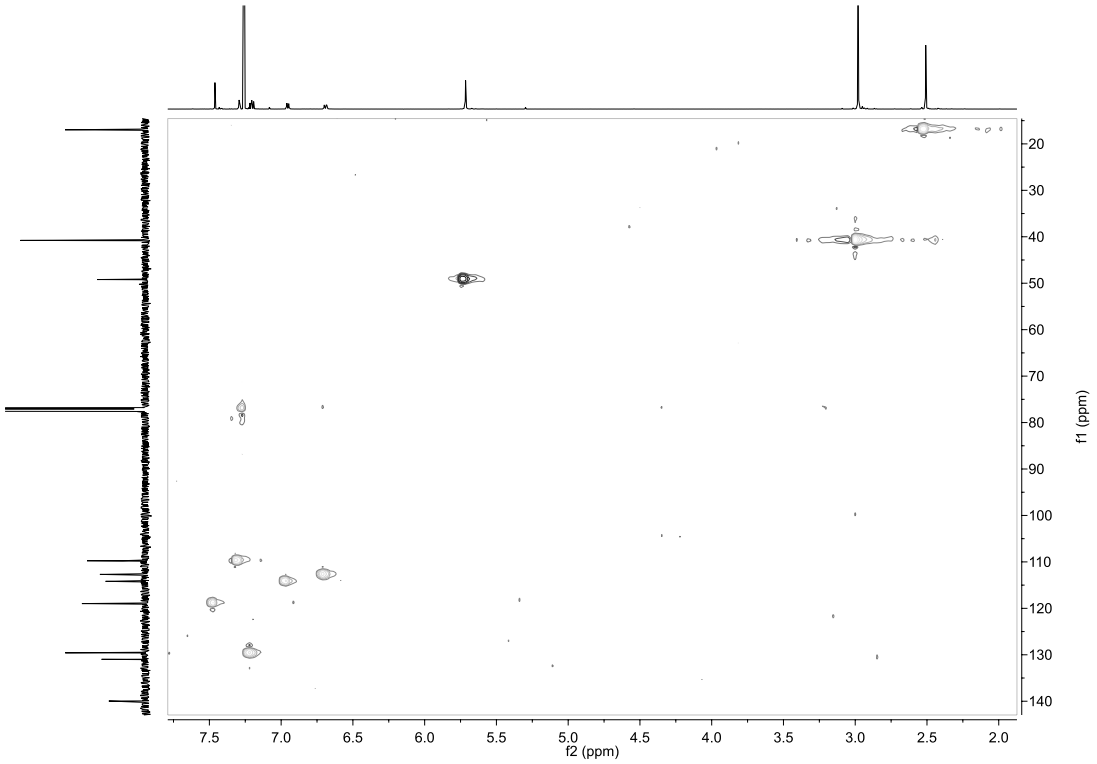

Figure D-52. HSQC NMR spectra for Tri-Click 3-ethynyl-*N,N*- dimethylaniline.

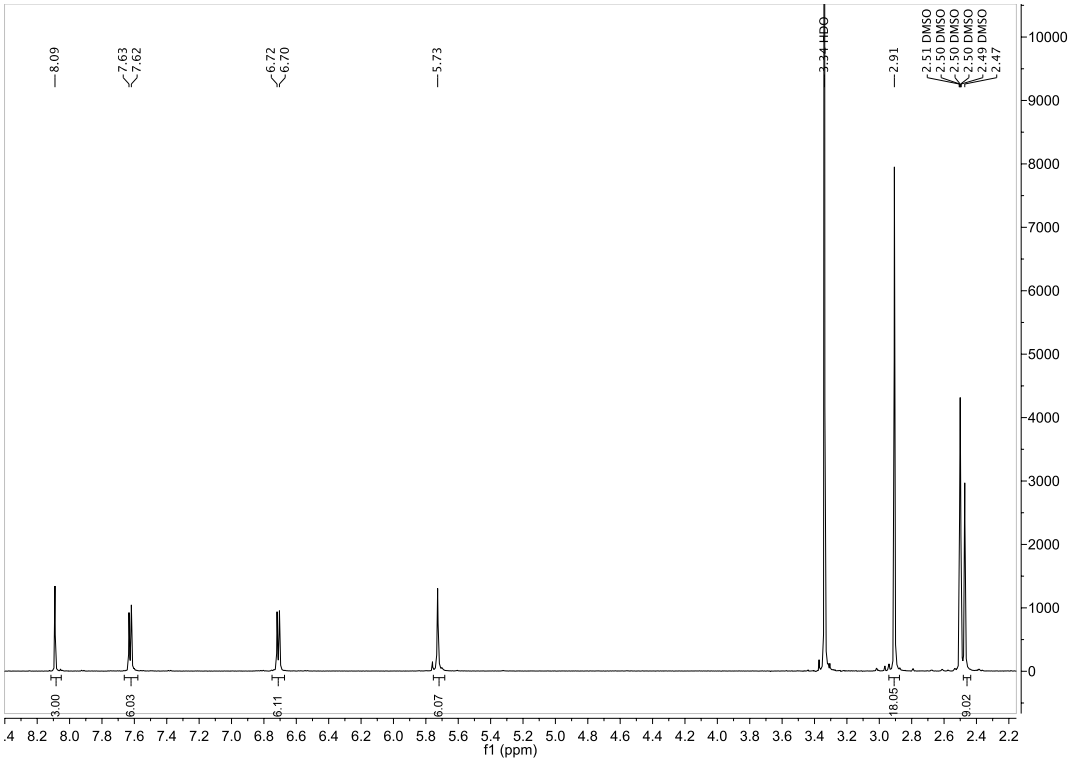

Figure D-53. ^{1}H NMR spectra for Tri-Click 4-ethynyl-*N*,*N*-dimethylaniline.

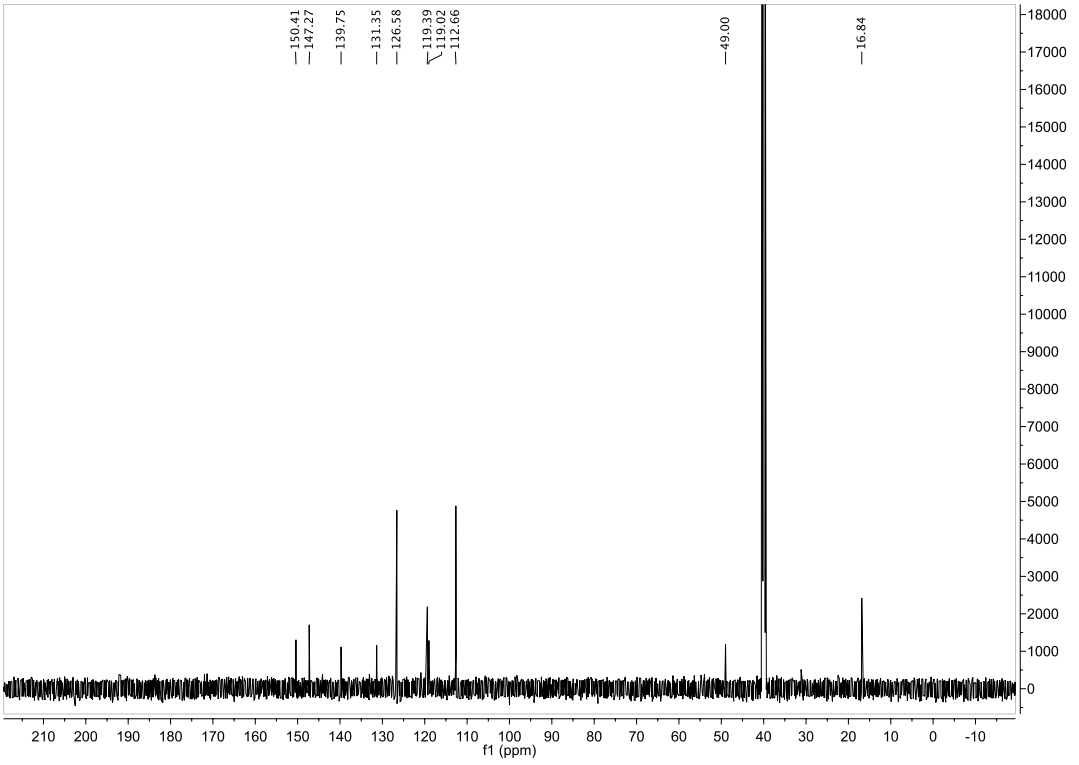

Figure D-54. ^{13}C NMR spectra for Tri-Click 4-ethynyl-*N*,*N*-dimethylaniline.

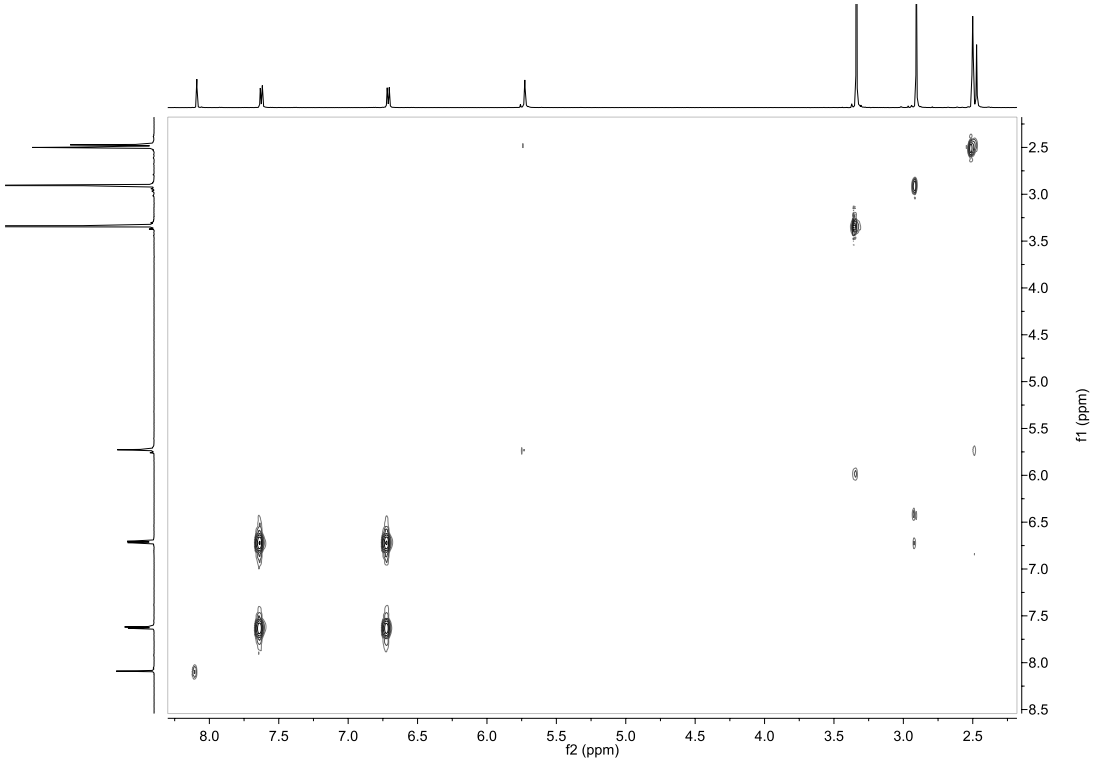

Figure D-55. COSY NMR spectra for Tri-Click 4-ethynyl-*N*,*N*-dimethylaniline.

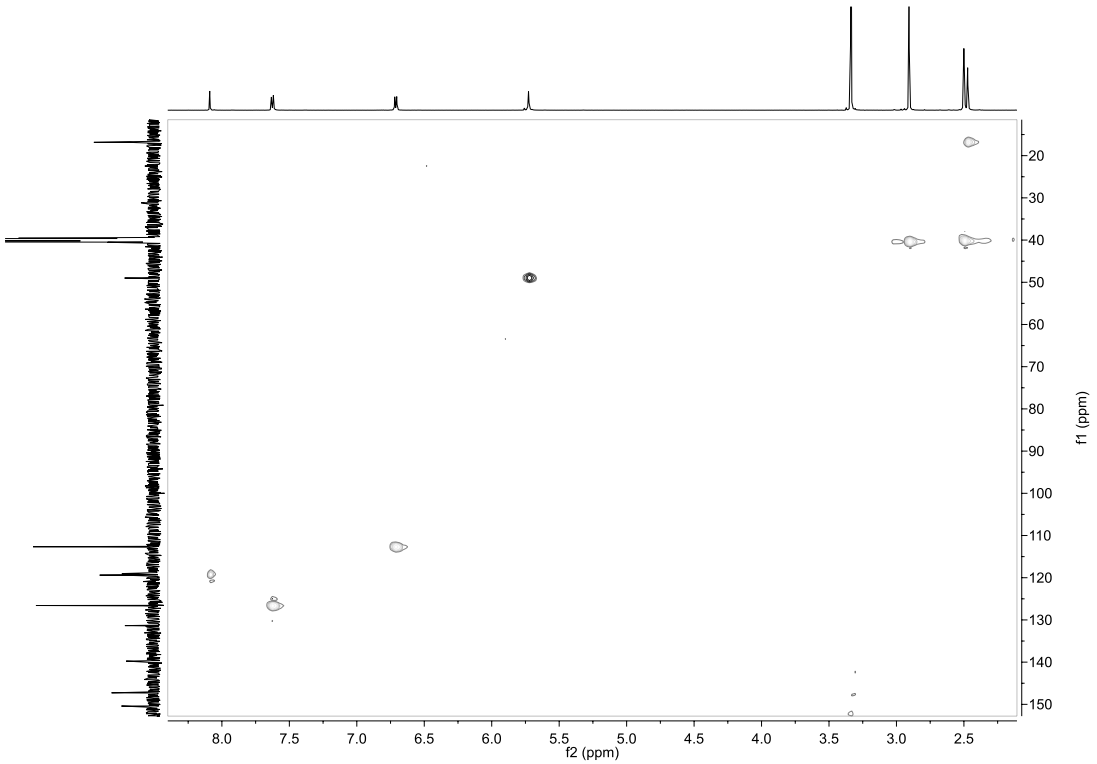

Figure D-56. HSQC NMR spectra for Tri-Click 4-ethynyl-*N*,*N*-dimethylaniline.

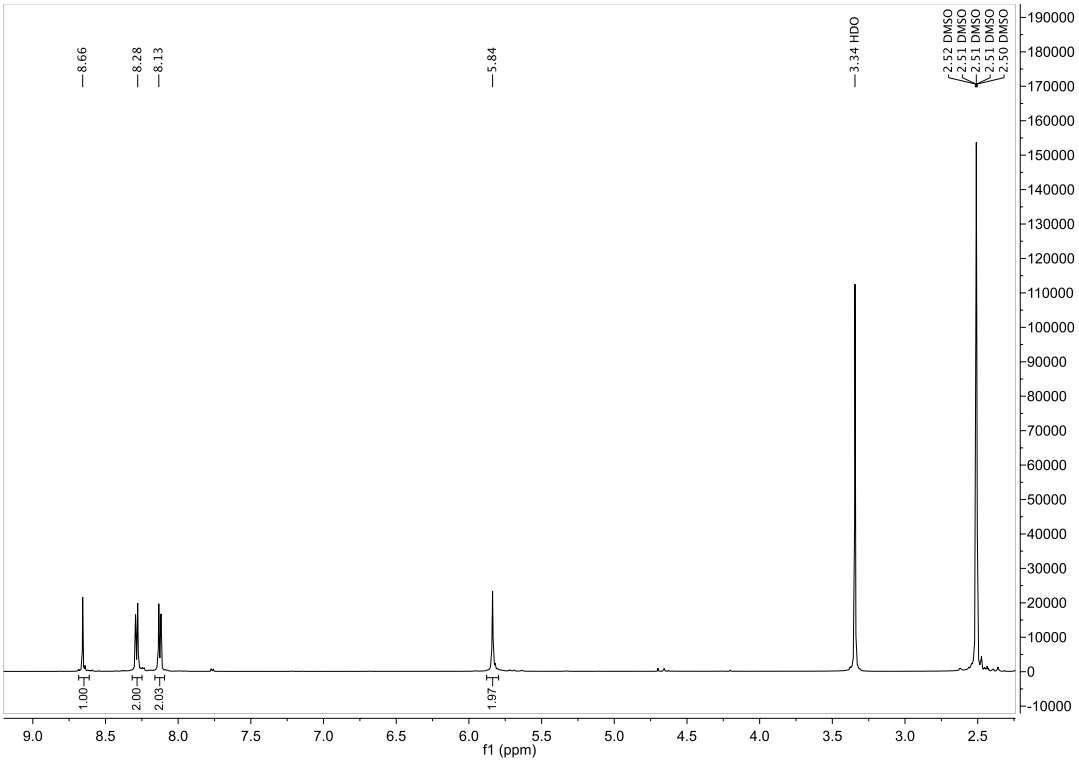

Figure D-57. ^{1}H NMR spectra for Tri-Click 1-ethynyl-4-nitrobenzene.

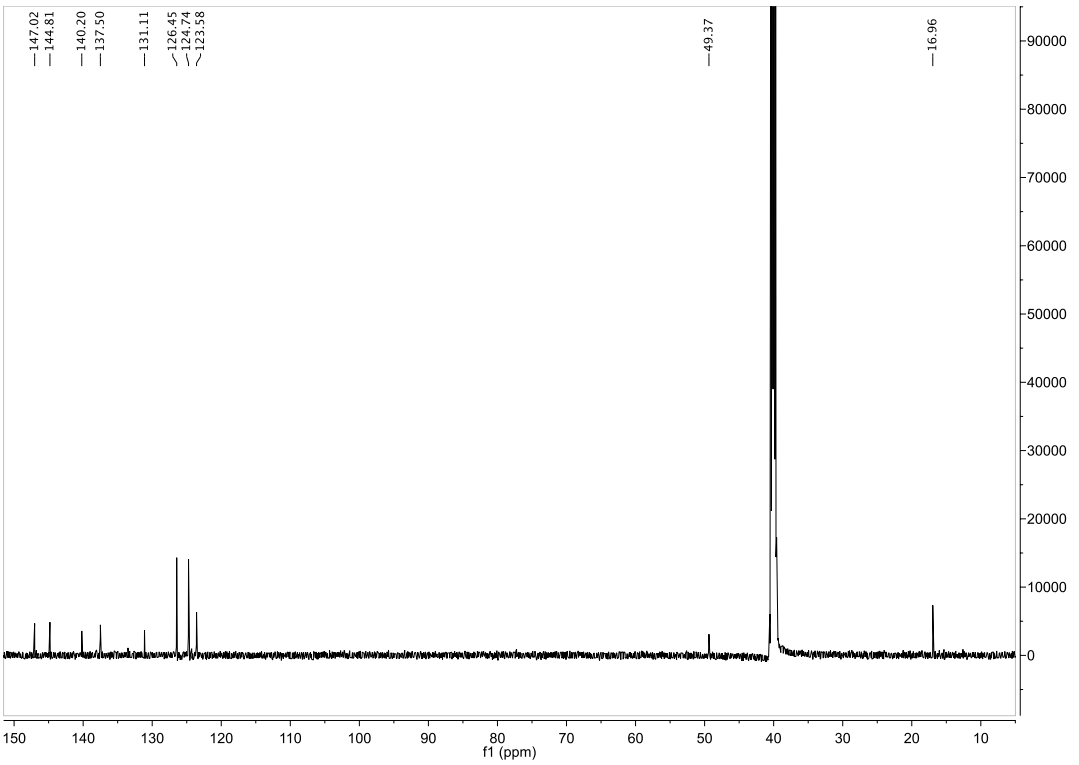

Figure D-58. ^{13}C NMR spectra for Tri-Click 1-ethynyl-4-nitrobenzene.

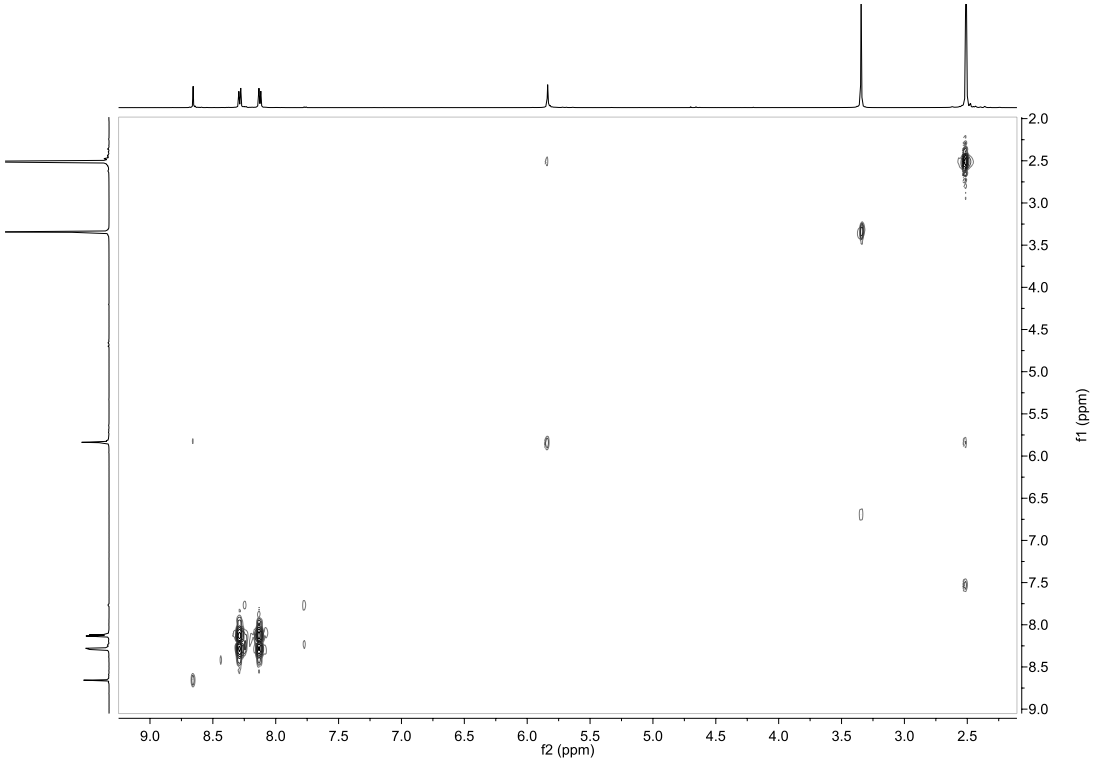

Figure D-59. COSY NMR spectra for Tri-Click 1-ethynyl-4-nitrobenzene.

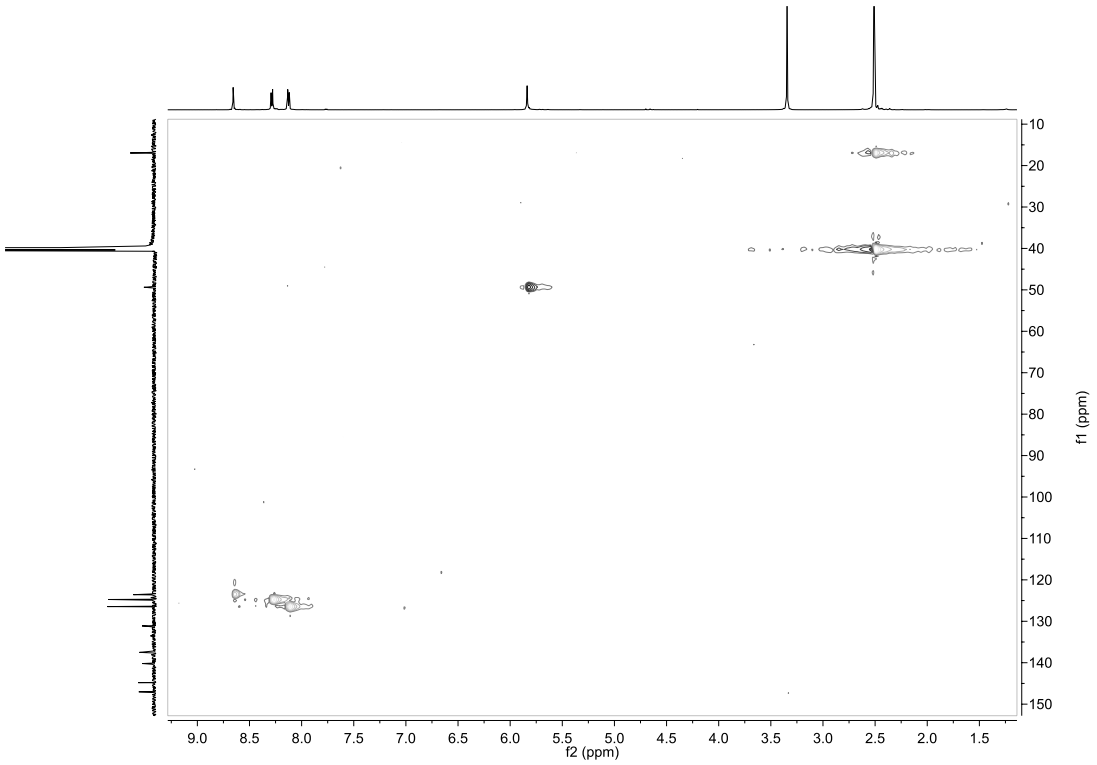

Figure D-60. HSQC NMR spectra for Tri-Click 1-ethynyl-4-nitrobenzene.

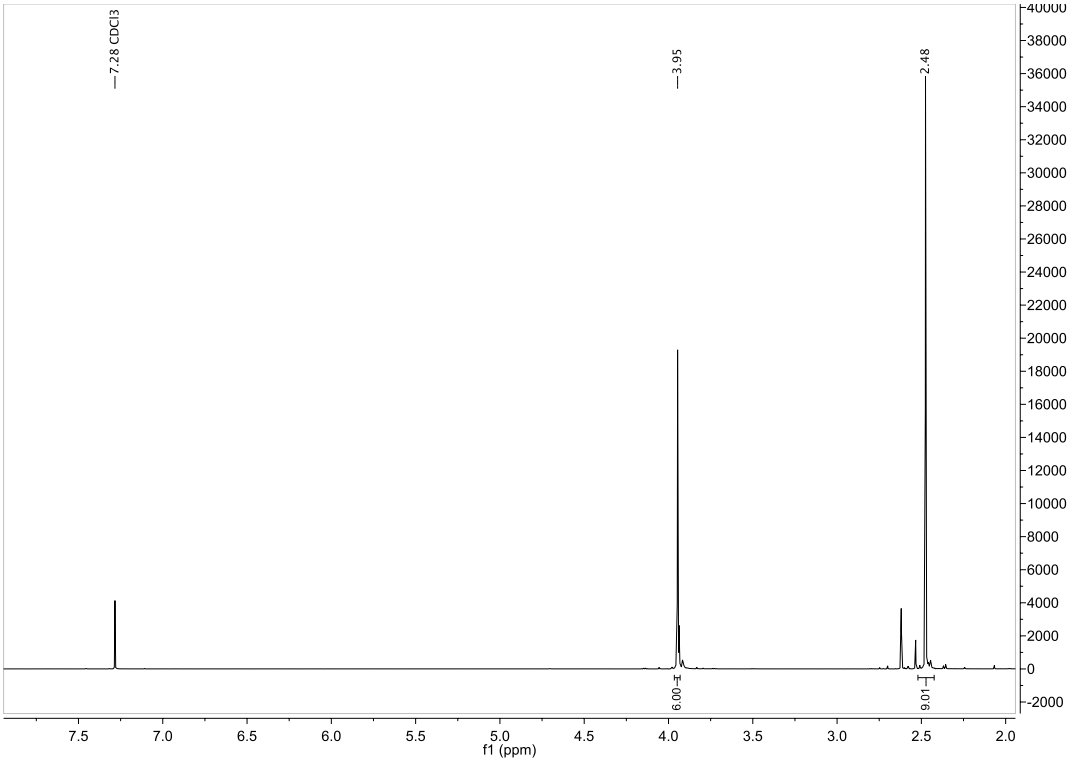

Figure D-61. ^{1}H NMR spectra for 1,3,5-tris(aminomethyl)-2,4,6-trimethyl benzene (triamine).

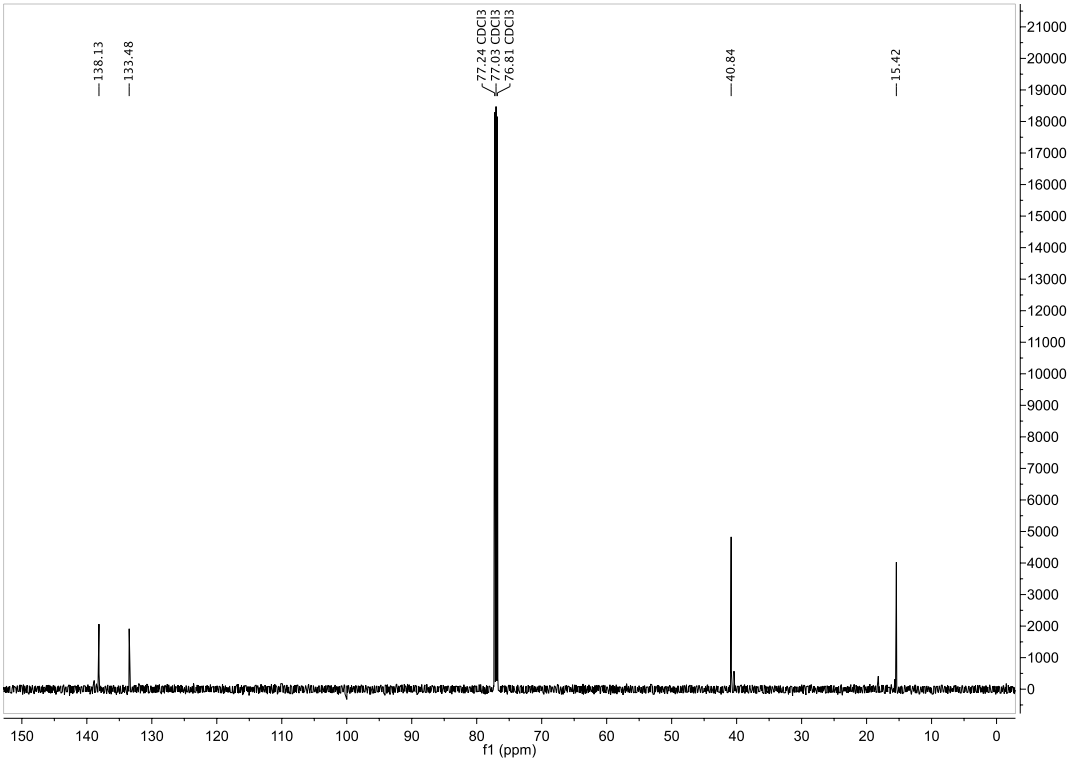

Figure D-62. ^{13}C NMR spectra for 1,3,5-tris(aminomethyl)-2,4,6-trimethyl benzene (triamine).

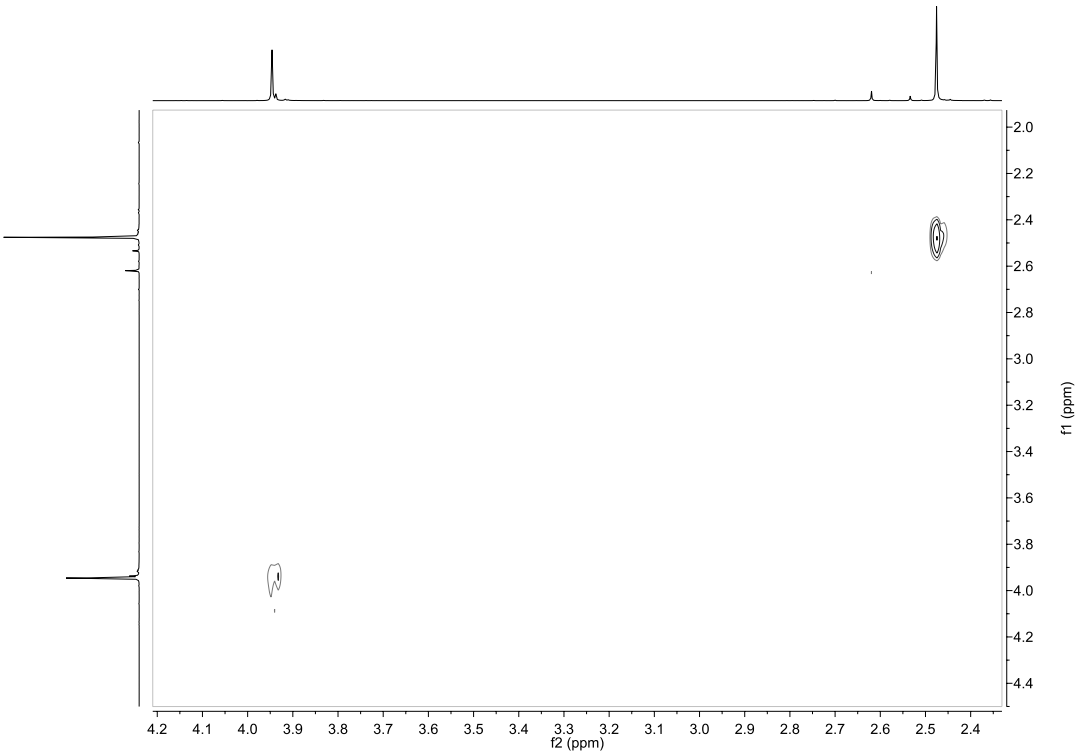

Figure D-63. COSY NMR spectra for 1,3,5-tris(aminomethyl)-2,4,6-trimethyl benzene (tri-amine).

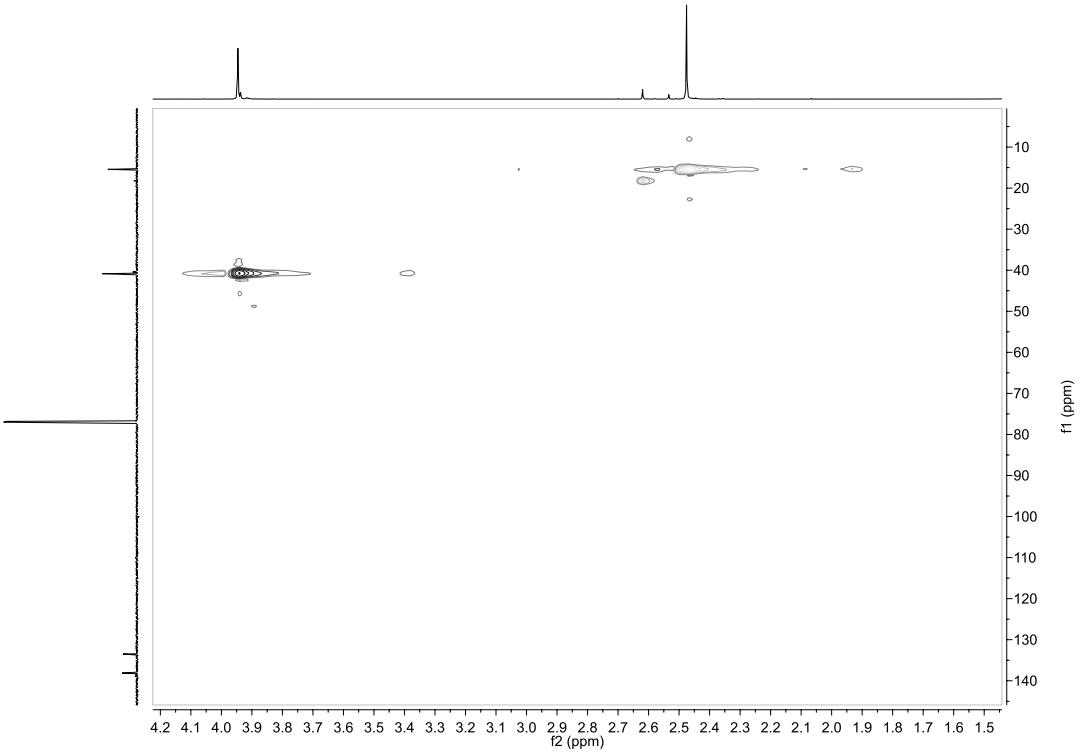

Figure D-64. HSQC NMR spectra for 1,3,5-tris(aminomethyl)-2,4,6-trimethyl benzene (tri-amine).

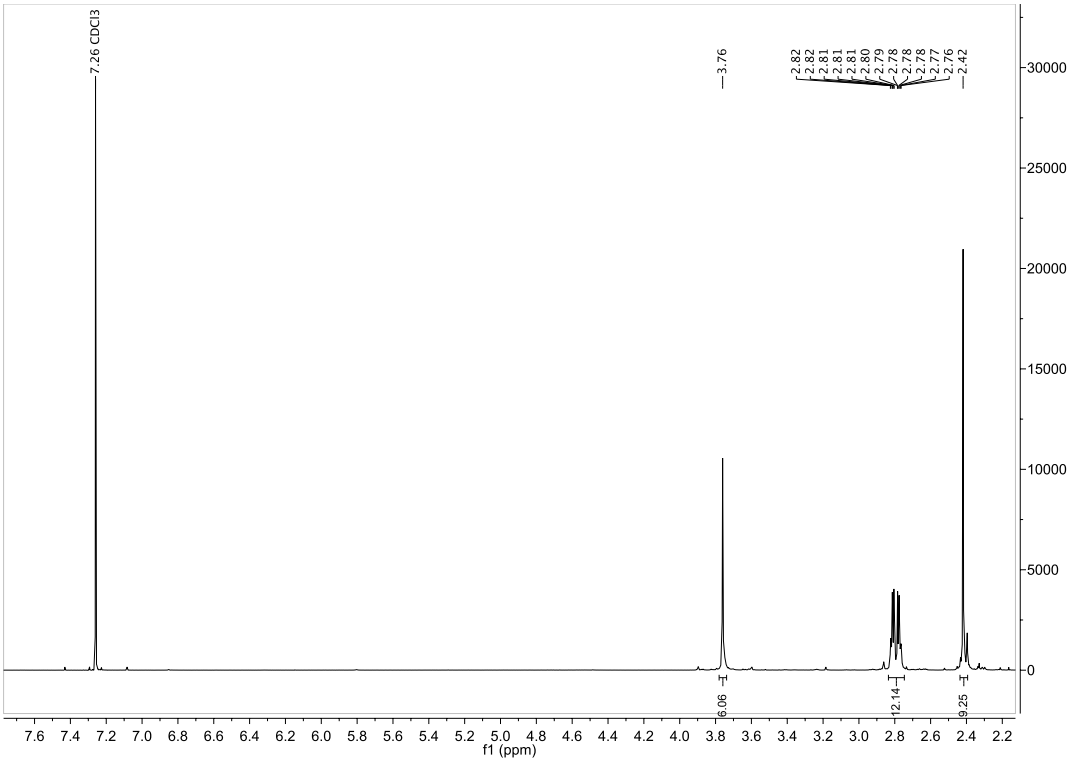

Figure D-65. ^{1}H NMR spectra for *N*^{1},*N*$^{1'}$,*N*$^{1''}$-((2,4,6-trimethylbenzene-1,3,5-triyl)tris(methylene)) tris(ethane-1,2-diamine) (NS234).

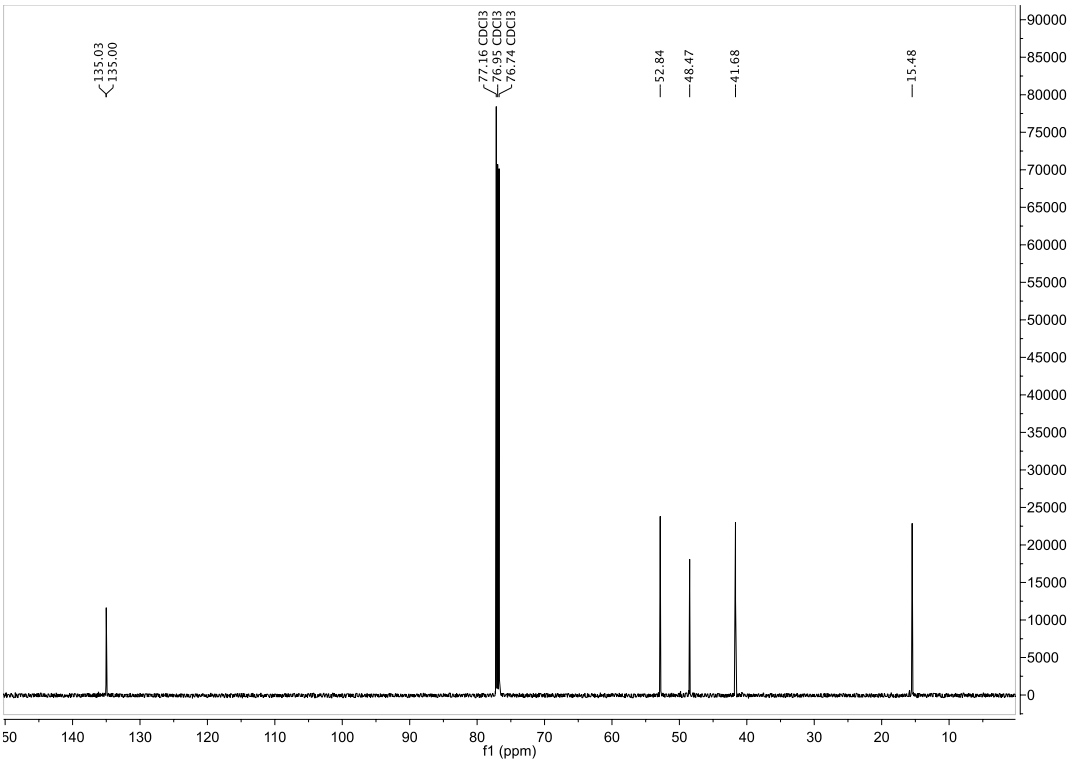

Figure D-66. ^{13}C NMR spectra for *N*^{1},*N*$^{1'}$,*N*$^{1''}$-((2,4,6-trimethylbenzene-1,3,5-triyl)tris(methylene)) tris(ethane-1,2-diamine) (NS234).

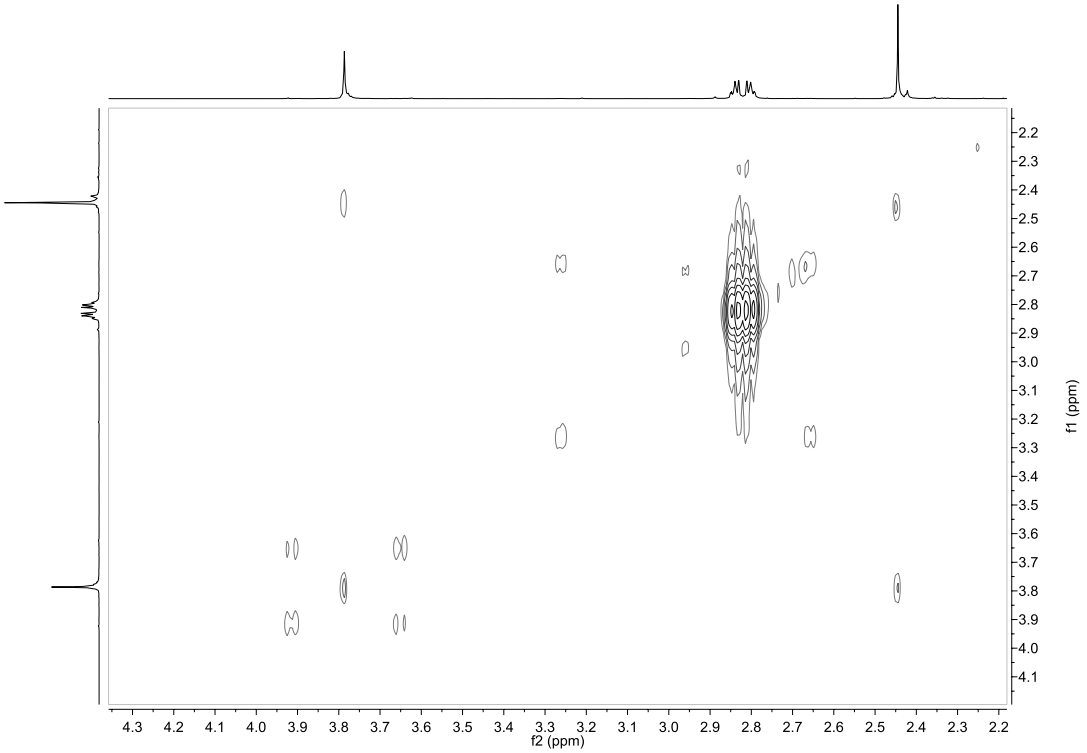

Figure D-67. COSY NMR spectra for *N*[1],*N*[1'],*N*[1'']-((2,4,6-trimethylbenzene-1,3,5-triyl)tris(methylene)) tris(ethane-1,2-diamine) (NS234).

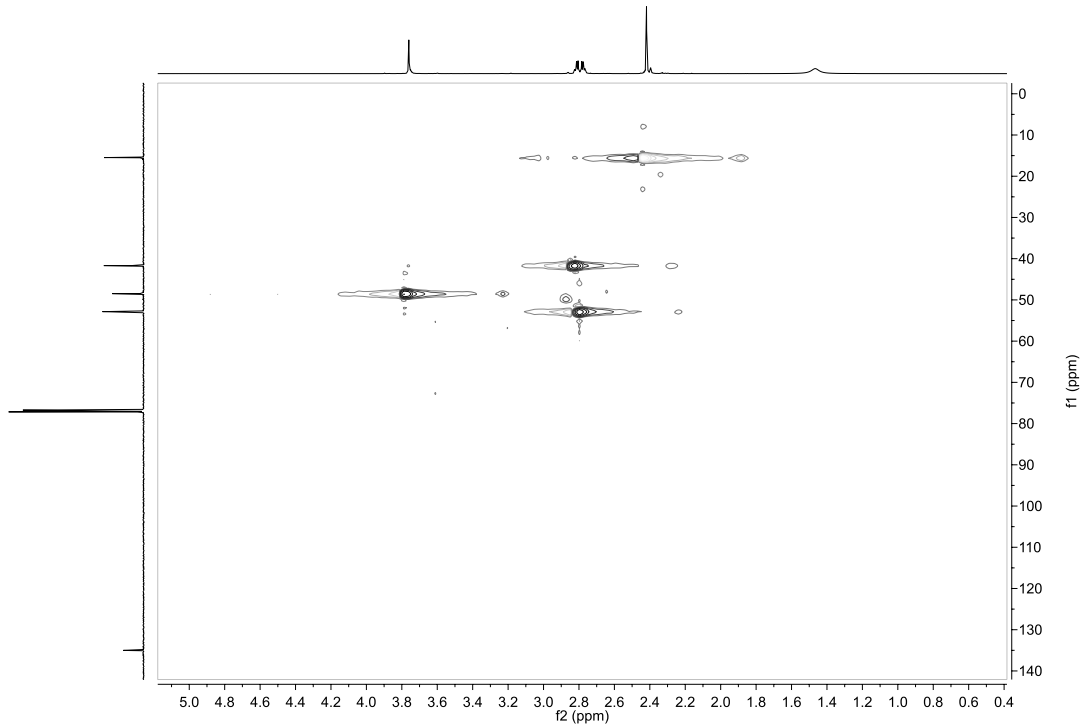

Figure D-68. HSQC NMR spectra for *N*[1],*N*[1'],*N*[1'']-((2,4,6-trimethylbenzene-1,3,5-triyl)tris(methylene)) tris(ethane-1,2-diamine) (NS234).

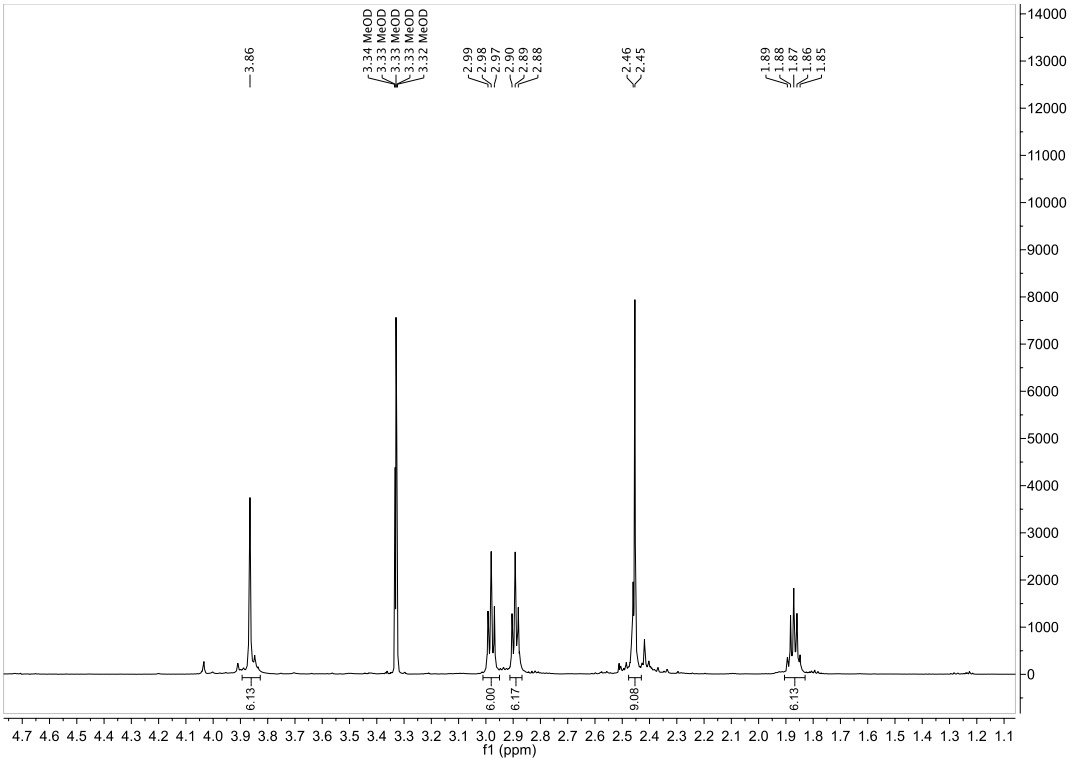

Figure D-69. ^{1}H NMR spectra for *N*^{1},*N*$^{1'}$,*N*$^{1''}$-((2,4,6-trimethylbenzene-1,3,5-triyl)tris(methylene)) tris(propane-1,3-diamine) (NS235).

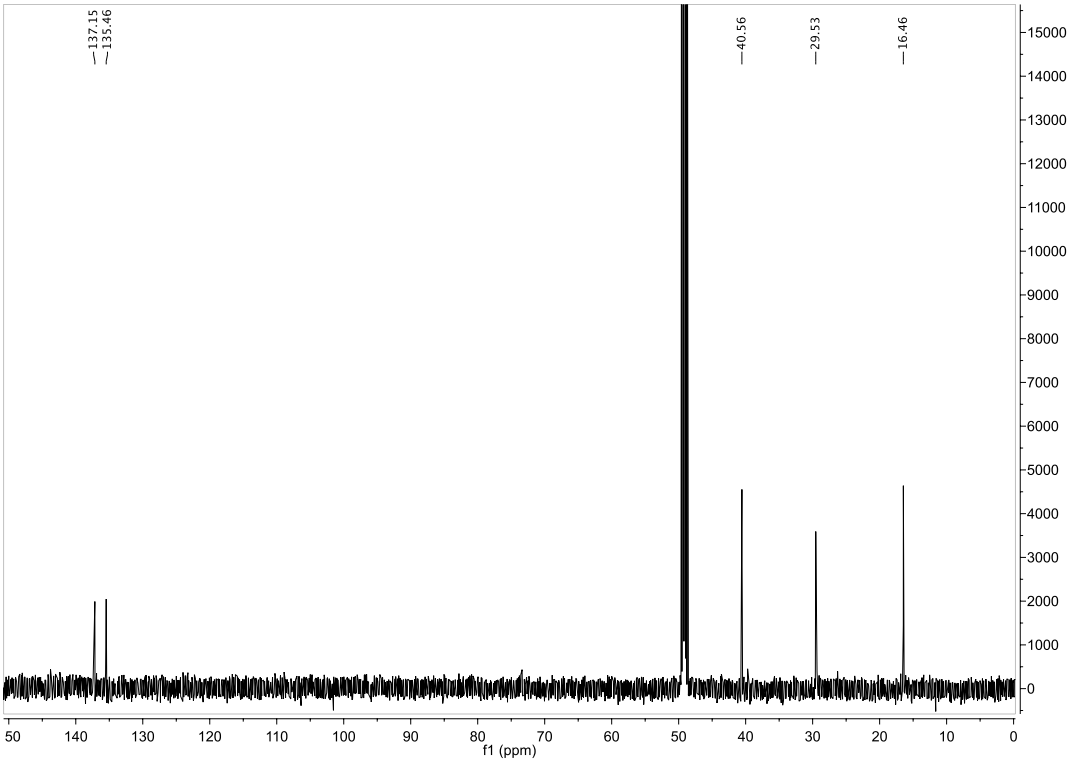

Figure D-70. ^{13}C NMR spectra for *N*^{1},*N*$^{1'}$,*N*$^{1''}$-((2,4,6-trimethylbenzene-1,3,5-triyl)tris(methylene)) tris(propane-1,3-diamine) (NS235).

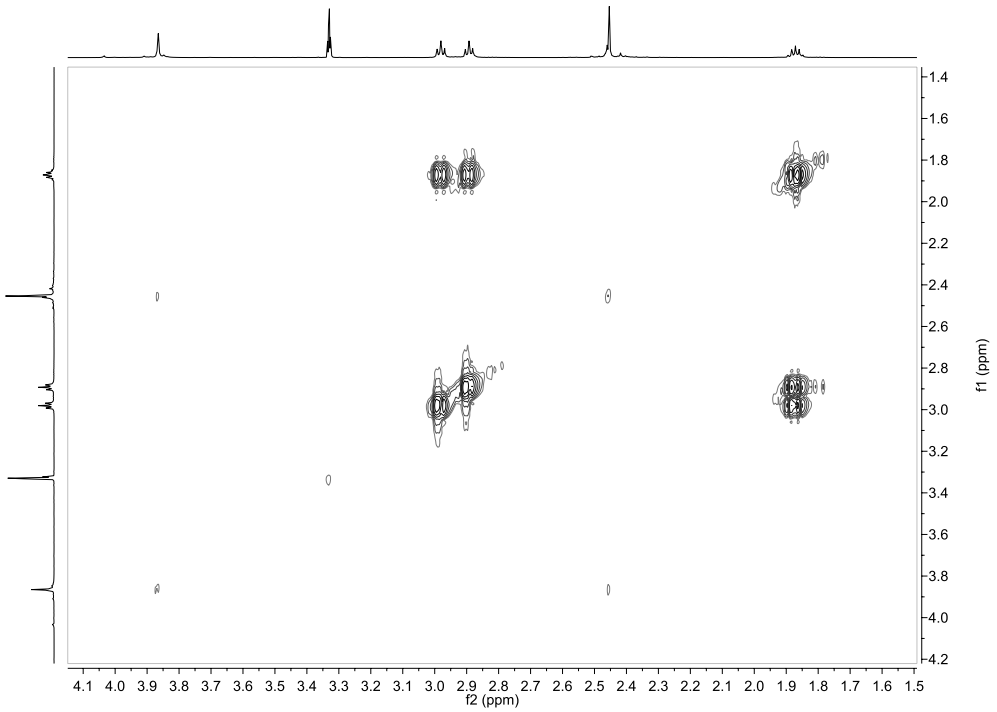

Figure D-71. COSY NMR spectra for $N^1,N^{1'},N^{1''}$-((2,4,6-trimethylbenzene-1,3,5-triyl)tris(methylene)) tris(propane-1,3-diamine) (NS235).

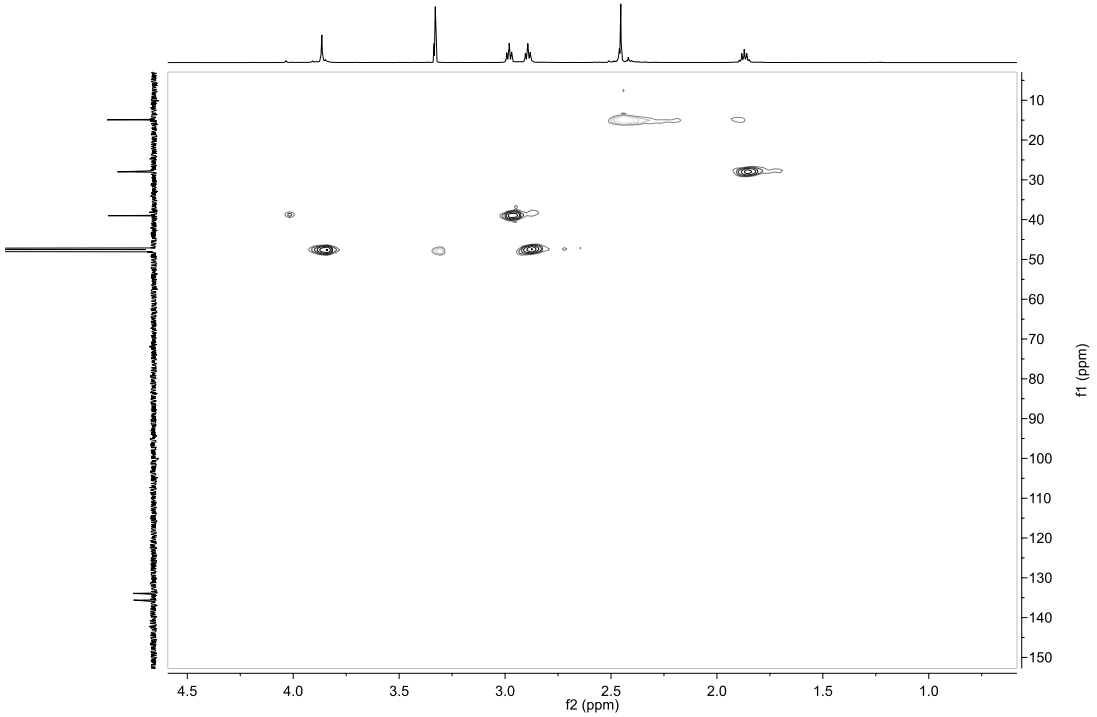

Figure D-72. HSQC NMR spectra for $N^1,N^{1'},N^{1''}$-((2,4,6-trimethylbenzene-1,3,5-triyl)tris(methylene)) tris(propane-1,3-diamine) (NS235).

D-5: References

1 J. Howarth and N. A. Al-Hashimy, *Tetrahedron Lett.*, **2001**, 42, 5777–5779.

2 N. Alhashimy, D. J. Brougham, J. Howarth, A. Farrell, B. Quilty and K. Nolan, *Tetrahedron Lett.*, **2007**, 48, 125–128.

3 T. H. J. Niedermeyer and M. Strohalm, *PLOS ONE,* **2012**, 7, e44913.

4 N. McStay, Z. Molphy, A. Coughlan, A. Cafolla, V. McKee, N. Gathergood and A. Kellett, *Nucleic Acids Res.*, **2017**, 45, 527–540.

5 J. L. Nallasivam and R. A. Fernandes, *Eur. J. Org. Chem.*, **2015**, 2012–2022.

6 J. R. Thomas, X. Liu and P. J. Hergenrother, *J. Am. Chem. Soc.*, **2005,** 127, 12434–12435.

7 X. Zhou, Y.-W. Yip, W.-H. Chan and A. W. M. Lee, *Beilstein J. Org. Chem.*, **2011**, 7, 75–81.

8 M. A. Tandiary, Y. Masui and M. Onaka, *RSC Adv.*, **2015**, 5, 15736–15739.

9 N.-H. Nguyen, J. W. Apriletti, J. D. Baxter and T. S. Scanlan, *J. Am. Chem. Soc.*, **2005**, 127, 4599–4608.

10 J. G. Rodríguez, A. Lafuente, R. Martín-Villamil and M. P. Martínez-Alcazar, *J. Phys. Org. Chem.*, **2001**, 14, 859–868.

11 G. A. Molander and F. Cadoret, *Tetrahedron Lett.*, **2011**, 52, 2199–2202.

12 M. Ishizaki and O. Hoshino, *Tetrahedron*, **2000**, 56, 8813–8819.

13 Y.-W. Yip, G.-L. Law and W.-T. Wong, *Dalton Trans*, **2016**, 45, 928–935.

14 G. Liu, Z. Xin, Z. Pei, P. J. Hajduk, C. Abad-Zapatero, C. W. Hutchins, H. Zhao, T. H. Lubben, S. J. Ballaron, D. L. Haasch, W. Kaszubska, C. M. Rondinone, J. M. Trevillyan and M. R. Jirousek, *J. Med. Chem.*, **2003**, 46, 4232–4235.

15 G. Macdonald, *Tetrahedron*, **1998**, 54, 9823–9836.

16 M. H. Y. Cheng, H. Savoie, F. Bryden and R. W. Boyle, *Photochem. Photobiol. Sci.*, **2017**, 16, 1260–1267.

17 P. M. Hergenrother, *J. Heterocycl. Chem.*, **1980**, 17, 5–10.

18 X. Wang and A. Studer, *Org. Lett.*, **2017**, 19, 2977–2980.

19 C. D. Jones, R. W. Luke, and W. McCoull, Pyrimidines with TIE2 activity, **2008**, United Kingdom, EP1737463.

20 T. T. Denton, X. Zhang and J. R. Cashman, *J. Med. Chem.*, **2005**, 48, 224–239.

21 N. De Rycke, F. Couty and O. R. P. David, *Tetrahedron Lett.*, **2012**, 53, 462–466.

22 J. N. Moorthy and S. Saha, *Eur. J. Org. Chem.*, **2010**, 6359–6365.

23 J. Podlaha, I. Císařová, D. Alexander, P. Holý, T. Kraus and J. Závada, *Collect. Czechoslov. Chem. Commun.*, **2000**, 65, 1587–1596.

24 M. Sawicki, D. Lecerclé, G. Grillon, B. Le Gall, A.-L. Sérandour, J.-L. Poncy, T. Bailly, R. Burgada, M. Lecouvey, V. Challeix, A. Leydier, S. Pellet-Rostaing, E. Ansoborlo and F. Taran, *Eur. J. Med. Chem.*, **2008**, 43, 2768–2777.

Appendix E

Supporting information accompanying Chapter V, DNA Recognition by Novel C_3-Symmetric “Tri-Click” Scaffolds.

E-1: Materials and Methods

The pH was monitored by a Mettler Toledo InLab Expert Pro-ISM pH probe.

E-2: DNA binding investigation (pUC19 scDNA)

DNA nuclease, condensation study.

This procedure was adapted from previously published protocols.[1] Tri-Click samples were initially prepared in DMF and further diluted in 80 mM HEPES buffer (Fisher). Reactions were carried out according to the following general procedure: in a total volume of 20 μL using HEPES buffer (80 mM) with 25 mM NaCl, 400 ng pUC19 (NEB, N3041) and varying concentrations of test compounds were incubated at 37°C for a defined period as per reaction either 90 min, 6 h, 12 h or 24 h. Reactions were quenched by adding 6x loading buffer (Fermentas) containing 10 mM Tris-HCl, 0.03% bromophenol blue, 0.03% xylene cyanole FF, 60% glycerol, 60 mM EDTA and samples were loaded onto an agarose gel (1.2%) containing 4 μL EtBr. Electrophoresis was completed at 70 V for 1 h in 1x TAE buffer, unless otherwise stated.

DNA nuclease in acidic and basic buffers.

A total of 400 ng of pUC19 DNA was treated as previously stated with slight modifications. Samples were incubated in acidic and basic buffers at pH 4.0 and 9.0, respectively. Sodium acetate (NaOAc, 80 mM) and Tris buffers (80 mM) were prepared and adjusted with HCl and NaOH accordingly to achieve the desired pH. Samples were loaded onto an agarose gel (1.2%) containing 4 μL EtBr. Electrophoresis was completed at 70 V for 60 min in 1x TAE buffer.

Metal Ion influence

Tri-Click samples (100 μM) were co-incubated with metal ions: copper(II) nitrate trihydrate, manganese (II) chloride tetrahydrate, and zinc acetate dihydrate (300 μM) for 30 mins prior to the addition to a total of 400 ng of pUC19 DNA treated as previously stated with slight modifications. Samples were incubated in HEPES (80 mM) or acidic buffer (NaOAc, 80 mM) for 90 mins prior to electrophoresis which was carried out as previously stated.

E-3: UV-Vis studies of TC1-Cu(II)

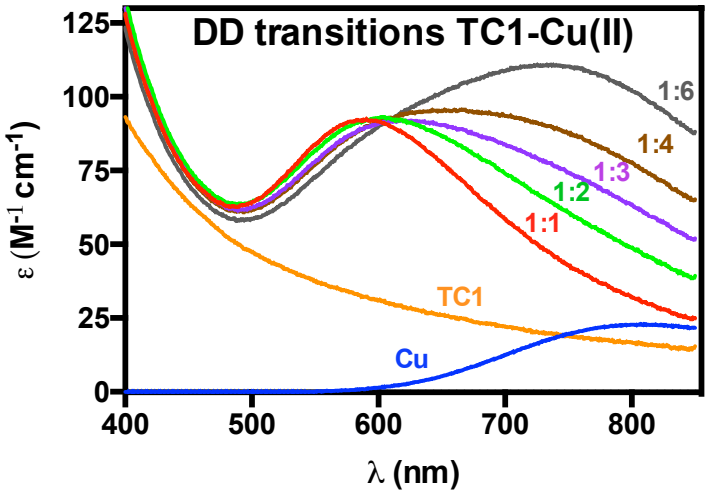

Figure E-1. UV Scans of **TC1**-Cu(II) complex at ratios of 1:1-4, and 1:6 (**TC1**:Cu) where the concentration of **TC1** is kept constant (2 mM) and the concentration of Cu(II) is varied from 2 mM up to 12 mM. The absorbance recorded were divided by the concentration and data were plotted against the extinction coefficient ε (M^{-1} cm^{-1}). Samples were incubated for 30 mins and each sample measured three times. **TC1** stock was prepared in DMF and diluted to its final concentration in H_2O, the percentage of DMF in water was <5 %, all copper(II) samples were prepared in H_2O.

E-4: DNA Damage Studies of TC1-Cu(II)

DNA cleavage

Stock solutions of the complex was initially prepared in DMF and further dilutions prepared in 80 mM HEPES buffer (pH 7.2). Superhelical pUC19 plasmid DNA (400 ng) was exposed to increasing concentrations of each **TC1**-Cu(II) in the presence of 25 mM NaCl. Reaction mixtures were mixed thoroughly and incubated at 37 ˚C. Reactions were quenched by the addition of 6× loading buffer (Fermentas) containing 10 mM Tris-HCl, 0.03% bromophenol blue, 0.03% xylene cyanole FF, 60% glycerol, 60 mM EDTA and subjected to gel electrophoresis as previously described.

DNA cleavage in the presence of added reductant

400 ng pUC19 plasmid was exposed to increasing concentrations of each **TC1**-Cu(II) in the presence of 25 mM NaCl and 1 mM Na-L-ascorbate. Reaction mixtures were vortexed and incubated at 37 ˚C for 30 min. Reactions were quenched with 6× loading buffer (Fermentas). Electrophoresis was carried out at 70 V for 90 minutes in 1× TAE buffer and photographed using a UV transilluminator.

Atomic Force Microscopy (AFM)

AFM samples were prepared according to the following general procedures detailed below in the presence and absence of exogenous reductant.

In the presence of reductant: A total volume of 20 μl containing pUC19 (200 ng), MgCl (10 mM), varying concentrations of test compound **TC1**-Cu(II) (0.5, 1.0, 7.5 and 10 μM) in the presence of Na-*L*-Ascrobate (1mM) were incubated for 25 min at 37°C. Samples were further diluted to a DNA concentration of 2-3 ng/μl in a final volume of 10 μl with nuclease free H_2O and incubated on freshly cleaved mica.
In the absence of reductant: A total volume of 10 μl final concentrations of 3 ng/μl of pUC19 (NEB, N3041), 5 mM MgCl and varying concentrations of test compound **TC1**-Cu(II) (5, 10 and 30 μM), samples were incubated at 37°C for 1 h.

Mica was freshly cleaved prior to incubating with samples (10 μl, 5 mins) and rinsed thoroughly with nuclease free water (500 μl). Samples were dried under compressed air. AFM examinations were performed in ambient air with a commercial microscope (Bruker Dimension Icon AFM), in tapping-mode, using super sharp silicon cantilevers (SSS-NCHR, Windsor Scientific Ltd) with a 40 N/m force constant. Topographic images are recorded at a scanning rate of >1 Hz, and a resonance frequency of about 300 kHz (nominal value). Images were processed using the WSxM software[2] to remove the background slope and normalize the z-scale across all images, no additional filtering was performed.

DNA cleavage in the presence of ROS scavengers

The assay was conducted according to the method recently reported.[3,4] Briefly, to a final volume of 20 μL, 80 mM HEPES, 25 mM NaCl, 1 mM Na-*L*-ascorbate, and 400 ng of pUC19 DNA were treated with varying drug concentrations **TC1**-Cu(II) (0.5, 1.0, 2.5, and 4.0 μM) in the presence ROS scavengers; sodium azide (NaN_3, 10 mM), KI (10 mM), DMSO (10 %), D_2O (77 %), 4,5-Dihydroxy-1,3-benzenedisulfonic acid (Tiron, 10 mM), D-Mannitol (10 mM), *N'*-dimethylthiourea (DMTU, 10 mM), and L-Methionine (10 mM). Reactions were vortexed and incubated at 37 °C for 30 min and electrophoresis carried out as previously stated.

DNA cleavage in the presence repair enzymes

The assay was conducted according to the method recently reported by Fantoni *et al.*[4] with slight modifications. Supercoiled pUC19 DNA (400 ng) in 80 mM HEPES, 25 mM NaCl, 1 mM Na-*L*-ascorbate in a final volume of 20 µL nuclease free H_2O, was pre- incubated with **TC1**-Cu(II) for 30 min at 37 ˚C at concentrations of 2.5, 5.0 and 7.5 μM. The following reactions were supplemented with associated buffers as per manufacturer recommendations; those with Fpg contained 1 mg/mL BSA and 1× NEB Buffer 1, Endo III with 1× NEB Buffer 1, Endo IV with 1× NEB Buffer 3, Endo V with 1× NEB Buffer 4 and hAAG with 1× ThermoPol. Subsequently, 2 units of repair enzymes FpG (NEB, M0240S), endonuclease (Endo) III (NEB, M0268S), Endo IV (NEB, M0304S), Endo V (NEB, M0305S) and hAAG (NEB, M0313S) were added to the reaction mixture and incubated for 30 min, 37 ˚C. Samples were denatured with 0.25 % SDS, 250 µg/mL proteinase K and heated to 50 ˚C for 20 min. Reactions were quenched by adding 6x loading buffer (Fermentas) containing 10 mM Tris-HCl, 0.03% bromophenol blue, 0.03% xylene cyanole FF, 60% glycerol, 60 mM EDTA and samples were loaded onto an agarose gel (1.2%) containing 4 µL EtBr. Electrophoresis was completed at 70 V for 1 h in 1x TAE buffer and imaged using UV transilluminator.

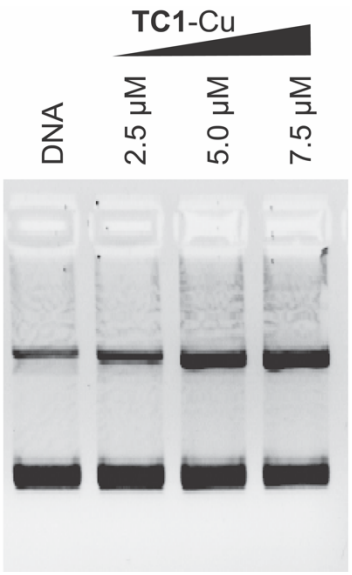

Figure E-2. TC1-Cu(II) (2.5, 5, and 7.5 µM; lanes 2-4) in the presence of 1 mM Na-*L*-ascorbate under the same conditions carried as per the repair enzyme protocol. Samples incubated for 30 min, 37 ˚C, prior to gel electrophoresis.

E-5: References

1 N. McStay, Z. Molphy, A. Coughlan, A. Cafolla, V. McKee, N. Gathergood and A. Kellett, *Nucleic Acids Res.*, **2017**, 45, 527–540.

2 I. Horcas, R. Fernández, J. M. Gómez-Rodríguez, J. Colchero, J. Gómez-Herrero and A. M. Baro, *Rev. Sci. Instrum.*, **2007**, 78, 013705.

3 C. Slator, Z. Molphy, V. McKee and A. Kellett, *Redox Biol.*, **2017**, 12, 150–161.

4 N. Z. Fantoni, Z. Molphy, C. Slator, G. Menounou, G. Toniolo, G. Mitrikas, V. McKee, C. Chatgilialoglu and A. Kellett, *Chem. Eur. J.*, **2018**, DOI:10.1002/chem.201804084.